# INSITU MEASUREMENT OF DYNAMIC SOIL PROPERTIES WITH EMPHASIS ON DAMPING

by

WILLIAM PATRICK STEWART

B.A.Sc.- Hons. (Civil Engineering)
University of British Columbia
M.Sc. (Civil Engineering - Geotechnical)
University of Alberta

A THESIS SUBMITTED IN PARTIAL FULFILLMENT OF

THE REQUIREMENTS FOR THE DEGREE OF

Doctor of Philosophy

in

THE FACULTY OF GRADUATE STUDIES

CIVIL ENGINEERING

We accept this thesis as conforming

to the required standard

THE UNIVERSITY OF BRITISH COLUMBIA

April 1992

Civil Engineering

The University of British Columbia
2075 Wesbrook Place
Vancouver, Canada
V6T 1W5

Date: 14 April 1992

## ABSTRACT

Measurements of the shear wave velocity ($V_s$) of near-surface soils by downhole and crosshole techniques have become fairly common, including the use of the seismic cone penetration test (SCPT) both at UBC and commercially. A full trace (typically in the order of 400ms long) of the received signal is normally recorded at selected depths, but traditionally only one point is used to determine $V_s$. This research is to determine if, these records could provide, at minimal cost, further information on soil properties. Initially alternate methods of $V_s$ calculation were investigated, but the main thrust of this research was use of the amplitude information in the signals to determine low-strain damping.

A variety of equipment; including three source types (mechanical swing hammer, Buffalo gun, and drop weight), three types of receivers (accelerometer, geophone, and bender), and the use of two cones; has been investigated and used for SCPT's at several sites.

The nature of the measured signals in both the time and frequency domain has been investigated and the importance of windowing to isolate the shear wave from the balance of the signal has been clearly demonstrated.

The cross-over method of velocity determination has been most commonly used at UBC. Two other methods (cross-correlation and phase of cross-spectrum) have been developed and compared. The recommended approach is the phase of the cross-spectrum method applied to windowed signals.

Five methods of damping calculation have been considered in some detail. Three of the methods (rise time, attenuation coefficient, and spectral ratio slope{SRS}) were available in the literature, and the other two methods (modified SHAKE and damping spiral) were developed as part of this research. The most general is the damping spiral method, and it can be shown that the SRS method is a special case of the damping spiral approach. The SRS method is applied simultaneously for several depths within a soil layer, eliminates geometric corrections and was found to be the most accurate approach.

Attempts were made to evaluate damping from actual earthquake records, both local (Pender Island earthquake, using SHAKE) and foreign (Lotung array, Taiwan, using the SRS method), but met with little success.

Specific recommendations have been developed for all three facets of the measurement and calculation of damping. It has been shown that these recommendations lead to results that are repeatable and that are consistent with both laboratory and published values, for both shear wave velocities and damping.

## TABLE OF CONTENTS

## LIST OF TABLES

**LIST OF FIGURES**

## LIST OF SYMBOLS

| | |
|---|---|
| A, $A_o$ | Amplitude of wave, amplitude at source (V or g) |
| a,b | Best-fit parameters (depend on base units) |
| c,d | Series to be fitted (slopes with frequency {s}, depths {m}) |
| c | Phase velocity (m/s) |
| CV | Coefficient of variation (decimal or %) |
| $CV_D$ | CV of damping |
| $CV_v$ | CV of velocity |
| $CV_z$ | CV of slope of Spectral Ratio Slope (SRS) with depth |
| Coh | Coherence function (decimal) |
| $D_s$, $D_l$ | Fraction of critical damping of shear, longitudinal waves (decimal or %) |
| d | Measure of damping (decimal or %) |
| $d_{cap}$ | damping capacity |
| $d_{log}$ | damping by logarithmic decrement |
| $d_{loss}$ | damping by loss coefficient |
| E, F | Amplitude Coefficients for SHAKE (m) |
| e | Deviation from best-fit (depends on base unit) |
| f | Frequency (Hz) |
| $f_A$, $f_B$ | resonant frequencies of layers A, B |
| $f_o$ | predominant frequency (frequency at greatest magnitude) |
| $f_r$ | resonant frequency |
| $f_1$, $f_2$ | frequencies at half-power points |

| | |
|---|---|
| FFT | Fast Fourier transform |
| $G$ | Shear modulus (kPa) |
| $G_{max}$ | maximum shear modulus (at small strain) |
| $G^*$ | complex shear modulus |
| $G$ | Total geometric correction |
| $G_1$ | - for near receiver |
| $G_2$ | - for far receiver |
| $G_{ij}$ | Average correlation function of signals (typ. $\{V/Hz\}^2$) |
| $G_{xx}, G_{yy}$ | average auto-correlation |
| $G_{yx}$ | average cross-correlation |
| $G_{yx}^*$ | conjugate of average |
| $\lvert H \rvert$ | Magnitude of transfer function (typ. $\{V/Hz\}$) |
| $h$ | Sample height (m) |
| $I$, $I_o$ | Mass moment of inertia of sample, of driving cap in resonant column test (kg-m$^2$) |
| $k$ | Wavenumber (1/m) (= $2\pi/L$) |
| $L$ | Wavelength (m) |
| $N$ | SPT blowcount (blows/0.3m) |
| O.C. | Overconsolidated |
| $p_a$ | Atmospheric pressure (101.3kPa) |
| $Q$, $Q^{-1}$ | Quality factor and its inverse, a measure of damping (dimensionless) |
| $q_c$ | Measured cone bearing (typ. bars) |

| | |
|---|---|
| r12 | Reflectivity coefficient for wave passing from layer 1 to layer 2 (decimal) |
| $S_{ij}$ | Spectral ratio slope computed using signals i/j (s) |
| $S_n$ | Average of noise spectra ($\{V/Hz\}^2$) |
| s | Standard deviation (depends on base unit) |
| $s_b^2$ | variance of slope of fit |
| $s_c^2$ | variance of fit with depth |
| $s_s^2$ | variance due to standard deviation of SRS |
| $s_T^2$ | variance of total (slope and standard deviations) |
| $s_u$ | Undrained shear strength (kPa) |
| T | Period (s) |
| | Travel time (s) in rise-time method (RTM) of analysis |
| t | Time (s) |
| | Rise time in RTM |
| t(f) | Time as a function of frequency |
| $t_o$ | rise time at source in RTM |
| $t_I$ | interval travel time |
| $t_{12}$ | Transmissivity coefficient for wave passing from layer 1 to layer 2 (decimal) |
| T&D | Combined transmissivity and divergence correction |
| $V_s$ | Shear wave velocity (m/s) |
| $V_n$ | shear wave velocity of layer n |
| $V_m$ | peak particle velocity |

| | |
|---|---|
| v(f) | Shear wave velocity as a function of frequency |
| w | Weighting factor (dimensionless) |
| x | Distance (m) |
| $x_1$ | - to near receiver |
| $x_2$ | - to far receiver |
| X(f) | Fast Fourier Transform (FFT) of a signal (typ. V/Hz) |
| z | Slope of SRS with depth (s/m) (= $\alpha$/f) |
| $\alpha$ | Attenuation coefficient (1/m) |
| $\gamma_p$ | Peak shear strain (decimal or %) |
| $\theta$ | Angle of incidence (typ. radians) |
| $\kappa$ | Real part of k (1/m) (= $\omega$/c) |
| $\rho$ | Soil density (kg/m$^3$) |
| $\sigma$ | Stress (kPa) |
| $\sigma_o$ | mean effective confining stress (Saxena and Reddy, 1989) |
| $\sigma_{3c}'$ | confining pressure (Zavoral, 1990) |
| $\Phi$ | Discontinuous phase (typ. radians) |
| $\phi$ | Phase (typ. radians) |
| $\omega$ | Angular frequency (rad/s), Resonant angular frequency - resonant column tests |

**ACKNOWLEDGEMENTS**

The writer wishes to thank his research advisor, Professor R.G. Campanella for providing the research equipment and facilities and for discussions and assistance throughout the period of this research. The writer would also like to acknowledge the other faculty in the Department of Civil Engineering at UBC, particularly Professor P.M. Byrne, for their helpful comments; and the technical staff , particularly Scott Jackson and Harald Schrempp, for their assistance. Discussions with other graduate students, particularly Mr. Alex Sy, were useful in the research and assistance with the field work was appreciated.

Financial assistance for this research was made possible through grants from the Canadian National Science and Engineering Research Council. Financial support was provided by UBC and through a GREAT Scholarship provided by the Science Council of B.C. with the support of Conetec Investigations Ltd.

Most importantly, the writer would like to acknowledge his wife Donna, who provided encouragement and support both to begin the program and throughout the research. This thesis is dedicated to her.

# CHAPTER 1

# INTRODUCTION

## *1.1 PURPOSE AND SCOPE*

The evaluation of civil engineering problems involving the transmission of waves through soil, such as seismic response under earthquake loading and foundation response under dynamic loading, requires a knowledge of the appropriate soil stiffness and damping properties. In contrast to static loading, dynamic or cyclic loading imposes stress reversals on the soil requiring a more detailed evaluation of the soil properties. In particular, for the earthquake problem, the primary concern is with horizontal waves passing vertically upwards from bedrock through the soil, i.e. shear waves, and the soil properties of greatest concern are the shear modulus, G, and the damping of shear waves, $D_s$.

Determination of these properties, as with other soil properties, has traditionally been carried out in the laboratory. Laboratory testing offers significant advantages in providing control of a wide range of stress and strain conditions. However sampling of the soil must cause some level of disturbance, and in granular soils, can cause a high level of disturbance. As well, it is difficult to reproduce the insitu stress conditions. Some studies (Richart et al, 1977) have shown that the small strain shear modulus, $G_{max}$, can be underestimated by laboratory testing, especially for clays.

The laboratory tests can be complemented with insitu soil tests. These tests offer the advantage of sampling a larger volume of soil that has been minimally disturbed by the insertion of the testing tool. Elastic theory has been used to show that $G_{max}$, can be determined from the shear wave velocity, $V_s$, and soil density, $\rho$ ( = unit weight, $\gamma$, divided by acceleration of gravity, g), as follows:

$$[1.1]\ G_{max} = \rho\, V_s^2 = (\gamma/g)V_s^2$$

The measurement of soil properties from insitu tests is based on wave propagation theory. A wave is characterized by the transport of energy through the soil by particle motion, without any permanent displacement of the soil itself. Waves can be broadly classified into surface and body waves. Surface waves may exist when there is a surface separating media of different properties (e.g. soil and air). Examples of surface waves are Rayleigh (vertically polarized) and Love (horizontally polarized) waves. Body waves are waves that can exist in an ideal full space, or travel in a region that is not affected by a free surface, and consist of compression (longitudinal, P-) waves and shear (transverse, S-) waves. The particle motion is in the direction of the wave propagation in P-waves, and is perpendicular to the direction of wave propagation in S-waves. Body waves can also be classified by the shape of the wavefronts, with the most commonly referenced shapes being plane and spherical.

If both P- and S-wave velocities can be measured, two elastic constants ( say G and Poisson's ratio , $\nu$) can be calculated. However at shallow depths in uncemented, saturated soils the P-wave is transmitted mainly by the water and measured values of the velocity, $V_p$, remain fairly constant at 1500-1600m/s (close to or slightly greater than that of water alone). However water cannot carry shear stresses, so that in saturated soils the S-wave is transmitted by the soil grains, and the wave velocity, $V_s$, is a measure of the soil deformability, $G_{max}$. Typical values of $V_s$ at different sites vary from about 50m/s to greater than 300m/s.

Because of the importance of shear loading, the use of shear modulus in many modelling techniques, and the ability of obtaining measurements in both saturated and partially saturated soils, measurements of $V_s$ have become fairly common, using downhole, crosshole, or spectral analysis of surface wave (SASW) techniques. Studies at the University of B.C. (UBC) have concentrated on downhole measurements with a receiver in a piezocone, i.e. the seismic cone penetration test, SCPT (beginning with Campanella and Robertson,1984). Generally speaking, a complete record of a signal is recorded at each depth. Determination of the shear wave velocity normally uses only one point in the signal; i.e. the shear wave arrival, cross-over, first peak, etc. and the balance of the signal is not used.

Two typical signals at different depths are shown in Fig.1.1. It can be observed that the time of arrival of the shear wave has shifted

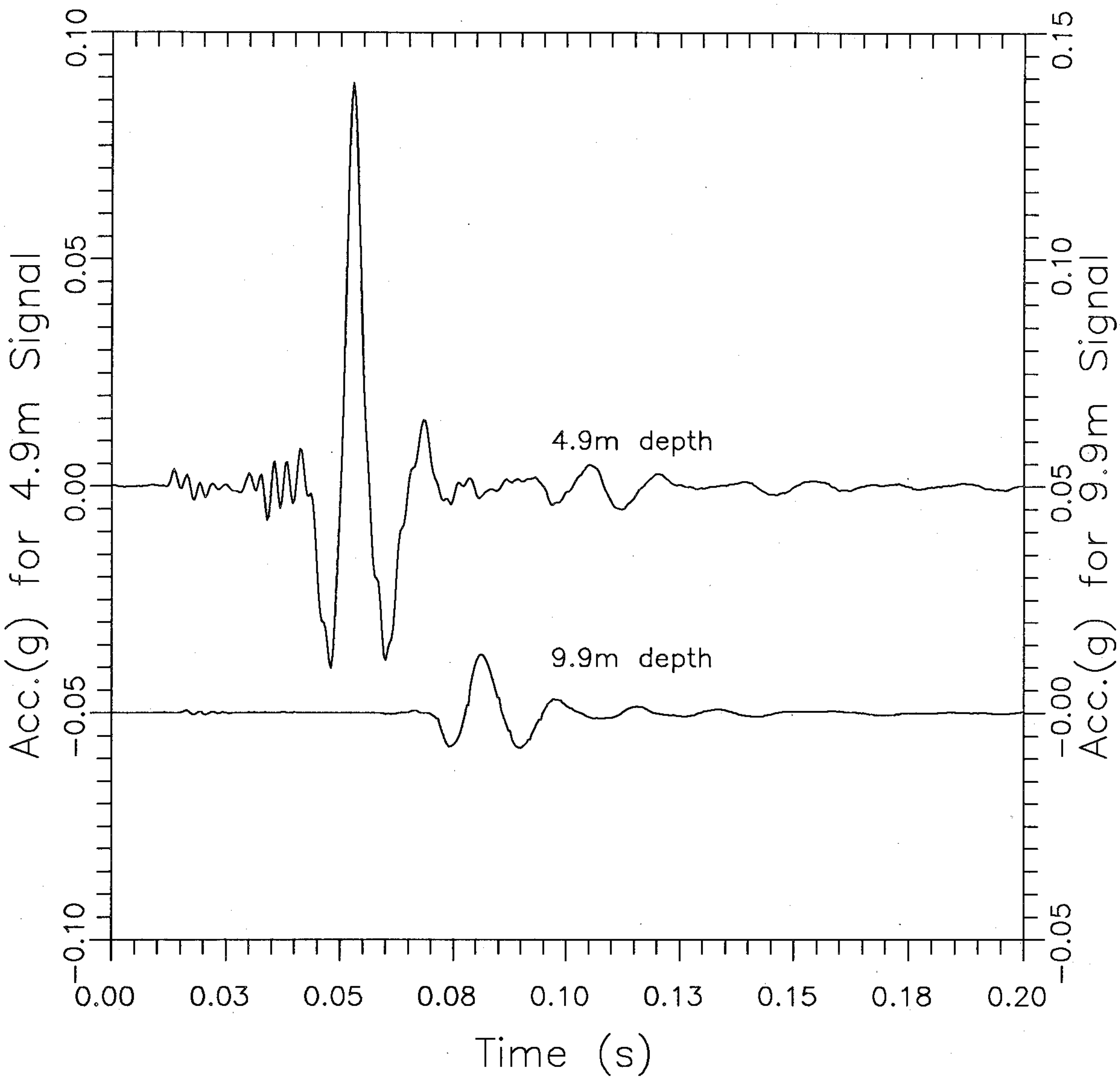


Fig.1.1 Typical Signals from Seismic Cone Penetration Test

about 28ms, and this information can be used to calculate the velocity. It can also be observed that the deeper signal is smaller; the peak is about seven times smaller than that of the upper signal. A more detailed look shows that the shape of the wave has changed slightly. The ratio of the peak to the trough as about 2.2 for the upper signal and about 1.8 for the lower signal, and the distance (time shift) between the troughs is slightly greater in the deeper signal.

The objective of the present research was to determine if records made for shear wave velocity measurements could provide, at minimal cost, further information on soil properties. Earlier research on the use of the crosscorrelation function for $V_S$ determination has been expanded, and use of the phase of the cross-spectrum to determine $V_S$ was investigated. However the main thrust of the research was the use of amplitude information in the signals to determine low-strain damping.

Measurement and calculation of amplitude information is inherently more difficult than simply picking the time an event occurs in a signal. However recent advances in instrumentation and signal analysis software have allowed progress in these areas, and thus in the insitu measurement of damping.

Development of the methodology required evaluation of the equipment (especially sources and receivers), field procedures, and calculation methods. Both existing and newly developed calculation methods were evaluated for stability (error analysis), repeatibility and confirmation with existing information. Four different research sites with soil conditions ranging from clay to sand were tested at various times over a two-year period. Standard equipment, procedures and calculation method were selected and successfully compared with laboratory and published results.

### *1.2 THESIS ORGANIZATION*

Chapter 2 gives a discussion on dynamic soil properties, provides definitions of terms used and formulations of the equations used in the calculations, and presents a discussion of transforms to and calculations in the frequency domain. A compilation of previous investigations provided in the literature is given in Chapter 3.

A description of the test sites investigated is provided in Chapter 4, followed by a discussion of the equipment used and the nature of the recorded signals in Chapter 5.

The measurements, methods of analysis and results for $V_s$ and $D_s$ are detailed in Chapters 6 and 7, and available means of confirmation of the results are provided in Chapter 8.

Chapter 9 presents the major findings of this thesis and offers recommendations for future research.

The appendices provide detailed analyses of the complex cepstrum method and of three approaches to damping calculations that ultimately proved unsuccessful as well as the main macros and programs used in this research.

## CHAPTER 2

## DYNAMIC PROPERTIES, FORMULATIONS, AND FREQUENCY DOMAIN

### *2.1 INTRODUCTION*

Both the general nature of, and the factors affecting, shear modulus and damping are discussed. Various definitions of damping that have been developed are explored. The equations of wave propagation are provided and extended in several ways to show various methods of damping calculation. A basic development of the fast Fourier transform is provided, with an introduction to frequency domain observations and calculations.

### *2.2 SHEAR MODULUS, G, WITH AN EMPHASIS ON $G_{MAX}$*

The stress-strain behaviour of soils is more complex than that of many man-made engineering materials. Fig.2.1 schematically presents a portion of a cyclic triaxial test on soil. For the first loading on the soil (shown dashed) the stress-strain curve tends to be hyperbolic, i.e. the secant modulus, G, decreases with strain. The initial slope of the curve is given by the low-strain modulus, $G_{max}$. Insitu tests are limited to small strains (usually < $5x10^{-3}$%), so that the modulus of concern is $G_{max}$. The stress-strain curve during unloading is not the same as that during loading, giving rise to a closed hysteresis loop. This is discussed in section 2.3.

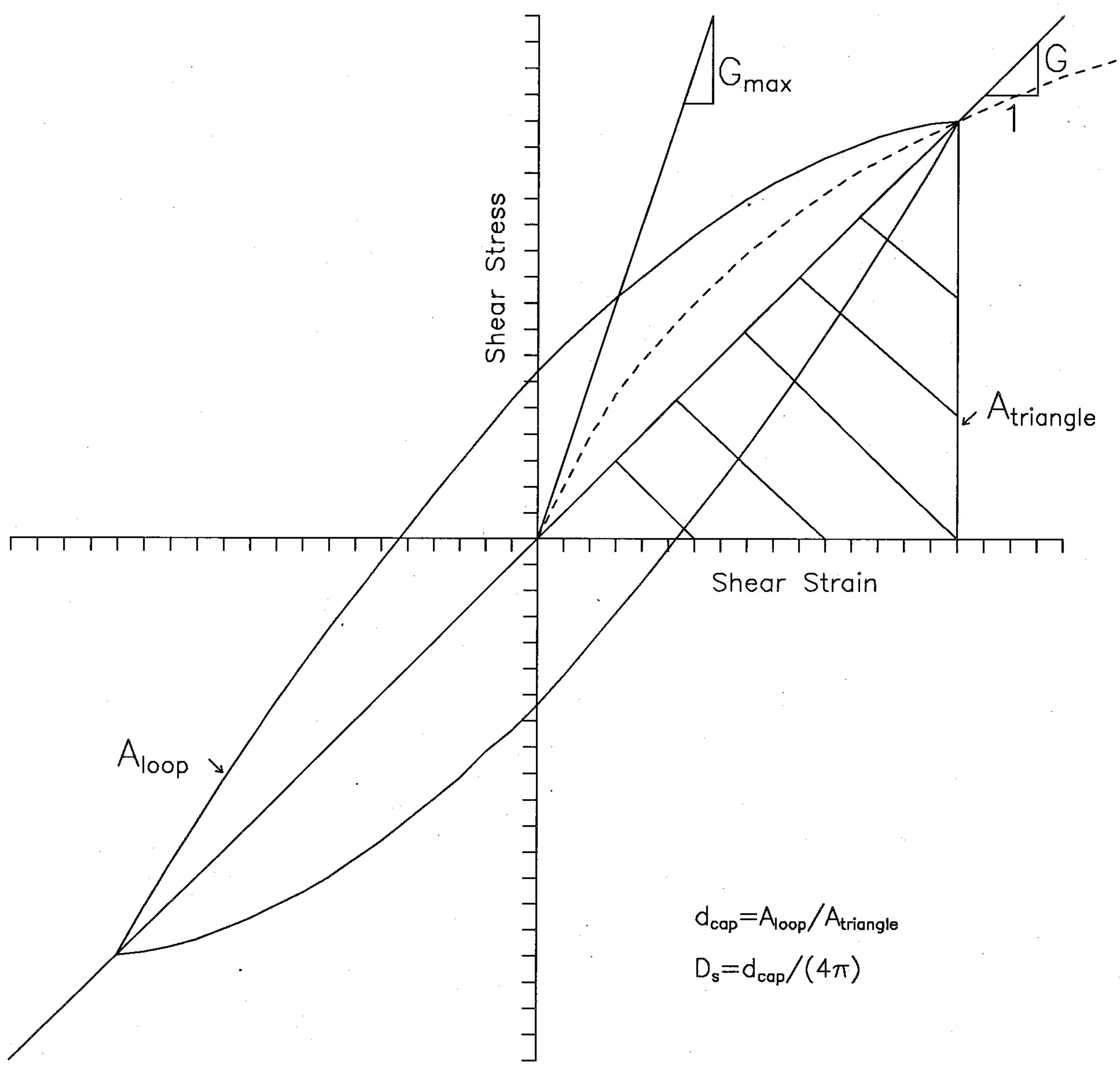


Fig.2.1 Stress—Strain Curve for Cyclic Loading of Soil

Hardin and Black (1968) list about ten factors with some influence on $G_{max}$. They found that for sands, $G_{max}$ depended primarily on void ratio and effective confining stress, with a small ageing effect. For clays they found that void ratio, confining pressure, ageing and clay mineralogy were important. For normally-consolidated clays they found that the small-strain modulus could be expressed as:

[2.1] $$G_{max} = K\ F(e)\ p_a\ (\sigma'_{3c}/p_a)^n$$

in which K is a dimensionless constant for each soil, F(e) is a function of void ratio which varies somewhat with different studies, $p_a$ is atmospheric pressure, $\sigma'_{3c}$ is the effective confining pressure, and n is an exponent of about 0.5 to 0.6. Zavoral (1990) gave a detailed review of the parameters affecting $G_{max}$ in clay. For his series of tests on normally-consolidated samples at increasing depths he expressed the results as:

[2.2] $$G_{max} = 292.1 p_a(\sigma'_{3c}/p_a)^{0.90}$$

Hardin and Drenevich (1972b) confirmed eqn.2.1 (with an additional term for overconsolidation ratio, OCR). This later study included sands, and they stated that the same equation could be applied to sands without the OCR term. They suggested the use of insitu tests or laboratory vibration tests for determining $G_{max}$. The typical shear wave velocities of 50 to 300m/s given in Chapter 1, with assumed densities of 1600 to 2100kg/m$^3$, would give $G_{max}$ of 4MPa to 189MPa.

*2.3 NATURE OF DAMPING*

Material damping refers to the energy dissipation within a soil mass during dynamic (cyclic) loading. Whitman (1970) provided one of the earlier summaries of material damping of soils (also termed internal damping, intrinsic damping, or simply damping). The stress-strain curve during unloading is not the same as that during loading, giving rise to a closed hysteresis loop (see Fig.2.1). The area of the loop is a measure of the energy lost during a cycle of unloading/reloading.

Corresponding to the bulk modulus and shear modulus, it is possible to measure a compressional damping and a shear damping. Saxena and Reddy(1989) gave results for longitudinal damping($D_l$, corresponding to Young's modulus E) of a sand. They found it was difficult to correlate $D_l$ to the test parameters and recommended two different values for low and high strain levels. The majority of present design methods emphasize shear loading, and this thesis will emphasize only damping under shear loading, $D_s$.

In general, it appears, from laboratory testing at least, that the material damping of soils is hysteretic (frequency independent) although tests on saturated cohesive soils show a slight increase in damping with frequency (Hardin and Drenevich,1972b). Palaniappan(1976) compared theoretical models of hysteretic and viscous damping with a cyclic triaxial test on a micaceous silt. The experimental results agreed very closely with the hysteretic model. Most authors seem to attribute material damping to particle sliding. Palaniappan, quoting others, states that for a constant friction (Coulomb) damping model the free vibration decay envelope is a straight line. Since the free decay envelope is found to be curved (possibly exponential), the source of damping must be more complex, likely involving particle movement and rotation as well as slip. It should be noted that the majority of soil models that have been developed use viscous damping (the dashpot model), and therefore measured damping must be re-expressed in a suitable form to be used in the models.

Whitman (1970) expresses the damping capacity, $d_{cap}$ as the ratio of energy lost in a cycle to the maximum strain energy introduced in the cycle,

[2.3] $d_{cap} = A_{loop}/A_{tri}$

where: $A_{loop}$ = Area of loop

$A_{tri}$ = Area of right triangle between strain axis and line from origin to point of loop

For purposes of analysis, he related $d_{cap}$ to viscous damping parameters (for small damping levels):

(a)logarithmic decrement, $d_{log}$

[2.4] $d_{log} = d_{cap}/2$

(b)loss coefficient (phase lag between force and displacement), $d_{loss}$

[2.5] $d_{loss} = d_{cap}/(2\pi)$

(c)damping ratio = ratio of actual viscous coefficient to critical value, $D_s$

[2.6] $D_s = d_{cap}/(4\pi)$

Whitman noted that the most important factors affecting damping, at least in sands, are shear strain and confining pressure. There was a slight increase in damping when water was introduced to dry sand, and damping in clay appeared to be less than in sand.

The geophysics literature most commonly refers to the measurement of attenuation as the quality factor, Q and its inverse $Q^{-1}$. Johnston and Toksoz (1981) define Q as the ratio of stored energy to dissipated energy ($2\pi W/\Delta W$). Thus Q can be related to $D_s$ (for the low-loss materials normally encountered) as :

[2.7] $Q = 1/(2D_s)$

Hardin and Drenevich (1972a) listed four "very important parameters" affecting damping in both sands and cohesive soils:

Strain amplitude

Effective mean principal stress

Void ratio

Number of cycles of loading.

The effect of degree of saturation in cohesive soils was given as not clearly known, although the effect on modulus is given as very important.

Damping was found to increase with strain, being "very small" for small strains of about $10^{-4}\%$ and approaching a maximum value, $D_{max}$, asymptotically at large strains. In a companion paper (1972b) they provided equations for $D_{max}$, which decreased with log(N), (N=number of cycles) for all soil types tested, and nonlinearly decreased with confining pressure and increased with frequency for cohesive soils. The damping ratio, at a given strain, decreased with confining stress and number of cycles, varying approximately with the square root of confining stress and the logarithm of number of cycles. Tests done on various soils show a decrease in damping with an increase in void ratio. It should be noted that the materials with higher void ratios were the more cohesive soils.

Seed and Idriss (1970) concluded that for sands, "an average damping ratio vs. shear strain relationship for an effective vertical stress of 2000 to 3000 psf (96 to 145kPa) would appear to be adequate for many practical purposes. Considering the scatter... an average relationship may be even more justified." For clays, they concluded that it was "difficult to determine the main factors influencing the damping ratio". Their average curves for sand and clay give slightly lower damping for clays for strains greater than about $10^{-2}$% and slightly higher for clays at lower strains. This finding was confirmed in later work by Sun et al(1988). Seed and Idriss assumed that damping for gravelly soils was the same as that for sands. This was confirmed in later testing (Seed et al,1986). For peats, they reported damping of about 10-13% for strains of about2-5x$10^{-3}$%, about 3 times that for clay.

More recently, a number of researchers (Lee and Stokoe,1986; Yan and Byrne,1990) have found that the stresses in the directions of propagation($\sigma_a$) and particle displacement($\sigma_b$) affect the shear modulus and that the "out-of-plane" stress($\sigma_c$) has at most a very minor effect. In addition, Ni(1987) measured damping of a sand under true triaxial conditions. He found that damping decreased slightly with increases in $\sigma_a$ and $\sigma_b$ and is nearly unaffected by changes in $\sigma_c$.

## *2.4 LABORATORY METHODS AND ANALYSIS FOR DAMPING*

The main laboratory tests used to determine damping appear to be the resonant column(RC) and cyclic triaxial(CT) (both compression and torsion) tests. Combined developments have included true triaxial conditions using a hollow cylinder sample. Earlier testing included the cyclic direct shear (Palaniappan,1976) but this is not generally used today because of the nonuniform stress/strain conditions induced in the sample. The cyclic simple shear apparatus (NGI and Cambridge designs) has been used by a number of researchers. Woods (1978) points out "internal complexities and uncertainties" with the test, and it appears that the test is not commonly used for damping measurements.

In the more traditional cyclic triaxial test, a sample is set up in the usual way and a vertical cyclic load (usually sinusoidal) is applied to the top cap. Damping can be calculated from the area of the hysteresis loop. Palaniappan extended this theory to include tests at other than the resonant frequency. However this test, and longitudinal testing with the RC apparatus, gives the longitudinal damping, $D_l$. Saxena and Reddy(1989) conducted RC tests on Monterey sand and found the following relationship between longitudinal($D_l$) and shear($D_s$) damping:

$$[2.8]\quad D_l = 1.08\, D_s \left|\frac{\sigma_o}{P_a}\right|^{0.25}$$

where: $\sigma_o$ = mean effective confining pressure

$P_a$ = atmospheric pressure (same units as $\sigma_o$)

Although they point out that the relationship is by no means perfect, it does suggest that measurements of $D_l$ can only be approximately equated to $D_s$ for stresses near atmospheric, and therefore it is desirable to measure $D_s$ directly.

The resonant column (torsional mode) and torsional shear triaxial tests can provide direct measurements of $D_s$. A combined test apparatus, including hollow cylinder samples has been described by Ni(1987).

Woods(1978) summarized the work of eight groups that developed similar equipment in the early 1970's and three other groups that used a short but variable (across the radius) height to reduce stress variations. For the RC test, damping can be calculated from decay under free vibrations as:

[2.9] $$d_{log} = \ln(a_n/a_{n+1})$$

where: $a_n$, $a_{n+1}$ = successive peaks in amplitude decay

[2.10a] $$D_s = \left|\frac{d_{log}^2}{4\pi^2 + d_{log}^2}\right|^{0.5}$$

or

[2.10b] $$D_s \text{ approx.} = d_{log}/(2\pi)$$

An alternate method to obtain damping in the RC test is the half-power bandwidth. The sample must be excited over a range of frequencies near the resonant frequency ($f_r$). A frequency response curve is calculated and the frequencies above ($f_2$) and below ($f_1$) resonance where the amplitudes are 0.707 times the peak amplitude are noted. The damping is then given by (Ni,1987):

[2.11] $$D = (f_2-f_1)/2f_r$$

For the torsional shear test, damping can be measured from the area of the hysteresis loop.

Zavoral (1990) used both resonant column and torsional shear equipment to test clay samples from a Lower Mainland test site (Lower 232 St.) and his results are compared with field measurements later in this thesis.

In order to test the Random Decrement Technique, Aggour et al (1982a) used a white noise signal generator in the RC test. Their results gave good agreement for the damping of a sand, compared with measurements using sinusoidal vibration.

Typical laboratory values of damping at small strains are given in Table 2.1.

| Soil Type | Strain,% | Damping,% | Source |
|---|---|---|---|
| Cohesive | $10^{-3}$ | 3 (1-5) | Sun *et al.*,1988 |
| Clay | $10^{-3}$ | 0.9-2.4 | Zavoral,1990 |
| Sand | $10^{-3}$ | 1.5 | Ishihara,1982 |
| Cohesionless | $10^{-4}$-$10^{-3}$ | 0.5-2 | Seed *et al.*,1986 |
| Sand | $10^{-3}$ | 1 | Saxena and Reddy,1989 |

TABLE 2.1. Laboratory Measurements of Damping

Thus the laboratory values of damping at small strains have been found to be about 0.5% to 2% for sand and typically 1% to 3% (but up to 5%) for clay.

In order to provide a range of values for analysis, the curves of Seed and Idriss show data to about 1% strain. However, among others, Saxena and Reddy give the range of strains for the RC test as $10^{-4}$ to $10^{-1}$%. Ni's data with the torsional shear test extended up to about $10^{-1}$%. He also found a high uncertainty in the measurement of damping in high-amplitude testing. It is not clear how reliable larger strain values of damping are.

### *2.5 FORMULATION FOR FIELD MEASUREMENTS*

This section will introduce the equations describing body waves and discuss factors affecting the amplitudes of such waves. First consider a simple sine wave with no damping travelling along a string with wavelength L and velocity v, then:

[2.12] $$A = A_o \sin \frac{2\pi}{L} (x-vt)$$

It is convenient to introduce the following terms:

[2.13] wave number, $k = \dfrac{2\pi}{L}$ and

[2.14] angular frequency, $\omega = \dfrac{2\pi}{T}$

where T is the period. (Some authors include the initial phase shift $\phi$ but only the relative phase is important to this discussion.)

Then the above equation becomes:

[2.15] $$A = A_o \sin(kx-\omega t)$$

or, in terms of the complex exponential:

[2.16] $$A = A_o \exp[i(kx-\omega t)]$$

This equation is for one-dimensional motion, in direction x only, such as along a string. Waves in soil can be plane waves, for example generated by an earthquake movement of flat-lying bedrock, or spherical waves, for example generated by a point source explosive device, or in general, a mix of these two wave types. For spherical waves in a homogeneous medium, neglecting near-field terms, White(1965) showed that the amplitude decayed inversely with distance,R i.e.

[2.17] $$A = A_o\ 1/R \exp[i(kx-\omega t)]$$

However, soil is rarely homogeneous and commonly layered. At the interface between two layers, the amplitude of spherical body waves can be affected in at least two ways: transmission/ reflection and divergence. As shown in Fig.2.2, the amplitude of the transmitted wave

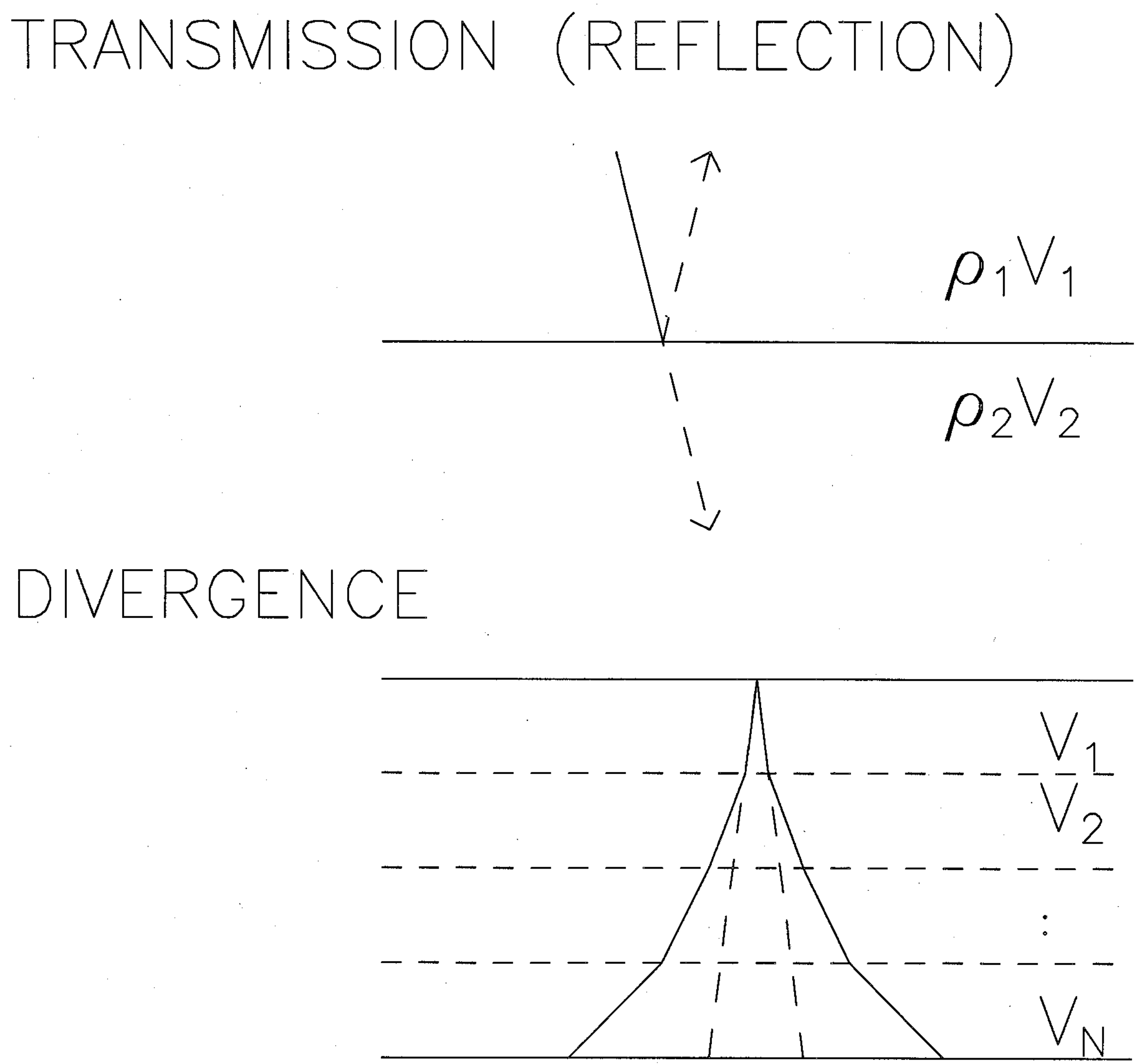

Fig.2.2 Amplitude Changes at Soil Layer Interfaces (after Stewart and Campanella, 1991)

is reduced because (1) part of the wave energy is reflected (for both plane and spherical waves), and (2) the wave front of spherical waves is refracted, decreasing the amplitude for increasing velocities.

The attenuation correction for transmission is a function of the change in acoustical impedance across an interface. The acoustical impedance of a layer is the product of the density, $\rho$ and velocity, V. The reflection coefficient, $r_{12}$, of the boundary between layers 1 and 2, is given by:

$$[2.18] \qquad r_{12} = (\rho_2 V_2 - \rho_1 V_1)\ /(\rho_2 V_2 + \rho_1 V_1)$$

and since the variation in density is often smaller than the variation in velocity, the reflection coefficient is often given as approximately $(V_2-V_1)/(V_2+V_1)$. The transmission coefficient, $t_{12}$, is given by $t_{12} = 1 - \mathrm{Abs}(r_{12})$, and $t_{12}$ is the attenuation correction.

The attenuation correction for divergence is somewhat more complex, and has been discussed by Mack(1966). Although it is not stated, the development is based on the principle of refraction as given by Snell's Law;

$$[2.19] \qquad \frac{\sin(\theta_1)}{\sin(\theta_2)} = \frac{V_1}{V_2} \text{ ; where } \theta = \text{angle of incidence}$$

The energy density ratio, e, will be given by the ratio of the areas with and without refraction. Since the energy is proportional to the square of the wave amplitude, the amplitude correction will be equal to the square root of e. If the region of interest consists of N horizontal layers of constant velocity Vn, over the depth from Z1 to Z2, then the attenuation correction at a depth of Z2 is given by the reciprocal of:

$$[2.20] \qquad \frac{1}{(Z_2-Z_1)V_1} \sum_{n=1}^{N} (V_n Z_n)$$

For his problem, Mack found the divergence factor to be 1/1.15, compared with 1/1.21 for the effects of reflection.

Johnston and Toksoz(1981) stated that damping can be introduced by making k complex, but do not give a theoretical basis. A more rigorous development in Appendix F shows that the use of a complex k leads to a reasonable approximation for $D_s$. Thus let:

[2.21] $k = \kappa + i\alpha$, where $\alpha$ = attenuation coefficient.

and the phase velocity, $c = \omega/\kappa$

Then the expression for the real component of amplitude becomes:

[2.22] $A = A_o \, 1/R \exp(-\alpha R)$

Mok *et al.*(1988) used this expression, considering two signals of amplitude $A_1,A_2$ at distances of $R_1,R_2$ from the source, to yield:

[2.23] $\alpha = \ln(A_1R_1/A_2R_2)/(R_2-R_1)$ or

[2.24] $D_s = \ln(A_1R_1/A_2R_2)/(2\pi t_I f)$

where: $t_I$ = interval travel time

$f$ = frequency of wave.

Tonuchi *et al.*(1983) used a downhole method with a shallow fixed receiver and moving deeper receiver, and computed the attenuation coefficient from:

[2.25] $$\alpha = \frac{\ln\{ (R_1B_{1f}/A_{1f}) \; / \; (R_2B_{2f}/A_{2f}) \}}{R_2 - R_1}$$

where: $A_{1f}$, $A_{2f}$ = FFTs of shallow signals for hits 1&2

$B_{1f}$, $B_{2f}$ = FFTs of deeper signals

FFT = Fast Fourier Transform of signal

A similar type of equation is used in the computer program SHAKE (Schnabel *et al.*, 1972):

[2.26] $u = E \exp[i(kx + \omega t)] + F \exp[-i(kx - \omega t)]$.

The amplitude coefficients (E,F) are calculated using the soil density and complex shear modulus $G^*$ given by:

[2.27] $$G^* = G(1 + 2iD_s) \quad \text{(original version)}$$

[2.28] $$G^* = G(1 - 2D_s^2 + 2iD_s[1 - D_s^2]^{1/2})$$

(revised version -Udaka and Lysmer, 1973)

An alternate development of eqn.2.17 can be followed if the imaginary portion of the equation is retained. In order to clearly show the dependence on distance, Eqn.2.17 can be expressed as:

[2.29] $$A(x,t) = \frac{A_o}{x} e^{i(kx-\omega t)}$$

In order to introduce damping (attenuation) allow the wavenumber to be complex as before in eqn.2.21:

[2.30] $$k = \kappa + i\alpha$$

with $\kappa = \omega/c$ , where c = phase velocity; so that eqn.2.29 becomes:

[2.31] $$A(x,t) = \frac{A_o}{x} e^{-\alpha x} e^{i\kappa x} e^{-i\omega t}$$

The attenuation coefficient, $\alpha$, can be related to the fraction of critical damping, D. For low values of damping, D is given by the ratio of the imaginary part of k to the real part or $D=\alpha/\kappa$ therefore $\alpha=D\kappa$ or:

$$\alpha = \frac{D\omega}{c} \tag{2.32}$$

Consider the ratio of two signals, measured at distances of $x_1$ and $x_2$ from the source, at the same time. Then:

$$\frac{A_2}{A_1} = \frac{x_1}{x_2} e^{-(D\omega/c)(x2-x1)} e^{(i\omega/c)(x2-x1)} \tag{2.33}$$

or:

$$\frac{A_2}{A_1} = \frac{x_1}{x_2} e^{-(D\omega/c)(x2-x1)} [COS((\omega/c)\{x_2-x_1\}) + i\ SIN((\omega/c)\{x_2-x_1\})] \tag{2.34}$$

When this equation is plotted in a Nyquist diagram (Imaginary part as a function of Real part), it is the equation of a spiral. The magnitude at zero frequency is given by the geometric spreading $(x_1/x_2)$. This factor could also include other frequency-independent terms such as transmissivity and divergence of spherical waves. The rate of spiraling with frequency is $(D/c)(x_2-x_1)$. For a given set of signals, the distance is fixed, and over a suitable frequency range, the velocity is constant. Therefore, the rate of spiralling is determined by the damping.

Redpath and his colleagues (1982,1986) used an approach similar to that of Mok *et al* (1988)except that they define the attenuation coefficient $\alpha$ as zf or $z = \alpha/f$. Therefore eqn.2.22 becomes:

$$A = A_o \, 1/R \, \exp(-zfR) \qquad [2.35]$$

If we consider signals measured at two distances from the source, $R_1$ and $R_2$ where $R_2$ is greater than $R_1$, then the ratio is:

$$\frac{A_2}{A_1} = \frac{R_1}{R_2} \exp[-zf\ (R_2 - R_1)] \qquad [2.36]$$

Taking natural logarithms of this equation gives:

$$\ln \frac{A_2}{A_1} = \ln \frac{R_1}{R_2} - zf(R_2 - R_1) \qquad [2.37]$$

Differentiating these terms with respect to f gives:

$$d[\ln\ (A_2/A_1)]\ /\ df = -z(R_2 - R_1) \qquad [2.38]$$

It can be noted that the term given as 1/R in eqn.2.35 is eliminated by differentiating. Any geometric term affecting the amplitude that does not depend on frequency will be similarly eliminated. This will include the transmission and reflection corrections described above if the velocities are independent of frequency, which is the case if the frequency range for the analysis is properly selected. If $R_1$ is held constant and $R_2$ (or simply R) is varied, we can differentiate with respect to R, giving:

$$\frac{d^2[\ln (A_2/A_1)]}{df\ dR} = -z \qquad [2.39]$$

The fraction of critical damping can be computed as:

$$D_s = \frac{zV_s}{2\pi} \qquad [2.40]$$

where $V_s$ = Average shear wave velocity of the layer.

This section began with the equation for a simple sine wave which was then expressed in terms of the complex exponential. Corrections for spherical waves and layered systems (geometric corrections) were discussed. Damping was introduced using the complex wave number. Using the real component of the resulting equation gives the basic equation (2.22) for the attenuation coefficient ($\alpha$) method., which requires previous calculation of the geometric corrections. In order to select a single value of damping it is also necessary to assume or show that $\alpha$ is a linear function of frequency. The complete (complex) form of the equation is used later in the damping spiral method which allows calculation of the geometric corrections. The basic equation (2.26) of the SHAKE program was given, and will be used later in a modified form, along with previously calculated geometric corrections, to calculate damping. The linear function form of $\alpha$ was used to compute the equation (2.35) for the spectral ratio slope method, which eliminates the need for geometric corrections. The above equations are the foundation for the damping calculations presented in Chapters 3 and 7.

## *2.6 FREQUENCY DOMAIN*

Signal measurement is normally carried out in the time domain i.e. variations in the value of some parameter are recorded as a function of time. However it has been found useful to carry out analyses of signals in terms of the frequency content of the signals, so it is desirable to transform the signals into the frequency domain.

In 1807 J.B.J. Fourier presented a lecture in which he claimed "any" periodic signal could be represented by a series of harmonically related sinusoids. Although his work was controversial, it spurred further development of his theories. The initial development was in terms of sinusoids, but most of the relationships provided today are given in terms of the complex exponential function. These are related by Euler's formula:

[2.41] $$e^{iz} = \cos(z) + i\,\sin(z), \text{ where } i=\sqrt{-1}$$

Most natural signals, or those passing through natural materials, contain a range of frequencies and detailed analysis of such signals awaited the development of computers and the digitization of signals. The Fourier transform of digitized signals is referred to as the discrete Fourier transform (DFT). In the mid-1960's an extremely fast algorithm to compute the DFT was developed, and became known as the fast Fourier transform (FFT). This algorithm has been used throughout this research and the transformed signals will be referred to as the FFT's of the signals.

Usually signals are digitized at a series of points equally spaced in time with a time step $\delta t$. Thus the signal can be given as $x(n)$ with $n=0,1,\ldots,N-1$ where N is the total number of points. Then the DFT, $X(k)$, can be expressed as (Oppenheim et al, 1983):

$$X(k) = \frac{1}{N} \sum_{n=0}^{N-1} x(n)e^{-ik(2\pi/N)n} \quad k=0,1,\ldots,N-1 \tag{2.42}$$

and the inverse transform by:

$$x(n) = \sum_{k=0}^{N-1} X(k)e^{ik(2\pi/N)n} \quad n=0,1,\ldots,N-1 \tag{2.43}$$

The frequency step between points in the transform is given by $\delta f = 1/(N\delta t)$ and the maximum (Nyquist) frequency is given by $1/(2\delta t)$. For a given number of points, the frequency step is inversely proportional to the time step, so that the time step should be selected with care.

It should be noted that these equations are not universally accepted. The program DADISP places the 1/N term in the inverse transform, not in the FFT. The program VU-POINT places a term of $\delta t$ at the front of the FFT, a term of $1/(N\delta t)$ in the inverse transform, and the negative sign in the exponential term is switched to the inverse transform. The units of the FFT thus become v/Hz for a time signal in

v. It should also be noted that the signal to be transformed is implicitly periodic, that is the algorithm assumes that the signal is repeated infinitely. Thus the last point in the signal is followed by the first point in the signal, and these points should therefore be close to or equal in value to avoid a "step" in the assumed periodic signal.

The sinusoid at a particular frequency in the Fourier transform has two parameters, an amplitude and time shift. This pair of values is normally calculated as a complex number, i.e. a real part (R) and an imaginary part (I). An alternate system is the polar representation with the magnitude and phase given as:

[2.44] $$|X| = \sqrt{R*R + I*I}$$

[2.45] $$\phi = \tan^{-1}(I/R)$$

Actual measured signals contain an almost continuous range of frequencies and are shown in detail later in this thesis. To clarify some of the above discussion, simplified signals, and their FFT's, have been prepared. Fig.2.3a shows three cosine waves with different frequencies and amplitudes. The three waves were added together and the sum is shown in Fig. 2.3b.

It is desired to resolve the frequencies in the signal in Fig.2.3b. The FFT of the signal was computed and the magnitude of the FFT (which is normally shown to the user in most signal analysis programs) is given in Fig.2.3c. The frequencies at the peak magnitudes (or peak frequencies) at 5, 10 and 15Hz can be clearly seen. Ideally

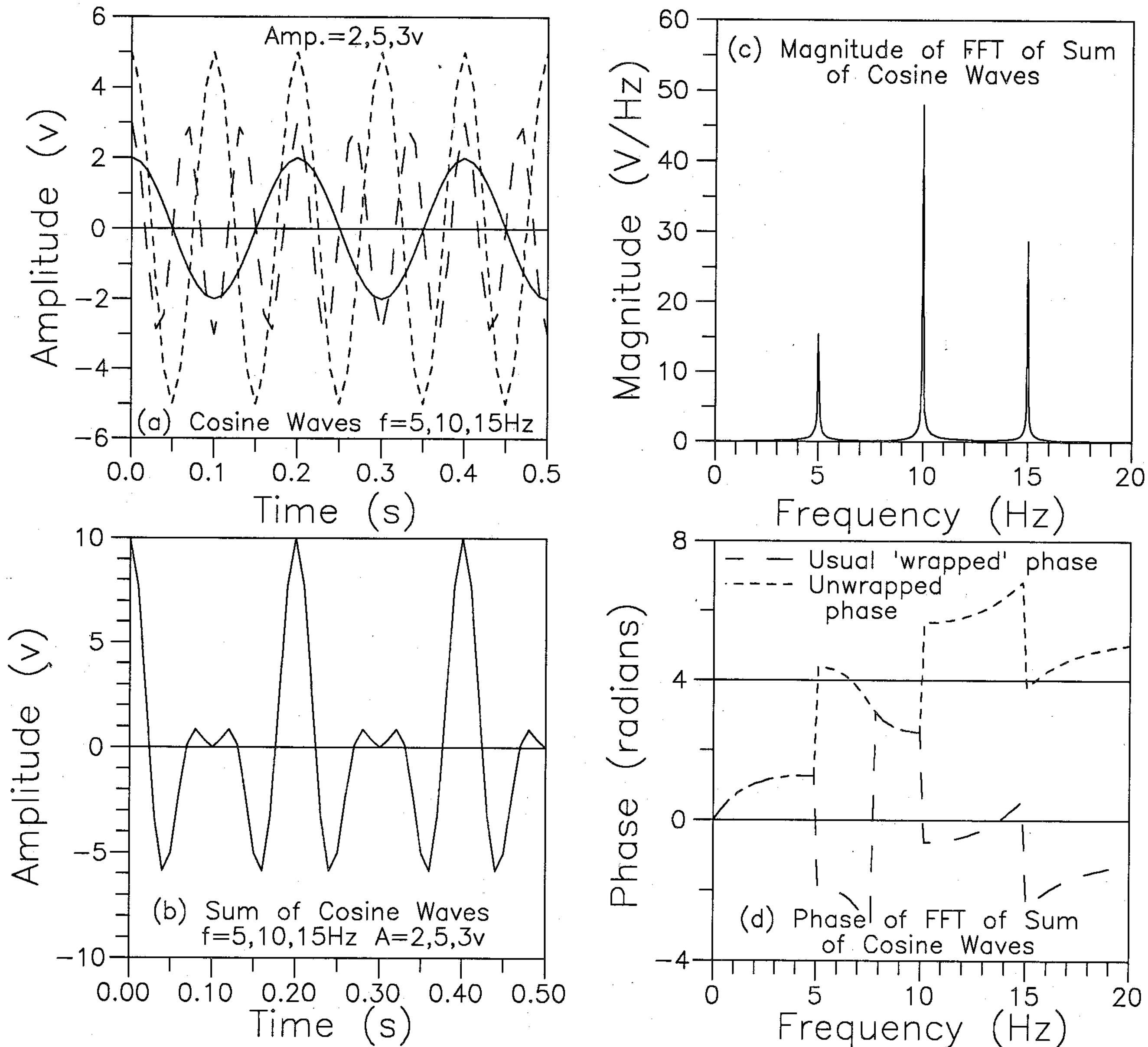


Fig.2.3 Frequency Domain Analysis of Simple Sum of Waves

the function would be three $\delta$-functions (of zero width) but this cannot be achieved numerically and the base of the peaks show some spreading. The peak values are in the correct order of size, but are not quite in the assigned 2:5:3 ratio because of the steps in the frequency function and numerical errors associated with the $\delta$-functions.

The phase of the FFT is provided in Fig.2.3d. The phase is shown in two ways, the usual 'wrapped' phase, and the unwrapped phase. Since the phase is computed from $\tan^{-1}(I/R)$ the results will fall in the range $-\pi$ to $\pi$ ( or 0 to $2\pi$, etc. depending on the program used). Alternately the phase can be unwrapped to extend outside this range. Phase unwrapping is discussed in more detail in section 5.6.2. It can be observed that a shift of $\pi$ radians occurs at each frequency in the signal. Unwrapping eliminates the 'spurious' step near 7.5Hz in the wrapped phase. Phase values between the three input frequencies are not meaningful in this case as there are no other frequencies present. Phase values are more useful when comparing two signals.

Fig. 2.4a shows two cosine waves at a frequency of 5Hz, with the second signal having an offset in time of 50ms. If we compute the FFT's of the two signals, the magnitude plots (given in Fig.2.4b) are exactly the same. However, the phase plots in Fig.2.4c are different. Each show a step of $\pi$ radians at 5Hz but if we look at the difference between the phase values (at 4.98Hz, the closest computed value to 5Hz) the difference is -1.56635rad. By the time-shift property of the DFT (Oppenheim et al, 1983):

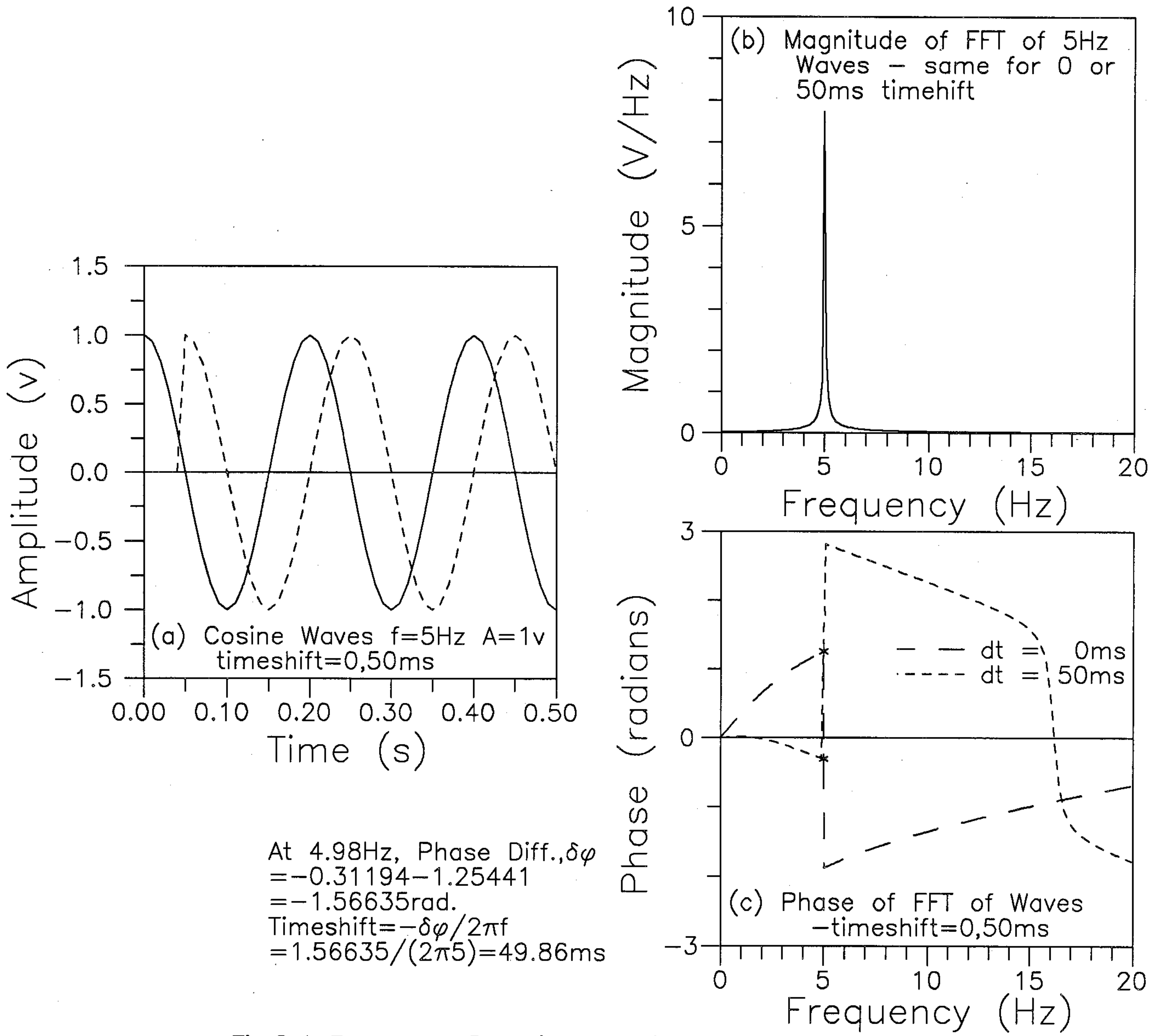


Fig.2.4 Frequency Domain Analysis of Sum of Shifted Waves

[2.40] $\delta t = -\delta\phi/\omega = -\delta\phi/(2\pi f)$

The calculated time shift from the phase difference, 49.86ms, is close to the actual value of 50ms, but is off slightly as the FFT was not calculated exactly at 5Hz.

An alternate approach, which avoids the separate calculation and comparison of two phases, is to calculate the cross-spectrum of the two FFT's. First the conjugate of the first (earlier) FFT is calculated by changing the sign of each imaginary part in the FFT (a+ib becomes a-ib), then the conjugate is multiplied by the second FFT, giving the cross-spectrum. Examining the phase of the cross-spectrum, as given in Fig.2.5, gives the phase at 4.98Hz as -1.5663rad., exactly the same as the difference found above. This was expected as the phase is additive when two FFT's are multiplied.

If the inverse FFT of the cross-spectrum is computed, the result is the cross-correlation of the two signals presented in Fig.2.6. The maximum peak in the cross-correlation occurs at 50ms, the input timeshift.

This section has presented a brief summary of transforming time-based signals into the frequency domain, with an emphasis on the FFT, and indicated some of the uses of the FFT in a simplified manner, as much of the work in this thesis relies heavily on the FFT and calculations in the frequency domain.

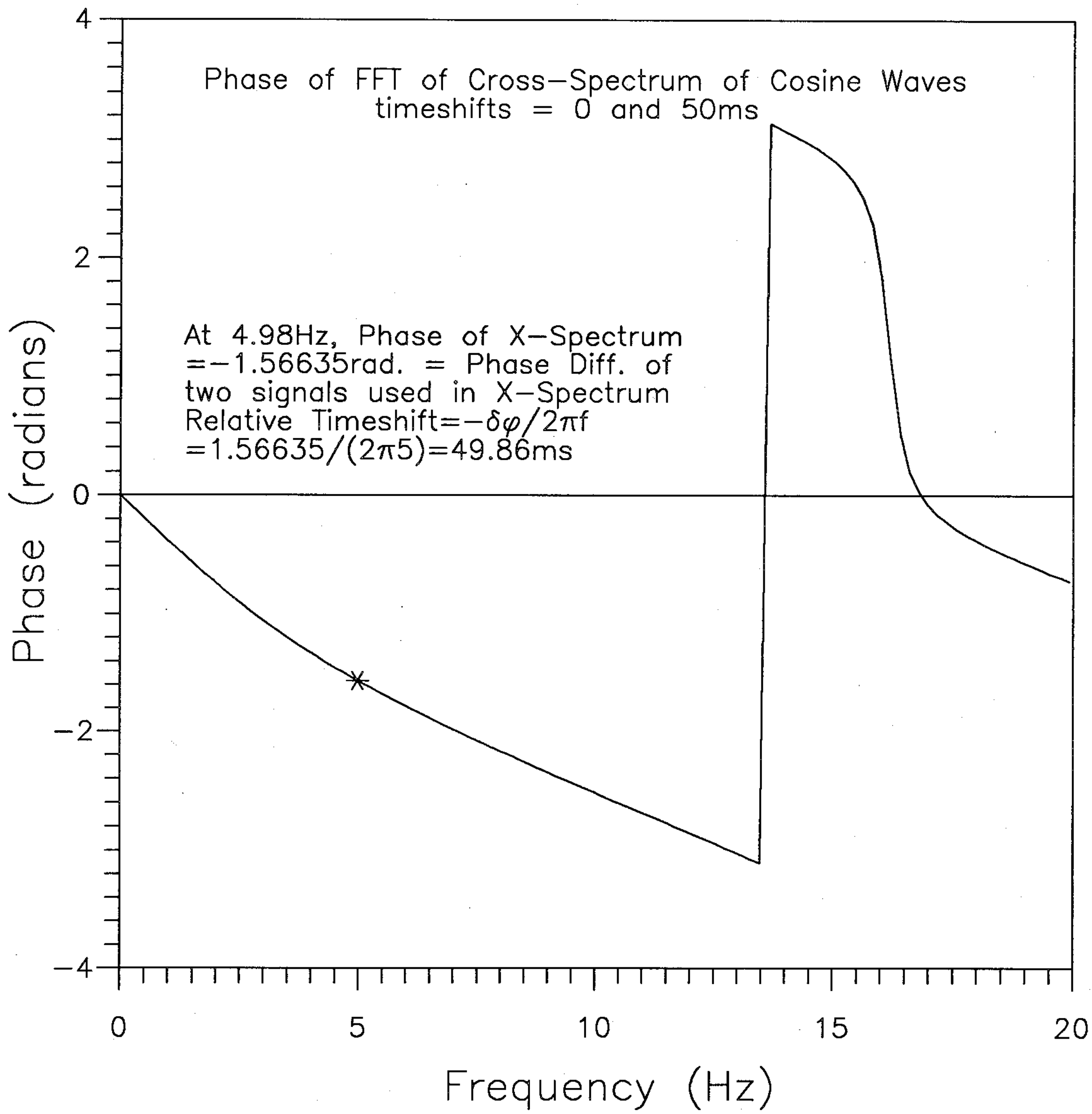


Fig.2.5 Phase of Cross–Spectrum of Shifted Waves

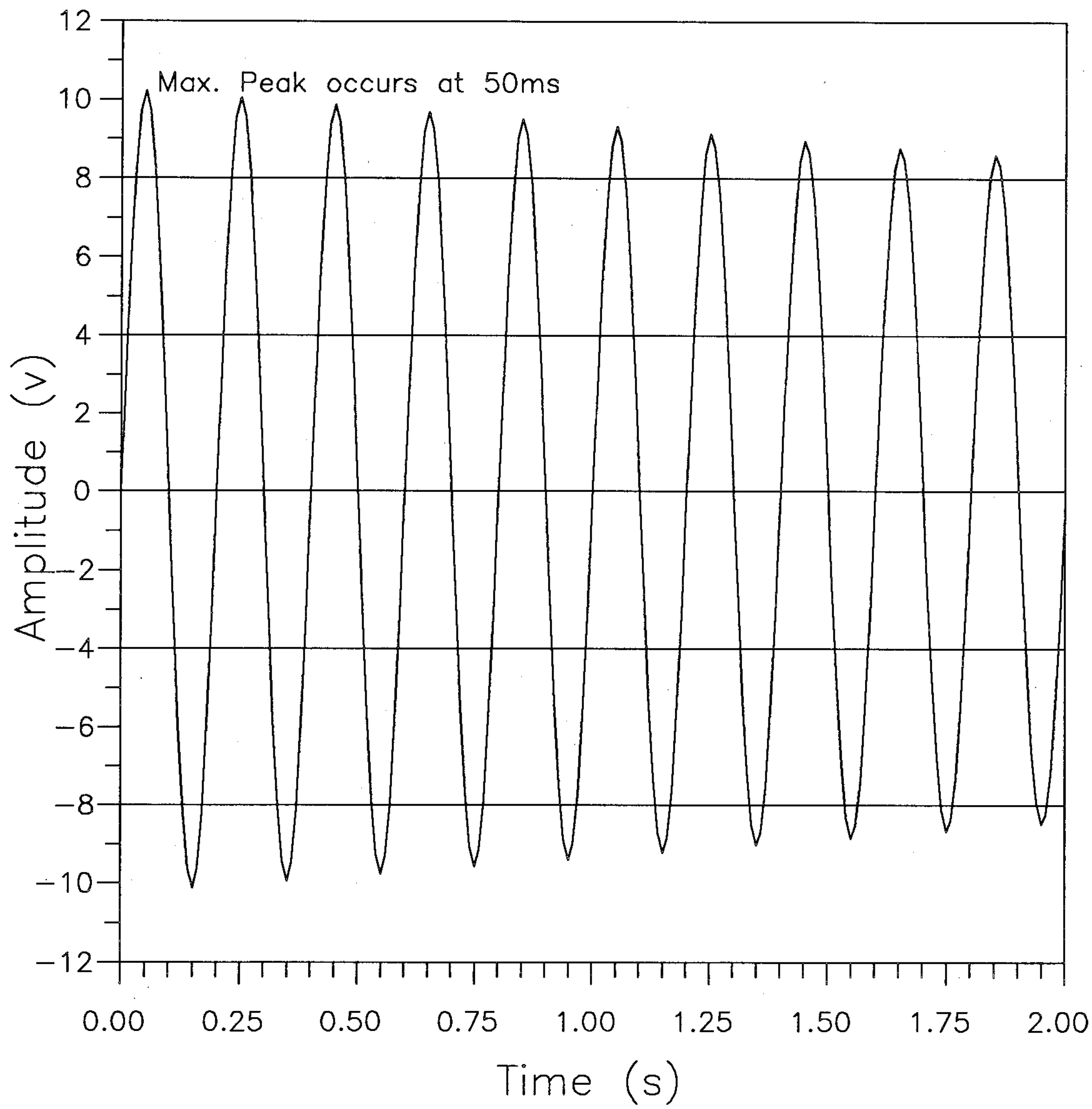


Fig.2.6 Cross—Correlation of Shifted Waves

# CHAPTER 3.

# PREVIOUS INVESTIGATIONS

### *3.1 SHEAR WAVE VELOCITIES*

The measurement of shear wave velocity in soils is now well established with specialist firms providing such measurements on a fairly routine basis. Warrick (1974) reported the results of downhole tests at a San Francisco bay mud site. In their Richart Commemorative lecture, Woods and Stokoe (1985) provided an update on shallow seismic testing with an emphasis on crosshole testing, discussed data interpretation, and described the spectral analysis of surface waves (SASW) technique. Robertson et al (1986) described the seismic cone penetration test (SCPT) and provided several examples that showed that crosshole and SCPT results were in good agreement. Sirles (1988) presented four case histories from nearly 50 crosshole investigations that the USBR had conducted up to that time.

Stokoe and his co-workers (e.g. Stokoe and Nazarian, 1985) have presented a number of papers on the SASW method. Basically, the method consists of the measurement of surface (Rayleigh) waves at two points at a variety of spacings and frequencies (variety of hammers), followed by the computation of the phase of the cross-power spectrum, the phase velocity, $V_\phi$, and the wavelength, $\lambda$, to give a field dispersion curve ($\lambda$ vs. $V_\phi$). A trial soil profile (a series of layers of assumed thickness and $V_s$) is varied in a computer program to match the field dispersion curve with the process being termed inversion. The method has apparently been successfully applied at a number of sites, including several where drilling or a cone sounding would be impractical. A variation using a triangular array of receivers and background noise as a source was described by Abbiss and Ashby (1983). In addition to velocity measurements, a recent article suggested the feasibility of damping measurements using SASW techniques. Al-Hunaidi (1991) discussed possible corrections required in using the SASW method to measure shear wave velocities. However, one of the equations he presented expressed the amplitudes of the signals in terms of an attenuation coefficient related to material damping. This raises the possibility that damping might be measured using the SASW technique. There is no further discussion of the SASW method in this thesis.

### *3.2 DAMPING MEASUREMENTS*

One time-domain approach, the rise-time method (RTM), has been used by others for calculating damping. The usual equation given for this method is:

[3.1] $t = t_o + 2CT^*D_s$

where: $t$ = rise time (time to reach first peak)

$t_o$ = rise time at source

$C$ = a constant

T = travel (arrival) time

$D_s$ = damping

The problem in using this method is the value of C. Redpath et al (1982) point out that the 'constant' C may be a function of damping. Other authors point that the range in the value of C is rather wide. Burkhardt et al (1986) quote values of 0.1 to 0.485 from numerical studies and 0.13 to 0.59 from laboratory studies and they found that the scatter of damping values is generally larger for the RTM than for any other method. Anderson and Reinke (1989) also observed that the highest measurement error resulted from the rise time techniques. Based on these observations, it was concluded that it was unlikely that the RTM could be successfully used for damping calculations.

Two separate methods of damping calculation based on frequency domain calculations are presented in the literature. The first is the attenuation coefficient method used by Hoar and Stokoe (1984) and Mok et al (1988), and the second is the spectral slope method as used by Redpath and colleagues (1982,1986) and others (Kudo and Shima,1981, Meissner and Theilen, 1986).

### 3.2.1 Attenuation Coefficient Method

Hoar and Stokoe (1984) presented the results of damping calculations from crosshole measurements using a vertical impulse source and three receivers in separate casings at a depth of 15 ft and spacings of 7.6, 15.5 and 23.8 ft from the source. They used the attenuation coefficient method, eqn.2.24, in two ways. First they manually selected points on the traces to determine the amplitudes and periods, and secondly they calculated the spectra and computed damping as a function of frequency. The first method gave damping values of 2.2% to 8.0% depending on the signals and points selected. The spectral approach gave damping values of about 0-4%, averaging about 2%. (and negative values for low frequencies, long wavelengths). They recommended the spectral approach.

Mok et al (1988) used a crosshole technique, so the generated waves were unlikely to encounter interfaces between layers of soil (although the method would be affected by nearby layers of high velocity). They pointed out that the use of windowing reduced the scatter in calculated damping. Their results are given in Table 3.1.

### 3.2.2 Spectral Ratio Slope Method

The second method used was the spectral slope method, based on eqn.2.39. The coefficient z can be determined by first finding the Fast Fourier Transform (FFT) of one signal at a reference depth, then for each deeper signal compute the FFT, the ratio of the FFTs, and the negative of the natural logarithm (ln) of the ratio. After finding the slope of −ln(ratio) versus frequency plot at each depth, these slopes are plotted versus depth.

The slope(s) of the depth plots give the coefficient z for each layer. The fraction of critical damping can be computed from eqn.2.40.

The spectral slope method avoids the need for interface corrections and gave relatively low scatter in the results when Redpath et al (1982) applied smoothing to the intermediate calculated values (both spectra and ratios).

### 3.2.3 Results of field measurements

Some reported field values of damping are given in Table 3.1.

| Soil Type | Damping,% | Source |
|---|---|---|
| Sand | 6 | Kudo and Shima,1981 |
| Silt | 2.5 | " |
| Alluvium | 12(<25m) | Redpath *et al.*,1982 |
| (Sand & Clay) | 3.5(deeper) | (lab.1.5-3.5%) |
| Sandy | 5 | Tonouchi *et al.*,1983 |
| Clayey | 1.7 | " |
| Fine sand | 1.7 | " |
| Sandy silt | 2.5 | " |
| Sand | 4 | Meissner and Theilen,1986 |
| Bay mud | 4 | Redpath and Lee, 1986 |
| | | (lab. 2.5%) |
| Clay | 4-7 | Mok *et al.*,1988 |
| Sand(P-wave) | 2-3 | " (lab. 0.7%) |

TABLE 3.1 Field Measurements of Damping

Small-strain damping values from field tests in the literature give damping values of 1.7% to 6% for sands, 1.7% to 7% for clays, about 2.5% for silts and 3.5% to 12% for "alluvium". Compared to laboratory values, these values are higher by about a factor of 3 for sands and 2 for clays. Laboratory results given by Redpath et al (1982) suggest the field values are higher by a factor of 2 to 3 for the alluvium. The results also suggest a larger scatter in field values. Both the field and laboratory results are compared with values from the present research in Chapter 8.

### *3.3 RANDOM DECREMENT TECHNIQUE*

Use of the random decrement technique to determine the damping of soil insitu was proposed by Aggour et al(1982b). As they explain "The basic concept of the 'Random Decrement signature' is based on the fact that the random response of a structure is composed of two parts...By averaging enough samples...the random part will average out...It can be shown that...the deterministic part that remains is the free decay response from which the damping can be measured." They state that the method was initially developed for structures and has been used for aircraft, machinery, piping, and offshore structures.

The method has apparently been successfully applied to measure damping of soils in the laboratory using a resonant column device (Aggour et al, 1982a), giving results similar to the usual resonant column method. The method has also been applied to earthquake acceleration records measured at soil sites to estimate the damping of the soil deposit (Yang et al,1989).

However it seems intuitively reasonable that the method will incorporate the effect of instrument response, perhaps overwhelmingly, in addition to soil response when applied to a single record. Other methods of damping measurement incorporate the effect of two or more measurements in the same calculation. Indeed as Aggour et al (1982b) stated "A problem that has not been solved as yet is the determination of the amount of energy dissipated in the sensor mechanism itself in addition to the hysteric(?) damping of the soil." It is not clear that the problem can be solved using the method as proposed.

# CHAPTER 4

# STRATIGRAPHY AND SOIL PROPERTIES AT RESEARCH SITES

## *4.1 INTRODUCTION*

Seismic cone penetration tests (SCPT's) to determine shear wave velocities have been conducted by UBC investigators at numerous sites throughout the Lower Mainland, in the Arctic, and in southern California. The locations of all UBC research sites in the Lower Mainland are shown in Fig.4.1. Descriptions of these sites have presented by Sully,1991; Zavoral,1990; Gillespie,1990; Hers,1989; LeClair,1988; Greig,1985 and others.

Four different test sites in the Lower Mainland were investigated during this research. These sites were underlain by sand, silt and clay layers in which the shear wave velocity and damping were measured. A summary description of these four sites is presented in Table 4.1. Greater details of each site, the stratigraphy, a cone log, available soil properties, and the testing done at each location are given below. For the cone logs the soil classifications were based on charts given by Robertson and Campanella (1986). The consistency of fine-grained soils was based on the undrained shear strength, $s_u$ computed from

[4.1] $s_u = (q_c - \sigma_o)/15$

where $q_c$ is the measured cone bearing

$\sigma_o$ is the insitu total vertical stress

and the consistency definitions given in the CFEM (1985).

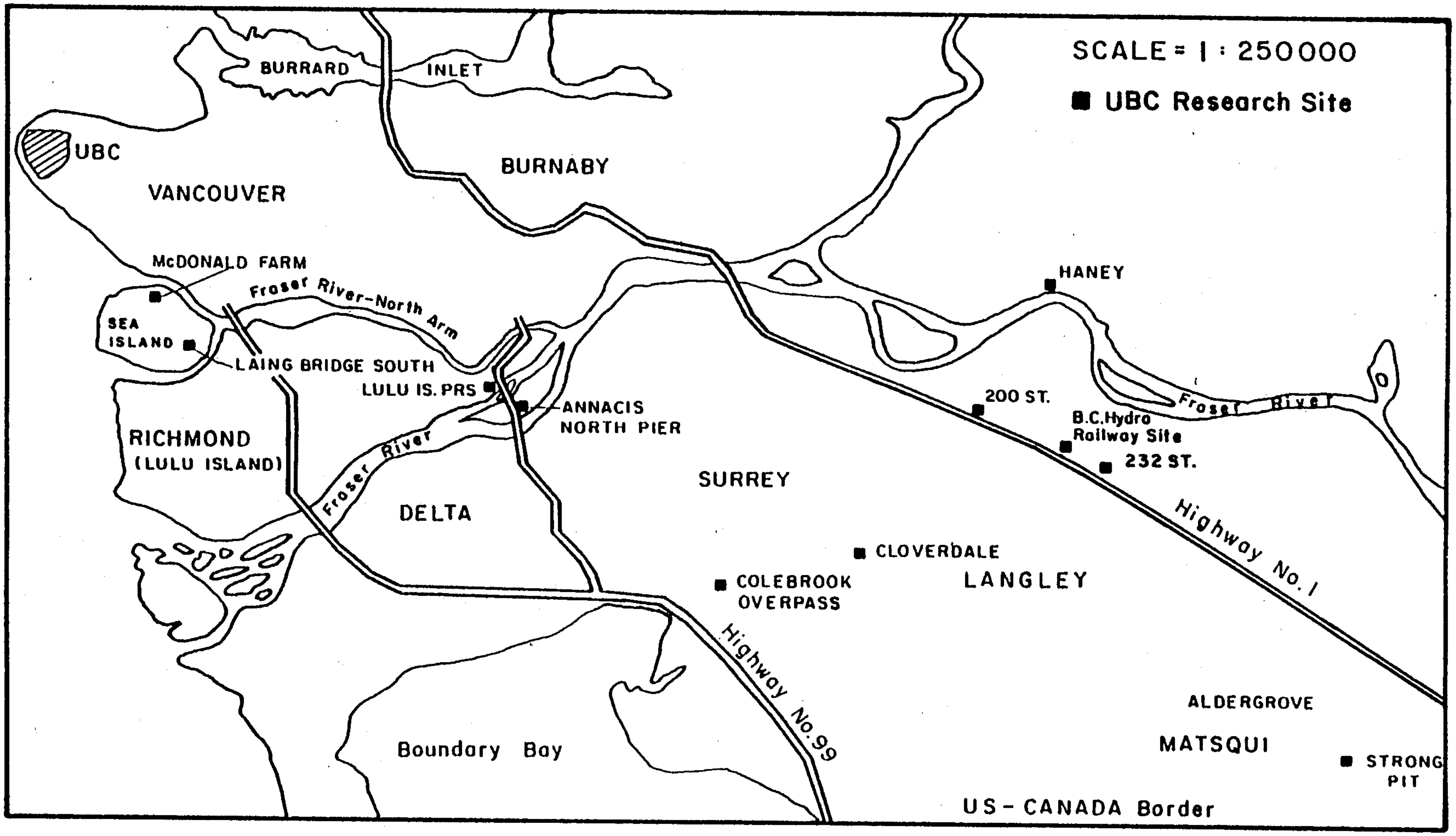


Fig.4.1 Location Plan for UBC Geotechnical Research Sites

| Site | Location | Main Soil Type(s)* |
|---|---|---|
| McDonald Farm (MF) | Sea Island, Richmond | SW over ML |
| Lower 232nd St. (L2) | Langley | CL (O.C. over upper 5m) |
| Annacis N.Pier (AN) | Annacis Is., Delta | SP (over ML) |
| Laing Bridge (LB) | Sea Island, Richmond | SP-SM (over ML) |

*Note: Soil types based on Unified Soil Classification System - see ASTM D2487-69 & D2488-69. (O.C. = over-consolidated).

TABLE 4.1 Research sites used for insitu measurements of damping

The density of granular soils was based on the relative density relationship for quartz sands given in Robertson and Campanella (1986) and the definitions given by Sowers and Sowers (1970). Consideration was also given to estimated SPT N-values calculated from

[4.2] $N = q_c/5$

and the density definitions in the CFEM (1985).

The MF, AN, and LB sites are located on the Fraser Delta and the L2 site is on an upland to the south of the Fraser River, in the Langley-Fort Langley corridor.

### *4. Stratigraphy and soil properties at research sites*

Armstrong (1990) provides a concise description of the geological framework of the Lower Mainland. Surficial geology maps prepared by the Geological Survey of Canada (Maps 1486a {1979},and 1484a, 1485a, and 1487a {1980}) provide basic information on geological history and surficial soil types in the Fraser Valley Lowlands west of the Rosedale-Agassiz area. Bedrock within the Lowlands is generally of Tertiary age, and is usually covered by a variable thickness of glacial drift. Growth of the Fraser Delta began during the regression of the last glaciation about 11,000 years ago. The evolution of the delta has been described by Blunden (1973) and Clague et al (1983). Delta growth has resulted in a generalized soil profile of marine silts, overlain by complex sandy deposits (marine, deltaic, and tidal flat), topped by silty overbank deposits (Wallis,1979; Sy et al,1991). Except near the surface, the post-glacial soils have mainly remained below the water table and therefore are usually normally consolidated. In many areas the upper metre or two has been reworked by man.

The Lower 232nd St. site is mapped by the GSC as Ce (Capilano sediments-mainly marine silt loam to clay loam with minor sand, silt and stony glaciomarine material). The site is just west of the area marked FLd (Fort Langley formation-marine silty clay to fine sand). The Fort Langley formation typically recorded at least three local advances of a valley glacier while the Capilano sediments were not overridden by ice. Consolidation results reported by Sully (1991) indicate that the soil is normally consolidated below 5m and is therefore correctly placed in the Capilano sediments.

## *4.2 MCDONALD FARM SITE*

### 4.2.1 Site description

The McDonald Farm (MF) site is on the north side of Sea Island, north of the Vancouver International Airport, and immediately south-west of the McDonald Park boat launch. The present site is just to the west of the former UBC research area. A general site map is provided in Fig.4.2. The surface dips slightly towards the drainage ditches, and it is believed that some fill was placed over the site during excavation of the ditches. The surface is generally covered by a heavy growth of grass. The groundwater table varies somewhat with the tidal level in the river just to the north, averaging about 1.5 metres below the surface.

### 4.2.2 Soil stratigraphy

The cone bearing and friction values obtained from three SCPT's at the site are given in Fig.4.3, along with the interpreted soil profile. Information gathered by Sully (1991) indicated that the sand is medium to coarse grained using the equivalent opening size (International) system with the break between coarse and medium sand as 0.6mm. However based on the sieve size (American-USBR) system with the break between

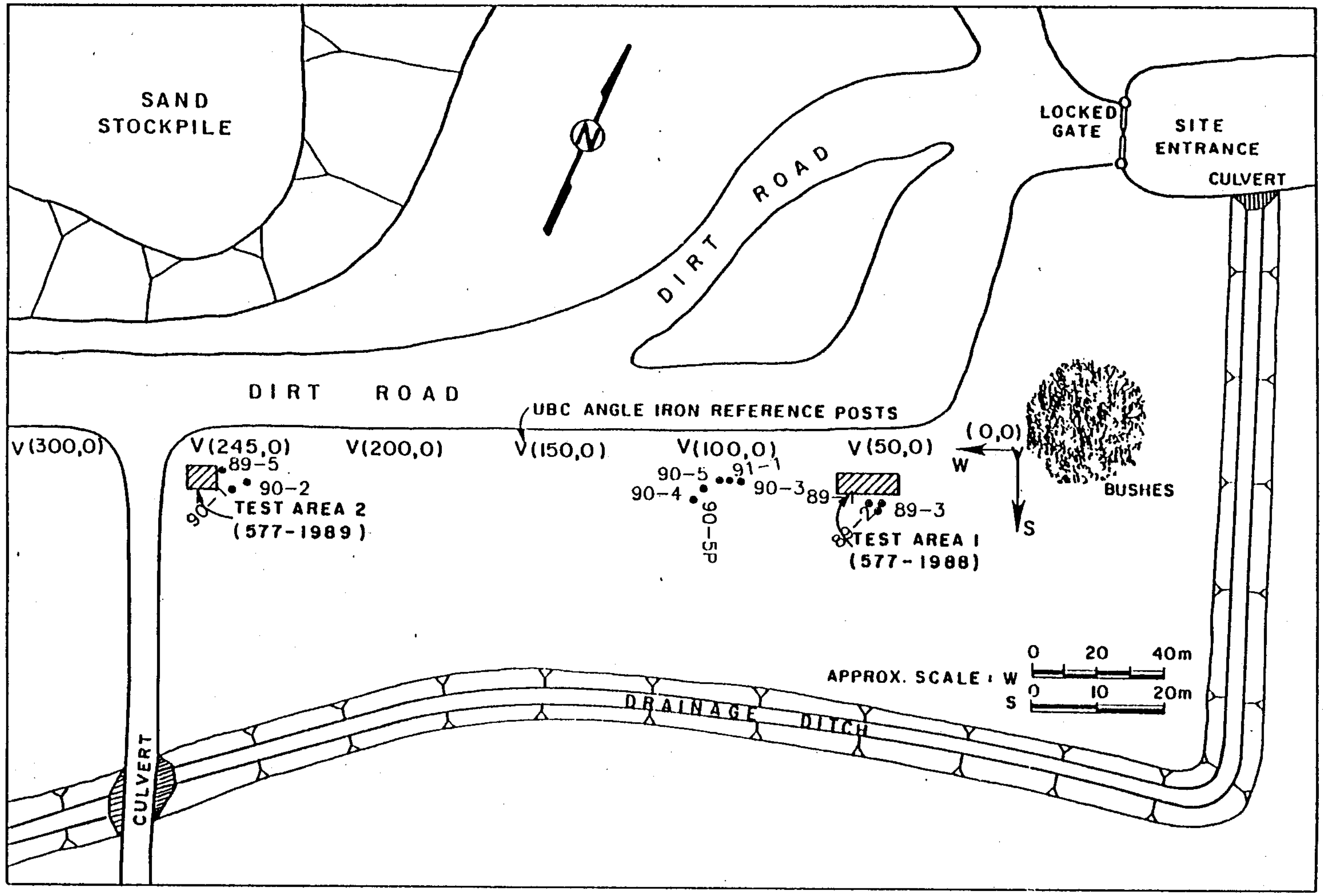


Fig.4.2 McDonald Farm Site Plan

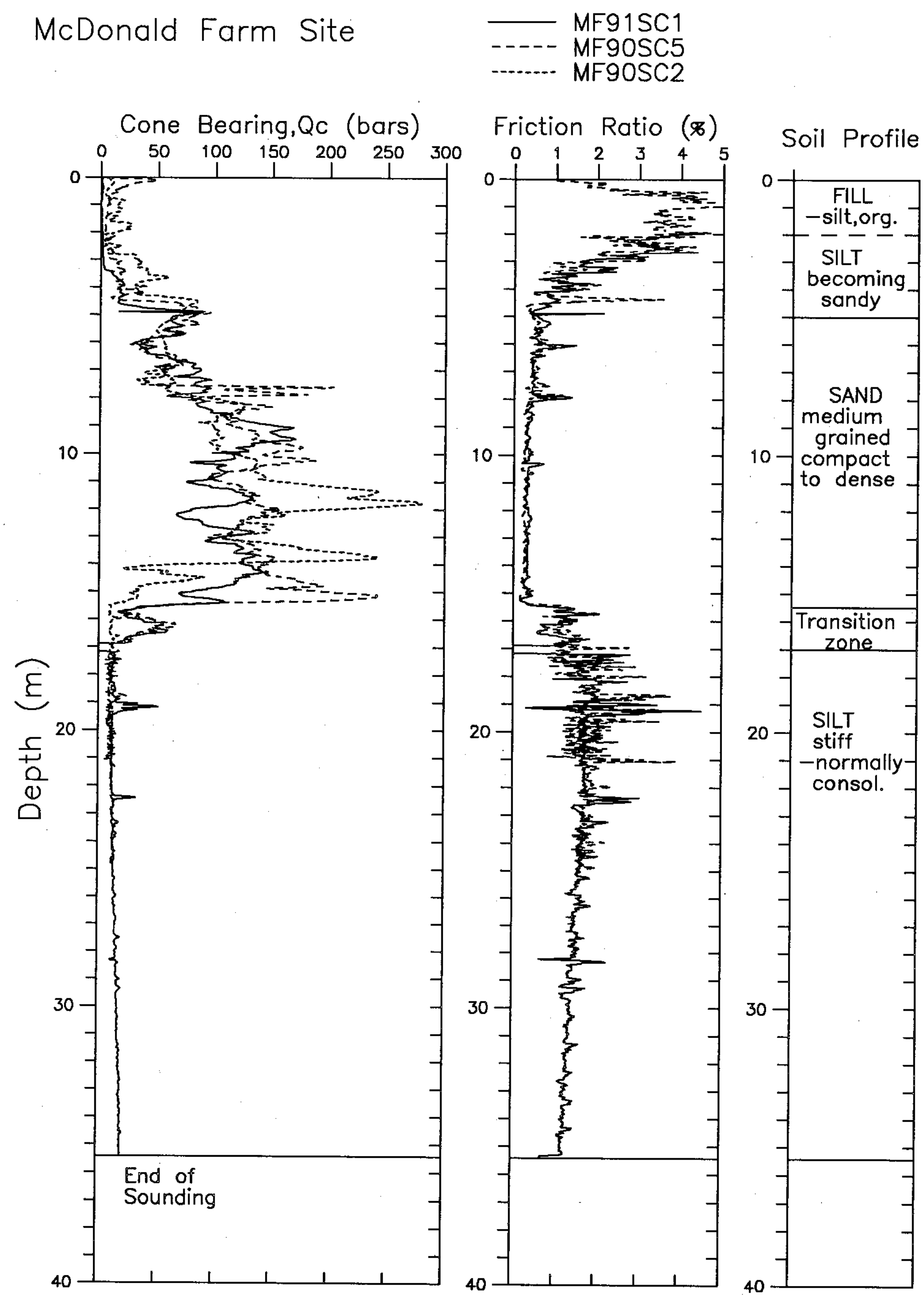


Fig.4.3 CPT Soundings — McDonald Farm Site

coarse and medium sand at the #10 sieve (1.68mm opening) the sand is fine to medium grained (see Fig.4.4). The silt contains about 10% sand sizes. The plasticity characteristics of the silt ($w_L$=35%, $w_P$=25%) place the soil very close to the A-line.

**4.2.3 Testing program**

The test program conducted at the McDonald Farm site is provided in Table 4.2. The locations of the tests are given in Fig.4.2.

*4.3 LOWER 232ND STREET SITE*

**4.3.1 Site description**

The Lower 232nd St. (L2) site is located on the northwest side of the intersection of Highway 1 (Trans-Canada Highway) and Highway 10 (232nd St.), south of Fort Langley. A general site map is provided in Fig.4.5. The site is roughly triangular in shape about 80m long and 40m wide. Testing was restricted to the eastern end, adjacent to the off-ramp from west-bound Highway 1. The site dips away from this part of the site to the drainage ditches, but in rainy periods the surface becomes soft enough to make driving difficult. The depth to the water table varies between 1m and 1.5m. The grass at the site has been regularly cut.

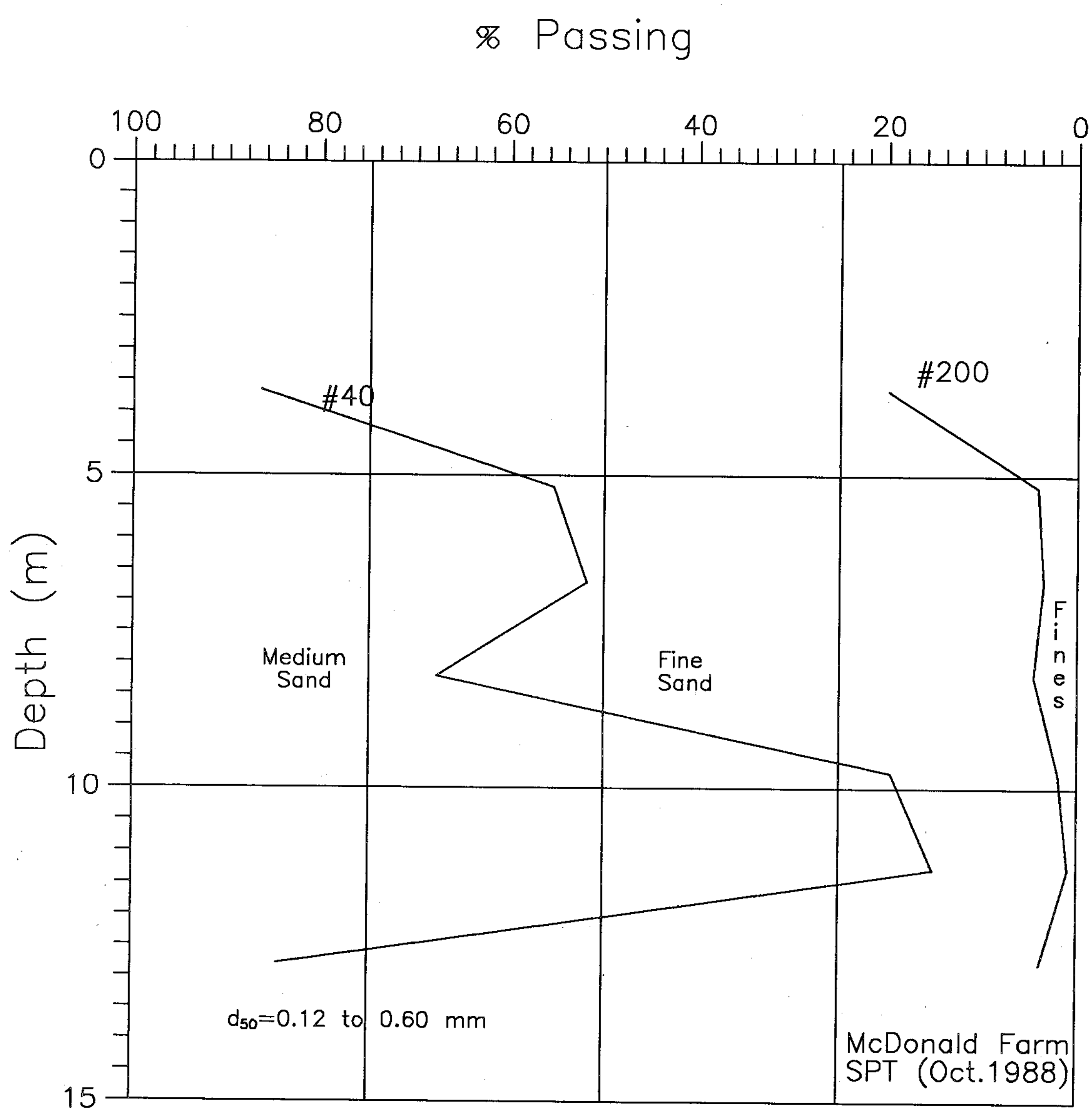


Fig.4.4 Grain Size Analyses – McDonald Farm Site

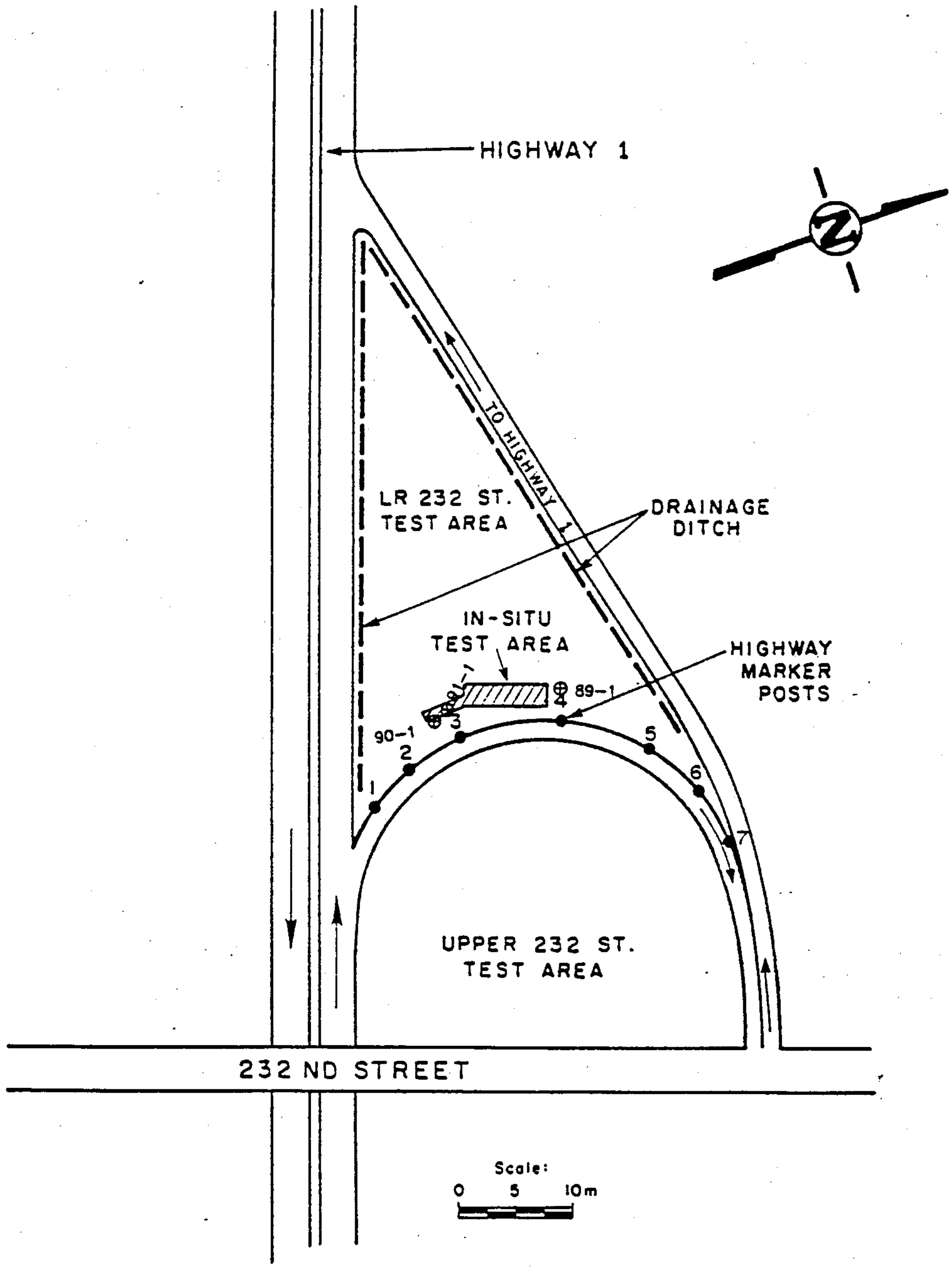


Fig.4.5 Lower 232nd St. Site Plan

| SCPT # | Date | Depth | Equipment | Comments |
|---|---|---|---|---|
| SC-89-M1 | May18/89 | 12m | B.,10g-A. | Too noisy |
| SC-89-M2 | May24/89 | 14m | B.,10g-A. | Too noisy |
| SC-89-M3 | Aug.15/89 | 30m | B.,2g-A. | Erratic noise |
| C77-89-5 | Oct.5/89 | 28m | 2-2g-A.(C&M) | |
| | | | -sledge hammer,BG | |
| MF90SC1 | Jan.11/90 | 14m | 2-2g-A.(C&M) | |
| MF90SC2 | Jan.19/90 | 20m | (C&M)-tried RC-Scope | |
| MF90SC3 | May1/90 | 25m | two cones-1fixed | -some noise |
| MF90SC4 | May17/90 | 1.9m | DW, cone | -various pads |
| | | | bender, geophone | on DW |
| MF90SC5 | May24/90 | 25m | cone only | |
| & 5P | | 15m | DW | |
| MF91SC1 | Apr.17/91 | 35m | cone only | |

Note: Mech. swing hammer used unless noted otherwise

B.=Bender A.=Accelerometer C=A. at top of cone

M=A. 1m above C BG=Buffalo Gun DW=drop weight

TABLE 4.2 Insitu Tests at McDonald Farm Site

### 4.3.2 Soil stratigraphy

The cone bearing and friction values obtained from three SCPT's at the site are given in Fig.4.6, along with the interpreted soil profile.

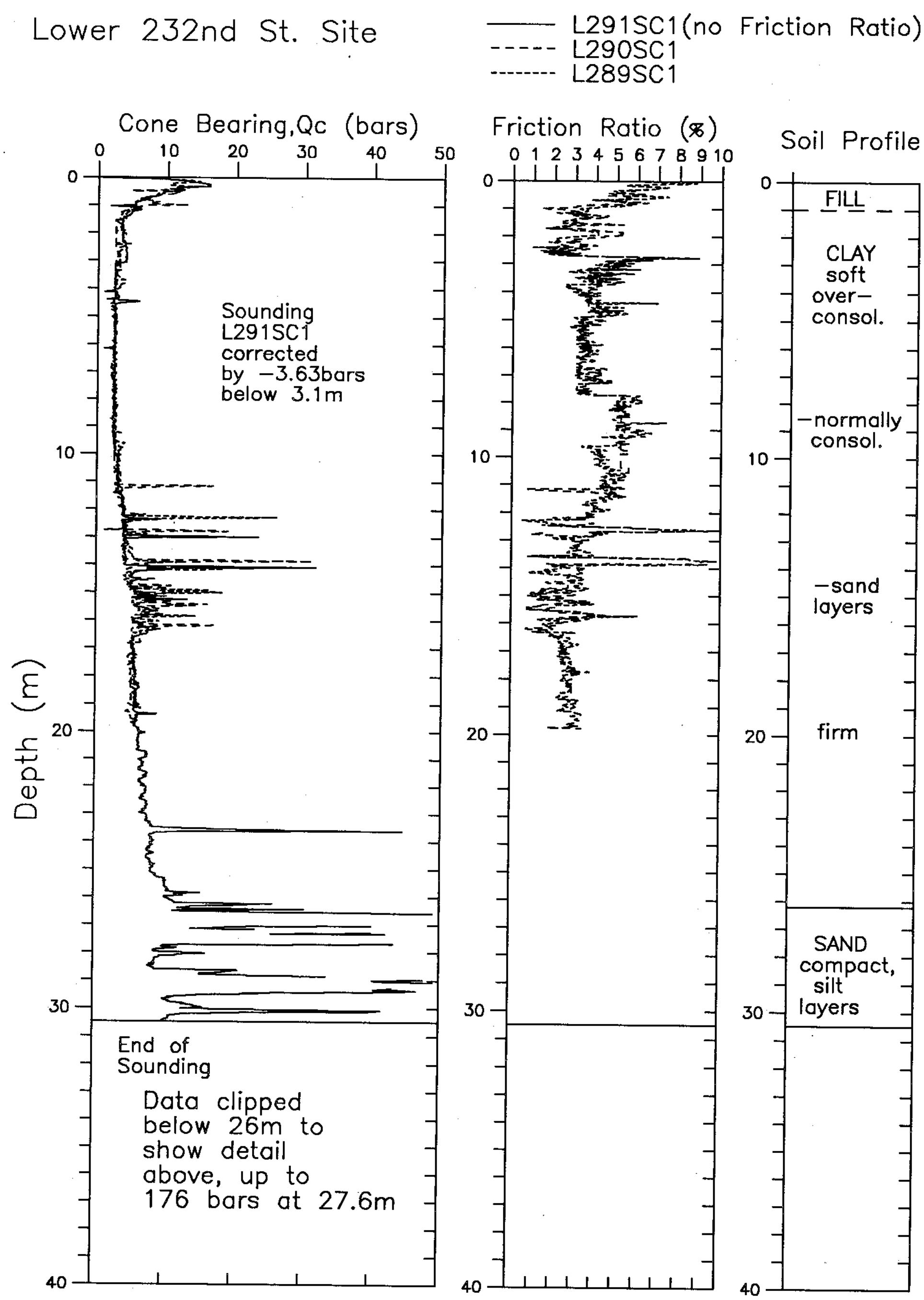


Fig.4.6 CPT Soundings – Lower 232nd St. Site

Information gathered by Zavoral (1990) indicated that the clay contains about 5% fine sand sizes and has water contents of 33 to 42%. The average plasticity characteristics of the clay ($w_L$=44%, $w_P$=20%) place the soil above the A-line and in the CL classification. Above the 2m depth, the limits are about 30% higher and the soil is CH. Data presented by Sully (1991) and Greig (1985) show that the field vane strength increases from about 20kPa at 4m to about 35kPa at 20m. The consolidation test results show that the clay is essentially normally consolidated below 5m.

### 4.3.3 Testing program

The test program conducted at the Lower 232nd St. site is provided in Table 4.3. The locations of the tests are given in Fig.4.5.

| SCPT # | Date | Depth | Equipment | Comments |
|---|---|---|---|---|
| L289SC1 | Dec.12/89 | 20m | C&M | |
| L290SC1 | Mar.19/90 | 20m | C&M | |
| L290SC2 | May30/90 | 22m | 2cones-1 fixed | -Noise with 2 Data Acq. Sys. |
| L291SC1 | May8/91 | 30m | Cone only | |

TABLE 4.3 Insitu Tests at Lower 232nd Street Site

*4.4 ANNACIS NORTH PIER SITE*

**4.4.1 Site description**

The Annacis North Pier (AN) site is located beneath the Alex Fraser Bridge on the eastern side of Annacis Island, which is in the South Arm of the Fraser River. Access is off Derwent Way. A general site map is provided in Fig.4.7. The surface dips slightly towards the gravel access road and towards the river. There are scattered clumps of grass and bushes around the site. It is expected that the groundwater table would vary somewhat with the tidal fluctuations in the Fraser River. Testing in the fall of 1990 indicated that the groundwater was at a depth of 5m to 6m. Bazett and McCammon (1986) indicated that artesian conditions exist at depth (increasing from about 40m to 80m depth). The 1990 testing also showed that about 3m of fill had been placed over the site.

**4.4.2 Soil stratigraphy**

The cone bearing and friction values obtained from one SCPT at the site are given in Fig.4.8, along with the interpreted soil profile. Grain size variation with depth is shown on Fig.4.9 (% passing #60 sieve shown as this was the size selected for testing). The sand contained a variety of sizes from coarse to fine grained. The samples were obtained from a Standard Penetration Test (SPT) boring and the blowcounts (N-values) are shown in Fig.4.10.

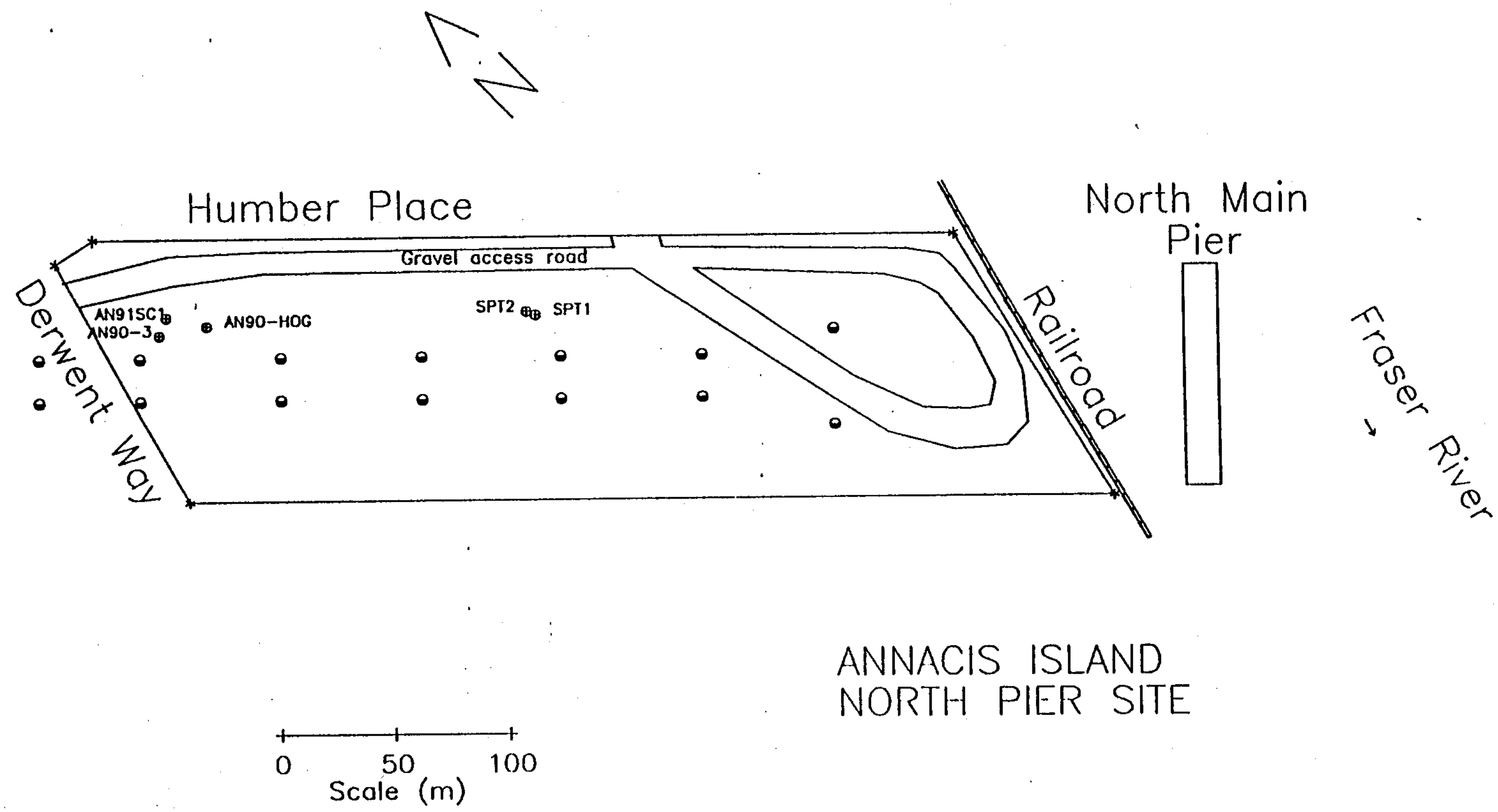


Fig.4.7 Annacis North Pier Site Plan

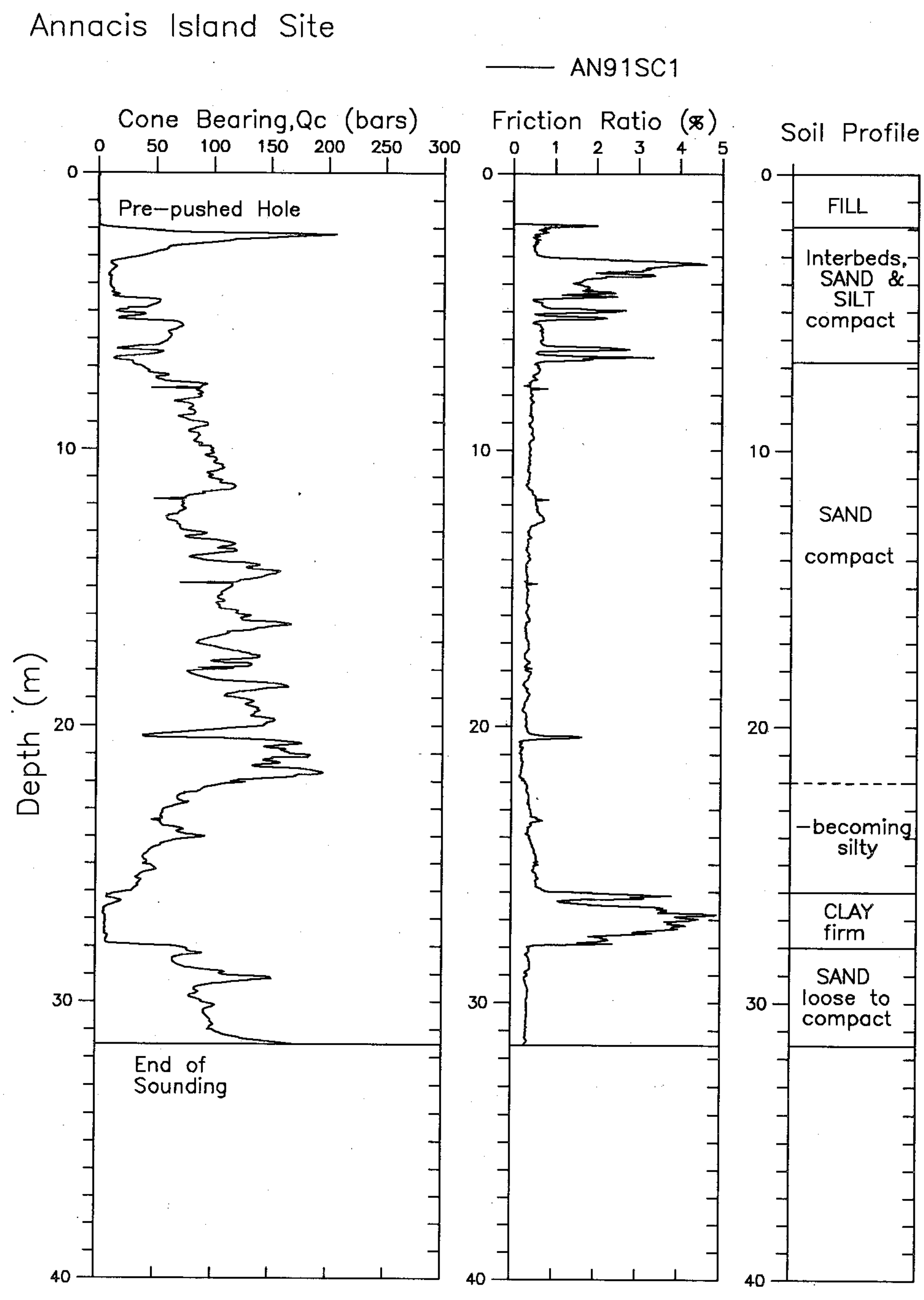


Fig.4.8 CPT Soundings — Annacis N.Pier Site

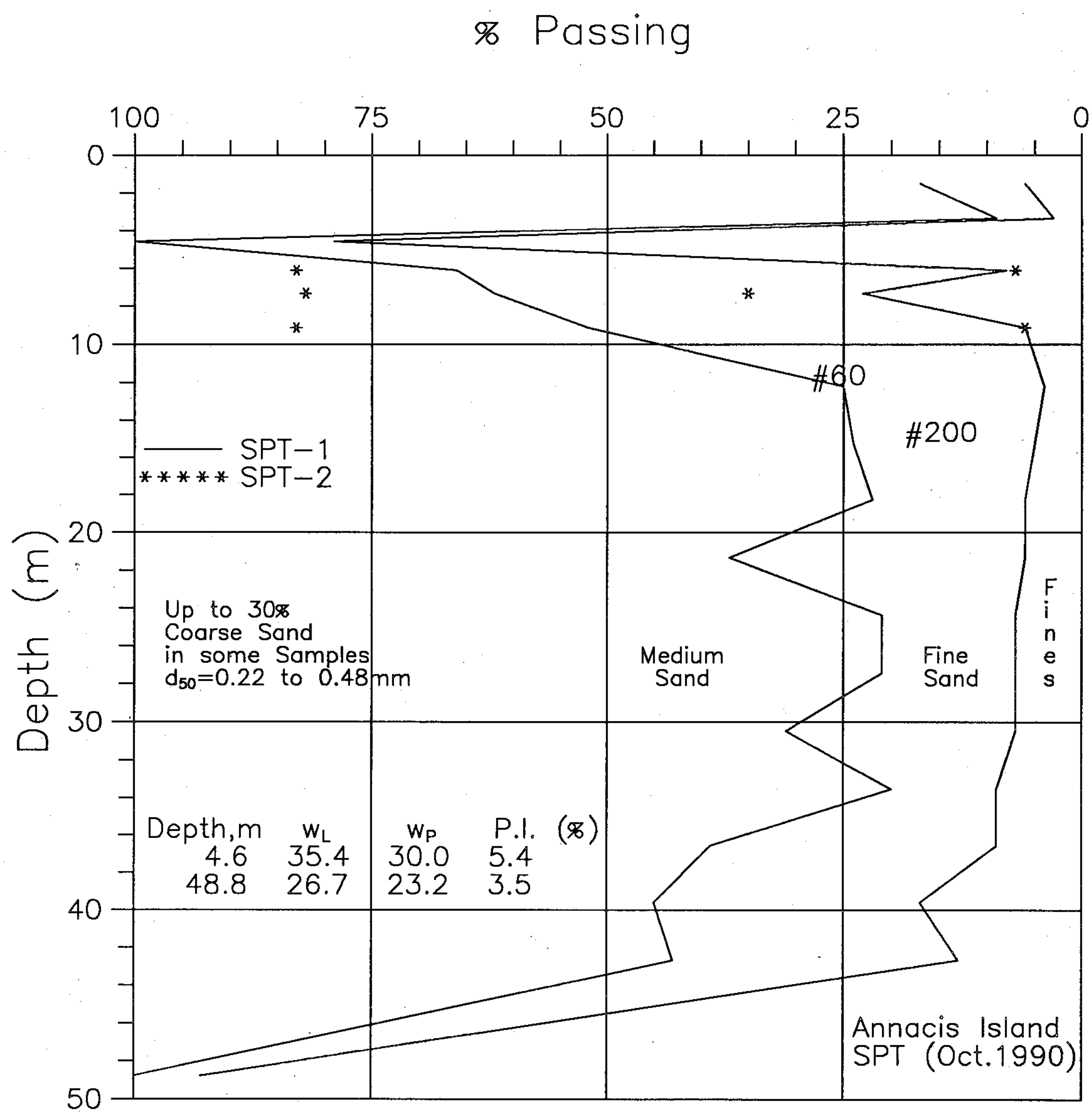


Fig.4.9 Grain Size Analyses — Annacis N.Pier Site

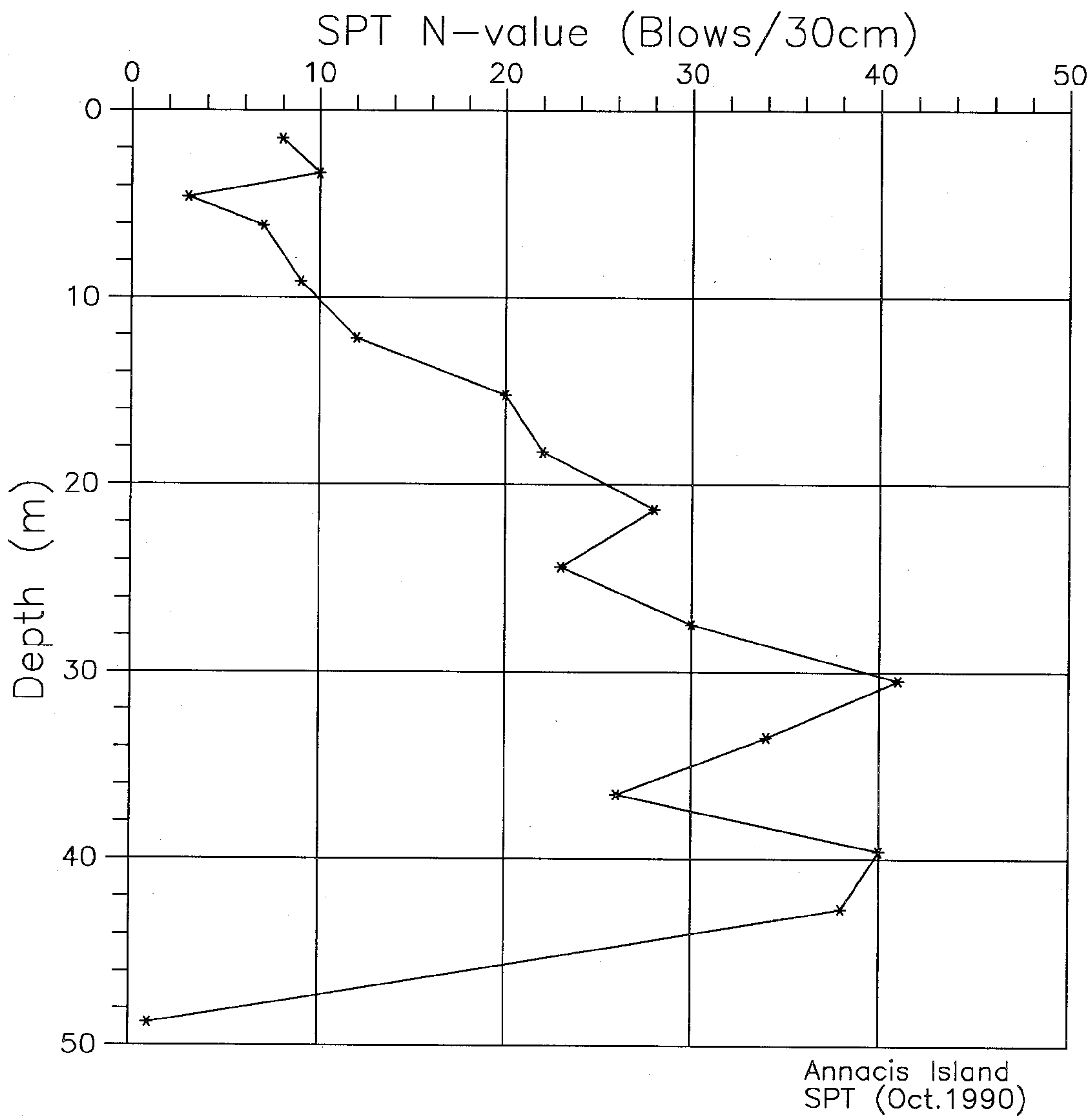


Fig.4.10 SPT Results – Annacis N.Pier Site

### 4.4.3 Testing program

The test program conducted at the Annacis North Pier site is provided in Table 4.4. The locations of the tests are given in Fig.4.7.

| SCPT # | Date | Depth | Equipment | Comments |
|---|---|---|---|---|
| AN90-HOG | Aug.28/90 | 20m | Geophone(Hog.Cone) | |
| AN90-3 | Sep.27/90 | 43m | C&M | Only upper 18m useful for $D_s$ |
| AN91SC1 | Apr.24/91 | 31m | Cone only | |

TABLE 4.4 Insitu Tests at Annacis North Pier Site

## *4.5 LAING BRIDGE SITE*

### 4.5.1 Site description

The Laing Bridge (LB) site is located just to the south of the south end of the Arthur Laing Bridge on the north-eastern side of Sea Island, about 4km from the McDonald Farm site. A general site map is provided in Fig.4.11. The site is about 70m wide and 340m long, with the test reported here conducted in the northeast corner of the site. The site is almost level with a slight slope for drainage. The grass covering the site is regularly cut. The groundwater table is about 1.2m deep.

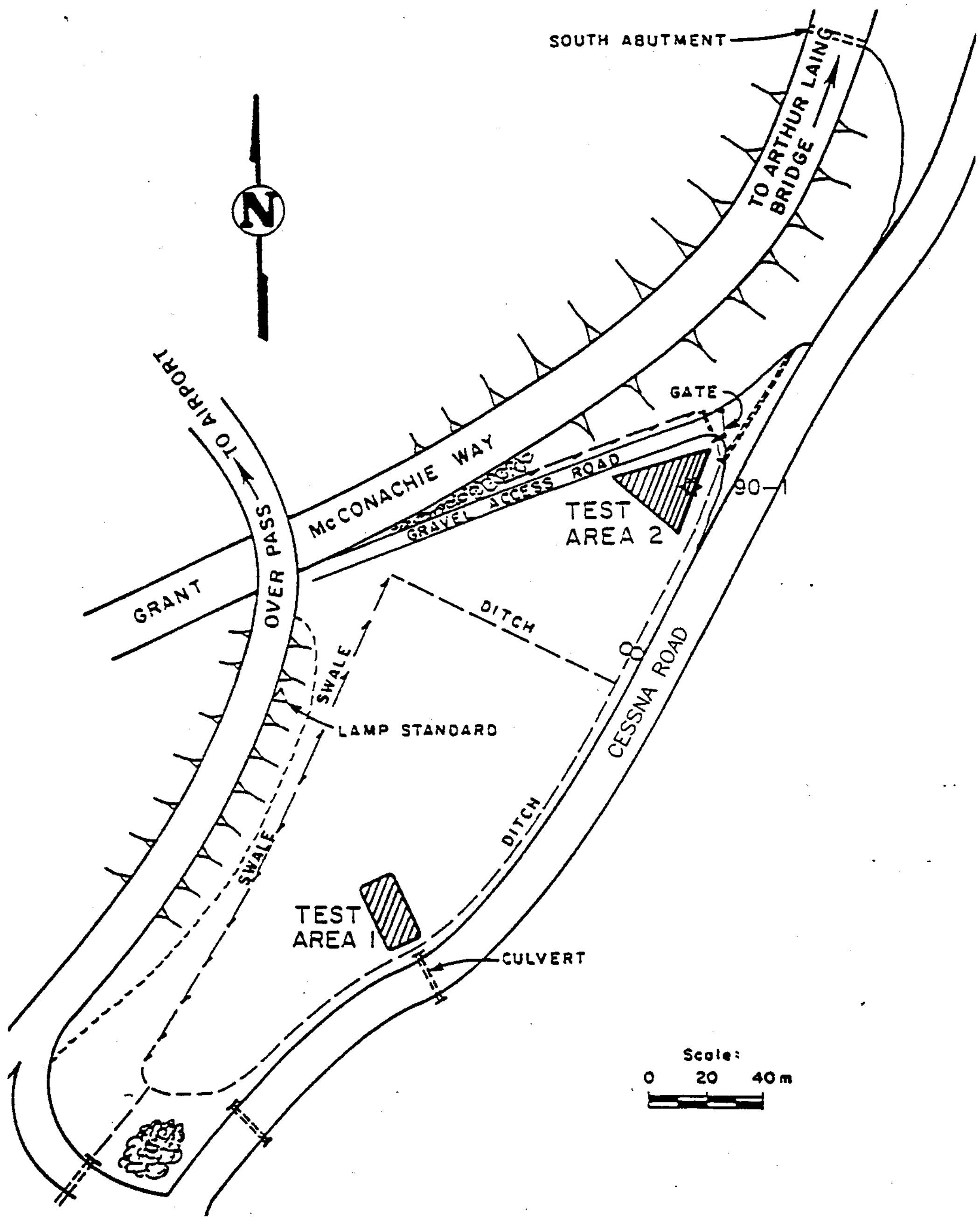


Fig.4.11 Laing Bridge Site Plan

### 4.5.2 Soil stratigraphy

The cone bearing and friction values obtained from one SCPT at the site are given in Fig.4.12, along with the interpreted soil profile. Grading curves provided by Sully (1991) indicate the sand is mainly fine-grained with an average $d_{50}$ size of 0.2mm. Deeper portions of the profile were described by LeClair (1988).

### 4.5.3 Testing program

The test program conducted at the Laing Bridge site is provided in Table 4.5. The location of the test is given in Fig.4.11.

| SCPT # | Date | Depth | Equipment | Comments |
|---|---|---|---|---|
| LB90SC1 | Aug.21/90 | 19m | Cone only-used Swing hammer, BG, and P-plate | |

TABLE 4.5 Insitu Test at Laing Bridge Site

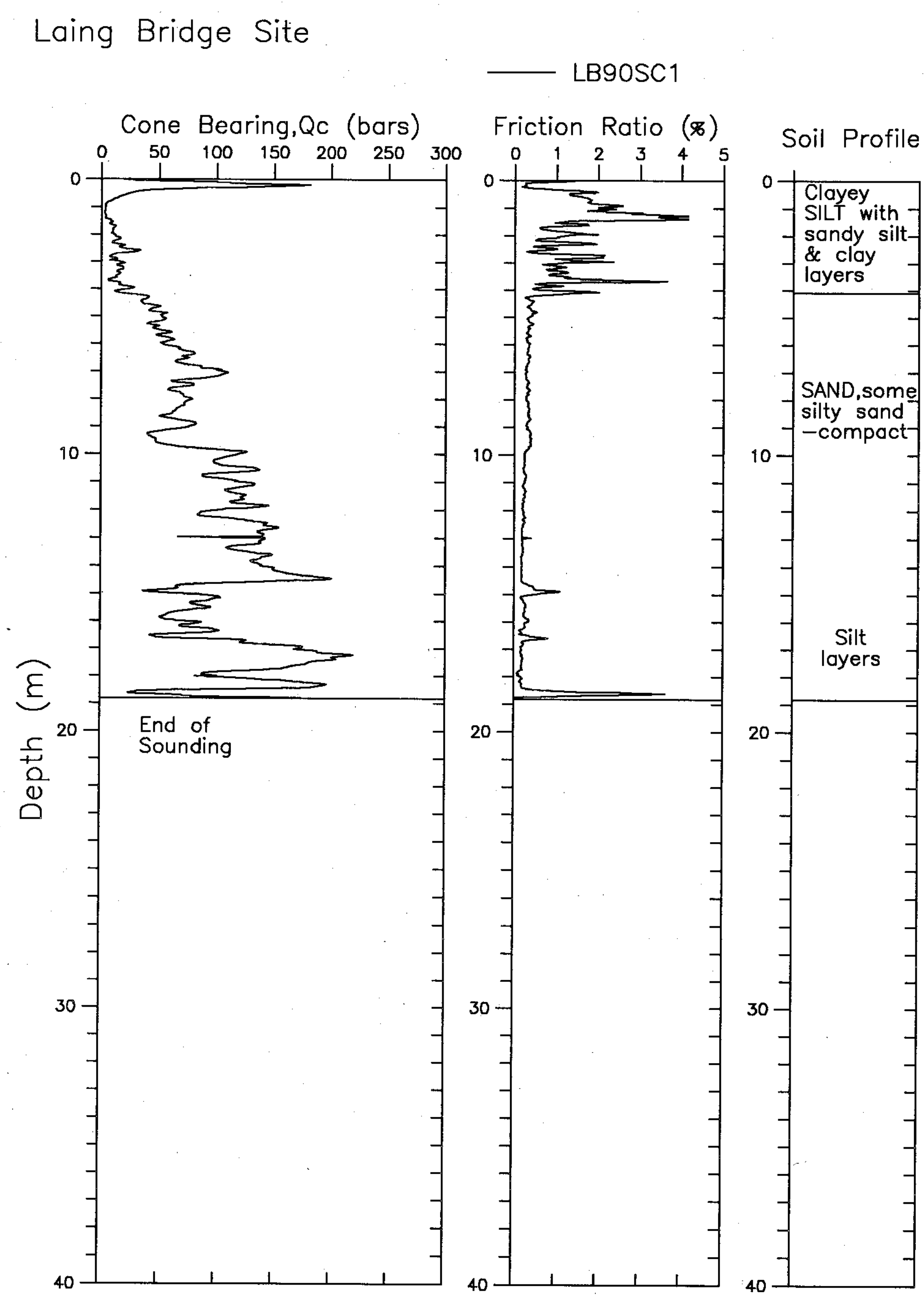


Fig.4.12 CPT Sounding – Laing Bridge Site

# CHAPTER 5

## EQUIPMENT, SIGNAL CHARACTERISTICS AND TEST PROCEDURE

### *5.1 INTRODUCTION*

Details of the cone equipment, test procedures, and interpretation to obtain a soil profile during a seismic cone penetration test were given by Gillespie (1990) and will not be repeated herein. Gillespie also discussed velocity measurements in the SCPT. Detailed discussions of the equipment used at UBC for the SCPT up to 1985 are given by Rice(1984) and Laing(1985). A schematic diagram showing the layout of the usual downhole test procedure is shown in Fig.5.1. A horizontally oriented seismic receiver is fixed into the cone body which is pushed vertically through the soil resulting in good coupling between the soil and the receiver. Testing is normally done in 1m increments as the pushing is stopped to add a rod for pushing the cone. Various aspects of the equipment used in this test, the characteristics of the signals measured, and a recommended procedure that has evolved over the course of this research will be discussed in this chapter.

### *5.2 SOURCES*

The primary source of shear waves has been a weighted plank (or beam) struck horizontally with a hammer. Initially a heavy wooden beam with steel ends, weighted with a van, was struck with a 7kgF (69N) sledge hammer. In a study of the factors contributing to optimal shear

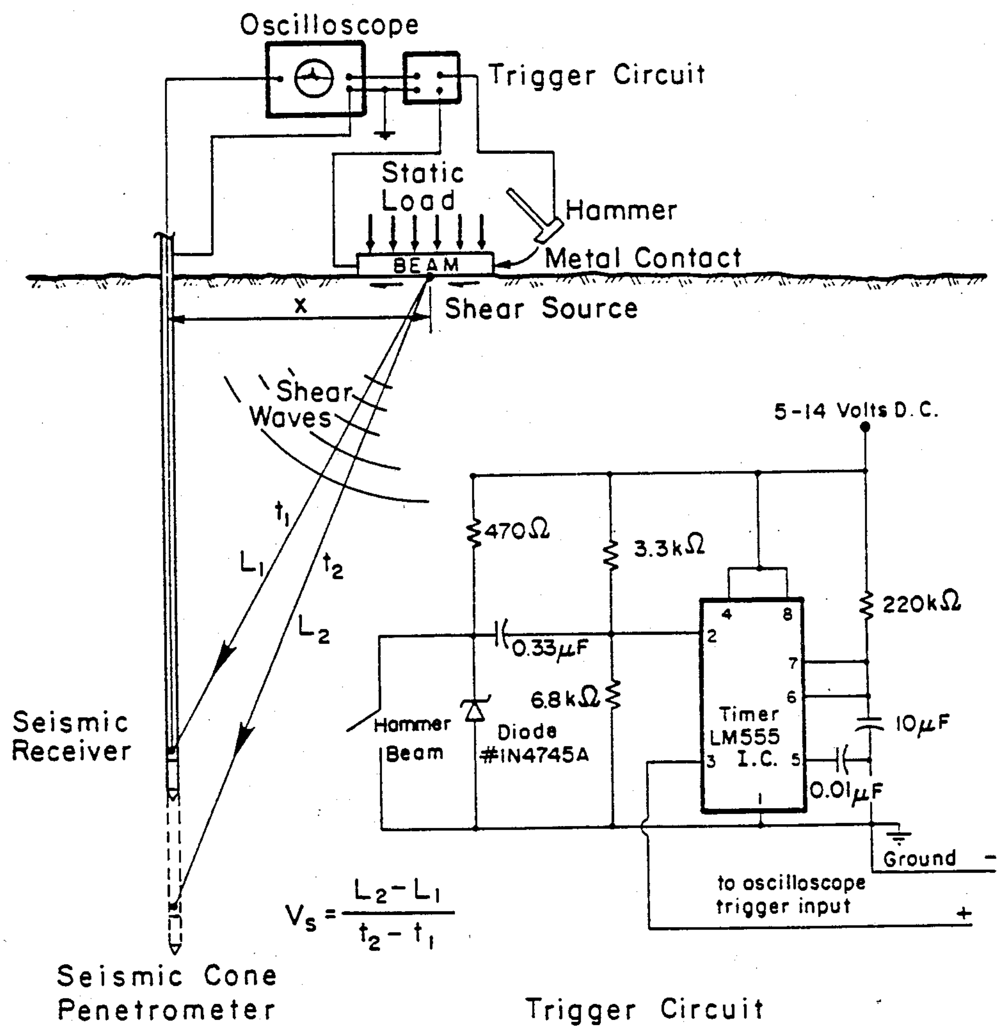


Fig.5.1 Schematic Diagram of Downhole SCPT Arrangement with Trigger (after Campanella and Stewart, 1990)

sources (Robertson, 1986), it was found that a very high normal load on the shear beam was absolutely essential. The high load maintains coupling with the ground so no energy is lost due to slippage when the beam is struck. It was subsequently found that the pads supporting the UBC cone truck, if suitably reinforced, could be struck without damaging the truck supports, and the pads are now used as the beam. At the present time an adjustable mechanical swing hammer weighing 12kgF (116N) is used to provide a highly repeatable or calibrated source for shear waves. The commonly used setting has an arm-length of about 2.25m, swinging through an arc of about 12.6$^{o}$, giving a vertical fall of about 56mm. This hammer is similar to one developed and used by Applied Research Associates (Shinn,1990). It should be noted that the end-plates of the pads, and a series of three vertical V-shaped plates just inside each end-plate, extend about 70mm below the pad. At a soil-surfaced site, these plates push into the ground surface and provide good contact. Discernable signals are clearly received to depths of at least 35m. On one site that had been covered with a dense gravel layer, the plates below the pads had essentially no penetration with the full weight of the truck on the pads, and the signals became difficult to discern below 15m.

A vertical hammer strike on a plate placed partly under the truck pad has been used to produce compression (P-) waves with limited success. Vertically oriented receiver can give erroneously very high velocity measurements (>6000m/s), possibly caused by a poor response to soil motion due to rod stiffness in the vertical direction or waves travelling in the rods. A horizontally oriented receiver gives very low signal to noise response and is not effective below a few meters depth. Recently a 136 Kgf (1.33kN) drop weight that is raised on an arm on the side of the UBC cone truck has been developed. It appears that P-waves from heavy drop weights are detectable to a depth of at least 15m.

An explosive source that has been routinely used for several years is the "Buffalo gun" (Pullan and MacAulay,1987). At UBC a 12 gauge shot gun shell is fired into the ground. A length of water pipe with fittings to hold the shotgun shell is placed in a narrow (38mm $\phi$) augured hole about 0.8m deep and flooded with water. The shell is fired by dropping a pointed rod into the pipe. Results of S-wave velocity measurements with the Buffalo gun are rather variable, sometimes in close agreement with the shear beam results, but often somewhat lower. Generally it is also possible to detect P-waves to a depth of about 10m with the buffalo gun. A high water table is needed to transmit the P-wave to depth.

For earlier offshore work from an ice sheet, seismic caps were used, exploded at three different locations; just below the ice, lowered to the mudline, and embedded in the mud. The limited number of tests suggested that the in-water seismic cap source signals, although difficult to interpret, gave reasonable results (Campanella et al, 1987).

Large strain sources have not been investigated in this research. The only known published work providing some details of equipment and calculations, with damping calculated using large-strain sources, is that of Shannon and Wilson (1980). An interesting surface source described by Layotte (1980) is the M3 Marthor hammer truck with a swinging hammer weighing 1700kg (16.7kN - over 100 times heavier than that used in this research). No details of the induced strains were provided.

## *5.3 USE AND TESTING OF RECEIVERS*

### 5.3.1 Types of receivers

A variety of receivers have been used in the research at UBC, including geophones and accelerometers of the piezoceramic and piezoresistive types. An important requirement of the receivers is that they fit within the cone to be used. The geophones used, manufactured by Geospace Corporation, are 1.7cm in diameter and have a natural frequency of 28Hz. In the 15 $cm^2$ cone a triaxial package was used, and in the 10 $cm^2$ cone a single horizontal geophone was used. When used with the shear beam source, they produce clear signals. However with the explosive sources it was found that the geophone did not provide clean signals, and it was difficult to detect the S-wave arrival. In recent studies to measure material damping in-situ, the natural frequency of the geophone was in the range of the shear wave of interest. Further, the calibration in the frequency domain was non-linear. For these reasons the use of accelerometers having natural frequencies from 300 to 3 kHz were pursued.

The piezoceramic bender units, manufactured by Piezo Electric Products, were 1.27cm square and had a natural frequency of about 3000Hz. Resonance of the undamped receiver caused noise on the signals, making interpretation difficult and requiring digital filtering. Two models of piezo-resistive accelerometers have also been used. These accelerometers can be calibrated statically. The first, manufactured by Kulite Semiconductor Products, has a range of +/-10g, is 0.95cm by 0.39cm has a natural frequency of about 550 Hz and is also undamped. Again resonance of the accelerometer caused noise on the signals. The second type, manufactured by IC Sensors, has a range of +/-2g, is 1.52cm square, has a natural frequency of about 600Hz and is critically damped. These have been successfully used for about 2 years.

Sensors with active axis oriented horizontally have been used singly, or in pairs separated by 1m along the cone rods. Velocities measured by a separated pair of sensors responding to a single impulse have been referred to as true interval measurements. Velocities measured by an advancing single receiver recording separate impulses have been referred to as pseudo interval measurements since timing is referenced to the trigger which must be repeatable. A detailed analysis by Rice (1984) showed that a comparison of pseudo to true interval methods gave a standard deviation less than 1.5% of the mean indicating that the methods are equivalent with a repeatable trigger.

### 5.3.2 Testing of receivers

The seismic cone signals measured with accelerometers typically have a frequency range of concern of less than 150Hz. The primary devices used to receive the signals in the cone were piezoresistive accelerometers, most commonly those manufactured by IC Sensors, model 3021-002-N. These piezoresistive accelerometers have a nominal capacity of 2g, a natural frequency of about 550-750 Hz, and a nominal damping of 70%. Thus the accelerometers provide a flat response over the frequency range of interest.

The response of some of the receiving devices was measured using a vibrator ("shaker") system. The available shaker was a Model V456 vibrator manufactured by Ling Dynamic Systems Ltd. With the bare table, the maximum output of the vibrator is governed by:

0-38 Hz Displacement

38-72 Hz Velocity

> 72 Hz Acceleration

With increasing load, these frequencies decrease and the range for which velocity governs disappears. The maximum useful frequency is 7500 Hz. The shaker output was controlled by a signal generator. A Zonic

AND Model 3525 FFT signal analyzer provided both the signal generator and the recording instrument.

A typical output of a swept sine test (nominally 0 to 500Hz) on an accelerometer is shown in Fig.5.2. The slope up to about 90 Hz and the variation beyond 400 Hz are expected results of the testing equipment and test procedure, respectively. In between it was anticipated that the response would be essentially flat (from the typical frequency response for an accelerometer as provided by the manufacturer given in Fig.5.3). It can be seen that the best fit line (shown dashed) is essentially flat but that the actual response is somewhat irregular, with steps based at about 260 Hz and 310 Hz. Further tests with another accelerometer of the same model, an earlier version (8060) of the same model, and an accelerometer from another manufacturer (Kulite Semiconductor Products Ltd. Model TGY 155 triaxial accelerometer) gave similar irregularities. It was concluded that these irregularities were likely part of the testing system. A similar test (0 to 200Hz) on a cone with an accelerometer installed is shown in Fig.5.4. The results are very similar with the steps occurring at lower frequencies, likely due to the increased mass on the shaker table.

Other receiving devices used included geophones and benders. A cone manufactured by Hogentogler & Co., Inc. containing a miniature geophone was tested. Based on swept-sine shaker tests on the cone, the geophone has a natural frequency of about 30 Hz and damping in the order of 15%. The manufacturer gives a natural frequency of 28 Hz and damping

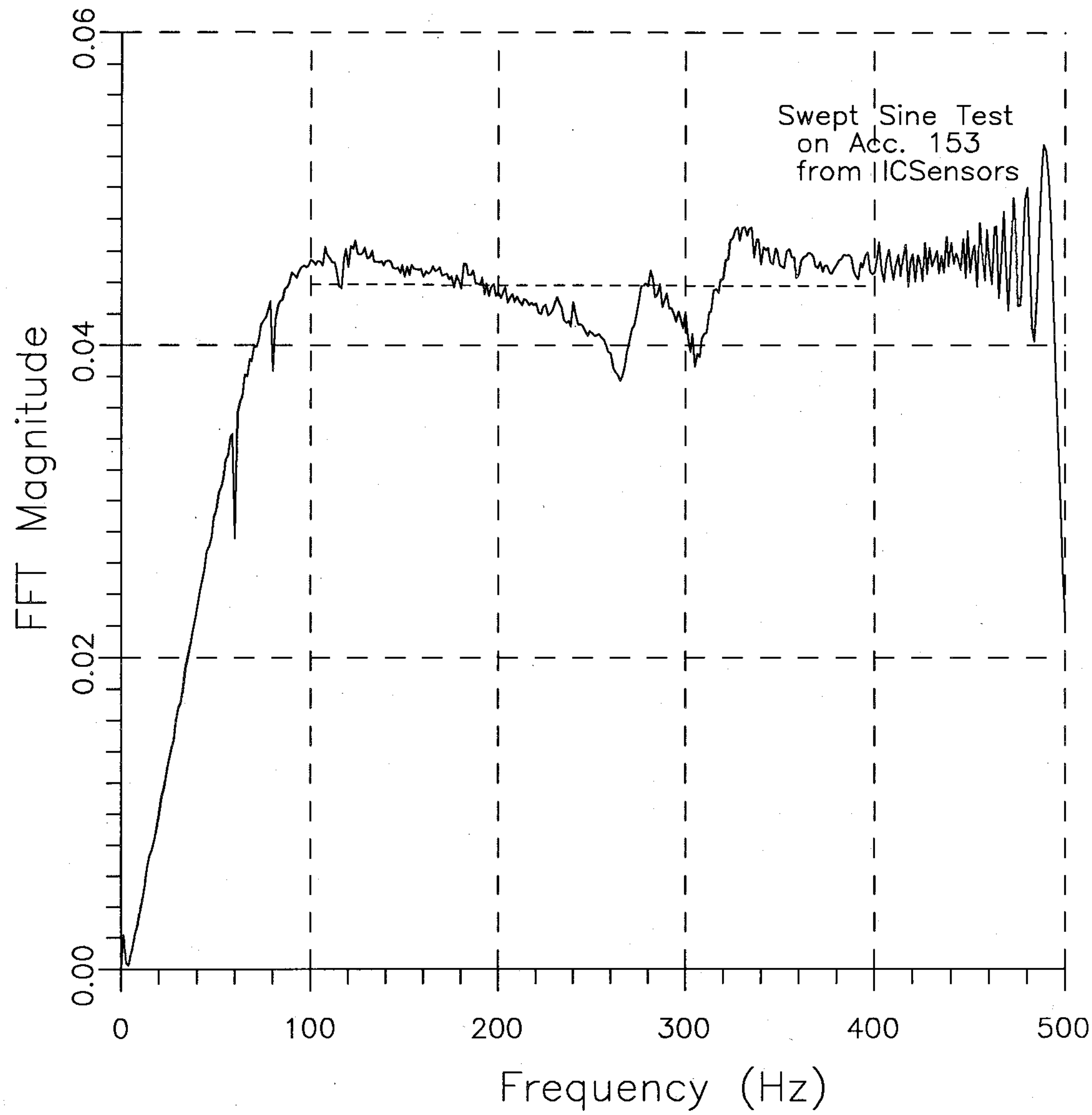


Fig.5.2 Swept Sine test on Accelerometer

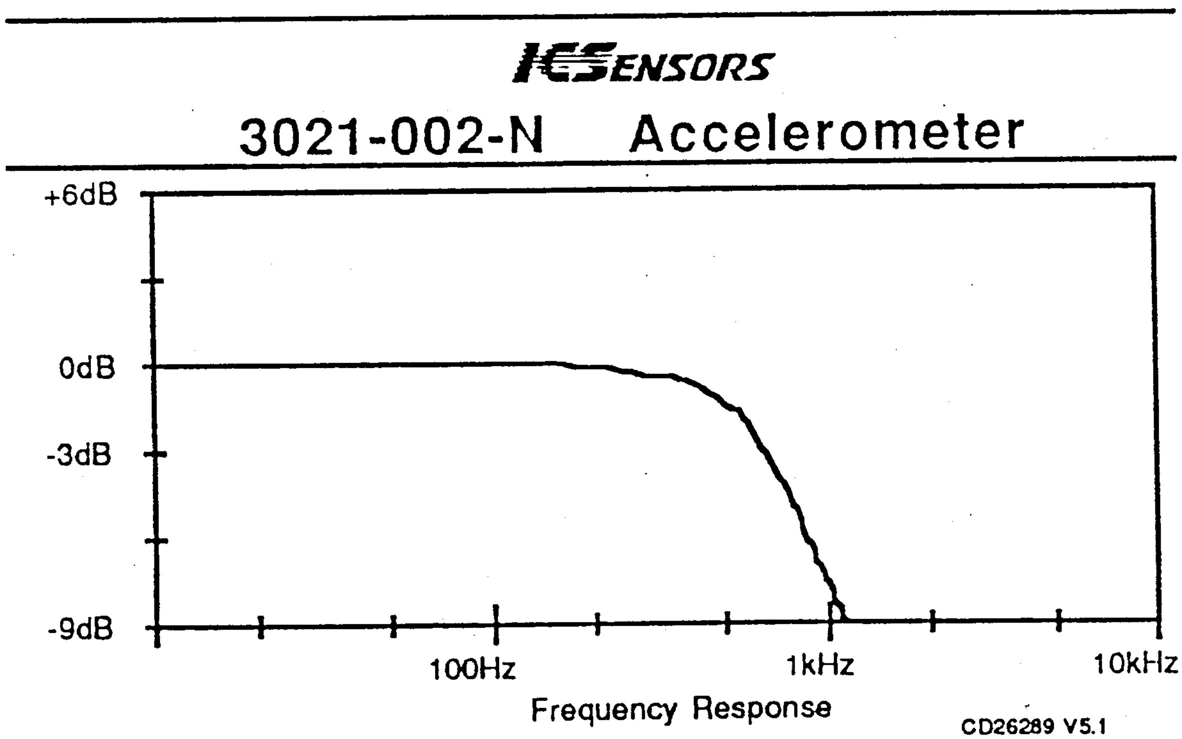


Fig.5.3 Accelerometer Frequency Response as Provided by Manufacturer

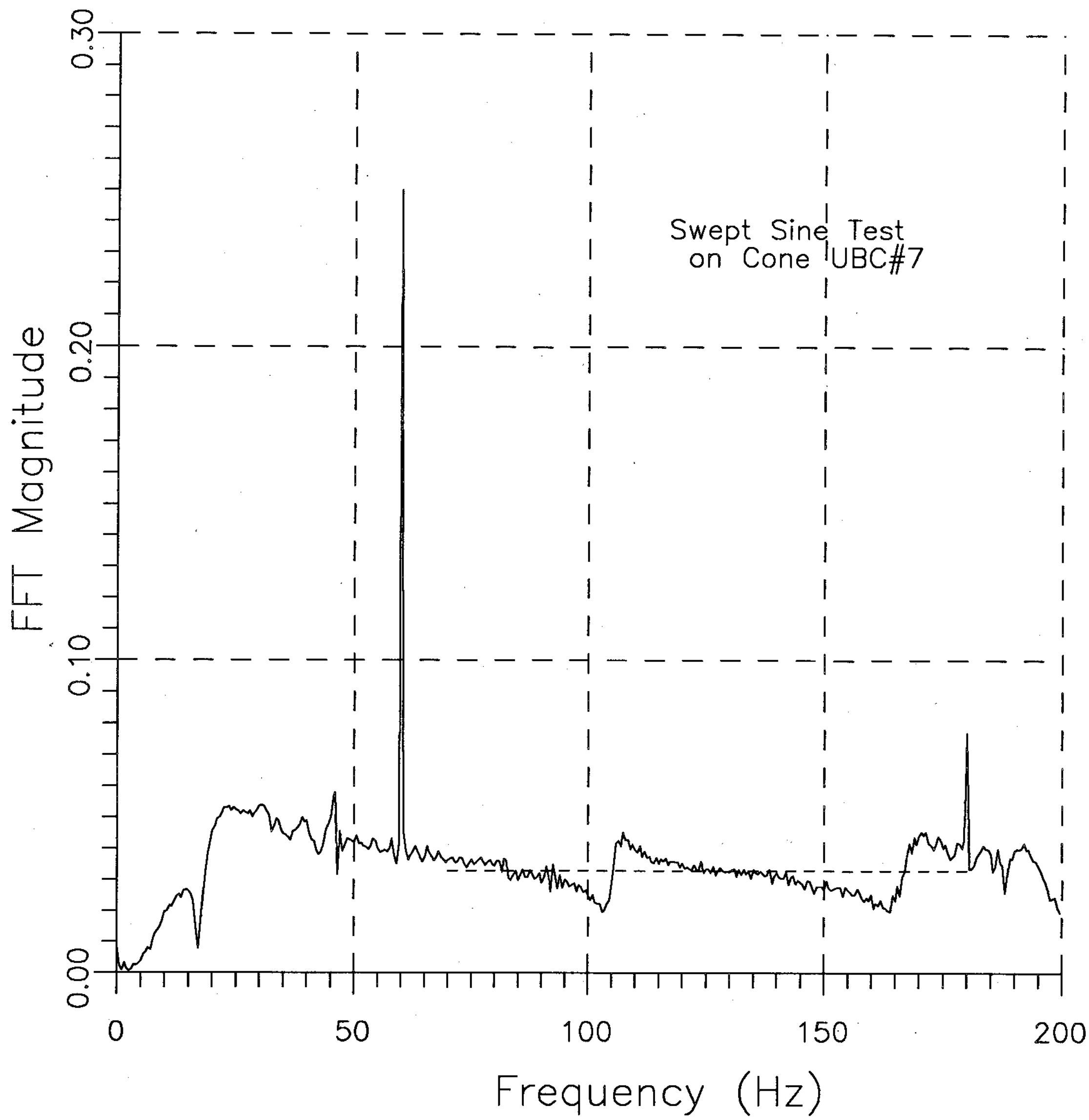


Fig.5.4 Swept Sine Test on Accelerometer Mounted in Cone (UBC#7)

of 18% (Geo Space Corp. Model GS-4-L3) and the frequency response curve provided is shown in Fig.5.5. Past the peak, the spectrum continued to fall (did not have a flat response) out to at least 300 Hz. A comparison of the signals, at similar depths, from the 18% damped geophone and a 70% damped accelerometer are presented in Fig.5.6. Observing the FFT's of the full signals, it can be seen that the peak amplitudes occur at the same frequency (about 73Hz). For the accelerometer record, the amplitudes decay with higher and lower frequencies. However for the geophone record, another significant peak occurs near the natural frequency, and this peak can be expected to affect calculations done in the frequency domain. The FFT's of the windowed signals do not show other peaks but the frequency for the peak amplitude is lower (about 61Hz) for the geophone record when compared to that (68Hz) for the accelerometer record. It should be noted that larger geophones have been successfully used in cased drillholes. Redpath et al (1982) used 10Hz geophones with damping of 0.7, and reported that these had a flat response from 15 to 200 Hz. They used a bandwidth of 40 to 100 Hz to measure damping.

The bender units used are piezoceramic transducers produced by Piezo Electric Products, Inc. They are 12.7mm X 12.7mm X 0.58mm thick (0.5"X0.5"X0.023"). When mounted as a cantilever, the resonant frequency is given as 1520 Hz. When mounted in the cone, the measured signals were frequently contaminated with noise (see Fig.5.7). As can be seen in Fig.5.8, the noise appeared to occur at multiples of 60 Hz.

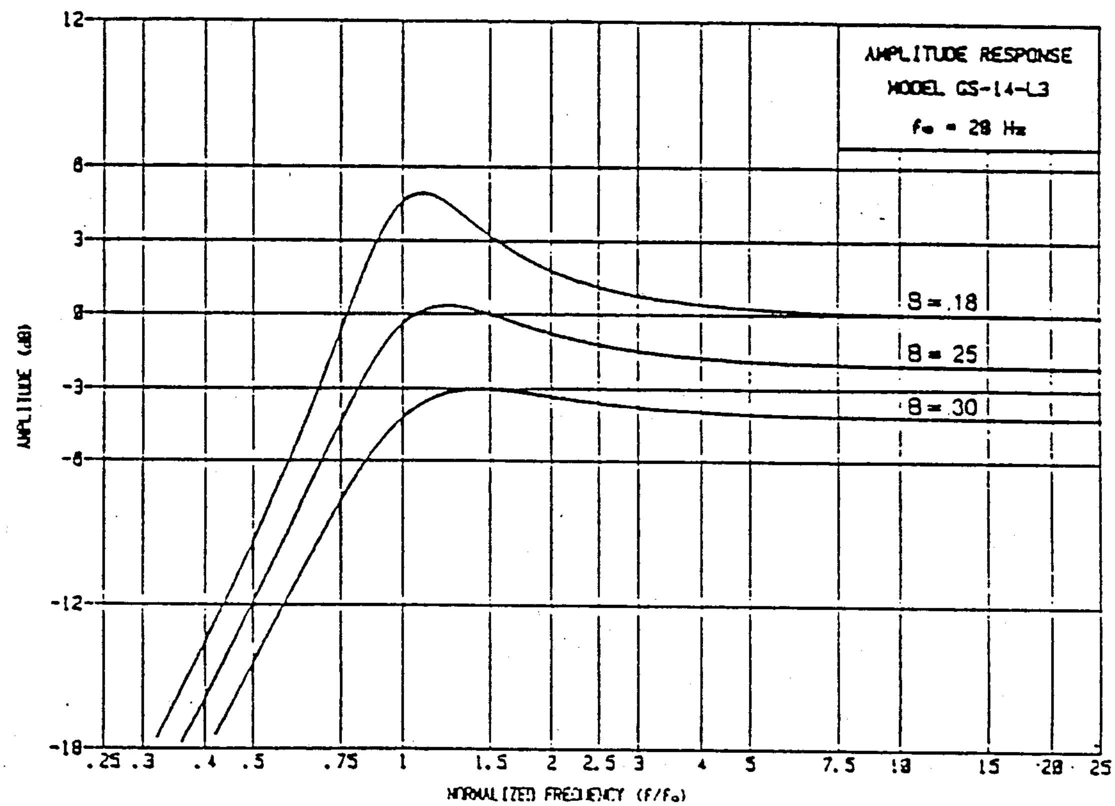


Fig.5.5 Geophone Frequency Response as Provided by Manufacturer

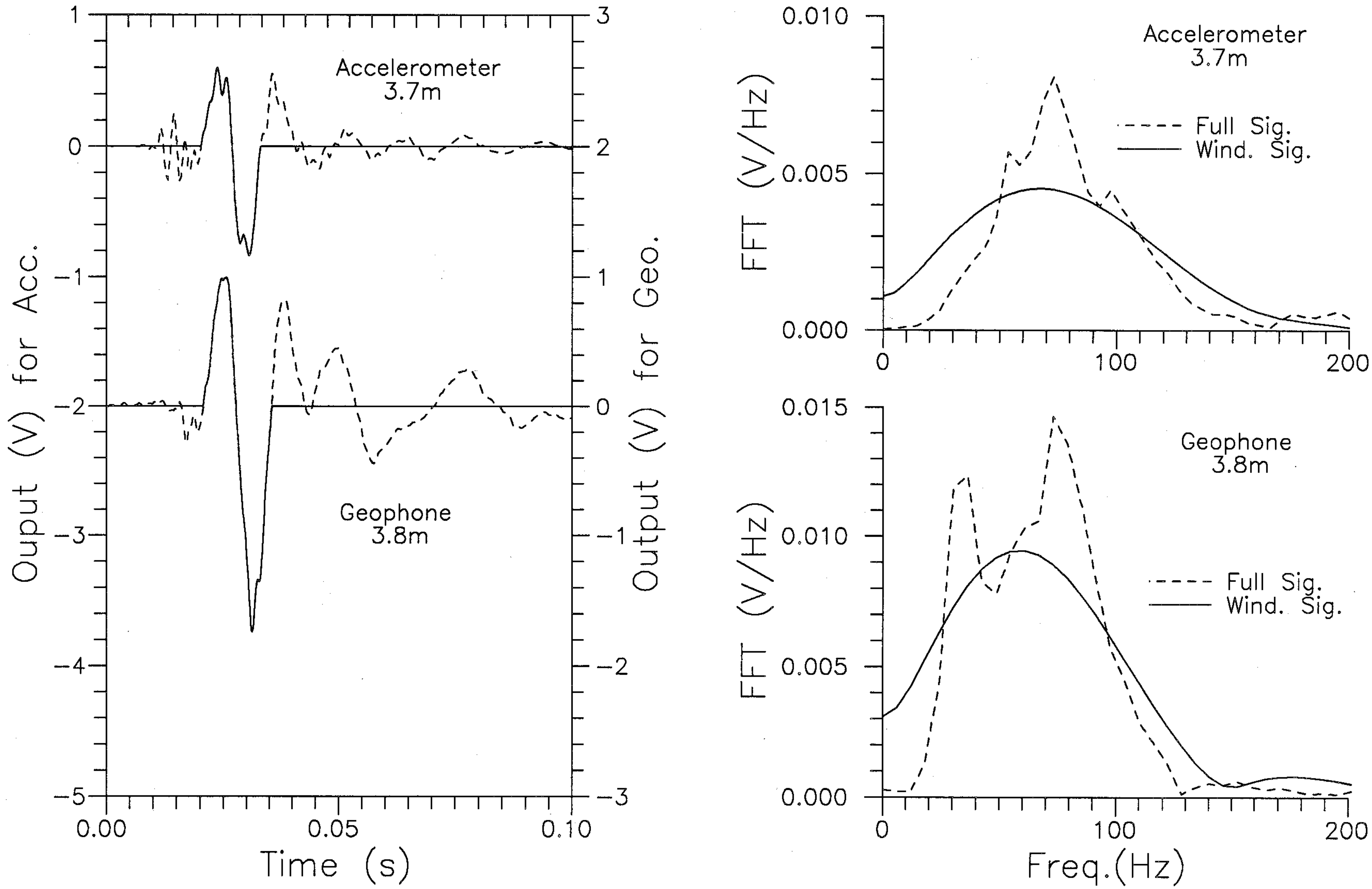


Fig.5.6 Comparison of Geophone and Accelerometer Signals

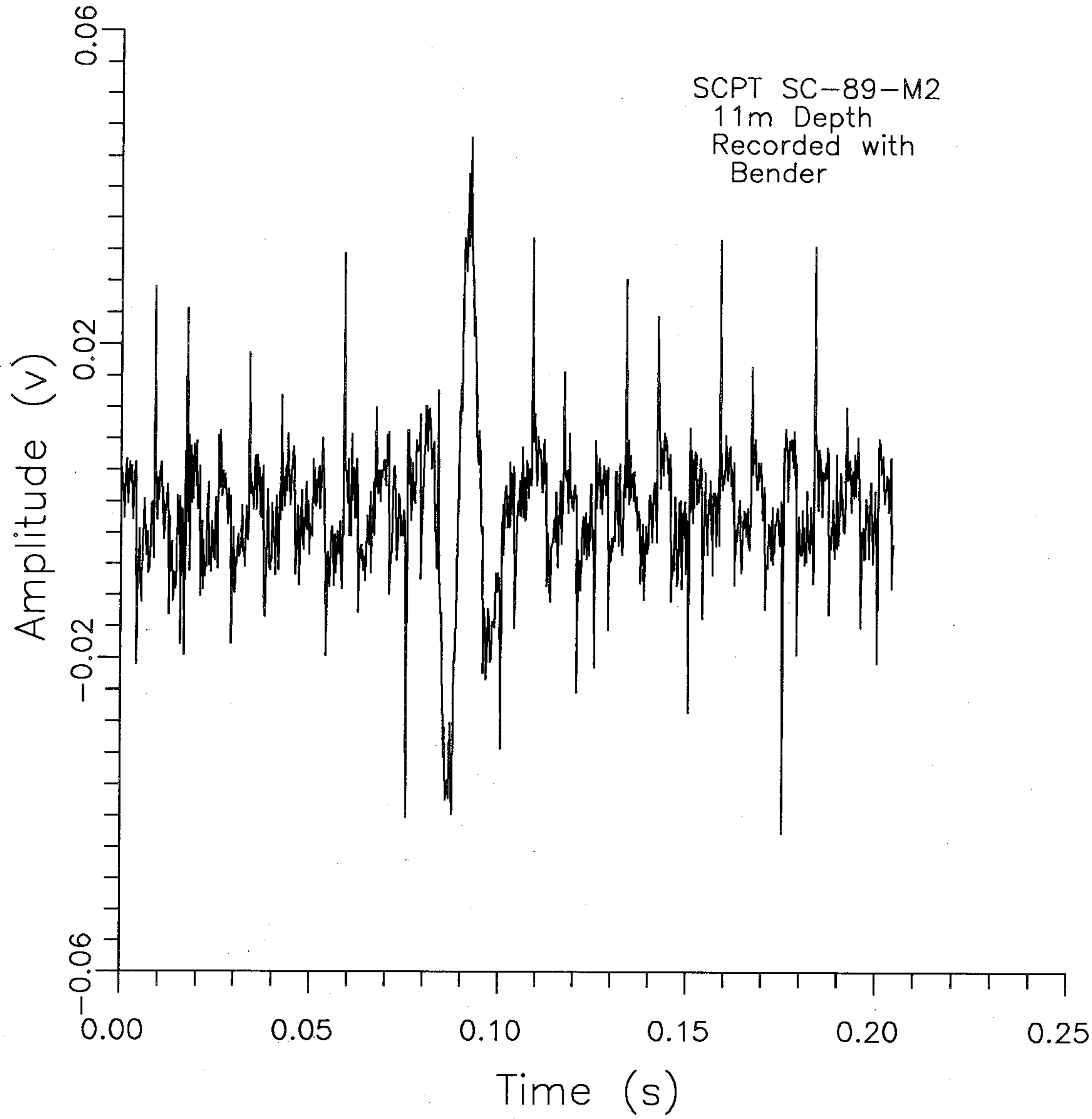


Fig.5.7 Typical SCPT Signal Recorded with Bender

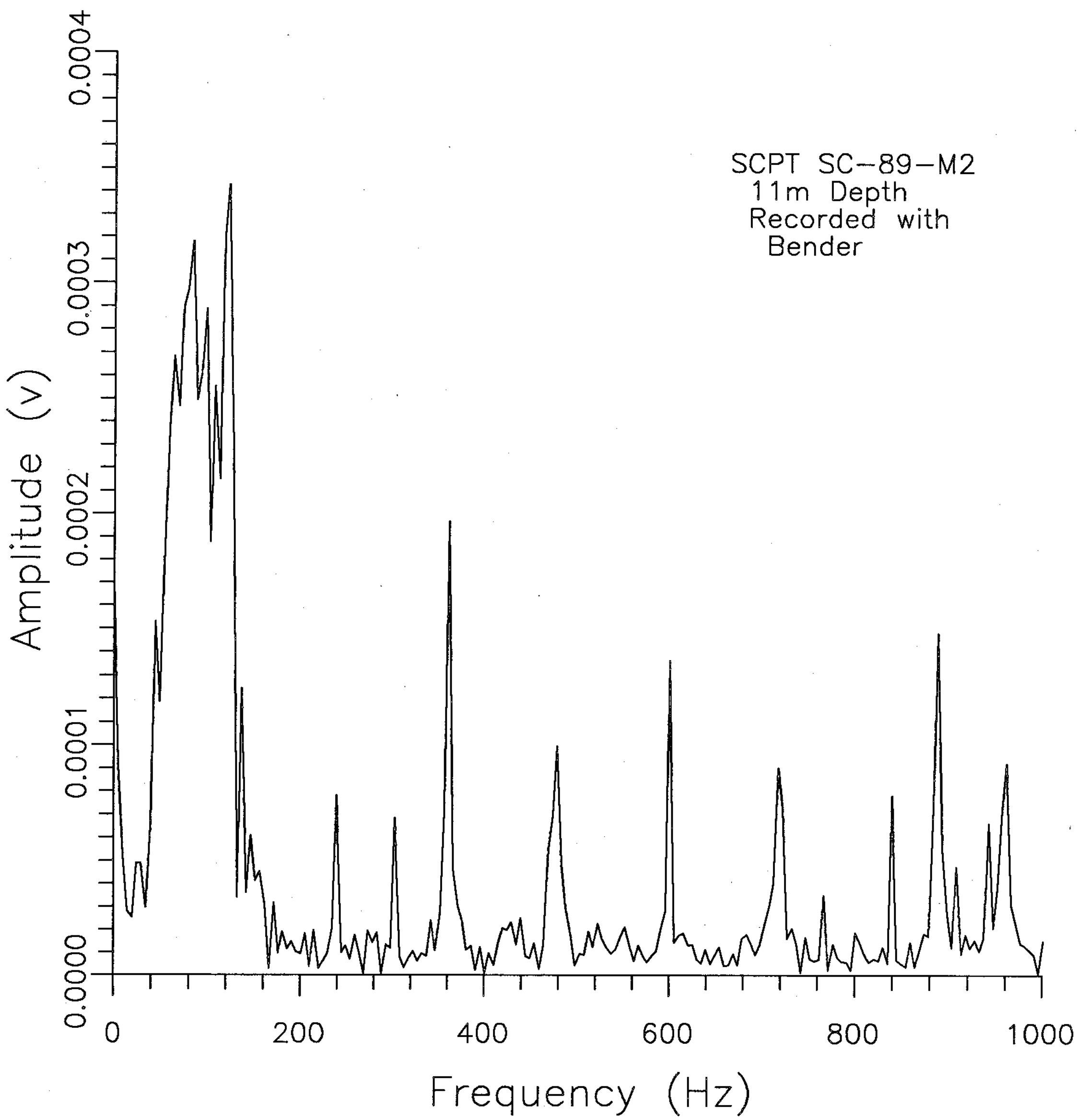


Fig.5.8 FFT of Signal Recorded with Bender

A shaker test on a bender unit is presented in Fig.5.9, which shows that there is not a flat response over the full range of the test.

### *5.4 TRIGGER AND RECORDER*

For velocity measurements that depend on separate impulses, the single most important factor is a repeatable trigger to begin the recording of signals. A variety of triggers have been studied; a receiver located in the soil near the source, an inertially activated switch also near the source and an electrical step trigger (Hoar and Stokoe,1978). For the receiver in the ground, especially a geophone, it was found that the rise time was both considerable and variable. The inertial switch itself had a small rise time but there was a longer and variable delay (0.3ms+/-0.05ms) before the oscilloscope was triggered. The delay was found to vary approximately inversely with the strength of the hammer blow.

A schematic diagram of the electrical step trigger used at UBC is shown in Fig.5.1. When the hammer makes contact with the metal pad on the shear beam, it completes an electrical circuit, allowing the discharge of a capacitor. This discharge causes the timer IC module to generate an output pulse of about 90% of the voltage source for about 2.4s duration. This duration negates the possible effects of bounces of the hammer. The rise time of the pulse is typically 100ns or 0.1$\mu$s. Once the pulse has finished, the circuit is automatically rearmed for

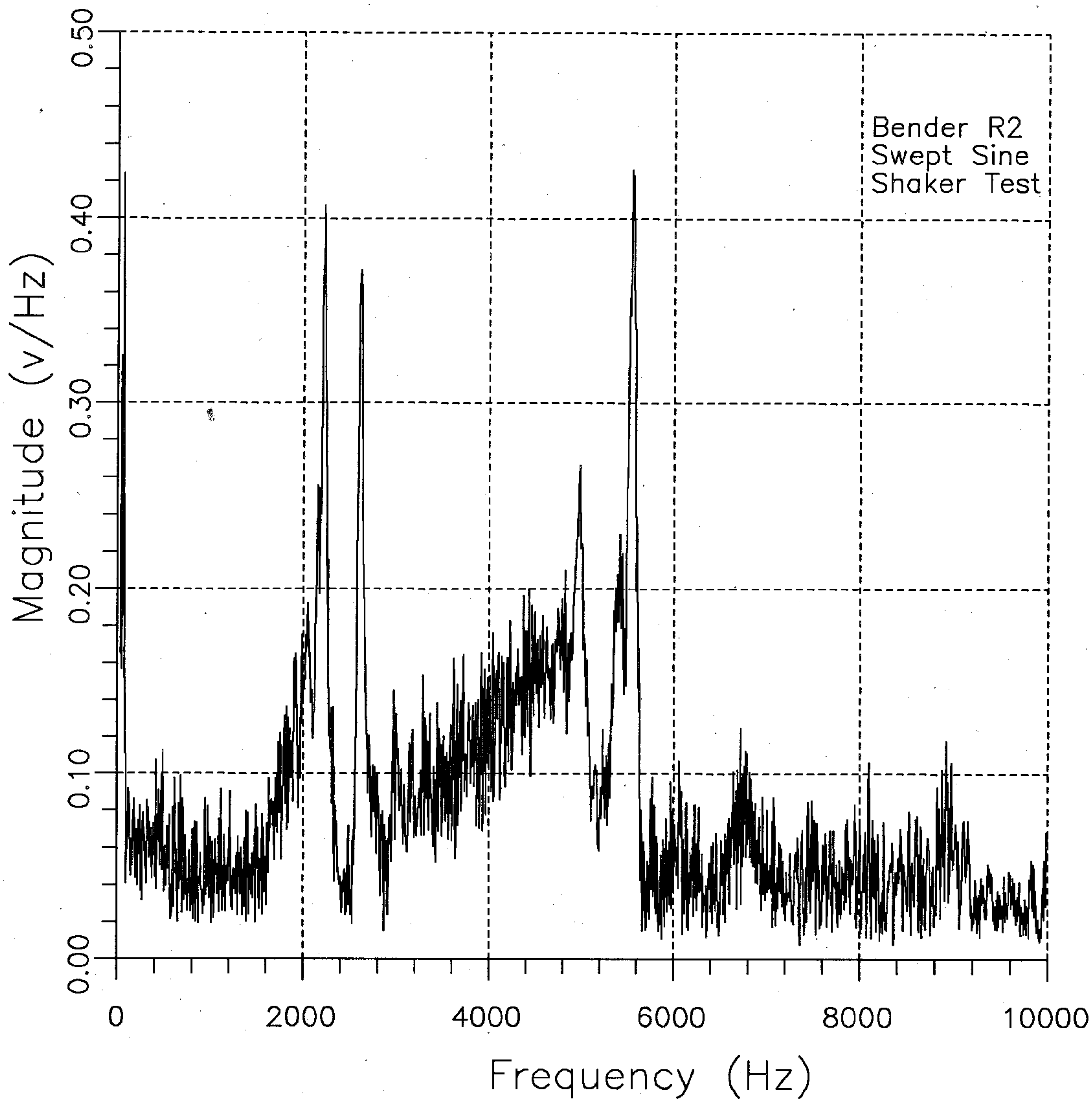


Fig.5.9 Swept Sine Test on Bender

another event. This trigger system has been used for several years with very good results. It is both repeatable and reliable.

The primary recording device used at UBC is a Nicolet 4094 digital oscilloscope with a CRT screen and floppy disk storage. The unit has a 15 bit amplitude resolution in the A/D (analogue to digital) converter and a time resolution down to $10\mu s$. This scope has been satisfactorily used for over eight years.

### *5.5 USE OF REFERENCE RECEIVERS*

It appears that most, if not all, previous investigators have used at least two receivers to measure a single waveform, in order to calculate damping. Some examples and quotations follow.

Redpath et al(1982) used a reference transducer at a depth of 20ft and a moving transducer at depths of 60 to 180ft.

Tonouchi et al (1983) stated that "The (damping factor measuring) method ...does not differ basically from ordinary PS logging. However, in order to normalize energy from the plank hammering vibration source, fixed measuring points were established at the ground surface." i.e. both a reference and moving receiver were used.

Meissner and Theilen(1986) stated that "For Q-determinations the emplacement of a reference geophone either within the same borehole or - preferably - in a secondary hole is of utmost importance...".

It appears that the idea that two receivers are necessary originated with the use of explosive sources that were not repeatable.

However the use of two receivers complicates both the installation and the measurement procedures in the field. With the simple mechanical swing hammer developed for seismic cone studies, it seemed that a highly repeatable source was available (see Fig.5.10) and that it should not be necessary to use two receivers. To confirm this hypothesis, field tests were run with two receivers, and the data was reduced two ways; firstly using the data from both receivers, and then using only data from the moving receiver.

For one of these tests (SCPT MF90SC3) a reference cone (UBC#8) was pushed to and left at a depth of 3.8m. The cable was threaded out under the truck, into the side door, and connected to one data acquisition system (DAS). The truck was driven ahead 0.25m and the moving cone (UBC#7), connected to a second DAS was pushed to the full depth of the test. Signals from both cones were recorded simultaneously. After testing it was necessary to reposition the truck back over the reference cone to remove it.

In order to evaluate the tests with one and two cones, the results were analyzed using the spectral ratio slope method. The method is based on Eqns.2.39 and 2.40, and the details are provided in section 7.2.6. The spectral ratios were computed first using the signal from the reference cone for each consecutive hit as the denominator of the ratio. Subsequently the ratios were calculated using the one signal from the moving cone recorded at the depth of the reference cone as the denominator. The results of the calculations are given in Fig.5.11.

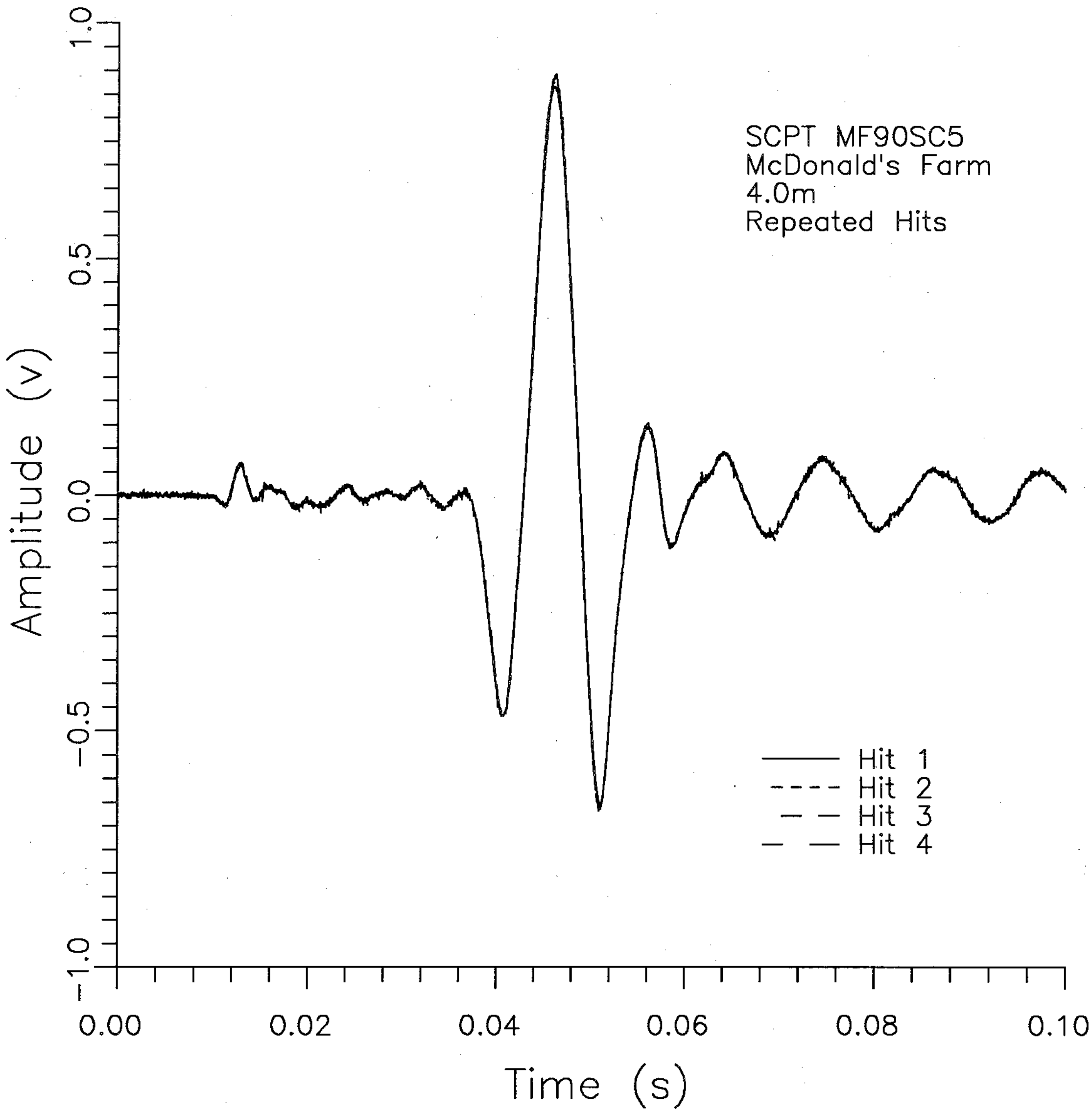


Fig.5.10 Repeatibility of Swing Hammer

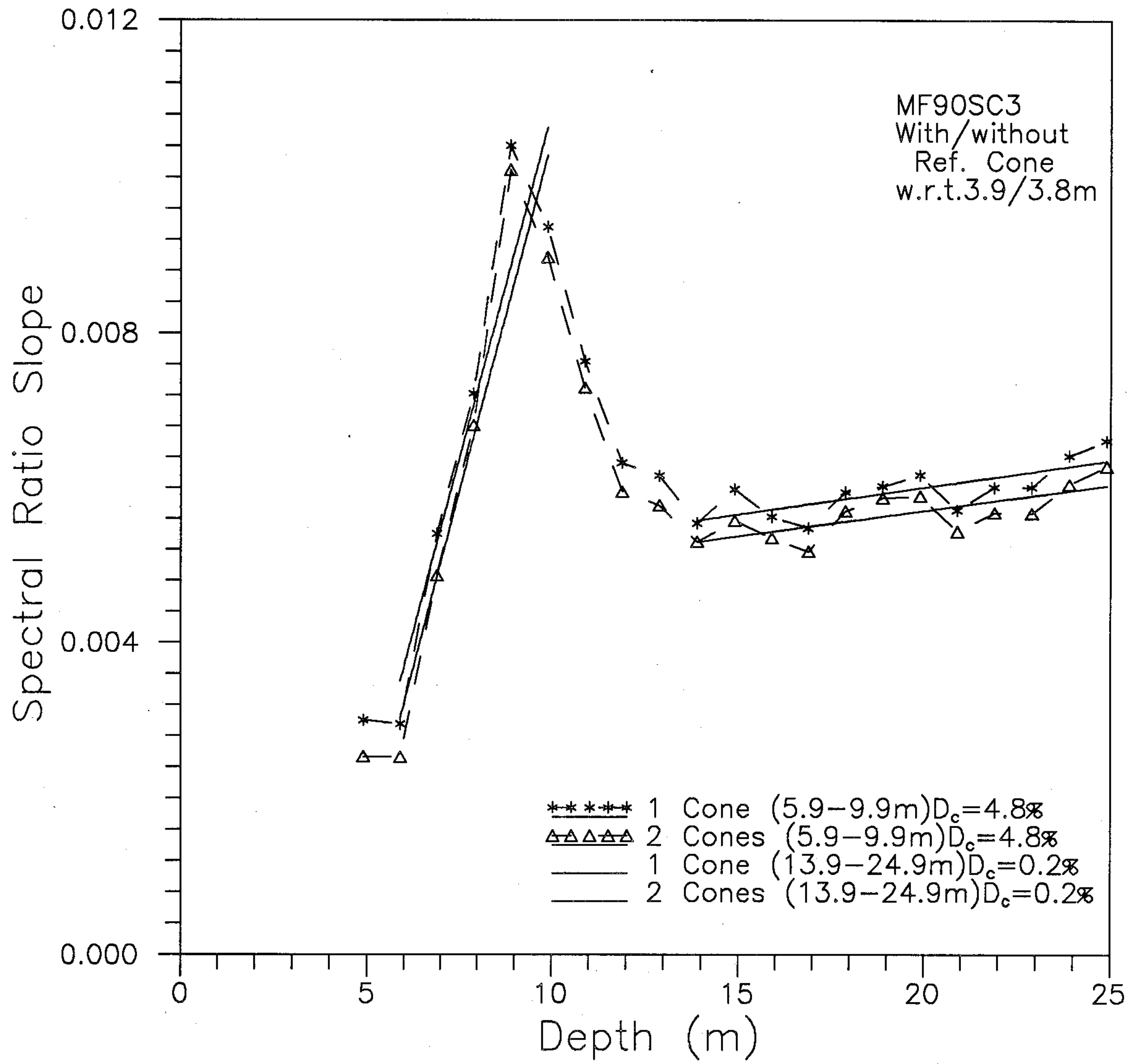


Fig.5.11 Comparison of Results With and Without Reference Cone

There is a slight offset of the two curves, but the slopes of the curves, which indicate the damping, are essentially the same.

However there appears to have been some slight noise (multiples of 60Hz) contamination in these tests, probably due to having two data acquisition systems hooked to a common power system. The computed damping values for the tests were not realistic, but it is believed that the results presented in Fig.5.11 indicate that the same results could be obtained with or without a reference cone, if the noise was not present. It is concluded, despite the comments of earlier reseachers, that with a repeatable source (and a consistent trigger) it is not necessary to use a reference receiver.

## *5.6 SEPARATION OF ACCELEROMETER SIGNALS*

### 5.6.1 Characteristics of Various Portions of Signals

In general the measured accelerometer signals can be seen as consisting of three components: (1)the underlying noise, that can be observed at the beginning and end of the signals, (2)the main shear wave pulse, and (3)a series of smaller pulses following the main pulse. The noise and the main pulse are expected in the signal, and the sources of each are easily explained. However the nature of the source or cause(s) of the smaller pulses is not clear, and the boundary between the main pulse and the smaller pulses is somewhat arbitrary. It is of interest to demonstrate the effects of the various parts of the signal on the transformation (FFT) of the signal to the frequency domain.

Fig.5.12 shows a fairly typical "clean" signal. The signal has been separated into the main shear wave (dotted line) and the balance of the signal. The FFT of the signal and its parts are shown in Fig.5.13. The full signal does show some irregularities which would affect calculations done in the frequency domain. By contrast, the FFT of the main shear wave only is smoothly changing. Most of the irregularities in the full signal appear to be caused by the balance of the signal.

The balance of the signal can be separated, somewhat arbitrarily, into the series of small pulses (dotted line) and the noise, as shown in Fig.5.14. Considering the FFT's of the balance of the signal and its parts (Fig.5.15), it can be seen that the series of small pulses constitute most of the major irregularities in the balance of the signal.

A deeper, more irregular signal is given in Fig.5.16 for comparison. It can be seen that the main shear wave is closer in size to the following pulses than in Fig.5.12. When considering the FFT's in Fig.5.17, it can be seen that the full signal is more irregular than in Fig.5.13. THe main shear wave is still smoothly varying with frequency. The balance of the signal still seems to contain the source of the irregularities in the full signal.

These examples of separating the accelerometer signals into the three component parts (main pulse, small pulses, and noise) do not

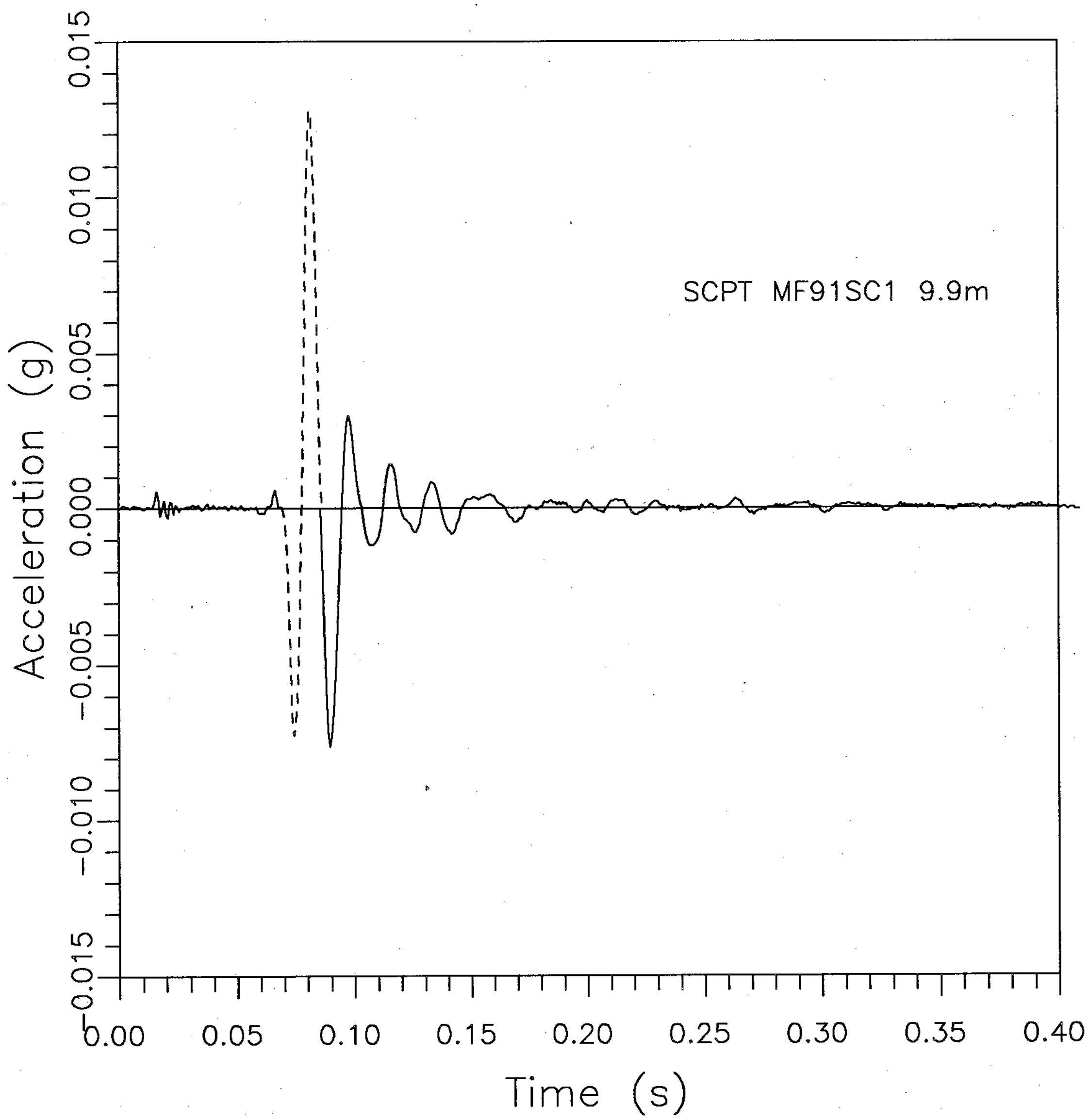


Fig.5.12 Separation of Signal into Shear Wave and Balance of Signal

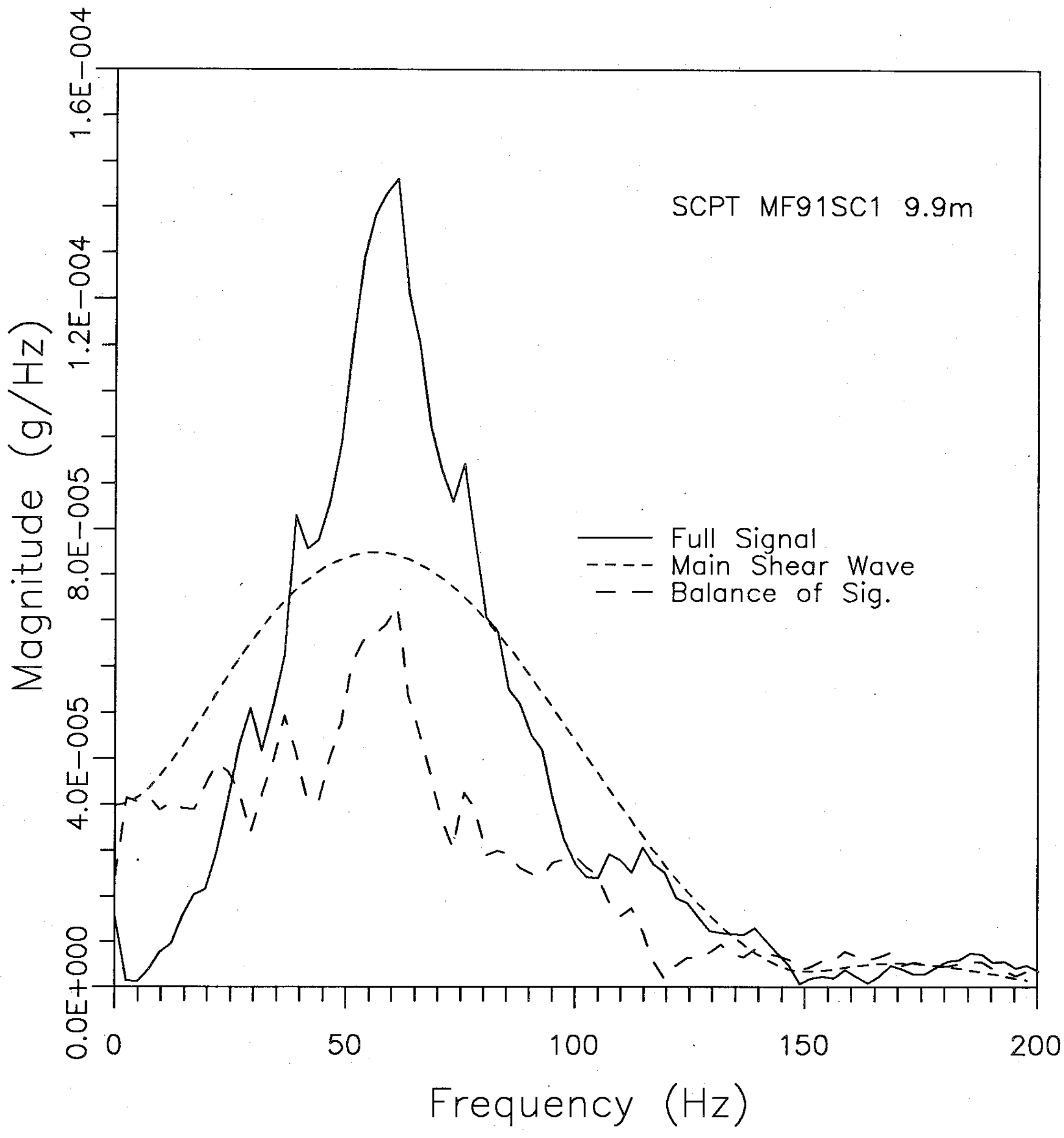


Fig.5.13 Fast Fourier Transforms (FFT's) of Wave and Balance of Signal

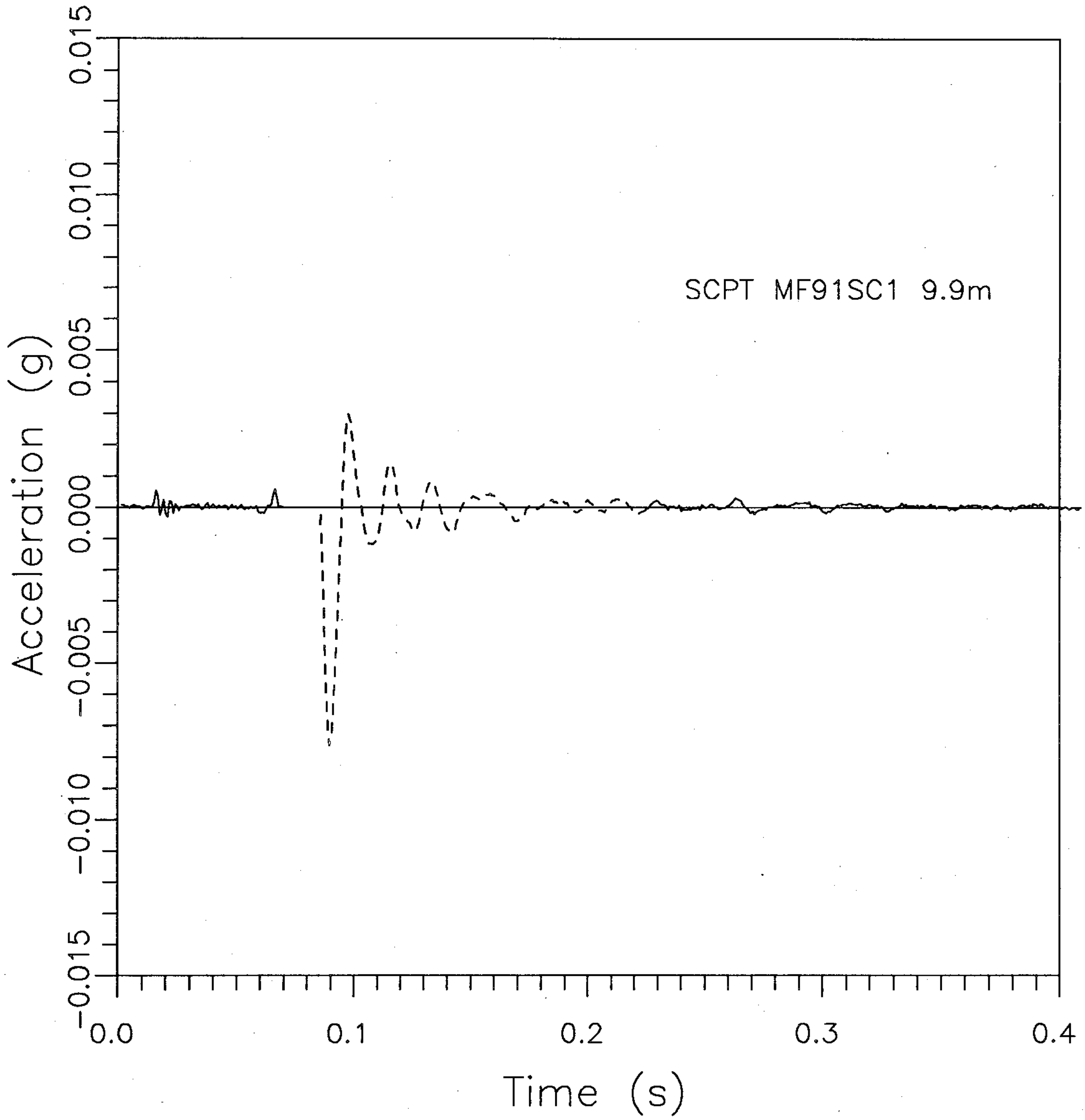


Fig.5.14 Further Separation of Signal

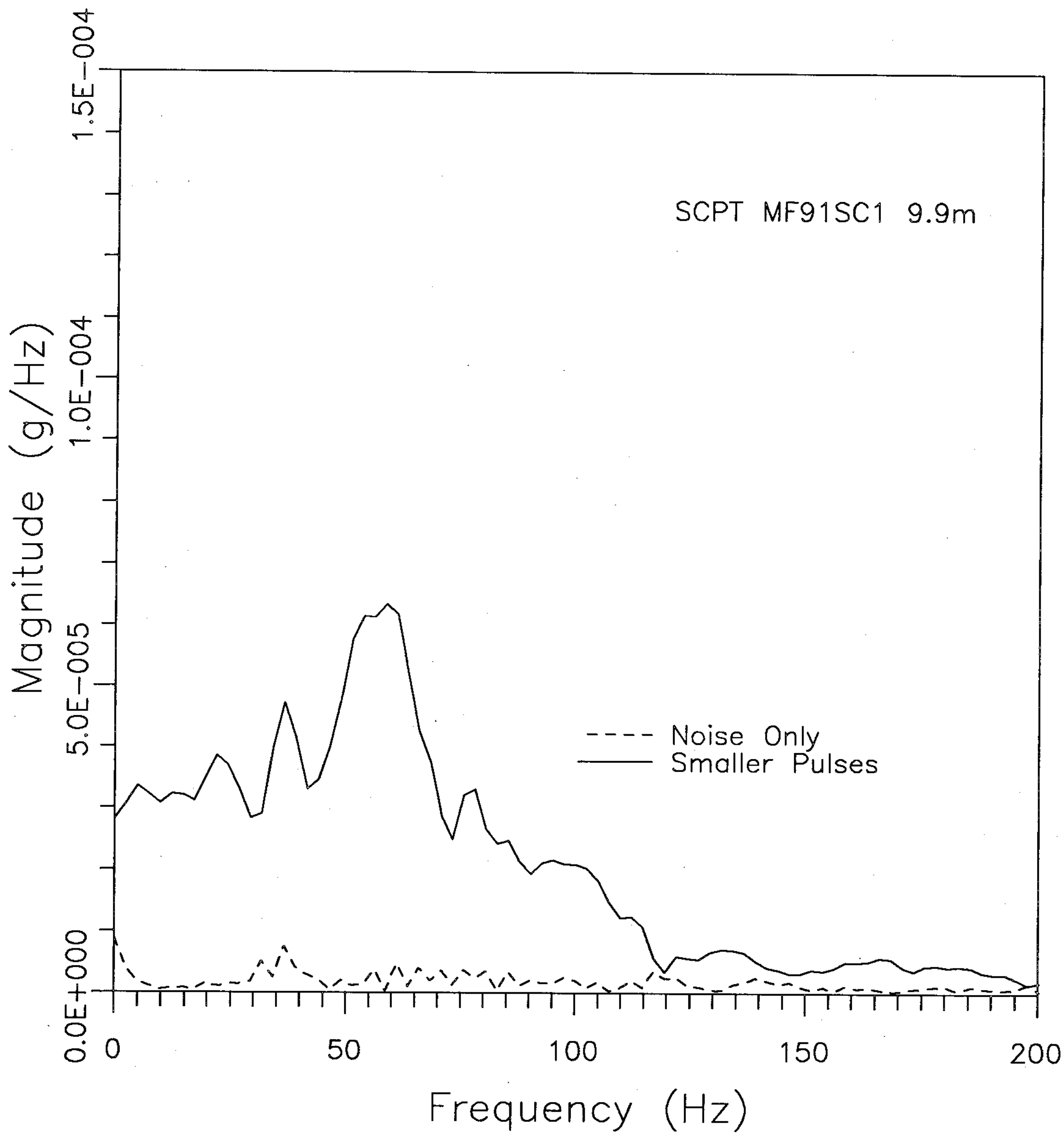


Fig.5.15 FFT's of Smaller Pulses and Noise

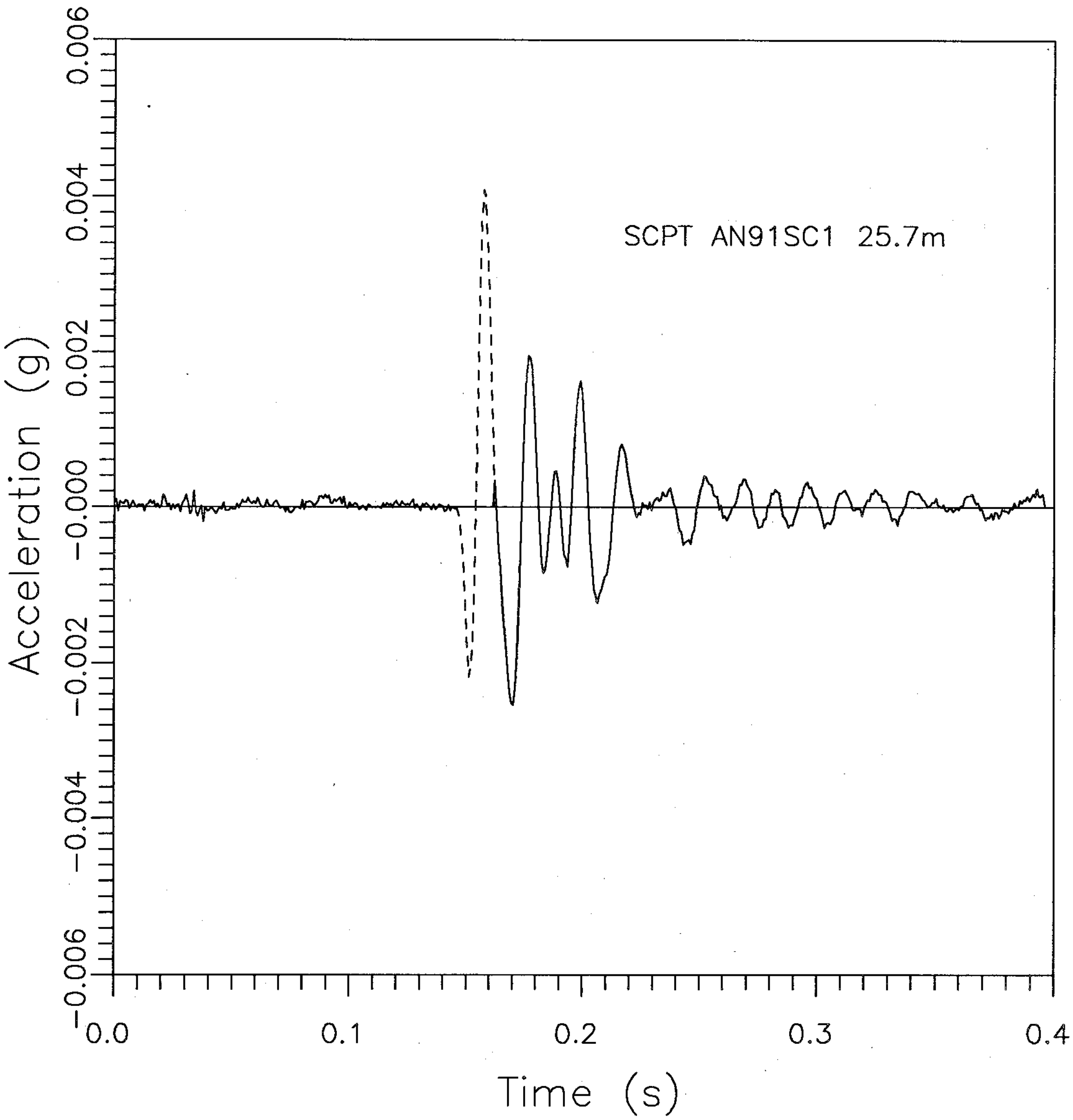


Fig.5.16 Separation of More Irregular Signal

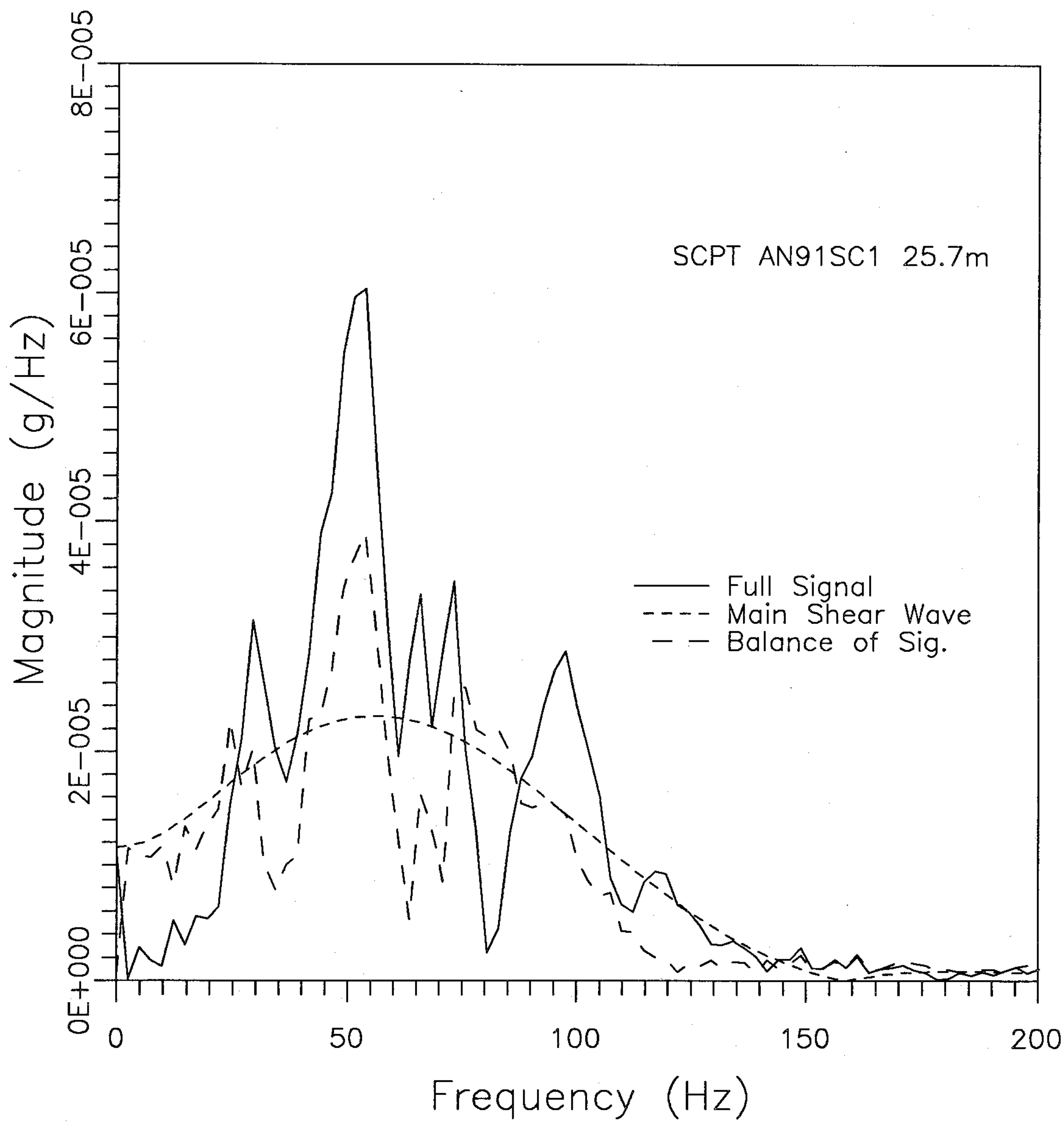


Fig.5.17 FFT's of Portions of More Irregular Signal

clarify the source or cause(s) of the small pulses. However, they do show that the main shear pulse should be isolated from the balance of the signal if "clean" FFT's are to be derived and used in further calculations.

### 5.6.2 Complex Cepstrum Method for Reflections

The previous section provided some indication of the complex nature of the complete measured signals. This complexity may be produced by the effects of many parameters including the effects of the source, material in the path of the signal, and the recording instrument. One of the simpler effects is a reflection included in the signal. The purpose of using the complex cepstrum is to separate reflections from a measured signal. This separation is done by transforming the combined signal into a signal which is a linear combination of, and which can be easily separated into, the two components. Many of the details of the method are presented in Appendix A and the reader is also referred to Ulrych(1971) and Oppenheim and Schafer(1975). Only a brief outline is presented here as the method could not be successfully applied.

In order to illustrate the method, a signal with a known reflection was created. Fig. 5.18 shoes a typical accelerometer signal from a shear beam source with the main shear wave pulse centred at about 45 milliseconds(ms). The second illustration in Fig.5.18 shows a signal, containing only the main pulse, which was formed by multiplying

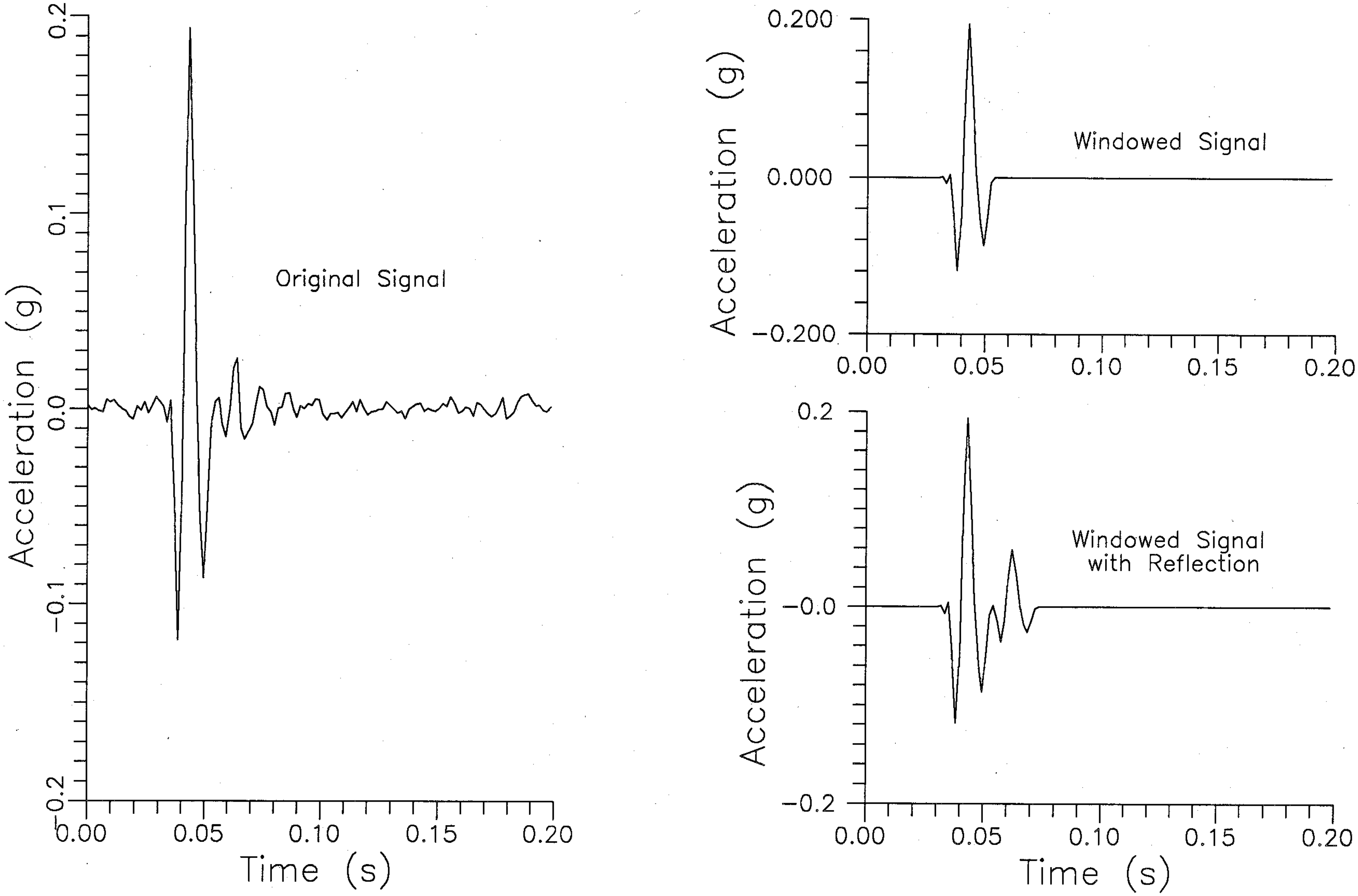


Fig.5.18 Calculation of Windowed Signal with Reflection

the full signal with a rectangular window. The windowed signal was convolved with a reflectivity series containing a spike of value 1.0 at 0.0ms to preserve the signal itself and a spike of value 0.3 at 19.2ms (nominal 20ms) to represent a reflector at a total extra distance travelled of about 3m (150m/s * 20ms). This time (distance) was selected to make the reflection clear in the signal and complex cepstrum. The third illustration in Fig.5.18 shows the result of the convolution, with the effect of the reflection to the right of the main pulse.

Calculation of the complex cepstrum involves several steps:

(1) Take FFT of signal

(2) Take natural logarithm of magnitude of FFT

(3) Unwrap phase and remove linear component

(4) Combine (2) and (3) and compute inverse FFT

At all steps it must be remembered that there are negative as well as positive values of frequency, and the magnitude is an even function, while the phase is an odd function. The complex cepstrum of the created signal with a reflection is shown at the top of Fig.5.19. Although the base units are the same as those for time, the cepstrum is usually referred to as being in the quefrency domain.

For this case the reflection is clearly obvious to the right (later time) of the main signal. If the reflection is clearly seen it can be removed by liftering (filtering in the quefrency domain), by simply using a low pass lifter (low-pass rectangular window just before

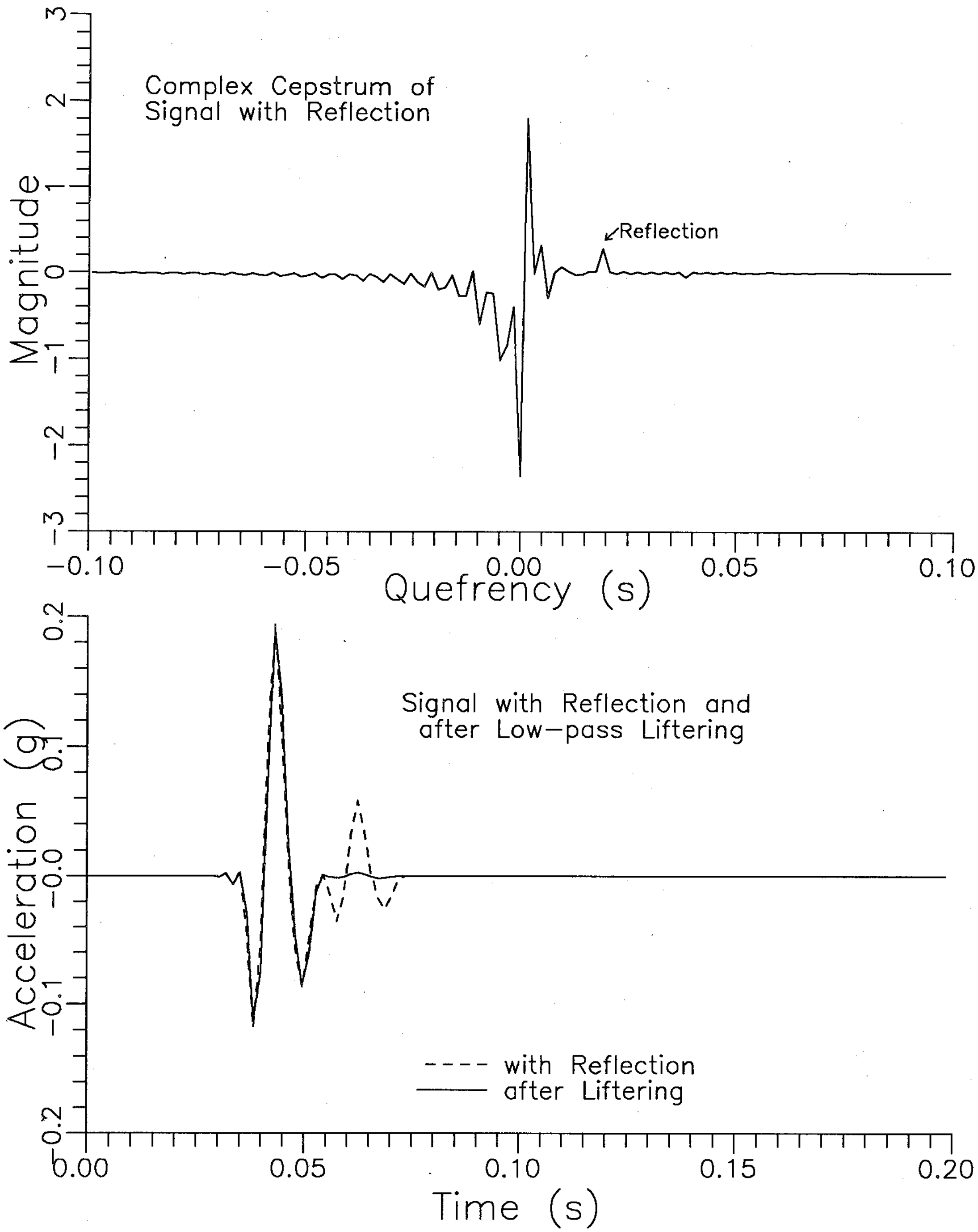


Fig.5.19 Complex Cepstrum and Inverted Signal after Liftering

the reflection). After liftering, the cepstrum must be returned to the time domain, by computing the FFT, taking the complex exponential, and computing the inverse FFT. The result is shown at the bottom of Fig.5.19, clearly showing that most of the reflection has been removed.

An example of the complex cepstrum of a measured signal from an SCPT is shown at the top of Fig.5.20. There is not a clear indication of a reflection. When this cepstrum was low-pass liftered at 9.6ms, and inverted to the time domain, the resulting signal contained additional pulses, rather than having had later pulses removed.

It is concluded that the smaller pulses following the main pulse in the accelerometer signals are not simple reflections, and thus the base signal cannot be recovered using the complex cepstrum approach.

Therefore it is necessary to assume an arbitrary cutoff to be applied to the signal for further calculations. It appears that the most practical basis is to use the first wavelength after the arrival of the shear-wave, to retain all of the frequencies in the incoming shear wave, and to exclude, as much as possible, the effects of reflections, instrument response, and other factors that may affect later portions of the signal.

## *5.7 SIGNAL PROCESSING CONSIDERATIONS*

The previous section showed that the portions of the signal other than the main shear wave strongly affect the FFT of the signal, and that these portions are not simple reflections of the shear wave that could

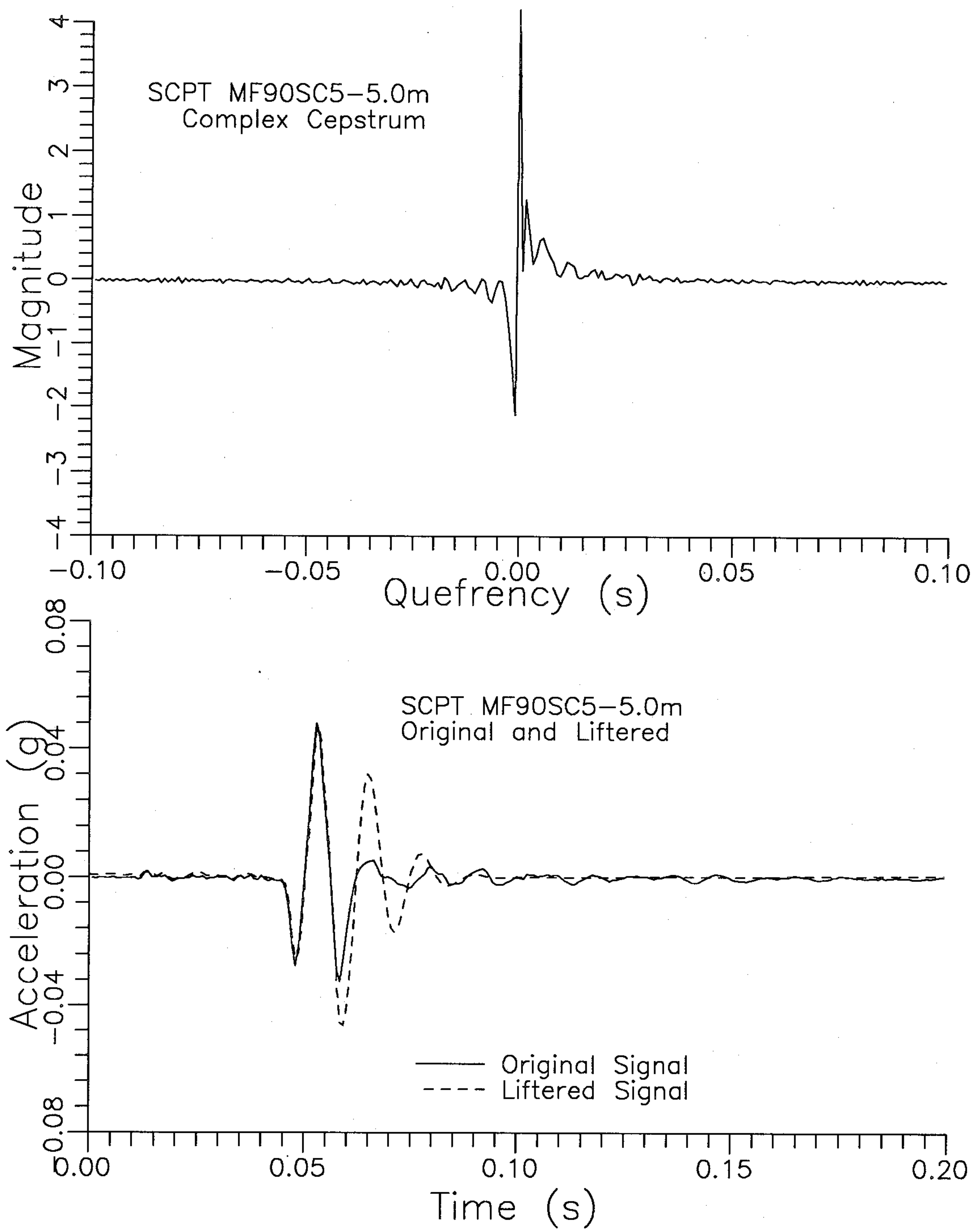


Fig.5.20 Complex Cepstrum Analysis of Measured Signal

be cleanly removed using a process such as the complex cepstrum. This section will discuss windowing to isolate the shear wave and also the coherence function.

The concept of windowing is of great importance in the spectral analysis of signals (Bath, 1974; Oppenheim et al, 1983). A window signal is formed along the same time scale as the original signal and a scale factor ranging from 0 to 1 is assigned at each time step. Windowing is simply the operation of multiplying the original signal by the window signal. The simplest window is the Uniform window, which has the value 1 at all time steps, and has no effect on the signal. A wide variety of window types; Bartlett, Hanning, Hamming, Flattop, Exponential, etc. have been developed for periodic signals. However, when applied to the full period of time measurement, these window types will distort transient signals, such as those measured for this work. It is simply desired to remove those parts of the signal that are extraneous to the measurement.

The next simplest window is a step function which has a value of 1 up to the end of the main pulse and 0 for the balance of the time period. Multiplying the original signal (Fig.21a) by this step window gives the chopped signal in Fig.5.21b. A rectangle window (see Fig.5.21d) has a value of 1 for the duration of the main pulse only and 0 before and after. Applying the rectangle window gives the windowed signal in Fig.5.21c. The FFT of a rectangle window contains side-lobes (related to Gibb's phenomenon), so that a tapered window (see Fig.5.21d)

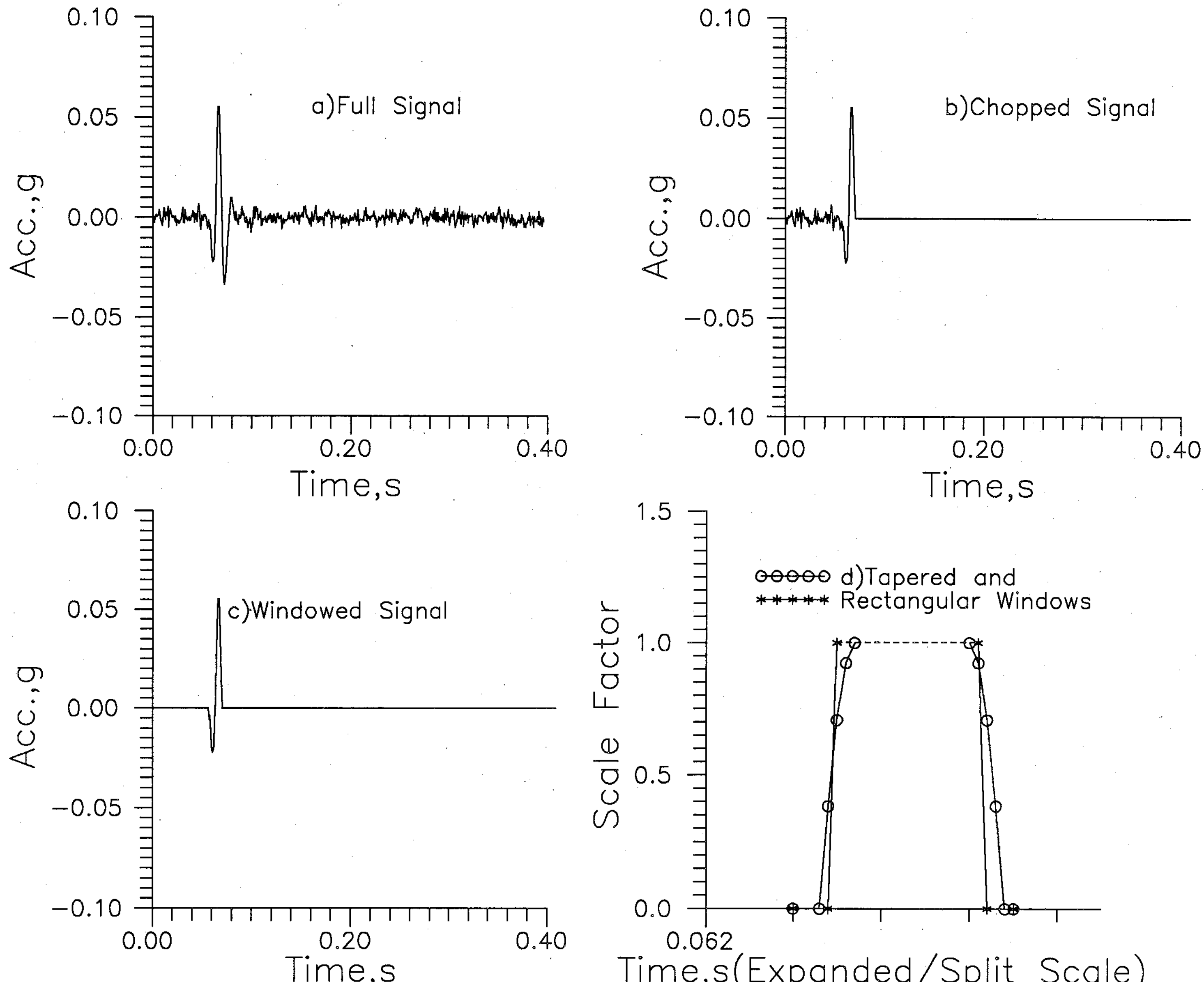

Fig.5.21 Signal Windowing (after Stewart and Campanella, 1991)

is sometimes used to reduce these possible effects. Mok et al(1988) used an "extended cosine-bell" (tapered) window for their geophone records.

For a sample signal, five different window types were considered to isolate the shear wave. Fig.5.22 shows rectangle, triangle, cosine, Hanning and Blackman windows. The latter two are raised cosine windows. In order to keep the distortion in the frequency domain to a minimum, Bath (1974) gives the following desired (but opposing) properties for the FFT of a window:

(1) A high concentration to the central (main) lobe, and

(2) Small or insignificant side-lobes

The FFT's of the windows are shown in Fig.5.23. The rectangle window best meets property 1, but has the highest side-lobes. The question remains if these are significant. The windows have been applied to a typical signal, and Fig.5.24 shows the results. The rectangle window leaves the time domain signal unchanged within the window. The other windows modify the shape of the signal, with the cosine and triangle causing the most change. Fig.5.25 presents the FFT's of the windowed signals. There does not appear to be significant differences at higher frequencies (>250Hz) at the scale shown. However if the frequency range is extended out to 500Hz to 1000Hz, and the vertical scale is expanded to show the details of the spectra in this range, the results are as shown in Fig.5.26. It can be seen that the signal multiplied by the Blackman window tends to best follow the

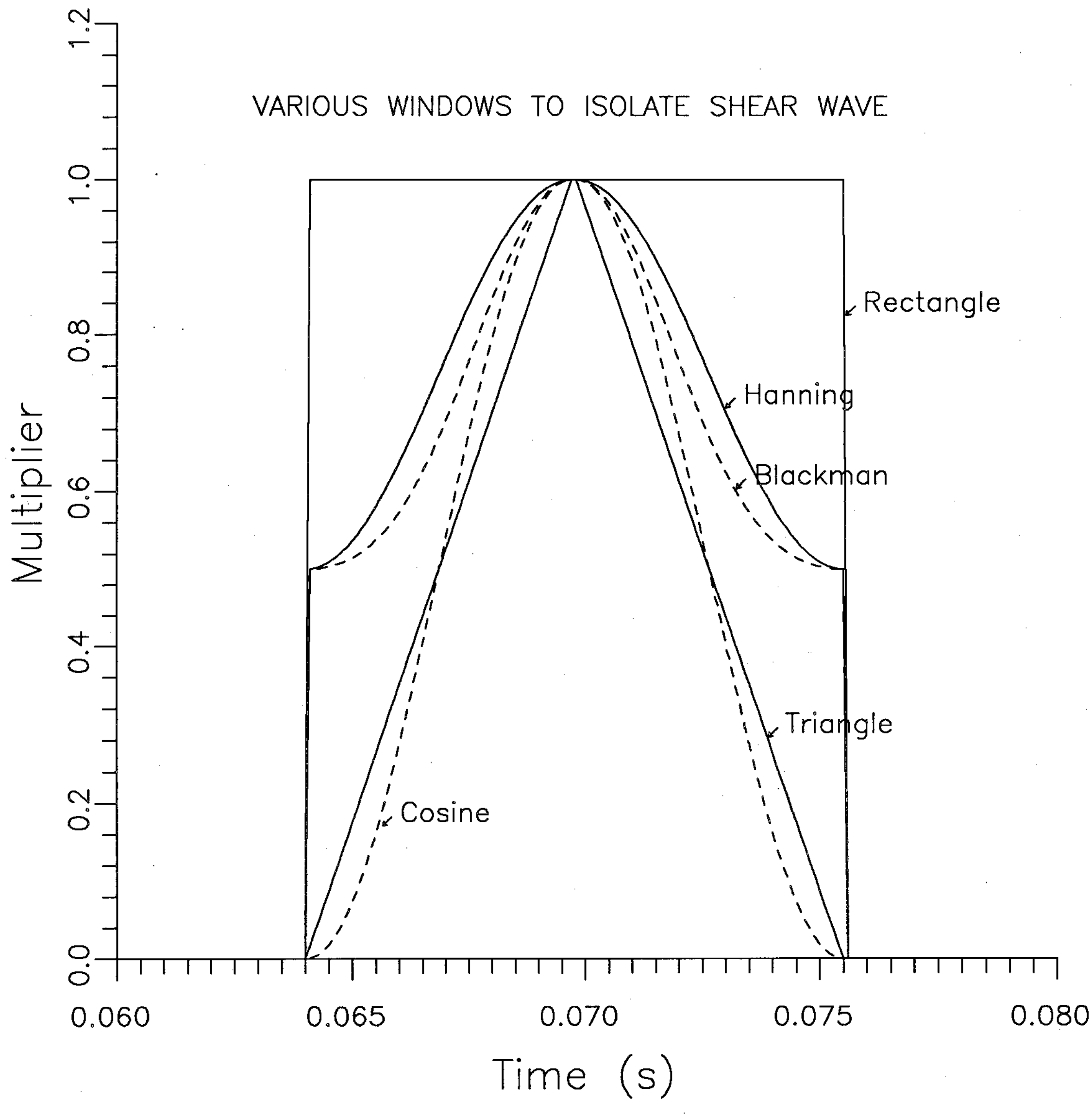


Fig.5.22 Various Windows to Isolate the Shear Wave

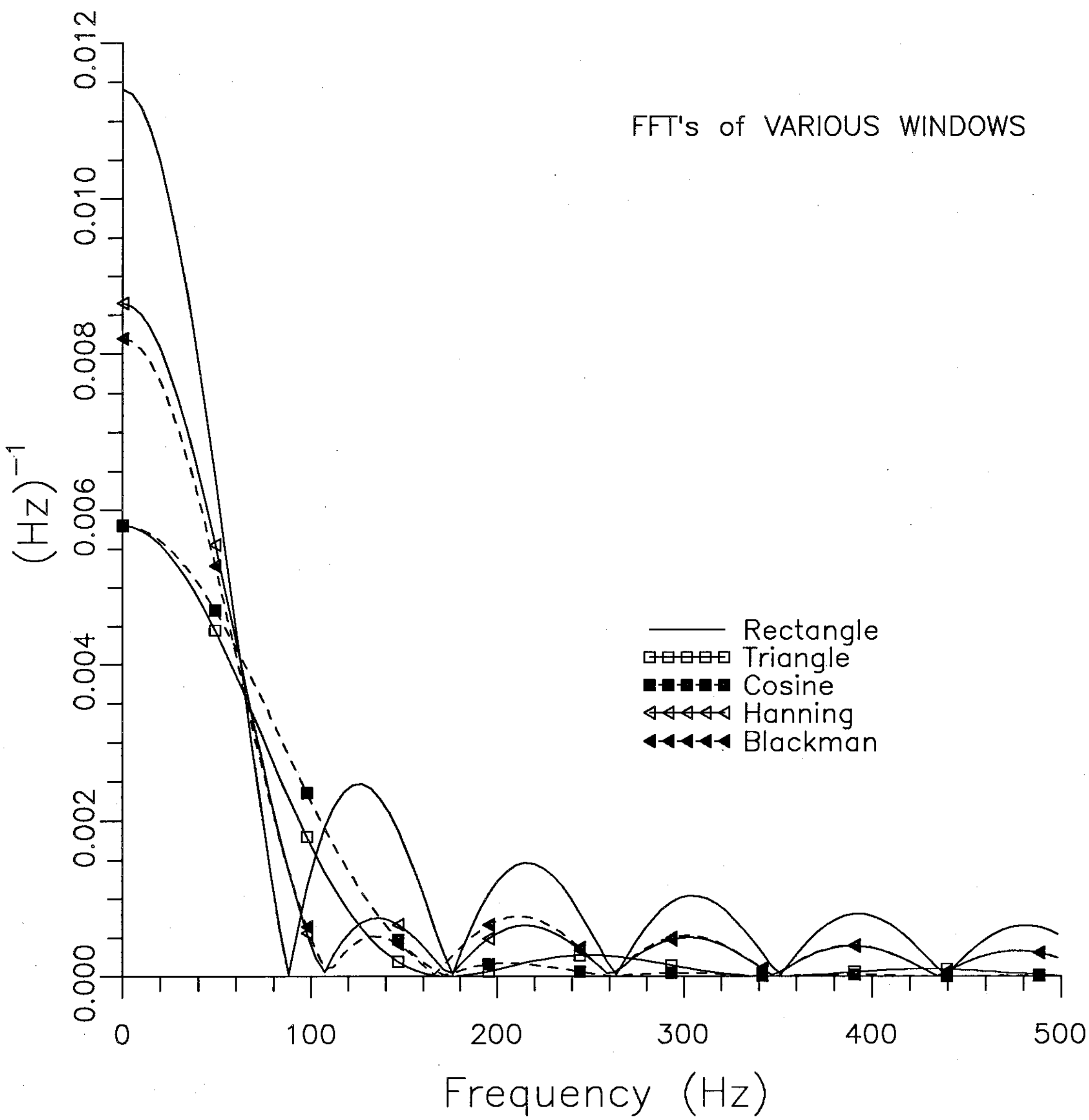


Fig.5.23 FFT's of Various Windows

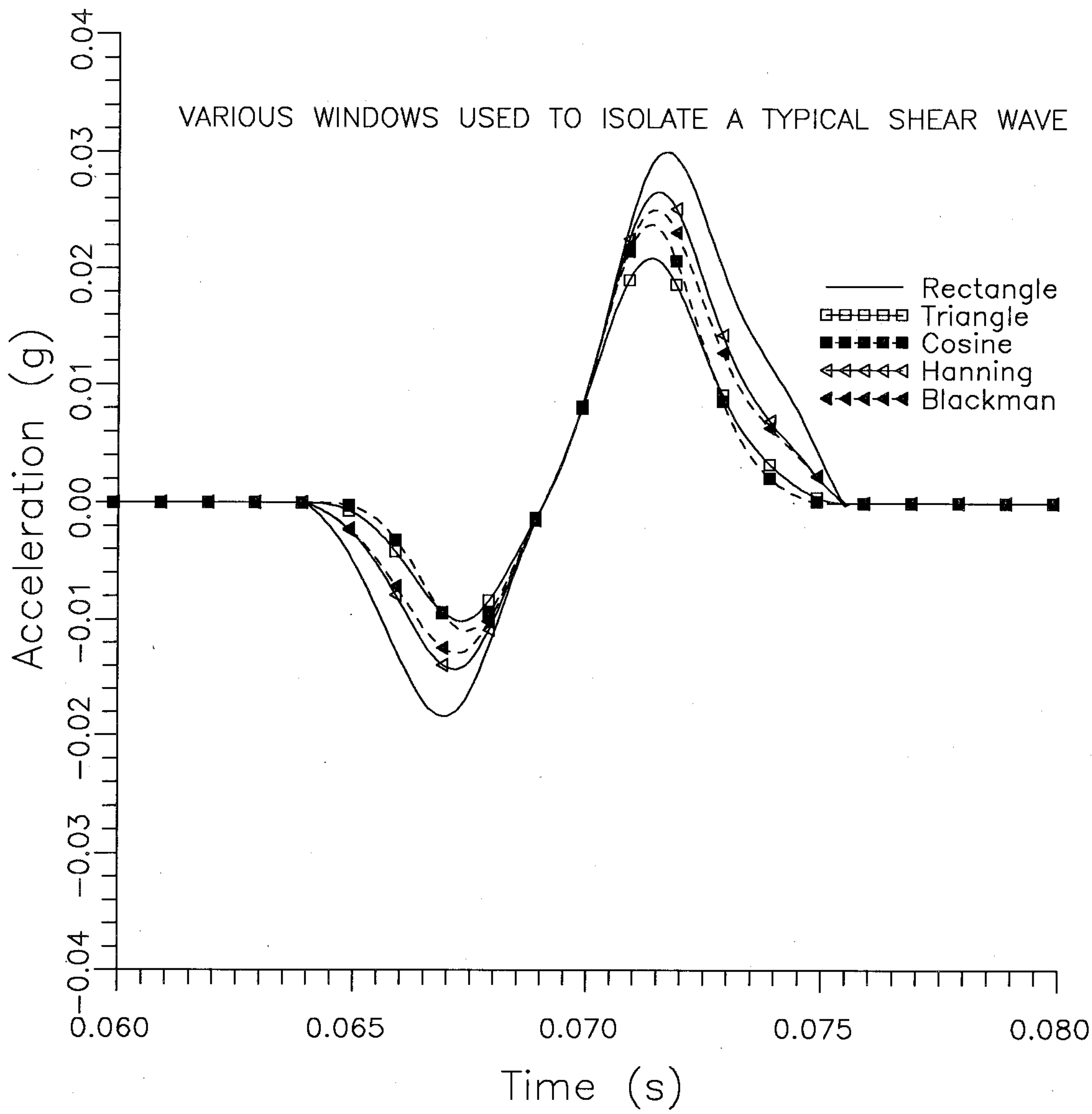


Fig.5.24 Shear Wave Forms after Windowing

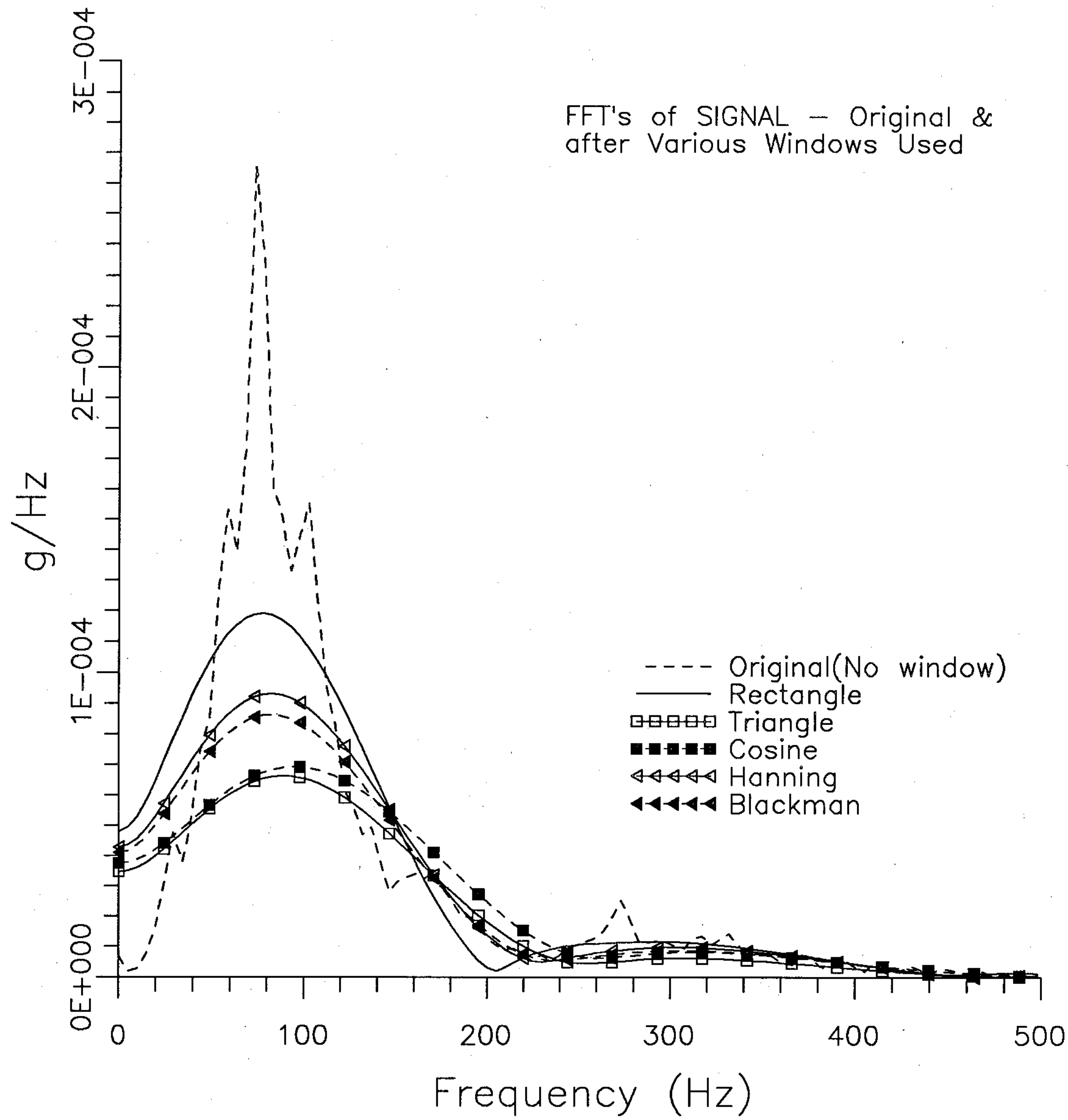


Fig.5.25 FFT's of Original and Windowed Signals (0–500Hz)

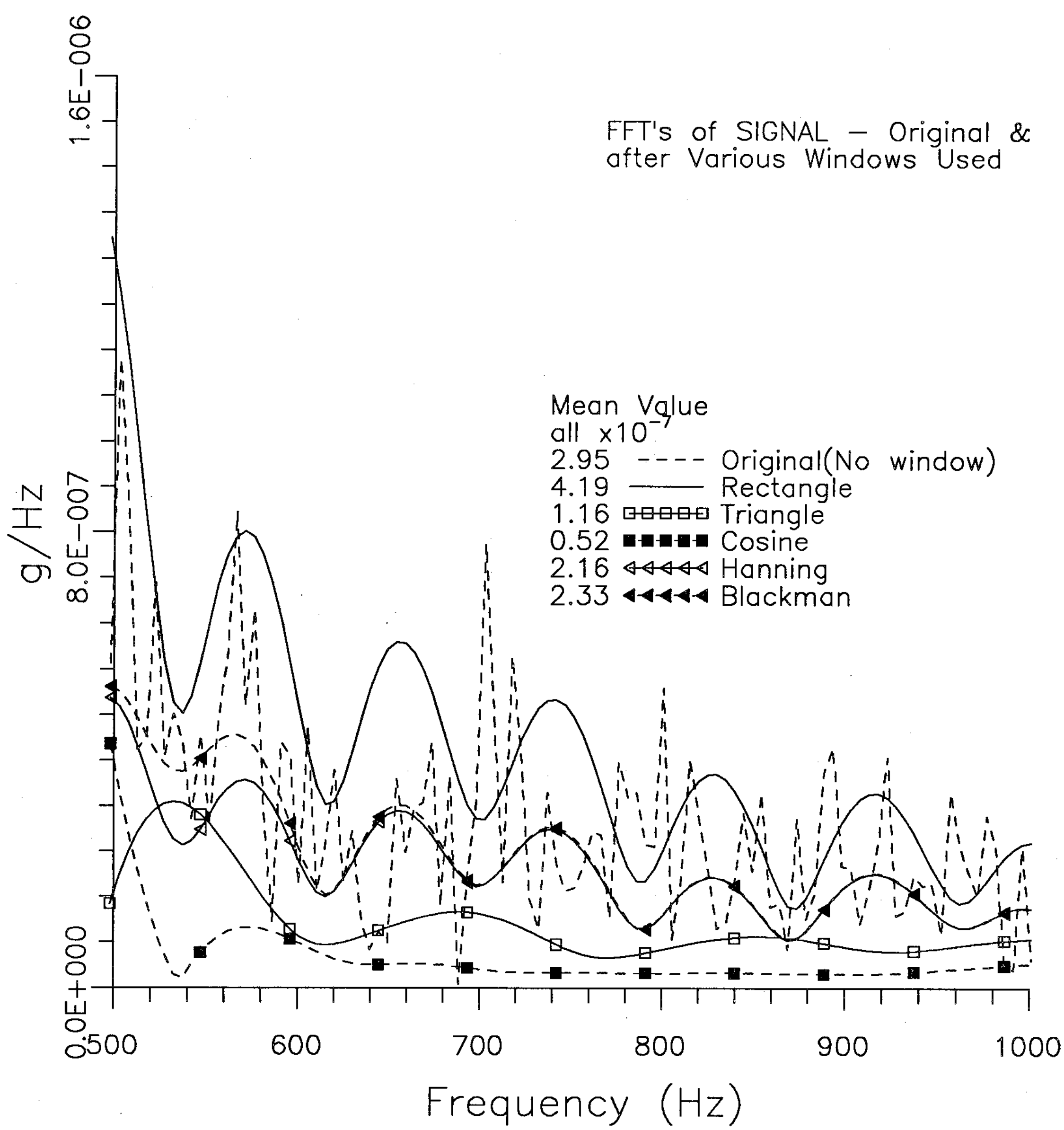


Fig.5.26 FFT's of Signals (500–1000Hz)

original signal, and thus the Blackman window may be the most appropriate for calculation in this frequency range.

However the bulk of the energy of the signals measured with the SCPT fall in a range of less than 200Hz, and the coherence (discussed below) usually drops in the 100Hz to 150Hz range. The FFT's in the 0Hz to 200Hz range are shown in Fig.5.27. It can be observed that the signal windowed with the rectangle is closest to the original (has the closest peak frequency and highest correlation with the original signal). It is concluded that the effect of the side-lobes is insignificant for our problem, and that the rectangular window is the best window to isolate the shear waves in the data in this research.

It is also necessary to determine the maximum bandwidth in the frequency domain to be used for further calculations. One method of determining a suitable bandwidth is to use the coherence function. Use of this method requires repeated hits at the same depth. Typically four hits at each depth have been used. The coherence function is defined as:

$$\text{[5.2]} \qquad Coh = \frac{G_{yx}\, G_{yx}^{*}}{G_{xx}\, G_{yy}}$$

where: $G_{yx}$ = Average of Cross-Correlation Spectra

$G_{yx}^{*}$ = Complex Conjugate of $G_{yx}$

$G_{xx}$ = Average of Autocorrelations of Upper Signal

$G_{yy}$ = Average of Autocorrelations of Lower Signal

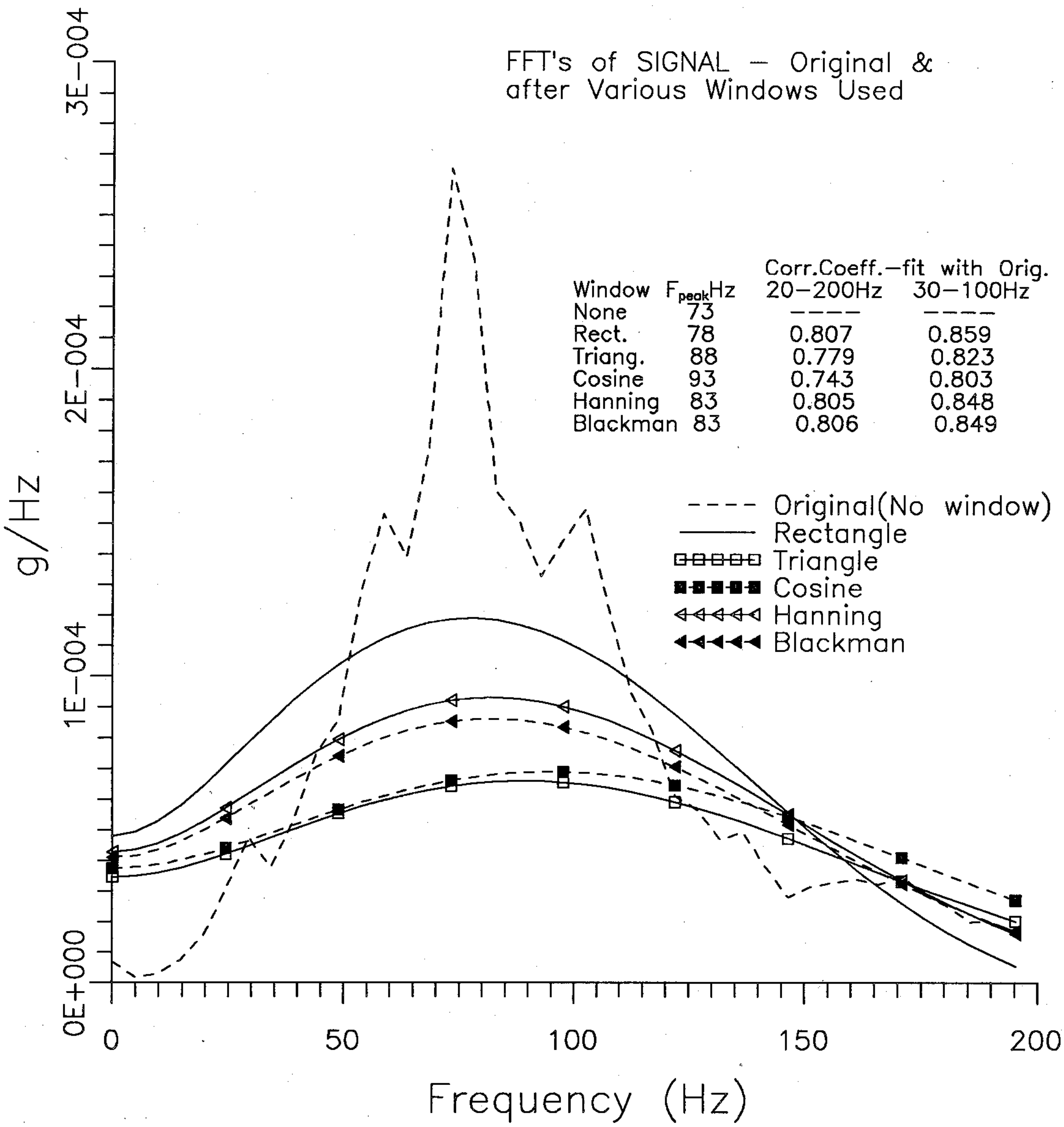


Fig.5.27 FFT's of Signals (0—200Hz)

Using the averages of several signals, it can be shown (Hewlett Packard, 1985) that the coherence can be expressed as:

$$[5.3] \quad Coh = \frac{|H|^2 G_{xx}}{|H|^2 G_{xx} + S_n^2}$$

where: $|H|$ = Magnitude of transfer function

$S_n$ = Average of noise spectra

Thus the coherence will be high at those frequencies where the effect of noise is minor, and it will be low where the noise dominates the signals.

Typical plots of the coherence function are shown in Fig.5.28. For the signals at shallow depth (5 to 6m), the coherence is very high (essentially 1.0) from about 30 Hz to 150 Hz. For the signals at greatest depth, the coherence is reasonably high (0.98 or greater) from about 40Hz to 105Hz. The choice of an acceptable coherence level will depend on the quality of the signals recorded. Generally a value of 0.95 or greater has been achieved over a reasonably wide bandwidth. The bandwidth given by the coherence function is the maximum that can be used for further calculations, and a narrower bandwidth may be required depending on the specific calculations to be done.

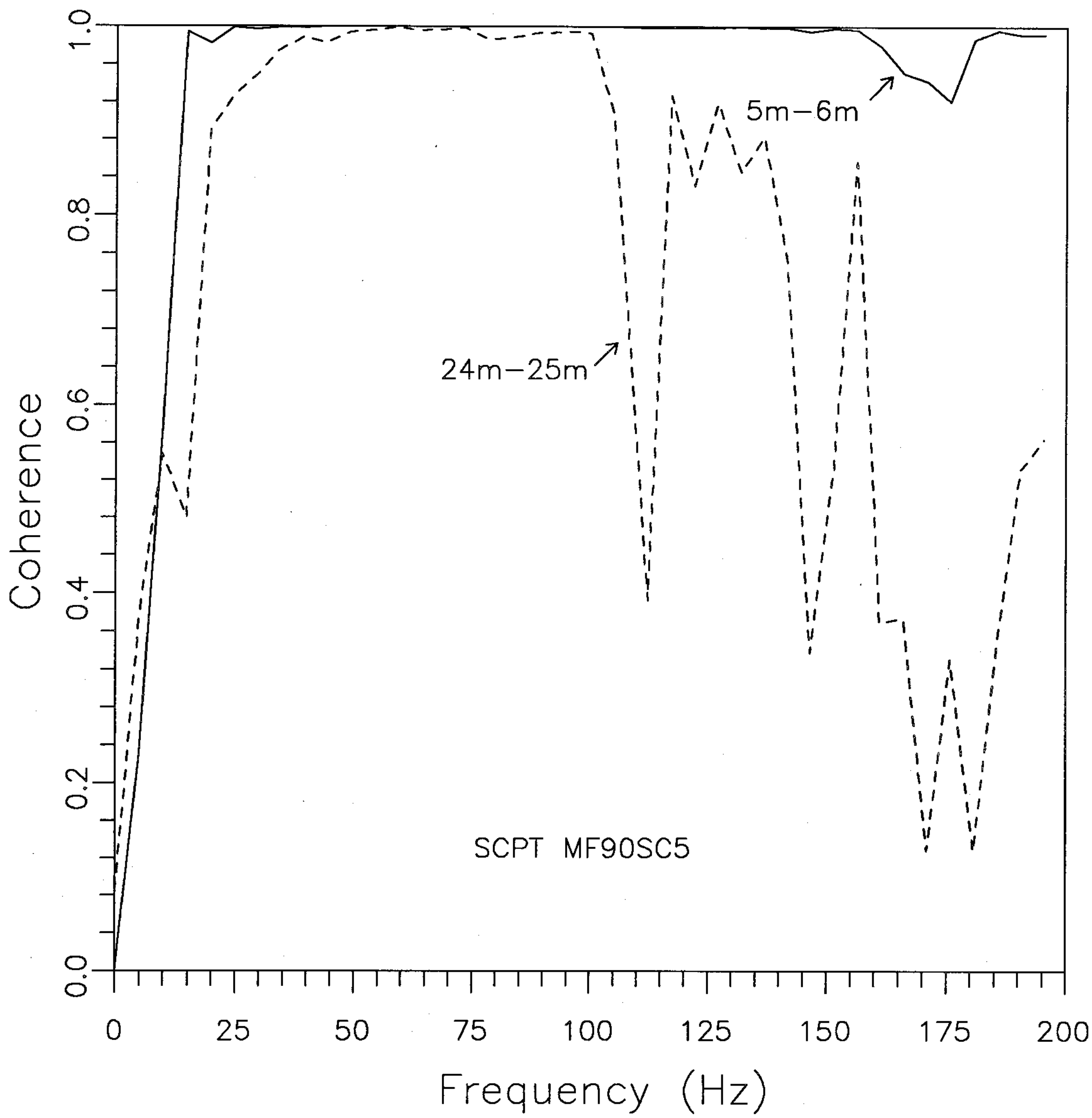


Fig.5.28 Coherence Function (after Stewart and and Campanella, 1991)

### *5.8 FREQUENCY CHARACTERISTICS OF MEASURED SIGNALS*

Investigations at four sites have allowed general observations on the frequency characteristics of the signals measured. The majority of these measurements used a shear beam source (and an accelerometer receiver), but results with other sources will be discussed.

Fig.5.29 shows the FFT's (fast Fourier transforms) for 8 signals recorded at increasing 1m depths from 2.7m to 9.7m, in a predominantly clay layer. The signals have been windowed to isolate the first shear wave. Except for 2.7m depth (which may include some surface effects), the peaks show a very gradual decrease in frequency (about 61Hz) with depth, and the FFT's have similar shapes. The frequency at the peak decreases to about 54Hz at 20m. Section 5.6.1 showed that windowing of the signals is required to obtain "clean" FFT's for analysis, but windowing of the signals tends to smooth the FFT's and a more complete visual comparison is provided if the full signals are used.

Fig.5.30 shows the FFT's of the same set of signals used in Fig.5.29 without windowing. Again the FFT's are of similar shape, with two peaks separated by a trough at about 75Hz. The frequency at the trough is similar down to 20m. Similar results for a predominantly sand site are shown in Fig.5.31. The FFT's at this site are again very similar with a single peak with a slowly decreasing frequency - about 75Hz down to about 70Hz. However the frequency at the peak does not decrease with further depth down to 20m. For the FFT's of the full signals, it appears that the predominant frequency is similar for both

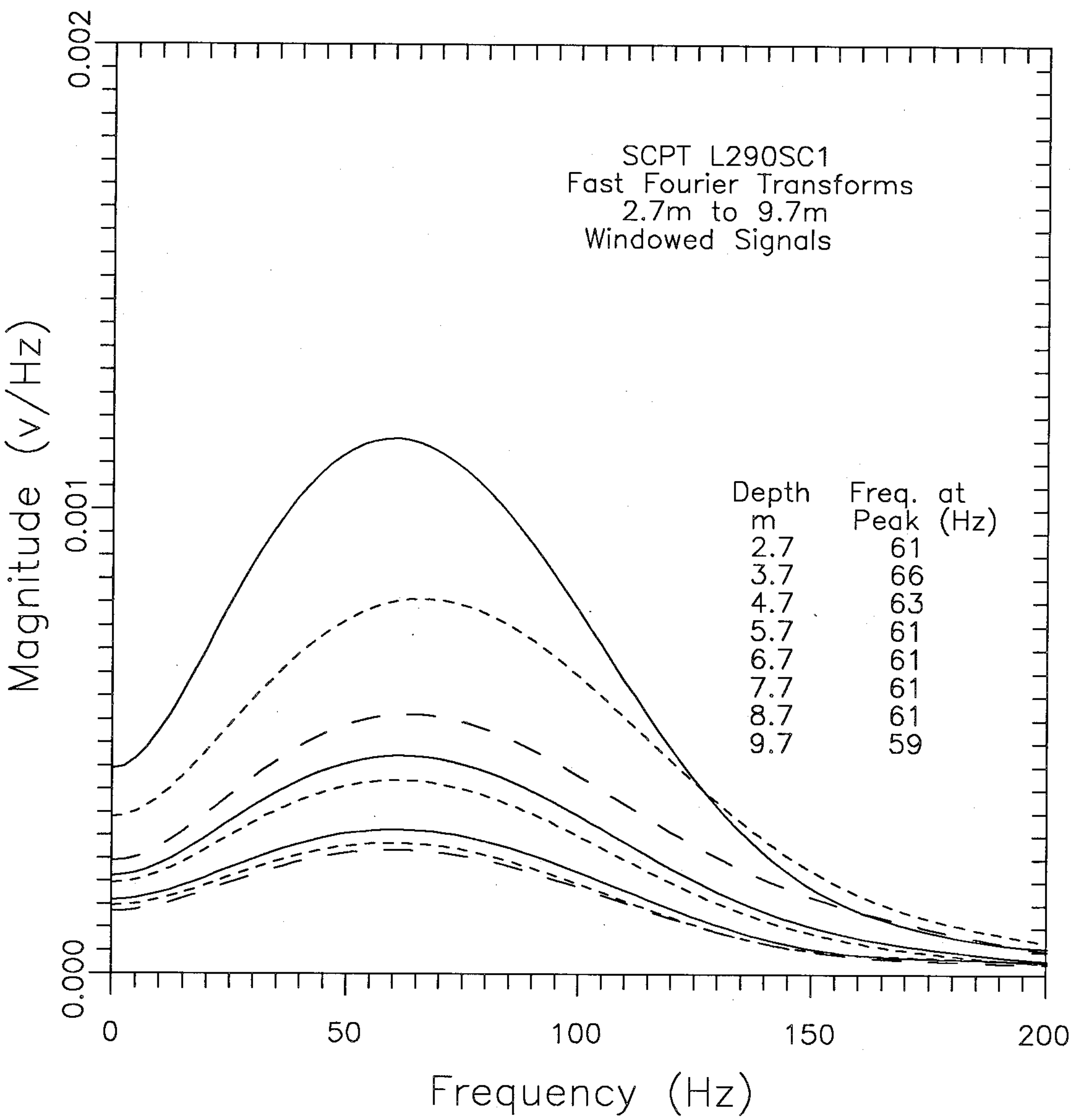


Fig.5.29 Variations in FFT Spectra with Depth for Windowed Signals in Clayey Soil

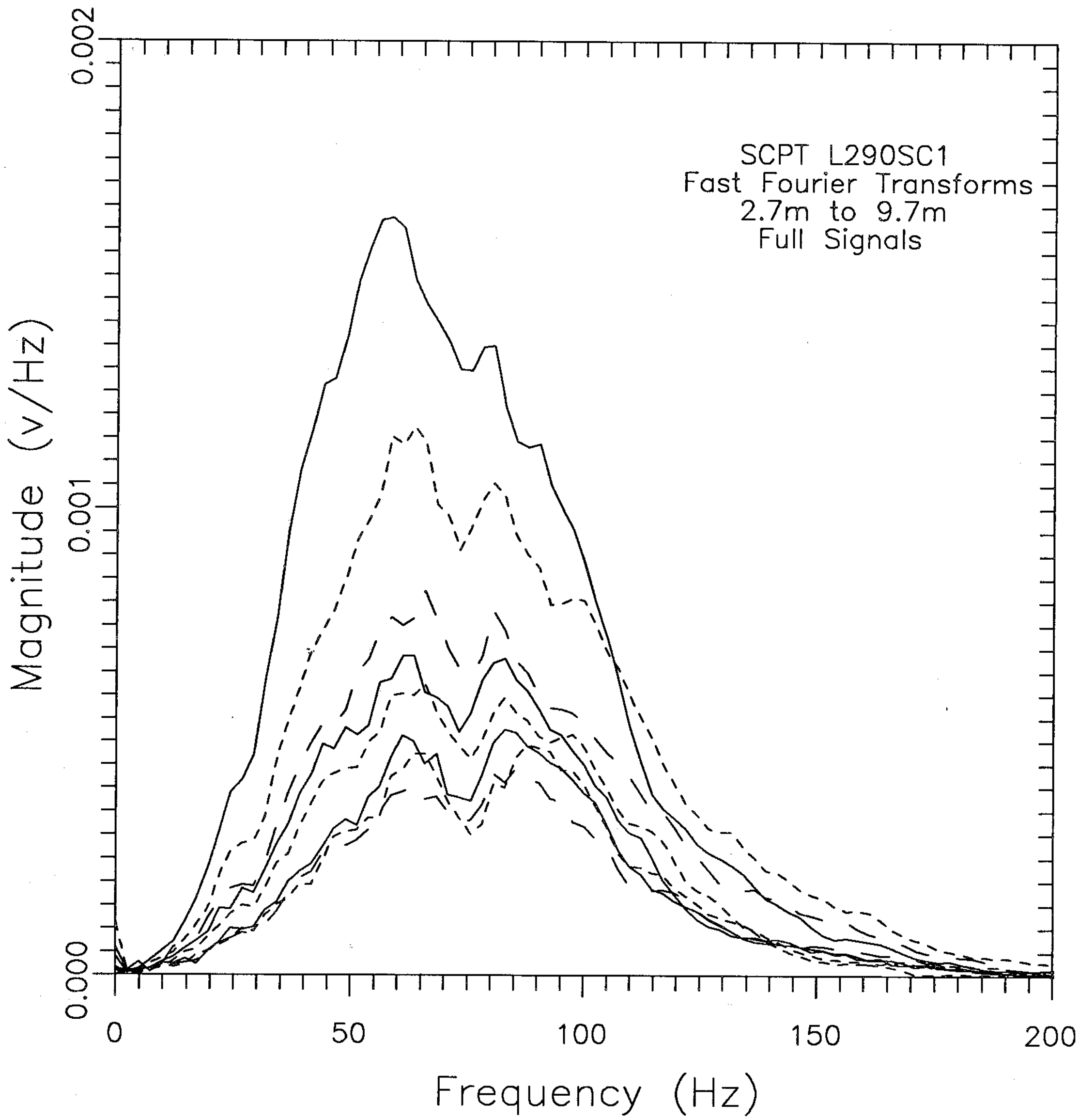


Fig.5.30 Variations in FFT Spectra with Depth for Full Signals in Clayey Soil (after Campanella and Stewart, 1990)

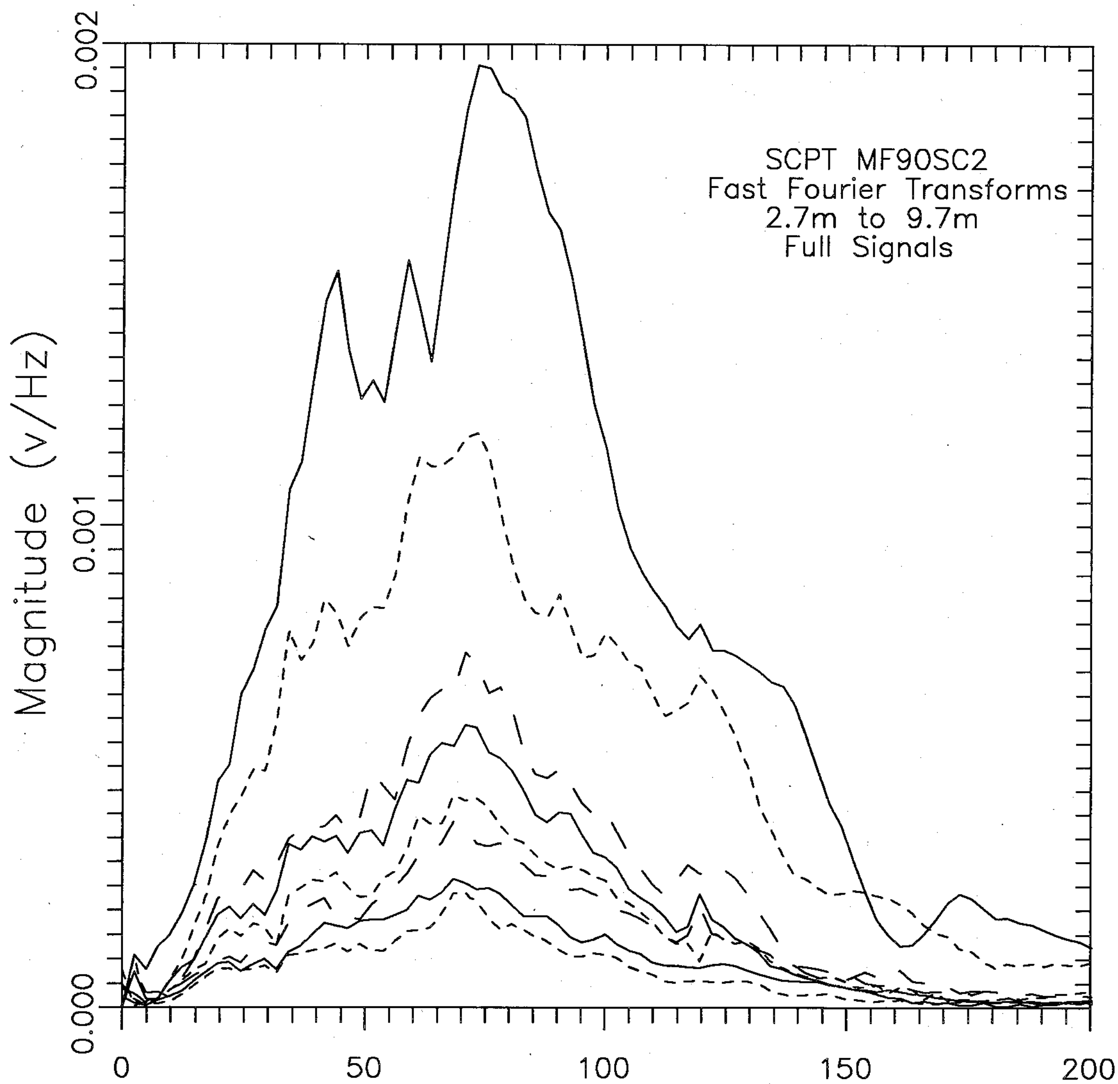


Fig.5.31 Variations in FFT Spectra with Depth for Full Signals in Sandy Soil (after Campanella and Stewart, 1990)

sand and clay sites, and that there is little reduction of the predominant frequency with depth to at least 20m.

It is of interest to review the frequency content of signals resulting from other sources. However, it is important to note that the sensitivity of the accelerometer receiver used drops off rapidly beyond 550Hz. Campanella et al (1989) reported P-wave frequencies of about 800-900Hz measured using a bender, and these frequencies would not be measured with the present accelerometer.

The buffalo gun was described in Section 5.2, and a typical signal is shown in Fig.5.32. A plot of the FFT's for signals at 1m increasing depths from 3.7m to 10.7m is provided in Fig.5.33. It is clear that the buffalo gun is not a repeatable source, as the magnitudes show a poor relationship with depth. The energy varies over a frequency range of about 30-170Hz as measured with the present system.

A 1.33kN drop weight source was also described in Section 5.2. A plot of FFT's with increasing depth recorded using the drop weight system is shown in Fig.5.34. It was observed that the drop weight source was more repeatable than the buffalo gun, but showed more scatter than the shear beam source. The frequency at the peak was generally around 45Hz, but with considerable energy in the range of 20Hz-95Hz. In another test a variety of pads were used between the drop weight and the base plate on the ground. Pads used for the drop weight testing included plywood (19mm), hard rubber belting (15mm) and soft silicone rubber (7mm). FFT's of the signals measured at one depth with the

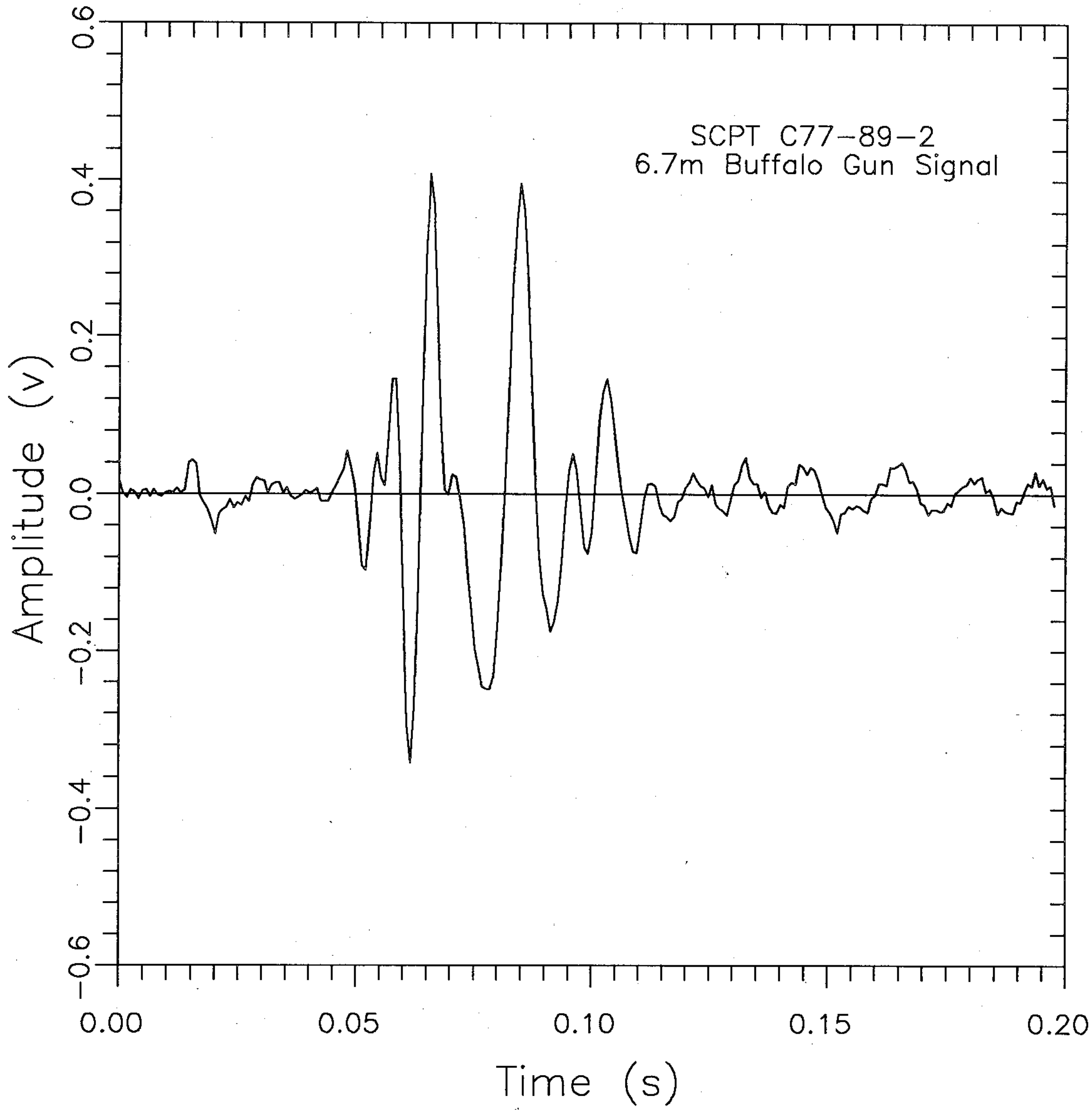


Fig.5.32 Typical Buffalo Gun Signal

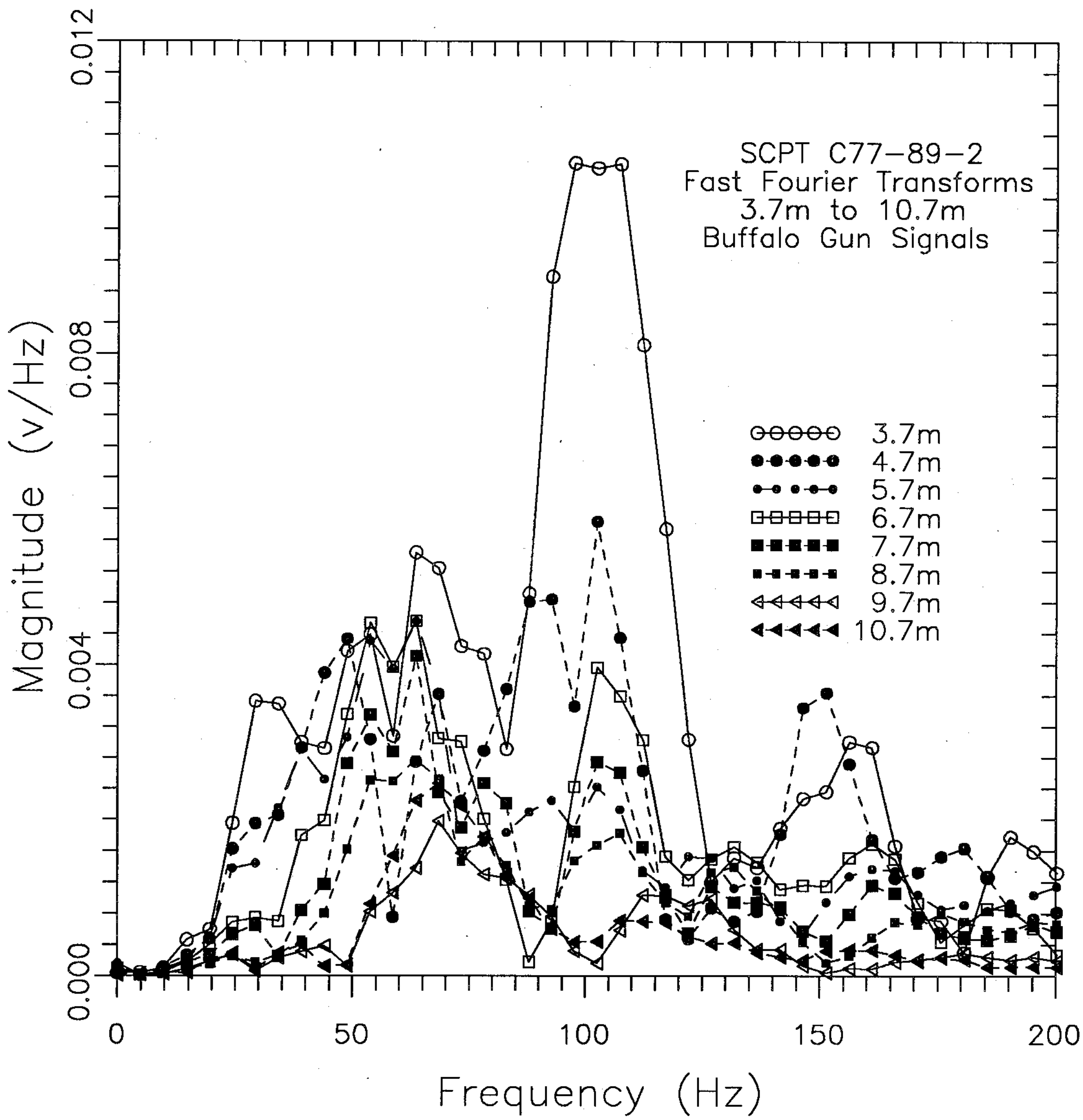


Fig.5.33 Variations in FFT Spectra with Depth for Signals from Buffalo Gun Source

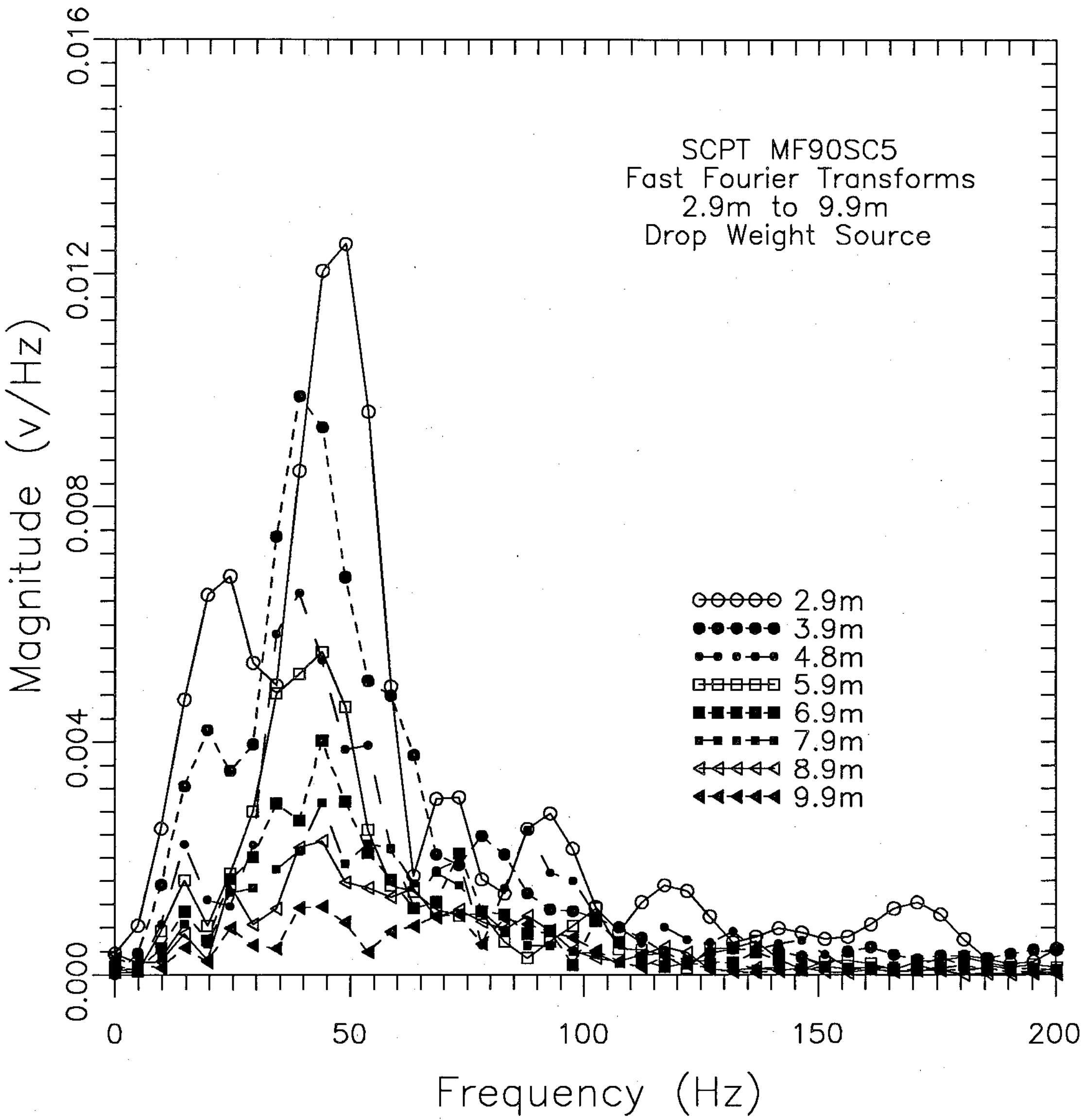


Fig.5.34 Variations in FFT Spectra with Depth for Signals from Drop Weight Source

various pads (and no pad) are presented in Fig.5.35. It was observed that there was little effect on the frequency content for any of the pads. The low frequency at the peak may be related to the shallow depth of the receiver during the testing.

Windowed signals generally show a slow decrease in the frequency at the peak of the FFT's. The full signals did not show this decrease, but do show the variations in the shape of the FFT that are smoothed by windowing. For the full signals, records in both sand and clay showed predominant frequencies of about 75Hz. The buffalo gun source (at least when using the accelerometer receiver) showed poor repeatibility and a wide frequency band (30-170Hz) with significant energy. The drop weight was more repeatable than the buffalo gun with a frequency at the peak of about 45Hz with some scatter. Use of various pads in the drop weight system had little effect on the frequency content of the measured signals

## *5.9 RECOMMENDED PROCEDURE FOR SEISMIC CONE PENETRATION TEST*

The seismic cone penetration test (SCPT) to measure shear wave velocities was well established at UBC at the start of this research. However, basically only the time information in the signals was used and the amplitude values were not considered in detail. In order to extend the test to damping measurements, it was necessary to accurately control and measure amplitude values. Recommendations on the equipment, test

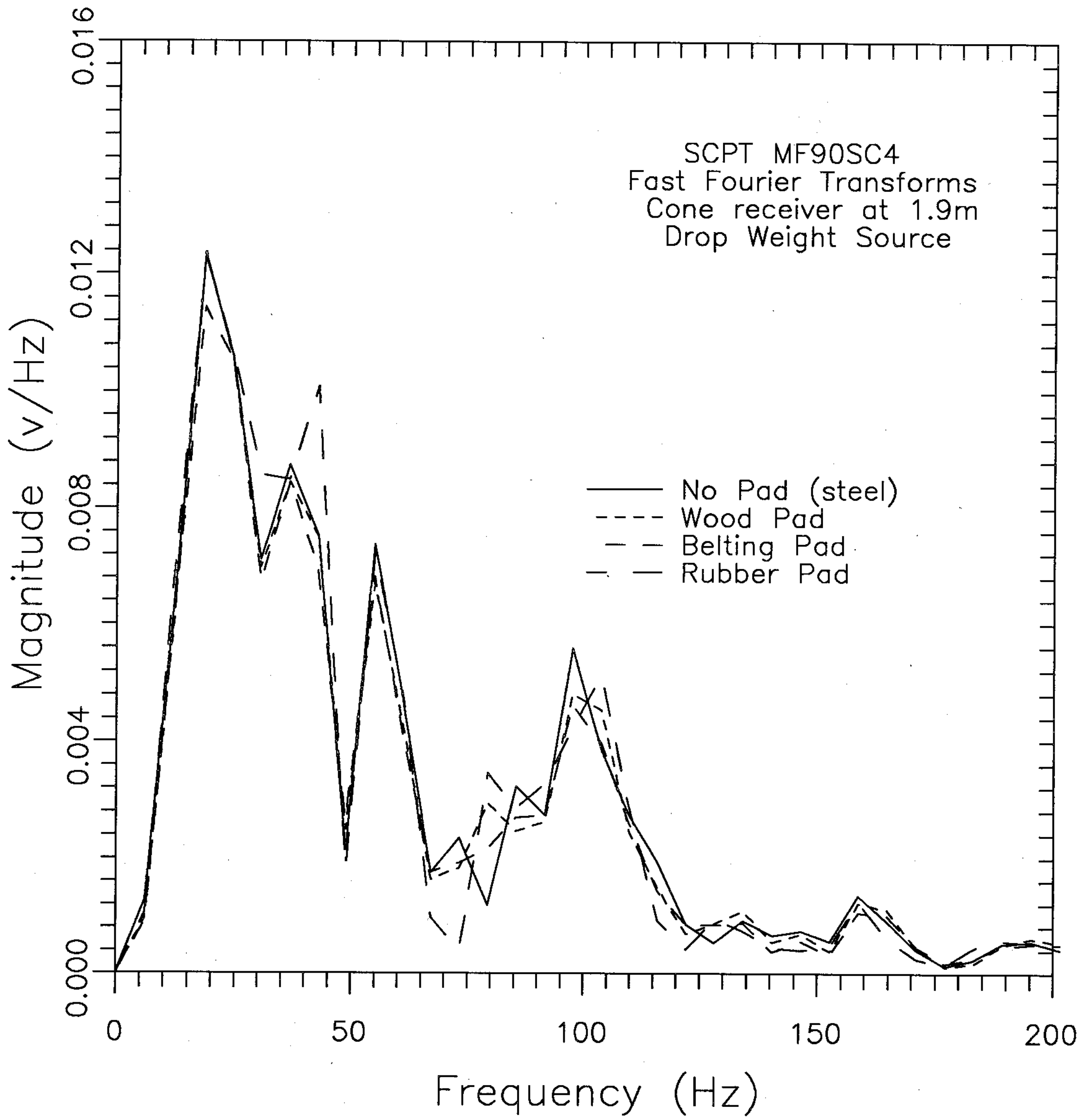


Fig.5.35 Variations in FFT Spectra for Signals from Drop Weight Source with Various Pads

procedure and signal processing have been developed and are outlined below.

New equipment requirements include a repeatable source and a receiver with a flat frequency response over the frequency range of interest (generally less than 200Hz). The mechanical swing hammer described in section 5.2 has been shown to provide a highly repeatable source (see Fig.5.10) and is recommended as the source for the SCPT. A fully damped (71% of critical damping) accelerometer is found to provide a flat frequency response (see Fig.5.3) and the model 3021-002-N by IC Sensors was successfully used.

The rods used are one metre in length, so testing is normally done in one-metre increments. The pushing head is moved to the bottom of its travel before each test. In order to reduce the possibility of waves travelling down the rods, the head is lifted clear of the rods before doing the test.

In order to provide a constant frequency step (increment between points of FFT) in the calculations, it is necessary to use the same time step for all of the depths. The time step to be used must be selected so that the shear wave can be recorded at the greatest depth expected. Typically time steps of 100$\mu$s or 200$\mu$s have been used. It has also been found useful to "AC-couple" the incoming signals to eliminate any zero offset.

During testing it has been found that the measured signals can be unexpectedly larger or smaller than anticipated. To overcome this problem it was found to be useful to record several signals at the same depth to ensure that the signal is repeatable. With the Nicolet oscilloscope, records can be easily divided into quarters, so that four records are normally stored at each depth.

After testing is complete, the signals must be processed. A plot of the cone data is also required to indicate the stratigraphy of the site. Initially, the four signals at each depth are reviewed to ensure that they are essentially the same. If one of the signals does not match the others it is removed. The signals are then averaged (see macro Avg4hits.mac in Appendix E). This gives a more representative signal and improves the signal to noise ratio. For plotting purposes the averaged signals are usually reduced in size by removing every second point. It has been found useful to plot, on one sheet, up to eight of these signals at increasing depths, in both the time and frequency domains. These plots can show any problems with the data set and can indicate depth zones (soil layers) to be used in the calculations. The averaged signals are then windowed to isolate the main shear wave (see macro Windclip.mac in Appendix E), and these windowed signals are used for the calculation of velocities and damping values (see other macros in Appendix E).

# CHAPTER 6

# VELOCITY DETERMINATION - METHODS AND MEASUREMENTS

## *6.1 METHODS OF VELOCITY DETERMINATION*

### 6.1.1 Introduction

Determination of body-wave (compression or shear wave) velocity has traditionally been done by eye, selecting the arrival point of the wave by observing the shape of the trace (sudden increase in amplitude) and selecting a certain instant of time as defining the arrival time. Fig.6.1 shows 4 wave traces, at depths of 3.7m and 4.7m, created by hammer hits to the left and right ends of the beam. The left hit signals show a significant drop before the upward pulse, whereas the right hit signals do not show a rise before the downward pulse. For deeper left hit signals, the drop before the upward pulse disappears. The width of the drop is 2ms to 3ms. Obviously, some experience, judgement and consistency must be applied in selecting the arrival time. For signals collected in offshore work, Gillespie (1990) found that, for a seismic cap source fired in the water, interpretation of the signals was only possible by using the recognition of a shear wave marker at depth, and extrapolating this marker upwards. Again judgement is required in selecting the arrival time.

Woods and Stokoe (1985) provided a brief summary of "direct time" (by eye) and "indirect time" methods of time measurement for velocity

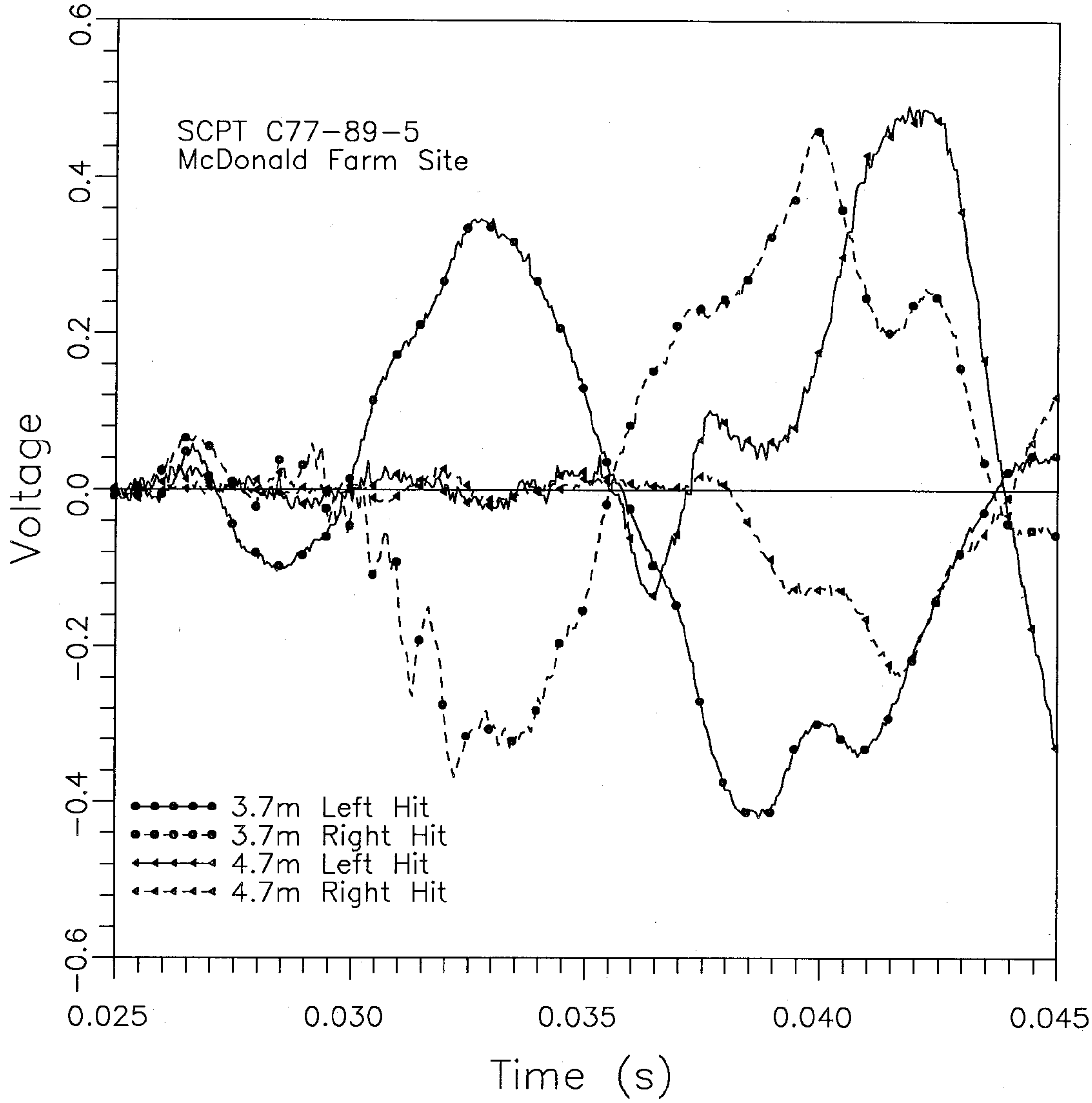


Fig.6.1 Typical Problems with Signals for Velocity Determination

calculation. For direct methods, they mention arrival, first peak/trough, and the cross-over (reversed polarity) approaches. Comparing the arrival and peak approaches for one example, they gave a difference of 2.7%.(237m/s vs. 230m/s) It can be noted in Fig.6.1 that the trough is poorly defined for the 3.7m deep right hit signal. The peaks/troughs are often flat and poorly defined.

For indirect time methods, they discuss the cross-correlation and the phase of the cross-spectrum approaches. They point out that the cross-correlation method was proposed as early as 1974. For the example discussed above, the cross-correlation method gave a velocity (235m/s) between the arrival and peak approaches. The phase of the cross-spectrum approach gave a velocity that varied somewhat with frequency, but averaged 229m/s, just under the peak method.

Woods and Stokoe (1985) concluded that, at least for crosshole testing, different approaches to calculating the shear wave velocities gave similar results, and that the main advantage of indirect (computed) methods is that they can be automated.

Robertson et al (1986), showed that the seismic cone downhole method gave the same results (similar velocities) as the more costly cross-hole method.

The cross-over, cross-correlation, and phase of cross-spectrum methods are discussed in more detail below.

### 6.1.2 Cross-over Method

Signals are normally recorded at depth intervals of 1m (the length of the cone rods). A significant advantage in using a shear beam source is that the signals are polarizable, that is the particle motion and the sign of the amplitude of the measured signal are reversed when the opposite end of the beam is struck. A fairly typical set of signals is shown in Fig.6.2 These signals were recorded with an accelerometer and digitally filtered (low pass at 300Hz) for clarity of presentation. Generally the time of the first cross-over of the two signals is clearly defined as in Fig.6.2. The time interval between two depths is found by subtracting the cross-over time at the shallower depth from that at the greater depth. The depth interval is calculated from the difference between the slant distances from the source to the receiver locations, as shown in Fig.5.1. The interval shear velocity, $V_S$, is given by the depth interval divided by the time interval. The cross-over method is thoroughly described by Robertson et al (1986).

### 6.1.3 Cross-correlation method

With some signals, the cross-over time can be shifted if the signal is perturbed near the cross-over location. The cross-over method only utilizes the time information in the signal at a single point. An alternate approach which utilizes all of the time information in the signals is the cross-correlation technique. In principle, the cross-correlation of signals at adjacent depths is determined by shifting the

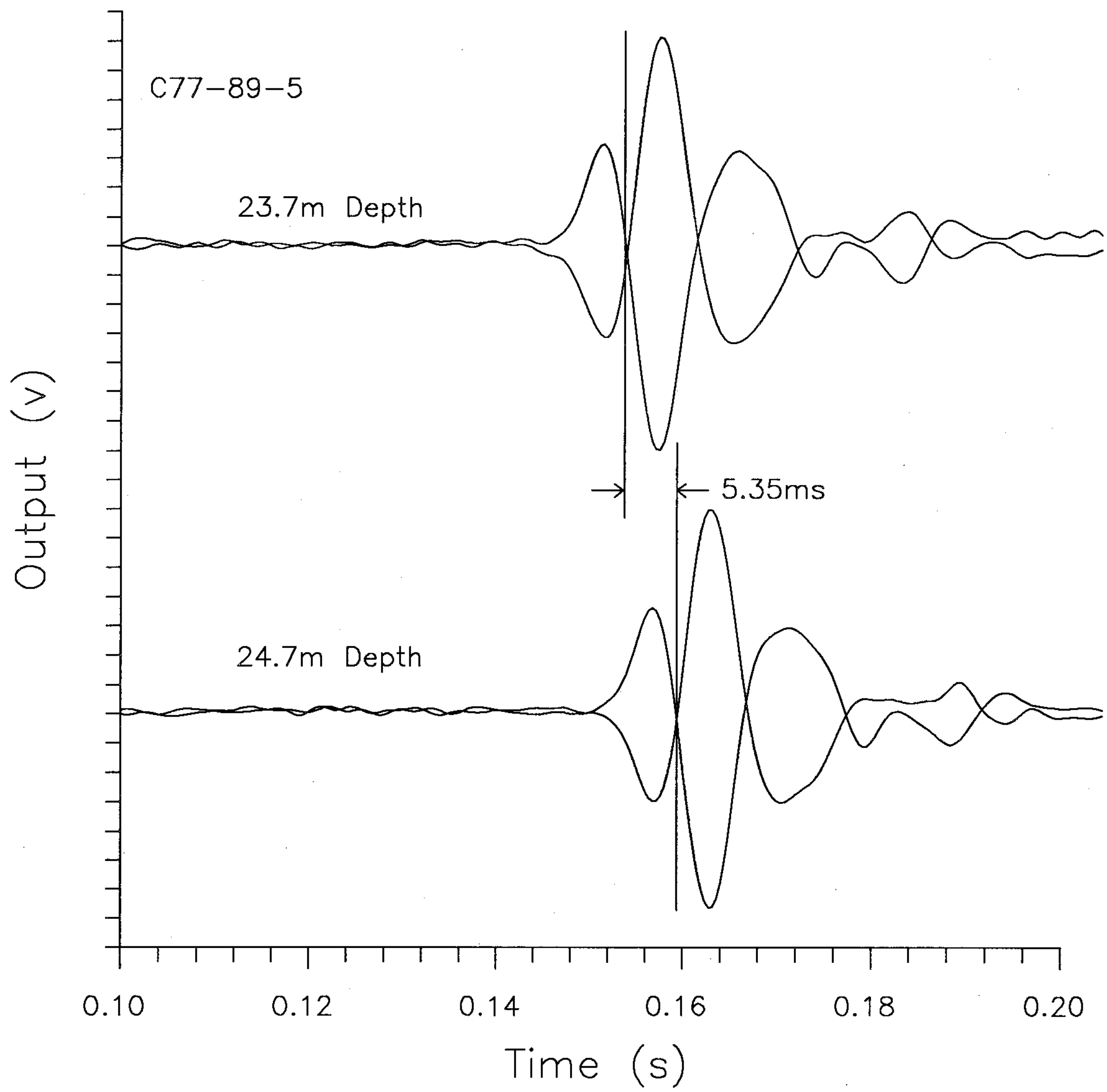


Fig.6.2 Cross-over Method for Time Interval
(after Campanella and Stewart, 1990)

lower signal, relative to the upper signal, in steps equal to the time interval between the digitized points of the signals. At each shift, the sum of the products of the signal amplitudes at each interval gives the cross-correlation for that shift. After shifting through all of the time intervals, the cross-correlation can be plotted versus the time shift, and the time shift giving the greatest sum is taken as the time interval to calculate the interval velocity. This process is shown schematically in Fig.6.3, where the lower signal has been shifted to the left and to the position giving the maximum correlation. The cross-correlation calculation can be done as outlined here, in the time domain, but it is very inefficient. A typical calculation for signals of nominally 2k(2048) points requires about 10 minutes on a 386 PC (25 MHz) with 387 coprocessor if the cross-correlation is done in the time domain.

An alternate method of calculation makes use of the frequency domain. In this procedure, which is outlined in Fig. 6.4, a Fast Fourier Transform (FFT) is used to convert each signal to the frequency domain. The complex conjugate of the upper signal FFT is calculated and multiplied by the lower signal FFT. The inverse FFT of the resultant is the cross-correlation of the signal. This calculation requires only about 20 seconds on the same 386 PC. The signals can be conveniently filtered before the multiplication, using a zero phase shift digital (cosine) filter (Campanella et al, 1989). The resulting cross-correlation can also be normalized by dividing by the square root of the

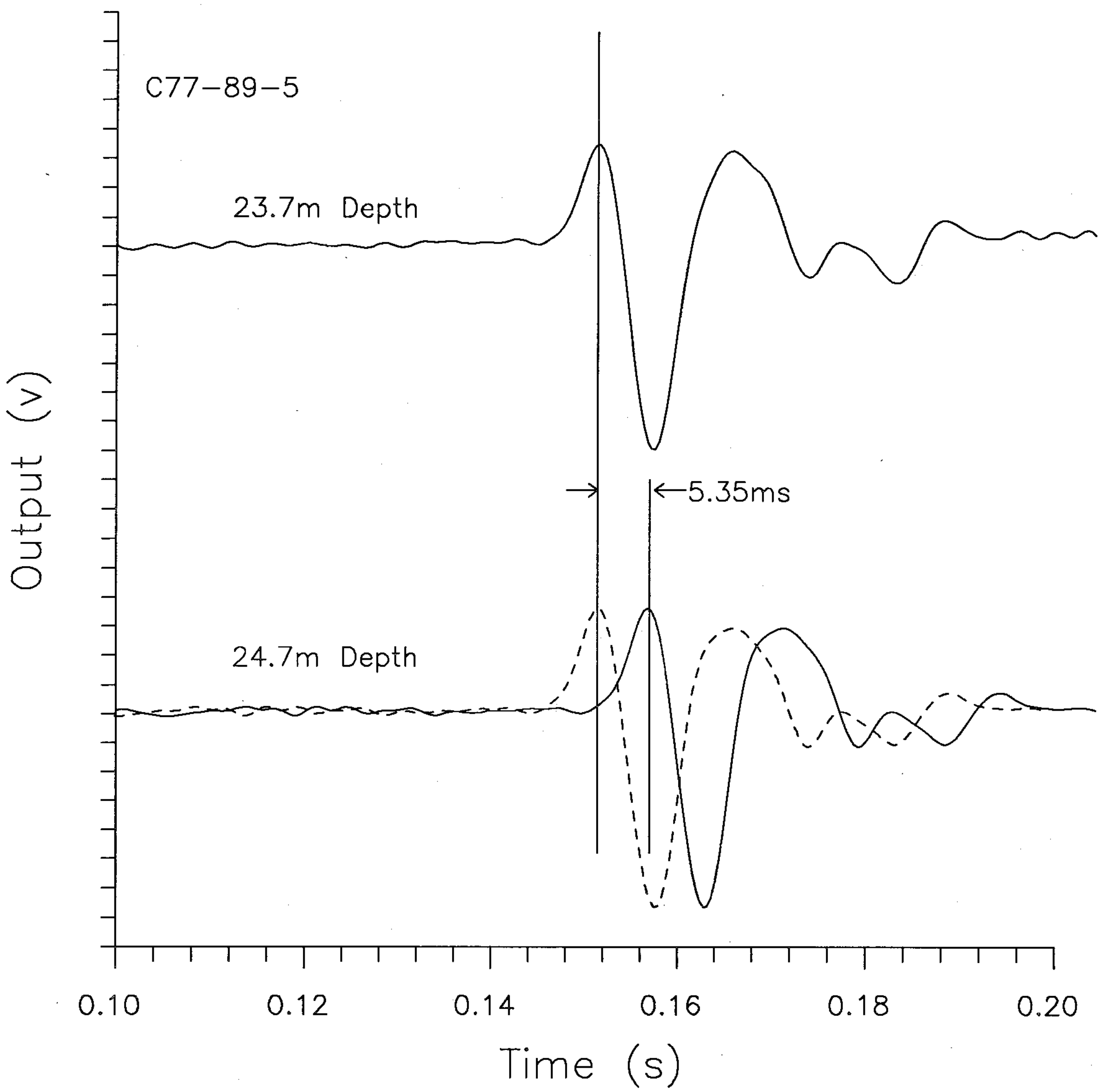


Fig.6.3 Cross-correlation Method for Time Interval
(after Campanella and Stewart, 1990)

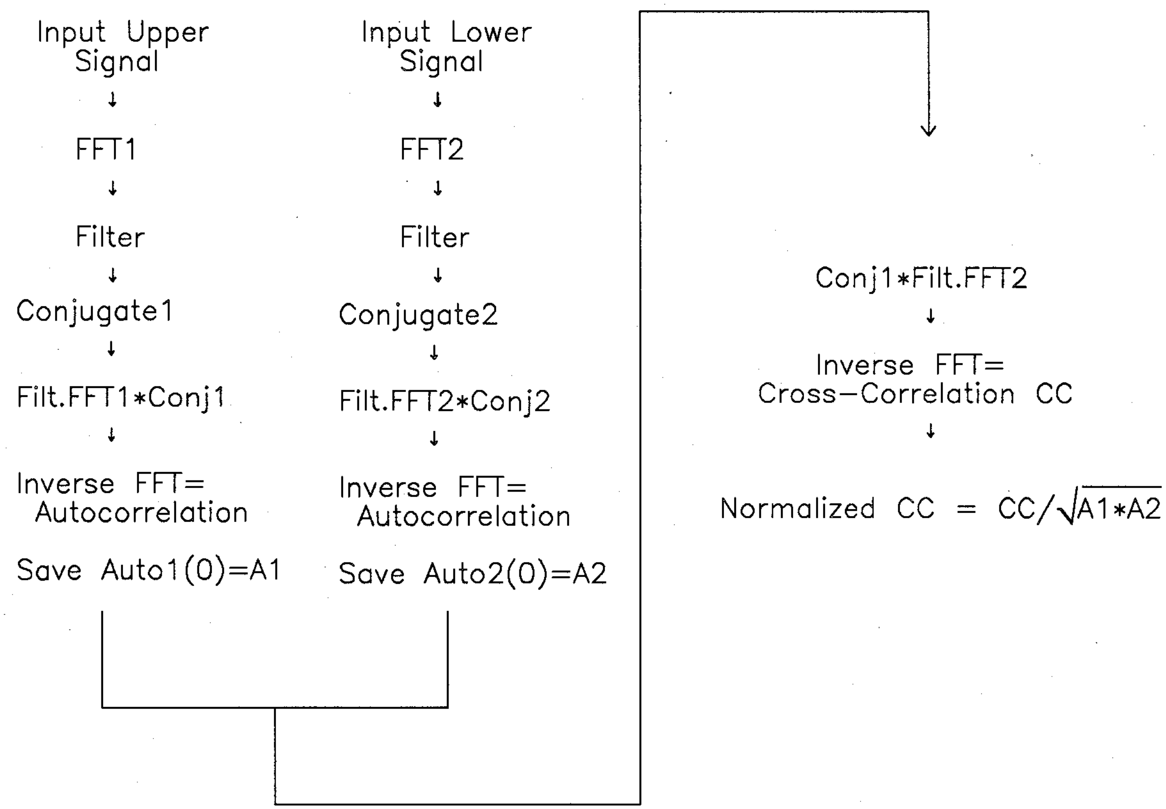


Fig.6.4 Flow Chart of Normalized Cross−correlation Procedure in the Frequency Domain (after Campanella and Stewart, 1990)

product of the autocorrelation of each signal evaluated at shift zero. The autocorrelation can be evaluated as the cross-correlation of a signal with itself, and has a maximum at a shift of zero.

The above procedure has been automated using a macro (automated sequence of keystrokes for a menu-driven program) with the commercially-available program called VU-POINT. A flow chart of the macro is shown in Fig.6.4 and a listing of the macro (Revnorm2.mac) in Appendix E. A typical output is shown in Fig.6.5, which gives a maximum correlation coefficient of 0.993 for a time of 5.35ms over a distance of 0.999m for a shear velocity of 189m/s. Further discussion is given in Campanella and Stewart (1992).

### 6.1.4 Phase of Cross-Spectrum Method

If desired, the cross-correlation approach can be extended to calculate the variation of velocity with frequency. Instead of computing the inverse FFT of the cross spectrum, the phase is calculated. Since the phase is periodic, it must be unwrapped (or stacked) to provide a continuous function, as discussed in Appendix A. For each frequency, f, the time interval can be calculated from:

$$t(f) = \frac{\text{phase}(^{\circ})}{360^{\circ} * f} = \frac{\text{phase(rad)}}{2\pi * f} \qquad [6.1]$$

where t(f) = time as a function of frequency, f.

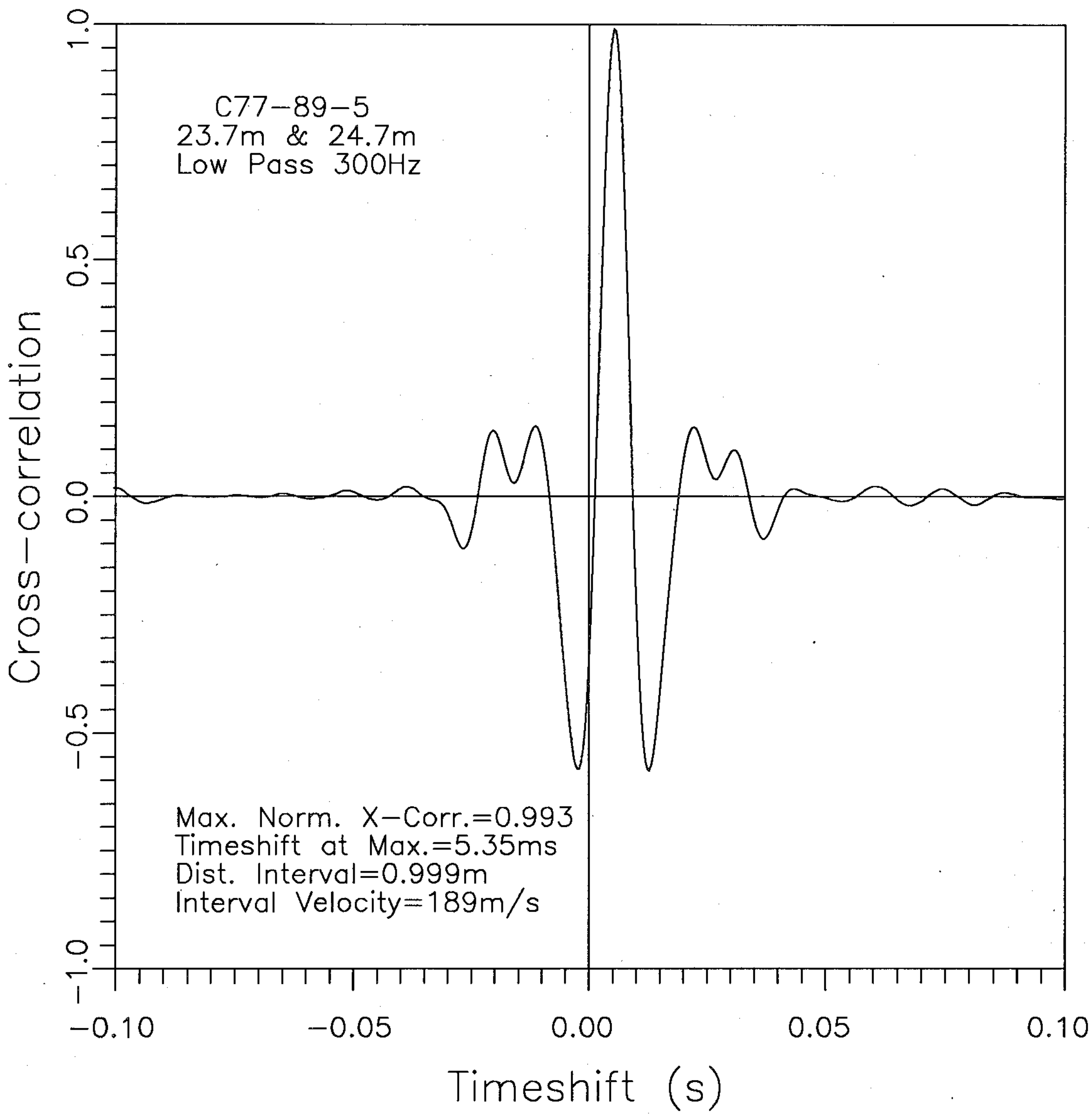


Fig.6.5 Typical Output of Cross-correlation Procedure
(after Campanella and Stewart, 1990)

and the velocity from:

$$v(f) = \frac{\text{distance}}{t(f)} \qquad [6.2]$$

A macro to calculate the velocity with this approach is given as Phvelfq2.mac in Appendix E. If we consider the same signals used in the previous examples, and unwrap the phase of the cross-spectrum, we find, for example, that the phase at 73.24Hz is 2.432rad. Dividing this phase by $2\pi f$ (460.2rad./s) gives a time of 5.28ms. For a distance interval of 0.999m, this time gives a velocity of 189.06m/s. The plot for a range of frequencies is shown in Fig.6.6 and it can be seen that the velocity determined by the cross-correlation is a reasonable average over the frequencies of interest (40 to about 120 Hz).

This method provides a direct representation of the variation of velocity with frequency, and allows direct selection of the frequency range to be used to compute the velocity. It also allows a direct calculation of the average velocity over the selected frequency range that is not restricted to discrete time steps as in the cross-correlation method. However, it is necessary to have access to a phase unwrapping function.

### *6.2 COMPARISON OF METHODS AND PROCESSING STEPS*

For comparing various methods and procedures, results from an early SCPT, C77-89-5, will be used as this sounding showed considerable variation when the various approaches were applied. Where required a

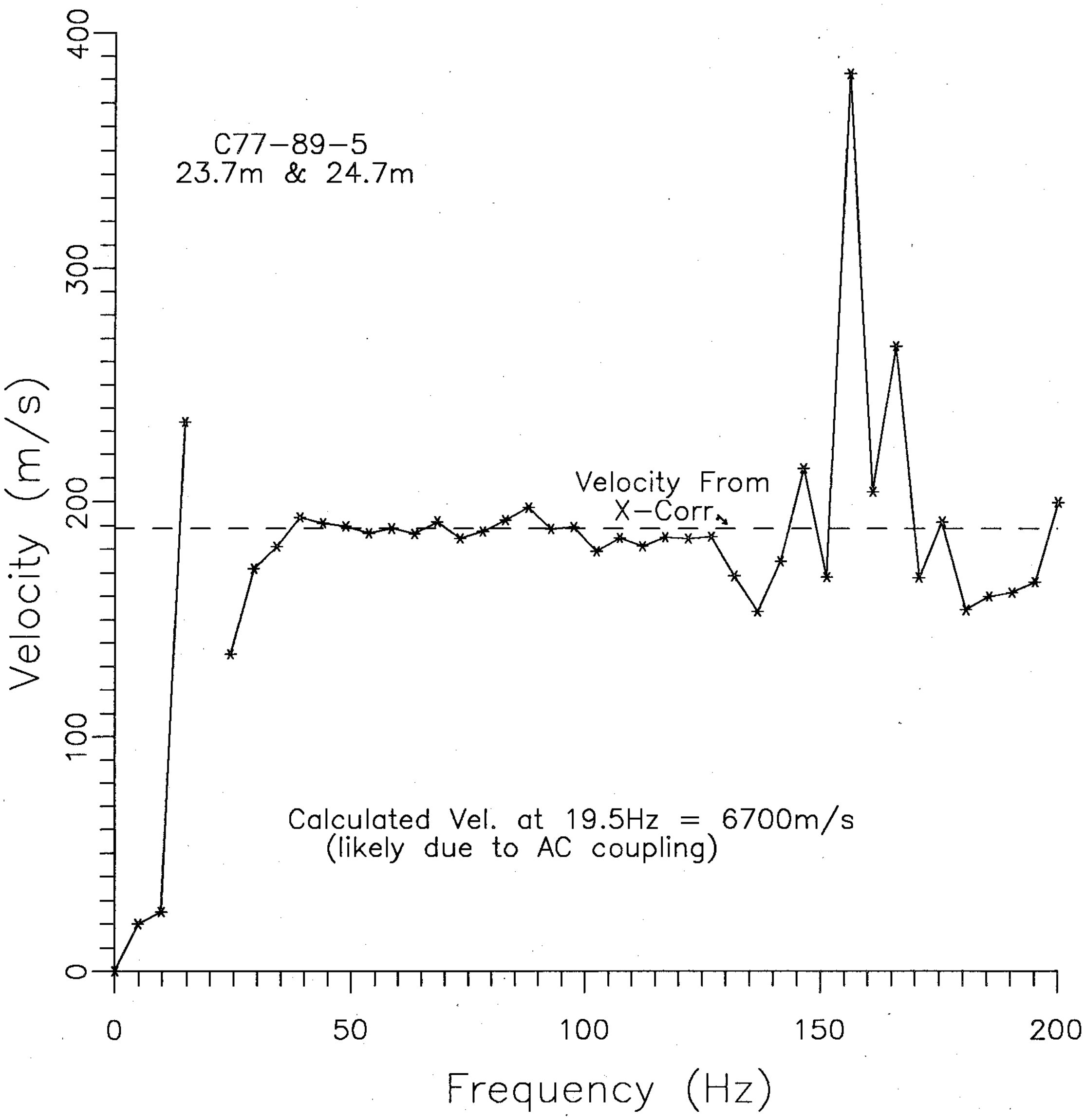


Fig.6.6 Velocity Variation with Frequency (modified from Campanella and Stewart, 1990)

frequency range of 40Hz to 100Hz was somewhat arbitrarily but consistently used. Results from other SCPT's are used to supplement this comparison.

### 6.2.1 Comparison of Cross-over and Cross-correlation Methods

A shear wave velocity profile comparing the results from cross-over and cross-correlation (applied to the full signal) methods is shown in Fig. 6.7. The velocities are in good agreement above 5m and below 14m. In between, the cross-over velocities are consistently less, within about 10%, except near 11m, where the difference is about 30% (depending on how one might select the cross-over point). The calculated cross-over velocity at this depth is affected by a "step" or distortion in the signal as shown in Fig.6.8. The cross-correlation velocity is not as affected by the localized step in the signal since the full signal is used to calculate the time shift. However, use of the full signal introduces parts of the signal that seem to be not directly related to the main shear wave as discussed in section 5.6, and these parts can affect the velocity calculation. Windowing to remove these effects is discussed in the next section.

### 6.2.2 Effect of Windowing on Cross-Correlation Velocities

Windowing of signals to separate the shear wave from the balance of the signal was discussed in sections 5.6 and 5.7. It was noted that the cause or nature of the smaller pulses after the main pulse could not

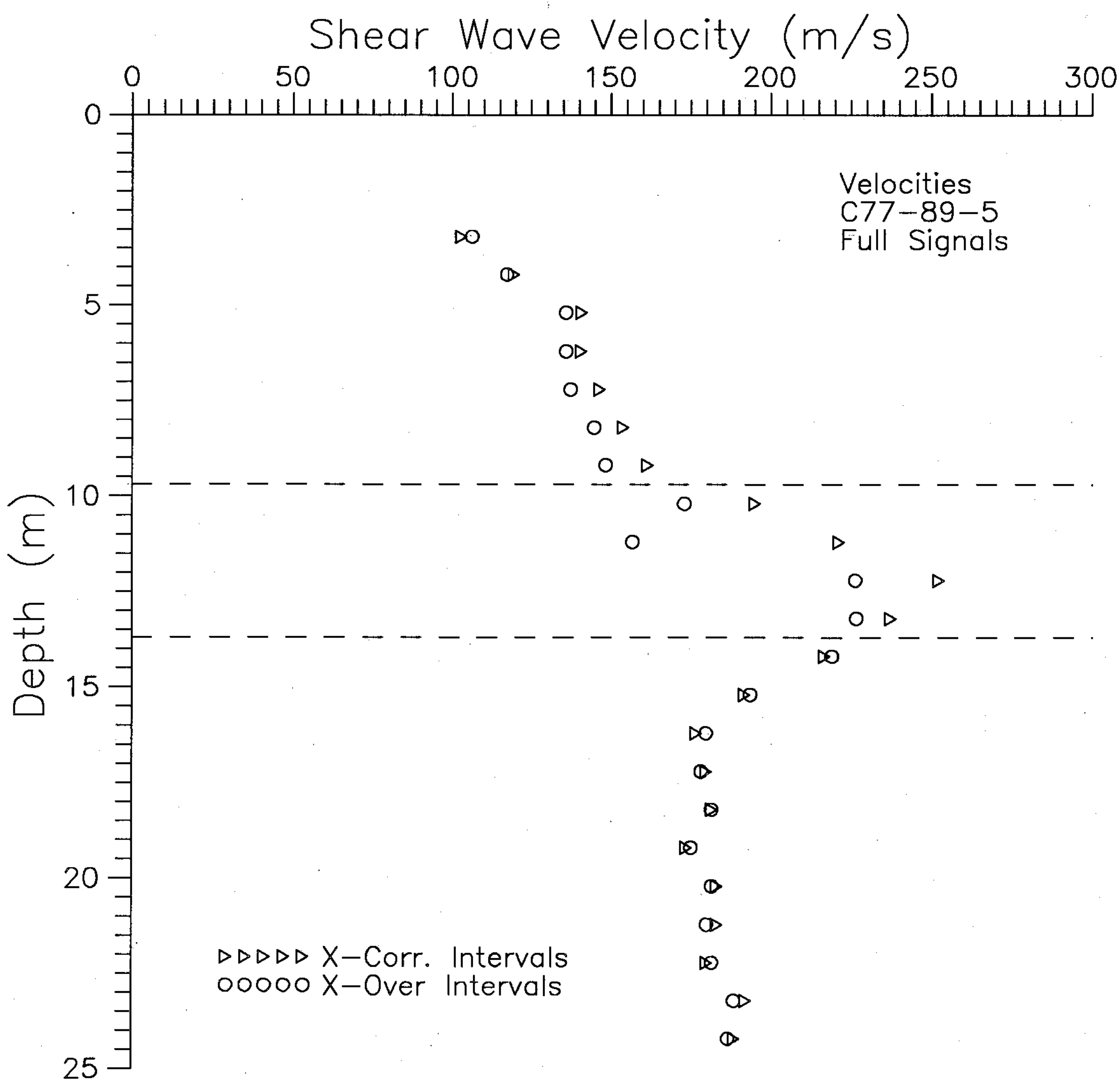


Fig.6.7 Comparison of Cross-over and Cross-Correlation Results using Full Signals (after Campanella and Stewart, 1990)

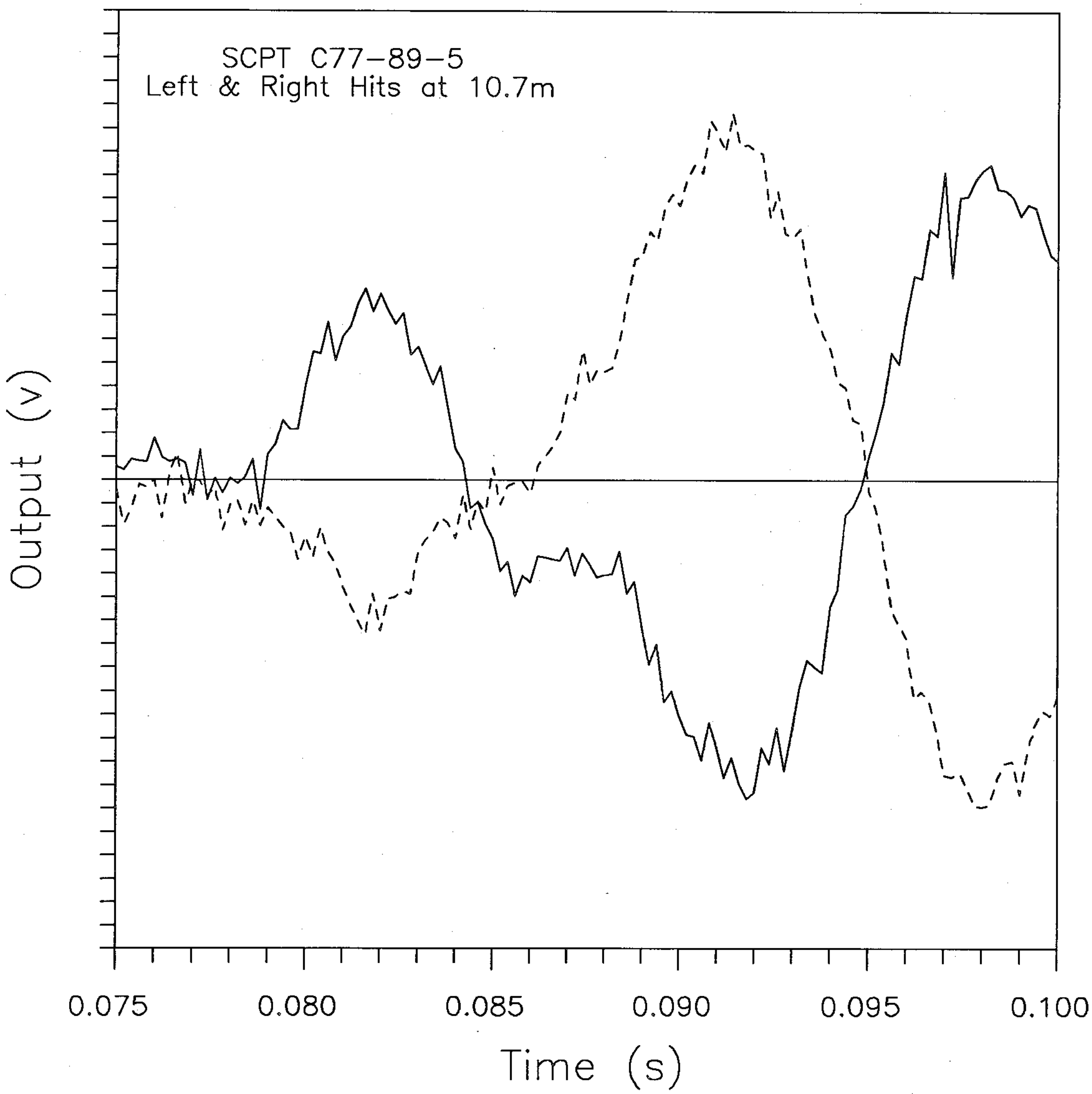


Fig.6.8 Signals from Polarized Hits showing 'Step' Effect
(after Campanella and Stewart, 1990)

be clearly identified, but if the shear wave alone is used the irregularities in the FFT are removed. The signals used in the previous section were windowed and the cross-correlation method was used to calculate velocities with the results shown in Fig.6.9. Again there is good agreement above 5m and below 14m. In between the velocities from the windowed signals are consistently less than those for the full signals, and vary higher and lower than the velocities from the cross-over method. It should be noted that having velocities from the full signals greater than those for the windowed shear wave suggests that the portions of the signal removed are not caused by reflections alone as there would have been longer travel times, or smaller velocities. Gillespie (1990) noted that "The optimum window of data to use for cross correlation appeared to be that obtained between the first arrival and the first crossover", that is, he used the first half shear wave.

Other comparisons using full and windowed signals are provided in Figs.6.10 to 6.12. The velocities in Fig.6.10 are for the lower 232nd St. site and show the windowed signals give velocities slightly less than for the full signals. Fig.6.11 shows velocities from the Laing Bridge site, and the windowed signal velocities are slightly greater than for the full signals, when digitally filtered (bandpass) over a 40Hz to 80Hz range. For a slightly wider filter (40-100Hz), the velocities in Fig.6.12 show that the results from the full and windowed signals are almost evenly split between high, low and equal values. It should be noted that the change in filter primarily affected the full

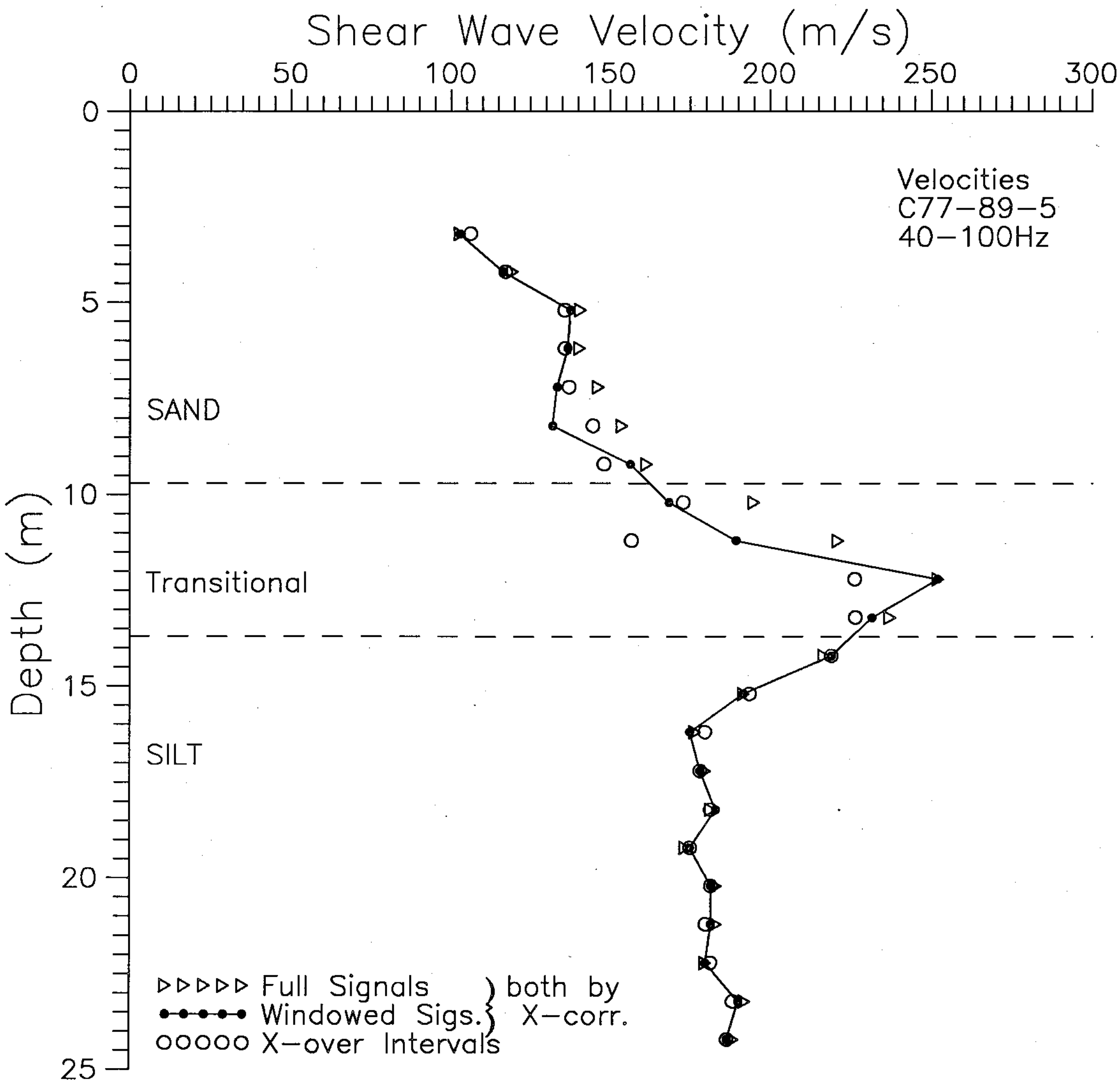


Fig.6.9 Comparison of Full and Windowed Signals used in Cross-correlation Method – McDonald Farm

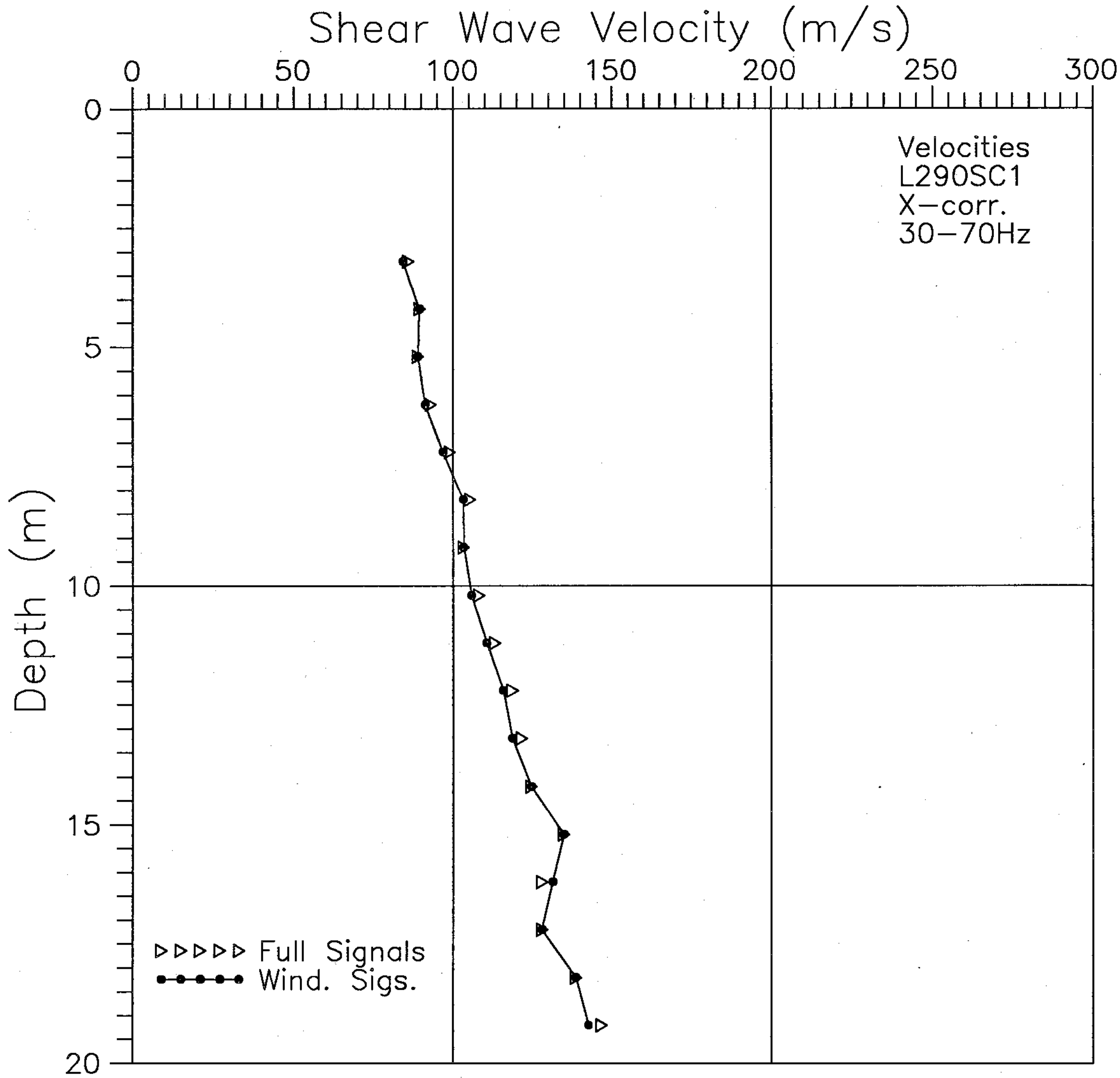


Fig.6.10 Comparison of Full and Windowed Signals
— Lower 232nd Street Site

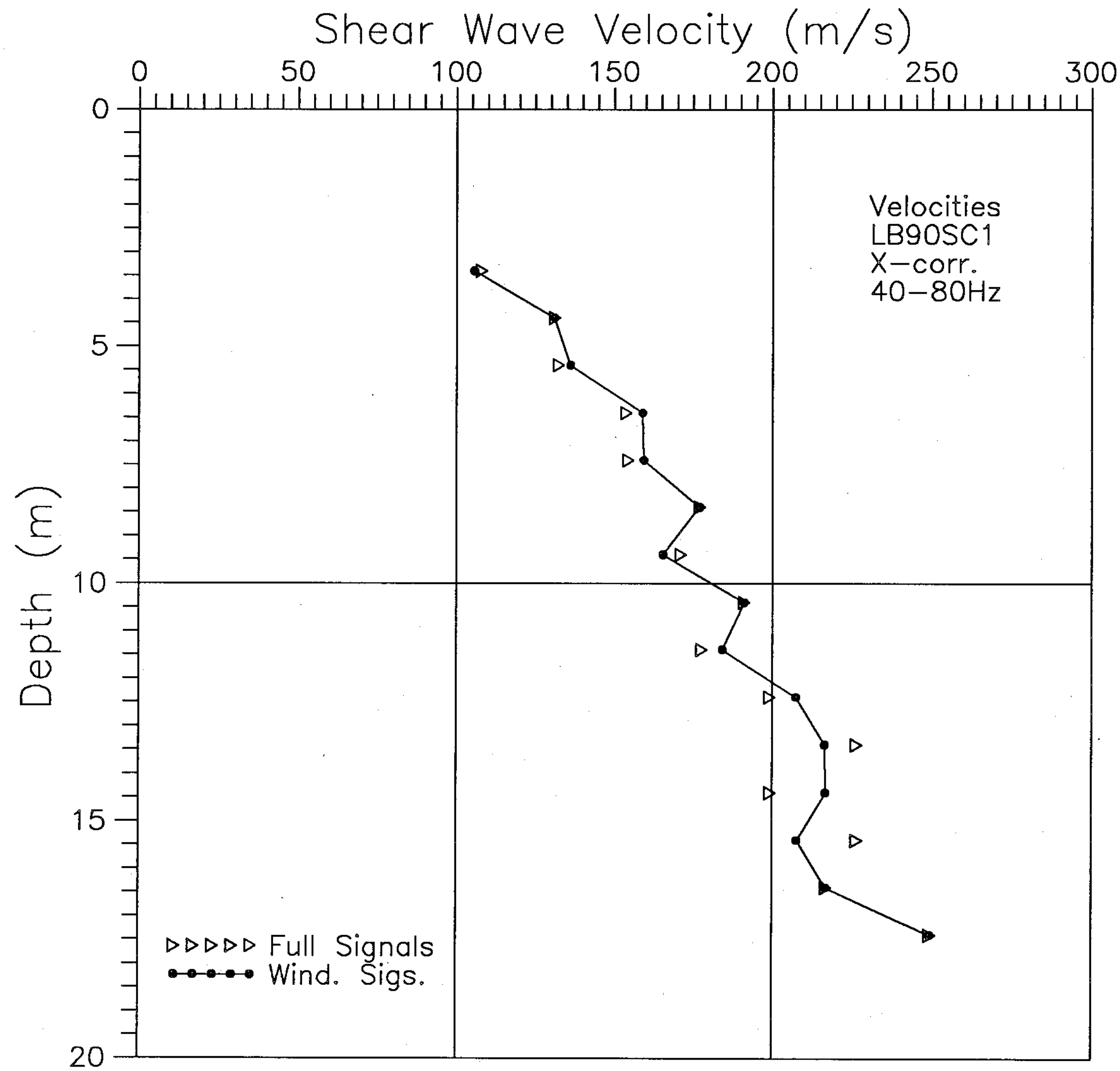


Fig.6.11 Comparison of Full and Windowed Signals
– Laing Bridge Site – 40Hz to 80Hz

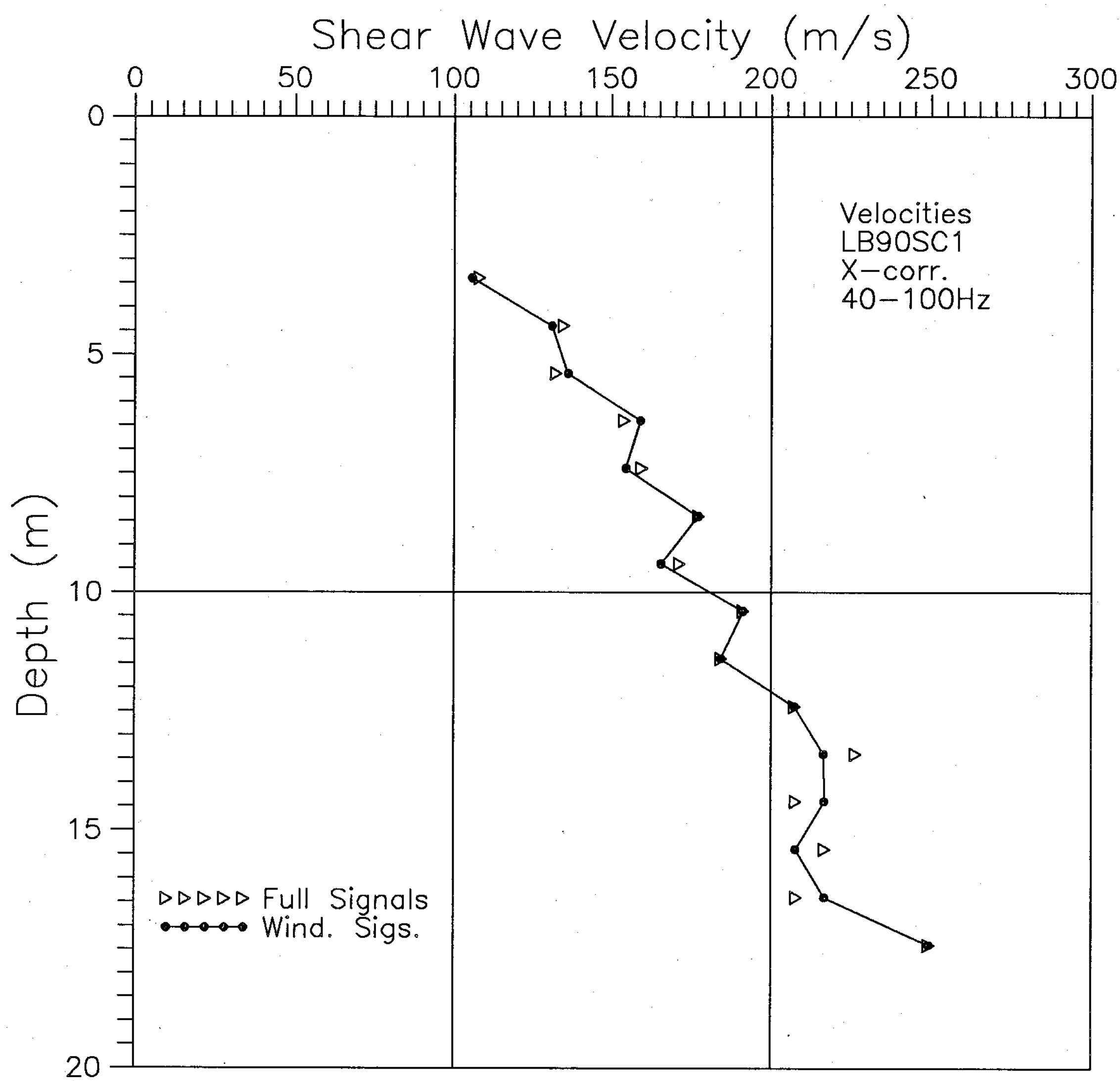


Fig.6.12 Comparison of Full and Windowed Signals
— Laing Bridge Site — 40Hz to 100Hz

signal values, with the velocity at only one depth being changed by one time step for the windowed signals.

It is concluded that there is no apparent consistent relationship between the velocities calculated using the full signals and those using windowed signals. Applying the cross-correlation method to the windowed signals removes the ambiguities in using the full signal (portions of which are poorly understood) and in using a single point in the signal (which can be affected by small local irregularities in the signal).

### 6.2.3 Phase of Cross-Spectrum Method

The phase of the cross-spectrum method has a significant advantage over the other methods discussed in that the variation of velocity with frequency is calculated, which can clarify understanding of the effects of different signal processing steps. For a single shear wave velocity, for example to calculate $G_{max}$, the velocity can be averaged over a suitable frequency range. Fig.6.13 shows the phase velocities over a 1m depth, using both the full signals and windowed signals, for a "poor" set of signals (C77-89-5) and a "good" pair of signals (MF91SC1). For the poor signals the velocities calculated from the full signals show a significant step at a frequency of about 75 Hz, dropping by a factor of about 2 (137m/s to 61m/s). The phase velocity from the windowed signals shows considerably less variation (120m/s before and 147m/s after). For the better signals, velocities for the full signals still show some variation (about 30 m/s over a frequency range of 40 to 80 Hz),

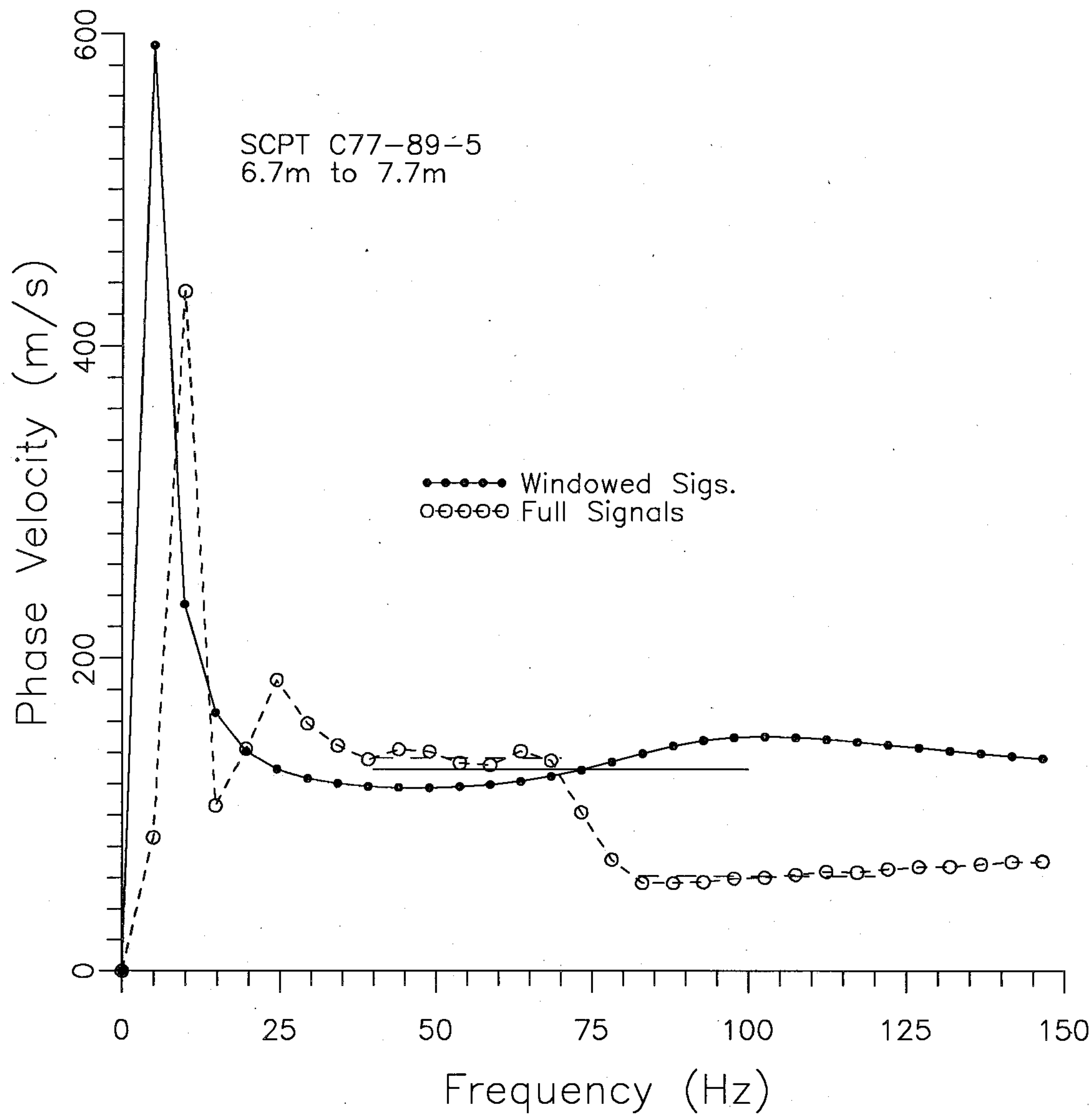


Fig.6.13 Comparison of Phase Velocities – Full and Windowed Signals

whereas velocities for the windowed signals are essentially constant for a typically-used frequency range of 40 to 80Hz.

A comparison of velocities calculated from windowed signals for the cross-correlation and phase methods is provided in Fig.6.14. It can be seen that the two methods give essentially the same velocities. As discussed in section 2.3, the phase velocity is the appropriate velocity for damping calculations. Velocities given in the remaining sections are the phase velocities for windowed signals.

### 6.2.4 Ray-Path Bending (Travel Path) Effects on Shear Wave Velocity Calculations

The effects of soil layering on the amplitudes of signals passing through the interface between layers was described in section 2.3. However, such interfaces will also affect the direction of propagation of waves passing through the layer, and thus the length of the travel path of the wave. The magnitude of the effect will depend on the relative values of the acoustical impedance of the layers. As indicated previously, the acoustical impedance ($\rho V$) is the product of the density, $\rho$, and the velocity, V. For this discussion, the changes in $\rho$ will be considered small relative to the changes in V, and thus the impedance will depend only on V.

Fig.6.15 shows a series of soil layers with velocities $V_0,\ldots,V_n$ and thicknesses $\Delta z_0,\ldots,\Delta z_n$. A seismic cone penetration test is carried out with a horizontal offset, X, from the source to the vertical rods.

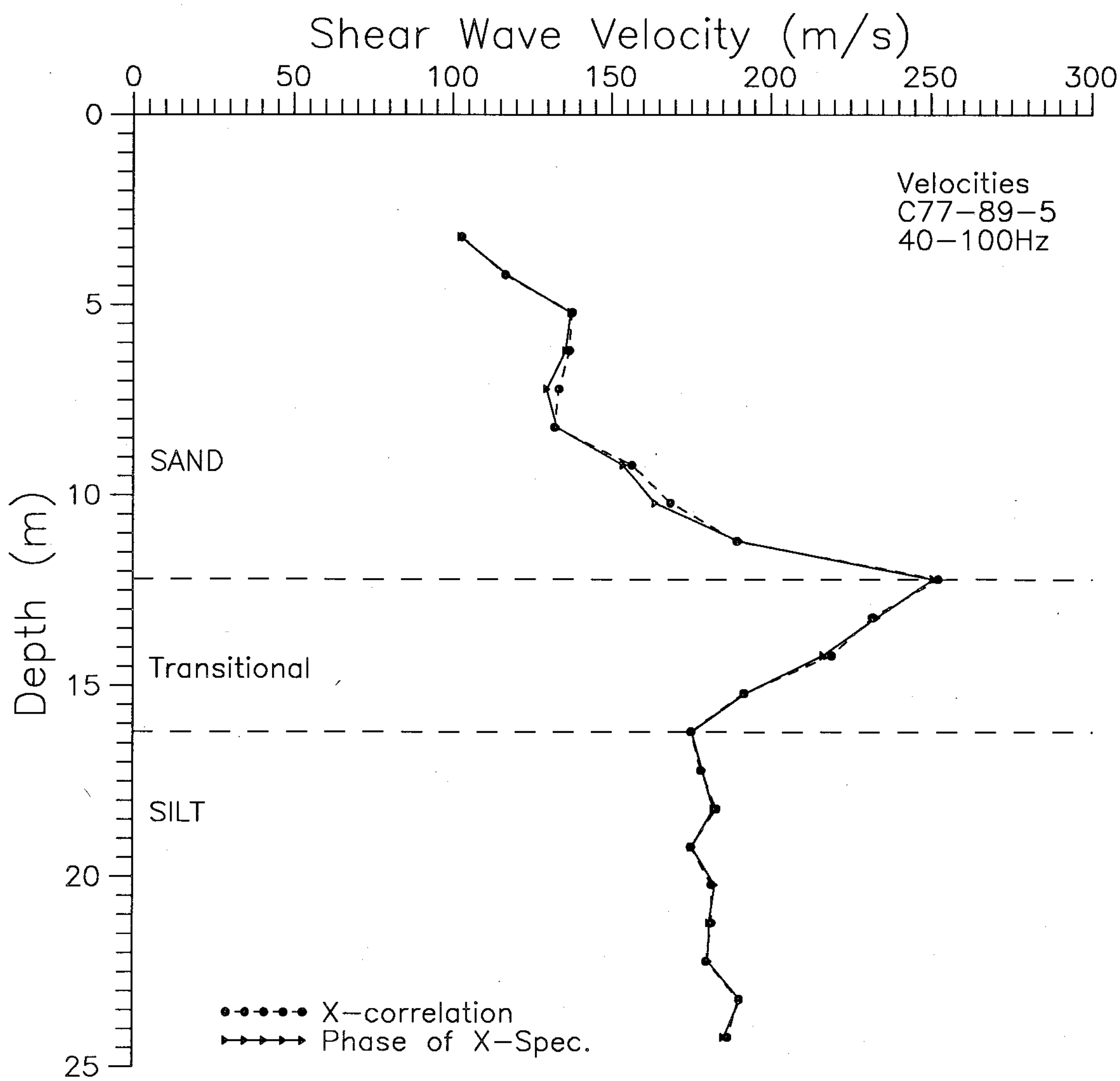


Fig.6.14 Comparison of Phase and Cross-correlation Methods with Windowed Signals

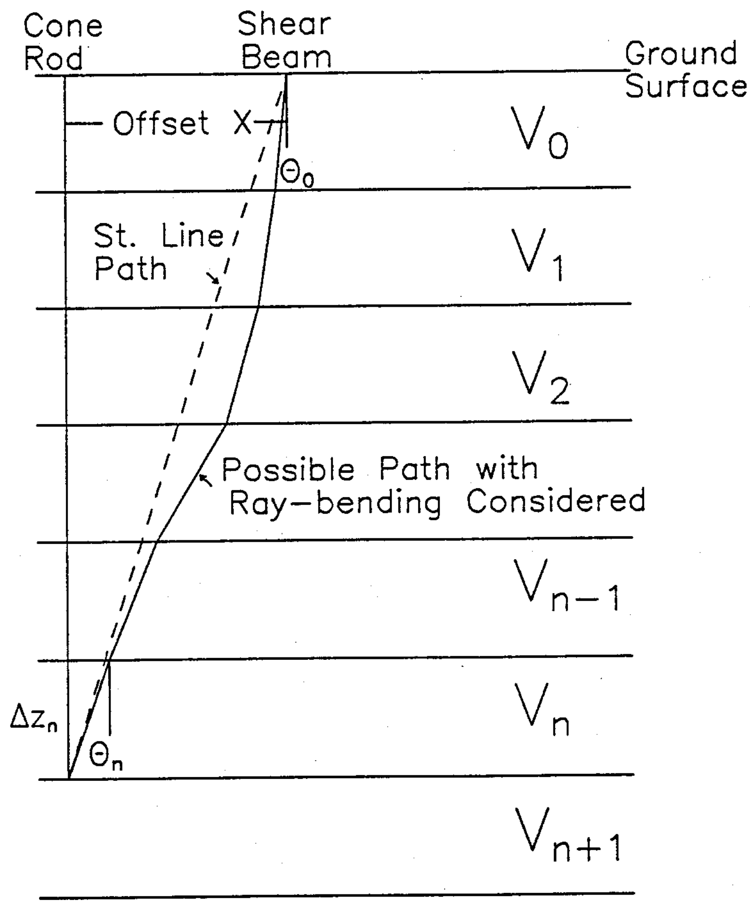


Fig.6.15 Ray-path Bending Effects in Layered Soil

Because of the offset (typically 1.1m), the rays (paths from source to receiver) will encounter the interfaces at an angle (to the normal), $\theta$, that will vary according to Snell's Law:

$$[6.3] \quad \frac{\sin \theta_n}{V_n} = \frac{\sin \theta_0}{V_0} = p$$

where p = a constant, the ray-path parameter.

In the nth layer, the layer travel time is given by:

$$[6.4] \quad \Delta t_n = \frac{\Delta z_n}{V_n \cos\theta_n}$$

and the horizontal distance moved in the layer is:

$$[6.5] \quad \Delta x_n = \Delta z_n \tan\theta_n$$

The development of the equations to this point follows Telford et al (1976), who subsequently considered infinitesimal layers. The balance of the development generally follows Rice (1984).

The above equations can be summed to give the total travel time and horizontal distance as:

$$[6.6] \quad T = \sum_0^n \frac{\Delta z}{V \cos\theta} = \sum_0^n \frac{\Delta z}{V \sqrt{1-\sin^2\theta}} = \sum_0^n \frac{\Delta z}{V \sqrt{1-(pV)^2}}$$

$$[6.7] \quad X = \sum_0^n \tan\theta \; \Delta z = \sum_0^n \frac{\sin\theta \; \Delta z}{\sqrt{1-\sin^2\theta}} = \sum_0^n \frac{pV \; \Delta z}{\sqrt{1-(pV)^2}}$$

or:

$$X = \sum_{i=0}^{n-1} \frac{pV_i \Delta z_i}{\sqrt{1-(pV_i)^2}} + \frac{pV_n \Delta z_n}{\sqrt{1-(pV_n)^2}}$$

To solve for $V_n$, let:

$$X - \sum_{i=0}^{n-1} \frac{pV_i \Delta z_i}{\sqrt{1-(pV_i)^2}} = J = \frac{pV_n \Delta z_n}{\sqrt{1-(pV_n)^2}} \quad \text{then:}$$

$$J^2 \{1-(pV_n)^2\} = (pV_n \Delta z_n)^2 \quad \text{or:} \quad V_n{}^2(p^2 \Delta z_n{}^2 + J^2p^2) = J^2$$

$$[6.8] \quad Vn = \left| \frac{J^2}{p^2 \Delta z_n{}^2 + J^2p^2} \right|^{0.5} = \left| \frac{(J/p\Delta z_n)^2}{1+(J/\Delta z_n)^2} \right|^{0.5}$$

To solve for the velocities accounting for ray-path bending, it is necessary to first solve for $V_0$ assuming a straight-line path. For each subsequent layer, an initial value of p is assumed (the value of p will decrease for deeper layers as the path becomes more vertical, and a reasonable approximation is required at each depth). The velocity is calculated from eqn.6.8, and is used in eqn.6.6 to calculate the total travel time. This calculated value is compared with the measured time and the value of p is adjusted, with the process continued until the times agree within a decided tolerance (1% was used). Then the process is continued for the next layer.

A program (see Appendix E) was written in Quick Basic to calculate the velocities accounting for ray-path bending and was applied to two sets of data from the McDonald Farm site. The data was windowed to isolate the first shear-wave, and the signals were then run through a cross-correlation program to get the time-shifts for each layer. Since it is not possible to measure the velocity from the source to the first receiver position, a velocity of 100m/s was estimated for the first layer by extrapolation from deeper measurements. The subsequent total travel times were calculated by summing the time shifts. Plots of the results are presented in Figs.6.16 and 6.17. The results are close whether ray-bending is taken into account or not. Secondary plots, of the percent differences between the methods, are given in Fig.6.18 and show the differences are generally less than 3%.

### *6.3 MEASUREMENTS OF VELOCITY*

Velocities calculated using the phase of the cross-spectrum method on windowed signals are presented for each of the four research sites. Generally the SCPT's selected are those used for damping calculations. The frequency range used to calculate the velocities were those over which the velocity was reasonably constant.

Fig.6.19 shows the results for the McDonald Farm site. The SCPT shown in Fig.6.14 (C77-89-5) is included. The soundings denoted as MF90SC5 and MF91SC1 are a few metres apart while MF90SC2 and C77-89-5 are located about 10m apart, but 140m to the west of the first pair. The velocities for the latter two tests are quite close, (correlation coefficient, R=0.97) while there is greater scatter in the former two tests (R=0.39). Velocities that appeared to be discrepancies were checked by the cross-correlation method and were confirmed. Scatter in the results is to be expected due to the variable layering in the sand and transition zone, as seen in the cone soundings. A brief comparison of velocities and cone bearing values indicated that, in a general

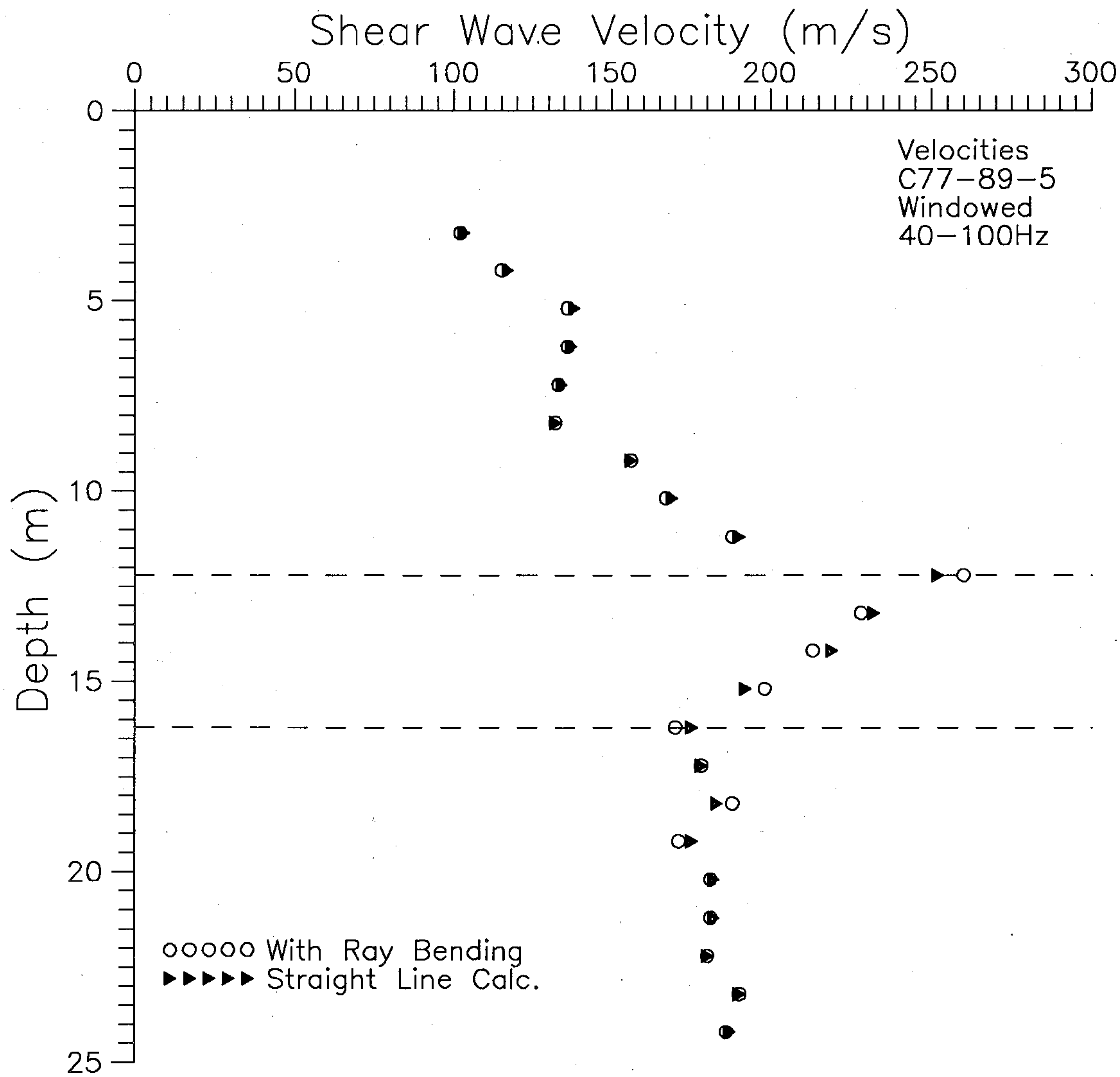


Fig.6.16 Comparison of Velocities With and Without Ray-Path Bending Considered - SCPT C77-89-5

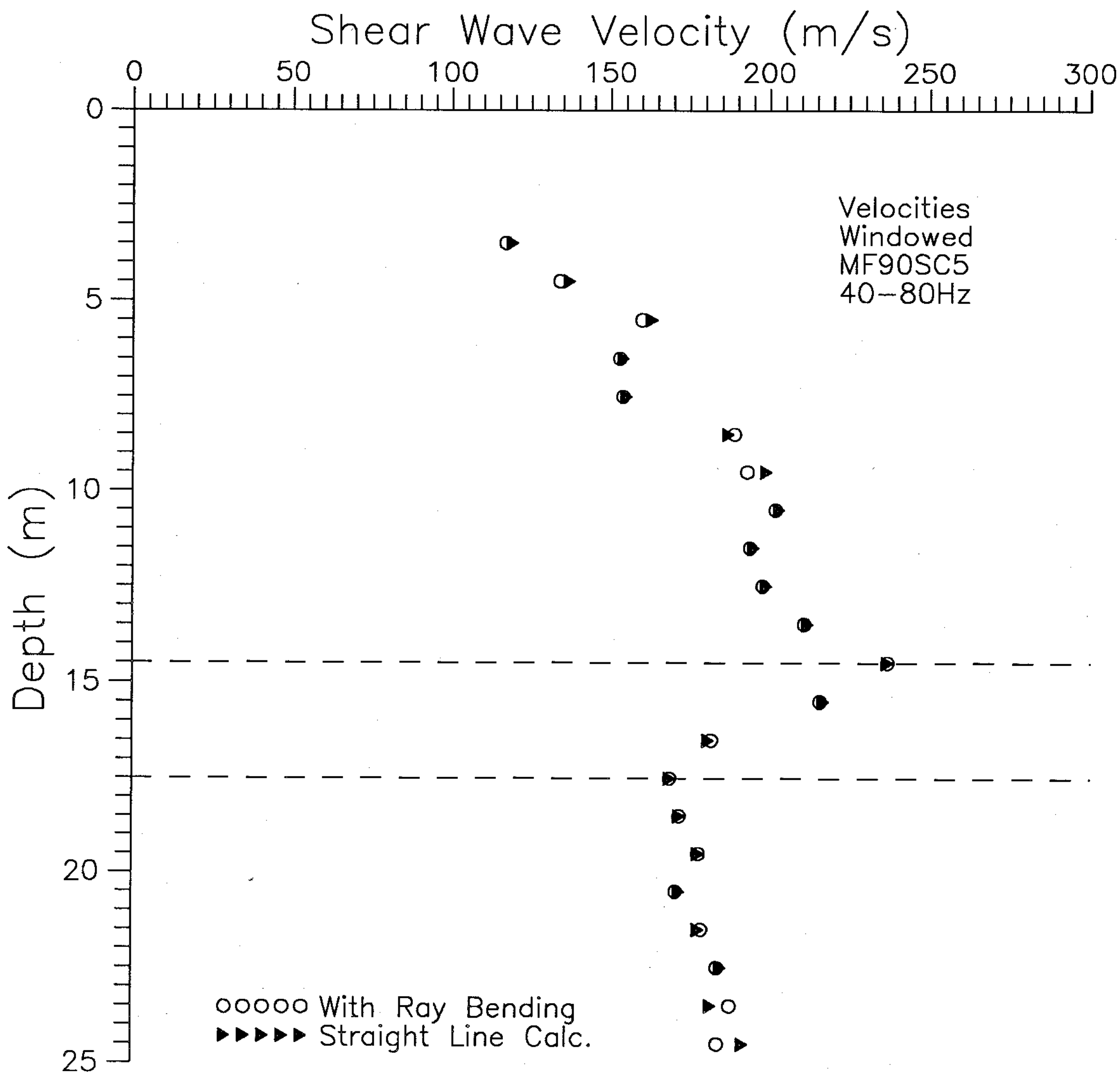


Fig.6.17 Comparison of Velocities With and Without Ray–Path Bending Considered – SCPT MF90SC5

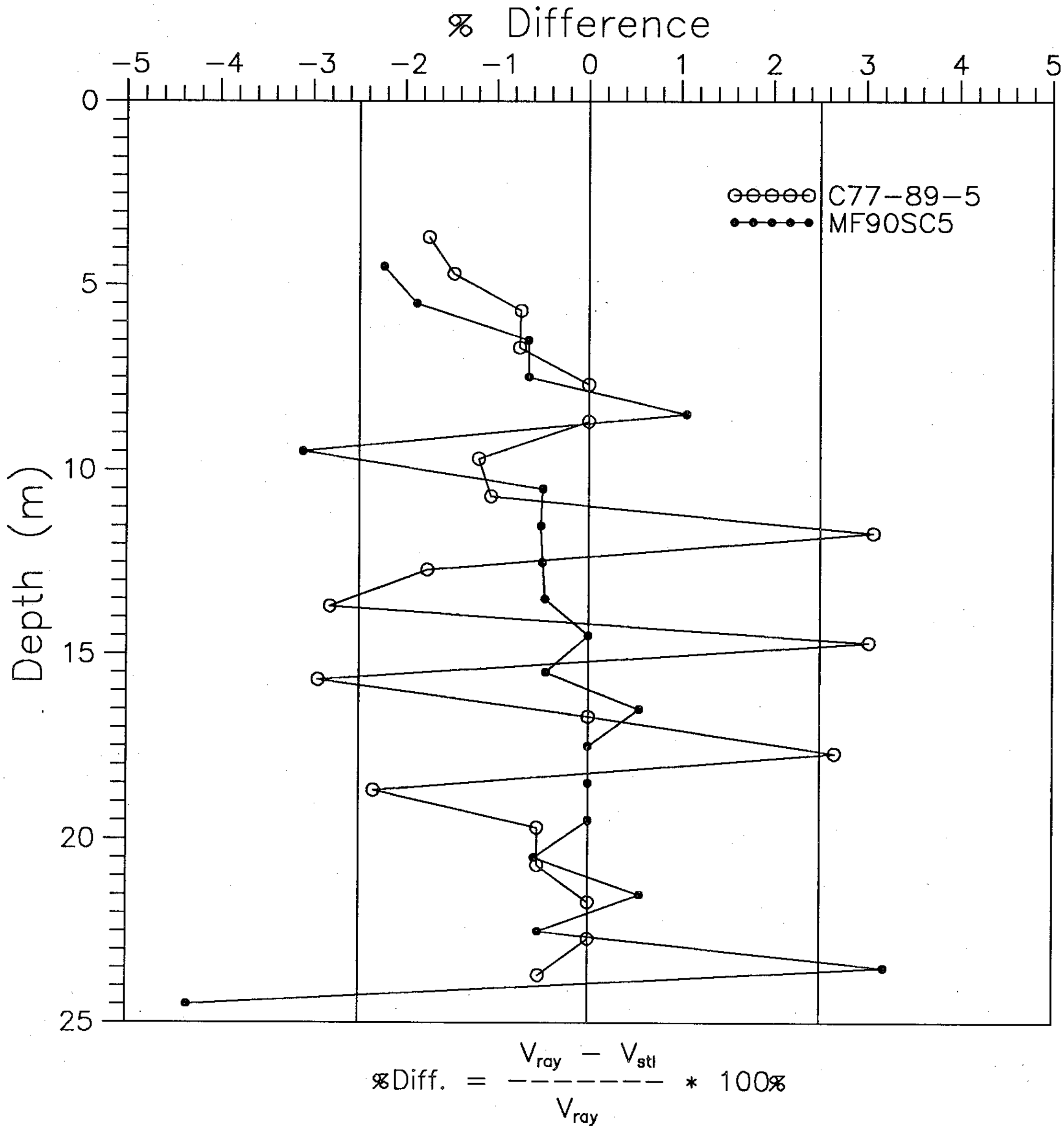


Fig.6.18 Percent Differences if Ray—Bending Consideded

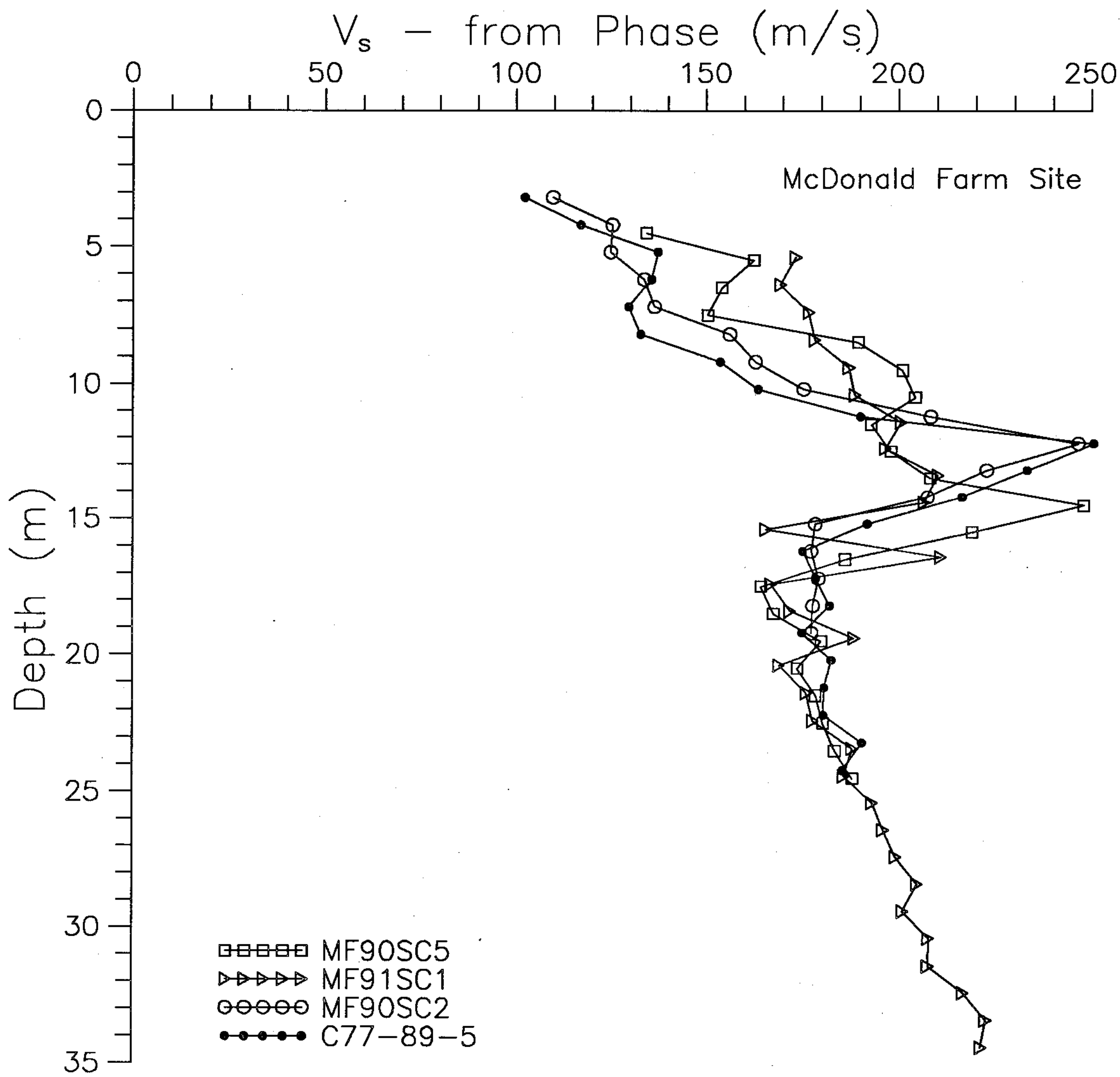


Fig.6.19 Phase Velocity Profiles – McDonald Farm Site

sense, a layer with lower average cone bearing had a lower average velocity, but comparisons over 1m depths ($V_s/q_c$ or $V_s^2/q_c$) did not improve the scatter in results.

Results for the Lower 232nd St. site are given in Fig.6.20. The SCPT marked as L289SC1 is near the north end of the test area, and the other two soundings are within a few metres of each other, about 20m to the south. The results for the latter two tests are very close (R=0.98), while the velocities for L289SC1 are generally about 10m/s higher.

Fig.6.21 presents the results of tests at the Annacis Island and Laing Bridge sites. Velocities for the two soundings at Annacis Island agreed closely (R=0.97), while the Laing Bridge gave somewhat higher velocities (about 0-50m/s).

In general the velocity measurements in adjacent soundings gave results that were close. With one exception, the correlation coefficients were 0.97 or greater. For the number of points used (12 to 17), this simply indicates that the signals are related with a confidence interval in excess of 99.95%. This does not imply that the measurements are the same, as the slopes of the correlation lines were 1.06, 0.95, and 1.17, not 1.0 as would be required for a perfect fit. The coefficients of variation for the slopes were 6.7%, 5.2%, and 8.0%, indicating a reasonably small scatter.

The rate of increase in the shear wave velocity was greater in the sands (about 12m/s/m) and less in the clays and silts (about 4m/s/m).

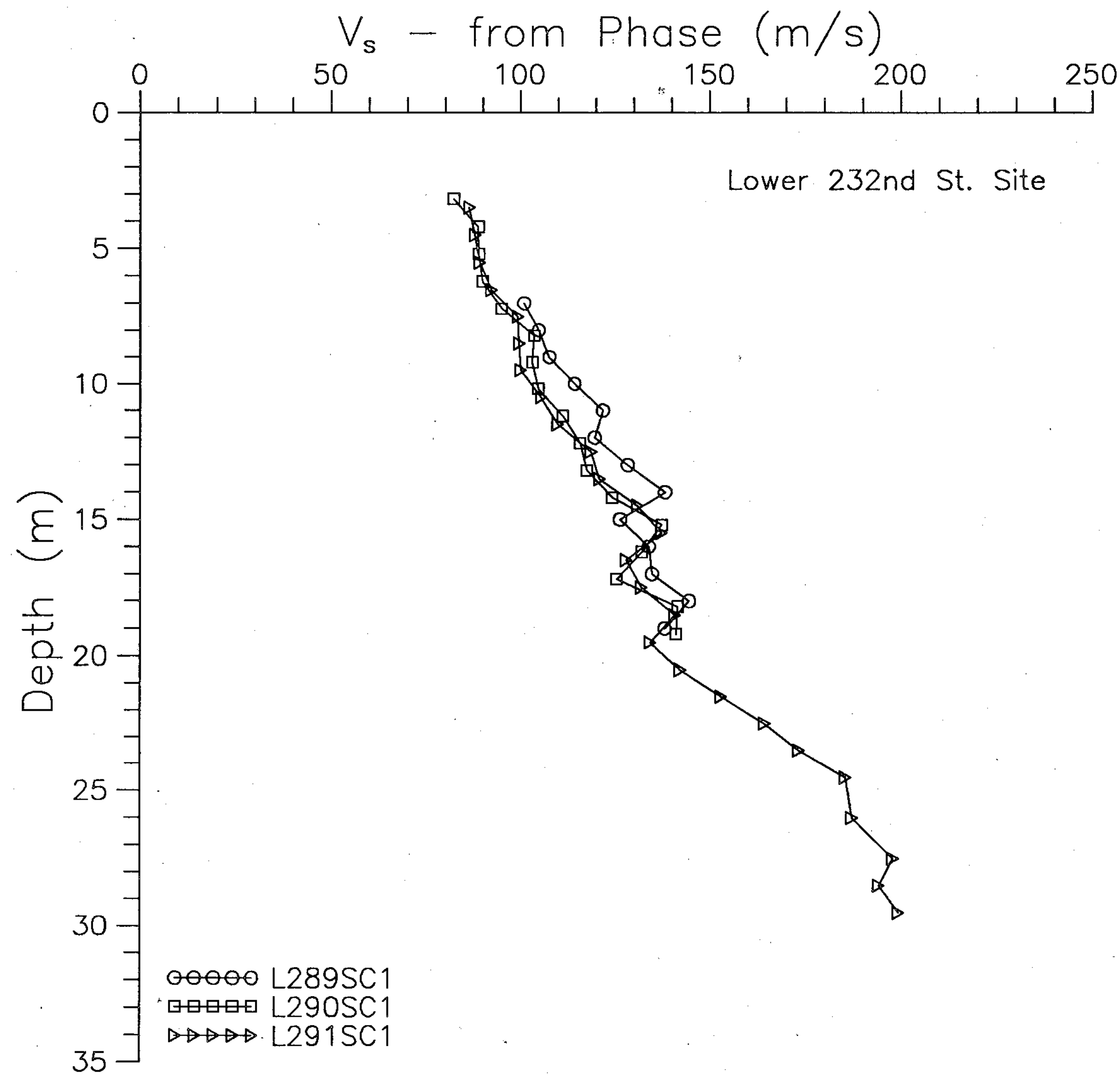


Fig.6.20 Phase Velocity Profiles − Lower 232nd St. Site

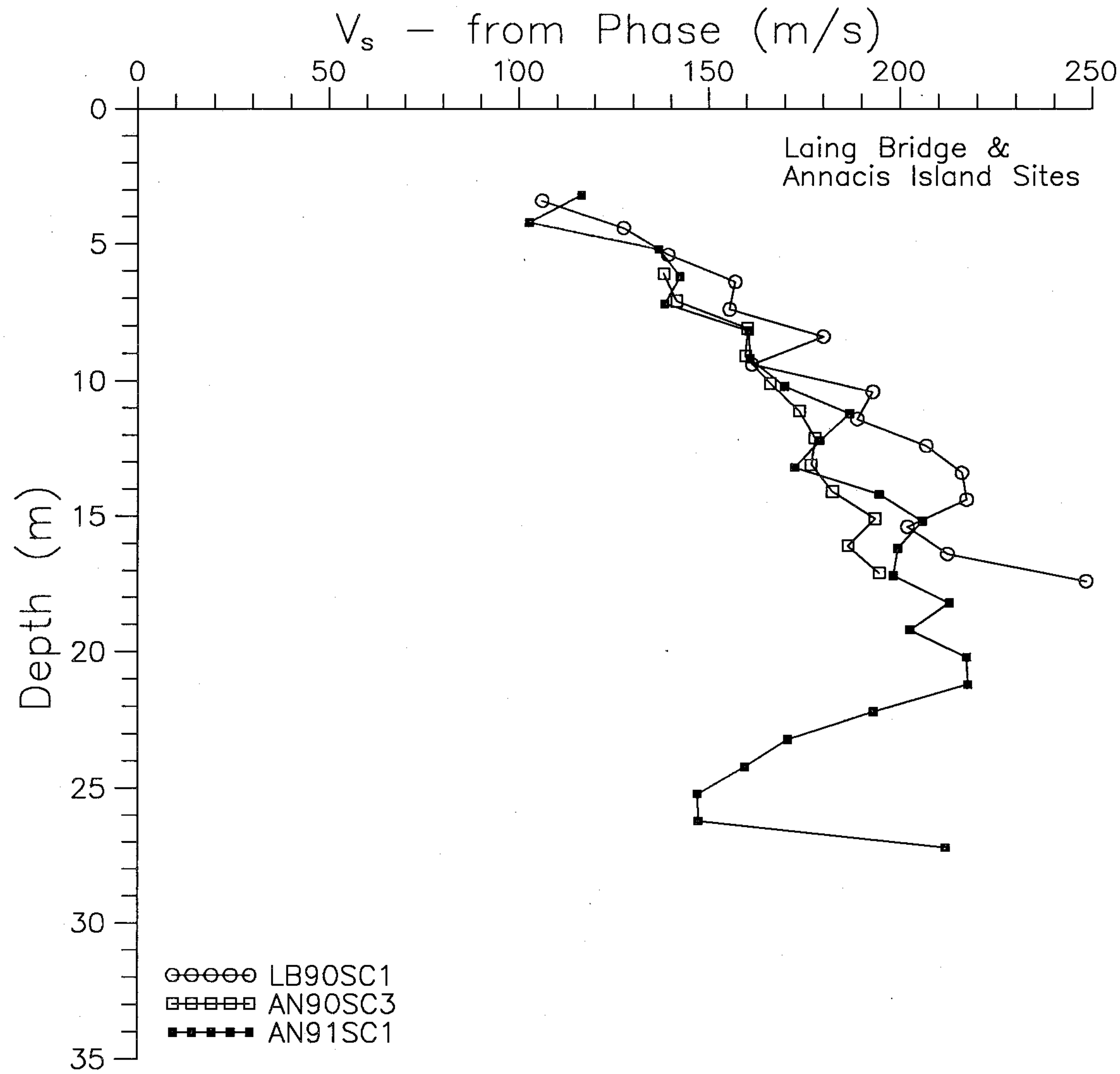


Fig.6.21 Phase Velocity Profiles – Annacis North Pier and Laing Bridge Sites

At the McDonald Farm site, the velocities decrease by about 75m/s to 85m/s at the base of the sand, followed by an increase in the silt.

### *6.4 SUMMARY OF VELOCITY DETERMINATION*

In general for "clean" signals, the shear wave velocity calculated by most methods will give similar results. For poorer signals, the recommended approach is to window the signals to isolate the main shear waves, then use the phase of the cross-spectrum method to obtain a plot of velocity versus frequency. Several plots over the depth of the sounding should be observed to select the frequency range for which the velocity is reasonably constant. The average velocity over the selected frequency range at each depth increment is the shear wave velocity for that increment.

Ray-path bending effects were investigated and it was found that differences in shear wave velocities were generally less than 3% whether or not ray-path bending was accounted for. For the balance of the results presented herein, ray-path bending effects were ignored.

Shear wave velocities from a total of ten SCPT's at four sites are presented. Tests within a few metres of each other generally gave highly repeatable results (correlation coefficient about 0.97), while tests at greater distances (20m to 140m) showed greater variation. Generally the velocities increased more rapidly in sand and less rapidly in clay and silt.

## CHAPTER 7

## DAMPING DETERMINATION - INSITU METHODS AND MEASUREMENTS

### *7.1 INTRODUCTION*

A portion of a typical suite of processed accelerometer records from a SCPT is shown in Fig.7.1. Repeatable hammer blows on a shear beam were the source for these records. The records are from SCPT MF90SC5 and have been windowed to isolate the first cycle of the shear wave. For clarity only seven selected signals at different depths have been shown. At this site the upper portion (about 3m to 15m depth) is primarily sand, and the lower portion (below about 17m) is primarily clayey silt. The signal peaks show a rapid attenuation in the shallow sands, and less rapid attenuation in the deeper silts. As discussed in Chapter 2 the attenuation is caused by both geometric effects and material damping, and the calculations discussed in this chapter must provide methods for separating these causes in order to measure the material damping.

Also discussed in Chapter 2 was the dependence of damping on strain level. Strains caused by the sources discussed in Chapter 5 are limited to relatively low strains. The peak strain levels, $\gamma_p$, caused by the shear waves can be calculated from the peak particle velocity, $V_m$, (calculated by integrating the accelerometer record) and the measured shear wave velocities, $V_s$, using the equation given by

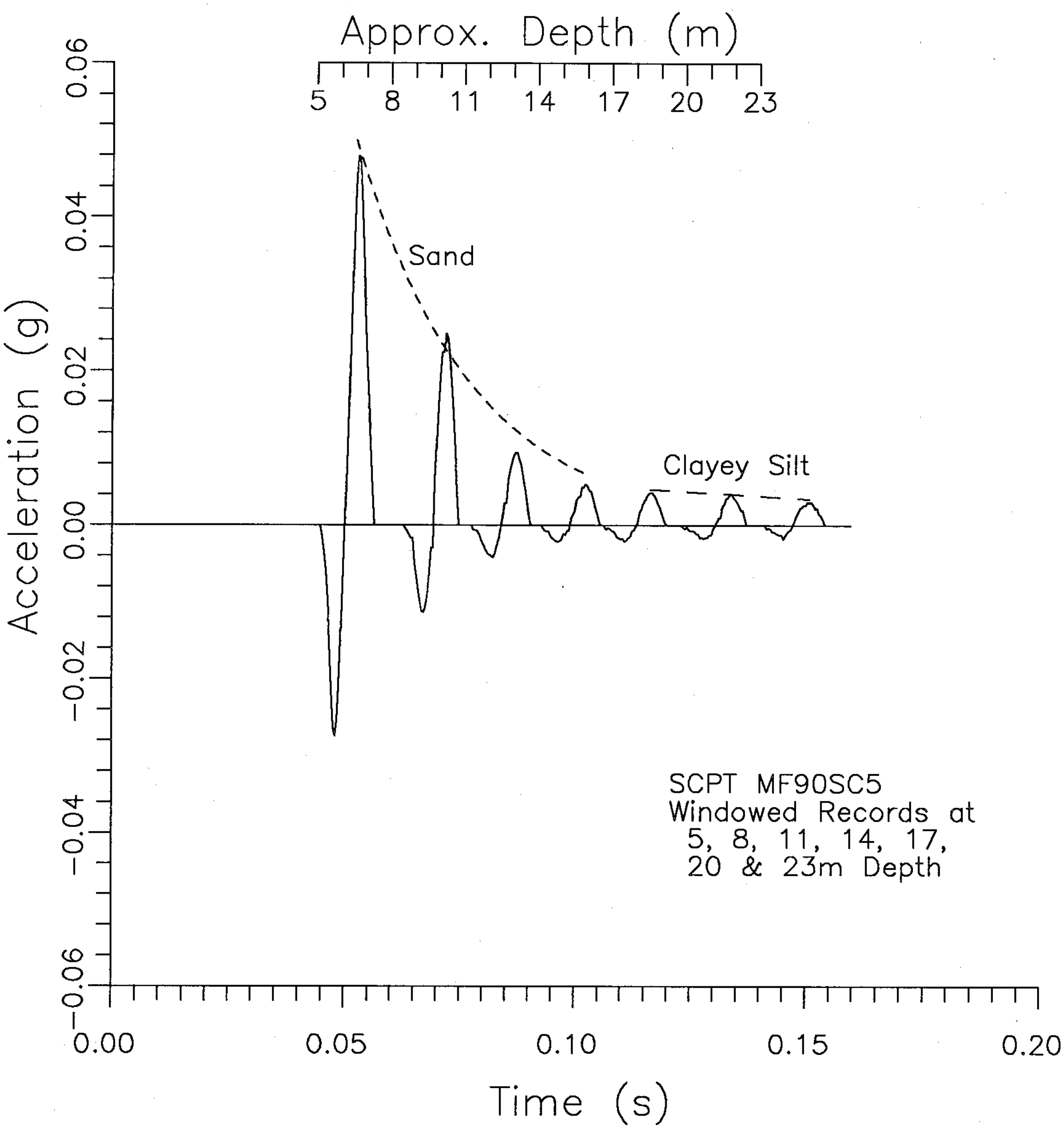


Fig.7.1 Portion (7 depths) of Suite of Processed Records (after Stewart and Campanella, 1991)

White(1965):

[7.1] $\gamma_p = V_m / V_s$

The relatively low peak strain levels calculated using eqn.7.1 decrease with depth, from about $2 \times 10^{-3}$% (clay site) and $6 \times 10^{-4}$% (sand sites) at 5m to about $5 \times 10^{-4}$% (clay site) and $3 \times 10^{-5}$% (sand and sand/silt sites) at 25m.

### *7.2 METHODS OF DAMPING CALCULATION*

A variety of methods have been proposed, mainly in the geophysical literature, to calculate damping from field measurements. Six methods of calculation are presented in this section. The first two methods are calculated in the time domain. The first is the rise-time method and the second is the random decrement approach. Neither of these methods could be successfully applied to the SCPT data.

Four separate methods of damping calculation in the frequency domain, based on the concepts given in Chapter 2, were fully evaluated as part of this study and are presented below. The first and last methods are variations of methods presented by others, and the other two were developed as part of this research. The first is the attenuation coefficient method, similar to the approach given by Mok et al (1988), the second is based on a modified version of the SHAKE program, the third is the damping spiral approach, and the fourth is the spectral slope method as used by Redpath and colleagues(1982,1986) and others (Kudo and Shima,1981, Meissner and Theilen, 1986). The first three are presented in the chronological order of their development and use. The spectral ratio method is presented last as it is the preferred method and will be used to analyze tests from all four sites.

In the downhole method used herein, the generated waves can be expected to pass through soil layers and the transmission and divergence effects described in Chapter 2 must be considered. It should be noted that in order to use all of the available data, it is necessary to calculate the damping on a metre by metre basis, and the corrections can only be calculated on the same basis. The shear wave velocity profile for SCPT MF90SC5 is given in Fig.7.2. Based on these velocities, the corrections for transmissivity and divergence were calculated using the program TRANSDIV given in appendix E. The results are presented in Fig.7.3 along with the combined effect of transmissivity & divergence and spherical spreading. It can be seen that the combined effect can be up to three times greater than the effect of spherical spreading alone, and therefore the effects of velocity variations must be considered.

### 7.2.1 Rise Time Method

A time-domain approach, the rise time method (RTM), was considered for calculating damping. Along with others, Redpath et al (1982) presented an equation for the method in terms of Q. Expressed in terms of $D_s$ the equation for this method becomes:

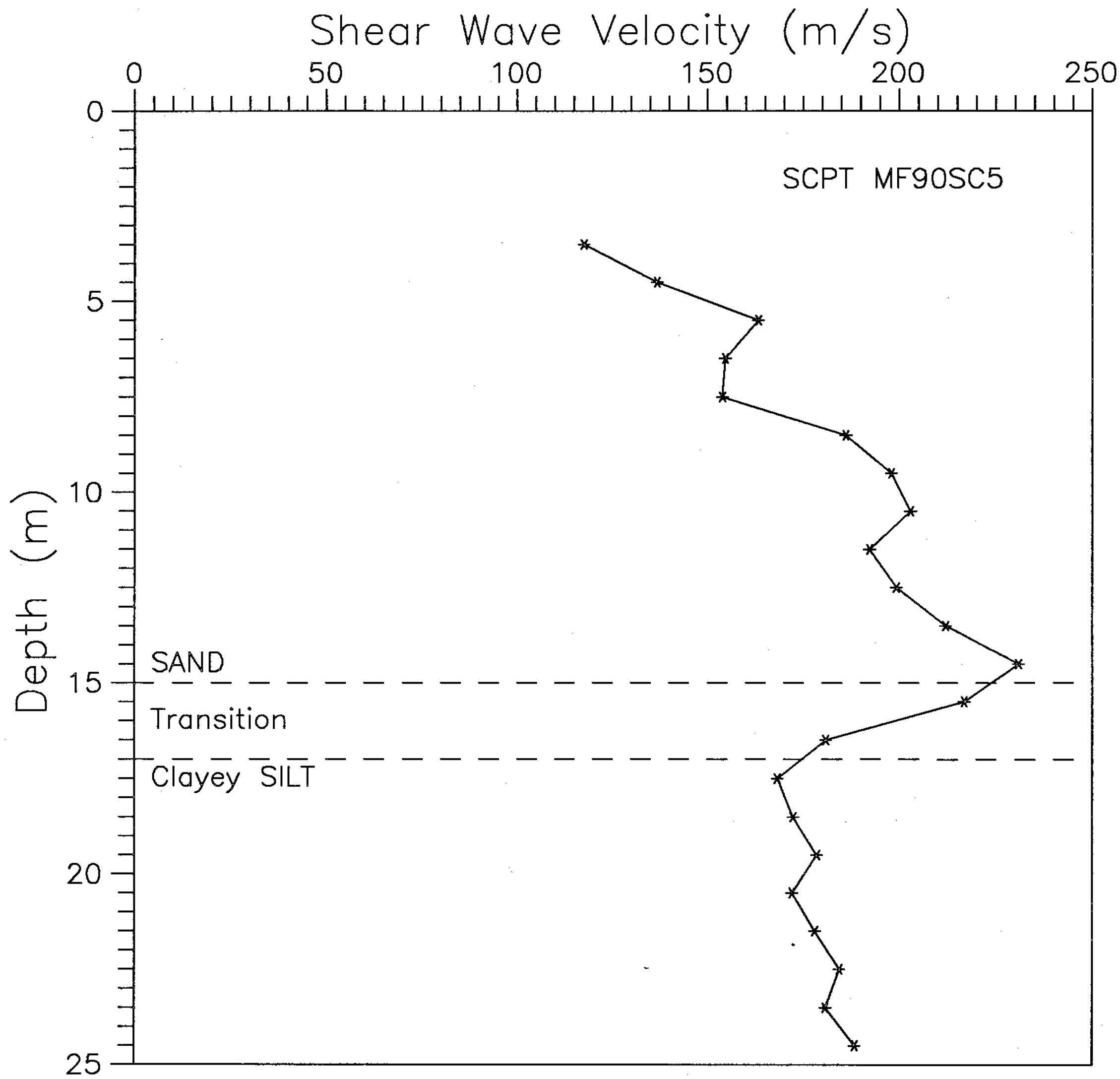


Fig.7.2 Shear Wave Velocity Profile for SCPT MF90SC5
(after Stewart and Campanella, 1991)

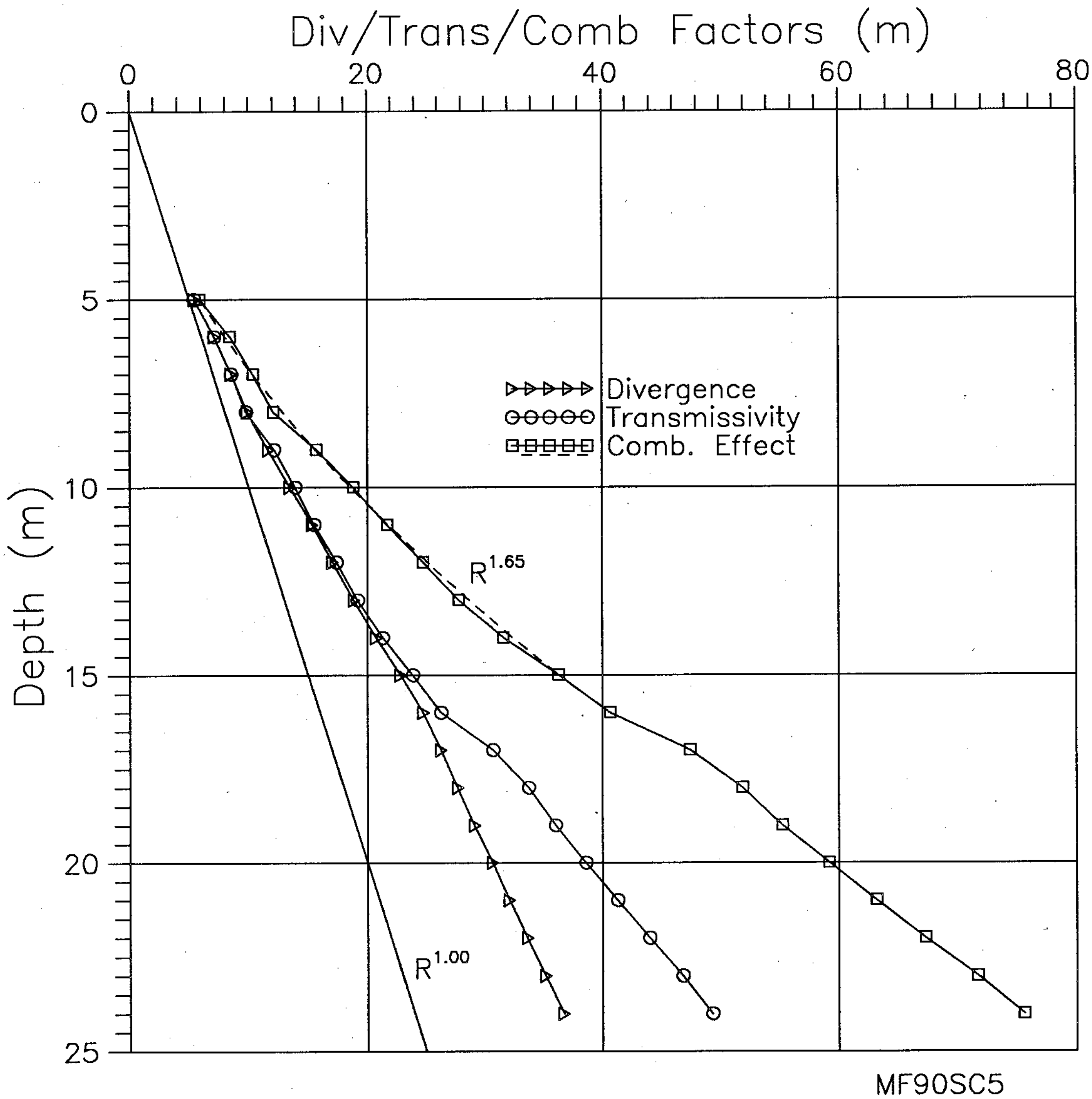


Fig.7.3 Amplitude Correction Factors based on Velocity Profile for SCPT MF90SC5 (after Stewart and Campanella, 1991)

[7.2] $t = t_o + 2CT*D_s$

where: $t$ = rise time (time to reach first peak)

$t_o$ = rise time at source

$C$ = a constant

$T$ = travel (arrival) time

$D_s$ = damping

If the rise time is plotted versus the travel time, the slope of the resulting line should be $2CD_s$. One of the major problems in using this method is the value of C. Burkhardt et al (1986) quote values of 0.1 to 0.485 from numerical studies and 0.13 to 0.59 from laboratory studies. Redpath et al (1982) point out that the 'constant' C may be a function of damping.

Other terms in the equation can also present difficulties. Section 6.1 discussed some problems with measuring arrival times. As well the rise time can be defined in a variety of ways and can be difficult to estimate as signals become noisy. Fig. 7.4 shows a portion of a signal around the first peak. Redpath et al (1982) define the rise time as the time required to move from the minimum (pre-arrival) level to the peak, along a best-fit line through the 'steepest portion' of the rise (time a). However other definitions could be used. We can define values at 10% of the rise, 50% of the rise, and 90% of the rise. The program VU-POINT has a waveform function that provides these values for a specified interval of a signal. An example is provided in Fig.7.5. Thus we could also define the rise time in Fig.7.4 along a best-fit line

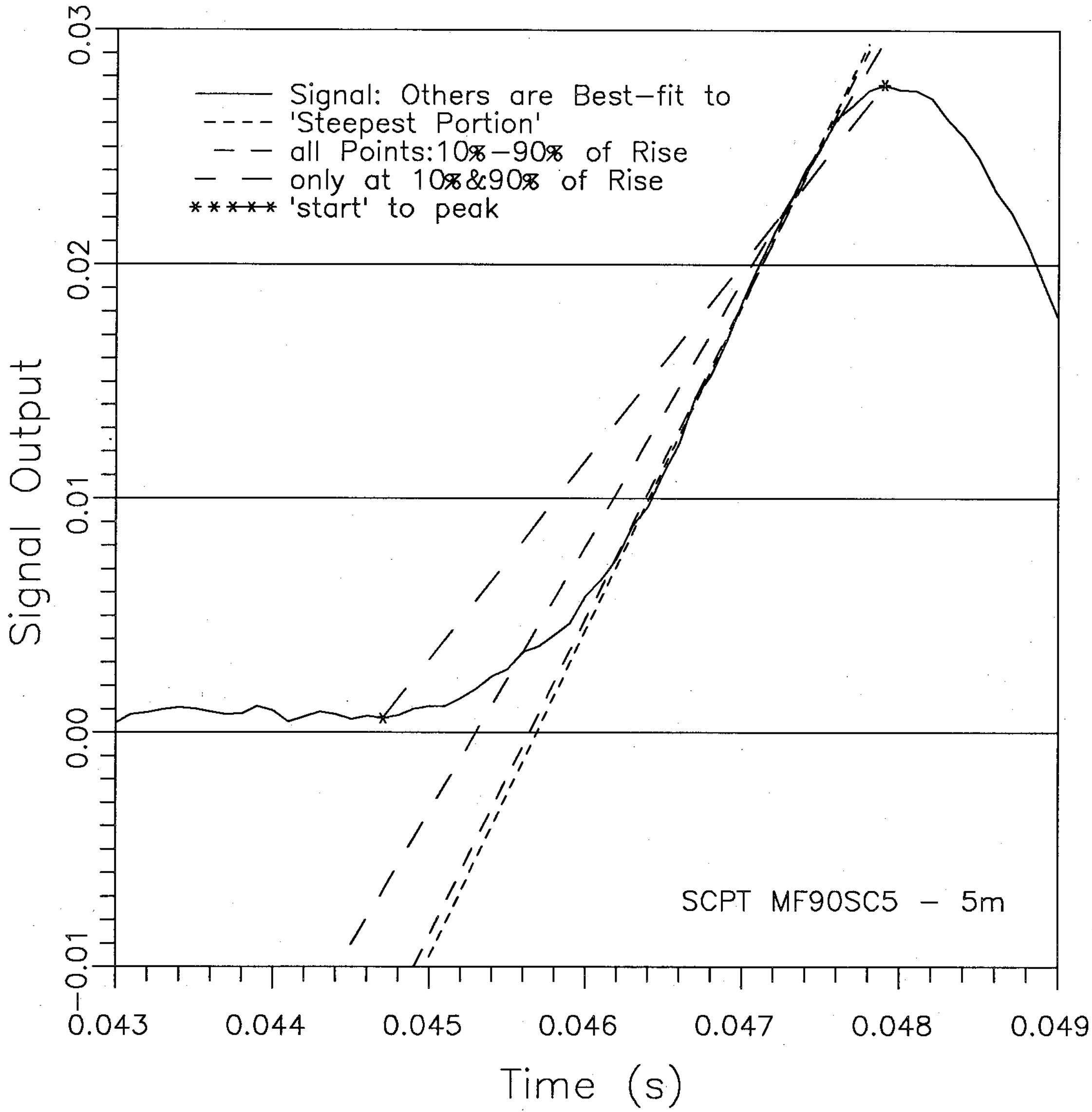


Fig.7.4 Various Definitions of Rise Time

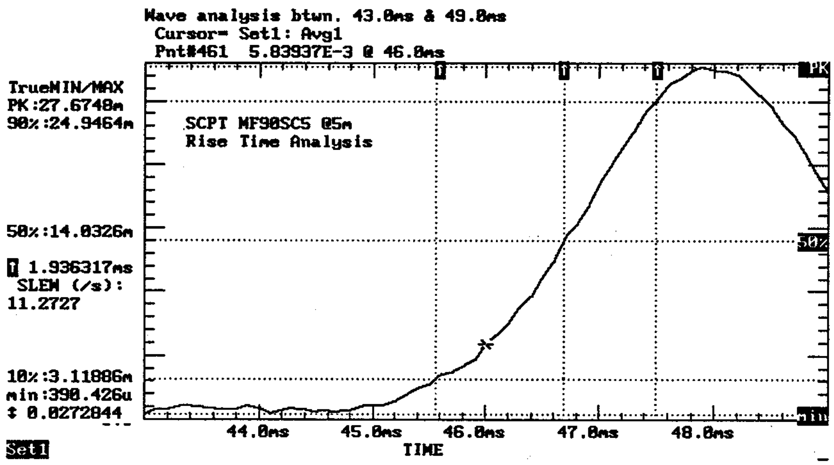


Fig.7.5 Rise Time Analysis using VU–POINT

to all the points between the 10% and 90% values (time b), or along a line between the 10% and 90% values only (time c). This is the method which the waveform function uses to calculate the 'slew' which is the slope of the line between the 10% and 90% points. From Fig.7.5, the rise time can be calculated from the minimum-peak value (0.0272844) given at the bottom of the left column of values divided by the slew (11.2727). Finally the rise time could be measured as the arrival to peak time (time d). For this particular signal, the calculated rise times are 1.85ms, 2.0ms, 2.42ms, and 5.2ms. Neglecting the last value, these times only differ by about 30%. Considering the wide range in the value of C, the range in the rise times are small. For convenience, rise times were calculated by method c, using VU-POINT.

Calculations were carried out for signals measured during SCPT MF90SC5 in the upper sand layer (6m to 13m) and are presented in Fig.7.6. Using the unfiltered signals, the calculations gave a slope of 0.0788 with a coefficient of variation (C. of V.) of 16%, indicating a reasonably small scatter. Assuming a C-value of 0.485 gives $D_s$ of 8.1%, which is somewhat higher than the laboratory values given in Table 2.1. It can also be seen that if the lowest suggested value of C (0.1) is used the damping increases to almost 40%. The signals were then filtered with a low-pass filter of 200Hz and reanalyzed. This reduced the scatter (C. of V.=11.9%) and the calculated value of damping (2.7%). Thus the filtering reduced the calculated $D_s$ by a factor of 3.

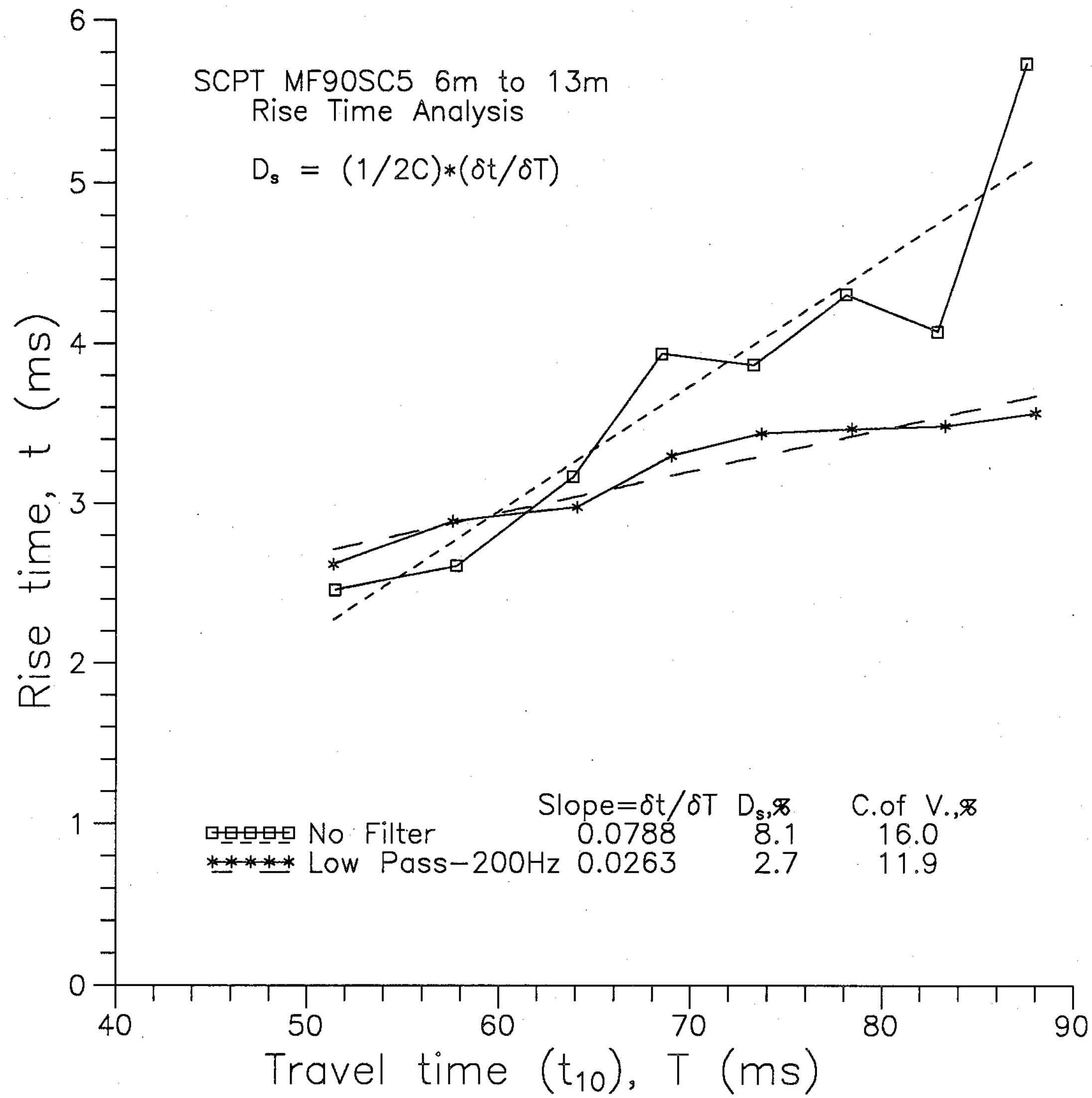


Fig.7.6 Rise Time Analysis– SCPT MF90SC5 – Unfiltered and Filtered

Another sounding at the same site (MF91SC1) was analyzed in the same manner and the results are presented, along with the previous results, in Fig.7.7. The calculated slope is actually slightly negative for this latter case. This finding indicates that the method is not repeatable at this site.

Several authors have indicated problems in using the rise-time method. Burkhardt et al (1986) state that "the scatter of calculated $Q_{eff}$-values (damping) is generally larger for the RTM than for any other method." Redpath et al (1982) used a theoretical value of 0.485 for C and found that the calculated values were 2 to 3 times lower for the RTM method,compared with other methods of calculation. They concluded that "estimates of damping based on rise times will be low for lossy materials (soils - with high damping compared to rock)." Anderson and Reinke (1989) also observed that "...the highest measurement error resulted from the rise time (Q=13 +/- 54%) and the pulse broadening (Q=10 +/- 55%) techniques." Based on the calculations presented above and these observations by others it was concluded that the RTM should not be pursued.

### 7.2.2 Random Decrement Method

Aggour and his colleagues (1982a,b) publicized the random decrement technique to calculate damping. The basic concept of the random decrement approach was discussed in section 3.3, and a detailed analysis of the method is presented in Appendix B. Calculations were

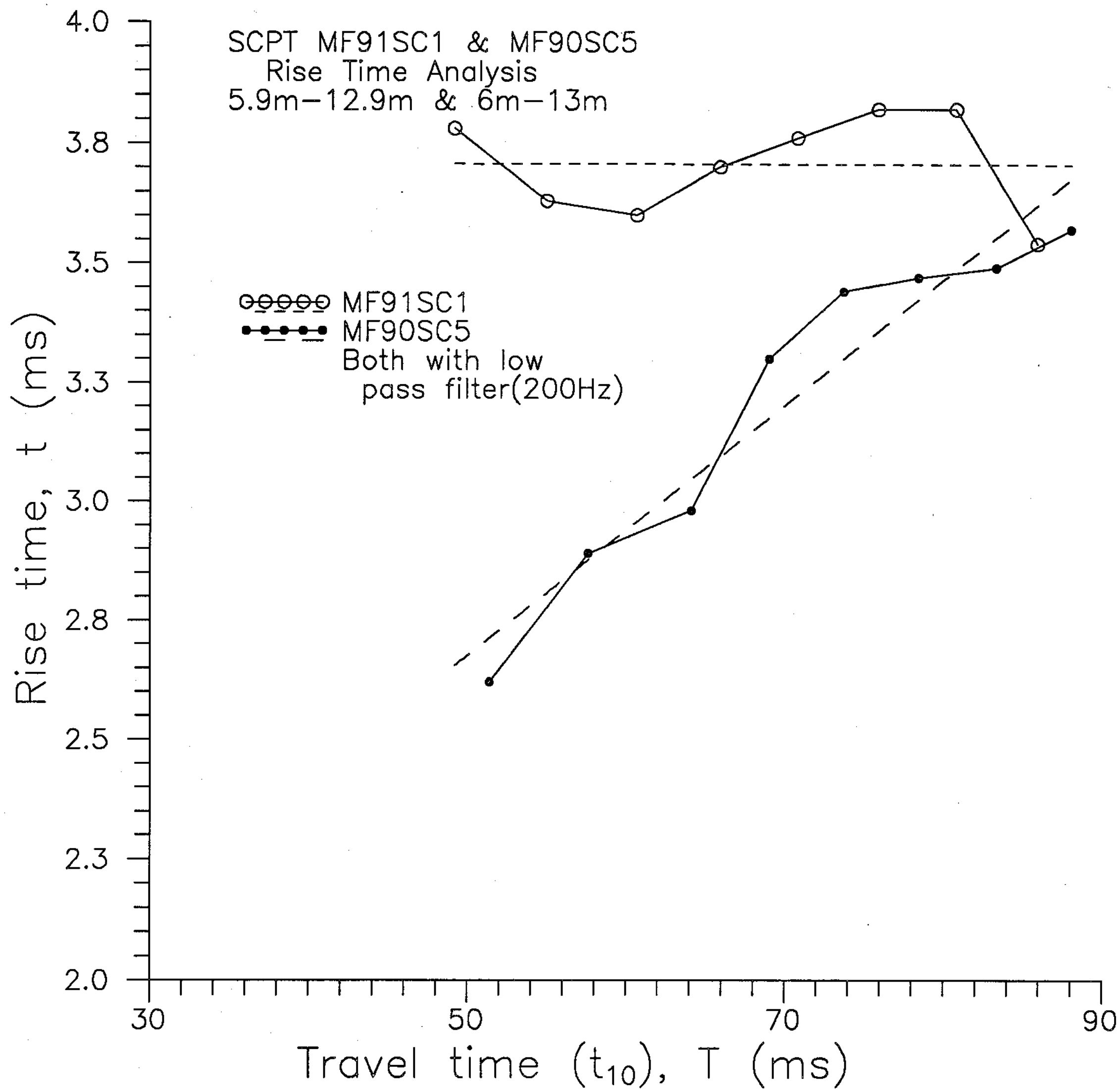


Fig.7.7 Rise Time Analysis – Two Soundings at McDonald Farm Site

carried out using the program RANDEC given in Appendix E. It was found that the calculated damping varied significantly with the degree of filtering (about 2% to 17%) and the number of cycles included in the calculation (about 3% to 30%) The method as proposed seems to incorporate system damping as well as material damping since a single record is analyzed. In an attempt to reduce or remove the effects of the measuring system, the method was applied to the inverse FFT of the ratio of the FFT's at differing depths, but this approach also gave a wide range of damping. It was concluded that this method also gives highly variable results and should not be pursued.

### 7.2.3 Attenuation Coefficient ($\alpha$) Method

This method makes use of eqn.2.24 which Mok et al (1988) used directly. However, they were using a crosshole technique and the generated waves were unlikely to encounter interfaces between layers of soil (although the method would be affected by nearby layers of high velocity). As indicated above for the SCPT method, the generated waves can be expected to pass through soil layers and the transmission and divergence effects must be considered. It will be assumed that only one interface (amplitude change) occurs within each interval, for one set of calculations, and that no interfaces occur (no correction) for a second set of calculations. The results of one calculation are shown in Fig.7.8, and show a slight decline in damping with frequency (about 0.01%/Hz) over the selected frequency range of 40 to 100Hz and a value

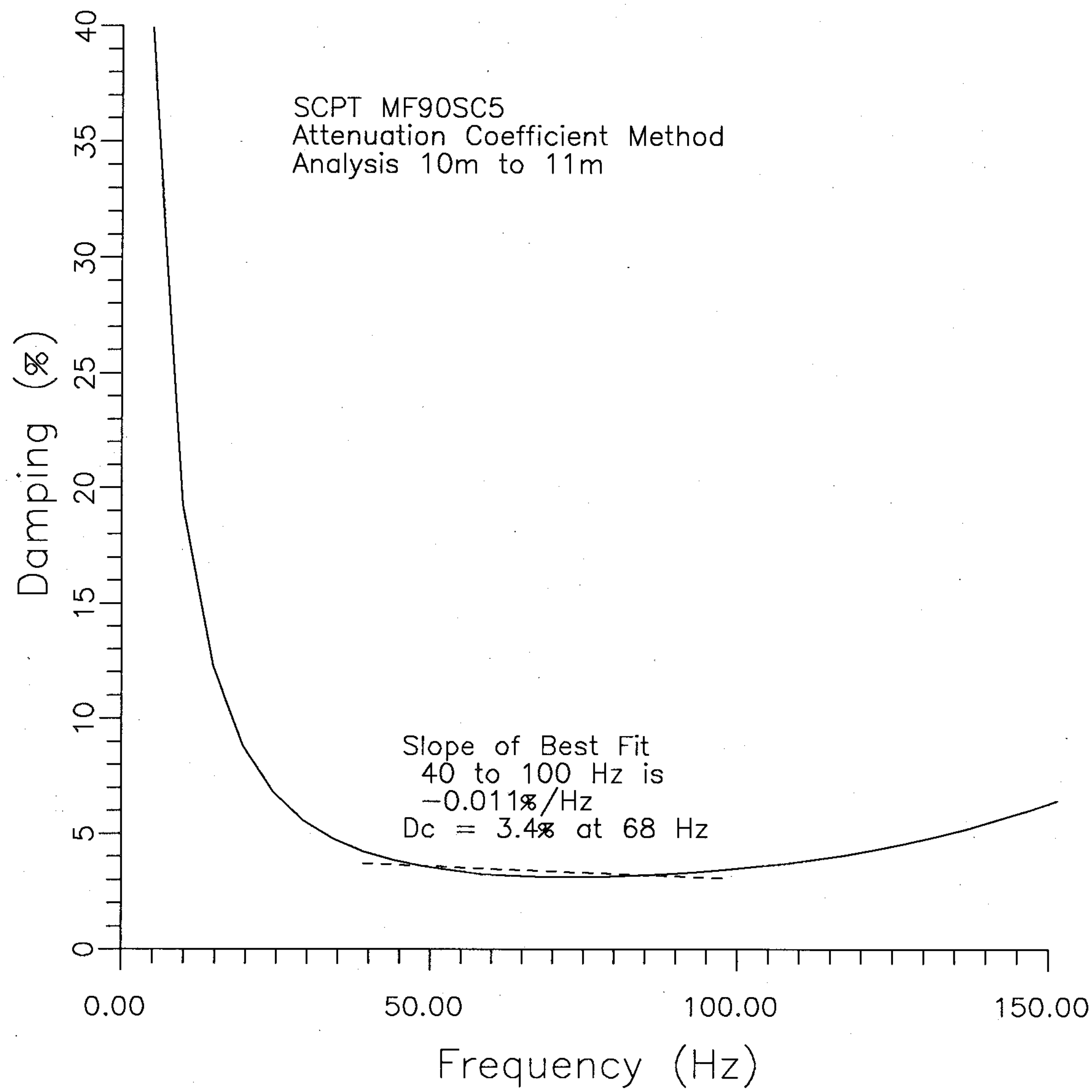


Fig.7.8 Damping by Attenuation Coefficient Method for 10m−11m Interval ( after Stewart and Campanella, 1991)

of 3.4% at the middle of this range. Calculations at other depths showed that the damping variation with frequency could be positive or negative. Results for a series of depths are shown in Fig.7.9, and indicate a large scatter in damping values (-7.6% to 7.0%), with a mean of 3.3% in the upper sands and -1.1% in the lower silts. The results also suggest a fairly constant average value with depth in the upper portion and an increase with depth in the lower portion. Also shown in Fig.7.9 is the effect of ignoring the transmission/divergence corrections which increases the damping values throughout the sounding with larger increases in the sand. It would appear that, if the transmission/ divergence corrections are included in the upper sand, but neglected in the lower silts, the resulting damping values are somewhat closer to the expected values.

The difficulty of applying the interface corrections, the very wide scatter in the results, and the negative values in the clayey silt, makes the attenuation coefficient method of little use to measure material damping insitu using downhole or SCPT methods. Although the sources of the scatter cannot be clearly identified, it is likely that geometric effects due to soil layering, which cannot be fully accounted for, are a major cause.

**7.2.4 Modified SHAKE Method**

This second frequency-domain method to calculate damping from insitu measurements is based on a modified version of the SHAKE program.

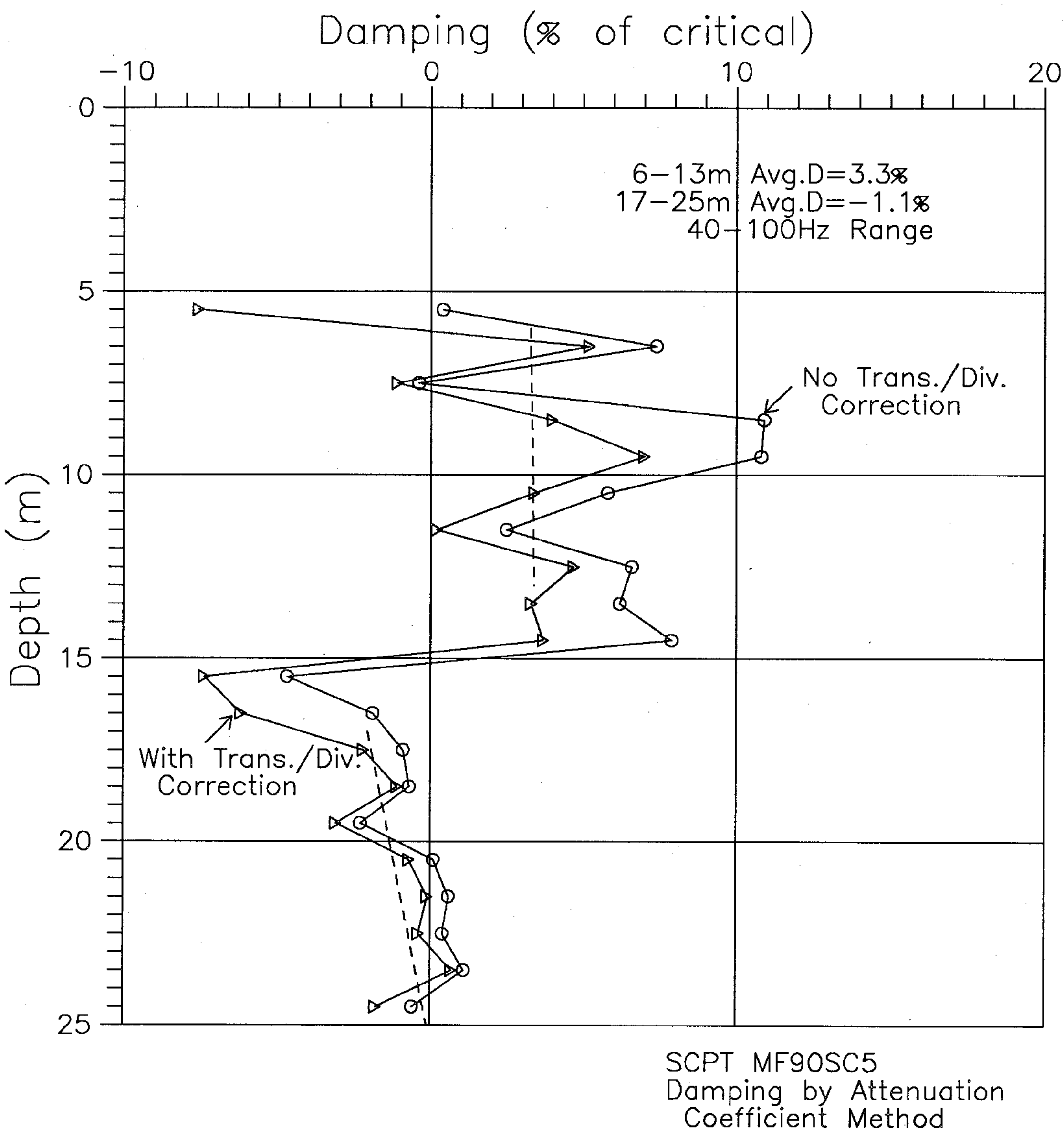


Fig.7.9 Damping by Attenuation Coefficient Method over Seismic Cone Profile (after Stewart and Campanella, 1991)

The original program was designed primarily to model earthquake motions moving upward from bedrock (Schnabel et al, 1972). The program does allow input of motions at an intermediate level in the soil, but the wave then spreads both up and down. In order to model the downhole tests, it was necessary to force the wave to propagate only downwards. This can be done by setting the coefficient E in eqn.2.26 equal to zero. In order to model the spherical wave in a layered soil, it was also necessary to make transmission and divergence corrections as in the first method. The value of damping is first estimated, and the acceleration response from the program is compared to the observed acceleration record at the greater depth. The damping is then adjusted to give a "best-fit" between the calculated and observed records.

Fig.7.10 shows the result of calculations between depths of 10 and 11 metres, using a low-pass filter of 100Hz on the recorded data. For this depth a damping of 5.5% was required to match the calculated peak to the measured peak. The results of a series of calculations for one seismic cone profile is shown in Fig.7.11. There is again a wide scatter in the results, especially in the upper sands, with negative values in the lower silts. The results suggest an increase in damping with depth in both the sands and silts. Calculations were also made for this method ignoring the transmission/ divergence corrections and these gave changes very similar to the first method. Again the sources of the scatter cannot be clearly identified, but it would seem that geometric effects due to soil layering, which cannot be fully accounted for, are a

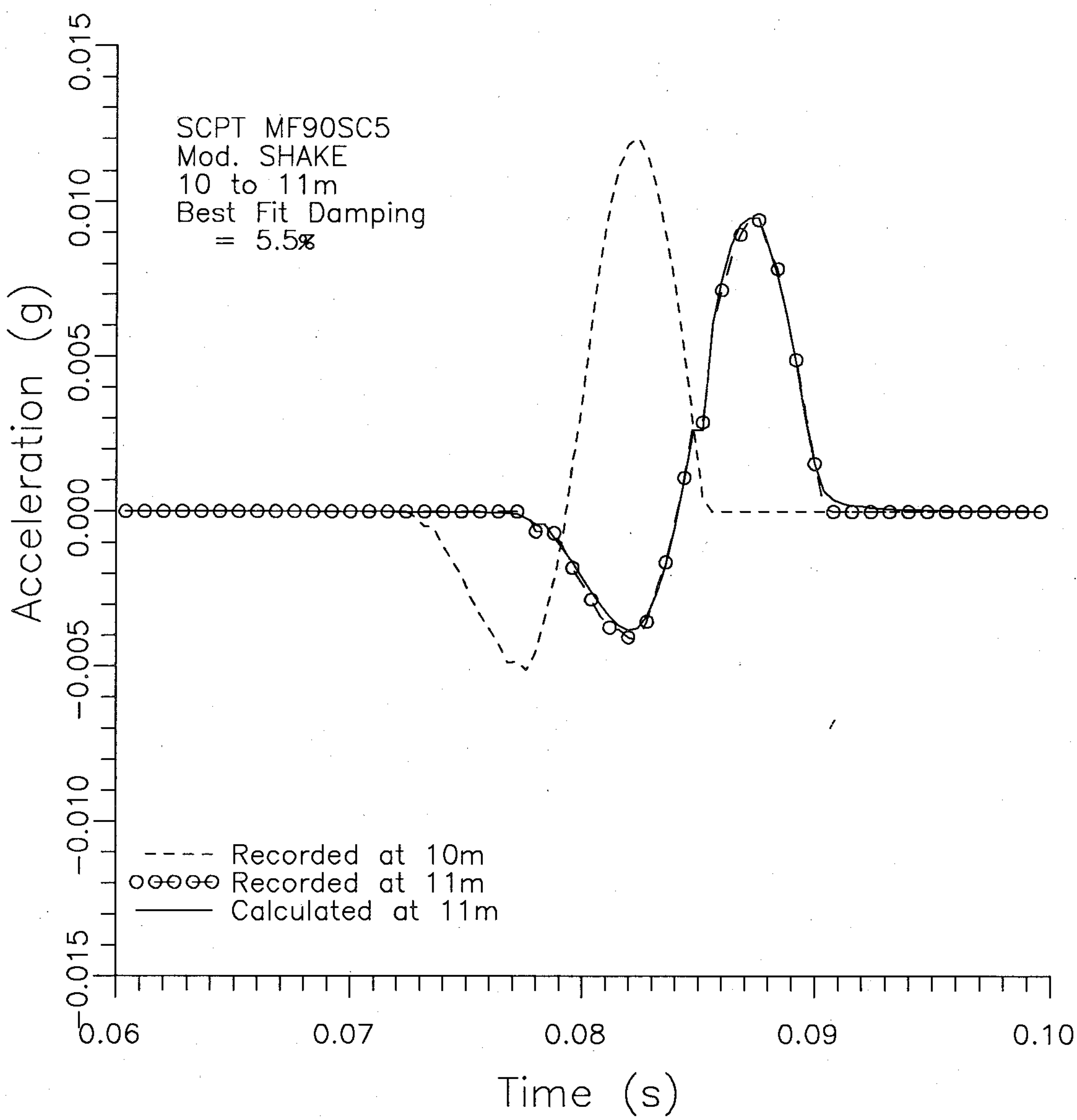


Fig.7.10 Damping by Modified SHAKE Method for 10m−11m Interval (after Stewart and Campanella, 1991)

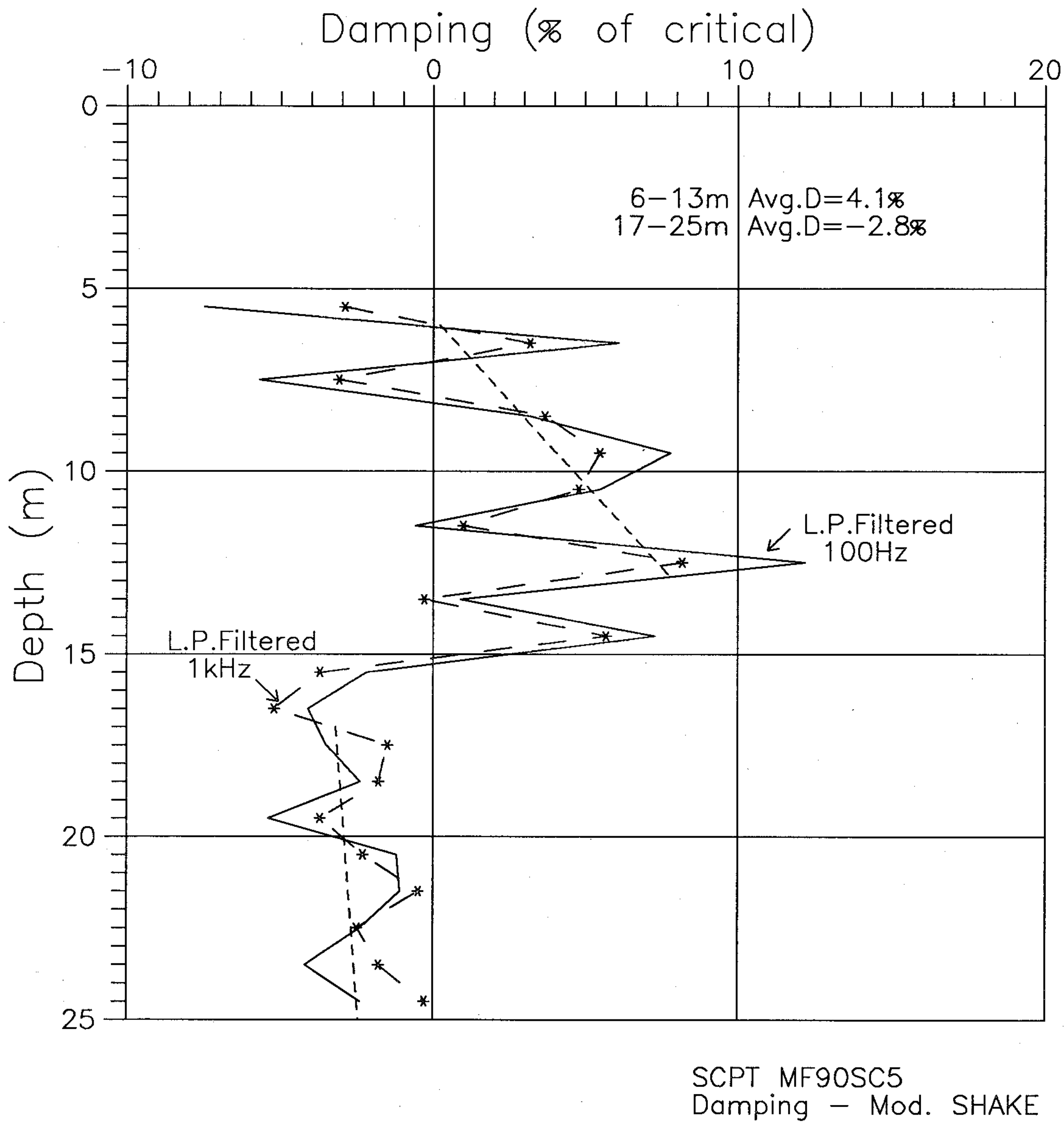


Fig.7.11 Damping by Modified SHAKE Method over Seismic Cone Profile (after Stewart and Campanella, 1991)

major cause. Also shown on Fig.7.11 are the results from a series of calculations with essentially no filtering of the signal (1000 Hz low pass filter). The trend of the results is very similar, but the scatter was reduced. Possibly the 100Hz low-pass filter has removed slightly too much of the signals. At any rate the scatter is unacceptable for either filter.

This method was found to be very time-consuming, compared to the other methods. The signals first had to be converted to the format required for the SHAKE program, then iteration of the damping values was performed. The other three methods were written into "macros" with the program VU-POINT which can read the signals directly as collected.

As for the $\alpha$ method, the difficulty of applying the interface corrections and the wide scatter in the results, including negative values, makes the modified SHAKE method of little use to measure material damping insitu using downhole or SCPT methods.

### 7.2.5 Damping Spiral Method

The damping spiral method is based on using the full complex expression for the wave equation as given in eqns. 2.33 or 2.34. The approach was developed from the modal circle method which is based on measurements at a fixed point, whereas the damping spiral uses measurements at two points separated by a fixed distance. The equations are repeated here:

[7.3] $$\frac{A_2}{A_1} = \frac{x_1}{x_2} e^{-(D\omega/c)(x2-x1)} e^{(i\omega/c)(x2-x1)}$$

or:

[7.4] $$\frac{A_2}{A_1} = \frac{x_1}{x_2} e^{-(D\omega/c)(x2-x1)} [\mathrm{COS}((\omega/c)\{x_2-x_1\}) + i\,\mathrm{SIN}((\omega/c)\{x_2-x_1\})]$$

When this equation is plotted in a Nyquist diagram (Imaginary part as a function of Real part), it is the equation of a spiral. The magnitude at zero frequency is given by the geometric spreading ($x_1/x_2$). This factor could also include other frequency-independent terms such as transmissivity and divergence of spherical waves. The rate of spiraling with frequency is $(D/c)(x_2-x_1)$. For a given set of signals, the distance is fixed, and over a suitable frequency range, the velocity is constant. Therefore, the rate of spiralling is determined by the damping.

A simple program was written to calculate eqn.7.4 at a number of points of varying frequency, for the given parameters of $x_1$, $x_2$, and c and for values of D varied to provide a match with the data (see program RIMSPIRL in Appendix E). The other factor that can be adjusted in the analysis is the geometric spreading (including transmissivity and divergence effects). This can be accomplished by a simple factor multiplying the $x_1/x_2$ ratio that has been termed the T&D correction. If the usable measured data extended down to zero Hz, this factor could be calculated directly. However, the usable data typically extends down to about 20Hz, so it is necessary to calculate the spiral for a given damping and then adjust the T&D factor to provide a match at the start of the usable spiral.

If signals separated by several metres (say 7m as in the following examples) are considered, the nature of the spiral is more clearly demonstrated, and the fit of the calculated and measured spirals can be more easily assessed. Fig.7.12 shows the data from tests at depths of 6 and 13m in the upper sand. It can be noted that a considerable T&D correction was required for the sand layers (expressed as 0.51 or almost a factor of 2). For Fig. 7.12, damping of 2% was assumed and it can be seen that the model does not spiral in at quite as fast a rate as the field data. Another calculation was done with a damping value of 2.2% and it can be seen in Fig.7.13 that this value gave a better match. Fig. 7.14 gives the results of a calculation from 17 to 24m with a damping value of 0.6%. Since the amount of damping is so small, the noise in the data makes a comparison difficult, but the model seems to be in fairly reasonable agreement.

The method of calculation used above clearly shows the spiral nature of the data but requires iteration of the damping and T&D correction values. These values can be calculated directly by separating the phase and magnitude of the ratio, and fitting lines to the separate curves. The phase curve gives the velocity, and the negative of the natural logarithm (-ln) of the magnitude curve gives both the geometric correction (intercept) and the damping (slope). The

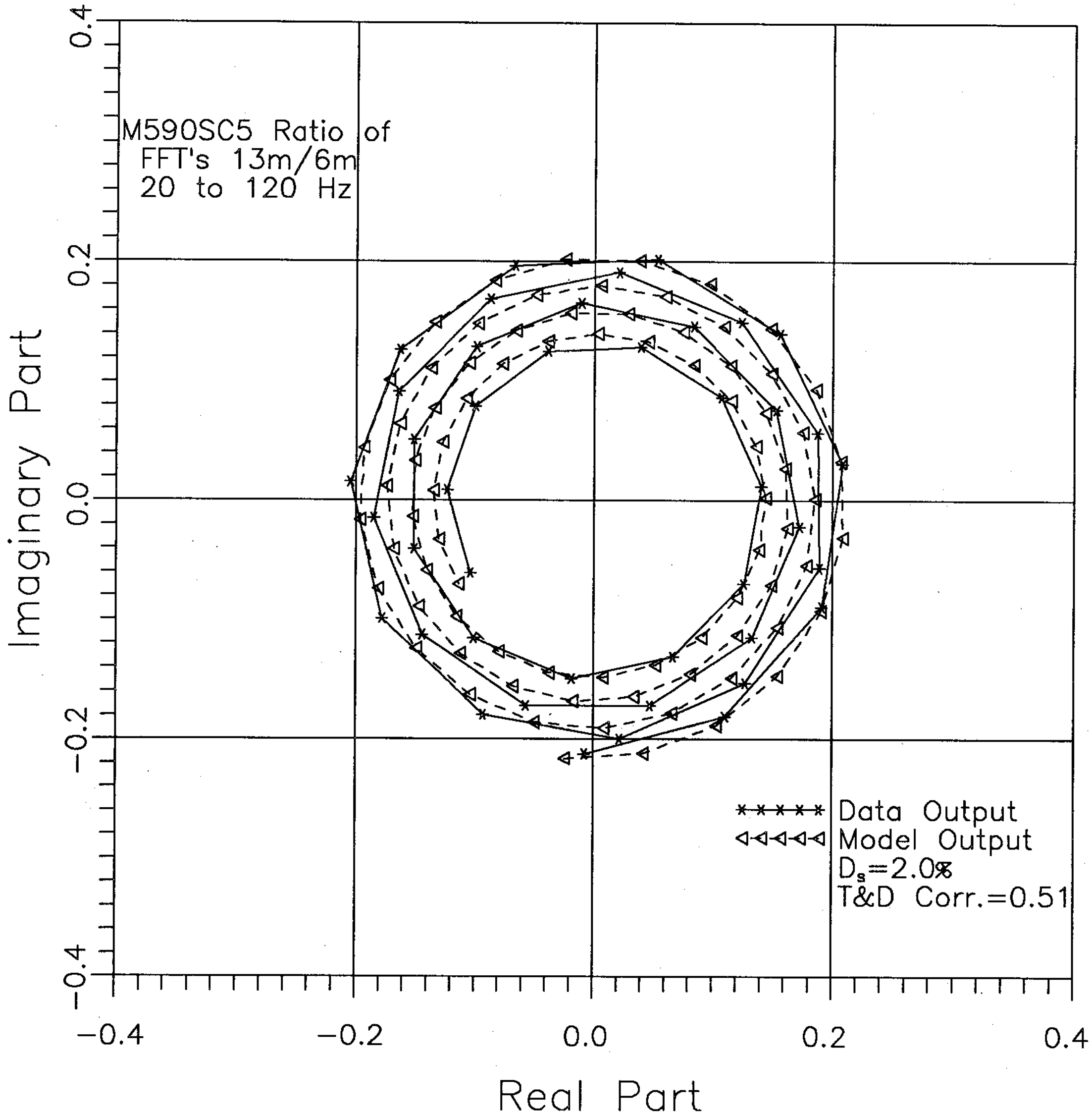


Fig.7.12 Damping by Damping Spiral Method for 6m–13m Interval – 2% Damping

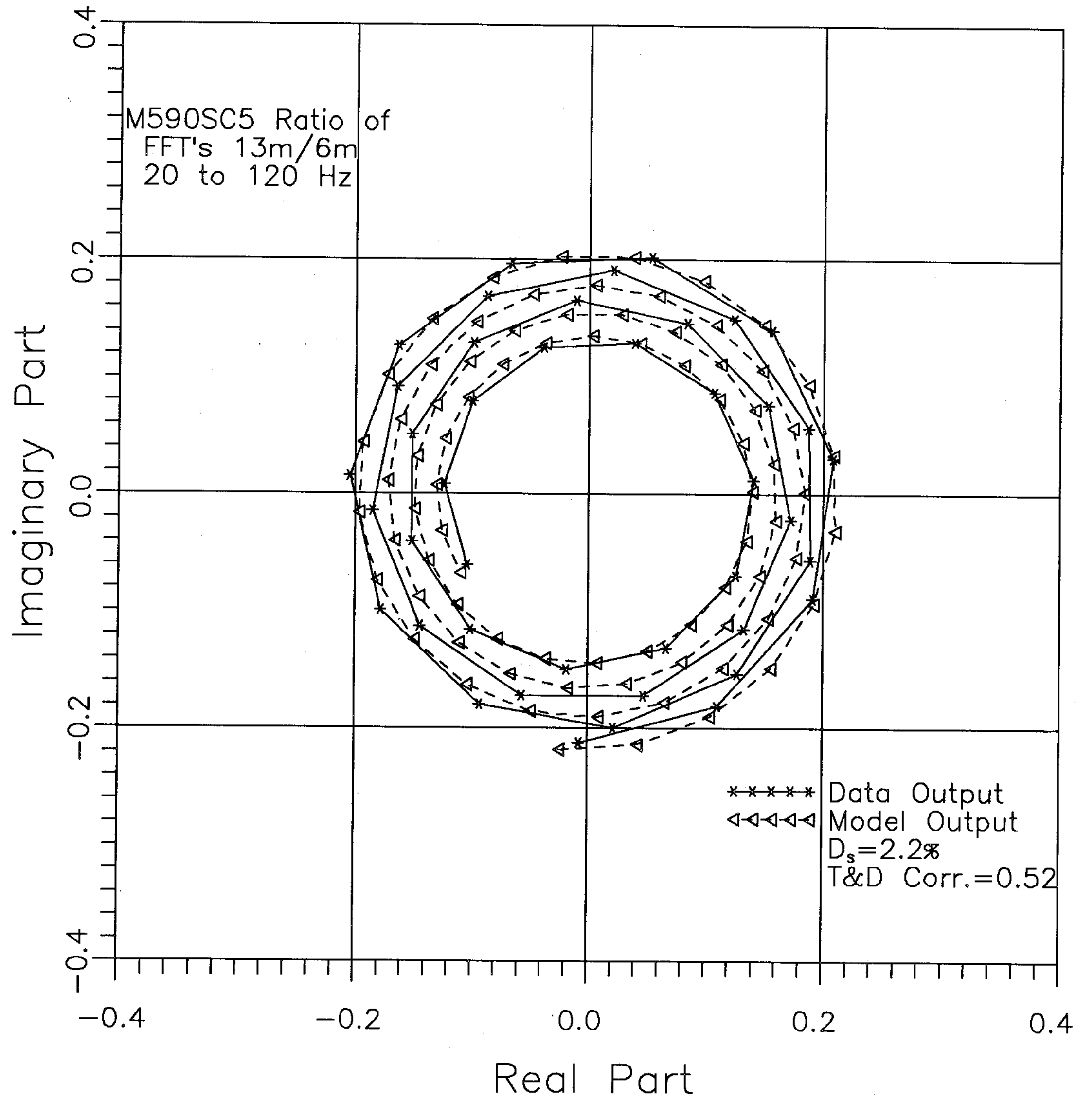


Fig.7.13 Damping by Damping Spiral Method for 6m–13m Interval – 2.2% Damping

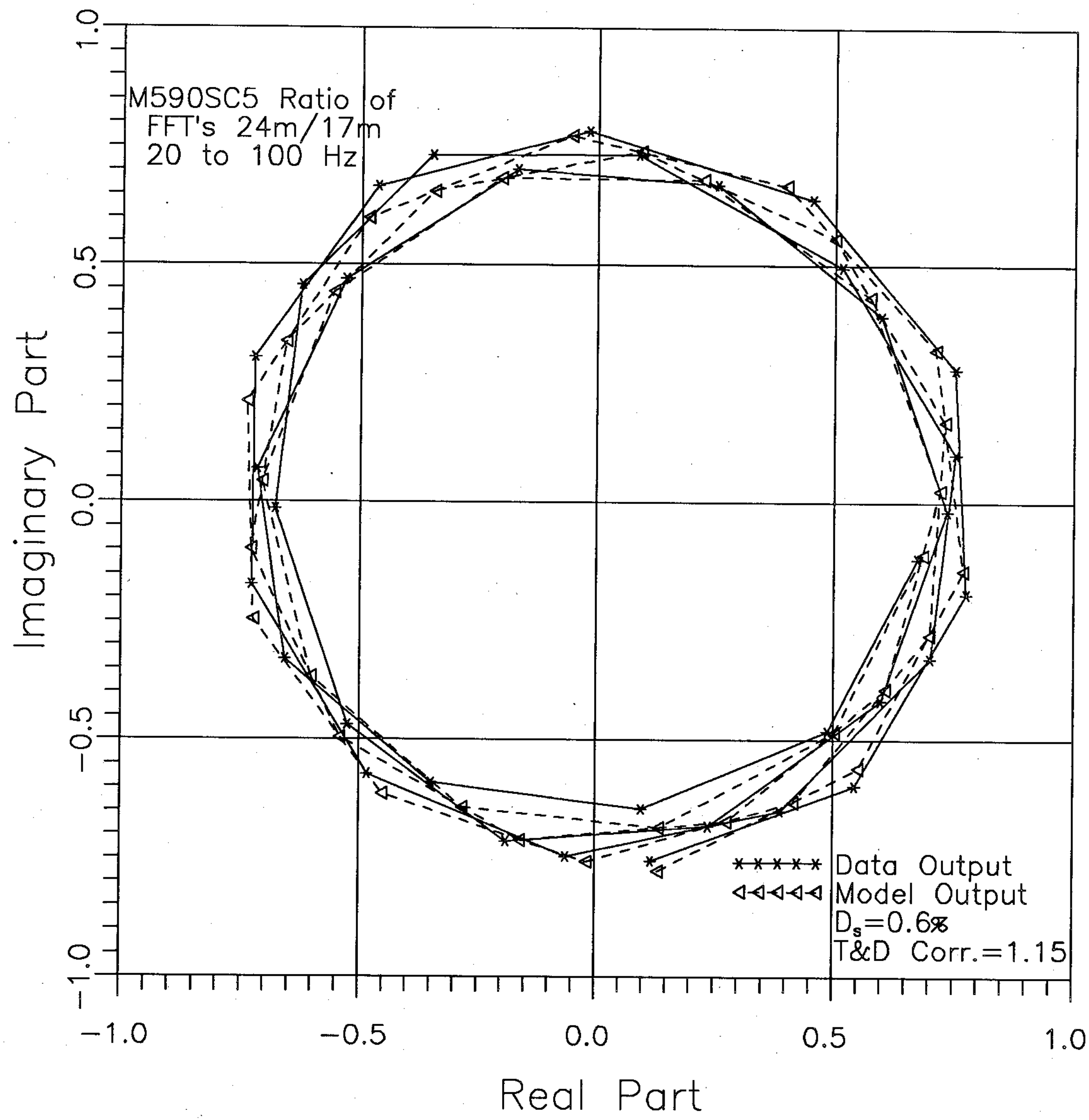


Fig.7.14 Damping by Damping Spiral Method for 17m−24m Interval − 0.64% Damping

final values used above were calculated in this way. The geometric corrections are discussed in greater detail in section 7.8.

Following the approach for the first two frequency domain methods, damping values were calculated on a metre-by-metre basis and the results are presented in Fig.7.15. The scatter in the results is considerably less than in the first two methods (less than half the range in values). The average damping in the sand is less than for the previous methods at 2.3% and is slightly higher than typical laboratory values (0.5-2%). The average value is larger (and positive) in the silt at 0.5%, although some of the intermediate calculated values are slightly negative. These negative values are likely caused by the scatter around the small measured damping value.

The damping spiral method is clearly the best of the first three frequency domain methods. The spectral ratio slope method discussed below is essentially a variation of the damping spiral method, with the advantages that the method is simpler and all of the signals measured in a layer are used for the calculation.

### 7.2.6 Spectral Ratio Slope (SRS) Method

#### *7.2.6.1 Description of method and results*

The fourth frequency-domain method used was the spectral slope method, based on eqn.2.40 $\{D_S = zV_S/(2\pi)\}$. The coefficient z can be determined by first finding the FFT of one windowed signal at a

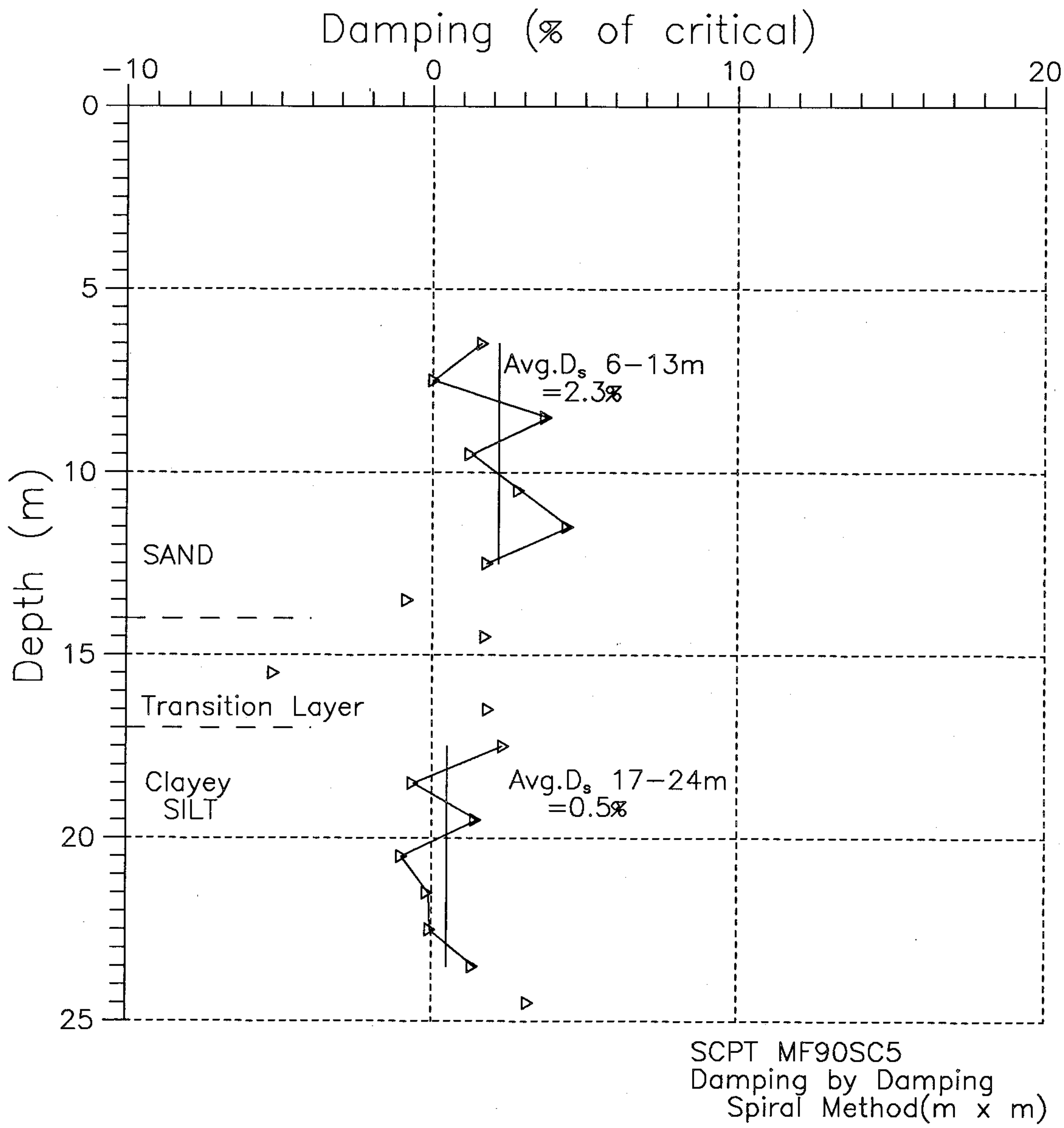


Fig.7.15 Damping by Damping Spiral Method over Seismic Cone Profile

reference depth, then for each deeper signal compute the FFT, the ratio of the FFTs, and the negative of the natural logarithm (-ln) of the ratio. A macro was written with the program VU-POINT (see Redwind2.mac in Appendix E) to facilitate the calculation of the slope of -ln(ratio) versus frequency at each depth and is outlined in Fig.7.16. After finding the slope of -ln(ratio) versus frequency plot at each depth (see Fig.7.17), these slopes are plotted versus depth (see Fig.7.18).

The slope(s) of the depth plots give the coefficient z for each layer. The fraction of critical damping can be computed from eqn.2.40. As shown in Fig.7.18, the method gives a damping value of 2.2% for the upper sands, and 0.5% for the lower silts.

Given a set of signals measured throughout a soil layer, it seems intuitive to carry out a calculation between each pair of signals and plot the results with depth. If there is no significant trend with depth, the average could be computed to represent the value for the entire layer. This was done in section 7.2.5 for the damping spiral method on a metre-by-metre basis.

The spectral slope method is similar to the damping spiral approach, but with one important advantage. It is implicitly assumed that the damping (or coefficient z) is constant throughout a layer, so that all of the information can be combined (not simply averaged) over the layer.

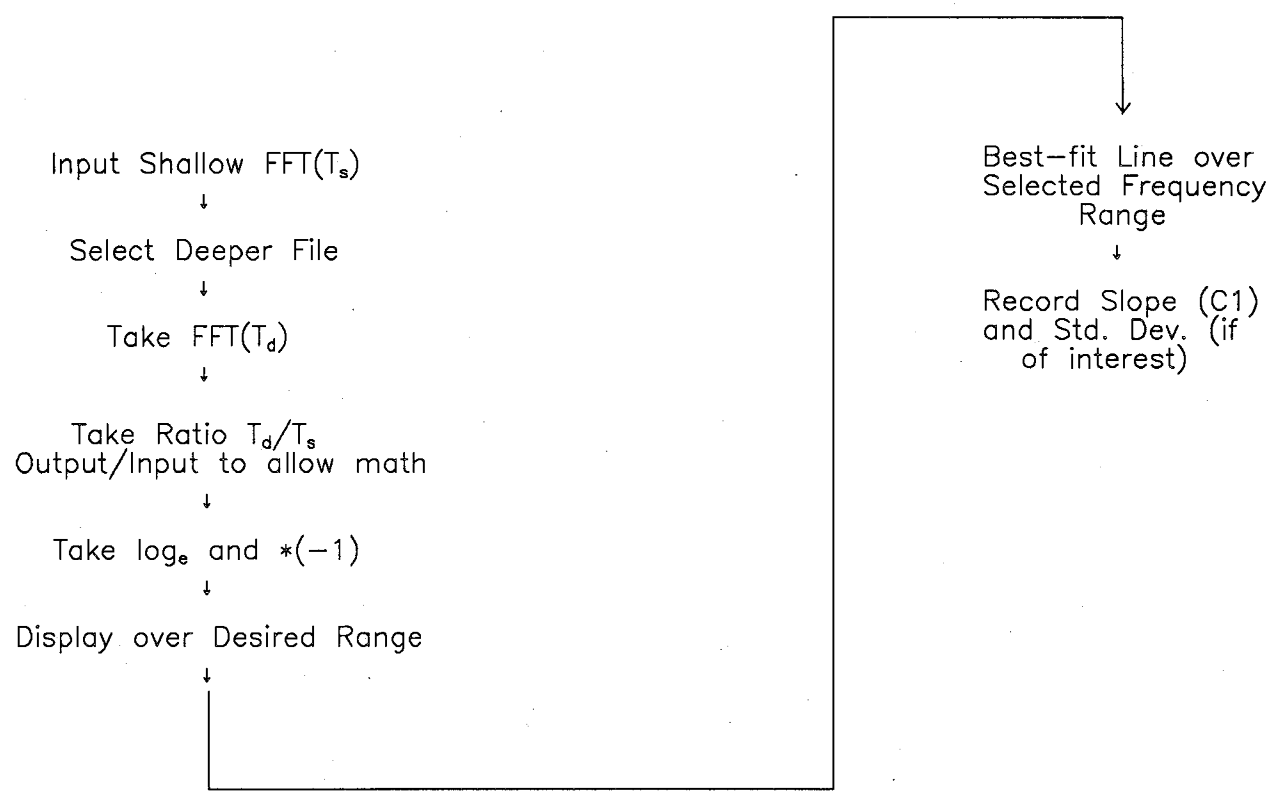


Fig.7.16 Flow Chart of Initial Phase of Spectral Ratio Slope Method

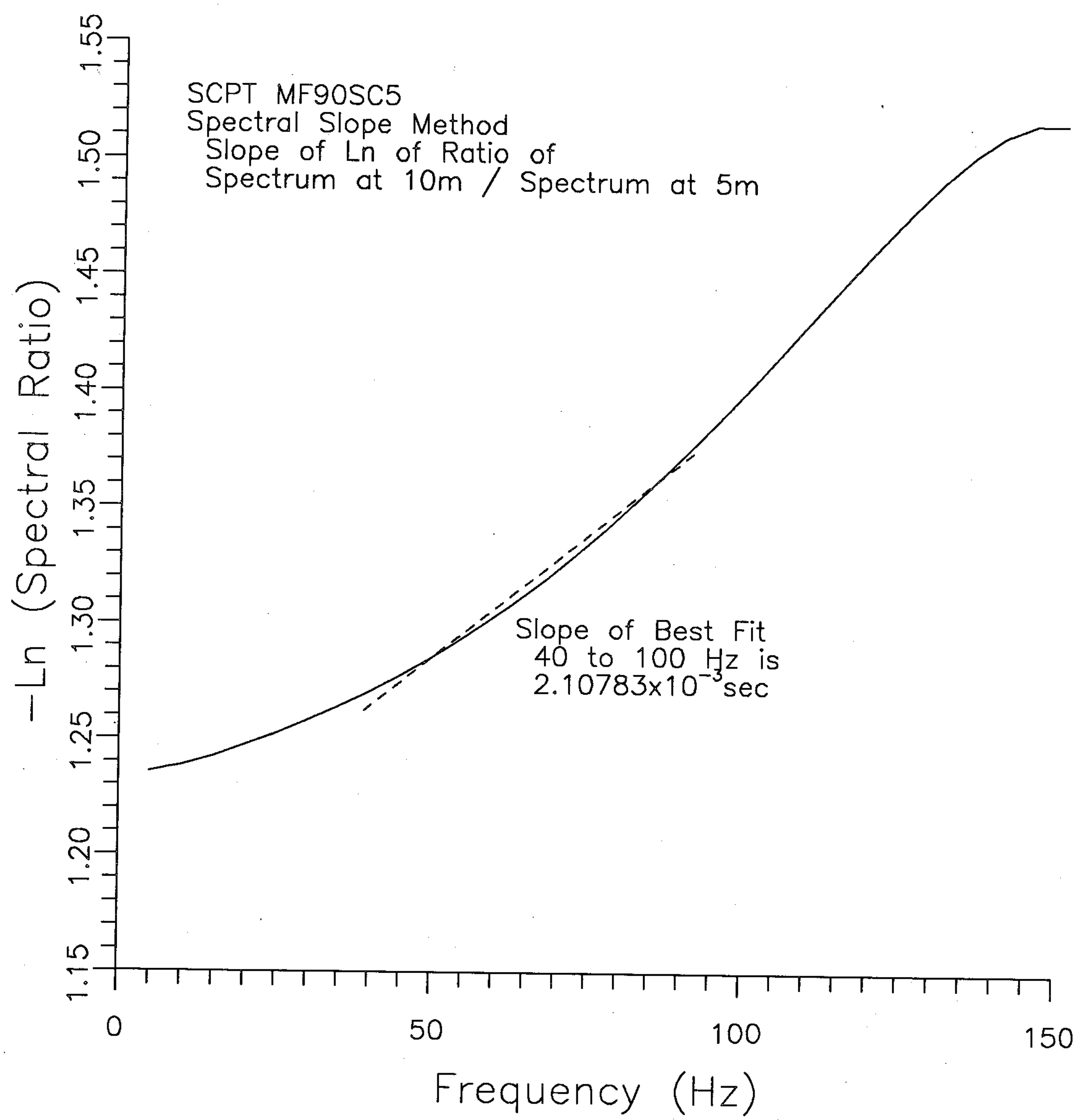


Fig.7.17 Damping by Spectral Ratio Slope Method for 10m Depth with 5m Depth as Reference (after Stewart and Campanella, 1991)

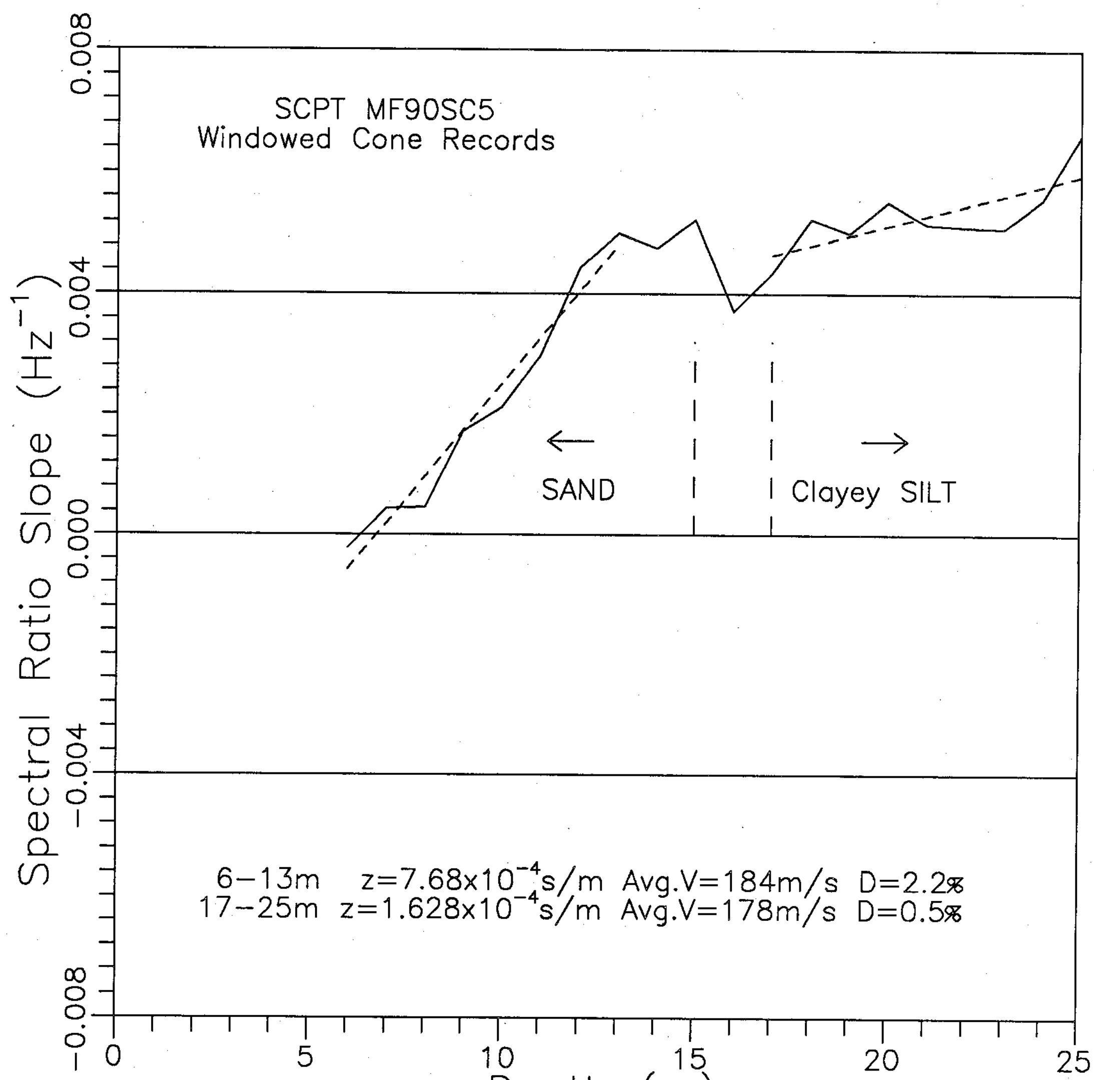


Fig.7.18 Damping by Spectral Ratio Slope Method over Seismic Cone Profile (after Stewart and Campanella, 1991)

To illustrate this advantage, consider 4 signals with amplitudes given by $A_0$, $A_1$, $A_2$, and $A_3$. The damping could be calculated by using either:

(A) The spectral slope method - each successive signal is divided by $A_0$, take natural logarithm (ln), plot -ln versus frequency (f), get slopes of -ln vs f-plots, $S_{i0}$, plot vs depth , get slope of $S_{i0}$ vs depth plot; or

(B) Metre-by metre method - each successive signal is divided by preceding signal, take ln, plot -ln versus frequency, get slopes of -ln vs f-plots, $S_{i,i-1}$, divide by depth difference to get local slopes, average local slopes to get average slope.

A simplified example is shown in Fig.7.19. Consider:

$$[7.5]\quad S_{20} = \frac{\delta(-\ln\{A_2/A_0\})}{\delta f} = \frac{\delta(-\ln\{A_2/A_1 * A_1/A_0\})}{\delta f}$$
$$= \frac{\delta-}{df}\left|\ln\frac{A_2}{A_1} + \ln\frac{A_1}{A_0}\right| = S_{21} + S_{10}$$

Therefore $S_{21} = S_{20} - S_{10}$ and similarly $S_{32} = S_{30} - S_{20}$. It can be noted that this calculation depends on the fact that the terms are logarithmic. When the sum is taken to compute the average in method B, we get:

$$[7.6]\Sigma\ S_{i,i-1} = S_{10}+S_{21}+S_{32} = S_{10}+(S_{20}-S_{10})+(S_{30}-S_{20}) = S_{30}$$

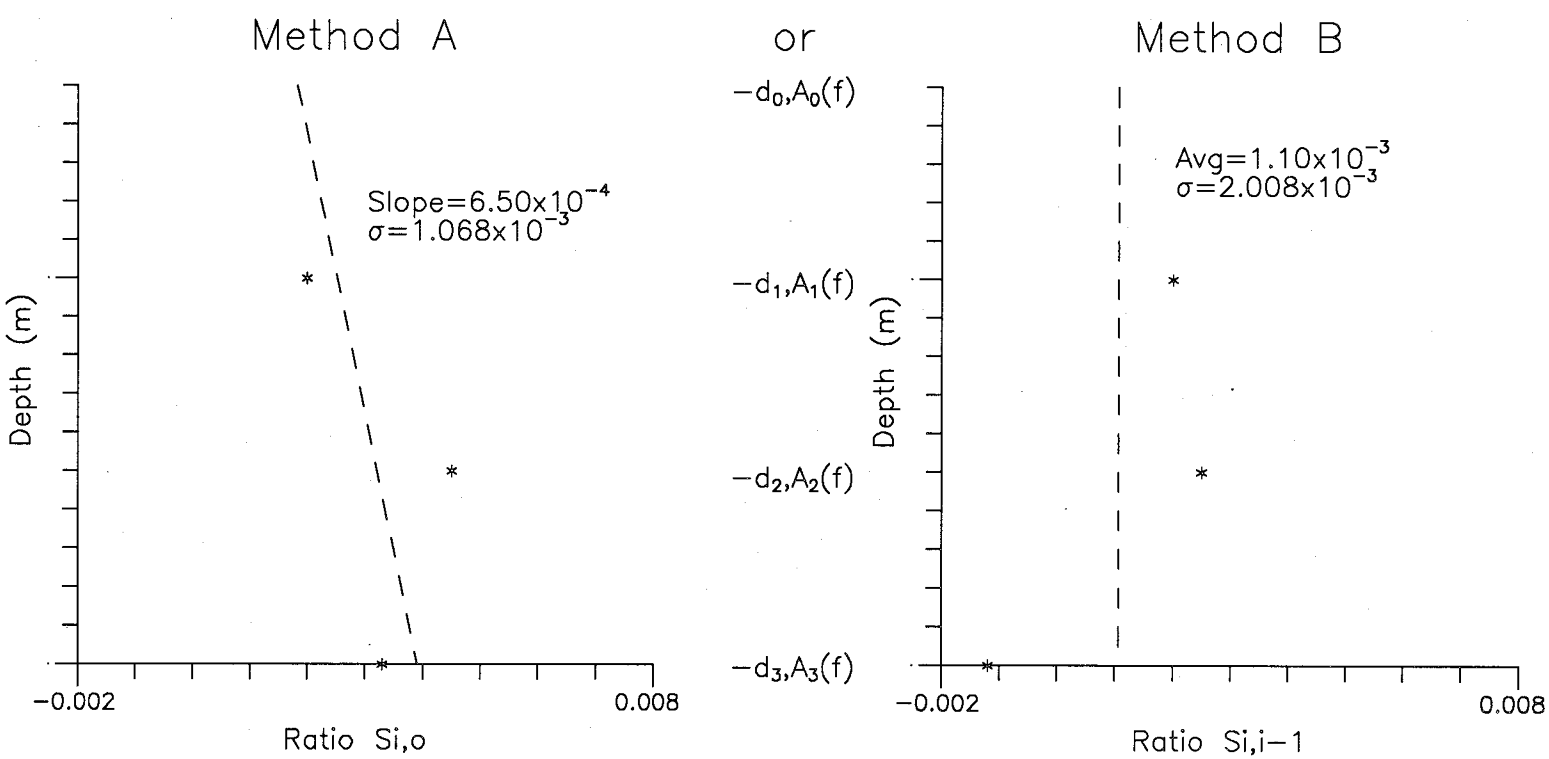


Fig.7.19 Simplified Example of Advantage of Spectral Ratio Slope (SRS) Method over Metre by Metre Approach

Therefore approach B (metre by metre) uses only the information in $S_{30}$ and consequently the scatter in the results (standard deviation) is greater. In contrast method A (spectral slope) uses all of the data ($S_{10}$, $S_{20}$, and $S_{30}$ in this simple example), and the standard deviation is only half of that for the method B calculation. As the number of points in a layer increase, the differences in errors also increase, which further shows the advantage of calculating damping for a complete layer, rather than averaging over sub-layers (metre by metre), in realistic soil profiles.

In summary, the calculation and plotting of damping on a metre-by-metre (mxm) basis allows the observation of any trend in the value with depth throughout a layer. If the trend is not significant, and a single value for the layer is to be calculated, an average of the mxm values should not be computed as only the first and last signals are effectively used. The spectral ratio slope method utilizes all of the signals in one calculation of the damping value, and therefore should be used for calculation of damping in a layer of soil.

#### *7.2.6.2 Error analysis for spectral slope method*

The spectral ratio slope method is the preferred method of analysis and will be used to analyze the results from all four research sites. Therefore it is necessary to properly analyze the numerical errors as the data is processed. Analysis of errors in the calculation of damping is complicated by the various steps required in the approach.

At each depth, a slope (of the -ln of the ratio of FFT's) with frequency is computed so that there is an error (standard deviation) associated with the slope value at each depth. Subsequently these points (slopes) are plotted versus depth and another line (or lines) is fitted, giving another standard deviation. This section outlines how these errors can be combined to calculate the standard deviation of the calculated damping values.

Consider a series of n points at depths, d, and slopes with frequency, c, and standard deviations, s. The fit (and error) with depth is relatively straightforward, and can be computed with VU-POINT directly. However weighting factors will be required for consideration of the individual standard deviations, so that the fitting process is outlined here following Neville and Kennedy (1964). We wish to find the coefficients to fit a line of the form: $c = a + bd$. Let the mean depth be $\bar{d}$ and $B = n\Sigma d^2 - (\Sigma d)^2$. Then:

[7.7] $a = \{\Sigma d^2 \Sigma c - \Sigma d \Sigma c\} / B$

[7.8] $b = \{n\Sigma dc - \Sigma d \Sigma c\} / B$

If we then compute the deviations, $\epsilon = c - (a + bd)$, we can compute the variance of the fit with depth:

[7.9] $s_c^2 = (\Sigma\epsilon^2)/(n-2)$

and the variance of the slope:

[7.10] $$s_b^2 = s_c^2 / \Sigma(d - \bar{d})^2$$

For the effect of the standard deviation, s, associated with each point, we must assign a weight which varies with the distance from the mean depth:

[7.11] $w = (nd-\Sigma d)/B$ then the associated variance is:

[7.12] $s_s^2 = \Sigma\, w^2 s^2$

and finally the total variance of the fit is simply:

[7.13] $s_T^2 = s_b^2 + s_s^2$

The standard deviation at each point of the fitting process is simply the square root of the variance, and the coefficient of variation ($CV_z$) is simply the ratio of the standard deviation to the mean. Subsequently the $CV_v$ of the velocity can be added to get the $CV_D$ for the damping i.e.

[7.14] $CV_D^2 = CV_z^2 + CV_v^2$

For the example given above (Fig.7.18) for the damping in the sand, the standard deviation of the fit of the slope, $\sigma_b$, is $5.889\mathrm{x}10^{-5}$s/m, and that due to the $\sigma$ at each point, $\sigma_s$, is $2.2567\mathrm{x}10^{-5}$s/m, for a total standard deviation on the coefficient z, $\sigma_z$, of $6.3061\mathrm{x}10^{-5}$s/m. For a slope of $7.68\mathrm{x}10^{-4}$s/m, the coefficient of variation is 8.2%. The average velocity over the layer is 184m/s with a $\sigma$ of 22.5m/s, so the coefficient of variation is 12.2%. When these values are combined to calculate damping the coefficient of variation is 14.7%. By contrast the approach given in section 7.2.5 (Fig.7.15), which showed far less scatter than the first two frequency-domain methods, gave a standard deviation of 1.52% or a coefficient of variation of 67.5%, more than 4 times that of the spectral slope method (If the trend is removed the standard deviation falls to 1.37% for a coefficient of variation of 61%, not a significant improvement.) Thus it is again concluded that calculation of damping over a layer significantly reduces the scatter in the final answer, compared with calculation on an averaged metre-by-metre basis.

### 7.2.7 Summary

Six methods of calculating damping from SCPT measurements have been discussed in detail and compared. The first two methods are applied in the time domain and both were found to give unacceptable results. The rise time method was shown to give very different answers for soundings at the same site and several other authors have rejected the method because of the scatter in the calculated values of damping. As expected, the random decrement method also gave a large scatter in results as the method as proposed uses the signals from a single record and must include the effects of the source and receiver system, as well as the soil.

Four methods of calculation in the frequency domain have been investigated. The attenuation coefficient method and the modified SHAKE method require previous estimates of the geometric corrections and consequently the scatter was large. The damping spiral method allows calculation of the geometric corrections and therefore reduces the scatter to an acceptable level. The method is essentially a more general form of the spectral ratio slope method which is simpler to apply and is the preferred method of calculation.

The spectral ratio slope method avoids the need for interface and spherical spreading corrections, uses the information from all of the signals in a layer, and has been shown to have less scatter in the results. Consequently this method has been used for the results reported in the rest of this thesis.

## *7.3 MEASUREMENTS OF DAMPING AT VARIOUS SITES*

### 7.3.1 Measured Values

Damping values using the spectral ratio slope method on windowed signals are presented for each of four research sites. The frequency ranges used for each soil layer at a given site were selected by viewing the -ln ratio vs. frequency plots over the range of depths and picking the linear portion that appeared on most of the plots. For each layer, the slope with depth is plotted, the average velocity is given, and the resulting damping is computed. Also shown are the coefficients of variation for each parameter.

Fig.7.20 shows the results for the McDonald Farm site. Soundings MF90SC5 and MF91SC1 are a few metres apart, and MF90SC2 is about 140m west of the other two. Results are limited to these three soundings as the other soundings had electrical noise in the signals. It is worthwhile to note that the soundings were done in a period of over one

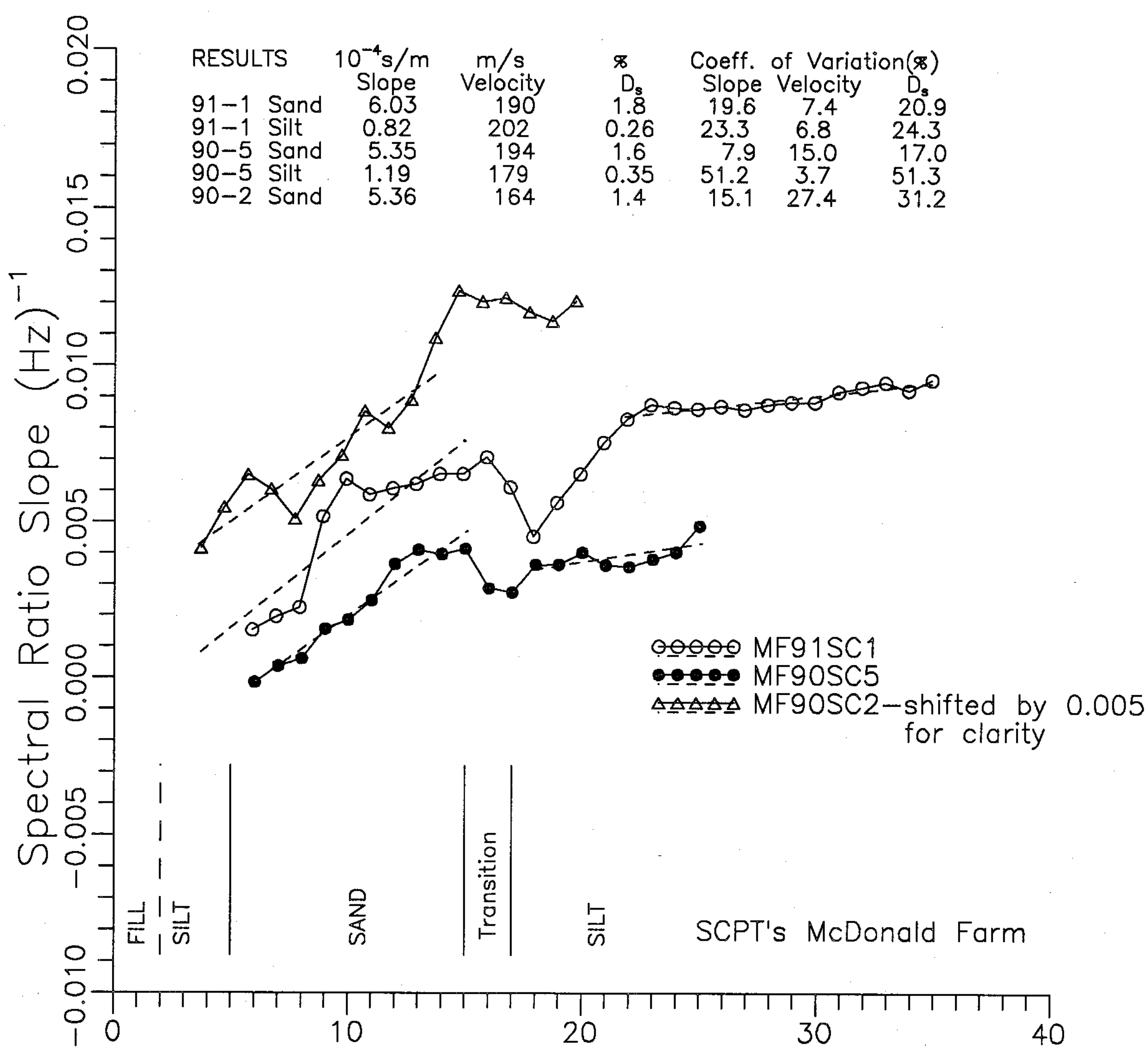


Fig.7.20 Damping from SRS Profiles — McDonald Farm Site

year. For the sand the calculated damping values were quite consistent at 1.8%, 1.6%, and 1.4%. The coefficients of variation were 21%, 17%, and 31%, indicating a reasonably small scatter in the results. The damping values for the silt were 0.26% and 0.35% (sounding MF90SC2 did not penetrate deeply enough to calculate a value). Although the standard deviations in the silt are about one-third of those in the sand, the coefficients of variation in the silt were larger (24% and 51%), as a result of the small damping measured.

Results for the Lower 232nd St. site are given in Fig.7.21. The soundings noted as L291SC1 and L290SC1 are within a few metres of each other and L289SC1 is about 20m to the north. The calculations were considered in two sections, above and below about 12m. The cone bearing values indicate sand layers at spacings of about 1m below this depth. Damping values for the upper sections agreed closely; 0.80%, 0.66%, and 0.84%. The coefficients of variation were fairly small (15% and 13%) for two of the tests, but considerably higher for L289SC1 at 39%. There were fewer points included in this calculation and the results showed greater irregularities. The calculated damping below 12m varied greatly, ranging from a negative value, through nearly zero (0.1%) to the value in the upper sections (0.8%). The sand layers have apparently disturbed the measurements.

Calculated damping values for the Annacis North Pier site are shown in Fig.7.22. The two soundings were within a few metres of each other and gave similar results. The damping values are 0.55% and 0.78%,

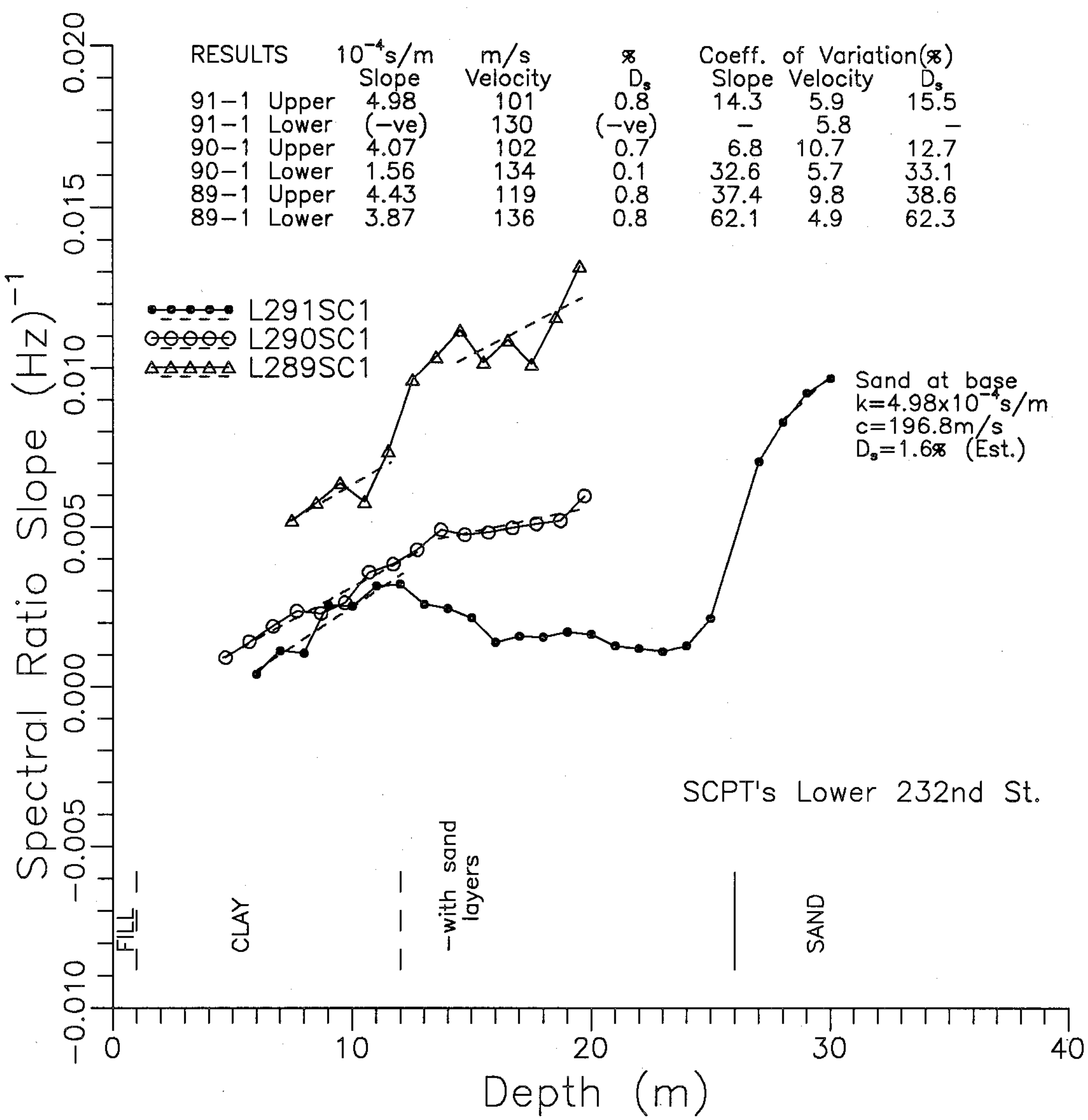


Fig.7.21 Damping from SRS Profiles − Lower 232nd St. Site

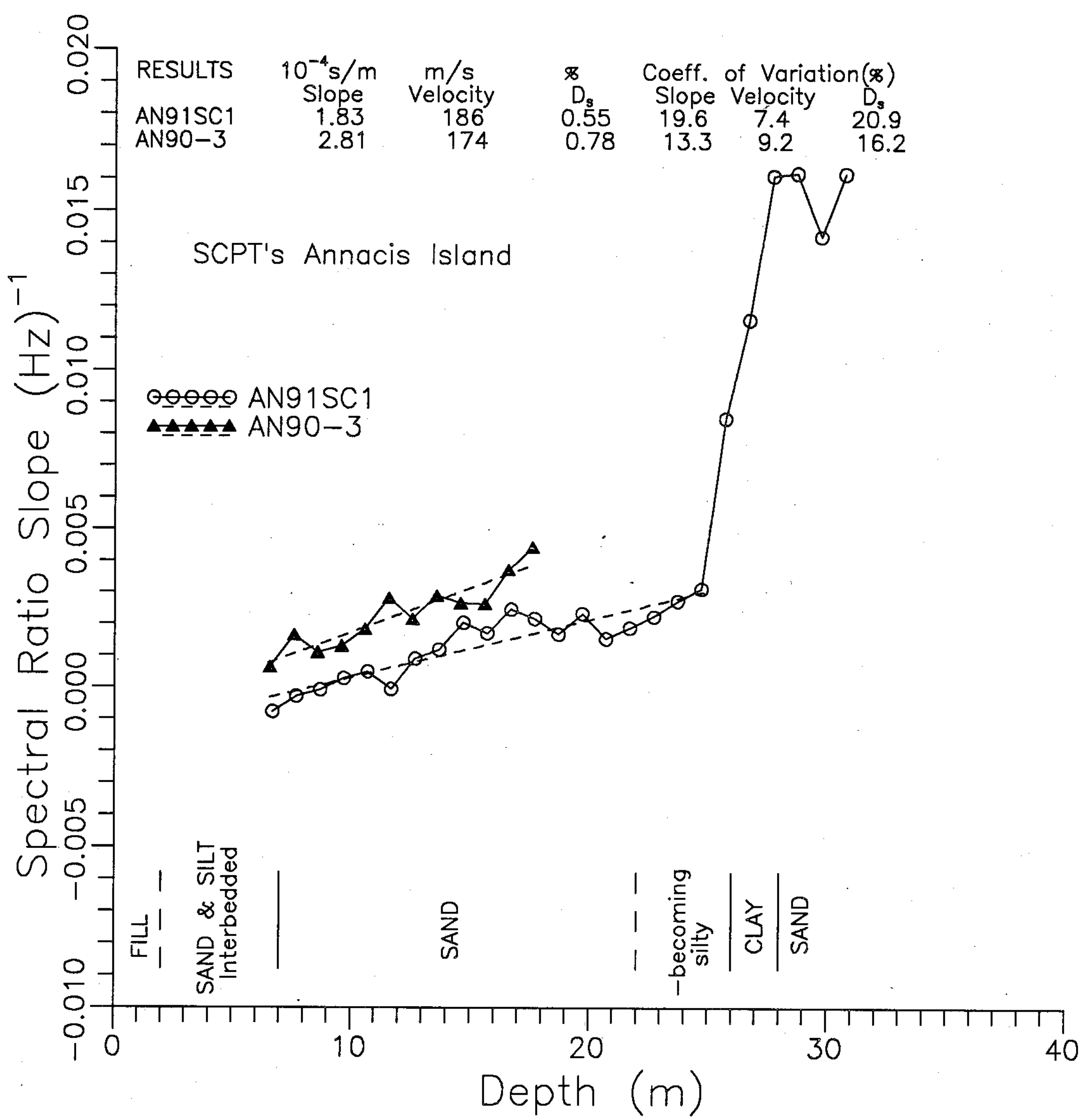


Fig.7.22 Damping from SRS Profiles – Annacis N.Pier Site

with the coefficients of variation being 21% and 16%. A large step in the spectral ratio slope curve can be seen as the sounding encountered a silt-clay layer, and the curve appears to be flattening off below this layer. The damping values are about 0.4 times those measured at the McDonald Farm site, yet both sets of data appear to be consistent. Fig.7.23 presents the results of a test at the Laing Bridge site. The damping is 0.62% with a coefficient of variation of 23%. This result agrees very closely with the Annacis results, although this site is closer to the McDonald Farm site.

A summary of all the successful damping measurements is provided in Table 7.1.

### 7.3.2 Damping Calculations using Data Measured by Others

In order to confirm that the success of the spectral ratio slope method was not limited to the SCPT system in use at UBC, two sets of data obtained by others, using similar equipment at a site in Ontario, have been analyzed. The main differences reported in the equipment are that the recording system had an equivalent accuracy of 12 bits (compared to 15 bits for the UBC system) and the height of the hammer drop was controlled by measurement rather than a mechanical catch. Macros were written to facilitate reading the data into VU-POINT, and these data files were then treated in the same manner as described above.

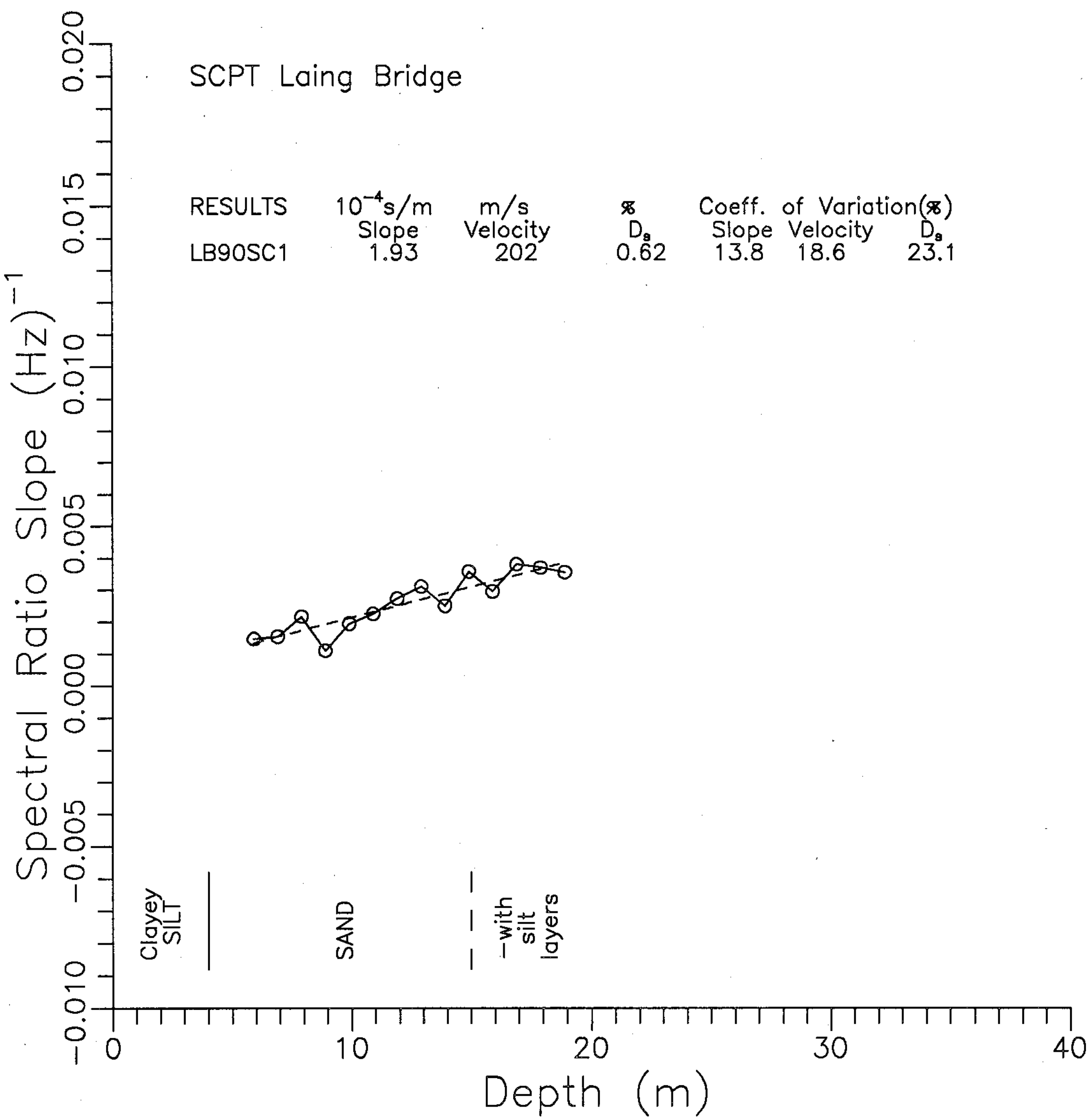


Fig.7.23 Damping from SRS Profile – Laing Bridge Site

| Sounding | Depth(m) | Soil | Avg.$V_s$(m/s) | Damping(%) |
|---|---|---|---|---|
| McDonald Farm Site | | | | |
| MF91SC1 | 5.9-14.9 | Sand | 190 | 1.8 |
| MF90SC5 | 6.0-15.0 | Sand | 194 | 1.6 |
| MF90SC2 | 3.7-13.7 | Sand | 164 | 1.4 |
| MF91SC1 | 21.9-34.9 | Silt | 202 | 0.3 |
| MF90SC5 | 18.0-25.0 | Silt | 179 | 0.4 |
| Annacis North Pier | | | | |
| AN91SC1 | 6.7-24.7 | Sand | 186 | 0.6 |
| AN90-3 | 6.6-17.6 | Sand | 174 | 0.8 |
| Laing Bridge | | | | |
| LB90SC1 | 5.9-18.9 | Sand | 202 | 0.6 |
| Lower 232nd Street | | | | |
| L291SC1 | 6.0-12.0 | Clay | 101 | 0.8 |
| L290SC1 | 4.7-12.7 | Clay | 102 | 0.7 |
| L289SC1 | 7.5-11.5 | Clay | 119 | 0.8 |

TABLE 7.1 Summary of Damping Measurements

Plots of shear wave velocities are given in Figs.7.24 and 7.25. For both sites, velocities using the phase and cross-over methods are shown, and for the second site velocities by cross-correlation are also shown. It can be seen that the phase and cross-correlation methods give almost identical answers, and that the cross-over velocities are fairly

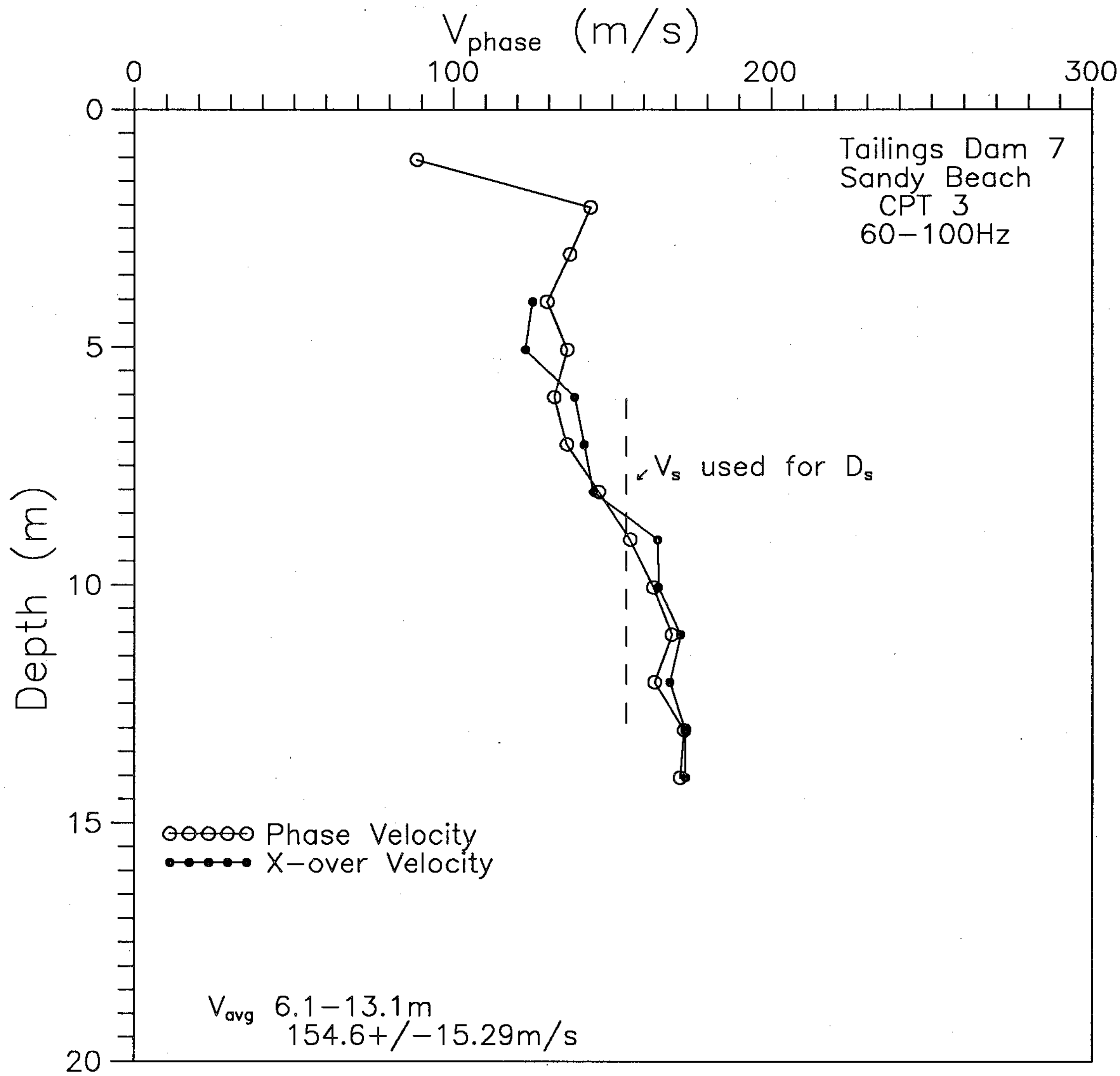


Fig.7.24 Shear Wave Velocities CPT 7–3

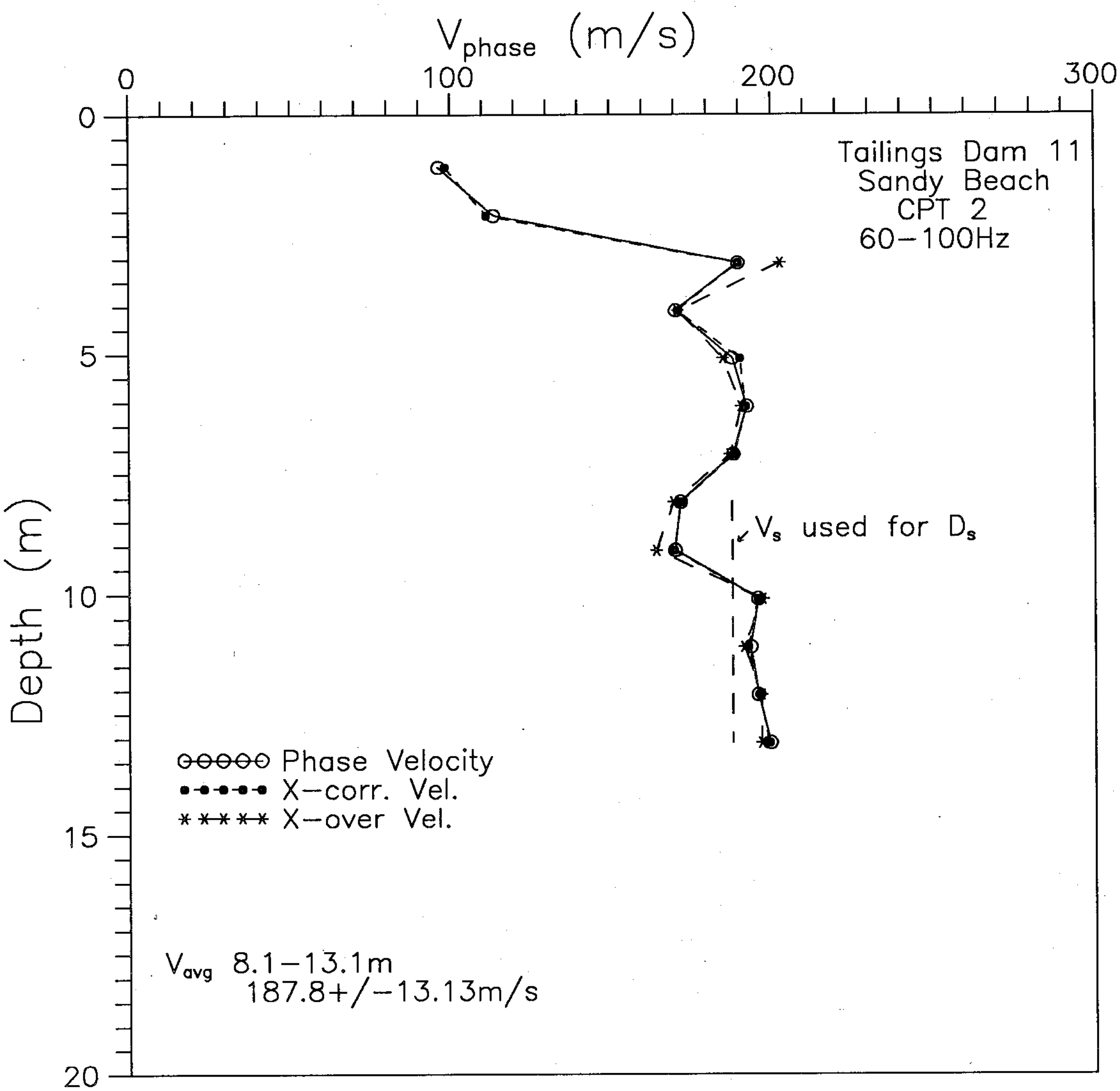


Fig.7.25 Shear Wave Velocities CPT 11−2

similar for these data sets. The cross-over times were not clearly defined for the first few metres.

The results of the damping calculations are shown in Figs.7.26 and 7.27. The damping values, 1.35% and 1.7% are similar to the values measured at the McDonald Farm site (1.4% to 1.8%) and the coefficients of variation, 16% and 17% are also very similar to those at the McDonald Farm site (17% and 21%).

For the first site, a series of calculations were done using the first recorded signal only, rather than the average of (typically) four signals, and the results are presented in Figs.7.28 and 7.29. Below 8m, the velocities are very similar using either the set of single signals or average signals. There was considerably more scatter in velocities using single signals above 8m. The spectral ratio slopes from the single signals also showed considerably more scatter above 7m and slightly more scatter below 7m. For calculations over the same depth range (7.6-14.6m), damping values were very similar (1.71% and 1.78%) with slightly more scatter with the single signals (coefficient of variation of 23% compared with 17% for the average signals).

It is concluded that the damping method developed was successfully applied to data obtained by others. For the one data set considered, use of a single set of records rather than the average of 4 signals at

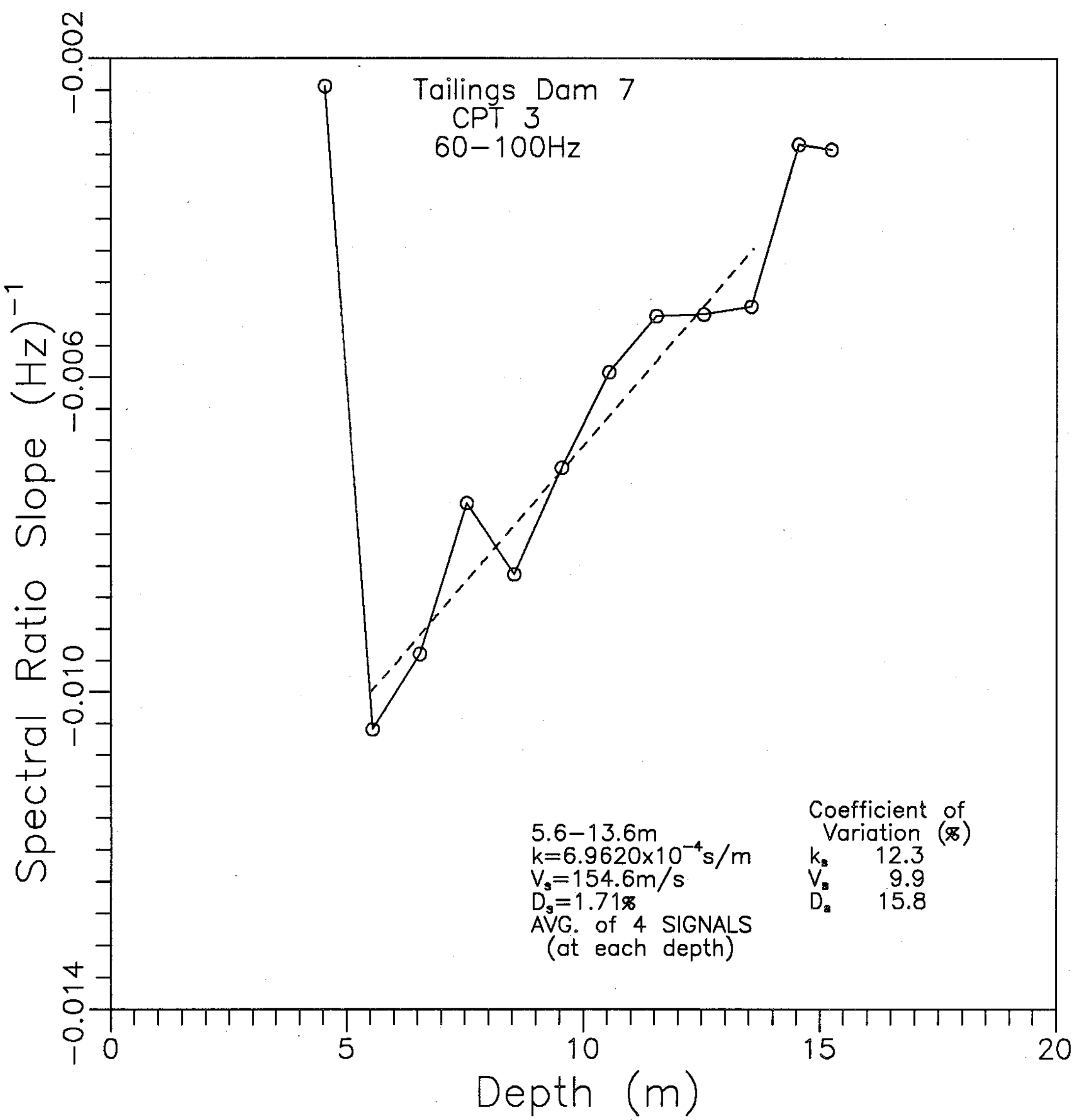


Fig.7.26 Damping from SRS Profile CPT 7−3

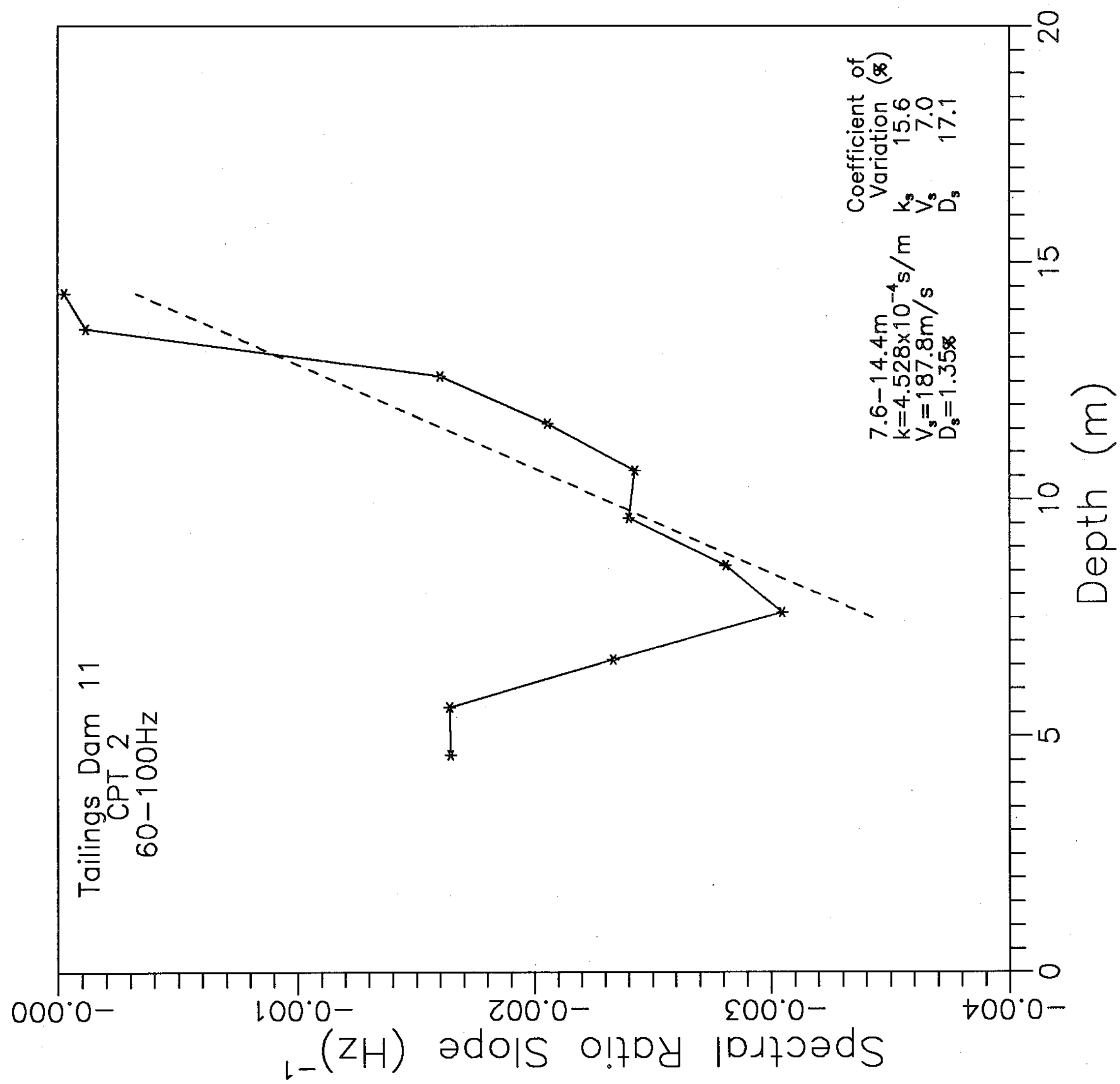


Fig.7.27 Damping from SRS Profile CPT 11−2

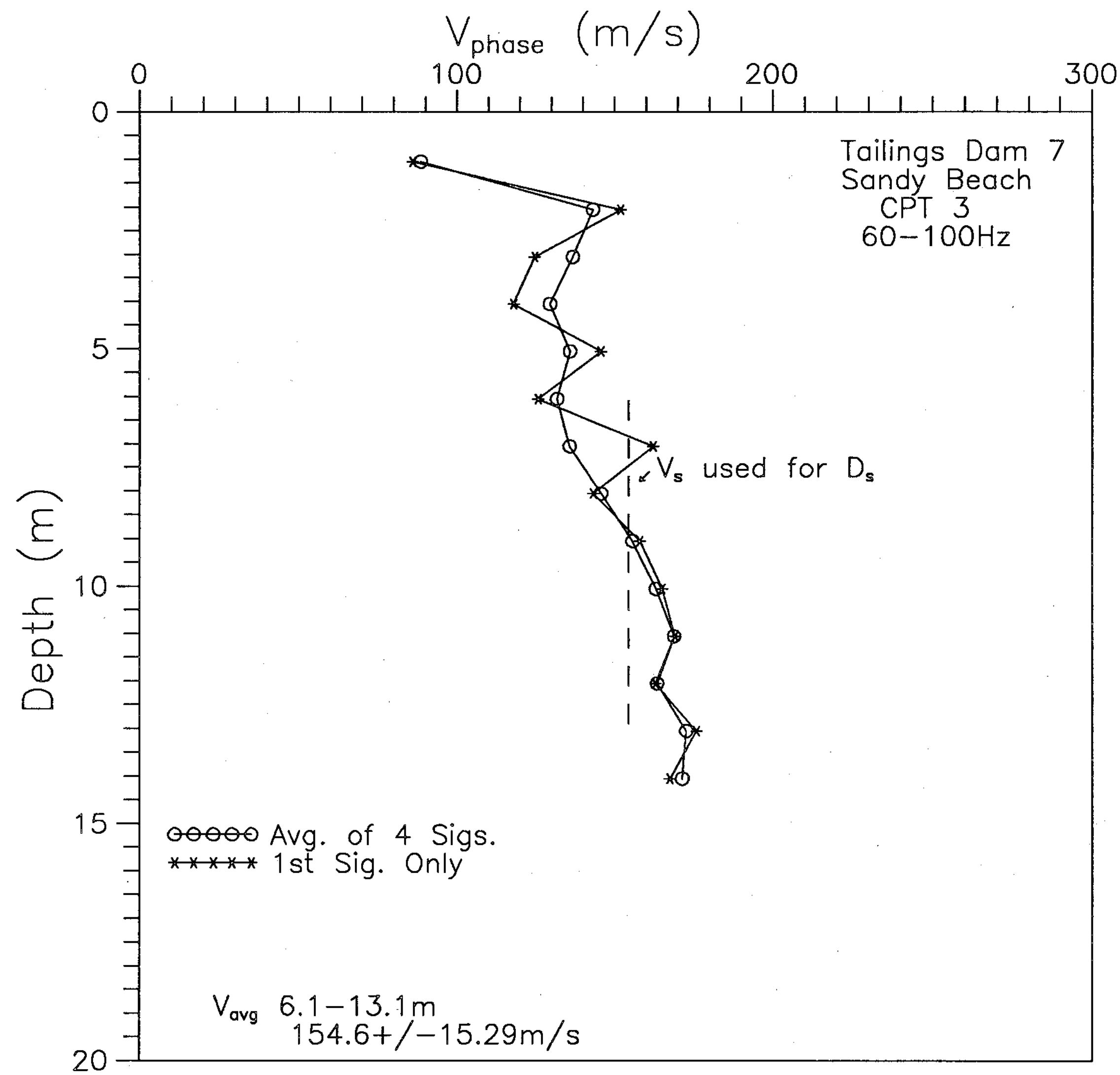


Fig.7.28 Comparison of $V_s$ – 1 Signal vs. Avg. of 4 Signals

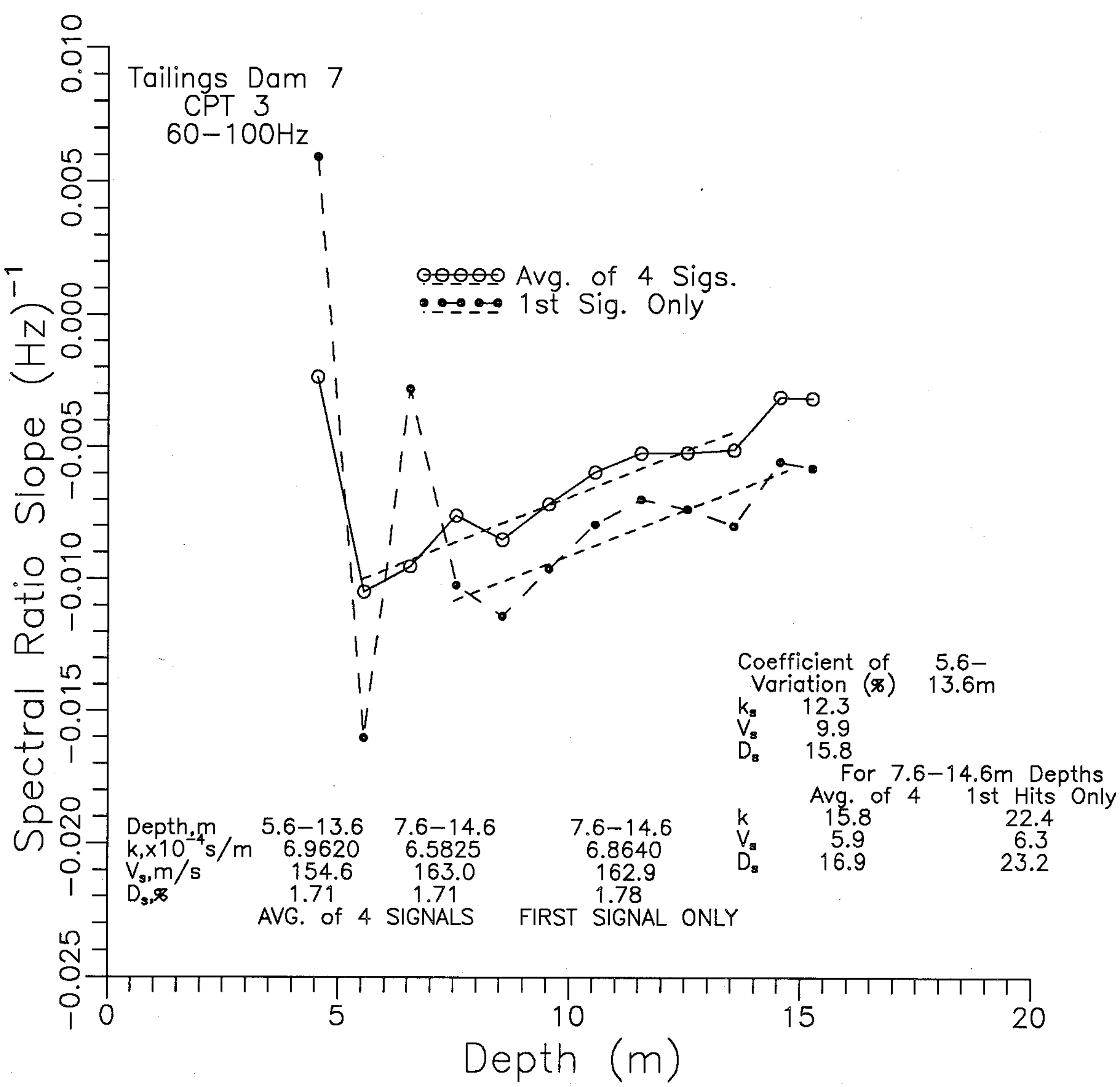


Fig.7.29 Comparison of SRS − 1 Signal vs. Avg. of 4 Signals

each depth gave comparable values for velocity and damping over a slightly smaller depth range with slightly more scatter.

### 7.3.3 Limitations of Method

A review of Figs.7.20 to 7.22 shows that the slopes of the spectral ratio slope curves are apparently undefined immediately below a soil layer interface or within interbedded soil layers. The data show that at least 6m, and preferably more, of relatively uniform soil is required to define the slope and thus the damping of the soil layer. The wavelength, L, of the signals used to calculate damping is given by the shear wave velocity, c and the predominant frequency, $f_o$, from:

[7.15] $L = c/f_o$

Typical predominant frequencies are in the 50 Hz to 70Hz range, and typical velocities are 100m/s to 200m/s. The wavelengths therefore range from about 1.5m to 4m, typically being about 3m. It is expected that measurements within one wavelength of an interface would be disrupted by the interface, and that at least one additional wavelength would be required to define the slope in the lower layer. Therefore at least 6m of relatively uniform soil is required for the damping measurement with the present equipment. It should be noted that this depth requirement is expected to be true even if measurements were to be made at intervals of less than the 1m increments used to date. Since the shear wave velocity of the soil is fixed, the only way to decrease the wavelength is to increase the frequency of the signals. It is not clear that signals at a significantly greater frequency would penetrate as deeply as the measurements are desired, so it may not be possible to overcome this depth requirement.

### *7.4 RELATIONSHIPS OF CPT PARAMETERS AND VELOCITIES TO DAMPING VARIATIONS*

In the above section it was found that damping values were repeatable at each site where two or more soundings were made. However the sand at the McDonald Farm site had an average damping value of about 1.6%, whereas the sand at Annacis and Laing Bridge had an average damping of about 0.65%, about 2.5 times less. Since the deposits are geologically similar, the reason for such a variation is not immediately obvious.

Other researchers have attempted to relate cone measurements to other soil properties. Campanella and Robertson (1986) provide curves of $G_{max}$ vs. $q_c$ for various values of the vertical effective stress. An attempt was made to relate the damping at sand sites in the present study to cone measurements. Fig.7.30 shows the relationship between damping and the average cone bearing over the depth of the damping calculation. It appears that the damping (at low strain) increases with the cone bearing, although there is considerable scatter. Damping is compared with sleeve friction and friction ratio in Fig.7.31, and there is no apparent relationship.

The relationship between damping and average shear wave velocity is shown in Fig.7.32. The slope of the relationship is essentially the

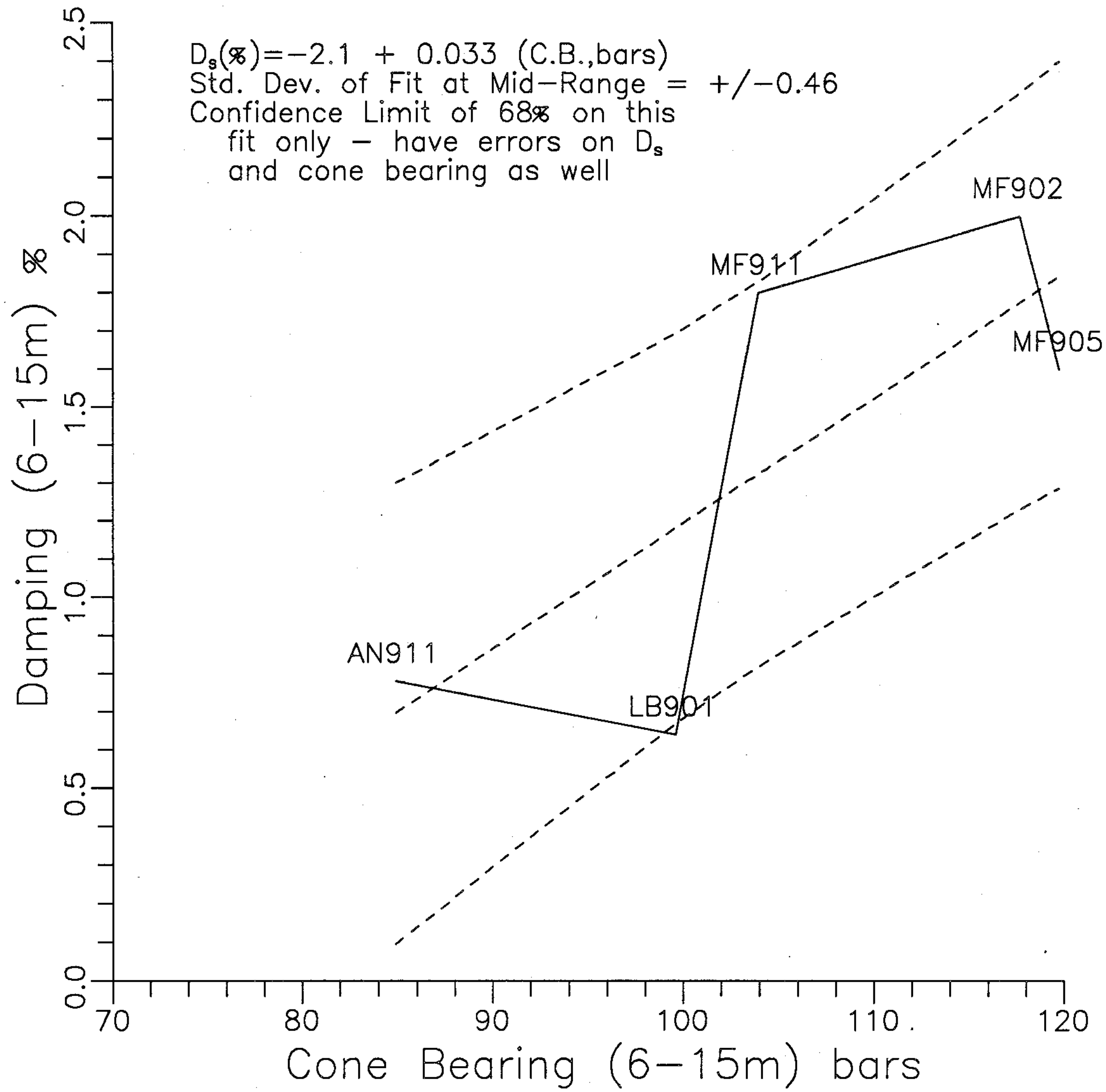


Fig.7.30 Damping Variation with Cone Bearing in Sand

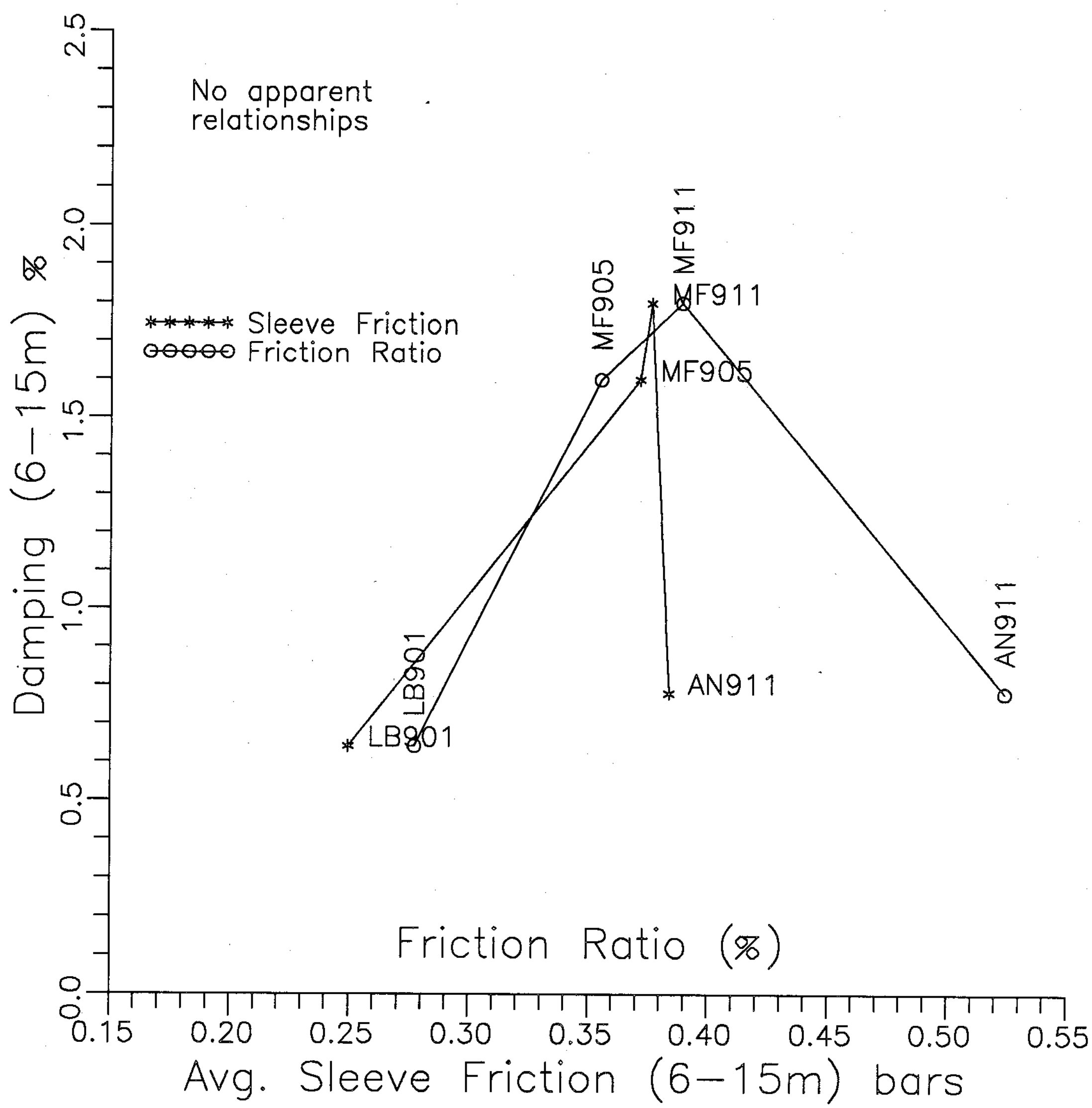


Fig.7.31 Damping Variation with Sleeve Friction and Friction Ratio in Sand

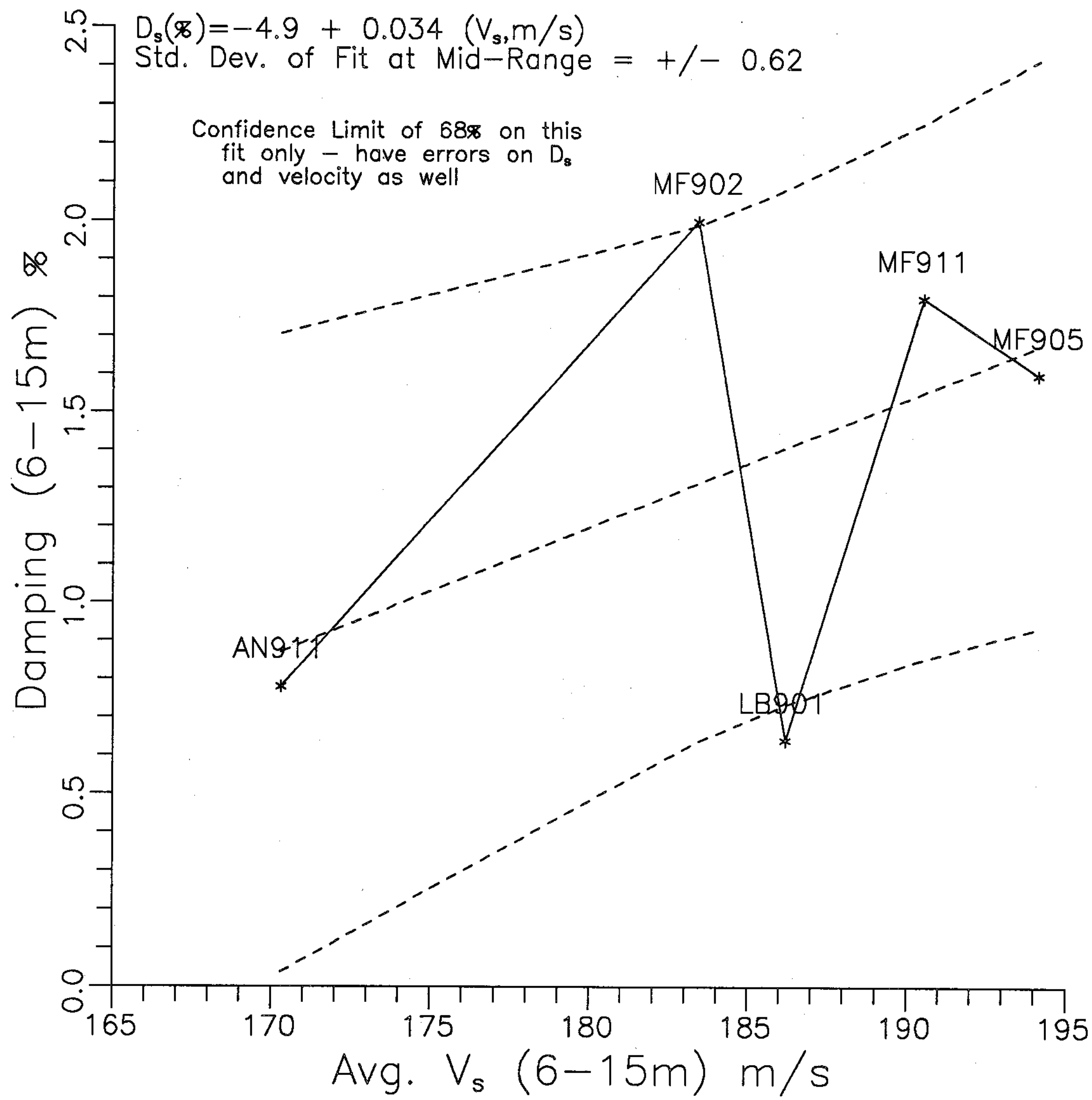


Fig.7.32 Damping Variation with Shear Wave Velocity in Sand

same as that for cone bearing. However the lowest damping site (at Laing Bridge) has a velocity near the middle of the range measured. It is interesting to note that the low-strain damping increases with velocity, whereas an inverse relationship is expected at higher strains.

Total damping (including geometric effects) is expected to increase with the variations in velocity, because of an increase in reflections. Fig.7.33 shows the variation of material damping with the standard deviation of the shear wave velocity over the depth of interest. There is a weak relationship, but the higher damping values occur at both the highest and lowest values of the standard deviation. It would appear that the standard deviation of the velocity is not a determining factor in the material damping calculations, and suggests that the geometric damping due to layering (which depends on the variations in velocity) has been removed as desired.

Although there is not enough data to form firm conclusions about the relationship of damping to other parameters, it appears that field measurements of damping in sand show an increase with an increase in cone bearing and shear wave velocity.

### *7.5 IMPORTANCE OF WINDOWING AND WINDOW SIZE ON DAMPING CALCULATIONS*

The results of damping calculations using windowed signals have been presented in the previous section, allowing comparisons to be made if different signal processing steps are taken. Mok et al (1988) windowed the shear wave in their analysis. Redpath et al (1982) give

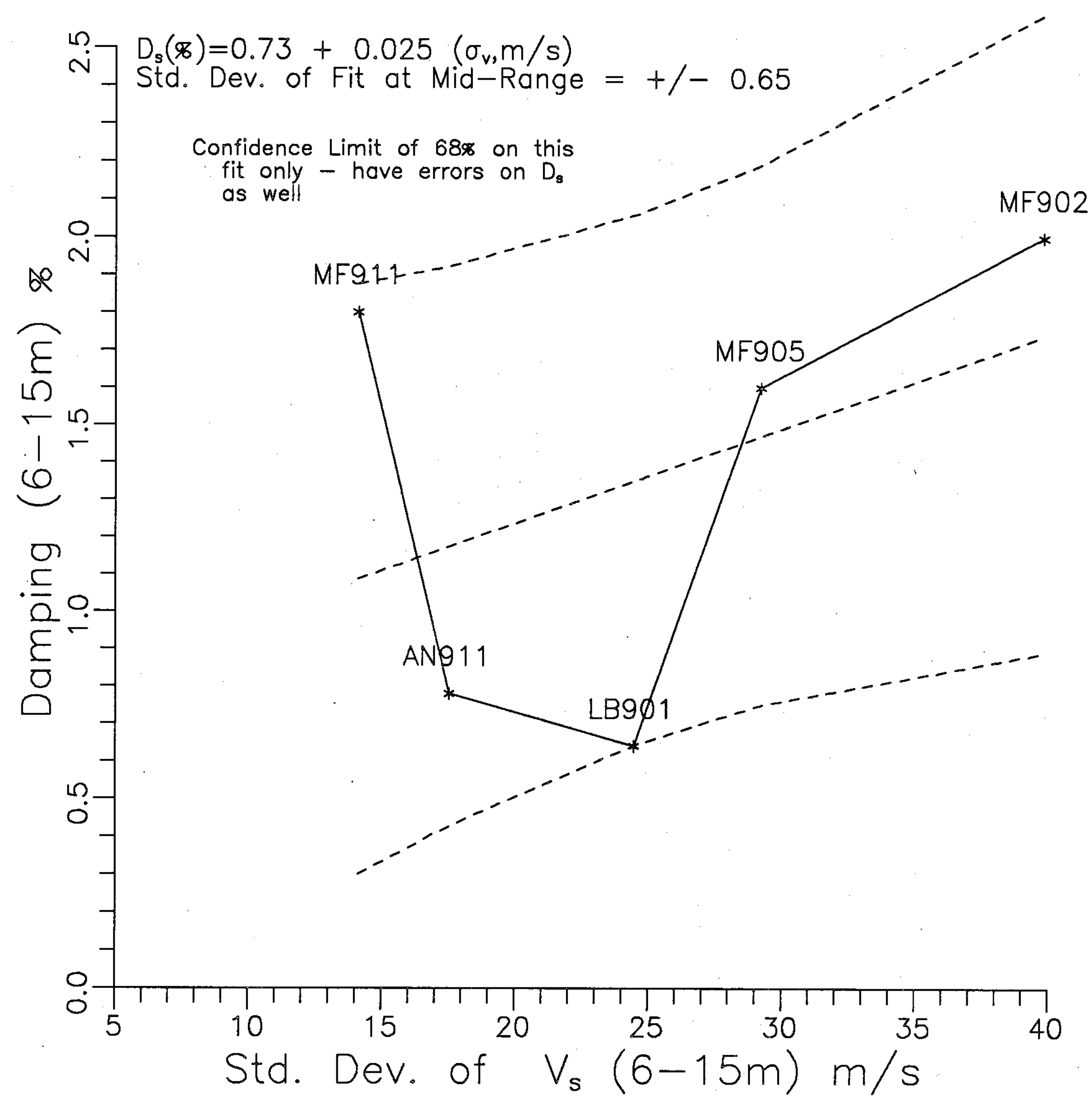


Fig.7.33 Damping Variation with Standard Deviation of $V_s$ Sand

considerable detail on the signal processing used (averaging, smoothing), but give no indication of windowing the shear wave. They found that damping values were "consistently higher" than the values from resonant column tests. In their 1986 report, Redpath and Lee specifically state that "the shear waves recorded down to bedrock depth were judged to be suitable for analysis without any windowing..." In this case their field measurements agreed fairly closely with laboratory results (which were at considerably higher strains).

In Fig.7.34, one of the SCPT's at the McDonald Farm site has been analyzed in three ways, using the full signals, the signals windowed to isolate the first wavelength of the shear wave, and windowed to isolate 1.5 wavelengths (in his discussion of wave propagation, White, 1965, uses waves of this shape). It can be seen that the calculations with the full signal gave a damping value about 3 times higher, with somewhat more scatter, and that the calculation with 1.5 wavelengths fell between the other two cases.

A similar analysis for a SCPT at the Annacis North Pier site, presented in Fig.7.35, shows the results of the full signal calculations are much more irregular, and it is difficult to find a straight section of the plot. An analysis carried out at the Lower 232nd St. site. is shown on Fig.7.36. In this case the slope of the full signals plot is large and negative.

For both the Annacis and Lower 232nd St. sites, the analyses using 1.5 wavelengths were again intermediate between the windowed and full

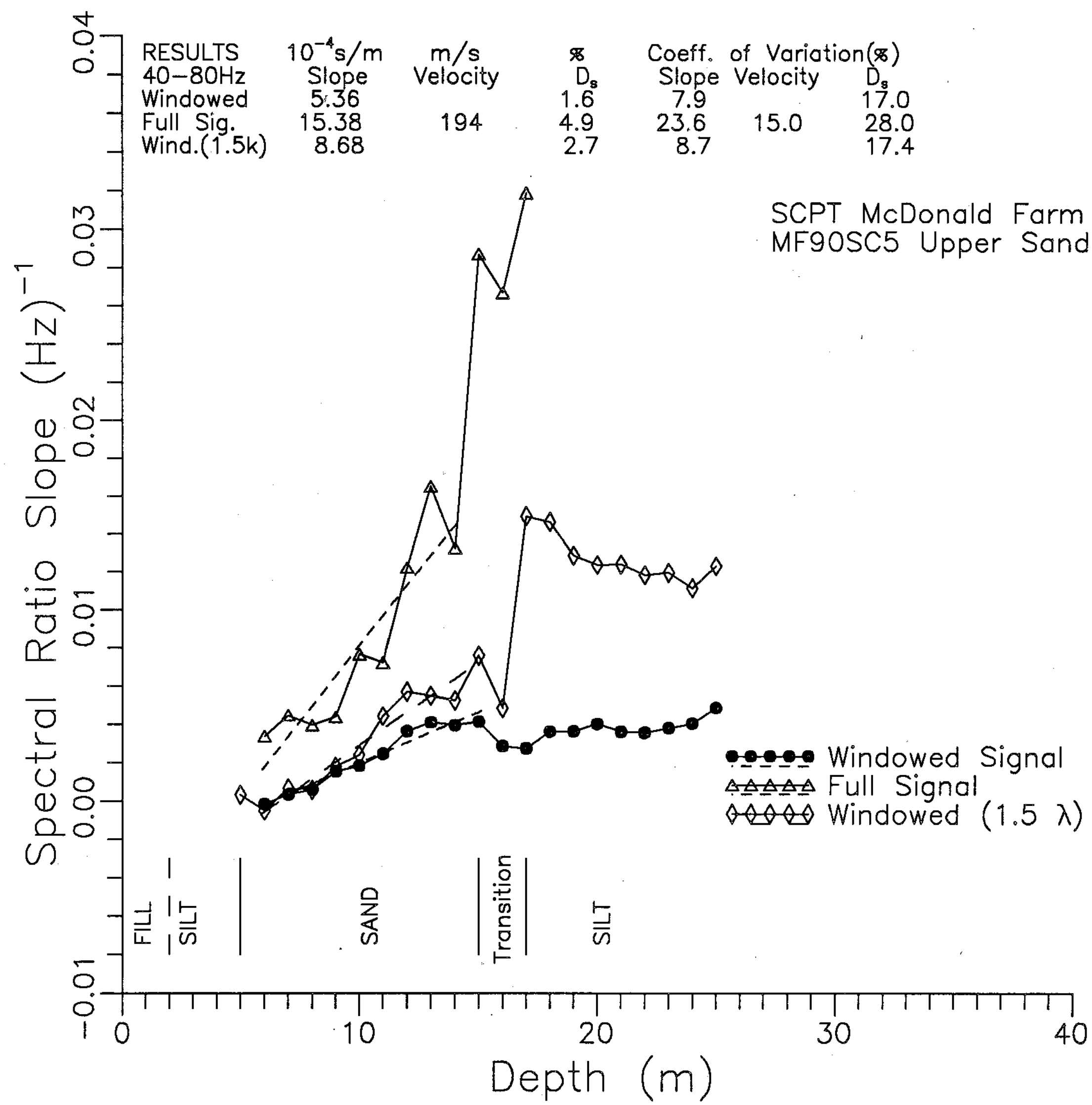

Fig.7.34 Effect of Signal Processing on Damping – McDonald Farm Site

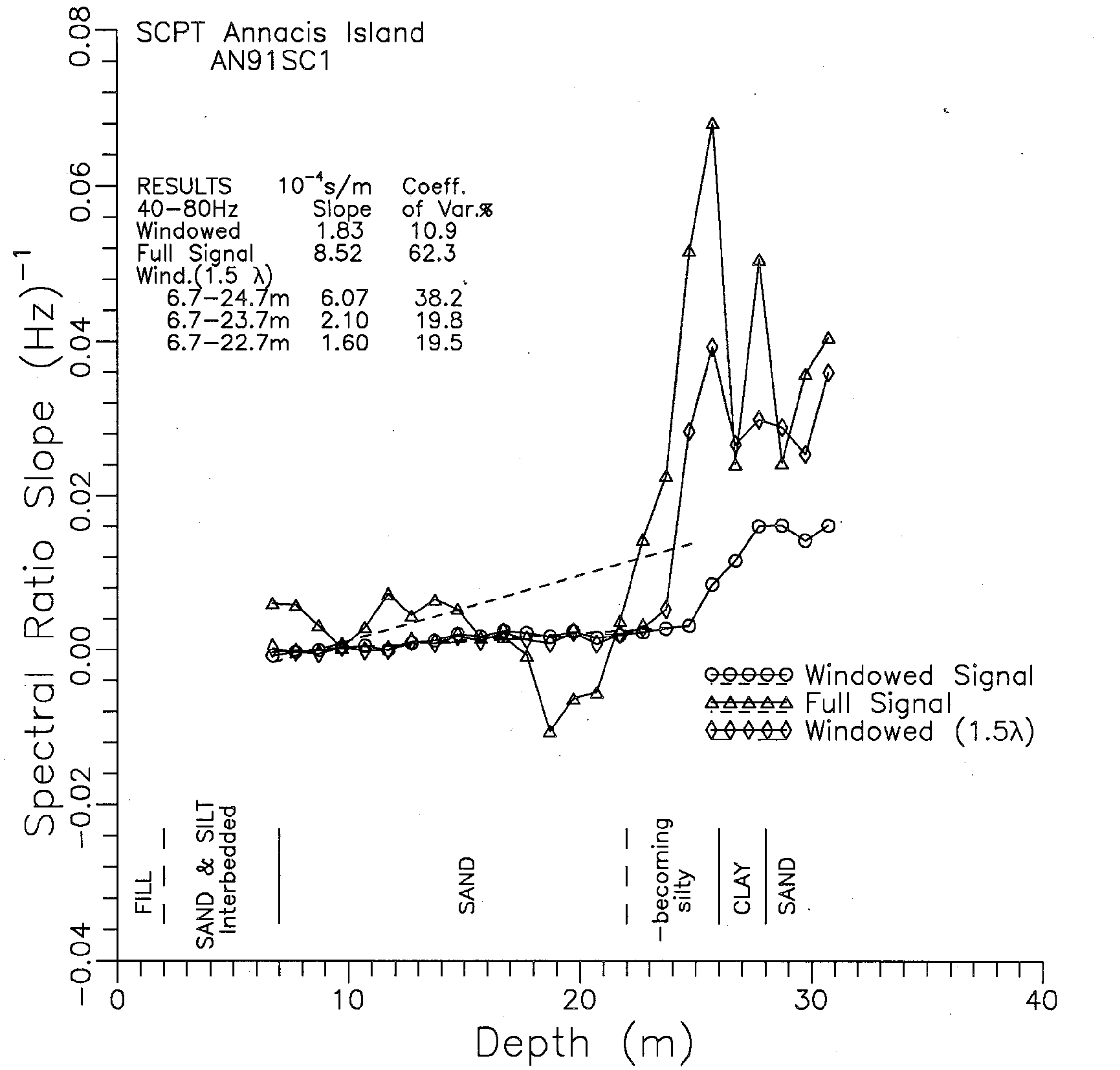


Fig.7.35 Effect of Signal Processing on Damping – Annacis N.Pier Site

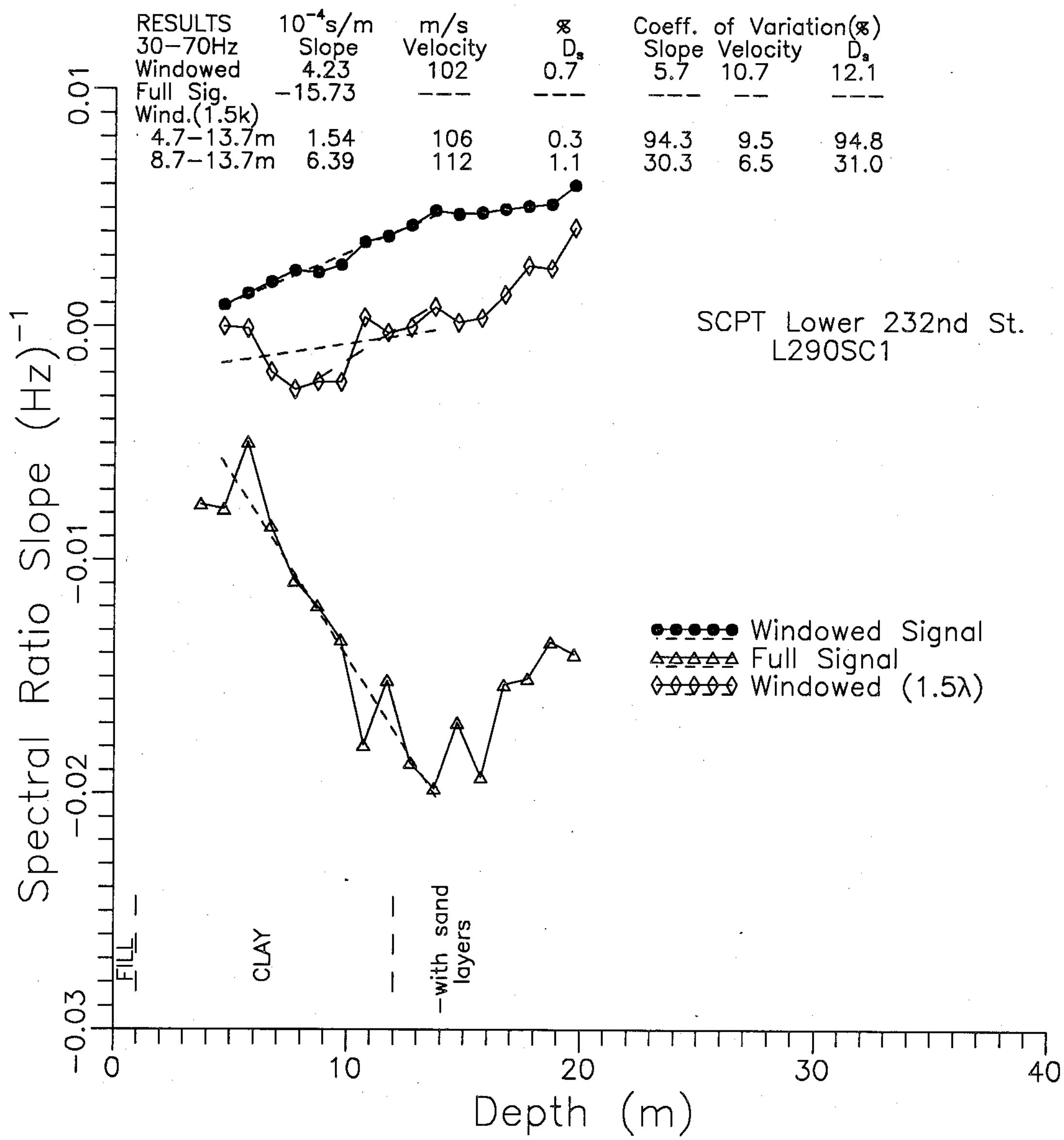


Fig.7.36 Effect of Signal Processing on Damping – Lower 232nd St. Site

signal analyses. The scatter was considerably greater than for the windowed case, with the coefficient of variation being from about 3.5 to more than 15 times greater.

As mentioned previously, the cause(s) of the oscillations after the main shear wave are not clear, but, for the system used for this research, it is clear from the erratic results using the full signals that the shear wave should be windowed to isolate the shear wave before further calculations are done. It is also clear that using a window length of 1.5 wavelengths generally gives more scatter and higher damping values. Chapter 8 will present a comparison of calculated damping values with available laboratory measurements and published recommendations. This comparison shows that the lower values of damping given by windowing over 1 wavelength compare more closely to available data. This finding, and the larger scatter using 1.5 wavelengths, indicate the window used on the data should not be longer than one wavelength.

### *7.6 SPECTRAL SMOOTHING-AN ALTERNATIVE TO WINDOWING?*

Some researchers (e.g.Redpath et al,1982) have used spectral smoothing as an alternative to windowing in damping calculations. Redpath et al stated that their "most common smoothing procedure was to use a 7-point running average on the individual spectra and a 15-point running average on the final ratio."

The magnitude of a typical signal is shown in Fig.7.37, along with the magnitude after smoothing with 5-point, 9-point, and 15-point triangular-weighted smoothing functions. Also shown is the magnitude of the signal after windowing. After applying the 5-point function the signal remains quite irregular. After applying the 9-point function the signal is only slightly more irregular than for the 15-point function. The signal resulting from the 15-point smoothing is visually as smooth as the windowed signal, but of rather different shape.

Standard triangular smoothing functions are effectively mild low-pass filters when applied to time domain data, and would be expected to operate similarly on the magnitude of the FFT which is simply a collection of real values equally spaced in frequency rather than time. If we consider the frequency axis as time, we can take the FFT of the magnitudes of signals. The resulting magnitudes, for no smoothing and with 15-point smoothing, are shown in Fig.7.38. There is obviously some type of low-pass "filtering" as a result of the smoothing. However, the physical result of the smoothing is not clear as the smoothed magnitude cannot be inverse transformed to the time domain, as the phase information has been lost.

For one of the SCPT's, damping calculations were carried out using both 9-point and 15-point smoothing on the FFT's of the full signals. Both the individual spectra and the resulting ratios were smoothed with one pass of the smoothing function. The resulting ratios, along with those for the windowed signal, are given in Fig.7.39. There was little

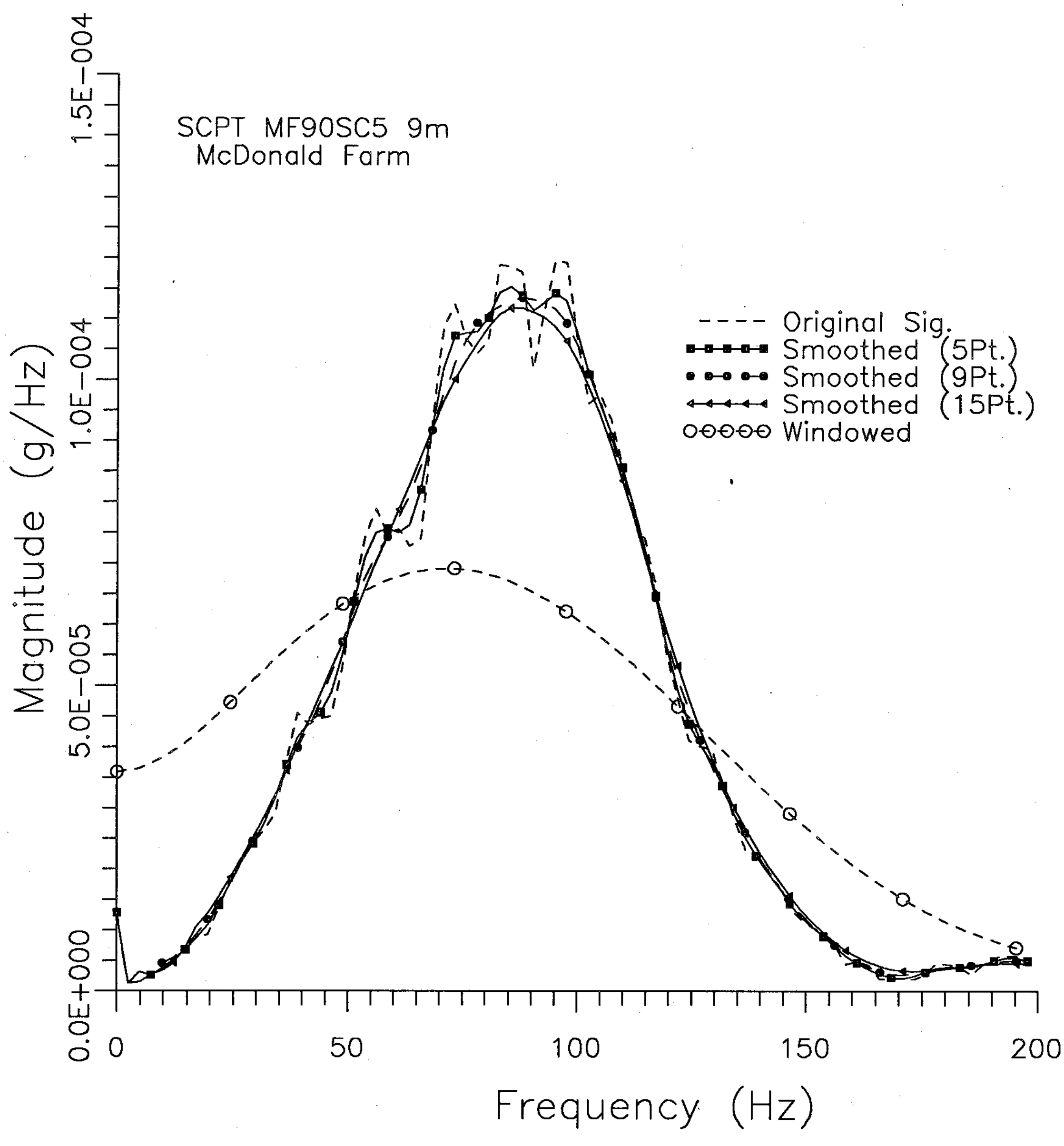


Fig.7.37 Effect of Size of Smoothing Function

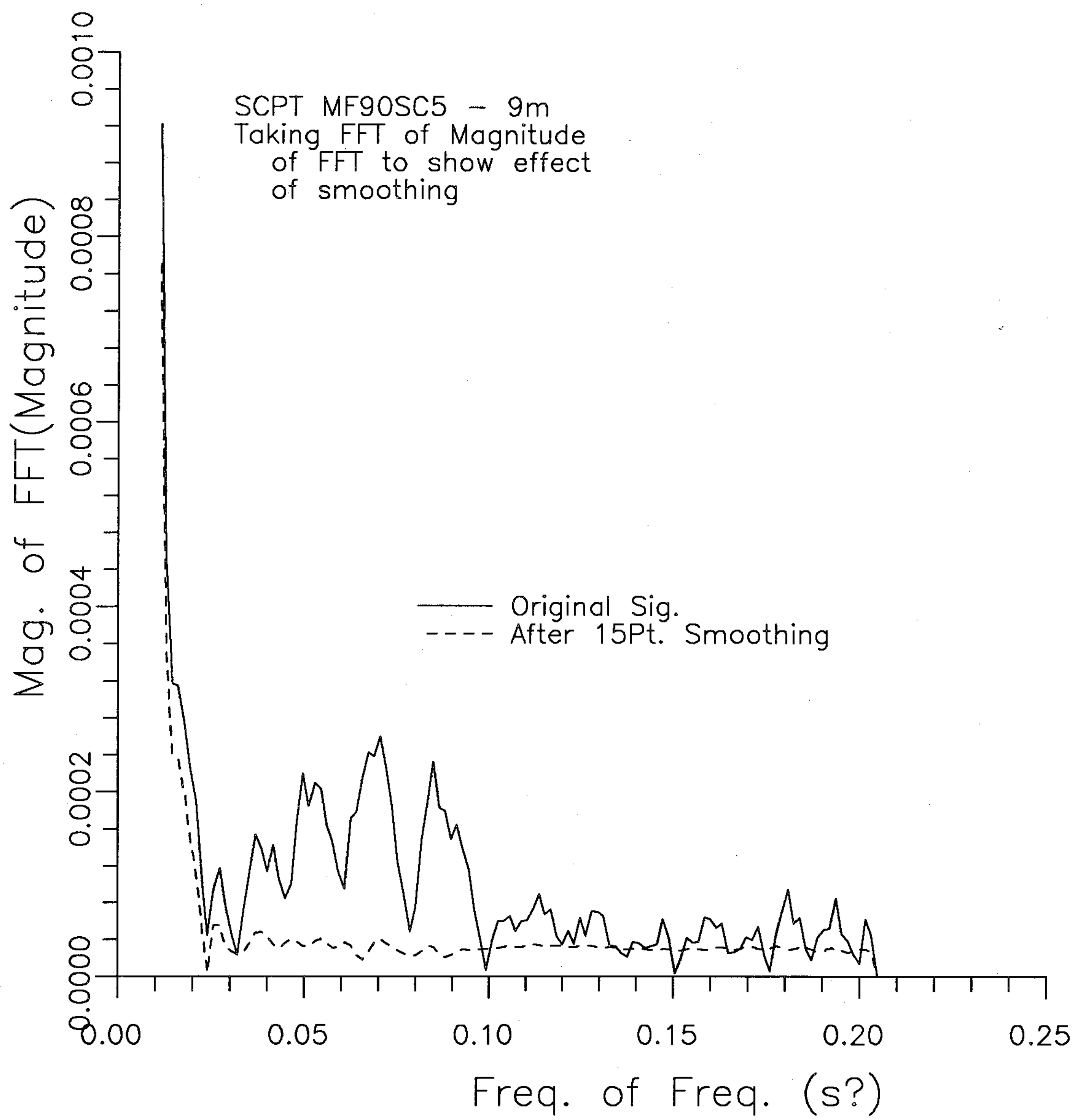


Fig.7.38 FFT's of Original and Smoothed Magnitude of FFT

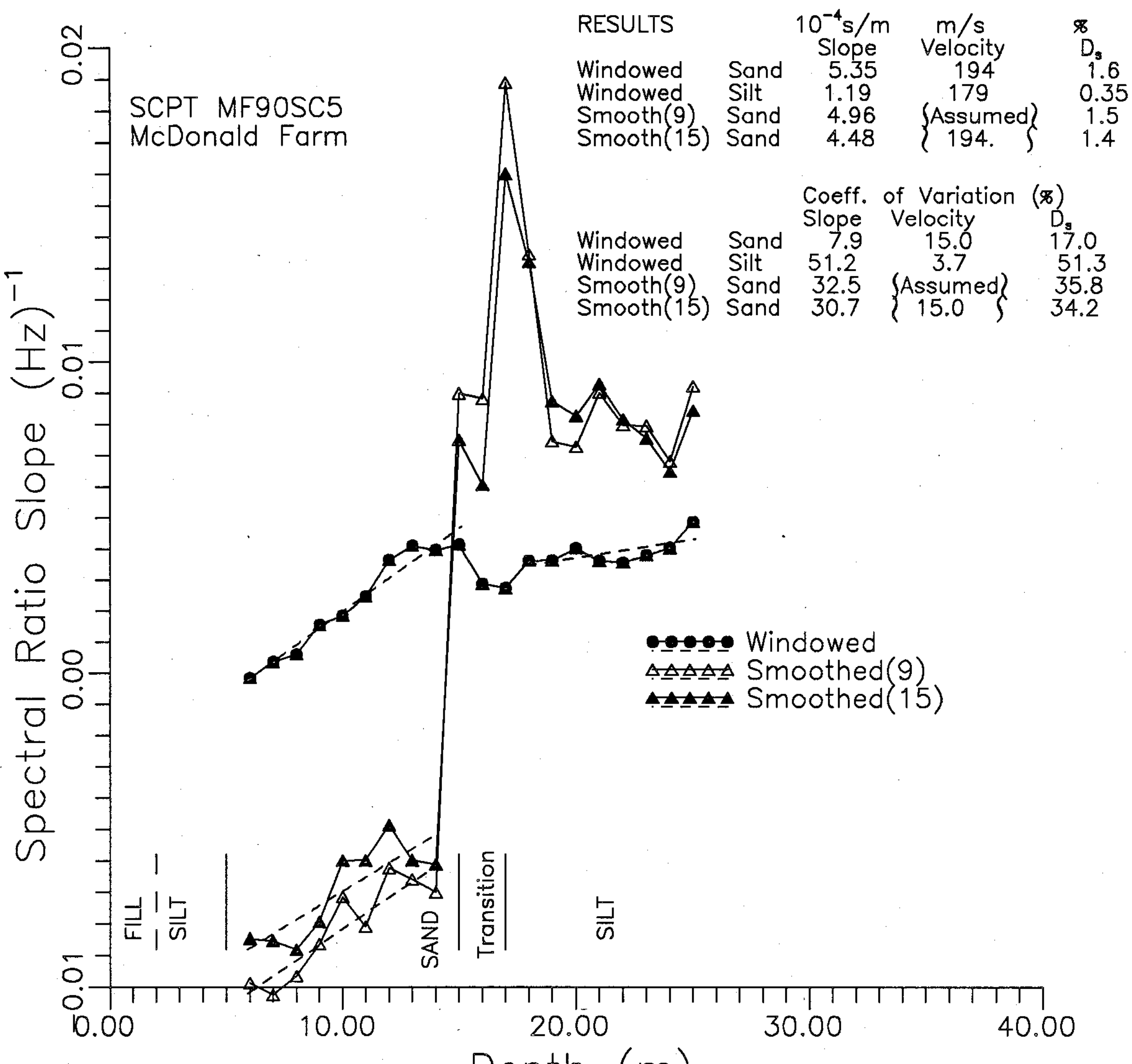

Fig.7.39 SRS Profiles — Windowed and Smoothed Analyses

difference between the results using 9-point and 15-point smoothing. In the upper sands, the calculated damping values were close to that for the windowed signal (1.5% and 1.4% compared to 1.6%). However there was considerably more scatter in the smoothed results; the coefficients of variation of the slopes were about 4 times greater. In the lower silts, the results of the smoothed calculations are not clear but would indicate a negative value for damping, whereas the windowed calculations clearly show a small yet positive value for damping.

The results of windowing the shear wave from a signal are physically clear (zeroing out of the rest of the signal), whereas the results of smoothing in the frequency domain are not intuitively clear. It has been shown, at least for this example, that the windowed calculation approach gave results with considerably less scatter (about one-half) and gave positive damping in the clayey silt. It is concluded that the windowed signal approach is preferable to smoothing of the spectra of the full signals.

## *7.7 DAMPING MEASUREMENTS WITH OTHER RECEIVERS*

Receivers that have been used in the SCPT were discussed in some detail in section 5.3. Attempts to calculate damping for receivers other than accelerometers are discussed in this section.

### 7.7.1 Geophones

A miniature geophone with a natural frequency of about 30Hz and damping in the order of 15% was installed in a cone for shear wave velocity measurements. This section provides an attempt to calculate damping from such measurements. The spectral ratio slope method was applied to records measured over a depth of 5 to 20m in a mainly sand deposit (Annacis North Pier site). The results given in Fig.7.40 show little or no damping from 5 to 10m then 4.5% damping from 10 to 20m. A nearby test using accelerometer records gave damping of 0.6% over the range of 5 to 17m. It appears that the damping of the geophone has increased the apparent damping measured and it is not obvious how these effects can be removed (see Fig.5.6). It should be noted again that larger geophones have been successfully used in cased drillholes. Redpath et al(1982) used 10Hz geophones with damping of 0.7, and reported that these had a flat response from 15 to 200 Hz. They used a bandwidth of 40 to 100 Hz to measure damping. It would appear that it may be possible to use a geophone in the SCPT if it could be critically damped.

### 7.7.2 Benders

The bender units used are piezoceramic transducers. When mounted as a cantilever in the cone the resonant frequency is 1520Hz and the receivers are undamped. The measured signals were frequently

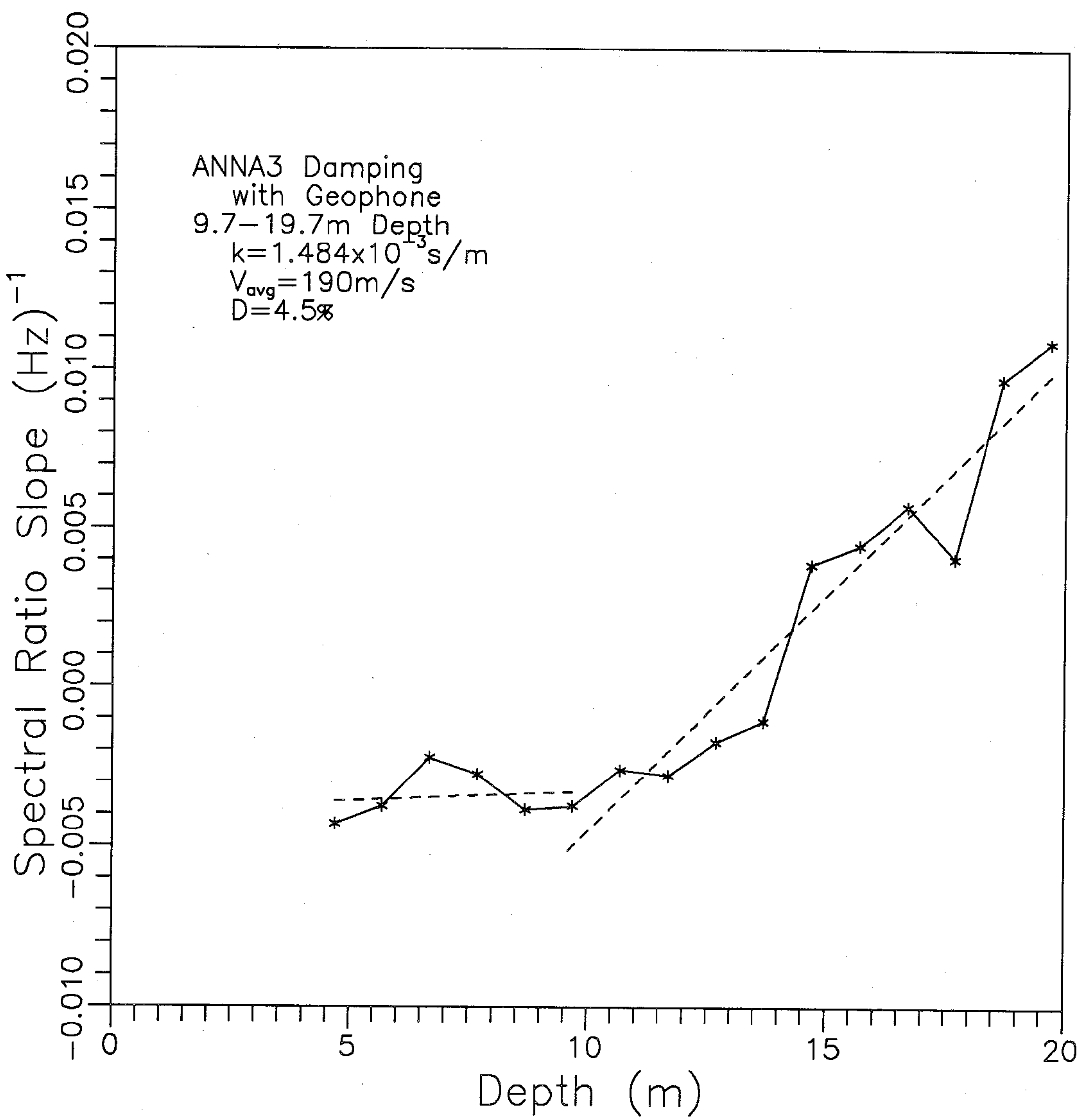

Fig.7.40 Damping Measurements with Geophone Receiver

contaminated with noise (see Fig.5.7). As can be seen in Fig.5.8, the noise appeared to occur at multiples of 60 Hz. A portion (4 to 10m) of one seismic cone penetration test using a bender (SC-89-M3) contained fairly clean signals. However the slope of the spectral ratio curve with depth was irregular, and trended to a negative value (see Fig.7.41).

Another attempt to use benders to calculate damping was made using data collected from the hydraulic gradient similitude (HGS) method testing reported by Yan and Byrne(1990). In this testing, one bender was used as the source and three as receivers. Since the test was done in a saturated soil, the benders were coated in epoxy to prevent wetting. This coating would have changed the natural frequencies of the benders and no testing was done to measure the new resonant frequency. Because of the relatively close spacing (35 to 55mm) of the receivers, a high frequency (10 kHz) source was used. A shaker test on a bender unit is presented in Fig.5.9, which shows that there is not a flat response over the full range of the test. From a HGS test with a gradient of 70, the average velocity was calculated to be 160m/s. The signal measured at the receiver nearest the source (S2) is shown in Fig.7.42. The time signals were multiplied by a rectangular window to isolate the main shear wave. The FFT of a resulting signal is given in Fig.7.43, with the peak just under 5 kHz, the main pulse from about 1500 to 8500 Hz, and very little energy beyond 20 kHz. The spectral ratio slope method was applied to the windowed signals. One step in the calculation is

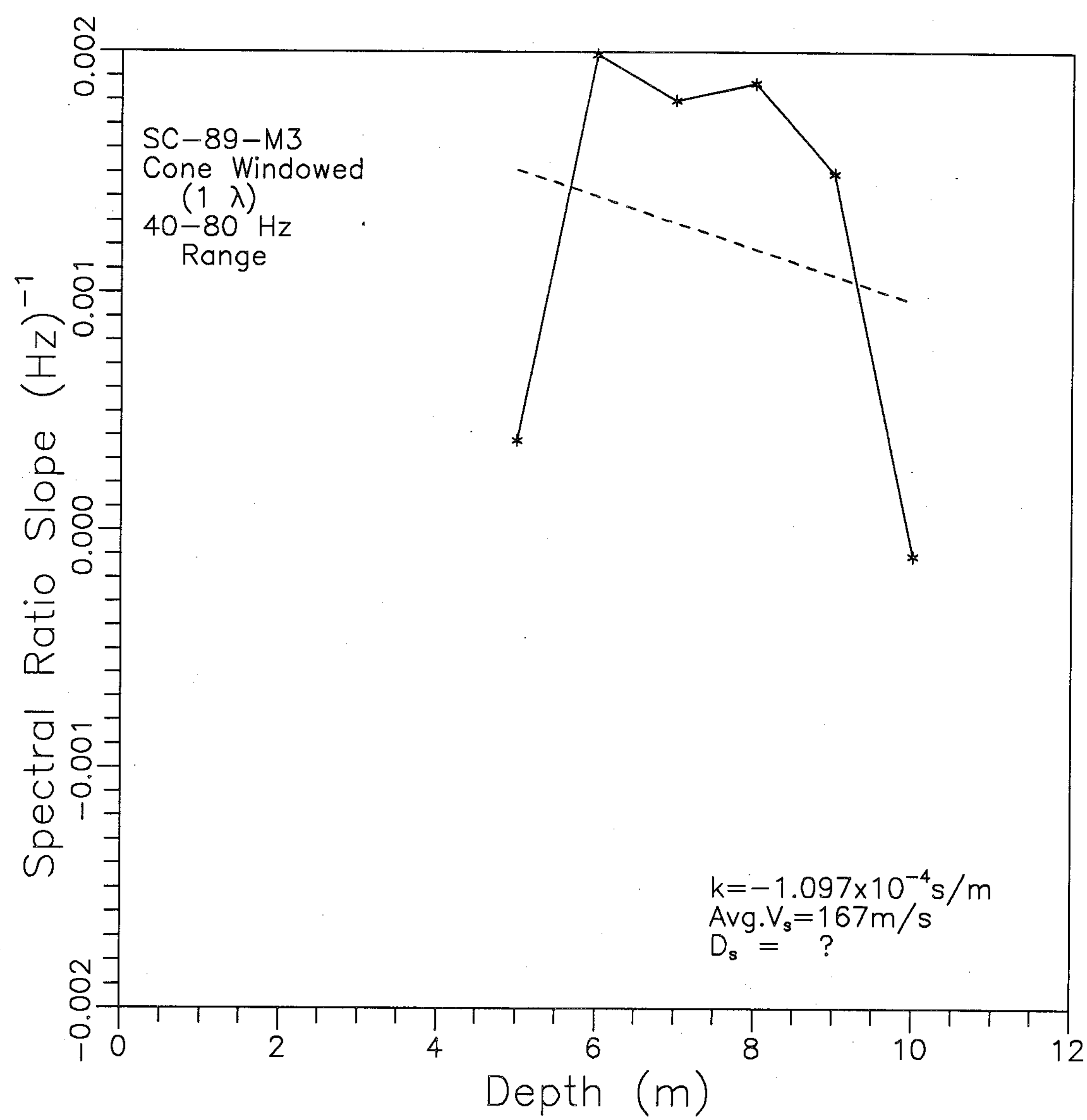

Fig.7.41 Damping Measurements with Bender Receiver

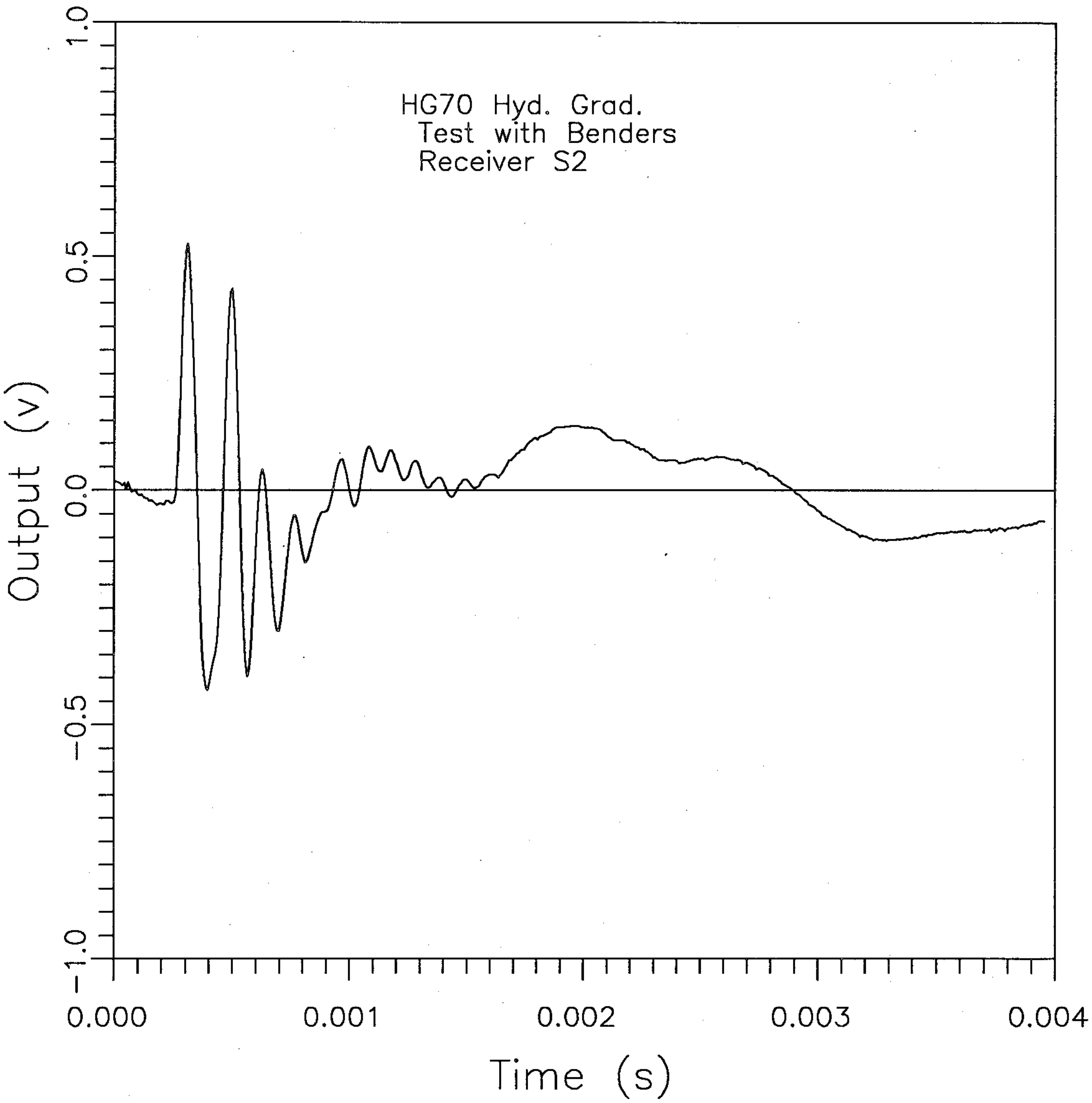


Fig.7.42 Bender Signal in HGS Test

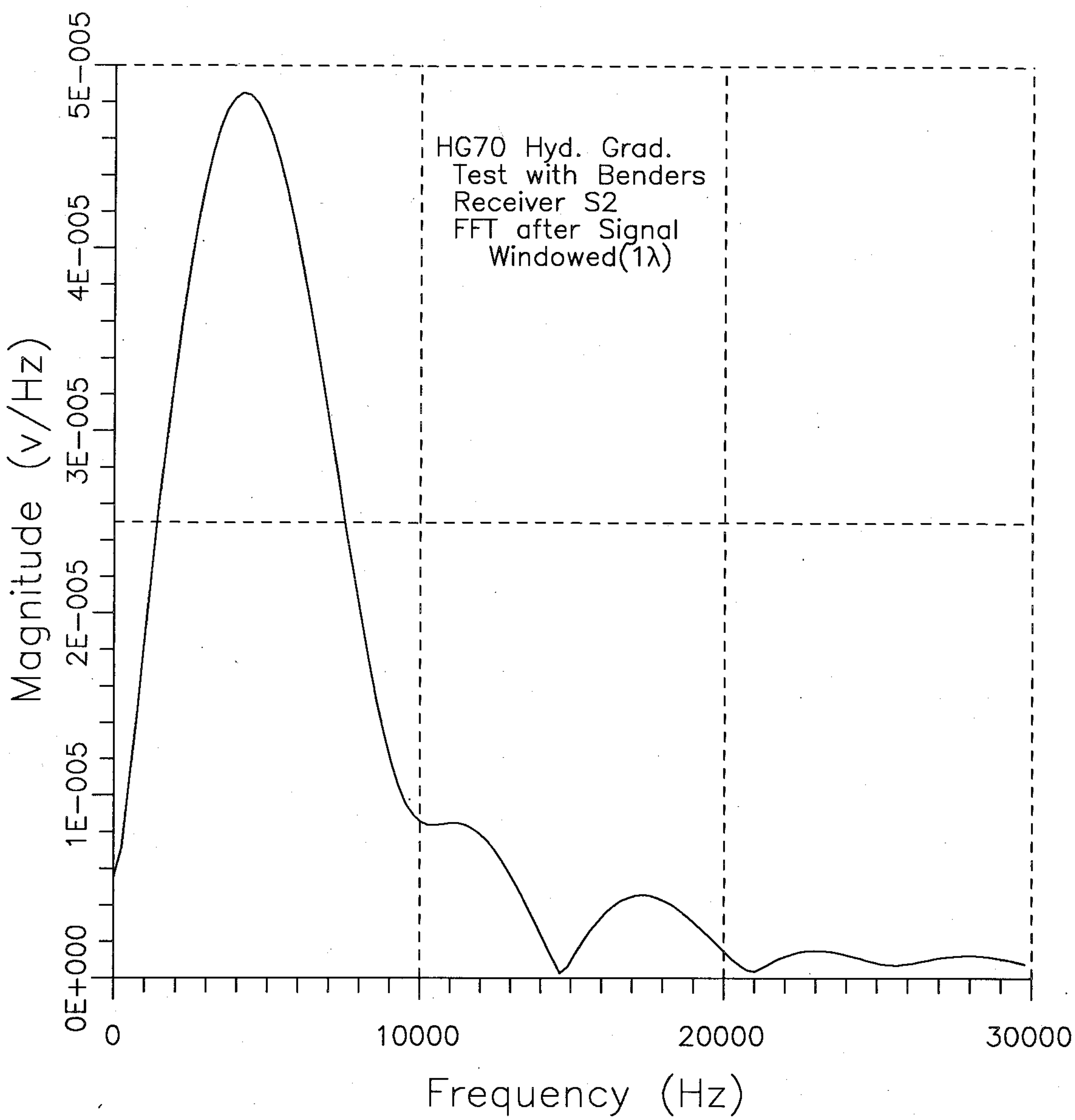


Fig.7.43 FFT of Bender Signal in HGS Test

shown in Fig.7.44. There is not an obvious frequency range over which to select a slope, as the curve is very irregular over the full range of 0 to 20 KHz shown. For the purpose of calculating a damping value a range of 4k to 9kHz was selected. The resulting values are shown in Fig.7.45, giving a damping value of 1.8%. The three points did not clearly form a line. Although the measured damping value is similar to those measured in sand in the field at the McDonald Farm site, this is considered somewhat fortuitous given the scatter shown in Fig.7.45.

## *7.8 GEOMETRIC CORRECTIONS FROM DAMPING SPIRAL METHOD*

The damping spiral method was discussed in section 7.2.5. This method allows the direct calculation of the geometric (frequency-independent) corrections that must have occurred between two measured signals. These can be compared with the spherical spreading correction, multiplied by the transmissivity and divergence corrections calculated from the measured velocities (or perhaps from some other basis). This allows a check on the validity of calculated values of the transmissivity and divergence corrections.

In complex exponential form, the basic equation for the method was given as eqn.7.3, which is repeated here:

$$[7.16] \qquad \frac{A_2}{A_1} = \frac{x_1}{x_2} \, e^{-(D\omega/c)(x2-x1)} \, e^{(i\omega/c)(x2-x1)}$$

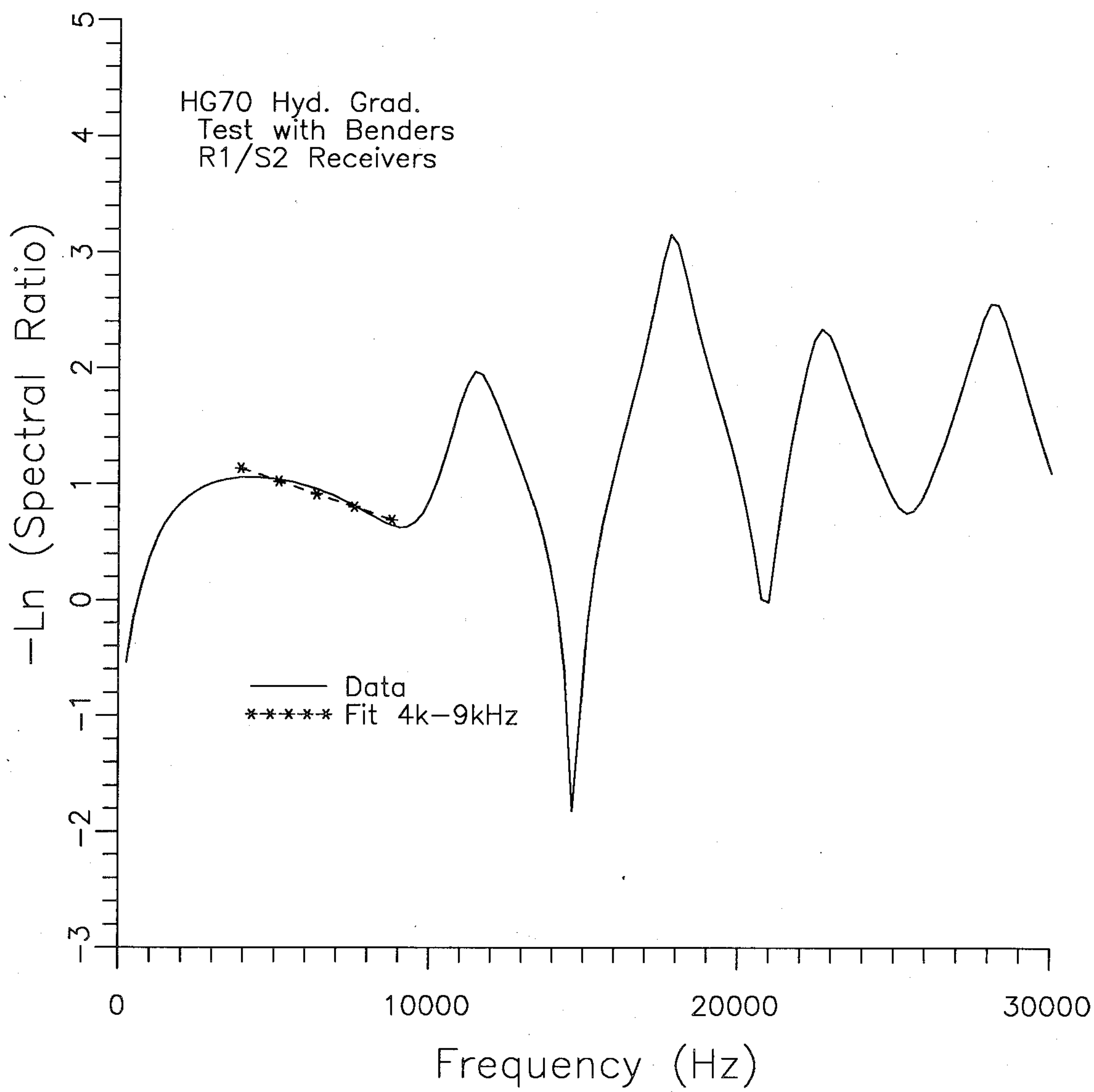


Fig.7.44 Variation of Ratio of FFT's with Frequency in HGS Test

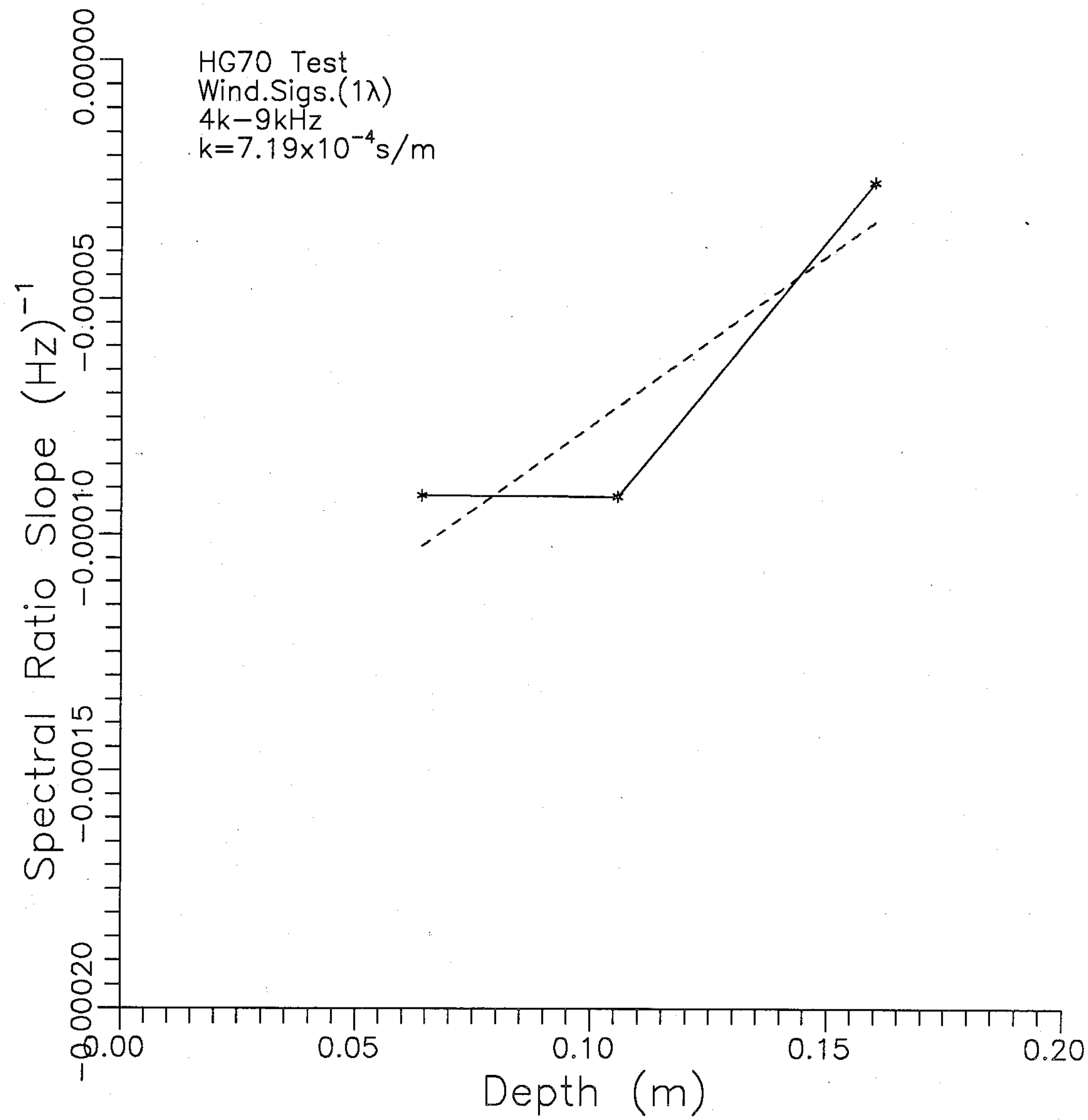


Fig.7.45 Damping in HGS Test

Taking natural logarithms, gives:

$$\ln\left|\frac{A_2}{A_1}\right| = \ln\left|\frac{x_1}{x_2}\right| -(D\omega/c)(x2-x1) + (i\omega/c)(x2-x1) \tag{7.17}$$

The term $x_1/x_2$ represents the geometric damping due to spherical spreading in a homogeneous material. In layered materials, as discussed in Section 2.5, there are additional geometric damping terms due to transmissivity and divergence (T&D corrections). For records obtained in layered soils, the total geometric damping includes the T&D corrections, so it is appropriate to replace the $x_1/x_2$, with $G_1/G_2$, where the terms in G represent the total geometric damping.

For damping calculations, it is convenient to plot the $-\ln(A_2/A_1)$ versus frequency, $\omega$. When the frequency is zero the latter two terms in eqn.7.17 are zero, thus the intercept is $-\ln(G_1/G_2)$ or $\ln(G_2/G_1)$. Taking the exponential of this term gives $G=G_2/G_1$. The depths of the records are known so that the corresponding term for spherical spreading, $x=x_2/x_1$, can be computed. The combined T&D correction is given by G/x. For plotting purposes, the T&D correction was multiplied by the corresponding depth to give a correction corresponding to an "equivalent depth" as was done previously for T&D corrections calculated from velocity measurements.

This method of calculating the T&D corrections was first applied to the sounding (MF90SC5) used for the calculations using velocities (Fig.7.3). The results from the damping spiral method (TDDS) are presented in Fig.7.46, along with the values calculated from velocities

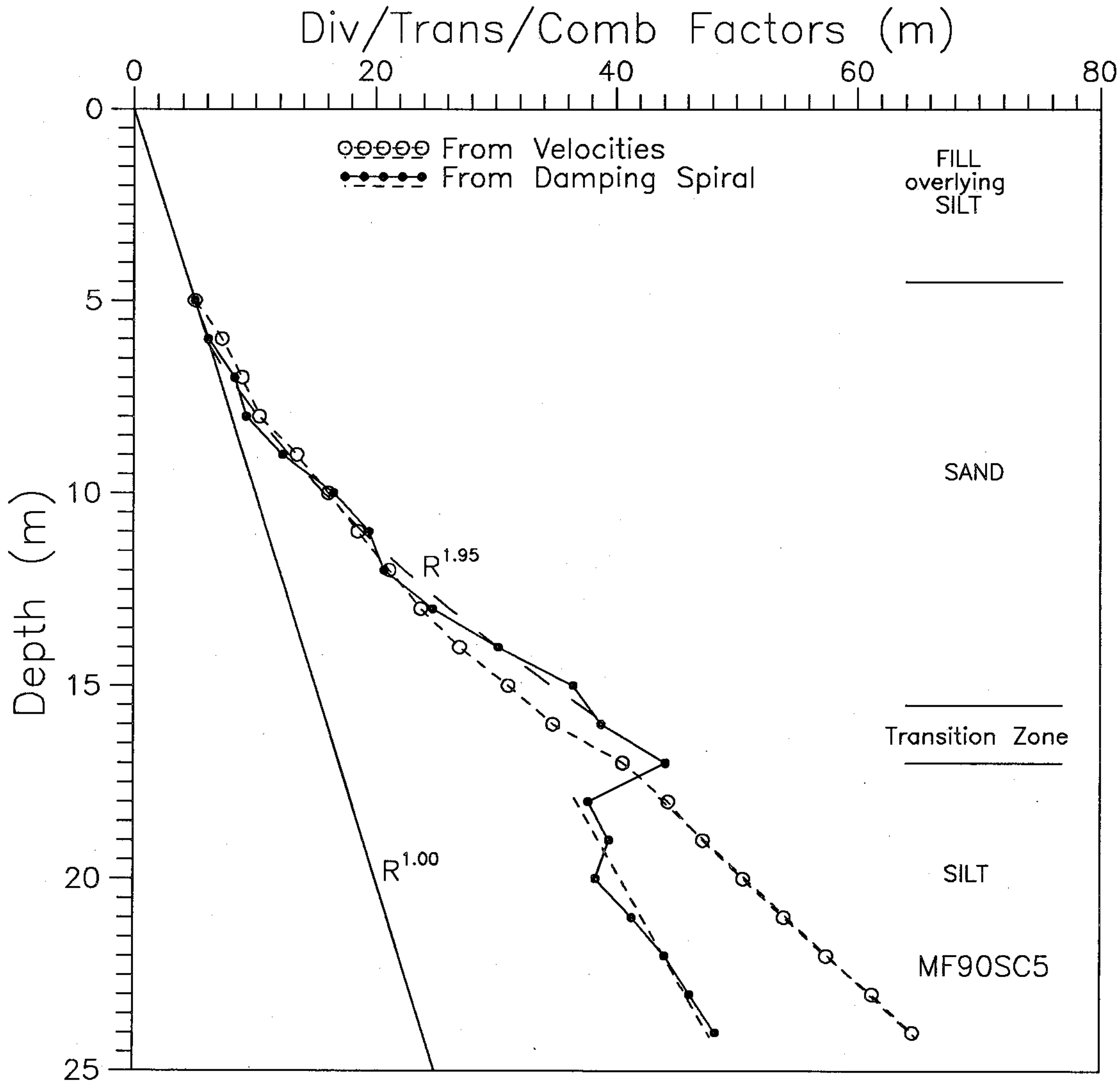


Fig.7.46 Comparison of Combined Transmissivity and Divergence (T&D) Calculations using Damping Spiral Method and from Velocities — SCPT MF90SC5

(TDV). The TDV values agreed fairly closely in the sand, but the equivalent exponent (1.65) was somewhat less than for the TDDS values (1.95). Calculations based on velocities could not predict the effects of the interfaces at the transition zone. In the underlying silt the TDV values had a steeper slope (3.41) than the slope (1.82) calculated directly from the records.

An adjacent sounding (MF91SC1) was analyzed and the results are compared with those for the previous sounding in Fig.7.47. The T&D values were in reasonable agreement in the sand, but differed by up to 40% in the transition zone. The slopes in the silt also differed considerably (0.83 for MF91SC1 and 1.82 for MF90SC5).

The results for an analysis for a site consisting mainly of clay (with scattered sand seams below about 12m) - SCPT L291SC1 - is shown in Fig.7.48. The resulting T&D corrections are small (ranging from 0.73 to 1.4). Corrections based on velocity measurements would seriously overestimate the T&D corrections. The results from another sounding about 20m to the north (L289SC1) are compared with the first set in Fig.7.49. and the findings are in reasonable agreement.

From the results presented above, it appears that damping spiral calculations for T&D corrections are fairly repeatable for the sand and clay, but not for the deeper silt. Differences in the silt may be caused by the low strain levels achieved. Calculations of T&D corrections using measured velocities appear to give reasonable results in the sand, but poor results in the clay and silt.

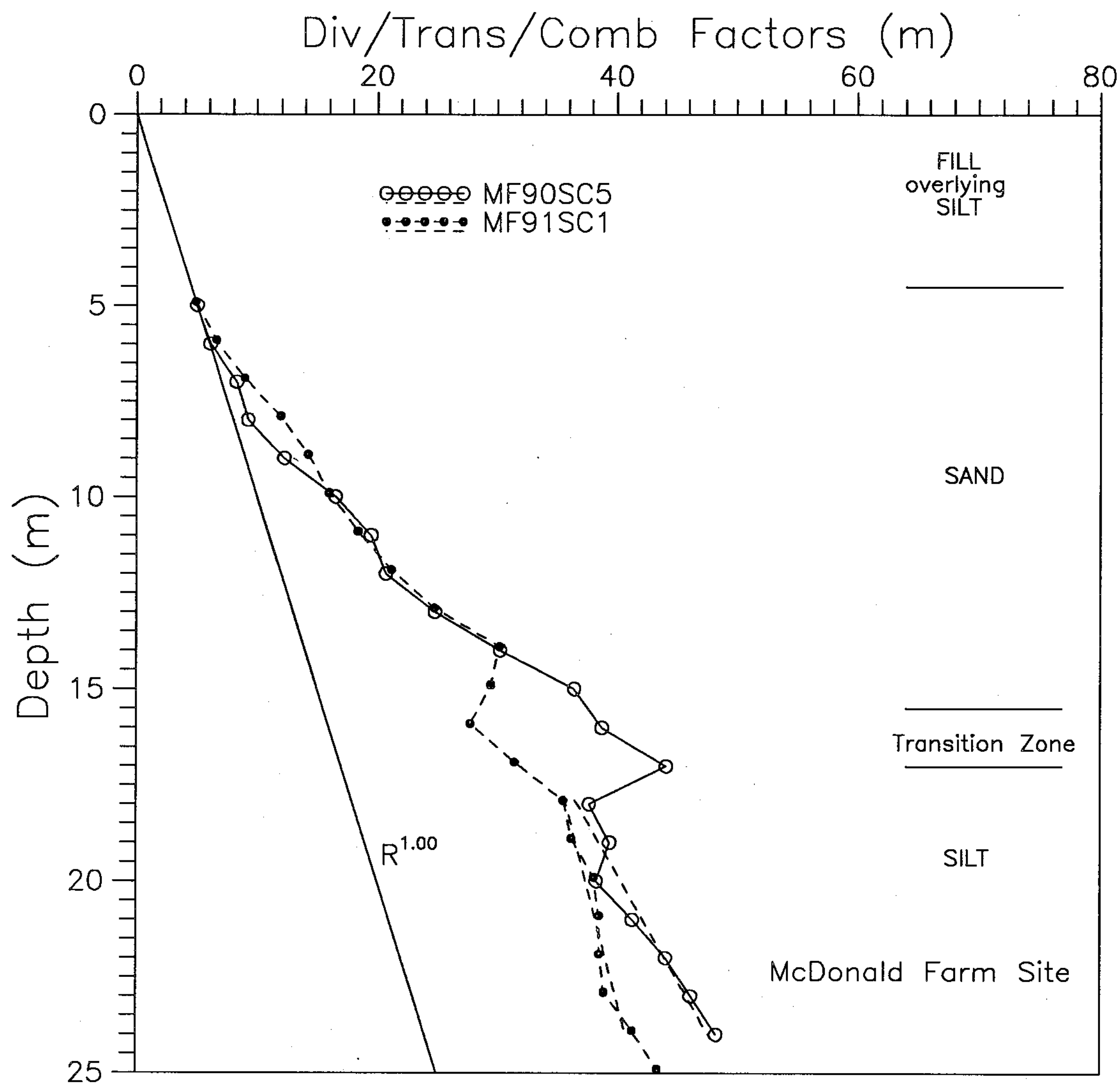


Fig.7.47 Comparison of T&D Calculations for Two SCPT's – McDonald Farm Site

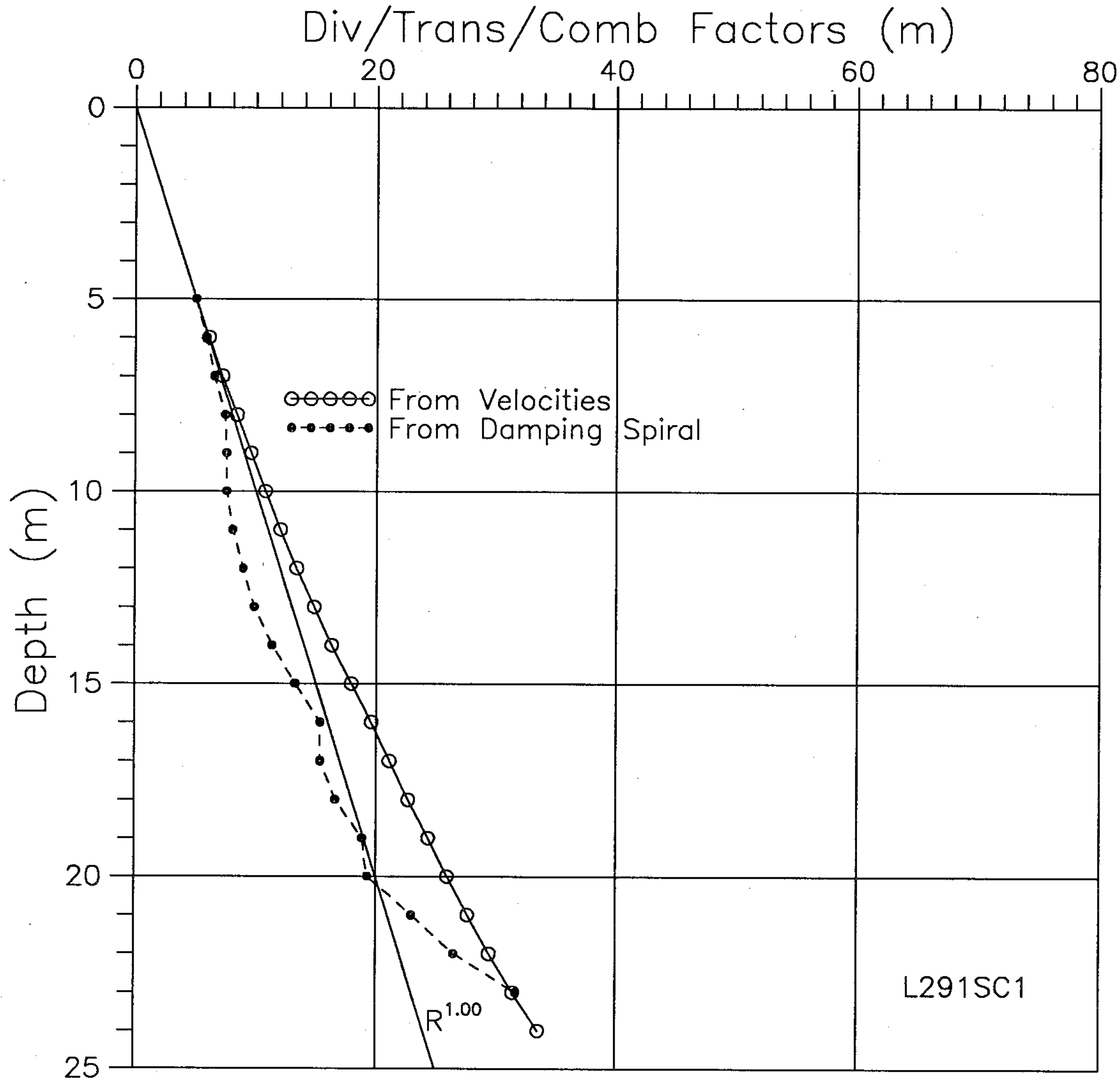


Fig.7.48 Comparison of T&D Calculations using Damping Spiral Method and from Velocities – SCPT L291SC1

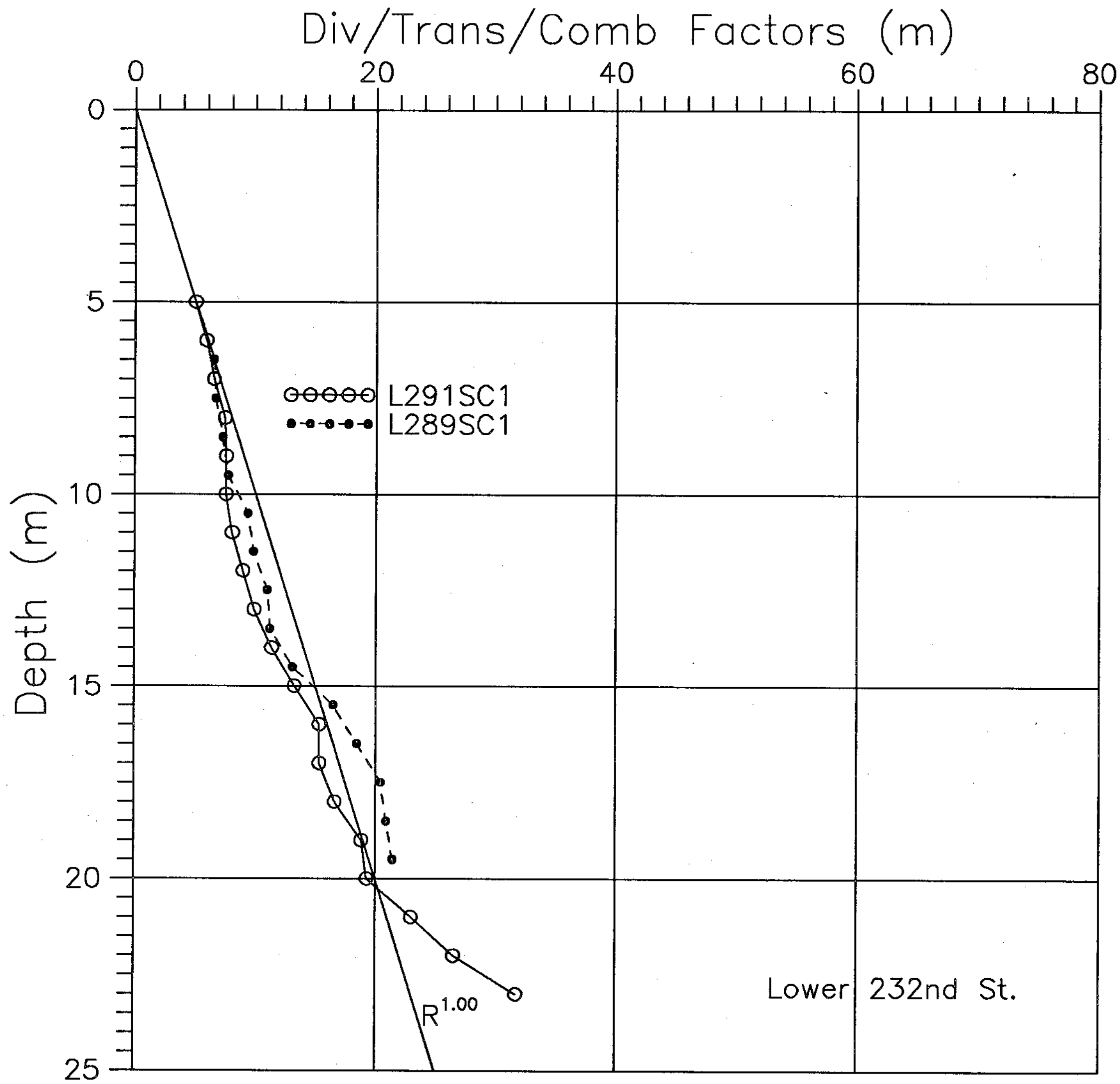


Fig.7.49 Comparison of T&D Calculations for Two SCPT's
– Lower 232nd St. Site

### *7.9 APPLICATION OF SRS METHOD TO EARTHQUAKE RECORDS*

Vertical arrays of accelerometers are being installed in earthquake-prone areas to measure simultaneous records of acceleration at various depths for various strain levels during earthquake shaking. It is of interest to determine if the damping methodology developed can be applied to these records. Details of the free-field downhole array (DHB) at the Lotung site in Taiwan are provided in Chang et al (1991). Basically the array consists of three-component accelerometers (N-S, E-W, and vertical) at the surface and depths of 6m, 11m, 17m, and 47m. Records for two of the events at the site were provided by the Geomatrix/EPRI group.

A more detailed review of the data is presented in Appendix C, with a summary of the findings presented here. A typical signal for event #7 had a peak acceleration of 107cm/s$^2$ (0.11g), and most of the energy of the signal was between 0.3 and 3Hz.

The first step in the calculation of damping is the calculation of the shear wave velocities. Since these signals involve larger strains it is not immediately obvious which method of calculating velocities is most appropriate. Chang et al (1991) used the signals to calculate velocities following the approach of Dobry et al (1976) which requires calculation of the resonant frequencies of the layers between the receivers. This approach was reviewed and the resulting velocities were confirmed.

However if damping calculations are to be based on windowed signals, it seems appropriate to calculate velocities using windowed shear waves. Velocities were calculated using the cross-correlation and phase methods. The results were similar and (except for the first layer) were about 80% of the values from the resonant frequency method. Presumably this effect can be explained as the strain in the peak wave was likely higher than that used in the resonant frequency method.

For the windowed shear wave signals it was observed that the time of the peak increased as the depth decreased, as expected for a wave moving upwards. It was also observed that the amplitude increases as the depth decreases. For planar waves moving upwards, it would be expected that there would be a slight decrease in amplitude due to damping. It would appear that there is some type of amplification occurring as the wave move upwards. A similar result was observed in the E-W component of the signals.

The spectral ratio slope method was applied to the windowed signals, using the 47m records as the reference signals, for both the N-S and E-W components from event #7. The slope given by the E-W records gave a negative value of damping. For the N-S records the slope from 6m to the surface only is similar to that for the E-W records, and it was observed that the amplification is much greater between these signals than it is for the lower three signals.

It is concluded that amplification, likely due to resonance effects, is occurring in the earthquake events, so that the method of damping calculation developed for SCPT results cannot be applied to earthquake records from an array. It is likely that the amplification is frequency-dependent, so that the spectral ratio slope method cannot remove the amplification effects. Application of more complex methods such as SHAKE or DESRA would require more complete information on the soil stratigraphy and properties.

# CHAPTER 8

# VERIFICATION OF RESULTS

Available means of verification of the results of calculations of velocities and damping values from insitu measurements include: site-specific and general area tests, including field and laboratory methods; published results and recommendations; and application of the results to the analysis of earthquake records. Since it is hoped that the methods developed will eventually be applied to the analysis of seismic problems, an analysis of a well-documented earthquake at a site where testing was conducted could provide valuable verification. For the other approaches to verification, the general order of applicability would be site-specific tests, general area tests, and published results and recommendations.

## *8.1 PENDER ISLAND EARTHQUAKE*

The best means of verification of the results would be a well-instrumented earthquake case history inducing strains near the level of the measurements. Such an ideal case history does not exist in this area , but records are available for the 1976 Pender Island quake. The Pender Island earthquake occurred on May 16,1976 and had a Richter magnitude of between 5.0 and 5.5. The epicentre was on Pender Island at longitude 123.34W and latitude 48.80N. The earthquake was recorded at several sites in the southwest corner of British Columbia. Two sites are of particular interest; Lake Cowichan where the site was underlain by rock, and Annacis Island where the site was underlain by a deep soil deposit where some detailed soil investigations have been carried out. Wallis (1979) analyzed these records as well as those from two other Lower Mainland sites. However, site specific dynamic test results were not available at that time.

A detailed analysis of the earthquake records is presented in Appendix D. Unfortunately, the evaluation of the results appears to indicate that the measured soil motion at Annacis Island could not result from the measured rock motion at Lake Cowichan, at least not with simple vertical propagation through the soil. The measured soil motion appears to have "excess energy" in the 0.8 to 1.8Hz range. Taylor et al (1983) attributed the difference between the measured and calculated response to the presence of surface waves. Although this may be the cause, it is also possible that the rock motion was different at the two locations. It is obvious that care must be exercised if the records are to be scaled to model larger earthquakes and that the records cannot be used to evaluate damping in the soil at Annacis Island.

## *8.2 VERIFICATION OF VELOCITY MEASUREMENTS*

### 8.2.1 Comparison with Laboratory Results

Zavoral (1990) carried out a series of tests on both block and tube samples of clay from the Lower 232nd St. site. The tests that apply to this discussion were resonant column tests conducted on tube samples retrieved over a variety of depths. Basically, the test measures the resonant frequency of a cylindrical sample at a certain strain level. Knowing the resonant frequency, $\omega$, the sample height, h, the mass moment of inertia of the sample, I (from the dimensions and weight), and the mass moment of inertia of the driving cap, $I_o$, the shear wave velocity, $V_s$, can be calculated from the frequency equation of motion (Drenevich et al, 1978):

[8.1] $I/I_o = (\omega h/V_s)\tan(\omega h/V_s)$

Computer programs have been developed to solve eqn.8.1.

The shear wave velocities are normally converted to shear modulus values using: $G_{max} = \rho V_s^2$. Resonant column tests were performed over a range of confining pressures and the data were fitted to give an equation relating the modulus to the confining pressure, $\sigma'_{3c}$, (normalized by the atmospheric pressure, $p_a$) as presented by Zavoral (1990):

[8.2] $G_{max} = 292.1\ p_a^{0.1}\ \sigma'_{3c}{}^{0.9}$

To apply this equation to the field, the insitu octahedral stress was calculated at several depths assuming an at rest lateral pressure coefficient of 0.55, and this stress was used in eqn.8.2, and the resulting values of $G_{max}$ were converted to shear wave velocities. The results are presented in Fig.8.1.

The laboratory values were about 7% less than the field measurements, but increase at about the same rate with depth. The shear strains were similar in both the field and laboratory tests. However

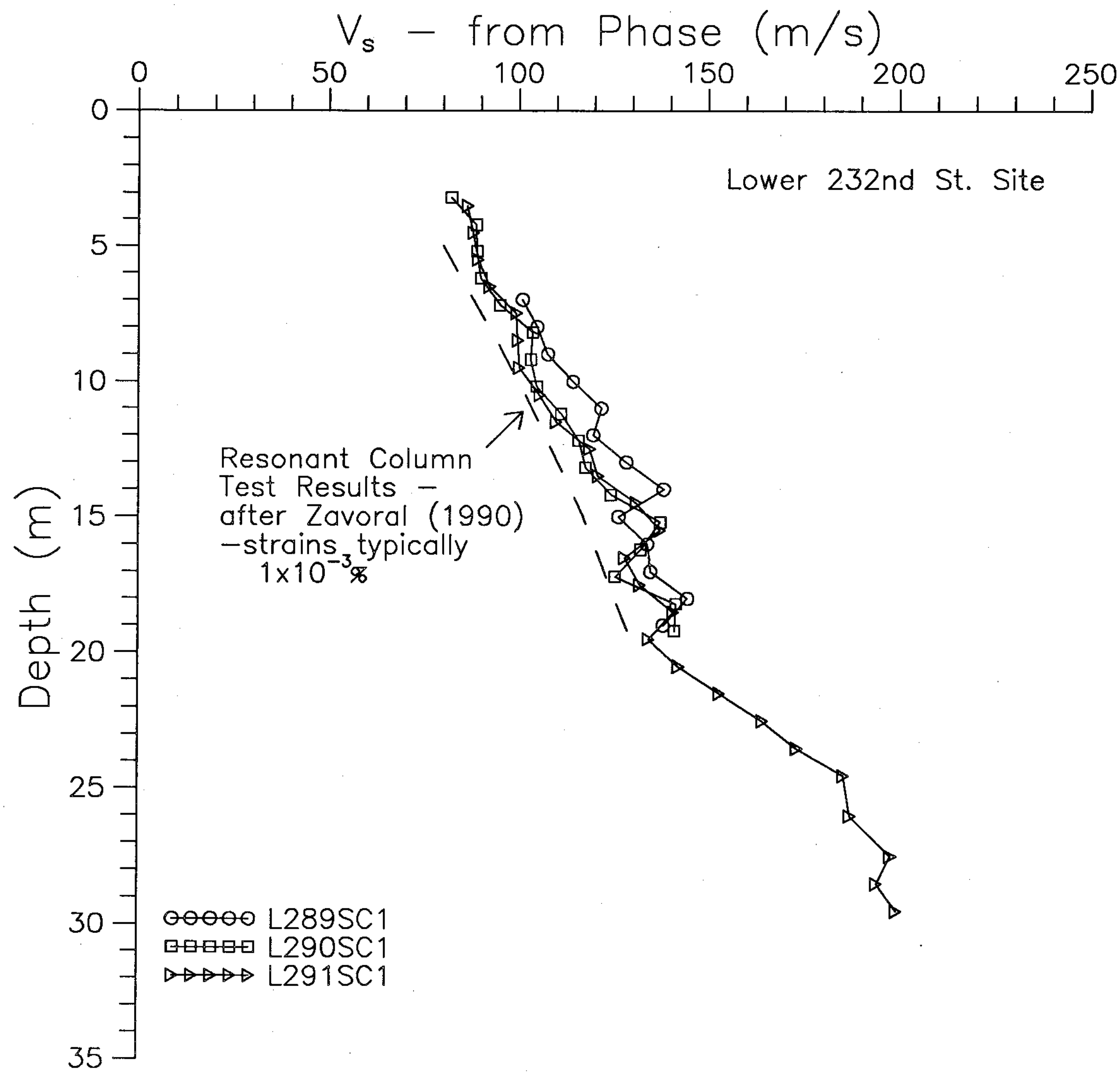


Fig.8.1 Comparison of Velocities with Laboratory Results

the laboratory values should still be expected to be somewhat less as they were typically determined after 1000min of sample confinement, and the field samples have aged for several thousands of years. Data presented by Richart et al (1977) suggested that, for normally consolidated clays, laboratory measurements of $G_{max}$ could be 70% (or less) of insitu values (this would indicate that $V_s$ would be 84% $\{=(0.7)^{0.5}\}$ or less). These values were essentially confirmed by Kokusho et al (1982) who related the normalized increase in shear modulus with time, ($N_G=\Delta G/G_{1000min}$) to plasticity index, $I_p$. For the clay at the Lower 232nd St. site, the $I_p$ reported by Zavoral(1990) was 24%, which would give an $N_G$ of 13%, compared with the 5% to 20% given by Richart et al (1977). Zavoral (1990) found values for $N_G$ for the Lower 232nd St. site to vary from about 14% to 24%, with an average of 18%. Thus the velocity values from the laboratory data might have been expected to be slightly lower than those measured insitu.

### 8.2.2 Comparison with Previous Seismic Cone Tests

Rice (1984) conducted shear wave velocity measurements at two of the research sites. The exact locations are not known but are believed to be in the general vicinity of the tests conducted for this research. He recorded between 30 and 40 blows at each depth and used the first cross-over points to determine the mean interval time. The comparisons are shown in Fig.8.2 for the McDonald Farm site and in Fig.8.3 for the Annacis North Pier site. At the McDonald Farm site , the velocities in

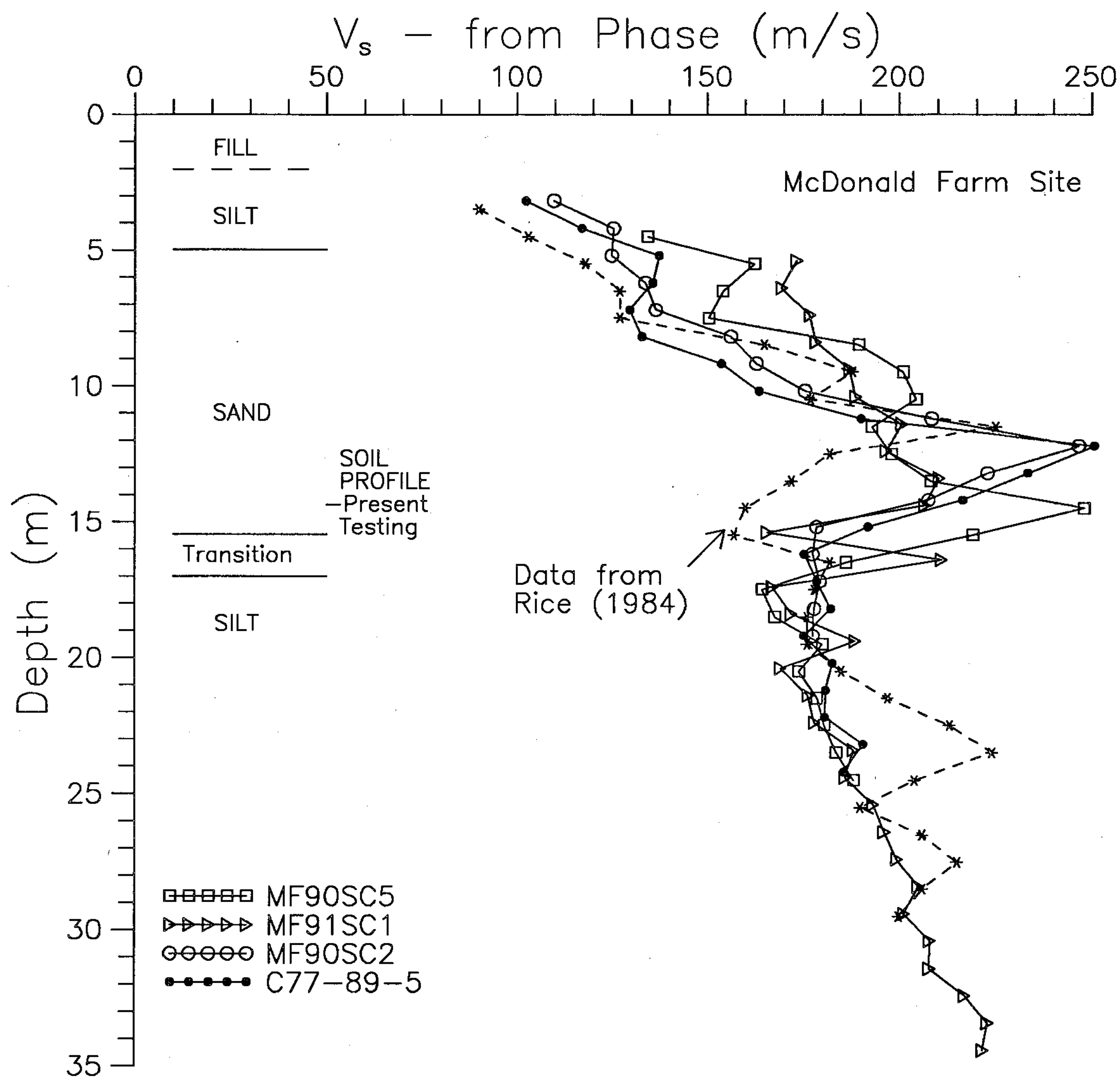


Fig.8.2 Comparison of Velocities with Earlier Measurements
— McDonald Farm Site

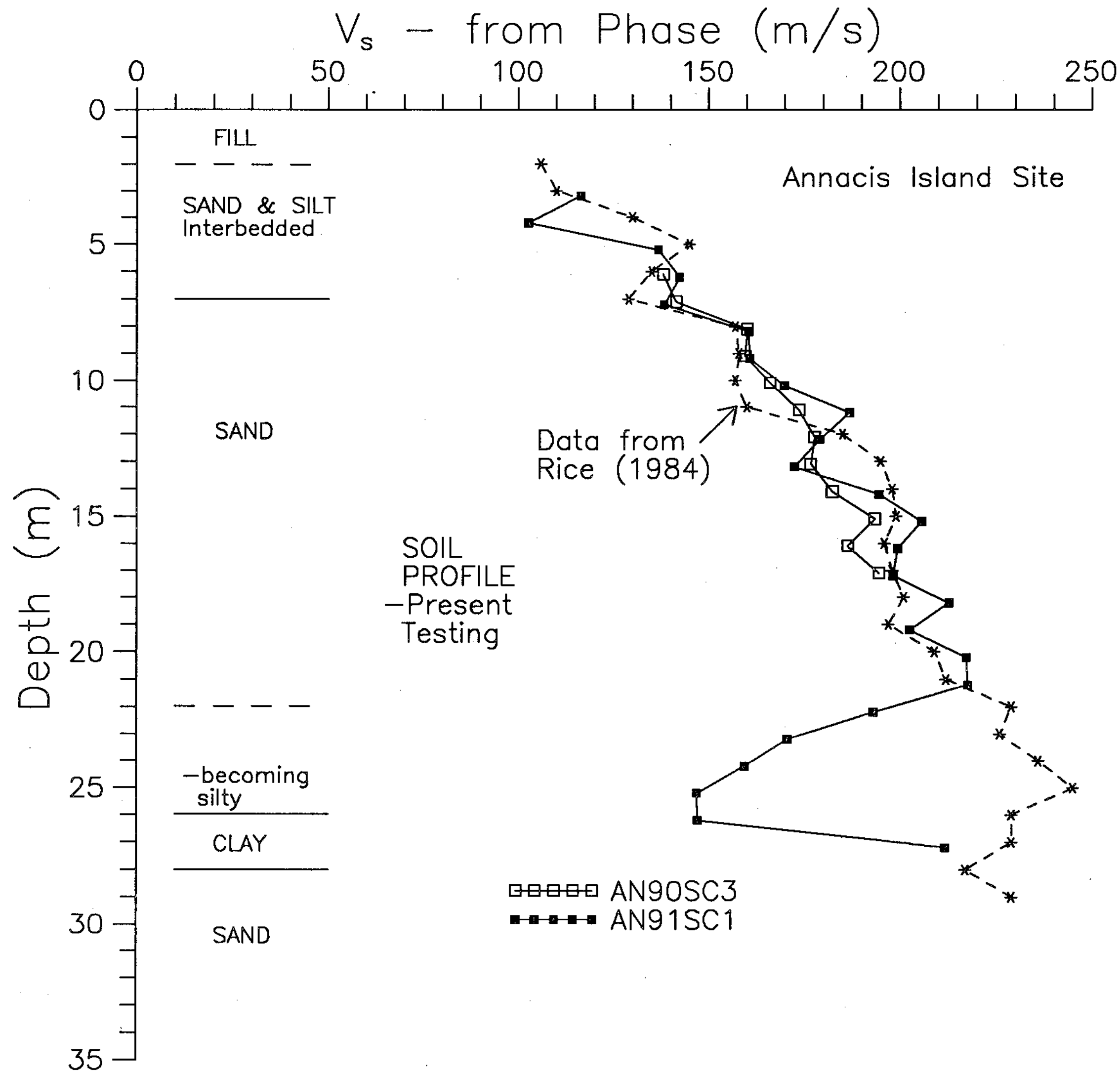


Fig.8.3 Comparison of Velocities with Earlier Measurements – Annacis N.Pier Site

the sand are in reasonable agreement, but his values are slightly lower above 7m. The transition zone occurs at a shallower depth. The velocities in the silt initially agree quite well, but show two peaks not encountered in the present testing. For the Annacis site also, the values agree quite well down to 21m. Below this depth the present sounding became increasingly silty. In general the ranges of velocities given by Rice (1984) were reproduced in this study.

### 8.2.3 Comparison with Other Results in the General Area

The Geological Survey of Canada (GSC) has recently been conducting surface measurements of shear wave velocities in the Fraser Delta area. Some results have been informally released for review. One data set is described as "1989 sites not encountering till - all forward & reverse shots - Fraser Delta". For this set, an approximate mean curve with depth and approximate envelope of all values are shown in Fig.8.4. Also shown on Fig.8.4 are the velocities measured in seven SCPT's in the Fraser Delta as part of this study. It can be seen that there is generally good agreement down to about 15m, and that the SCPT values are on the low side of the GSC envelope below this depth. This latter discrepancy is not unexpected as it is understood that the simple surface measurements used by the GSC cannot detect a decrease in velocity with depth.

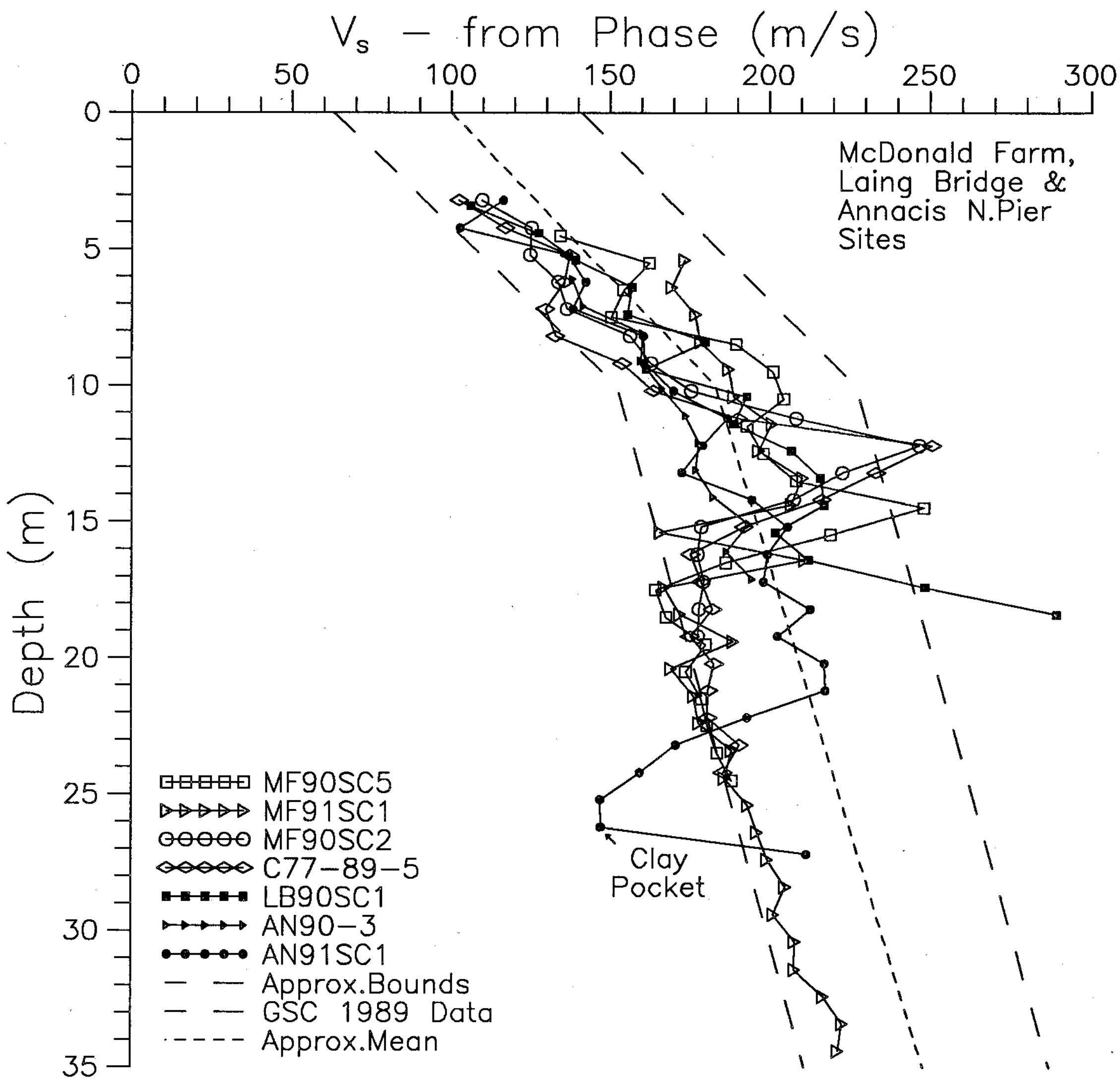


Fig.8.4 Comparison of Velocities with Other Measurements on the Fraser Delta

## *8.3 VERIFICATION OF DAMPING MEASUREMENTS*

### 8.3.1 Sand

Due to the difficulties of obtaining and handling sand samples, no site specific laboratory testing results exist for comparison with the insitu measurements of damping in sand deposits. All insitu damping measurements in sand deposits are shown in Fig.8.5, along with available laboratory results for a sample identified as a grey, clean fine to medium-grained sand (SP) from another site in the Fraser delta (Tilbury Island) provided by Klohn Leonoff Ltd.(1981) and published global values from Seed and Idriss (1970) and Idriss (1990). The Annacis North Pier and Laing Bridge results fall between the recommendations of Seed and Idriss and those of Idriss, and are in good agreement with the laboratory results. The results from the McDonald Farm site are 2 to 3 times higher and fall just above the recommendations of Seed and Idriss. In section 7.4 it was noted that the cone bearing was higher at the McDonald Farm site and the damping increased with cone bearing. The good agreement between the Annacis North Pier and Laing Bridge results and the available laboratory data indicates that the insitu damping results are comparable to those obtained in the laboratory.

### 8.3.2 Silt

Damping measurements in a clayey silt were only at the McDonald Farm site, and again no site-specific comparisons were available. Since

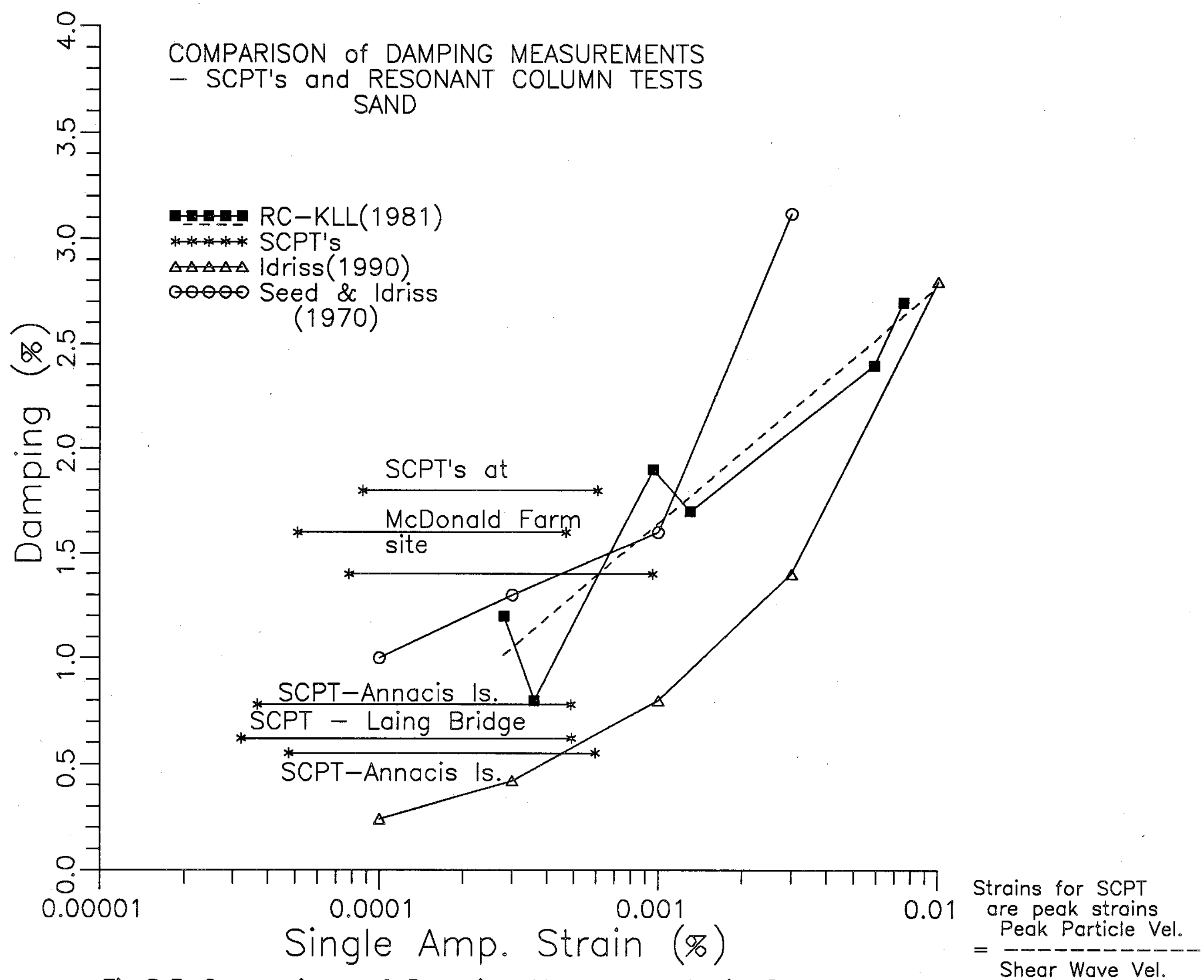

Fig.8.5 Comparison of Damping Measurements in Sand

the silt is located beneath a sand layer (>15m deep) the damping was at very low strain levels (<$6x10^{-4}$%). The results are shown in Fig.8.6, along with laboratory results from a Tilbury Island site for Klohn Leonoff Ltd. (1981) and an Annacis Island site for Golder Associates (1982), and a single curve of suggested values for both sand and clay (and presumably silt) from Idriss (1990). It can be seen that the laboratory values are in reasonable agreement, and that the Idriss curve plots near the middle of the laboratory data. Neither the Idriss curve or the laboratory data extend down to the strain levels of the field data, but the field damping values are close to the values of both the Idriss curve and the lowest of the laboratory values. The results are in general agreement with the values given by Idriss, so that the field measurements of damping are in the expected range.

### 8.3.3 Clay

Damping measurements in clay are reported for the upper portion (above 12m) of the Lower 232nd St. site. Fig.8.7 shows the field measurements, laboratory measurements by Zavoral (1990) and recommendations by Idriss (1990), and Sun at al (1988) (following Seed and Idriss, 1970). The laboratory data generally fall close to the recommendations of Idriss. A review of the soil profile provided in Fig.4.6 shows that sand layers exist below about 11m or 12m, and field values were only used to about 11m to 12m.. If the lowest-strain laboratory results from only above 11m (at 2.6m and 8.2m) are compared

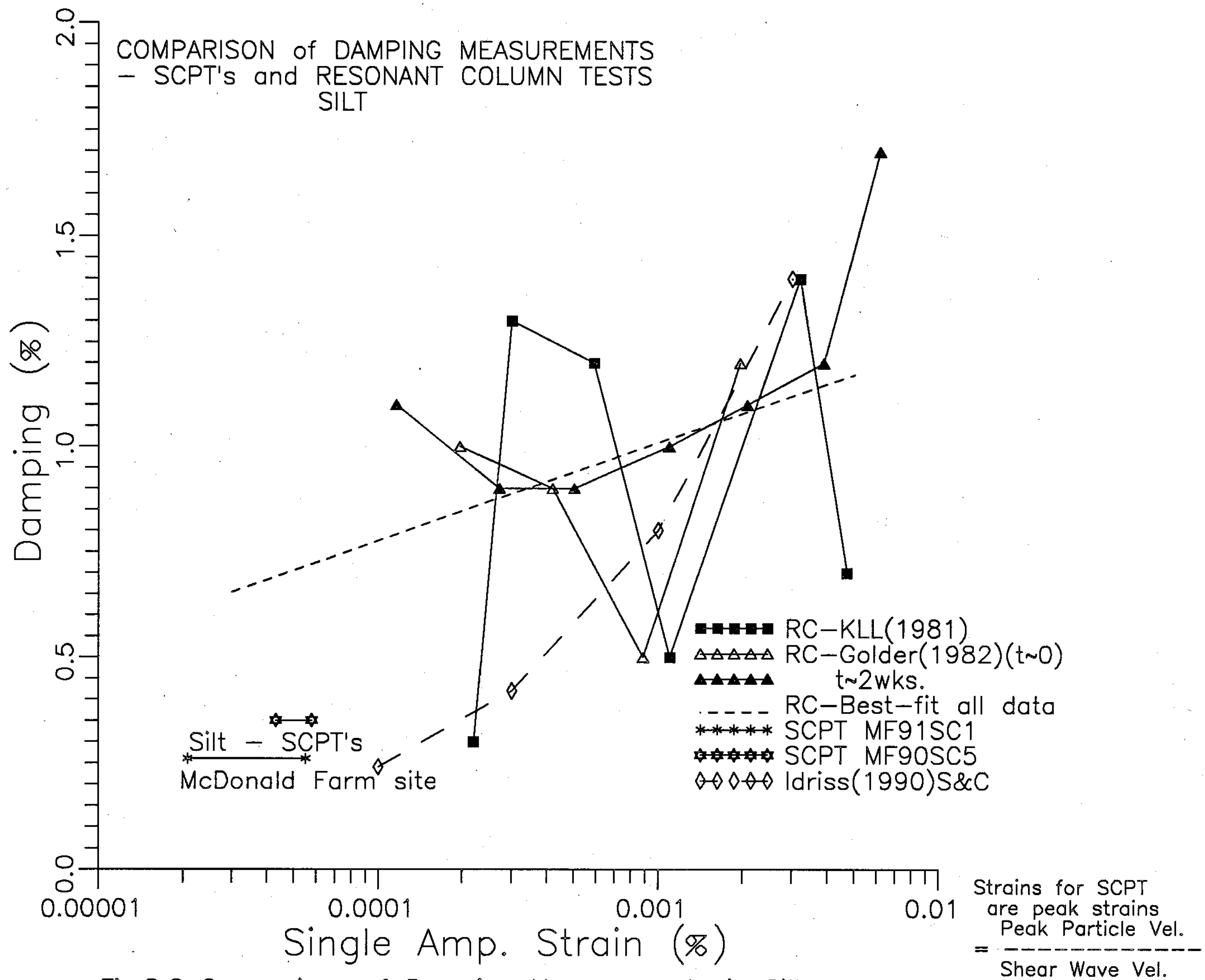


Fig.8.6 Comparison of Damping Measurements in Silt

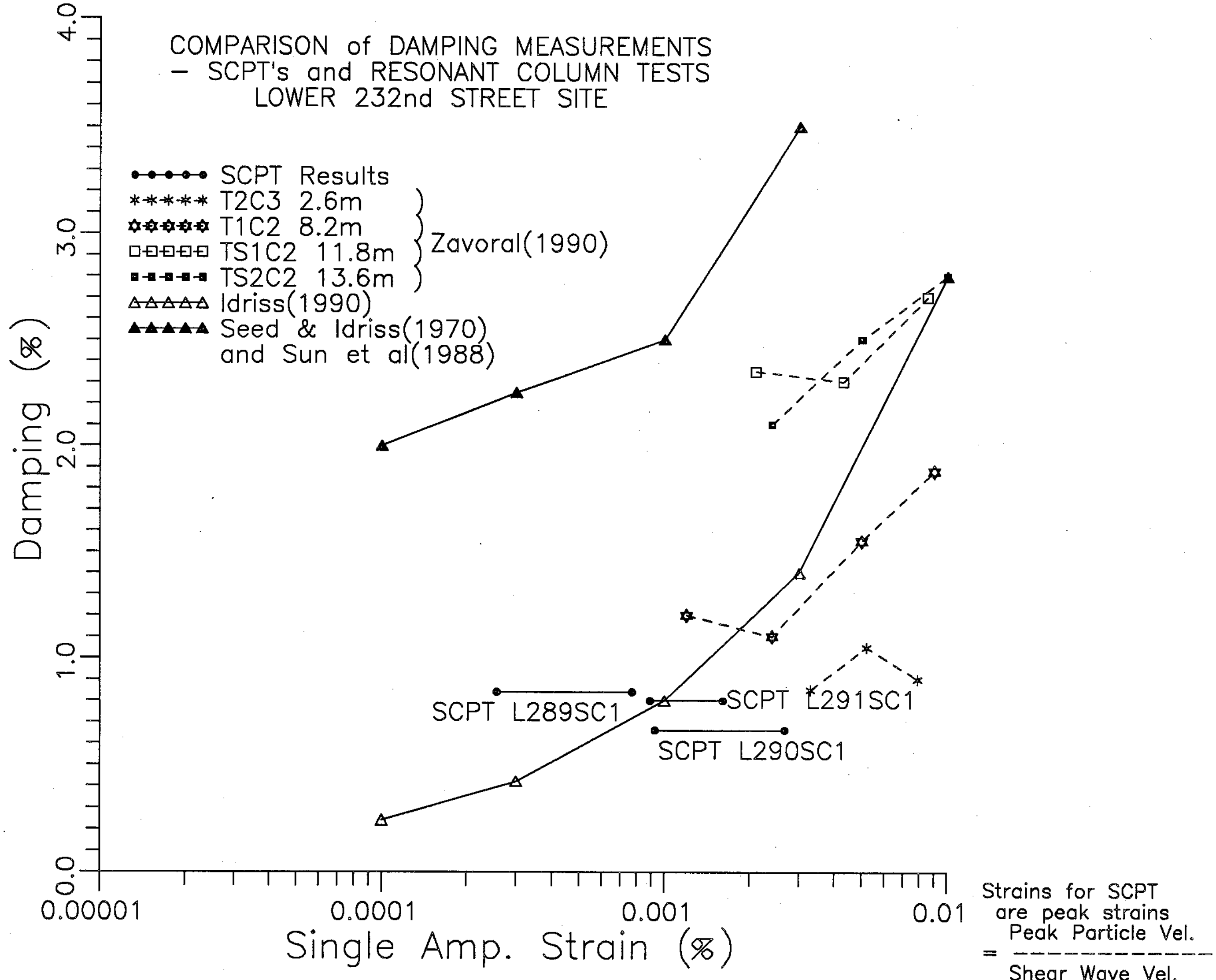


Fig.8.7 Comparison of Damping Measurements in Clay

with the field data there is close agreement (averaging about 1.0% for the laboratory and 0.8% for the field). This close agreement confirms the value of the field measurements.

### 8.3.4 Comparison with Typical Reported Values

A listing of reported values of damping at low strain from laboratory testing was provided earlier in Table 2.1. The values can be summarized as ranging from about 0.5% to 2% for sands and 1% to 5% for clays. The results from the present field measurements generally fall within the range of values reported for sand, but were at the low end of the range of values reported for clay.

Damping values from field measurements reported by others were provided earlier in Table 3.1, ranging from about 1.7% to 6% for sands, 1.7% to 7% for clays, about 2.5% for silts, and 3.5% and 12% for alluvium. Damping values from this study are lower than those reported by others. Sections 7.5 to 7.7 discussed the effects of signal processing and receiver type on the calculated damping values, and it appears that theses factors may have affected earlier results.

### 8.3.5 Summary

Except for the results in the sand at the McDonald Farm site which were somewhat higher, the field measurements of damping reported herein are in general agreement with the values of available laboratory data and with the recommendations of Idriss (1990). For the Lower 232nd St.

site, site-specific laboratory test results agreed closely with the insitu measurements of damping.

CHAPTER 9.

# SUMMARY AND CONCLUSIONS

The purpose of this research was to determine if seismic cone penetration test (SCPT) records made for shear wave velocity measurements could provide further information on dynamic soil properties. Initially several methods were investigated for calculation of shear wave velocities, particularly for measured signals which were noisy or of irregular shape. The main thrust of the research was to investigate the insitu measurement and calculation of intrinsic soil damping. The major findings of this study are presented below.

## *9.1 VELOCITY MEASUREMENTS-SCPT PROCEDURE*

1. If only one receiver is used, an accurate, repeatable trigger is required. The electrical step trigger was found to give a highly repeatable signal to start the records.
2. If smooth clean signals are measured, most methods of velocity calculation will give similar, satisfactory results. "Indirect time" methods (cross-correlation, phase of cross-spectrum) should be applied to the shear wave alone, not the full recorded signal.
3. If noisy, irregular signals are measured, it can be difficult to apply "direct time" methods (arrival, first peak, cross-over). Low-pass digital filtering may be helpful to reduce noise, but irregularities in the signals may create considerable difficulty in selecting the appropriate single point for calculation.

4. The recommended procedure for velocity determination in SCPT testing is:

a. For all signals, isolate the shear wave with a rectangular window.

b. Use the phase of the cross-spectrum method, giving the velocity variation with frequency.

c. Review the velocity vs. frequency plots for a number of depths and select the frequency range with a reasonably constant value at all depths. Select the average shear wave velocity over this frequency range at all depths.

5. Measured insitu velocities were found to be about 7% higher than laboratory values for the same clay. It was anticipated that the insitu velocities would be somewhat greater due to ageing of the insitu soil.

## *9.2 DAMPING MEASUREMENTS-SCPT PROCEDURE*

### 9.2.1 Equipment

1. As indicated above, an accurate trigger is required if a single receiver is used.

2. Since damping measurements are based on amplitude relationships, a highly repeatable source is required. A mechanical swing hammer (weight of 12kgF, arm-length of 2.25m) with the initial position controlled by a latch and the pivot swinging on plastic bushings, performed very satisfactorily.

3. In order that the receiver does not affect the measurements, a receiver that has a flat response over the frequency range of concern is required. A critically damped (70.7%) accelerometer with resonance well above the frequencies of interest can provide this response At the start of this research the only available damped accelerometer that would fit in the cone was the model 3021-002 accelerometer from ICSensors. This accelerometer has been successfully used for over two years.

4. In the past most investigators (Redpath et al,1982, Tonouchi et al,1983, Meissner and Theilen,1986) have used two receivers, one fixed near the surface and the other moving to increasing depth. It has been shown that with a repeatable source and accurate trigger, it is not necessary to use two receivers.

### 9.2.2 Calculations and Signal Processing

1. The rise time method was investigated and was shown to give very different damping values for soundings at the same site. The rise-time approach and other time-based methods of damping calculation were not pursued further as several authors have also indicated considerably more scatter compared with frequency-based methods.

2. The random decrement method which is based on the analysis of single records does not lead to reasonable or consistent damping values. An attempt at extending the method to the ratio of signals was not successful.

3. The attenuation coefficient method has been used by others, e.g. Mok et al,1988, especially for crosshole data. (Unfortunately some authors have referred to the procedure designated herein as the attenuation coefficient method by the term the spectral ratio slope method. This latter term has been used for method 6, following Redpath and his colleagues,1982,1986) When the attenuation coefficient method is applied to the SCPT, geometric corrections - spreading, transmissivity, and divergence - (which are not straightforward) are required, and considerable scatter was found in the results. This large scatter and negative damping values in the deeper silt deposits led to rejection of this method for damping calculations in the SCPT.

4. The first method developed as part of this research and applied to damping calculations was the modified SHAKE method. The modified SHAKE method also requires application of geometric corrections and had a similarly large scatter and negative damping values in the deeper silt deposits. Similarly this method was rejected for damping calculations in the SCPT.

5. The second method developed as part of this research and applied to damping calculations was the damping spiral method. The damping spiral method allows calculation of the geometric correction between each pair of signals. It can be applied on a metre by metre basis or on a layer basis using the uppermost signal in a layer for a reference. When applied on a metre by metre basis, the scatter is reduced considerably compared to methods 3 and 4, but is still large compared to the spectral

ratio slope (SRS) method. When applied on a layer basis, the method is essentially the same as the SRS method.

6. The spectral ratio slope (SRS) method eliminates the geometric corrections and allows simultaneous use of the information at all depths within a layer. This greatly reduces the scatter in the damping calculations, and the SRS method is the recommended method of damping calculation.

7. The shear wave (one wavelength long) should be isolated for use in the damping calculation by applying a rectangular window.

8. Windowing gave less scatter in the results than smoothing of the FFT of the full signal and therefore smoothing is not recommended as an alternative to windowing.

9. The above recommendations gave results that closely matched available laboratory data and published recommendations (Idriss,1990).

10. The method as developed is limited to small strains; about $3x10^{-3}$% at shallow depths to about $3x10^{-5}$% for greater depths.

11. The wavelength of measured signals is typically about 3m. Measurements in the first few metres will be affected by the interface, and several measurements are required to establish a slope of the SRS curve, therefore a relatively uniform layer of soil of at least 6m is required for the insitu measurement of damping.

12. Due to amplification of the signals, the SRS method cannot be applied to earthquake records measured in downhole arrays.

13. It was shown that considerable care must be exercised in analysis of local earthquake records. Rock and surface records may not contain similar frequency spectra, perhaps due to surface wave effects.

### 9.2.3 Summary

The spectral ratio slope (SRS) method was found to have the lowest scatter of all the methods investigated and is the recommended method of damping calculation. When applied to SCPT soundings the SRS method gave highly repeatable damping values over periods of one to two years. The calculated damping values were generally similar to those for available laboratory testing and published recommendations (Idriss,1990).

## *9.3 RECOMMENDATIONS FOR EXTENDING RESEARCH*

Woods (1991) provided a summary on the state of soil dynamics, including measurement of dynamic soil properties. He stated that " for small strain phenomena, the parameters affecting shear modulus (and $V_S$) are quite well known." Insitu measurements of $V_S$ of soils have been conducted for almost 20 years, and the measurement and calculation procedures are well developed.

On the other hand Woods(1991) stated that "Some major gaps still exist with respect to our ability to measure important dynamic soil properties in situ. There is not yet a method to measure material damping in situ...". This thesis does present the SRS method to measure and calculate small-strain damping insitu, but it is obvious that much work is required to have the method widely accepted. Recommendations for extending this research include:

1. Laboratory testing could be useful to confirm the differences in measured damping (e.g. McDonald Farm and Annacis North Pier values) and to establish whether these differences extend to higher strains. For cohesionless soils, consideration might be given to recovering frozen samples to minimize sample disturbance.

2. It would be desirable to extend the insitu measurement of damping to measure thinner layers. In order to reduce the wavelength, higher frequencies would be required. An alternate source would likely be required to propagate the higher frequencies to depth. In addition to the shear beam, two alternate sources (buffalo gun and drop weight) have been investigated, but both gave a larger scatter in frequencies and the frequencies at the peak magnitude were in the same general range (about 100Hz and 45Hz) as for the shear beam source. At this time, the nature of a source that would be capable of transmitting higher frequencies through soil is not clear. If such a source is developed, it may be necessary to acquire a damped accelerometer with a higher natural frequency.

3. For larger strains (0.1% and greater) other approaches such as cyclic pressuremeter testing can be used to measure damping. However, it would be desirable to extend the field measurements using the SCPT from the present level (generally less than $10^{-3}$%) to higher strain levels ($10^{-2}$% to $10^{-1}$%). Again an alternate source would likely be required. A much

larger hammer-on-beam source might achieve these levels, but may not be practical for routine testing.

4. Further testing may allow the development of correlations between other cone measurements and damping.

5. The spectral ratio slope method for damping calculation works well for small-strain waves passing down into the ground as body waves. However it cannot be applied to larger-strain waves passing upwards to a free surface due to the amplification of the waves. It would be desirable to formulate an equation including amplification effects, so that damping might be extracted directly from earthquake records from an accelerometer array.

6. In a recent paper Al-Hunaidi (1991) discussed the SASW method to measure shear-wave velocities and one of the equations he presented expressed the amplitudes of the signals in terms of an attenuation coefficient. This raises the possibility that damping might be measured using the SASW technique.

## BIBLIOGRAPHY


ASTM Standard D2487-69. Classification of soils for engineering purposes. ASTM Standards, Part 11. ASTM, Philadelphia.

ASTM Standard D2488-69. Description of soils. ASTM Standards, Part 11. ASTM, Philadelphia.

Abbiss,C.P. and Ashby,K.D. 1983. Determination of ground moduli by a seismic noise technique on land and on the sea bed. Tech. Note, Geotechnique, Vol.33, No.4, pp.445-450.

Aggour,M.S., Yang,J.C.S., and Al-Sanad,H. 1982a. Application of the random decrement technique in the Determination of damping of soils. 7th European Conf. on Earthquake Eng., Athens, Greece. Sept. Vol.2.

Aggour,M.S., Yang,J.C.S., Chen,J., Amer,M.I., and Al-Sanad,H. 1982b. In-situ determination of damping of soils. 7th Symp. on Earthquake Eng., Roorkee, India. Nov. Vol.I.

Al-Hunaidi,M.O. 1991. Nondestructive profiling of pavement sites using the surface wave method: a case study. Preprints, 44th Can. Geot. Conf., Vol.1, Paper12, Calgary.

Anderson,K.R. and Reinke,R.E. 1989. Validation of Q estimation techniques in a highly attenuative environment. 84th Annual Meeting, Seis. Soc. Am., Seismological Research Letters, Vol.60, No.1, April.

Armstrong,J.E. 1990. Vancouver geology. Geological Assn. of Canada, Cordilleran Section, Vancouver.

Bath,M. 1974. Spectral analysis in geophysics. Elsevier Scientific Pub. Co., New York.

Bazett,D.J. and McCammon,N.R. 1986. Foundations of the Annacis cable-stayed bridge. Can. Geot. Jnl. Vol.23,pp.458-471.

Baldwin,R. 1990. Personal communication.

Bland, D.R. 1960. The theory of linear viscoelasticity. Pergamon Press, New York.

Blunden,R.H. 1973. Urban geology of Richmond, B.C. Dept. of Geology Report No. 15, University of British Columbia.

Burkhardt,H., Paffenholz,J. and Schutt,R. 1986. Absorption of seismic waves (ASW). Final Report - DGMK project 254 - for the Federal Minister of Research and Technology. Hamburg. March.

Byrne,P. 1988. Course notes for CIVL581.

Byrne,P.M., Yan,L. and Lee,M. 1991. Seismic response, liquefaction, and resulting earthquake induced displacements in the Fraser Delta. 6th Can. Conf. on Earthquake Eng., Toronto, June.

Campanella,R.G., Robertson,P.K., Gillespie,D., Laing,N. and Kurfurst,P.J. 1987. Seismic CPT in the near offshore of the MacKenzie Delta. NWT. Canadian Geotechnical Jnl., Vol.24,No.1,pp.154-160.

Campanella,R.G., Baziw,E.J. and Sully,J.P. 1989. Interpretation of seismic cone data using digital filtering techniques. 12th Int. Conf. on Soil Mech. and Foundation Eng. Rio de Janeiro, Brazil. August.

Campanella,R.G. and Robertson,P.K. 1984. A seismic cone penetrometer to measure engineering properties of soil. 54th Annual Meeting, Soc. Exp. Geop., Atlanta,Ga., Dec.

Campanella,R.G. and Robertson,P.K. 1986. Guidelines for use, interpretation and application of the CPT and CPTU. Soil Mech. Series No.105, Dept. of Civil Eng., University of BC.

Campanella,R.G. and Stewart,W.P. 1990. Seismic cone analysis using digital signal processing for dynamic site characterization. Proc. 43rd Can. Geot. Conf., Quebec, Vol.II,pp.603-611.

CFEM 1985. The Canadian foundation engineering manual. 2nd Ed. Can. Geot. Soc. c/o Bitech Pub., Vancouver.

Chang,C.-Y., Mok,C.M., Power,M.S., Tang,Y.K., Tang,H.T., and Stepp,J.C. 1991. Development of shear modulus reduction curves based on Lotung downhole ground motion data. Proc. 2nd Int. Conf. on Recent Advances in Geot. Earthquake Eng. and Soil Dynamics, St.Louis, Paper No.1.44.

Clague,J.J., Luternauer,J.L. and Hebda,R.J. 1983. Sedimentary environments and postglacial history of the Fraser Delta and lower Fraser Valley, British Columbia. Can.J.Earth Sci., Vol.20, pp1314-1326.

Dobry,R., Oweis,I., and Urzua,A. 1976. Simplified procedures for estimating the fundamental period of a soil profile. Bull. Seis. Soc. America, Vol.66, No.4, pp1293-1321, Aug.

GSC 1979. Surficial Geology, Vancouver, British Columbia. Map 1486A. Geological Survey of Canada.

GSC 1980. Surficial Geology, New Westminster, British Columbia. Map 1484A; Surficial Geology, Mission, British Columbia. Map1485A; Surficial Geology, Chilliwack, British Columbia. Map1487A. Geological Survey of Canada.

Gillespie,D.G. 1990. Evaluating the shear wave velocity and pore pressure data from the seismic cone penetration test. Ph.D. thesis, Dept. of Civil Eng., University of British Columbia, 201p.

Golder Assoc. 1982. Resonant column test results on sample 5B from elev. -39.1m from boring GA-111F, Annacis Island, Delta, B.C. (testing by Geotechnical Engineers Inc.-Project 81867).

Greig,J.W. 1985. Estimating undrained shear strength of clay from cone penetration tests. M.A.Sc. thesis, Dept of Civil Eng., University of British Columbia.

Hardin,B.O. and Black,A.M.(1968). Vibration modulus of normally consolidated clay. JSMFD, ASCE, Vol.94,No.SM2, March, pp.353-369.

Hardin,B.O. and Drenevich,V.P.(1972a). Shear modulus and damping in soils: measurement and parameter effects. JSMFD, ASCE, Vol.98,No.SM6,June,pp.603-624.

Hardin,B.O. and Drenevich,V.P.(1972b). Shear modulus and damping in soils: design equations and curves. JSMFD, ASCE, Vol.98,No.SM7,July,pp.667-692.

Hers,I. 1989. The analysis and interpretation of the cone pressuremeter in cohesive soils. M.A.Sc. thesis, Dept. of Civil Eng., University of British Columbia.

Hewlett Packard 1985. The fundamentals of signal analysis. Application note 243. Feb.

Hoar, R.J. and Stokoe , K.H.II. 1978. Generation and measurement of shear waves *in-situ*. Dynamic Geotechnical Testing. ASTM STP 654, pp.3-29.

Hoar,R.J. and Stokoe,K.H.II 1984. Field and laboratory measurements of material damping of soil in shear. Proc. 8th World Conf. on Earthquake Eng., San Francisco. Vol.III, pp.47-54.

Horner,R. 1990. Personal communication.

Idriss,I.M. 1990. Response of soft soil sites during earthquakes. Proc. H. Bolton Seed Memorial Symp., Berkeley, Vol.2, pp.273-289.

Idriss,I.M. and Seed,H.B. 1968. Seismic response of horizontal layers. JSMFD, ASCE, Vol.94, No.SM4, July., pp.1003-1031.

Ishihara,K. 1982. Evaluation of soil properties for use in earthquake response analysis. Int. Symp. on Numerical Models in Geomechanics. Zurich.

Johnston,D.H. and Toksoz,M.N. 1981. Definitions and terminology. in Seismic Wave Attenuation. Geophysics reprint series No.2. Soc. Exp. Geophy. pp.1-5.

Klohn Leonoff Ltd. 1981. Resonant column tests on sample 20 (sand - 56ft.) and sample 42 (silt - 275ft.) from TH-1014, Tilbury Island, Delta, B.C. (testing by Shannon & Wilson, Inc. Job W-3786-01).

Kjartansson,E. 1979. Constant Q - wave propagation and attenuation. Jnl of Geophysical Research. Vol.84, pp.4737-4748.

Kokusho,T., Yoshida,Y. and Esashi, Y. 1982. Dynamic properties of soft clay for wide strain range. Soils and Foundations, Vol.22, No.4, Dec., pp1-18.

Kudo,K. and Shima,E. 1981. Attenuation of shear waves in soil. in Seismic Wave Attenuation. Geophysics reprint series No.2. Soc. Exp. Geophy. pp.325-338.

Laing,N.L. 1985. Sources and receivers with the seismic cone test. M.A.Sc. Thesis, Dept. of Civil Eng., University of British Columbia, 108 pgs.

Layotte,P.C. 1987. Marthor: an S-wave impulse source. in Shear Wave Exploration, ed. by Danbom,S.H. and Domenico,S.N. Geophysical Development Series, Vol.1, Society of Exp. Geophysicists.

LeClair,D.G. 1988. Prediction of embankment performance using in-situ tests. M.A.Sc. Thesis, Dept. of Civil Eng., University of British Columbia.

Lee,H.F.S. and Stokoe,K.H.II 1986. Investigation of low-amplitude shear wave velocity in anisotropic material Geotech. Eng. Rpt. GR86-6, Civil Eng, Dept., The University of Texas at Austin, Austin, TX.

Lysmer,J. 1980. Foundation vibrations with soil damping. Proc. 2nd ASCE Conf. on Civil Eng. and Nuclear Power, Knoxville, TN, Vol.II, Paper 10-4, pp.1-18.

Mack,H. 1966. Attenuation of controlled wave seismograph signals observed in cased boreholes. Geophysics, Vol.XXXI, No.1, Feb., pp.243-252.

Meissner,R. and Theilen,F. 1986. Experimental studies of the absorption of seismic waves. in "Absorption of Seismic Waves(ASW)". DGMK-Project 254. DGMK, Hamburg.

Mok,Y.J., Sanchez-Salinero,I., Stokoe,K.H.II, and Roesset,J.M. 1988. In situ damping measurements by crosshole seismic method. Earthquake Eng. and Soil Dynamics II. ASCE Spec. Conf., Park City, Utah. GSP No.20, pp.305-320.

Morrison,K.I. 1991. Personal communication.

Mueller,J.E. 1975. Victoria Map-area, British Columbia (92B). Geol Surv. Can., Paper 75-1, Part A.

Neville,A.M. and Kennedy,J.B. 1964. Basic statistical methods for engineers and scientists. International Textbook Co.,Scranton, Penn.

Ni,S-H. 1987. Dynamic properties of sand under true triaxial stress states from resonant/column torsional shear tests. Ph. D., The University of Texas at Austin.

O'Connell,R.J. and Budiansky,B. 1978. Measures of dissipation in viscoelastic media. Geophysical Research Letters, Vol. 5, No. 1, Jan., pp.5-8.

Oppenheim,A.V. and Schafer,R.W. 1975. Digital signal processing. Prentice-Hall Inc., Englewood Cliffs, N.J.

Oppenheim,A.V., Willsky,A.S., and Young,I.T. 1983. Signals and systems. Prentice-Hall Inc., Englewood Cliffs, N.J.

Palaniappan,E. 1976. Shear modulus and damping characteristics of soils. Ph.D., Georgia Institute of Technology.

Pullan, S.E. and Macaulay, H.A. 1987. An inhole shotgun source for engineering seismic surveys. Geophysics, Vol.52, No.7, July.

Redpath,B.B., Edwards,R.B., Hale,R.J., and Kintzer,F.C. 1982. Development of field techniques to measure damping values for near-surface rocks and soils. Prepared for NSF Grant No. PFR-7900192.

Redpath,B.B. and Lee,R.C. 1986. In-situ measurements of shear-wave attenuation at a strong-motion recording site. Prepared for USGS Contract No. 14-08-001-21823.

Rice, A.H. 1984. The seismic cone penetrometer. M.A.Sc. Thesis, Dept. of Civil Eng., University of British Columbia, 112 pgs.

Richart,F.E.Jr., Anderson,D.G. and Stokoe,K.H. 1977. Predicting insitu strain-dependent shear moduli of soil. Proc. 6th World Conf. on Earthquake Eng., New Delhi, India, Vol.III. Jan.

Robertson, M.D. 1986. Principles and parameters for the design of a portable shear wave source. B.A.Sc. Thesis, Geological Engineering Program, University of British Columbia, 79 pgs.

Robertson,P.K., Campanella,R.G., Gillespie,D., and Rice,A. 1986. Seismic CPT to measure in-situ shear wave velocity. J.Geotech.Eng.Div., ASCE, Vol.112, No.8, pp.791-804.

Robertson,P.K. and Campanella,R.G. 1986. Guidelines for use, interpretation, and application of the CPT and CPTU. Soil Mech. Series No.105, Civil Eng., University of British Columbia.

Saxena,S.K. and Reddy,K.R. 1989. Dynamic moduli and damping ratios for Monterey No.0 sand by resonant column method. Soils and Foundations. Vol.29, No.2, June, pp.37-51.

Schnabel,P.B., Lysmer,J. and Seed,H.B. 1972. SHAKE a computer program for earthquake response analysis of horizontally layered sites. Report No. EERC 72-12. University of California, Berkeley. Dec.

Seed,H.B. and Idriss,I.M. 1970. Soil moduli and damping factors for dynamic response analyses. Report No. UCB/EERC-70/10. University of California, Berkeley. Dec.

Seed,H.B., Wong,R.T., Idriss,I.M., and Tokimatsu,K. 1986. Moduli and damping factors for dynamic analyses of cohesionless soils. JGED, ASCE, Vol.112, No.11, Nov., pp.1016-1032.

Shannon and Wilson Inc. 1980. Evaluation of in-situ damping characteristics. Prepared for U.S. Nuclear Reg. Comm., NUREG/CR-1638.

Shinn,J.D. 1990. Personal communication

Sirles,P.C. 1988. Shear wave velocity measurements in embankment dams. Earthquake Eng. and Soil Dynamics II. ASCE Spec. Conf., Park City, Utah. GSP No.20, pp.248-263.

Sowers,G.B. and Sowers, G.F. 1970. Introductory soil mechanics and foundations. 3rd Ed. MacMillan Co., New York.

Stewart,W.P. and Campanella,R.G. 1991. Insitu measurement of damping of soils.Proc. 2nd Int. Conf. on Recent Advances in Geot. Earthquake Eng. and Soil Dynamics, St.Louis, Vol.I,pp.83-92.

Stokoe,K.H. II and Nazarian,S. 1985. Use of Rayleigh waves in liquefaction studies. Measurement and Use of Shear Wave Velocity for Evaluating Dynamic Soil Properties. ASCE-GED session, ASCE Convention, Denver. May. pp.1-17.

Sully,J.P. 1991. Measurement of in situ lateral stress during full-displacement penetration tests. Ph.D. thesis, Dept. of Civil Eng., University of British Columbia, 468p.

Sun,J.I., Golesorkhi,R., and Seed,H.B. 1988. Dynamic moduli and damping ratios for cohesive soils. Report No. UCB/EERC-88/15. EERC UC Berkeley.

Sy,A., Henderson,P.W., Lo,R.C., Siu,D.Y., Finn,W.D.L., and Heidebrecht,A.C. 1991. Ground motion response for Fraser delta, British Columbia. 4th Int. Conf. on Seismic Zonation. Stanford, CA. Aug.

Taylor,P.R., van Selset,A.M., Hodge,W.E., and Sexsmith,R.G. 1983. Annacis Island cable-stayed bridge - design for earthquake. Proc. 4th Can. Conf. on Earthquake Eng., Vancouver, June.

Tonouchi,K., Sakayama,T., and Imai,T. 1983. S wave velocity and the damping factor. Bull. Int. Assoc. Eng. Geol. No.26-27, Paris. pp.327-333.

Udaka,T. and Lysmer, J. 1973. Supplement to computer program SHAKE. EERC UC Berkeley.

Ulrych,T.J. 1971. Application of homomorphic deconvolution to seismology. Geophysics, Vol.36, No.4, Aug. pp.650-660.

Wallis,D.M. 1979. Ground surface motions in the Fraser Delta due to earthquakes. M.A.Sc thesis, Dept. of Civil Eng., University of British Columbia, 199p.

Warrick,R.E. 1974. Seismic investigation of a San Francisco bay mud site. Bull. Seis. Soc. of America, Vol.64,No.2, pp.375-385.

White,J.E. 1965. Seismic waves. McGraw-Hill, New York.

Whitman,R.V. 1970. Site evaluation and dynamic analysis of nuclear power plants. M.I.T. Press.

Woods,R.D. 1978. Measurement of dynamic soil properties. ASCE GED Speciality Conf. on Earthquake Eng. and Soil Dynamics. Pasadena,CA. Vol.1, pp.91-178.

Woods,R.D. 1991. Soil dynamics - a maturing discipline. Geotechnical News. Vol.9,No.3, Sept., pp.21-22.

Woods, R.D. and Stokoe, K.H.II. 1985. Shallow seismic exploration in soil dynamics. Richart Commerative Lectures, ASCE. pp.120-156.

Yan,L. and Byrne,P.M. 1990. Simulation of downhole and crosshole seismic tests on sand using the hydraulic gradient similitude method. Can. Geot. Jnl., Vol.27, No.4, Aug., pp.441-460.

Yang,J.C.S., Qi,G.Z., Pavlin,V., Durelli,A.J., and Esteva,L. 1989. In-situ determination of soil damping in the lake deposit area of Mexico City. Soil Dynamics and Earthquake Eng., Vol.8,No.1,pp.43-52.

Zavoral,D. 1990. Dynamic properties of an undisturbed clay from resonant column tests. M.A.Sc. thesis, Dept. of Civil Eng., University of British Columbia, 246p.

# APPENDIX A

## COMPLEX CEPSTRUM METHOD

### *A.1 INTRODUCTION*

In general, a measured signal may contain the effects of many parameters including the effects of the source, material in the path of the signal, and the recording instrument. One of the simpler effects is one or more reflections included in the signal. The purpose of using the complex cepstrum is to separate reflections from a measured signal. If this separation is possible, a clearer indication of the nature of the measured signal and its components can be obtained. This separation is done by transforming the combined signal (base signal and reflections) into a signal which is a linear combination of, and which can be easily separated into, the two components. The discussion presented here is somewhat simplified for clarity and the reader is referred to Ulrych(1971) and Oppenheim and Schafer(1975) for a more detailed approach.

A measured signal x(t) may have been formed by convolution of a wavelet (base signal) and a reflection which will be offset by a time given by the distance of the reflector divided by the velocity of the wavelet. Convolution can be performed by multiplication of the Fourier transforms (FT's) of the wavelet and the reflection (represented as a function of time). Thus the FT of the measured signal is the product of the FT's of the wavelet and the reflection(s). In order to illustrate the process, a signal was created which contained a known reflection.

*A.2 METHOD USING AN ARTIFICIAL SIGNAL*

A typical accelerometer signal from a shear beam source is given in Fig.A.1, and shows some noise at the start and end of the signal, the main shear wave pulse centred at about 45 milliseconds(ms), and some smaller pulses after the main pulse. Fig.A.2 shows a signal, containing only the main pulse, which was formed by multiplying the signal in Fig.A.1 with a rectangular window. The signal in Fig.A.2 was convolved with a reflectivity series containing a spike of value 1.0 at 0.0ms to preserve the signal itself and a spike of value 0.3 at 19.2ms (nominal 20ms) to represent a reflector at a total extra distance travelled of about 3m (150m/s * 20ms). This time (distance) was selected to make the reflection clear in the signal and complex cepstrum. Fig.A.3 shows the result of the convolution, with the effect of the reflection to the right of the main pulse.

The signals of concern here consist of a finite number of discrete real values at equally spaced time intervals. The transform of interest is then the discrete Fourier transform pair calculated using the Fast Fourier Transform algorithm (FFT). The FFT of the signal in Fig.A.3 is represented in Fig.A.4 and Fig.A.5 which give the magnitude and phase respectively.

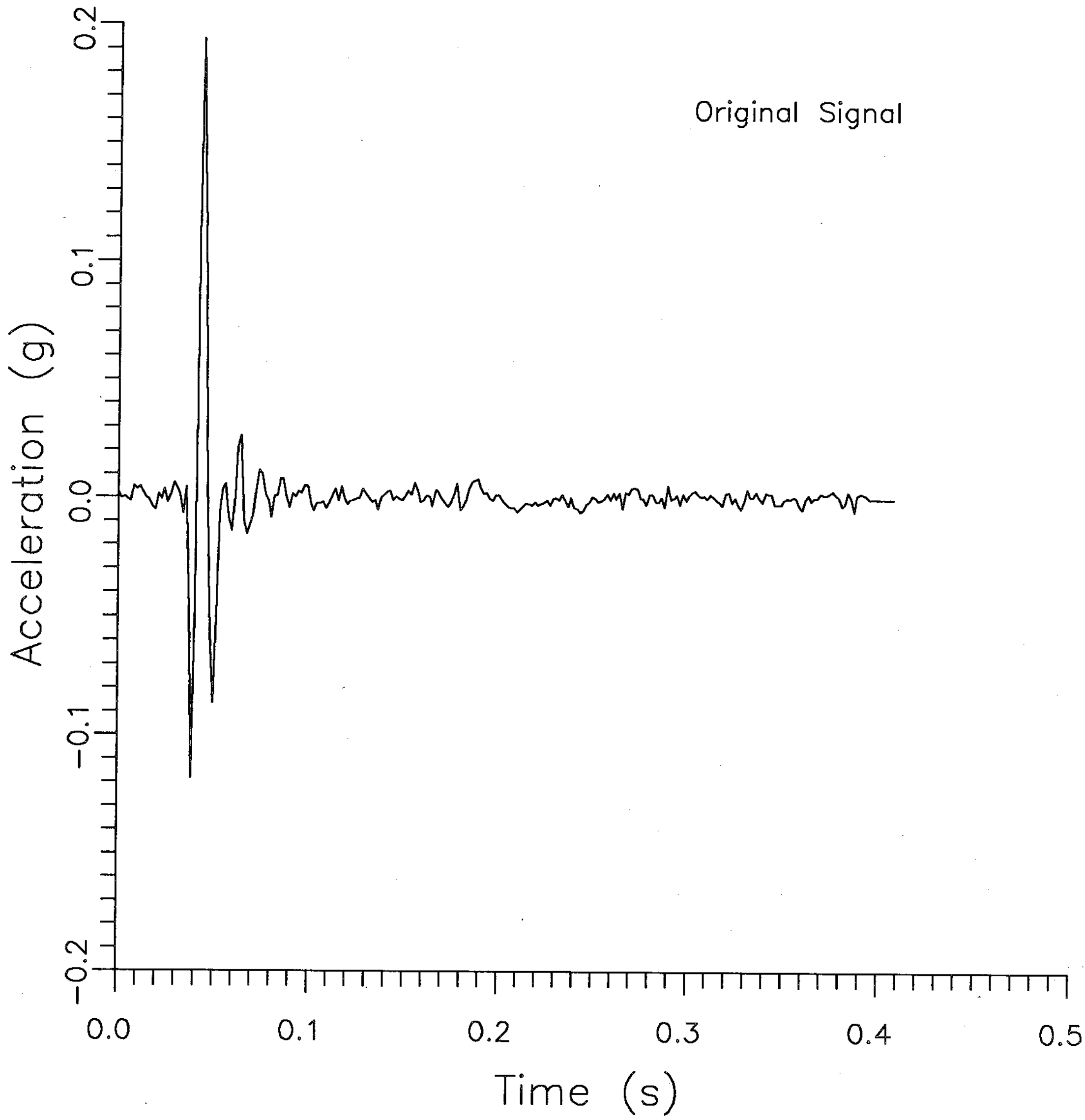


Fig.A.1 Typical Accelerometer Signal to be Analyzed

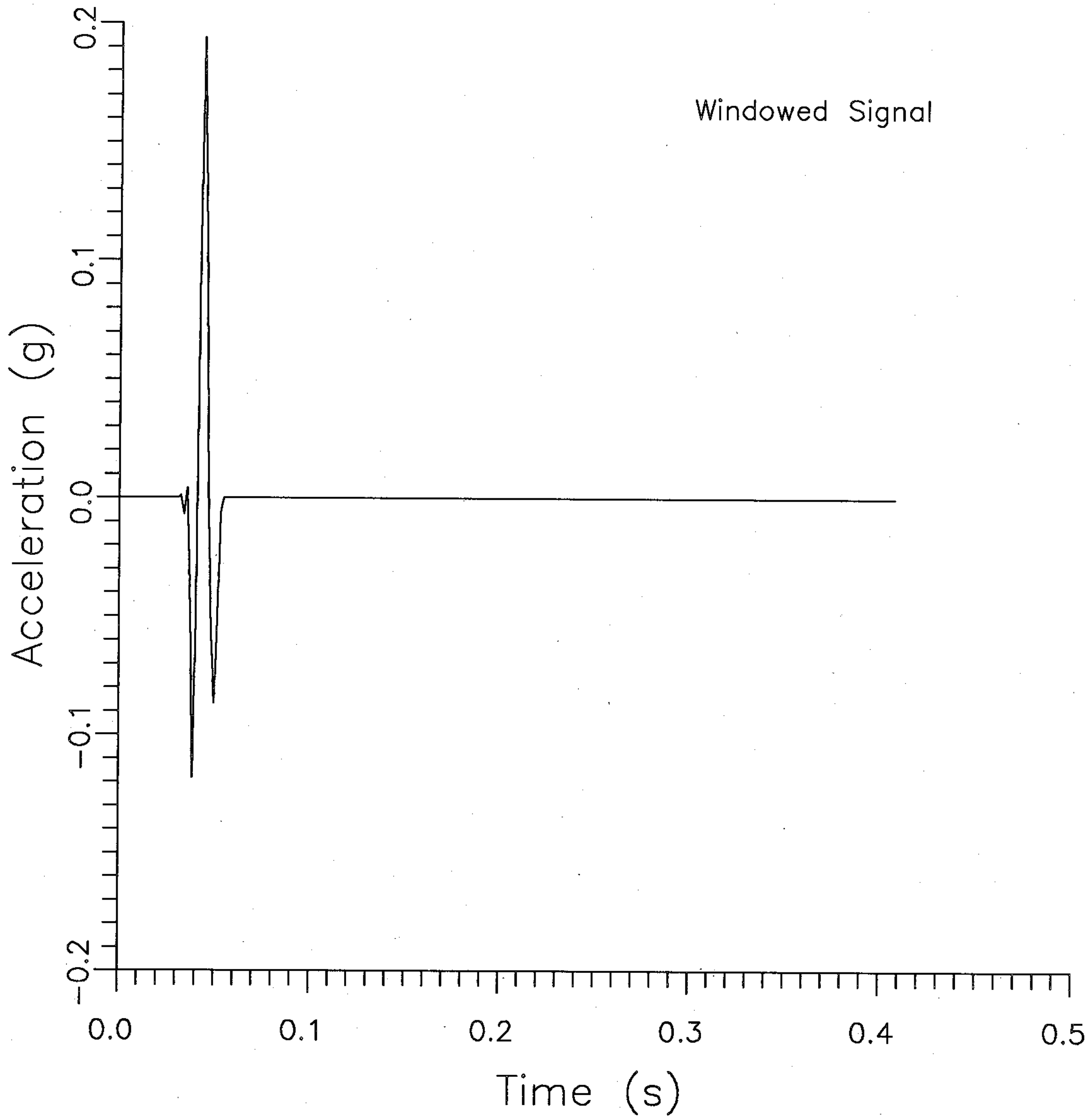


Fig.A.2 Shear Wave Separated from Typical Signal

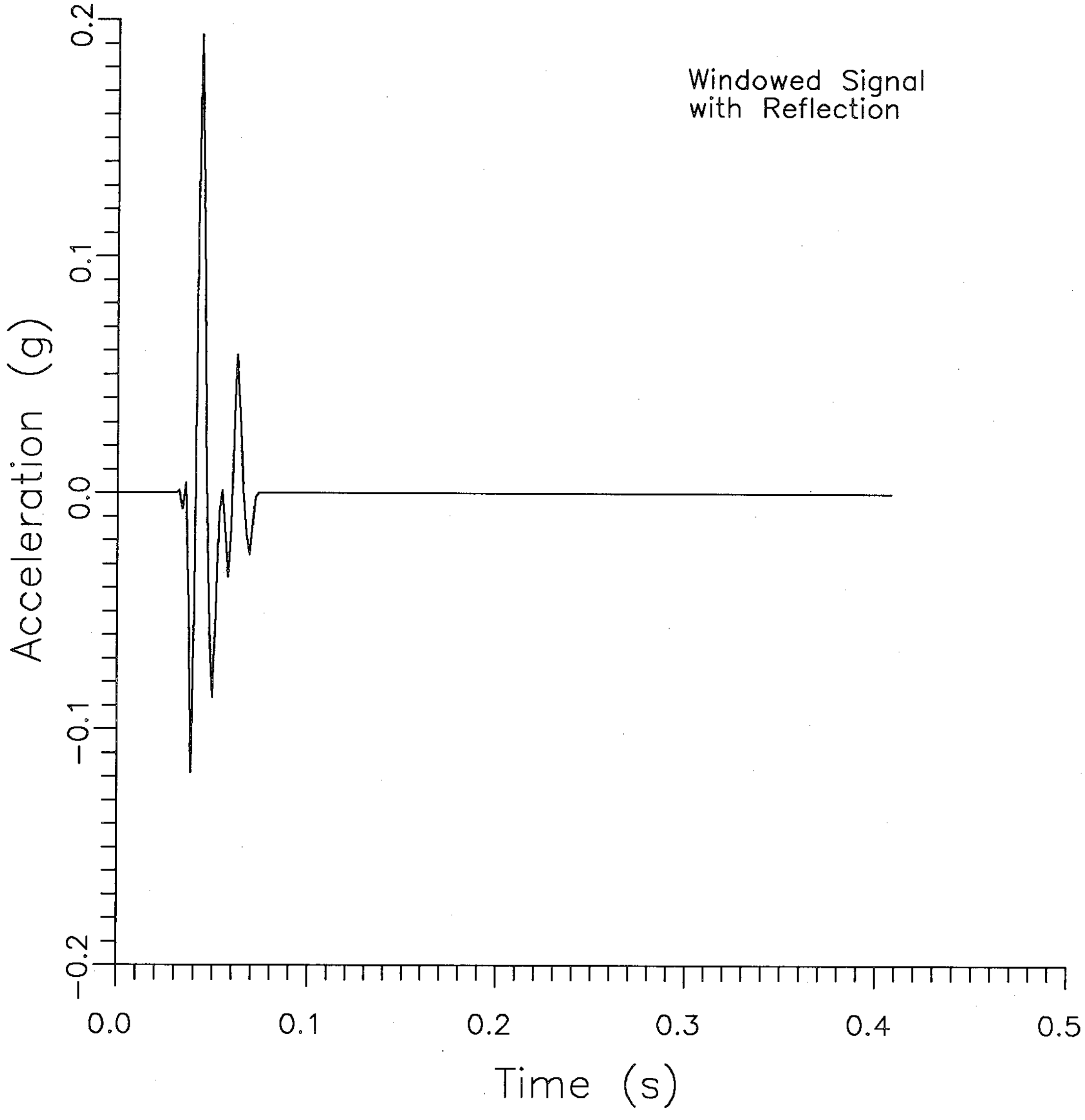


Fig.A.3 Shear Wave with Reflection

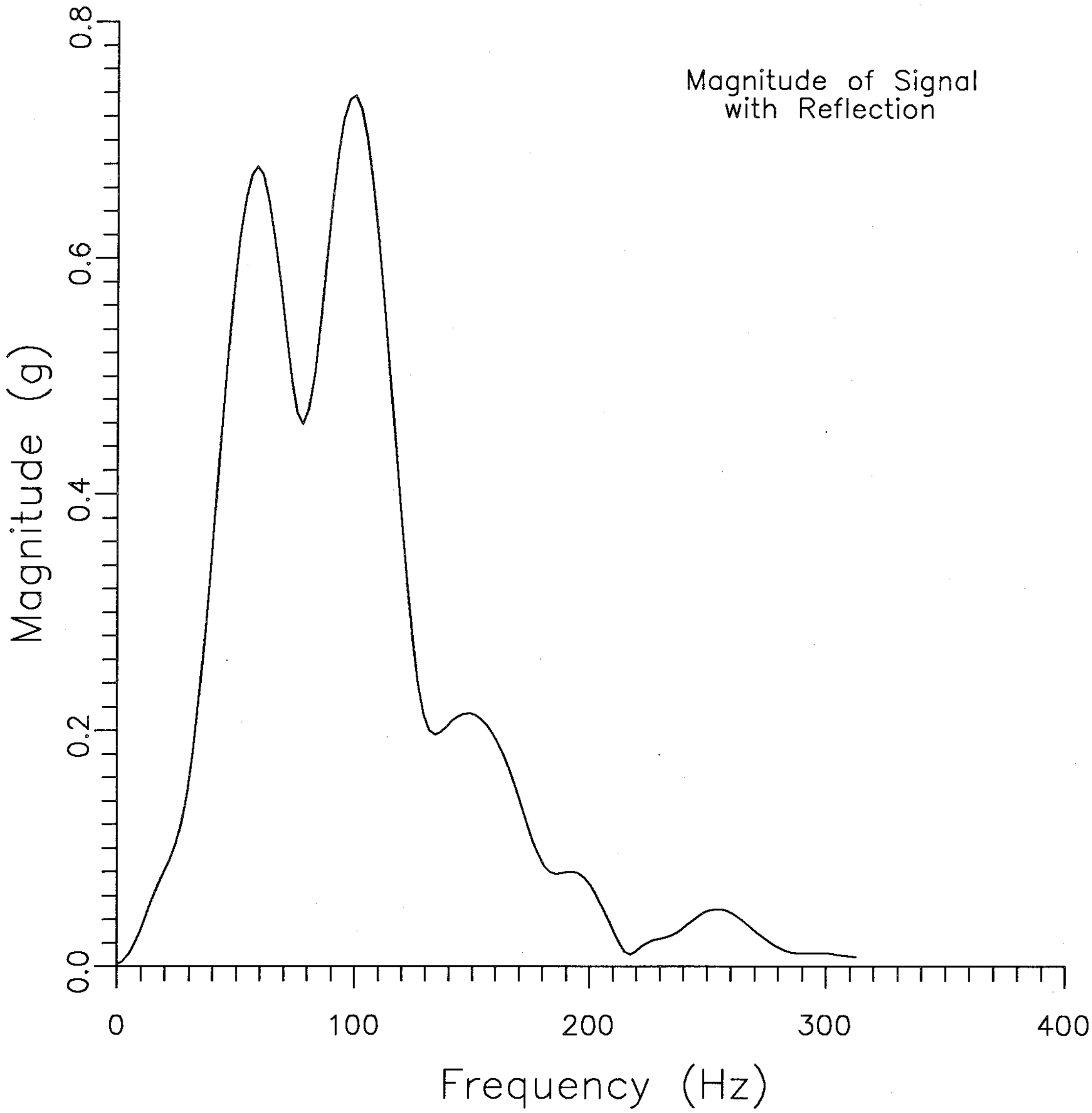


Fig.A.4 Magnitude of FFT of Shear Wave with Reflection

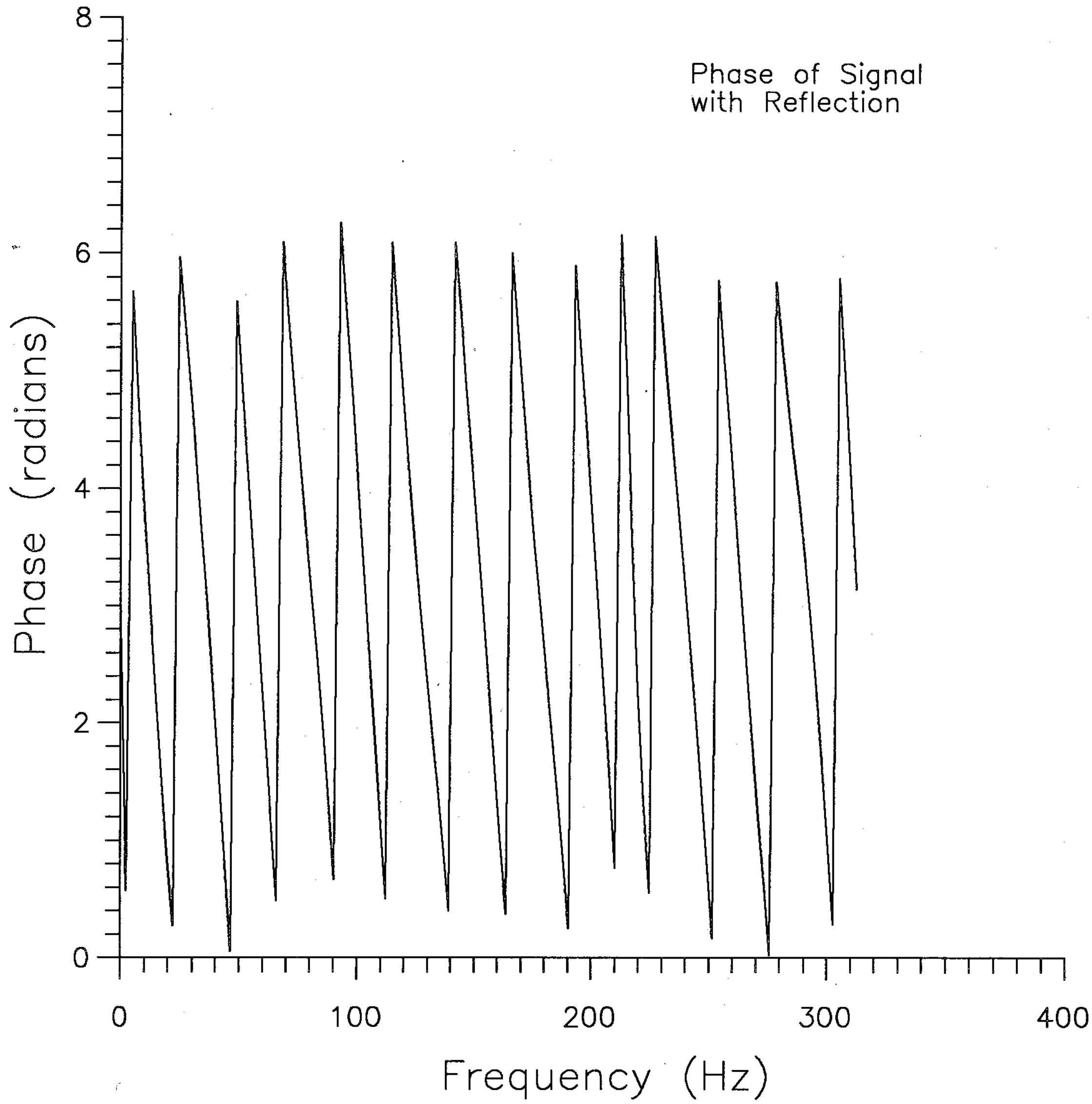


Fig.A.5 Phase of FFT of Shear Wave with Reflection

The first step in forming the complex cepstrum is to find the FFT of the measured signal. The signal can now be considered to be in the form of a product, which can be simplified to a sum by taking the logarithm of the FFT. Taking the inverse FFT restores the signal to a real sequence, which is in an additive space. The signal basis is again time but, since the logarithm was used to obtain the cepstrum, the signal basis is sometimes referred to as the quefrency domain.

The cepstrum calculated in the above manner is referred to as the complex cepstrum as the logarithm is applied to both the magnitude and phase of the FFT of the signal. A related calculation, called the real cepstrum, applies the logarithm to only the magnitude of the FFT and is used to analyze the periodicity of a signal. There are several additional computational considerations when calculating the complex cepstrum.

The logarithm of a series of complex numbers (the FFT of the measured signal) can be expressed in terms of the magnitude and phase as:

$$[5.1] \quad \ln[X(f)] = \ln|X(f)| + i\phi[X(f)]$$

where:

$$\phi[X(f)] = \Phi[X(f) +/- i2\pi n]$$

$$n=0,1,2... \text{ and } -\pi < \Phi[X(f)] < \pi$$

It can be seen that the complex logarithm is not uniquely defined and that $\Phi[X(f)]$ is a discontinuous function. In order to overcome these problems the phase can be "unwrapped" to provide a continuous function. The upper portion of Fig.A.6 shows the phase from Fig.A.5, and the lower portion shows the partially unwrapped phase. The first two "steps" in the phase have been removed by subtracting an amount of $2\pi$ from the balance of the signal beyond the step. The completely unwrapped phase in shown in Fig.A.7.

However the linear component of the unwrapped phase dominates the phase contribution to the complex cepstrum or as Ulrych states "...the effect...is to swamp the interesting information contained in the complex cepstrum". Thus it is necessary to remove the linear phase component. It should be noted that the removal of the linear phase component amounts to a shift of the output sequence, and therefore the linear portion removed should have a value that is a integer multiple of $\pi$ at the Nyquist frequency. An appropriate line is shown in Fig.A.7. This integer multiple will correspond to the number of points which the output sequence will have to be shifted after completion of the calculations.

The final phase to be used in the cepstrum is shown in Fig.A.8, and the natural logarithm of the magnitude is shown in Fig.A.9. It should be noted that the values are shown only for positive frequencies. The magnitude (or logarithm of magnitude) is an even function of frequency and thus is a simple mirror image around f=0(amplitude axis).

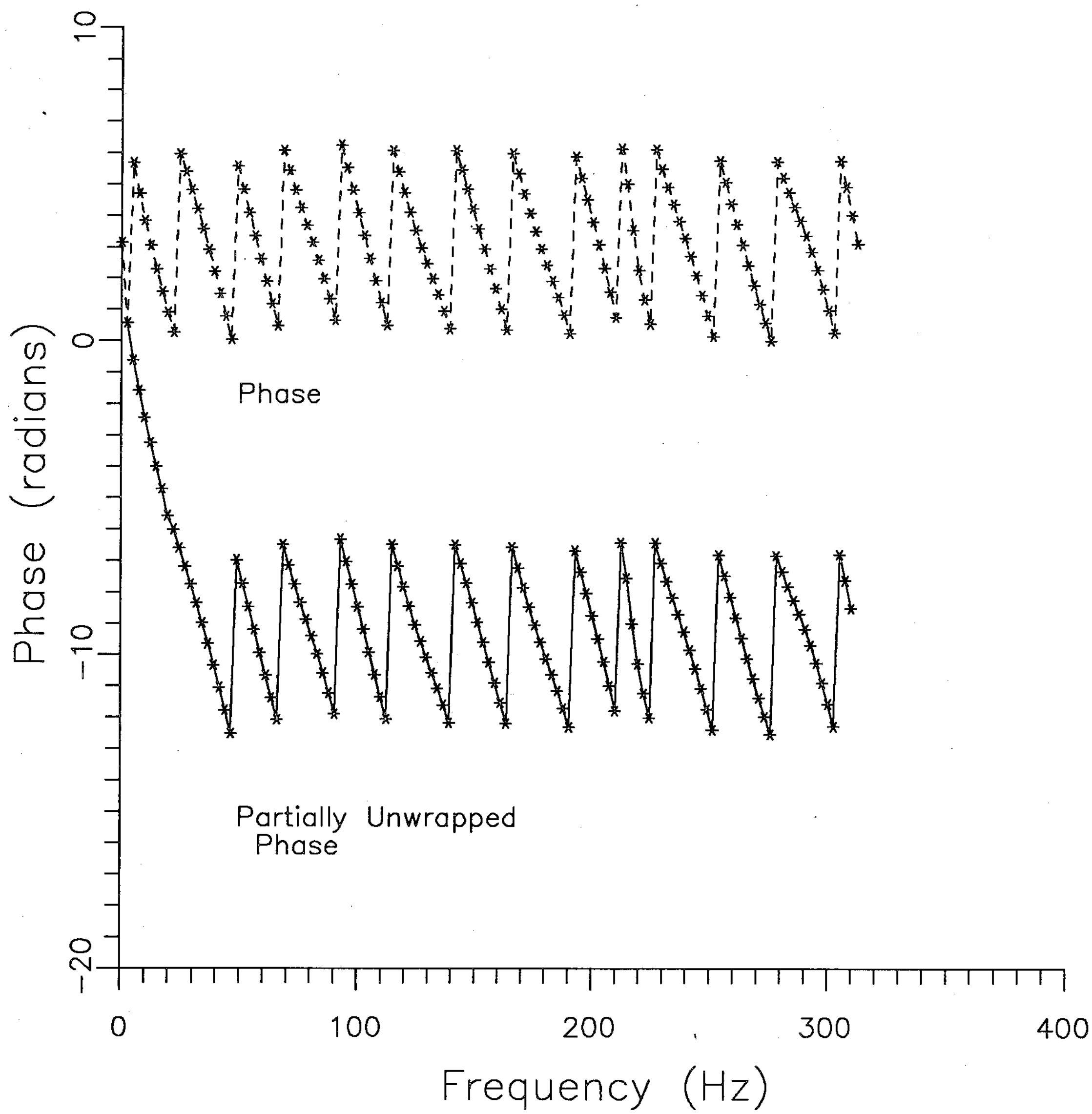


Fig.A.6 Partially Unwrapped Phase of FFT

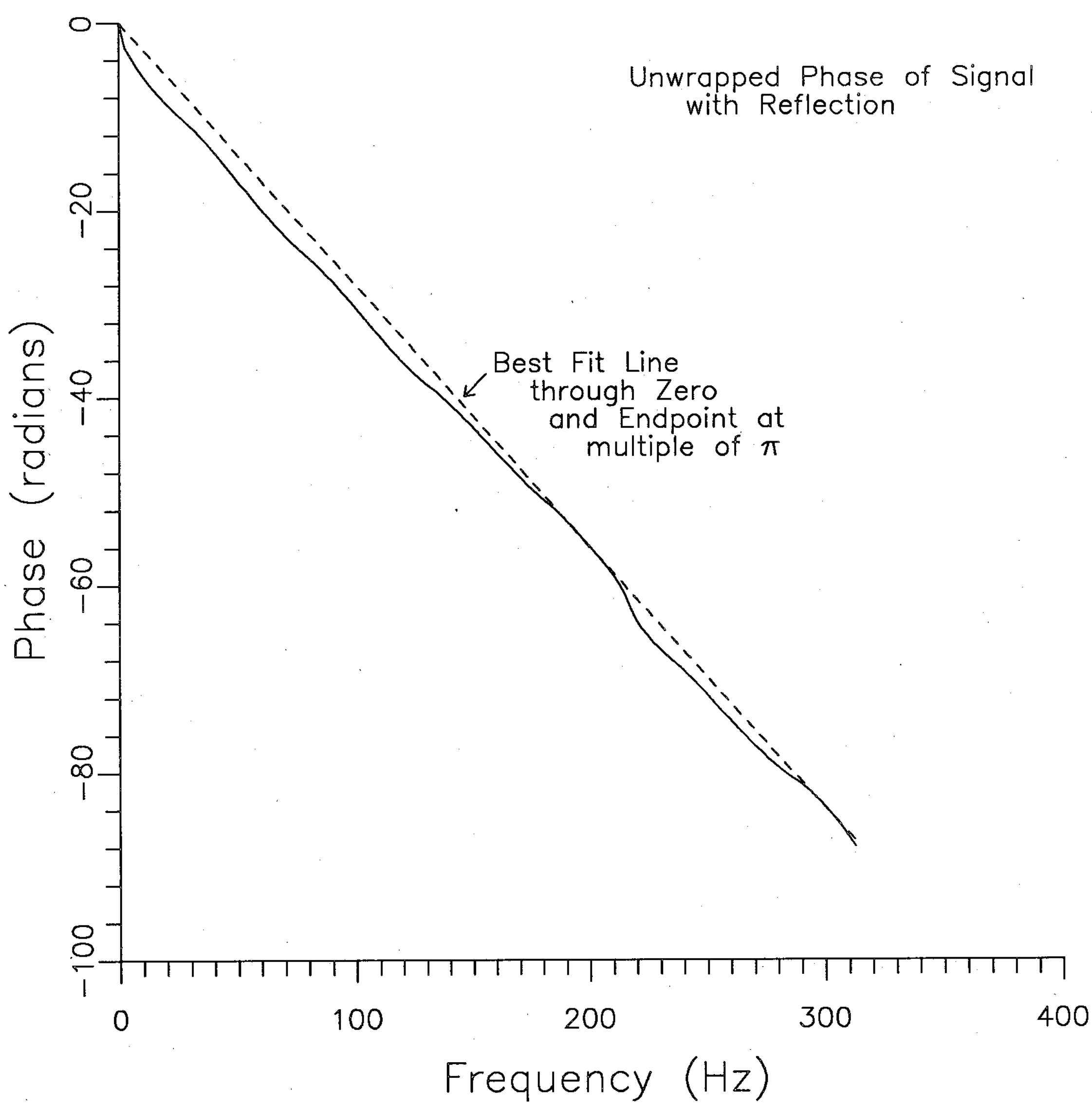


Fig.A.7 Fully Unwrapped Phase with Best-fit Line

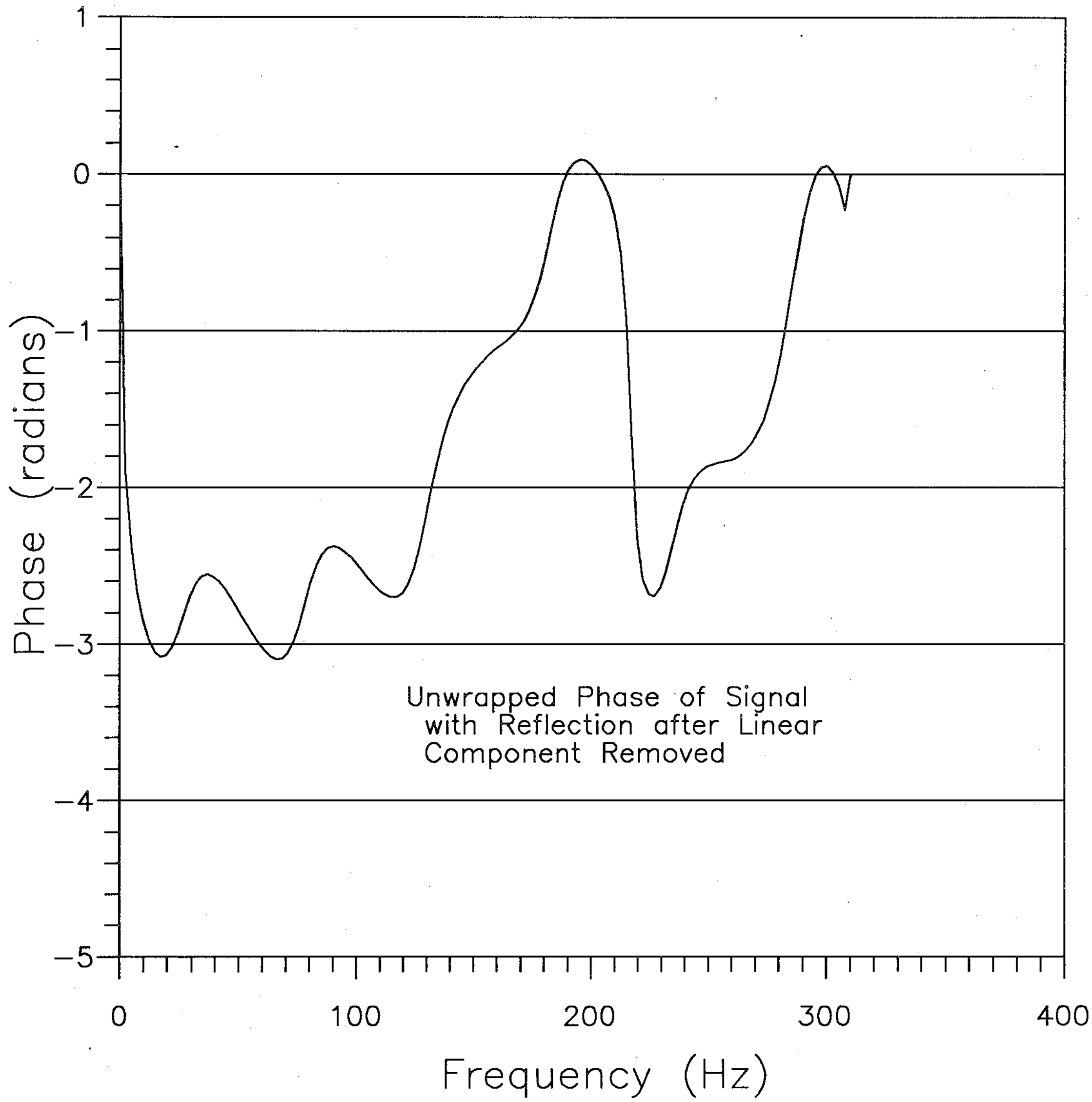


Fig.A.8 Unwrapped Phase with Linear Component Removed

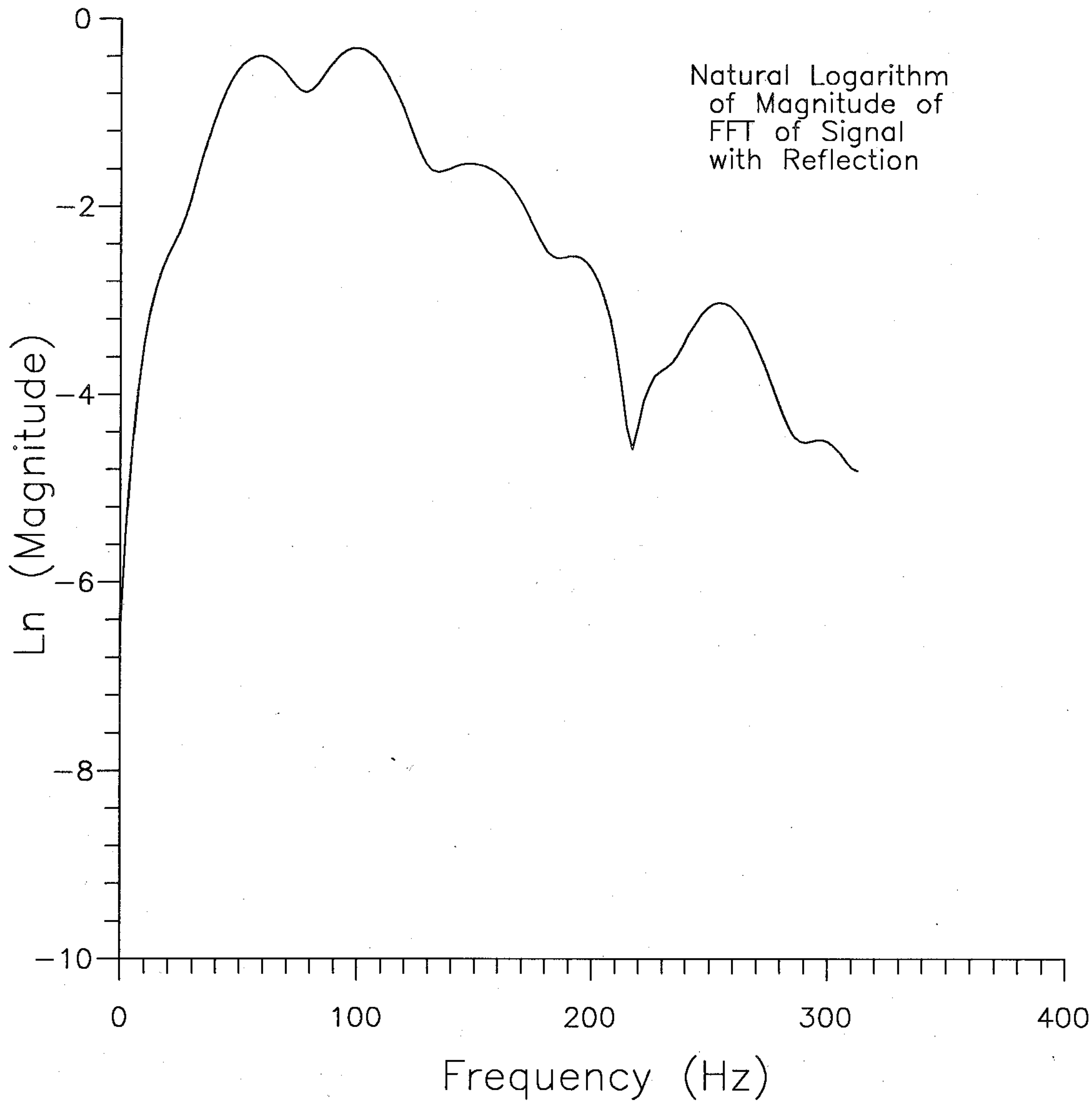


Fig.A.9 Natural Logarithm (Ln) of Magnitude of FFT

However, the phase is an odd function, and must also be mirrored around the frequency axis. These can be combined in the complex logarithm as given in eqn 5.1. Then the inverse FFT is calculated to give the complex cepstrum shown in Fig.A.10. The reflection at 19.2ms can be clearly seen. Fig.A.11 shows the corresponding cepstrum if the linear phase component is not removed. It is obvious that the information of interest near the origin is completely hidden.

Oppenheim and Schafer(1975) give an alternate realization of the complex cepstrum calculation using the logarithmic derivative. Although this method avoids the problems of computing the complex logarithm, they point out that there is more severe aliasing in this method. For a given number of sample points, it is expected that the above method using the complex logarithm will give a more accurate representation of the complex cepstrum.

After computing the complex cepstrum, the output is studied for indications of reflections on the positive side of the quefrency domain, as reflections, by definition, can only occur after the base signal. The reflection can be seen in Fig.A.10. The cepstrum can be "liftered" (filtered in quefrency domain) by using a simple rectangular window. The cepstrum was liftered using a low-pass window at 17.6ms (one time step before the reflection). The complex cepstrum must then be returned to the time domain. This is done by computing the FFT of the liftered cepstrum, taking the complex exponential (straightforward compared to complex logarithm), and computing the inverse FFT.

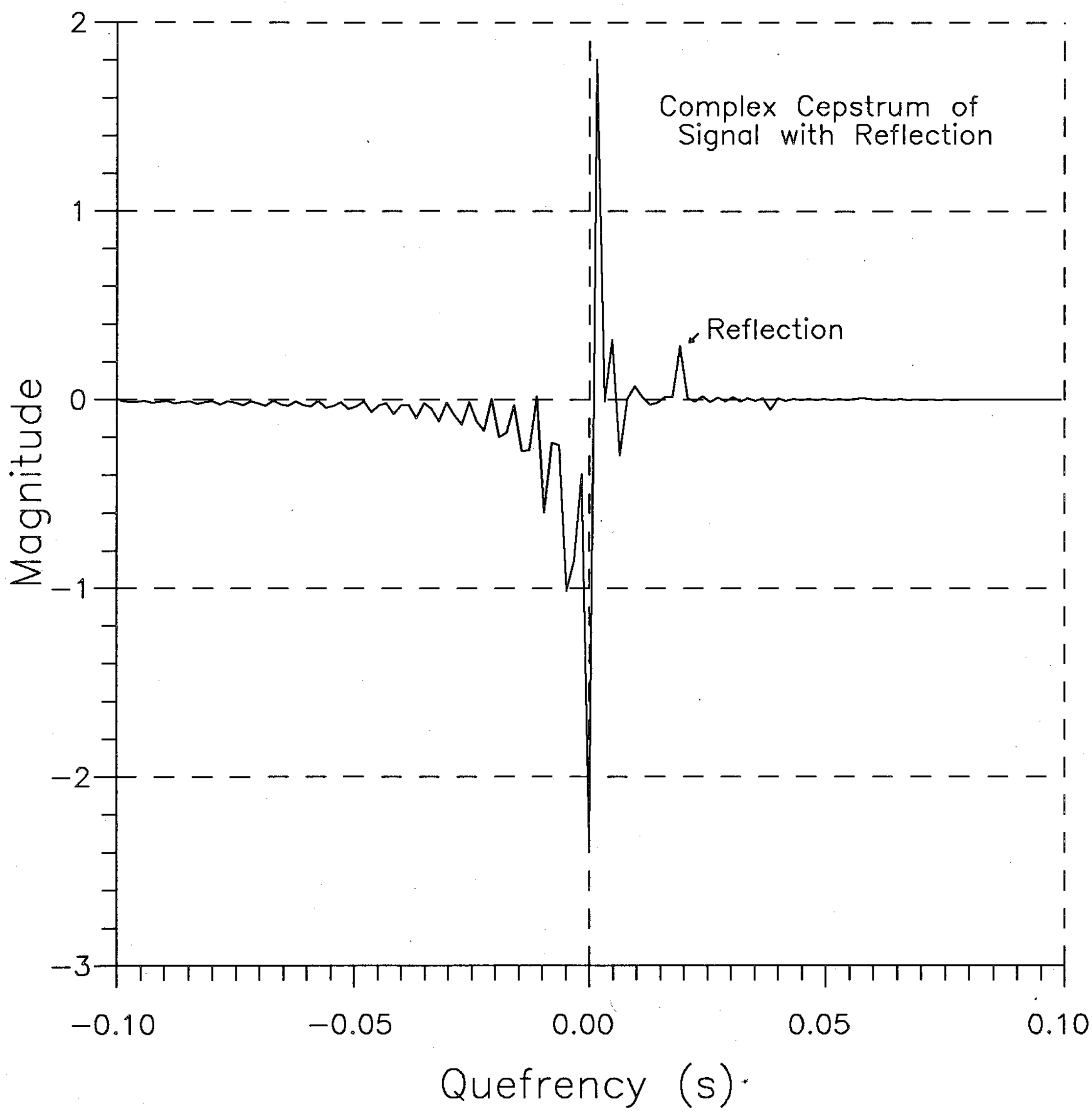


Fig.A.10 Complex Cepstrum of Signal with Reflection

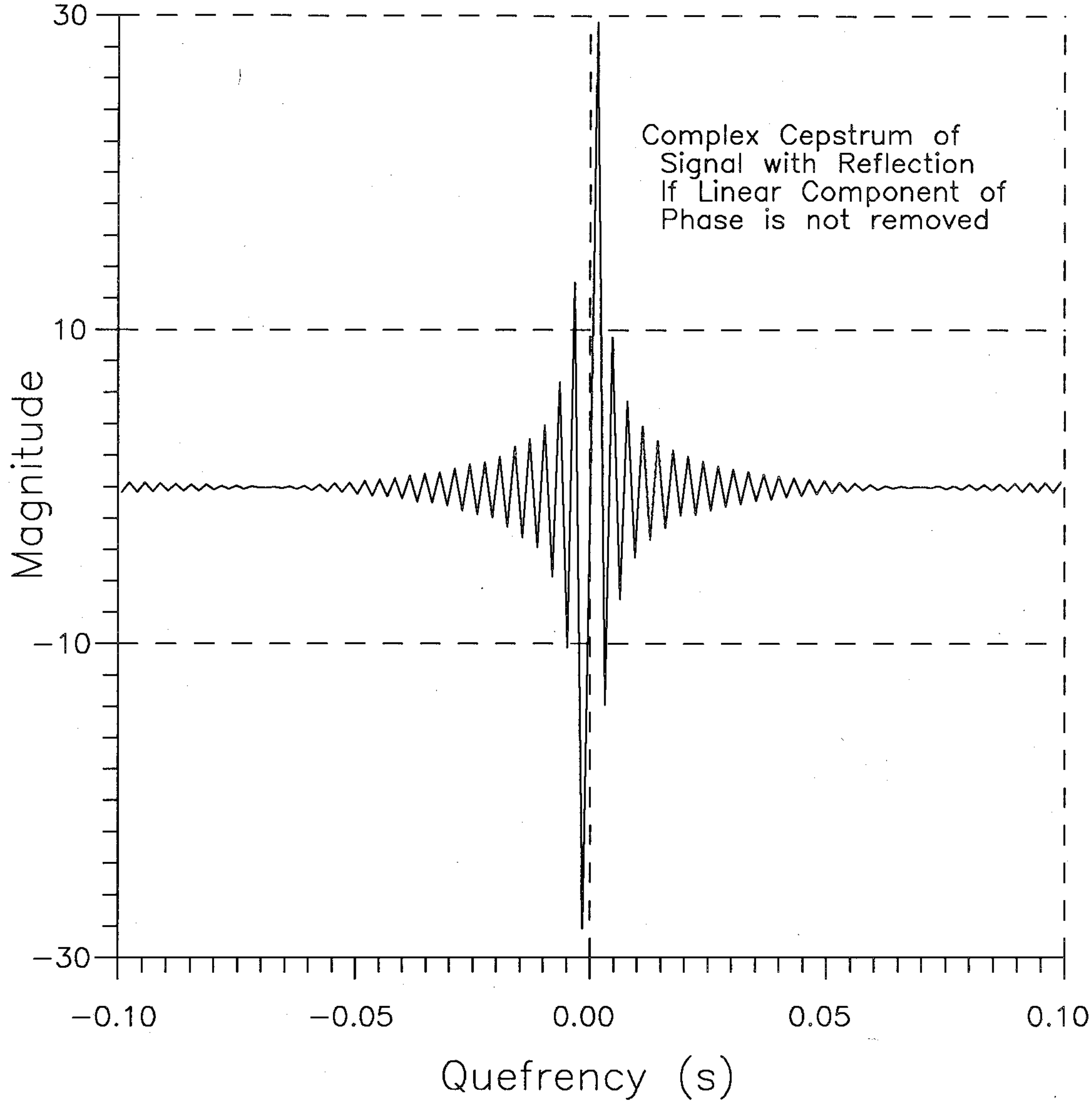


Fig.A.11 Complex Cepstrum of Signal if Linear Component not Removed

The resulting signal is shown in Fig.A.12, along with the original signal used in the calculation. It can be seen that the reflection is almost completely removed, and the original signal recovered. It also possible to use a high-pass lifter on the cepstrum and then use the inverse cepstrum calculation. The result of this calculation is shown in Fig.A.13, and most of the original reflectivity series is returned.

### *A.3 METHOD APPLIED TO MEASURED SIGNALS*

Examples of several complex cepstra of actual accelerometer signals are given in Fig.A.14 to Fig.A.16. None of these show a clear indication of reflections which stand out in the cepstra. The cepstrum in Fig.A.16 was liftered at 9.6ms, and converted back to the time domain. The resulting signal is compared with the original signal in Fig.A.17. The liftering process seems to have added to the original signal, rather than removing reflections.

It is concluded that the smaller pulses following the main pulse in the accelerometer signals are not simple reflections, and thus the base signal cannot be recovered using the complex cepstrum approach.

Therefore it is necessary to assume an arbitrary cutoff to be applied to the signal for further calculations. It appears that the most practical basis is to use the first wavelength after the arrival of the shear-wave, to retain all of the frequencies in the incoming shear wave, and to exclude, as much as possible, the effects of reflections,

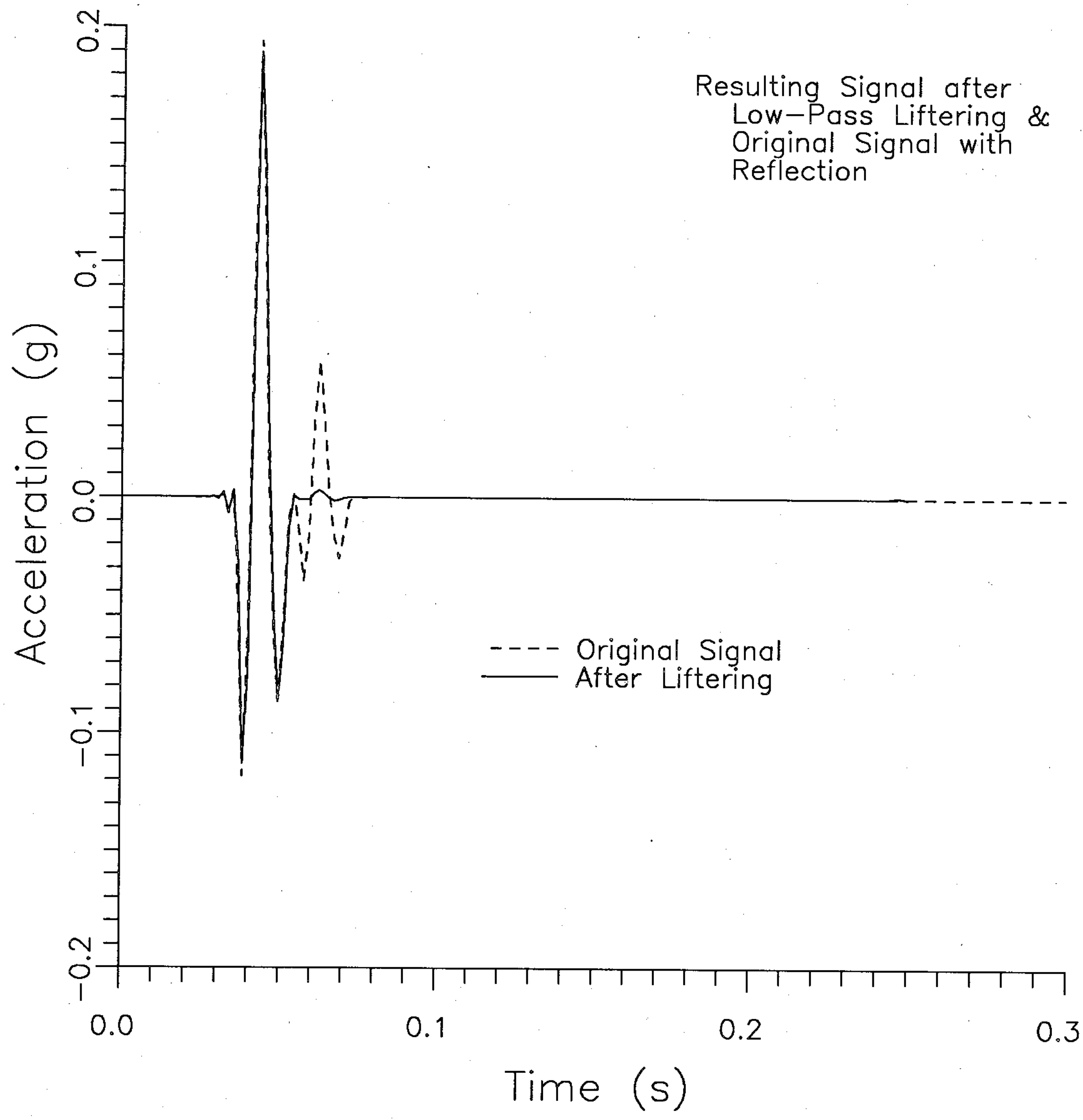


Fig.A.12 Liftered Signal with Reflection Removed

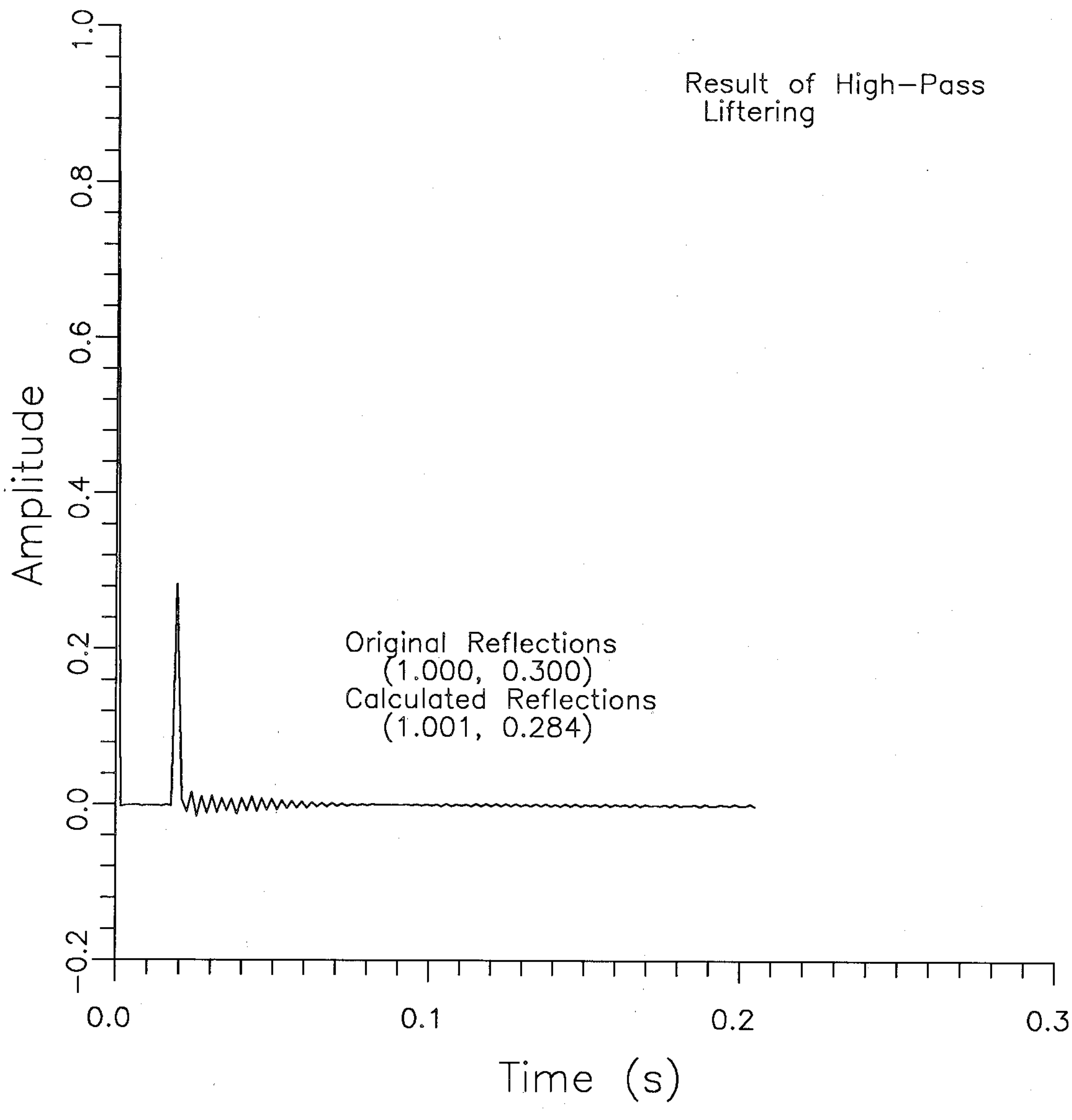


Fig.A.13 High-pass Liftered Signal to Recover Reflection

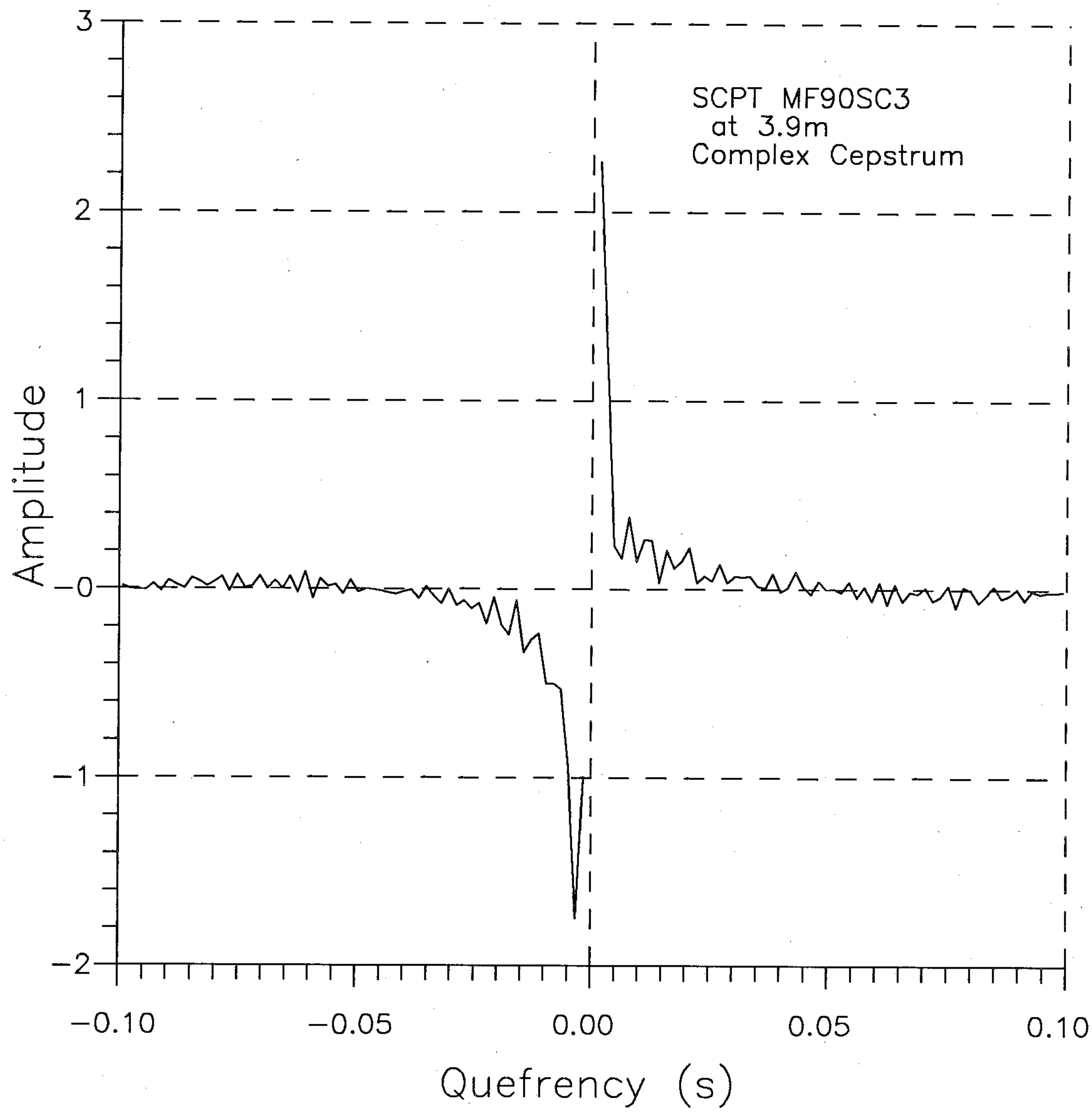


Fig.A.14 Complex Cepstrum of Recorded Signal at 3.9m

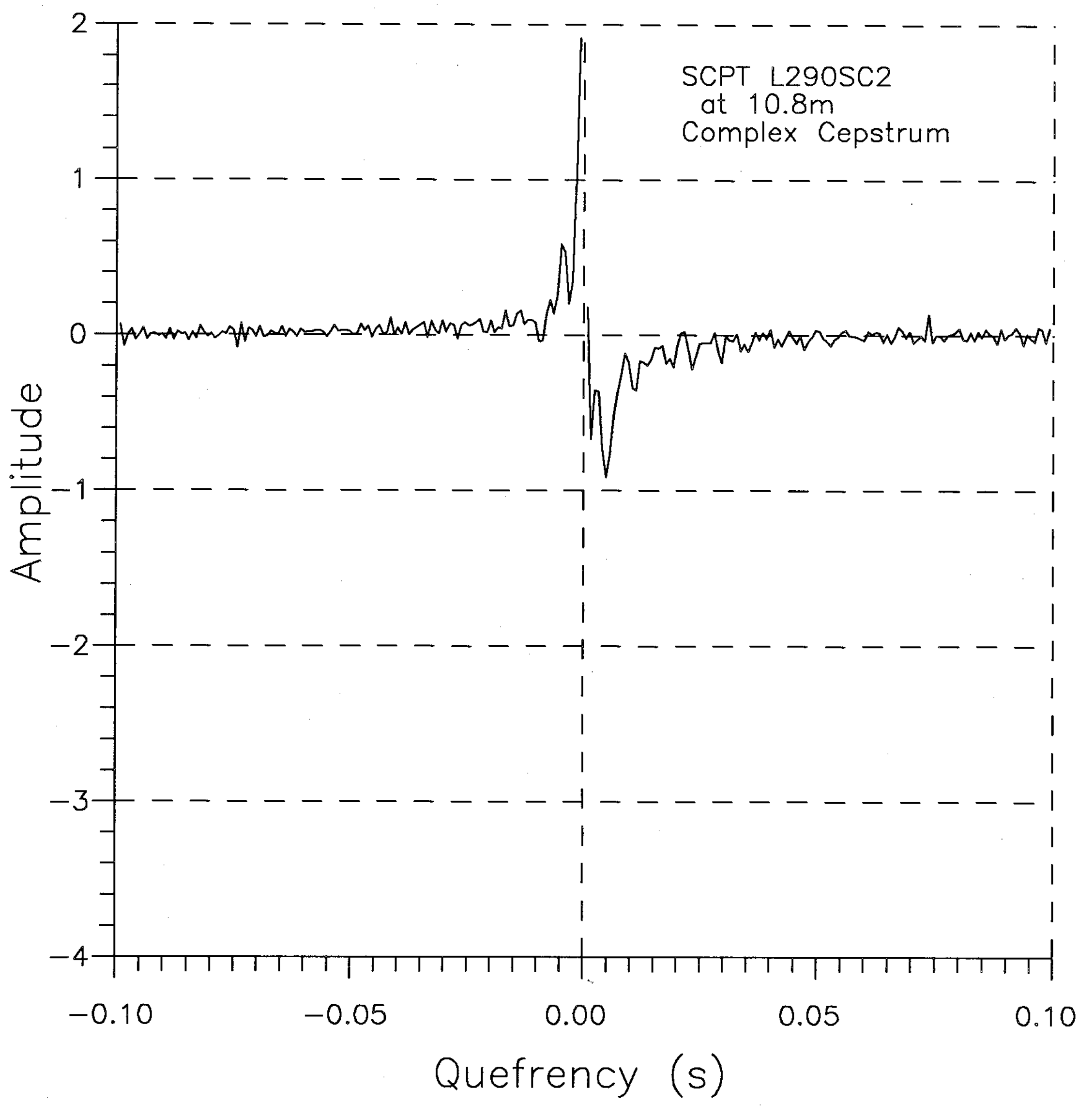


Fig.A.15 Complex Cepstrum of Recorded Signal at 10.8m

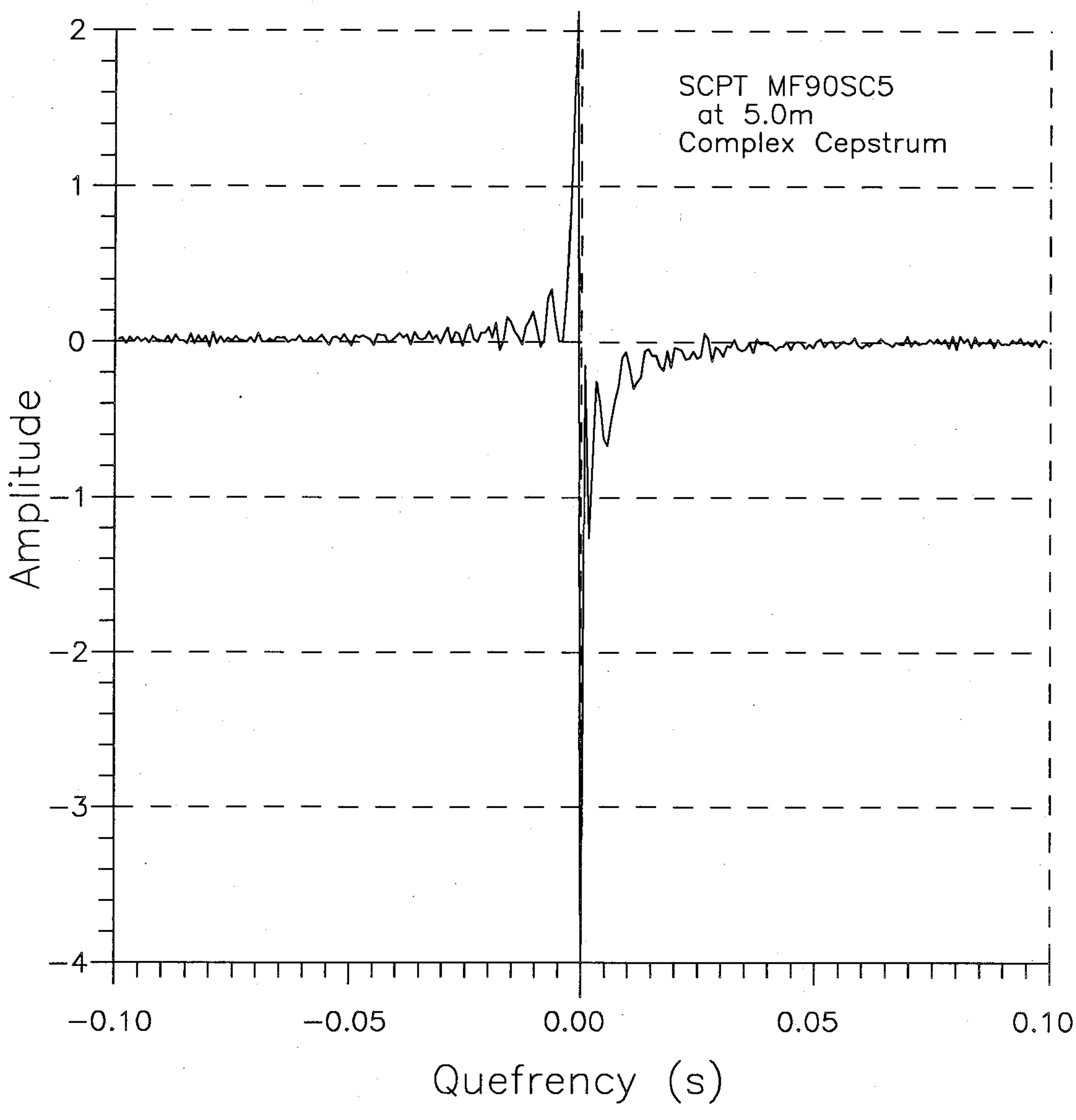


Fig.A.16 Complex Cepstrum of Recorded Signal at 5.0m

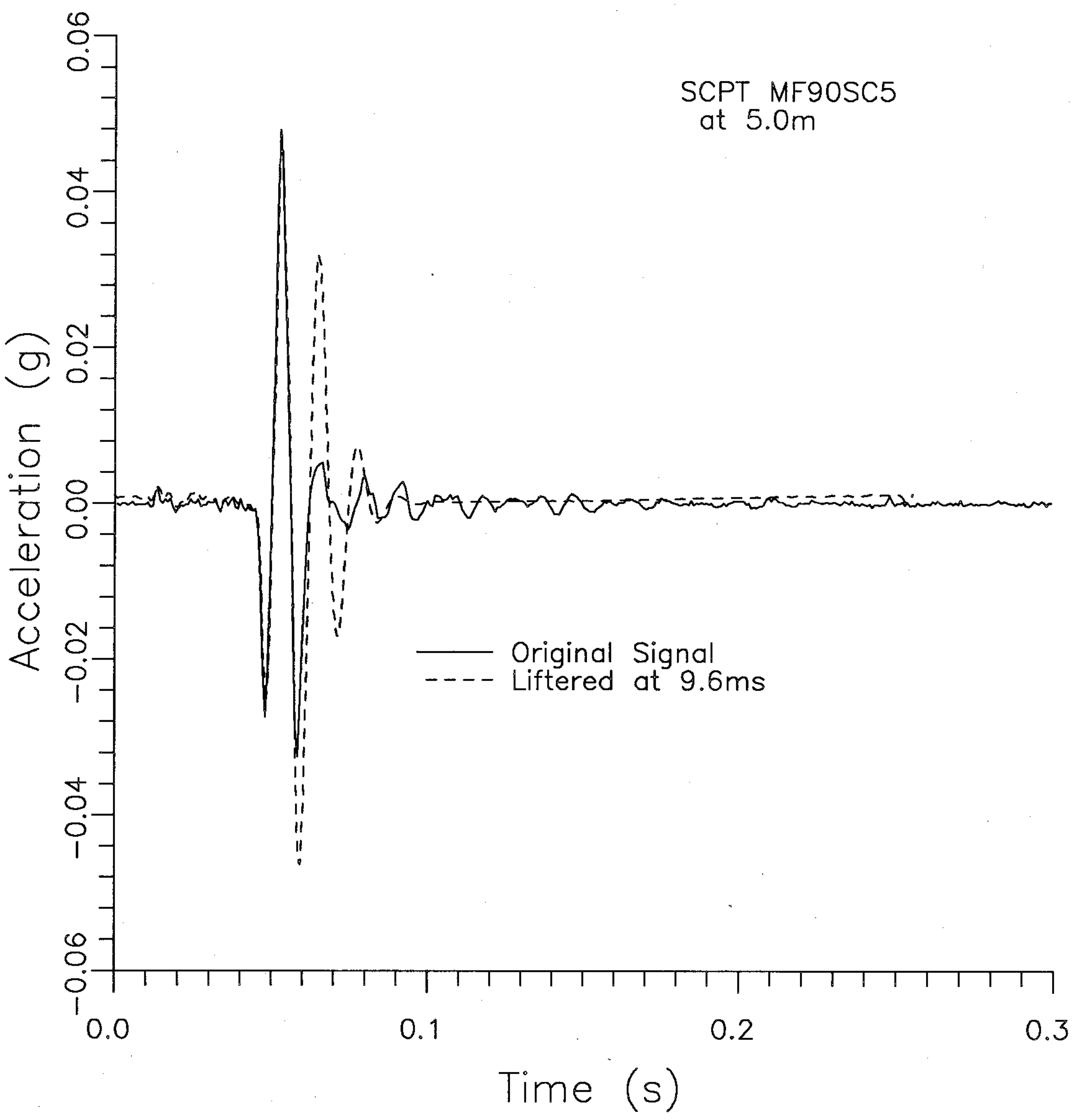


Fig.A.17 Liftered Signal of Cepstrum of Signal at 5.0m instrument response, and other factors that may affect later portions of the signal.

## APPENIX B

## RANDOM DECREMENT APPROACH

The basic concept of the random decrement approach was discussed in section 3.3 and it was pointed out that the method as proposed seemed to inherently incorporate instrument damping. This appendix provides some details of the method and provides some results.

A typical accelerometer signal which has been filtered (low pass 180Hz) is shown in Fig.B.1. In addition to the main shear pulse, a number of smaller pulses can be seen. In applying other methods, these smaller pulses (and the balance of the signal) are removed, since the causes of these pulses are not clear and these pulses tend to "contaminate" the "frequency signature" of the signal. However in the random decrement procedure these pulses form an integral part of the method and cannot be removed.

The random decrement procedure can be briefly explained in reference to Fig.B.1. Basically the procedure is to first filter the signal, then select an arbitrary amplitude for the analysis. The amplitude is selected to give a reasonable number of intercepts along the curve (8 in the case shown). At each intercept, equal arbitrary length segments (0.1sec or 501 points in this case) are duplicated from the signal. The segments are shifted to start at zero time and then averaged (Fig.B.2). The resultant "randec sum" shown in Fig.B.3 has an initial amplitude essentially equal to the arbitrary selected amplitude. A program to generate the randec sum is given in Appendix E. The method

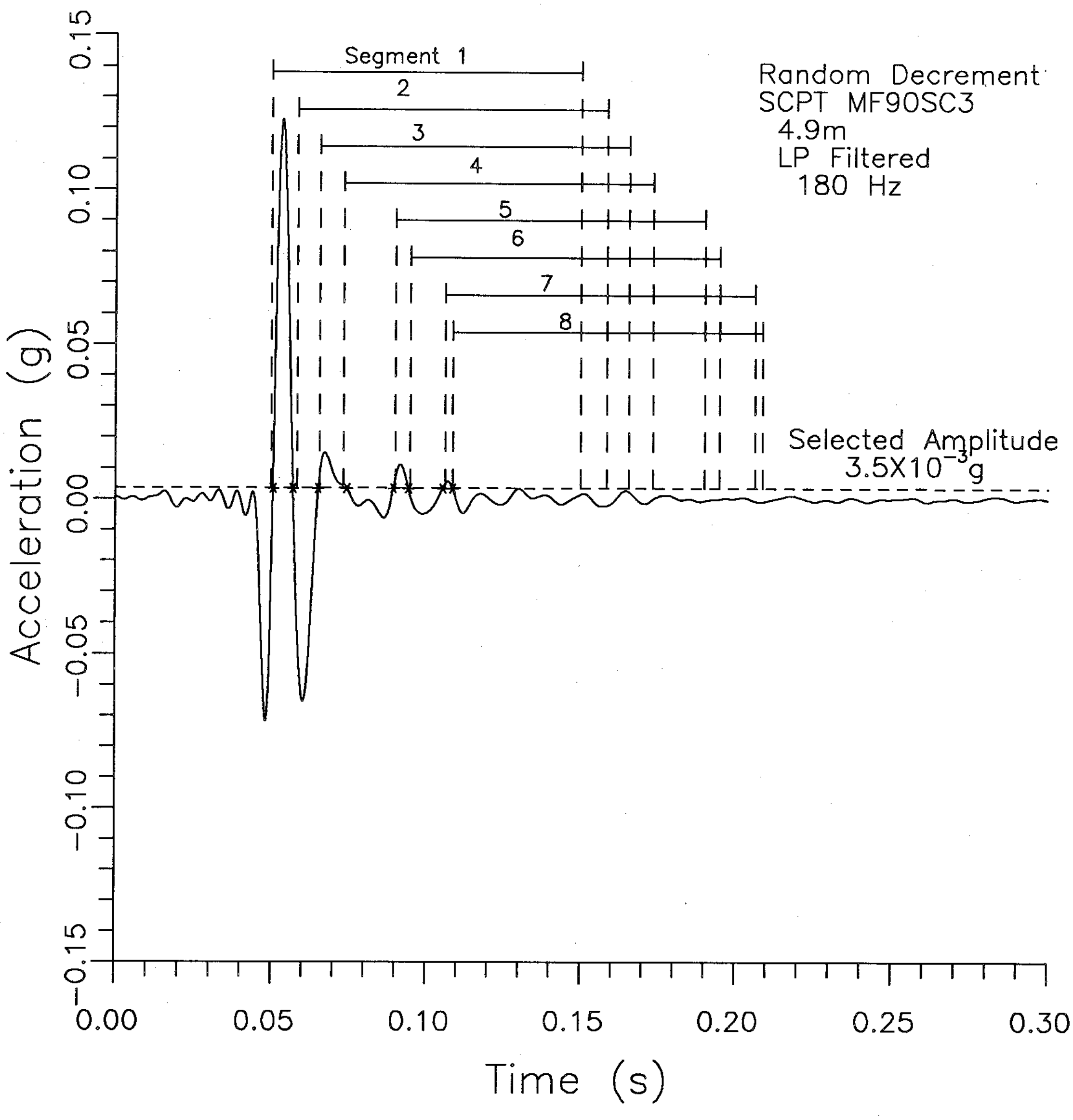


Fig.B.1 Random Decrement Method — Segment Selection

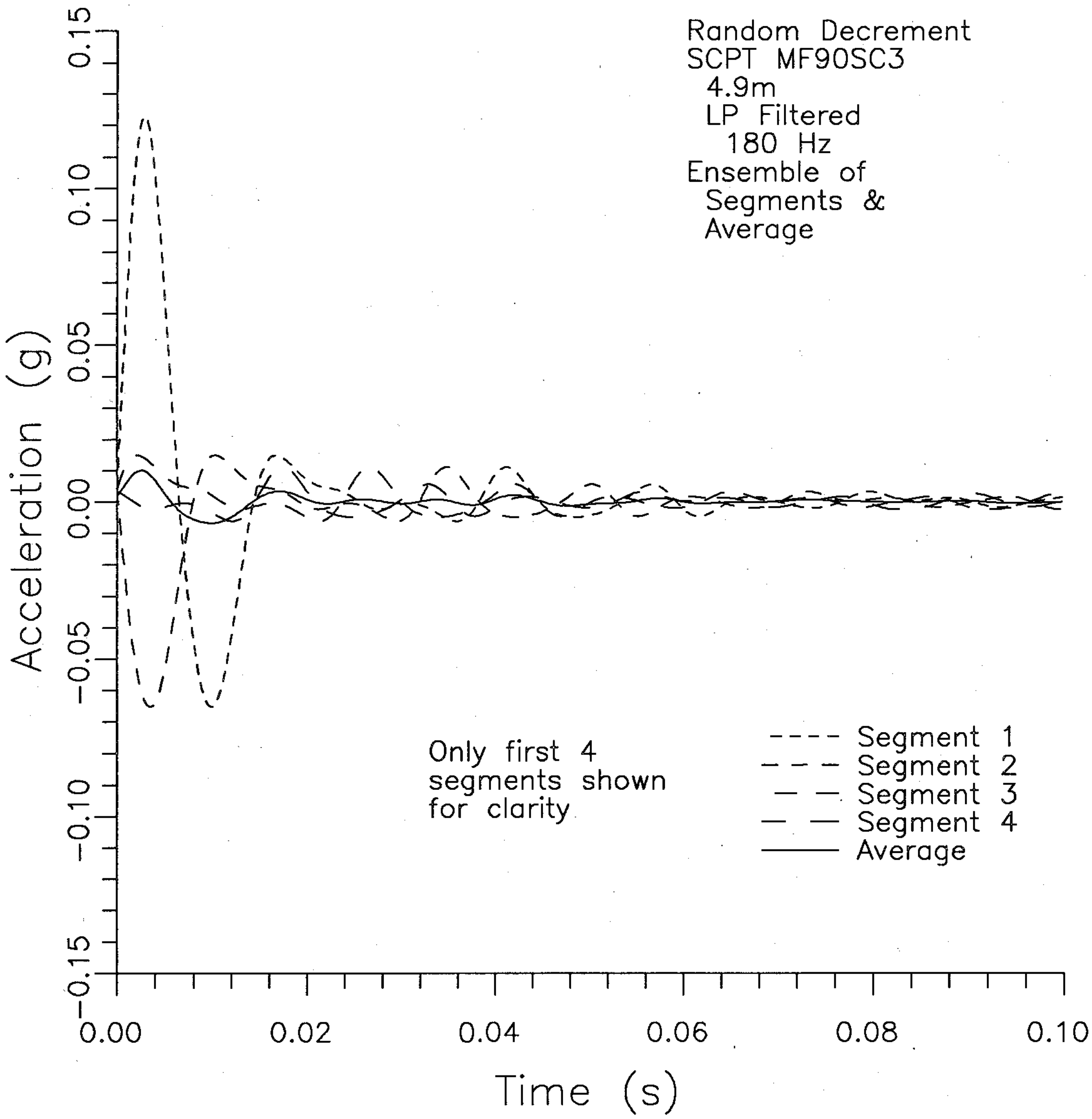


Fig.B.2 Random Decrement Method — Segment Ensemble

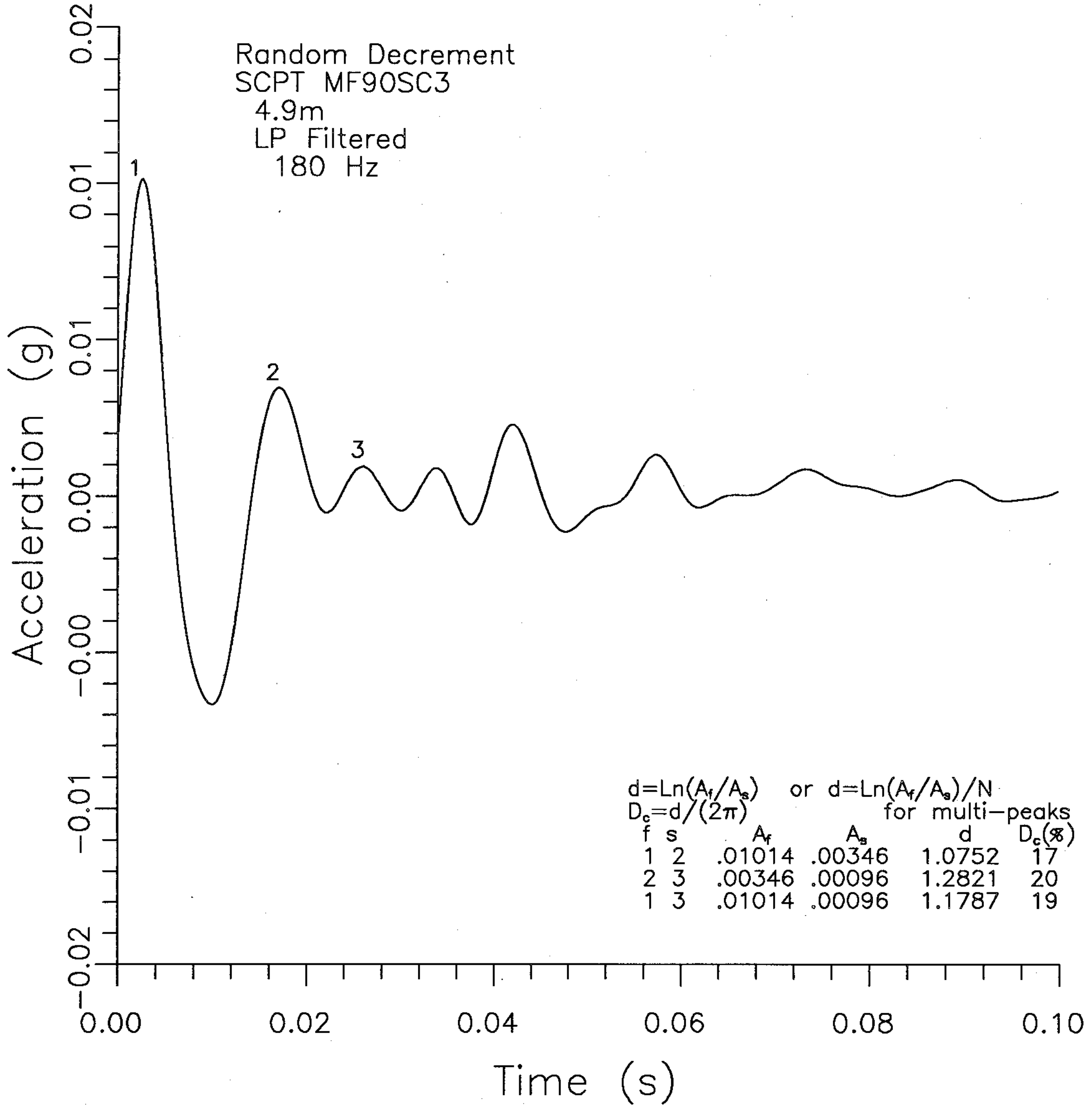


Fig.B.3 Random Decrement Method (Randec Sum) assumes that the initial slope will be equal to zero, since an equal number of positive and negative slopes will generally average to zero. In the case shown, and in the examples shown by Aggour et al (1982a,b) the initial slope is not zero as the initial pulse dominates the average. The peaks in the resultant signal are then analyzed to give the logarithmic decrement and the damping as shown in Fig.B.3. The resultant damping values were 17-20% as compared to the expected value of less than 2%. It seems that the method incorporates the effect of the instrument response, in addition to the soil damping.

In the 1982b paper, Aggour et al refer to the use of "appropriate narrow band filters" but do not give any details of the filters used. Yang et al(1989) used a bandwidth of 0.12Hz with a central frequency of 0.49Hz (bandwidth,$w_b$ approximately 25% of central frequency,$f_o$). The above analysis had a $w_b/f_o$ of about 200%, so that narrower bandwidths were considered. The inverse FFT after using a filter of 67-84Hz ($w_b/f_o$ about 23%) is shown in Fig.B.4. It can be seen that the shape of the signal has been drastically changed by the filtering. The resulting randec sum in Fig.B.5 shows an initial damping closer to the expected value, but the damping increases rapidly across the randec sum. An intermediate filter (54-98Hz, $w_b/f_o$ about 58%) was also used. The results shown in Figs.B.6 and B.7 are between the first two cases. The three cases are summarized in Table B.1.

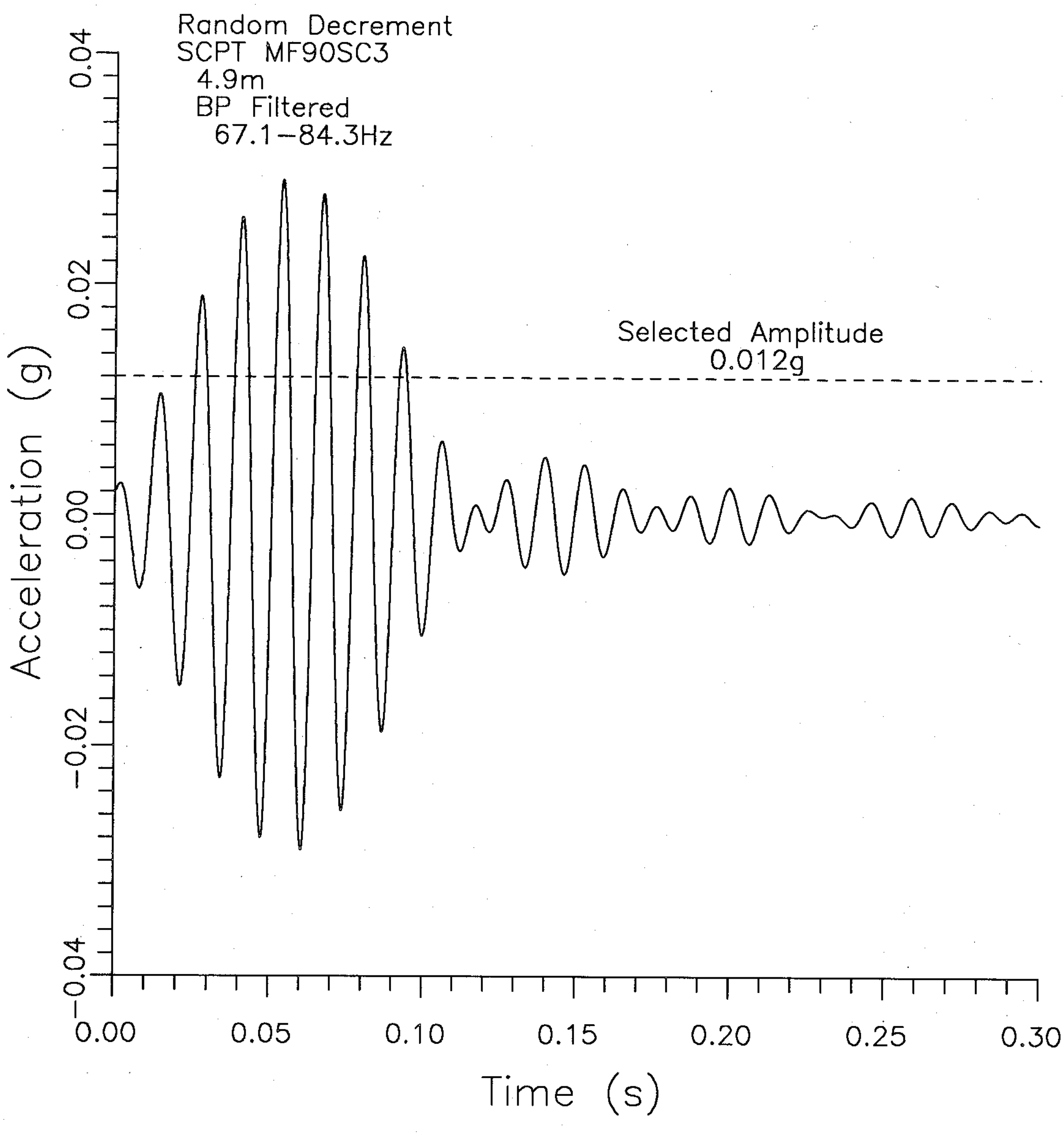


Fig.B.4 Random Decrement – Selection after Narrow Bandpass Filter (BPF)

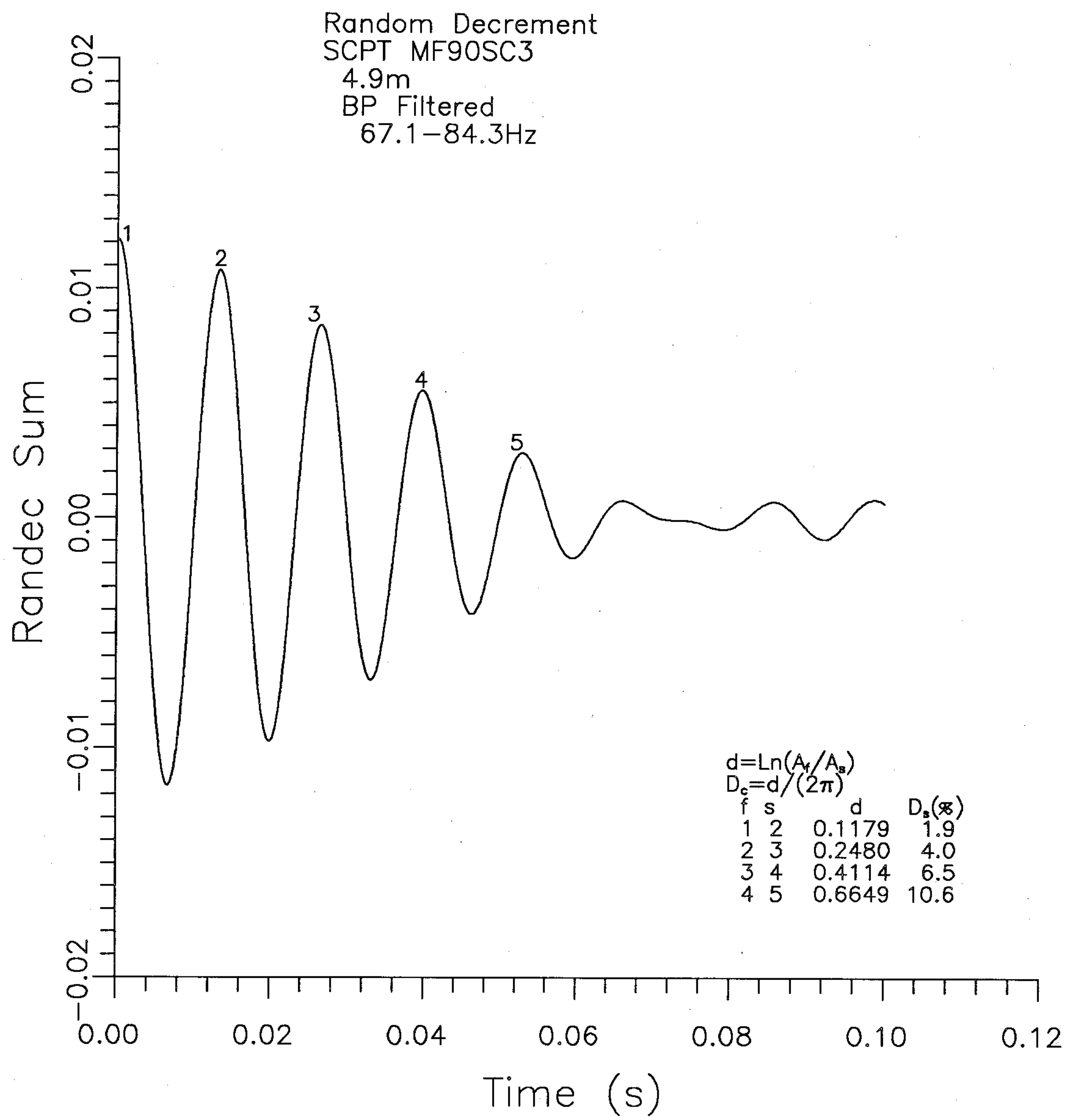


Fig.B.5 Signature after Narrow BPF

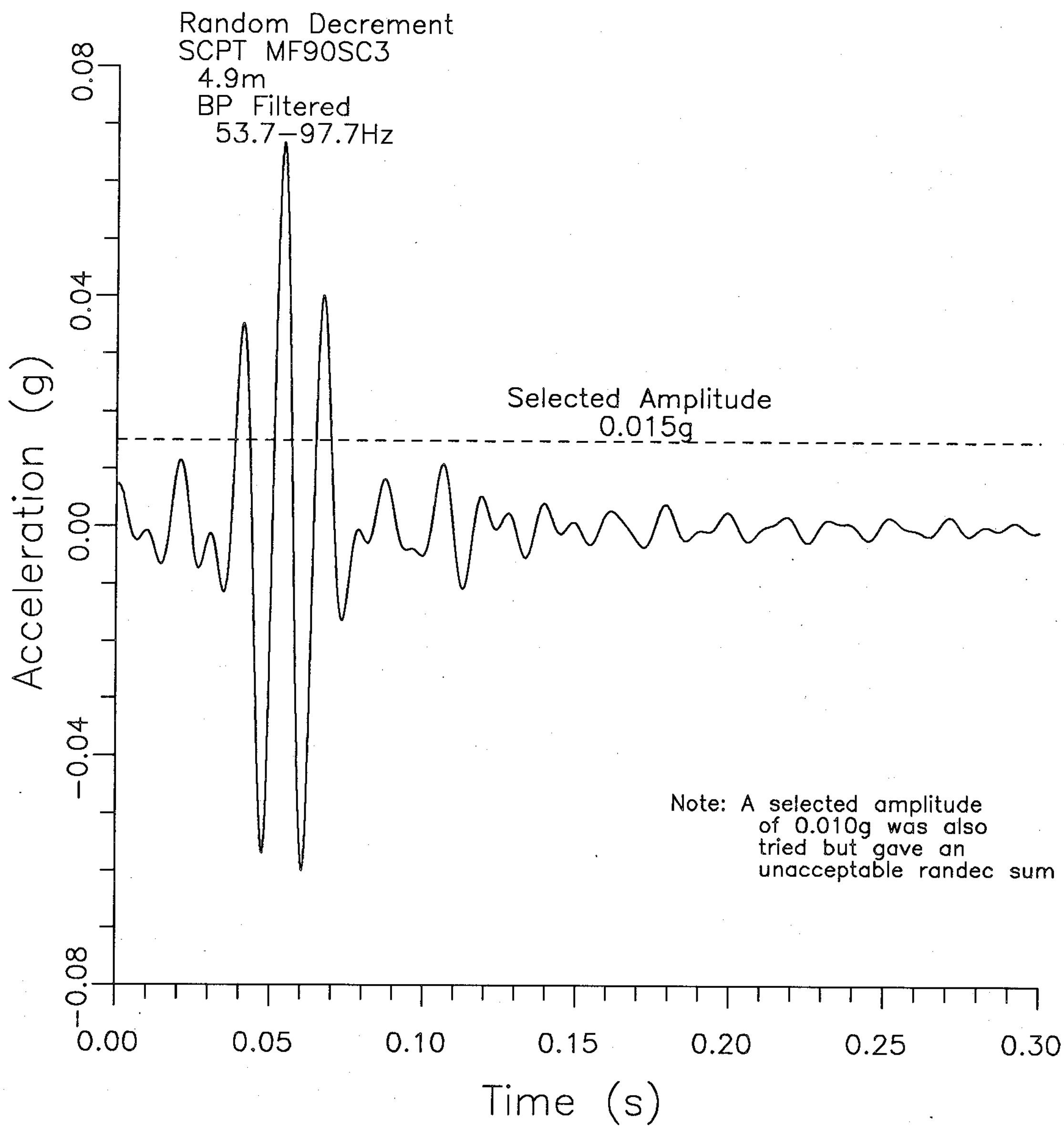


Fig.B.6 Selection after Intermediate BPF

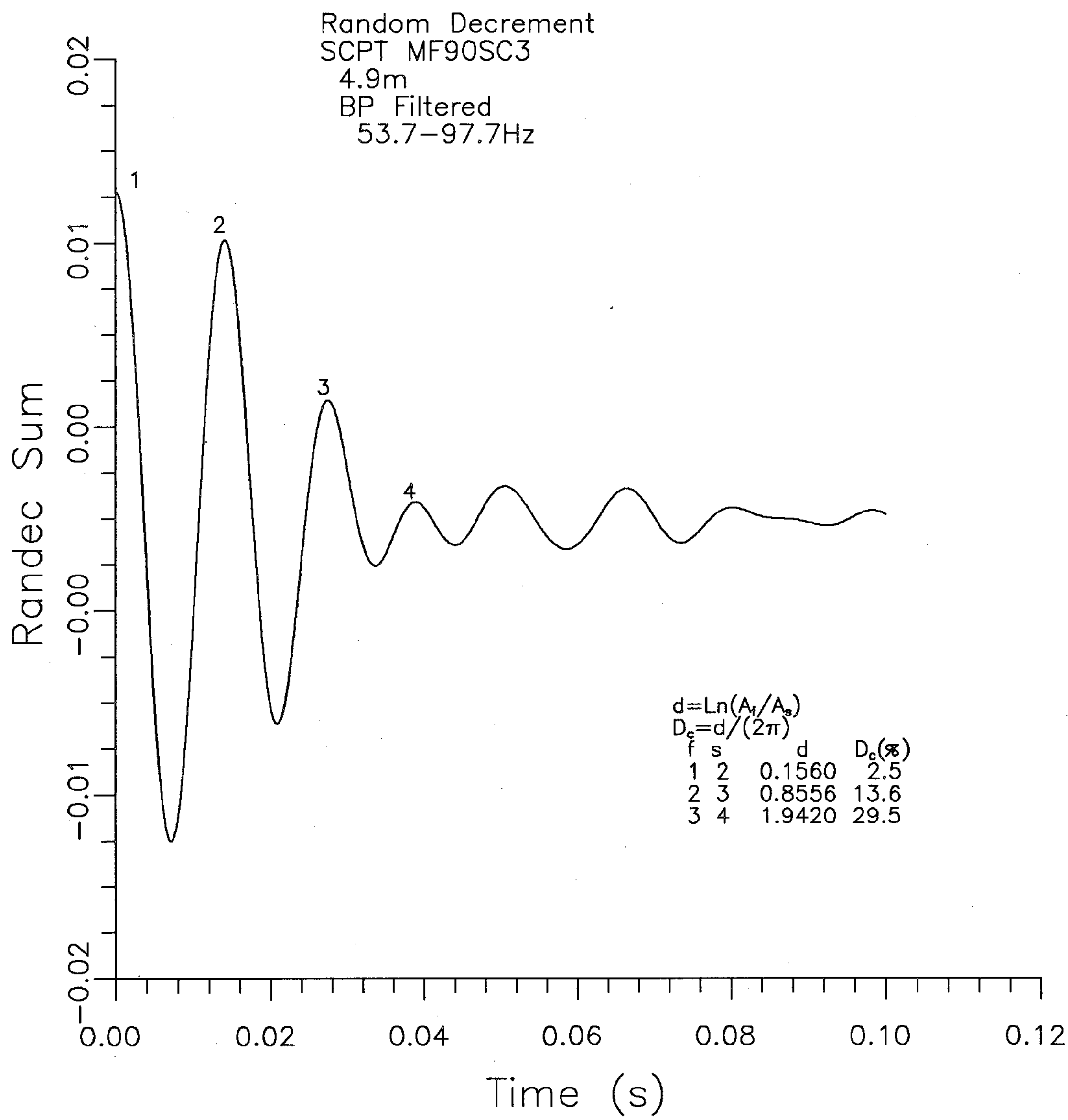


Fig.B.7 Signature after Intermediate BPF

Table B.1. Variation in Damping(%) with Filter Bandwidth

| Filter | Width | $w_b/f_o$ | Peaks used for Damping Calc. | | | |
|---|---|---|---|---|---|---|
| Hz | | % | 1-2 | 2-3 | 3-4 | 4-5 |
| 0-180 | 180 | 200 | 17 | 20 | 19 | |
| 54-98 | 44 | 58 | 2.5 | 13.6 | 29.5 | |
| 67-84 | 17 | 23 | 1.9 | 4.0 | 6.5 | 10.6 |

It can be clearly seen that for at least the first two increments that the damping decreases significantly with the bandwidth of the filter. In addition, for the last two cases, the damping increases significantly with time (number of "cycles").

Examples of similar large bandwidth calculations for a predominantly clay site are given in Figs.B.8 and B.9, giving damping of 29-32% compared with an expected value of less than 2%. Fig.B.9 shows an example where the first peak can be negative if the selected amplitude intercepts a peak in the signal before the main peak.

An attempt was made to expand on the method by considering the inverse transform of the ratio of the FFTs of two signals. It was hoped that this would give a signal that was more representative of the soil damping, and less affected by the instrument. The ratio of the FFTs is shown in Fig.B.10. A large peak can be observed at 220Hz so that the initial bandpass filter selected was 200-240Hz. The inverse FFT is shown in Fig.B.11 and the resulting randec sum is shown in Fig.B.12. The resulting damping calculated was very small (all less than 0.3%).

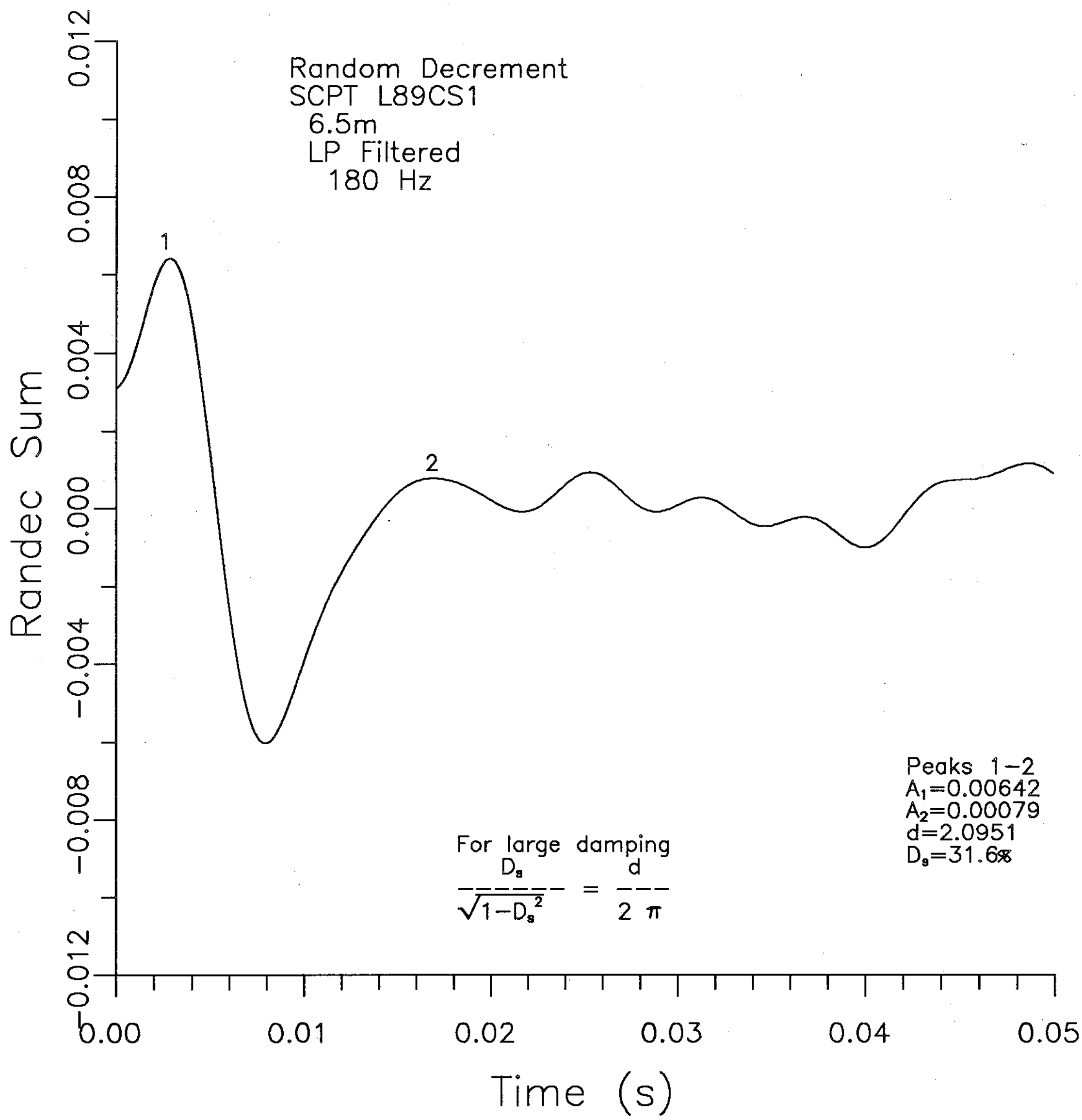


Fig.B.8 Signature from Lowpass Filter (LPF) Signal 1 at Clay Site

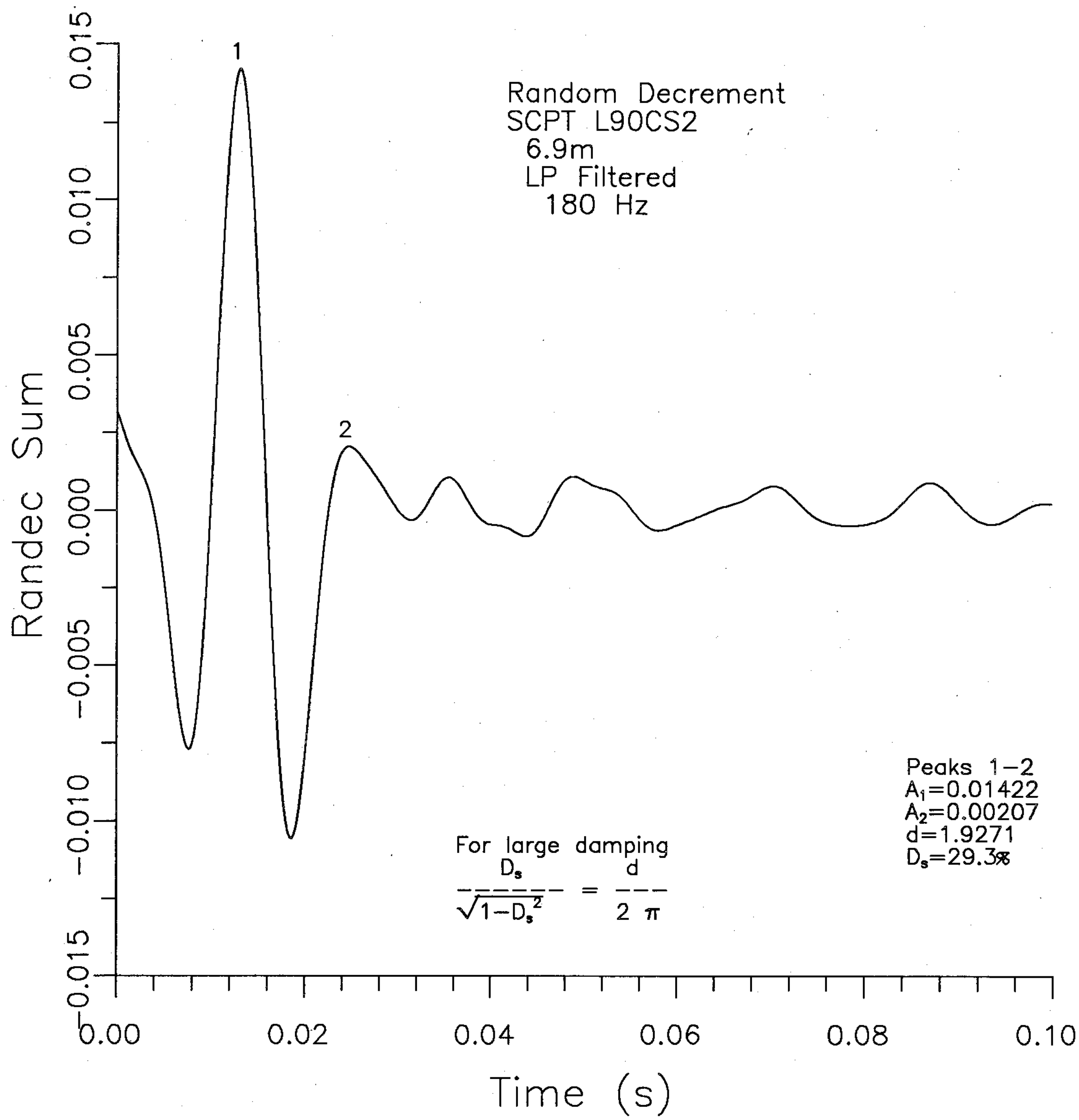


Fig.B.9 Signature from Lowpass Filter (LPF) Signal 2 at Clay Site

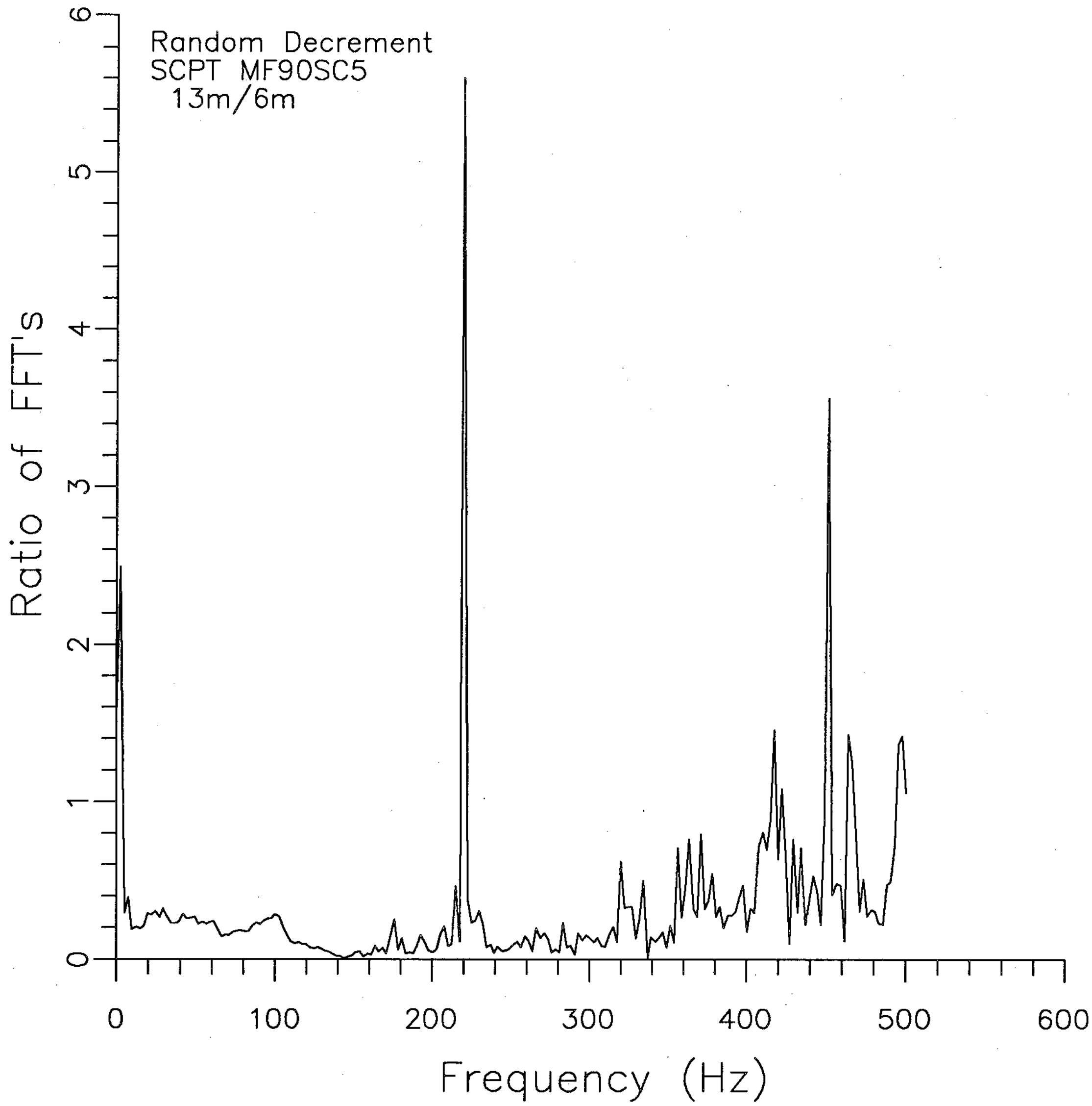


Fig.B.10 Ratio of FFT's of Two Signals to be Used for Random Decrement Calculations

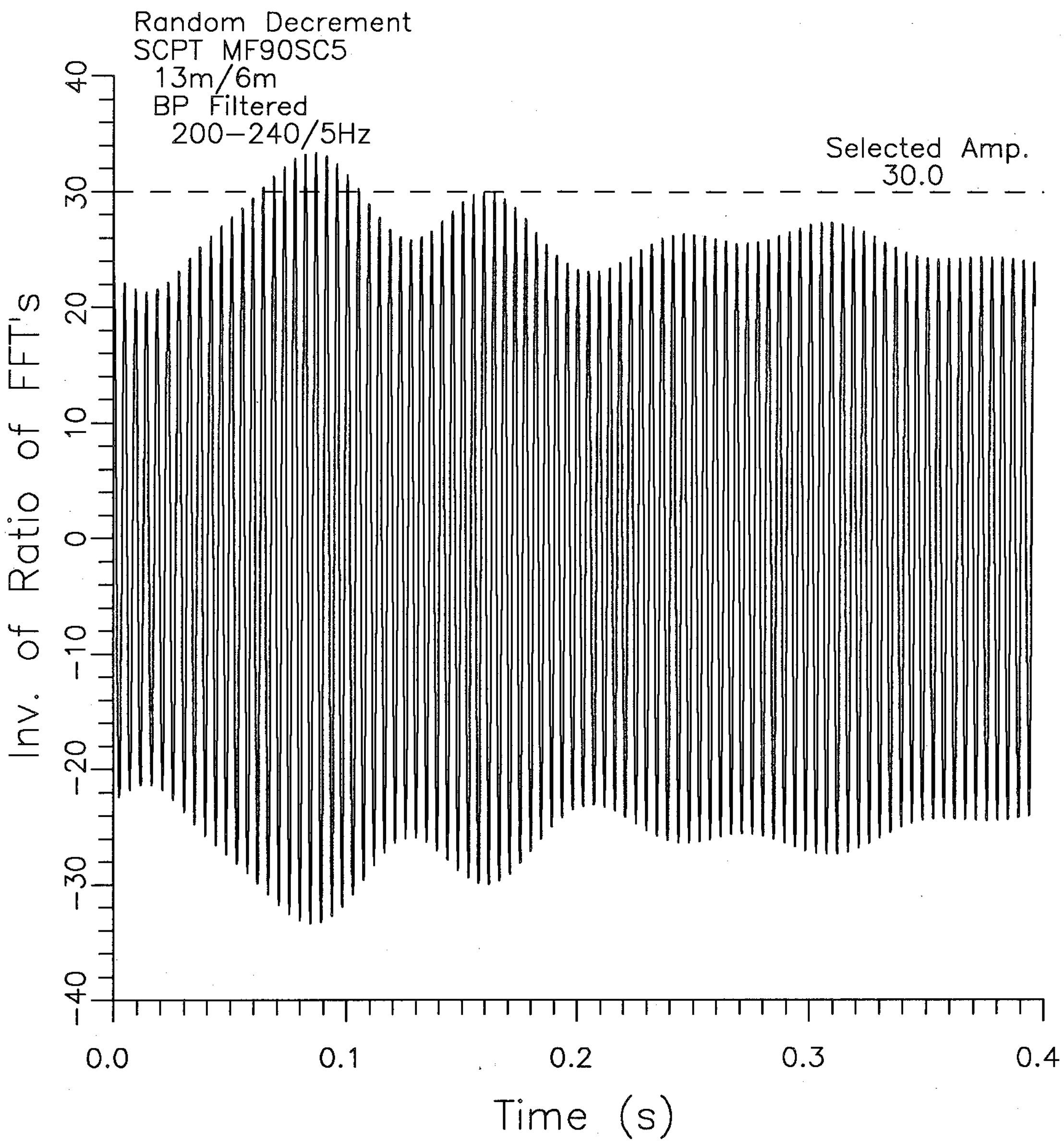


Fig.B.11 Inverse of Ratio of FFT's Filtered at 200–240Hz

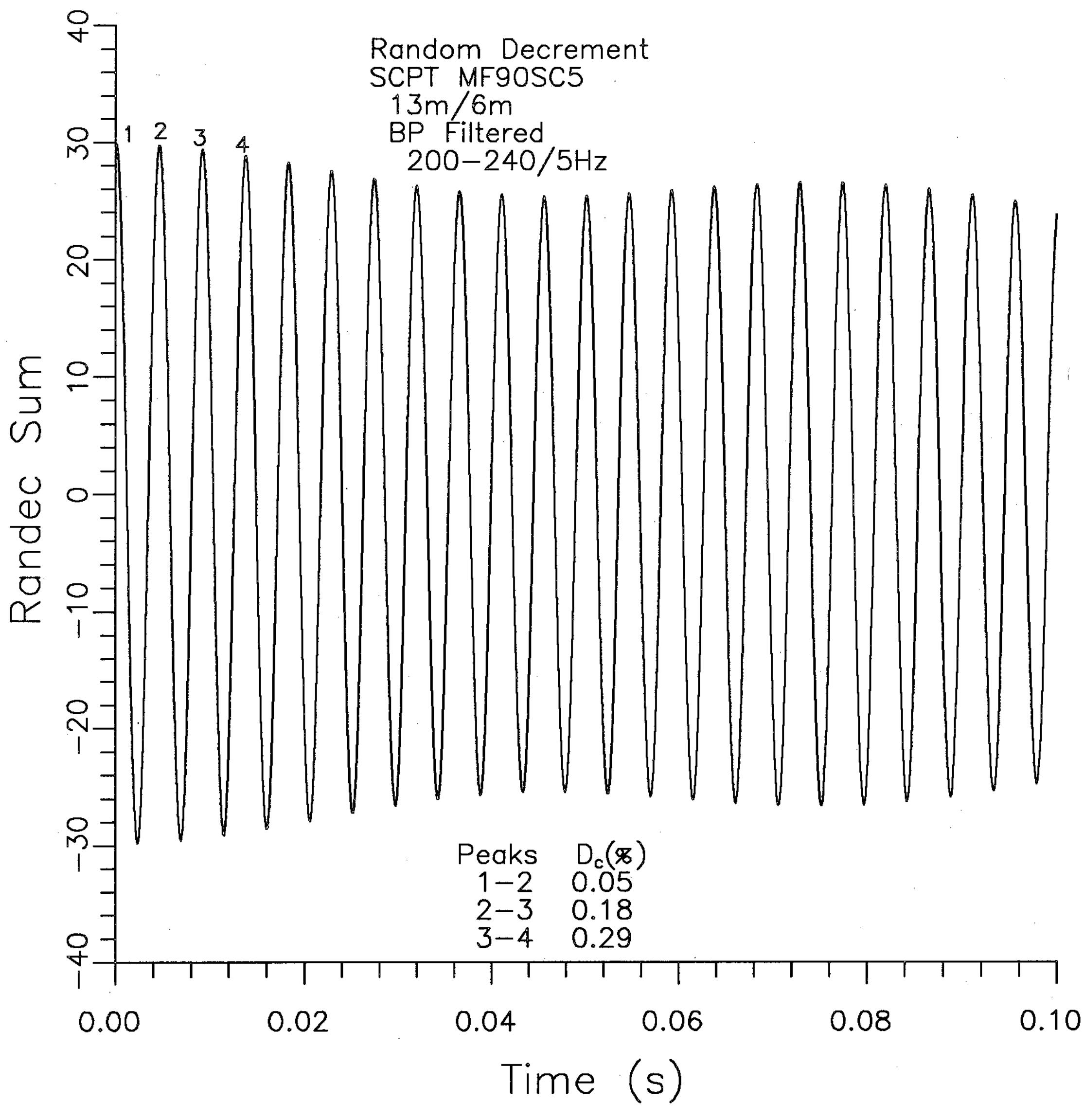


Fig.B.12 Signature from Ratio Filtered at 200–240Hz

Previous work with these signals indicated that the coherence was high for a frequency range of 40-100Hz or slightly wider. The inverse FFT after bandpass filtering at 40-100Hz is given in Fig.B.13. The shape of the resulting signal is somewhat similar to the initial signals, but with some added variations to the smaller peaks. The randec sum is shown in Fig.B.14 with damping varying from about 3-13%. These results show that the method is not improved by using the ratio of the FFT's of two signals.

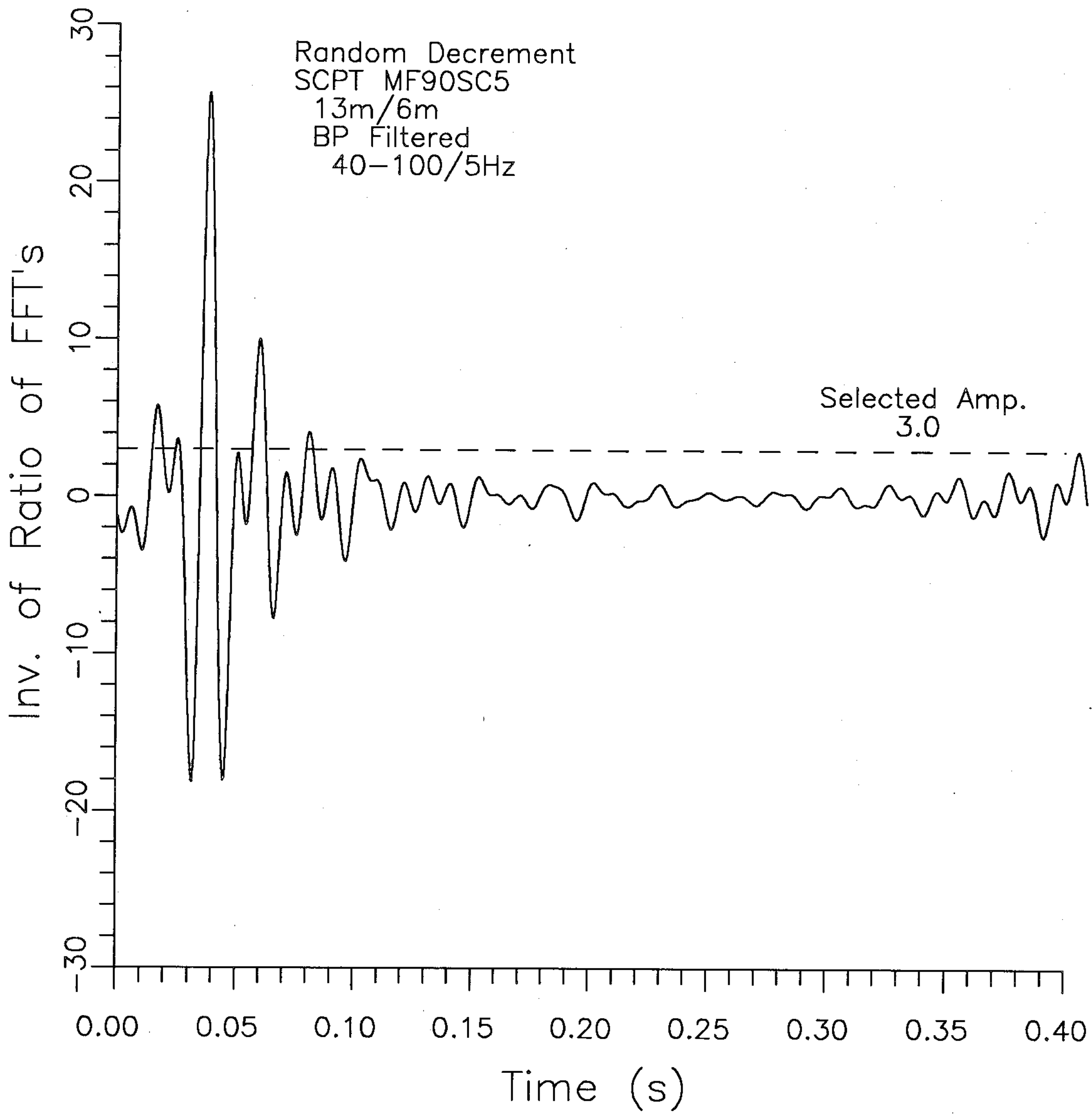


Fig.B.13 Inverse of Ratio of FFT's Filtered at 40–100Hz

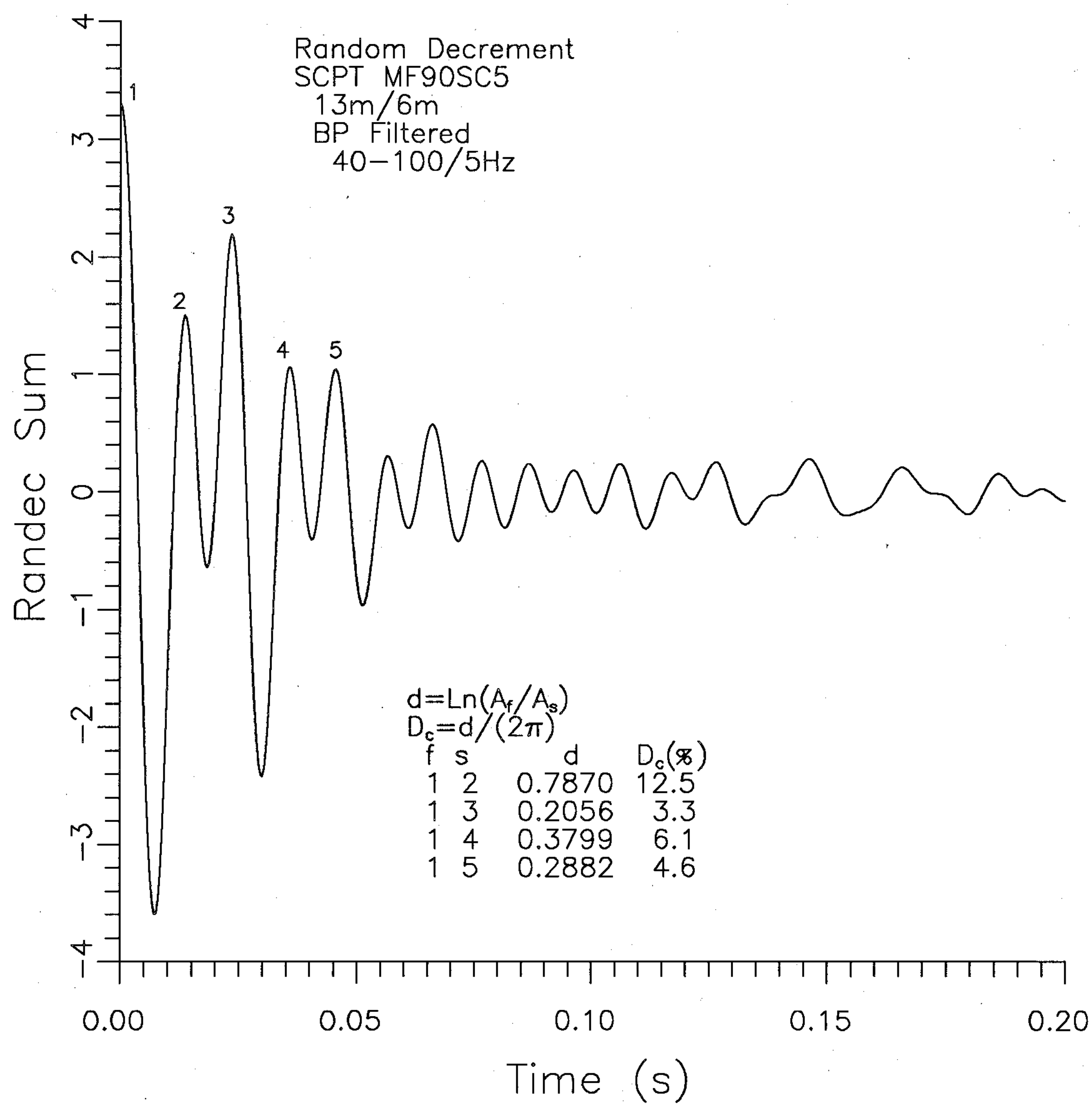


Fig.B.14 Signature from Ratio Filtered at 40–100Hz

## APPENDIX C

## APPLICATION OF SPECTRAL RATIO SLOPE METHOD TO LOTUNG ARRAY EARTHQUAKE RECORDS

Vertical arrays of accelerometers are being installed in earthquake-prone areas to measure simultaneous records of acceleration at various depths for various strain levels during earthquake shaking. It is of interest to determine if the damping methodology developed can be applied to these records.

Details of the free-field downhole array (DHB) at the Lotung site in Taiwan are provided in Chang et al (1991). Basically the array consists of three-component accelerometers (N-S, E-W, and vertical) at the surface and depths of 6m, 11m, 17m, and 47m. Records for two of the events at the site were provided by the Geomatrix/EPRI group. These earthquakes were summarized by Chang et al (1991) as follows:

TABLE C.1 Summary of Ground Motion Data

| Event | Date | Mag. | Epic. Dist.(km) | Focal Depth(km) | Peak Surface Acc.(g) EW | NS | Vert. |
|---|---|---|---|---|---|---|---|
| LSST#7 | 5/20/86 | 6.5 | 66.2 | 15.8 | 0.16 | 0.21 | 0.04 |
| LSST#16 | 11/14/86 | 7.0 | 77.9 | 6.9 | 0.13 | 0.17 | 0.10 |

A typical signal for event #7 is given in Fig.C.1, with the FFT provided in Fig.C.2. The peak acceleration is 107cm/s$^2$ (0.11g), and most of the energy of the signal is between 0.3 and 3Hz.

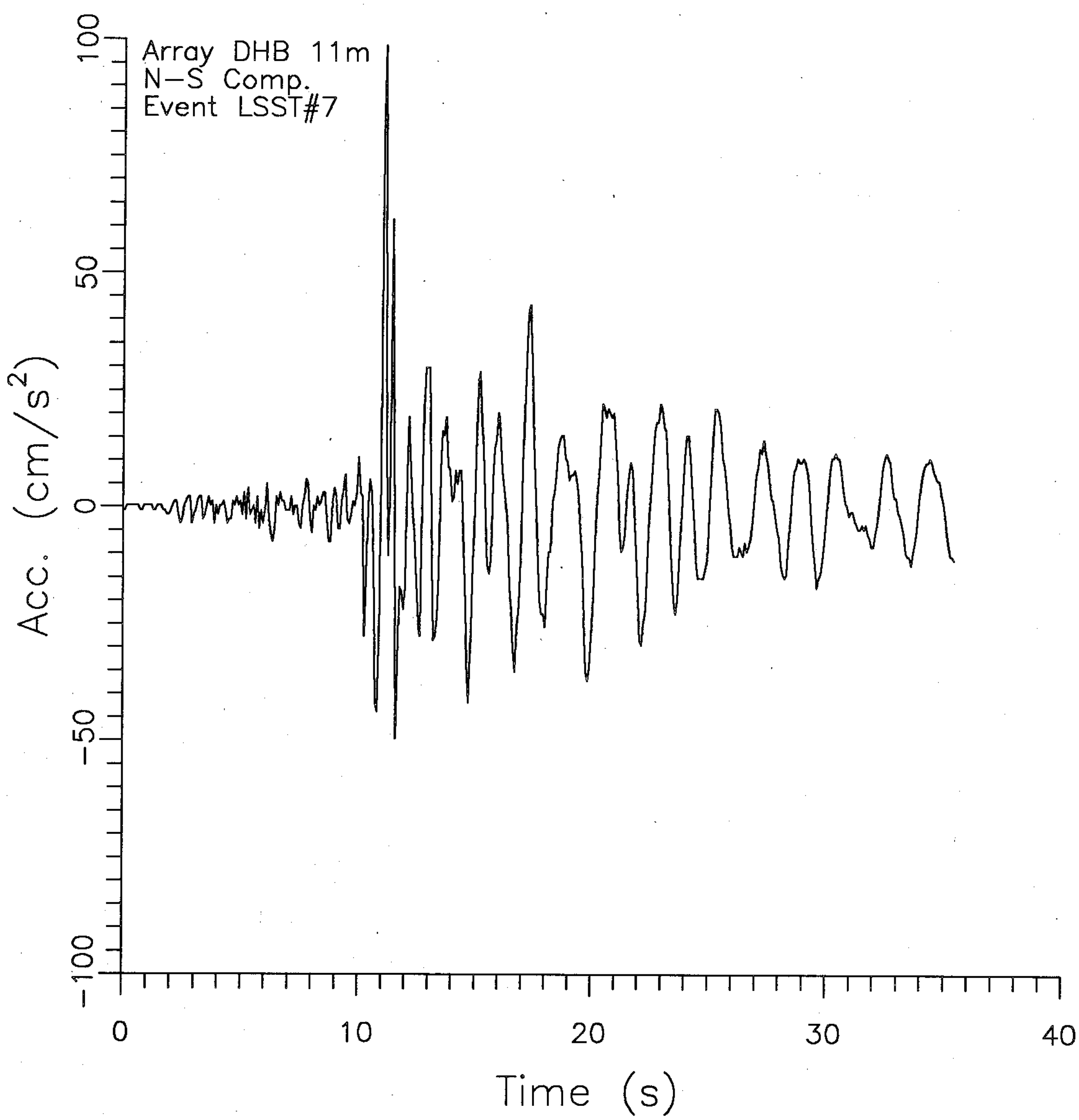


Fig.C.1 Time Signal – Array DHB – 11m – NS Comp – Event #7

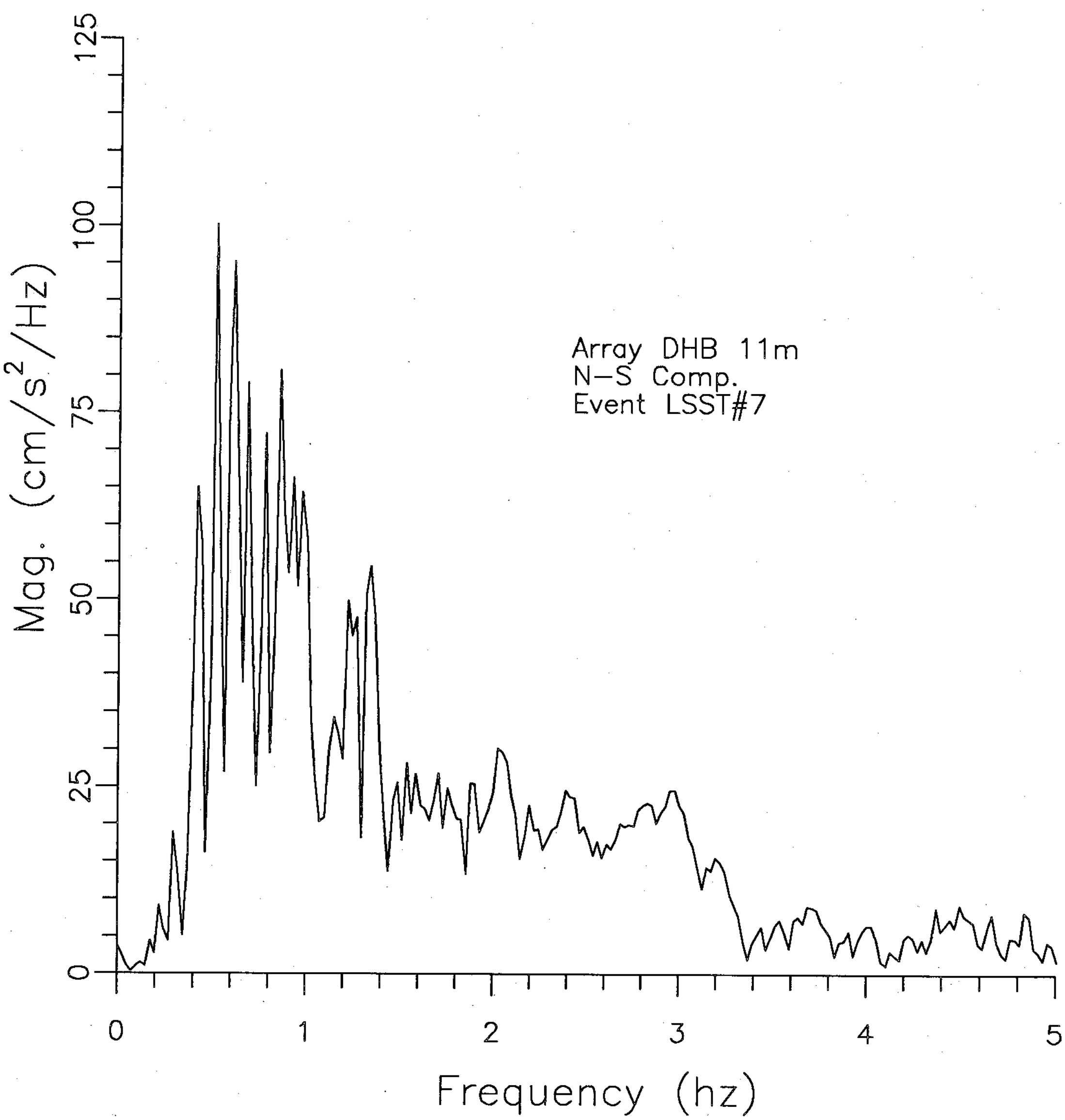


Fig.C.2 FFT – Array DHB – 11m – NS Comp – Event #7

## C.Application to Lotung Array

The first step in the calculation of damping is the calculation of the shear wave velocities. Since these signals involve larger strains it is not immediately obvious which method of calculating velocities is most appropriate. Chang et al (1991) used the signals to calculate velocities following the approach of Dobry et al (1976). For a two-layer system (layer A over layer B over rock), they showed that:

$$[C.1] \quad \tan \left|\frac{\pi f}{2f_A}\right| \tan \left|\frac{\pi f}{2f_B}\right| = \frac{\rho_B H_B f_B}{\rho_A H_A f_A}$$

where: $f_A$, $f_B$, $f$ = resonant frequencies of layer A, layer B and combined layer

$\rho_A$, $\rho_B$ = densities of layers A and B

$H_A$, $H_B$ = thicknesses of layers A and B

The method assumes that there is no damping, but since the solution is in terms of resonant frequencies, the errors are expected to be small. For a single degree-of-freedom system the damped frequency is computed from the undamped natural frequency by $\omega_D = \omega_n(1-D^2)^{0.5}$, and for a damping of 10%, the change is only 0.5%.

In order to find the velocities, it is necessary that $\rho_A$, $\rho_B$ are known or assumed (likely equal), and that $H_A$, $H_B$ are known. The ratios of the FFT's of the signal at the surface to that at each successive depth are computed. These ratios are examined to give the resonant frequencies $f_A$ and $f$. These values are used to solve eqn.C.1 for $f_B$, and the shear wave velocities for the two layers are calculated from

$V_s = 4Hf$. Dobry et al (1976) provided a nomograph for solving eqn.C.1 in terms of the resonant periods.

Possibly the most difficult step in the method is to determine the resonant frequencies. An example is shown in Fig.C.3. The magnitudes of the FFT's at the surface and at 11m were smoothed with two passes of a 5-point smoothing function. The ratio was computed and again smoothed with 2 passes. The resulting curve shows a peak at 5.76Hz, and about 5 other smaller peaks in the 0-10Hz range. A useful guide in selecting the resonant frequency and its multiples is suggested by the work of Idriss and Seed (1968). They point out that the solution for the earthquake response problem for a uniform layer gives the modal frequencies as: $\omega_n = (2n-1)\pi V/2H$. Thus, the frequencies will increase as 1, 3, 5, etc.

It was noted that the spectrum of the surface signal had a local maximum at 5.76Hz which was missing in the deeper signals. If we select the peak at 8.96Hz as a multiple of 5, giving a resonant frequency of 1.79 Hz, and the peak at 1.71Hz as the resonant frequency, then an estimate would be the average as 1.75Hz. This value gives a velocity close to that computed by Chang et al. Chang et al noted that the velocities calculated by this procedure were about one-half of the velocities measured by cross-hole geophysical tests, due to the larger strain during event #7. Both sets of velocities (Geomatrix-EPRI [GM-EP] for N-S component and cross-hole values) are given in Fig.C.4.

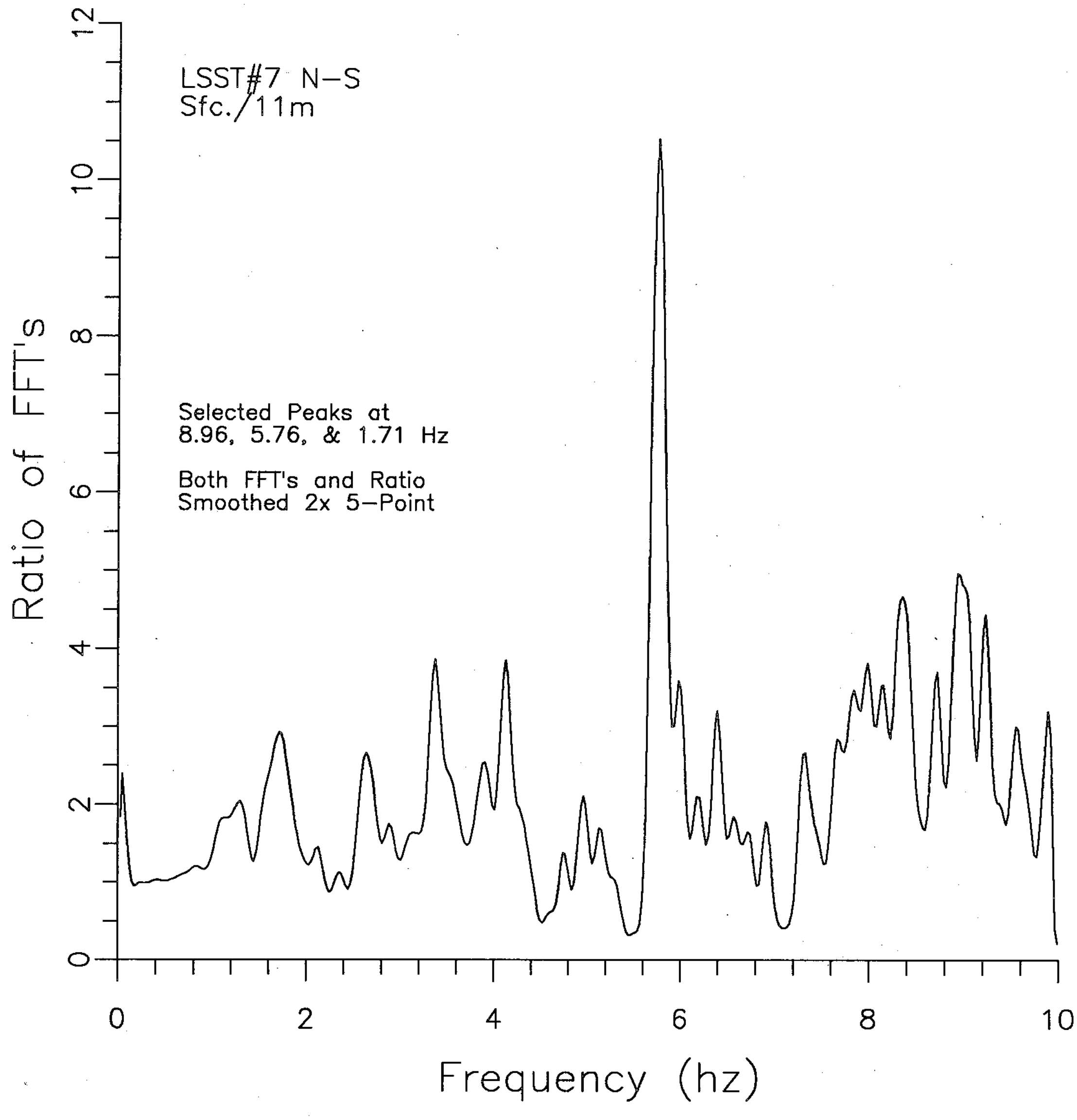


Fig.C.3 Ratio of FFT's – DHB – Surface/11m – NS – #7

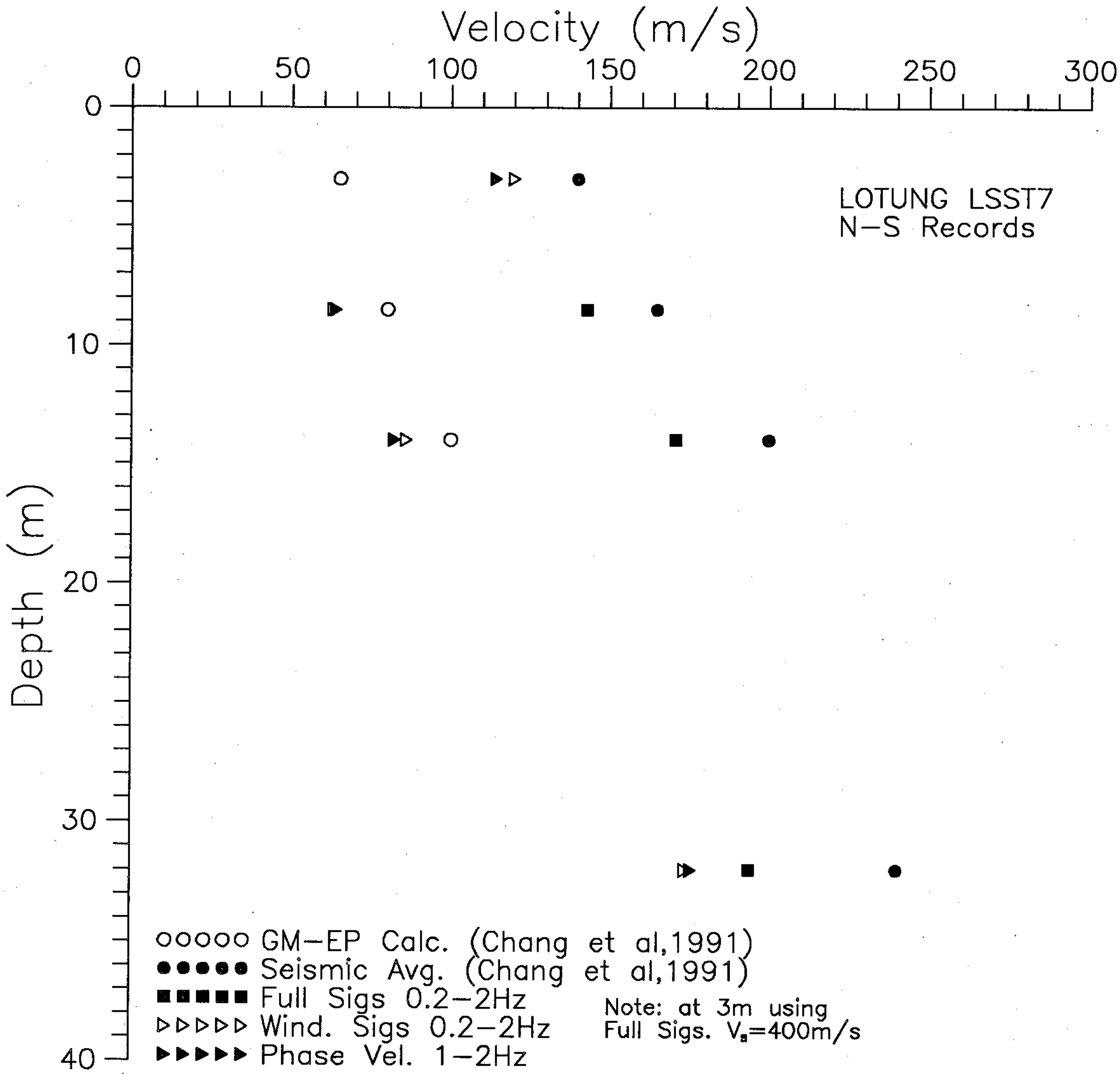


Fig.C.4 Velocities from Event #7 – Various Methods

After confirming the values given by Chang et al (1991), the methods presented in Chapter 6 were used to calculate velocities from the signals. Initially the cross-correlation method was applied to the full signals using a band-pass filter of 0.2-2.0Hz (selected from observation of the FFT in Fig.C.2). These results are also shown in Fig.C.4, and (except for the first layer) are about 85% of the cross-hole values and about 70% greater than the values calculated by Chang et al. Presumably the strain involved is less than that at the resonant frequencies, while still greater than that for the geophysical tests.

As can be seen in Fig.C.1, there is a peak acceleration just after 10s. This peak occurs in all of the event #7 records, and was isolated by windowing of the signals, as shown in Fig.C.5. For event #16, the peaks were proportionally less, as can be seen in the example in Fig.C.6. As well, when the peaks were windowed, the resulting waves were "contaminated" by other motions, as shown by the example in Fig.C.7. Consequently no further calculations were done for the event #16 records.

In Fig.C.5, it can be seen that the time of the peak increases as the depth decreases, as expected for a wave moving upwards. It can also be seen that the amplitude increases as the depth decreases. For planar waves moving upwards, it would be expected that there would be a slight decrease in amplitude due to damping. It would appear that there is some type of amplification occurring as the wave move upwards. A similar result was observed in the E-W component of the signals.

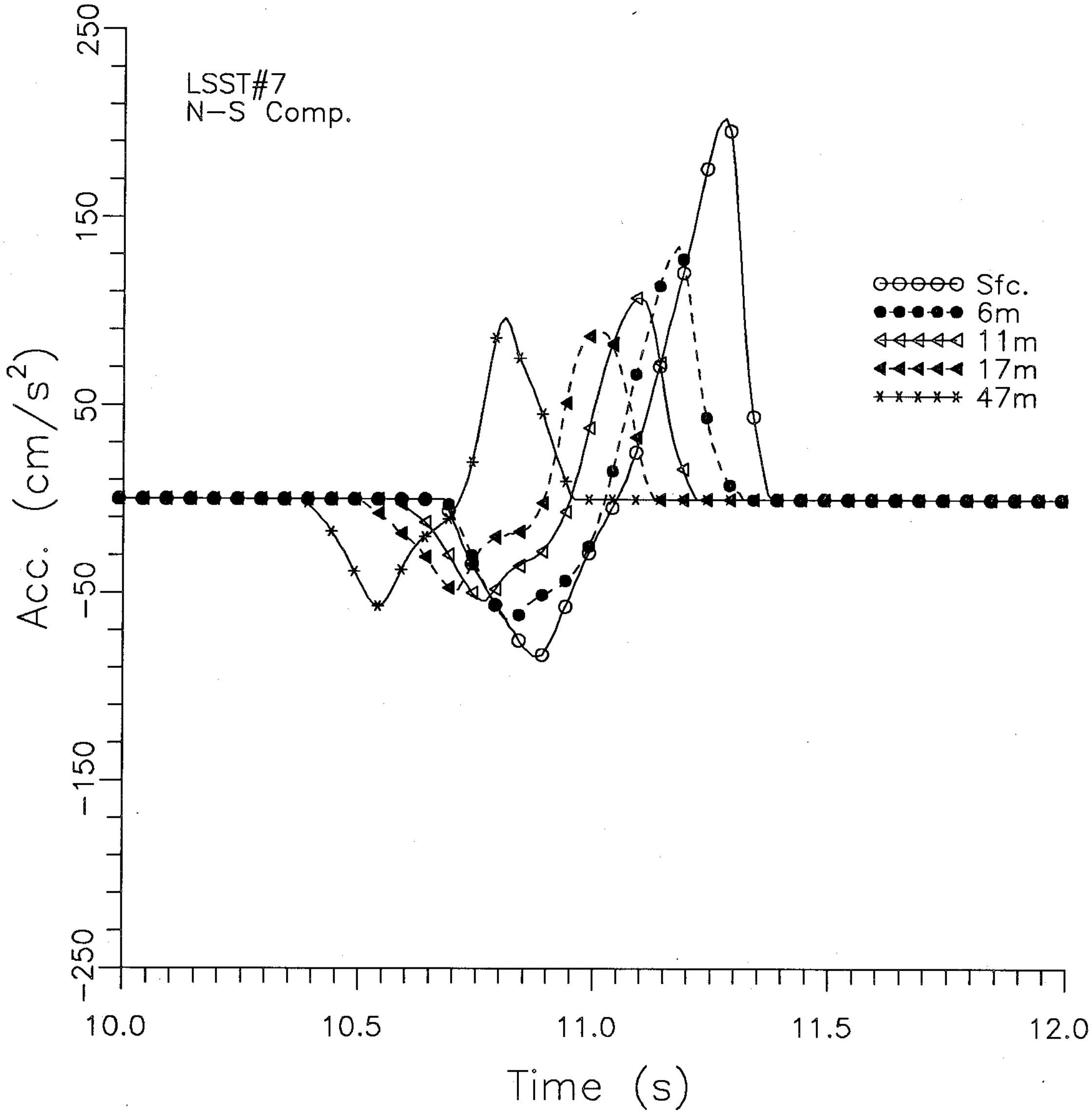


Fig.C.5 Windowed Signals – DHB – NS comp. – #7

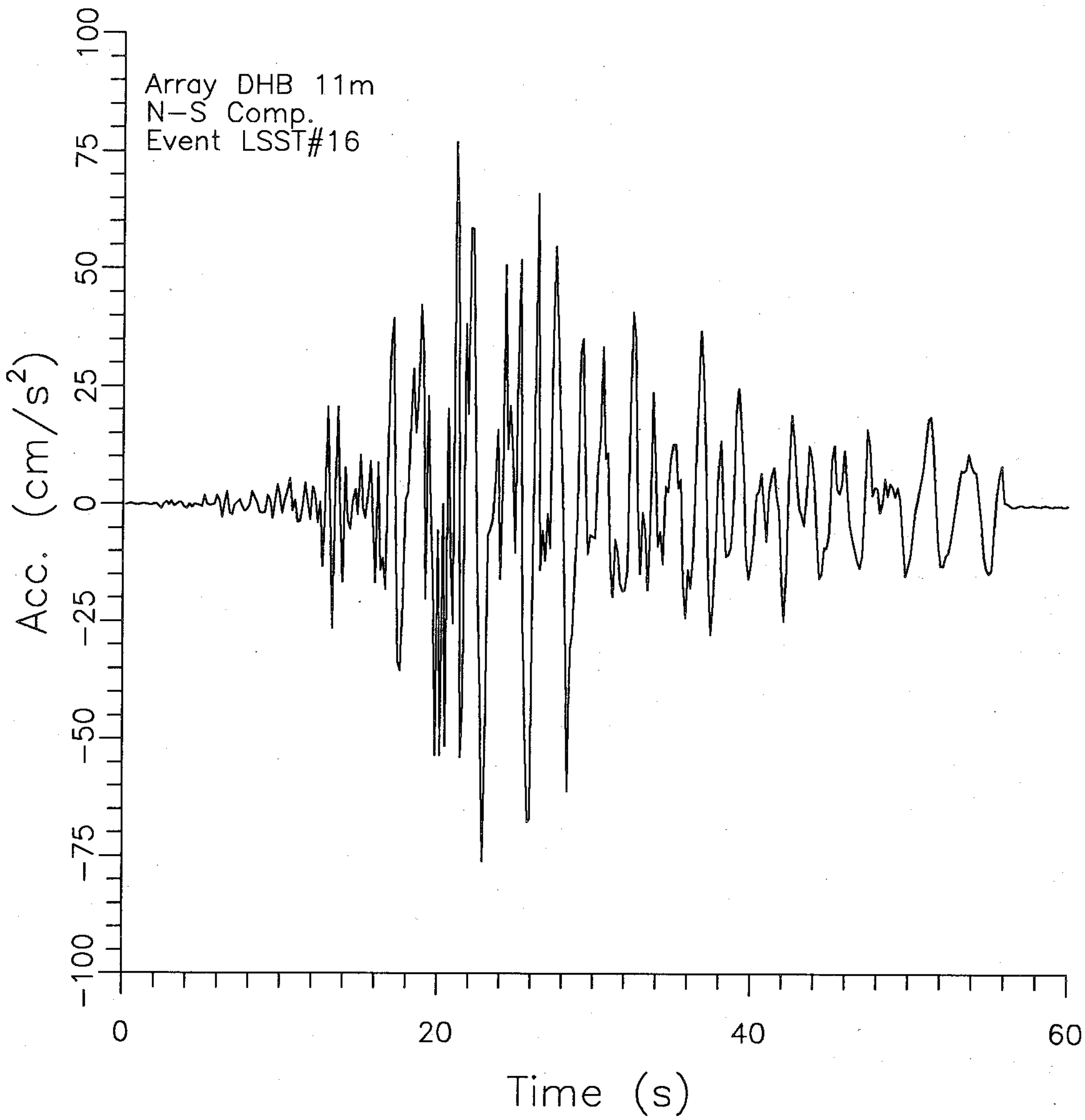


Fig.C.6 Full Signal – DHB – 11m – NS comp. – Event #16

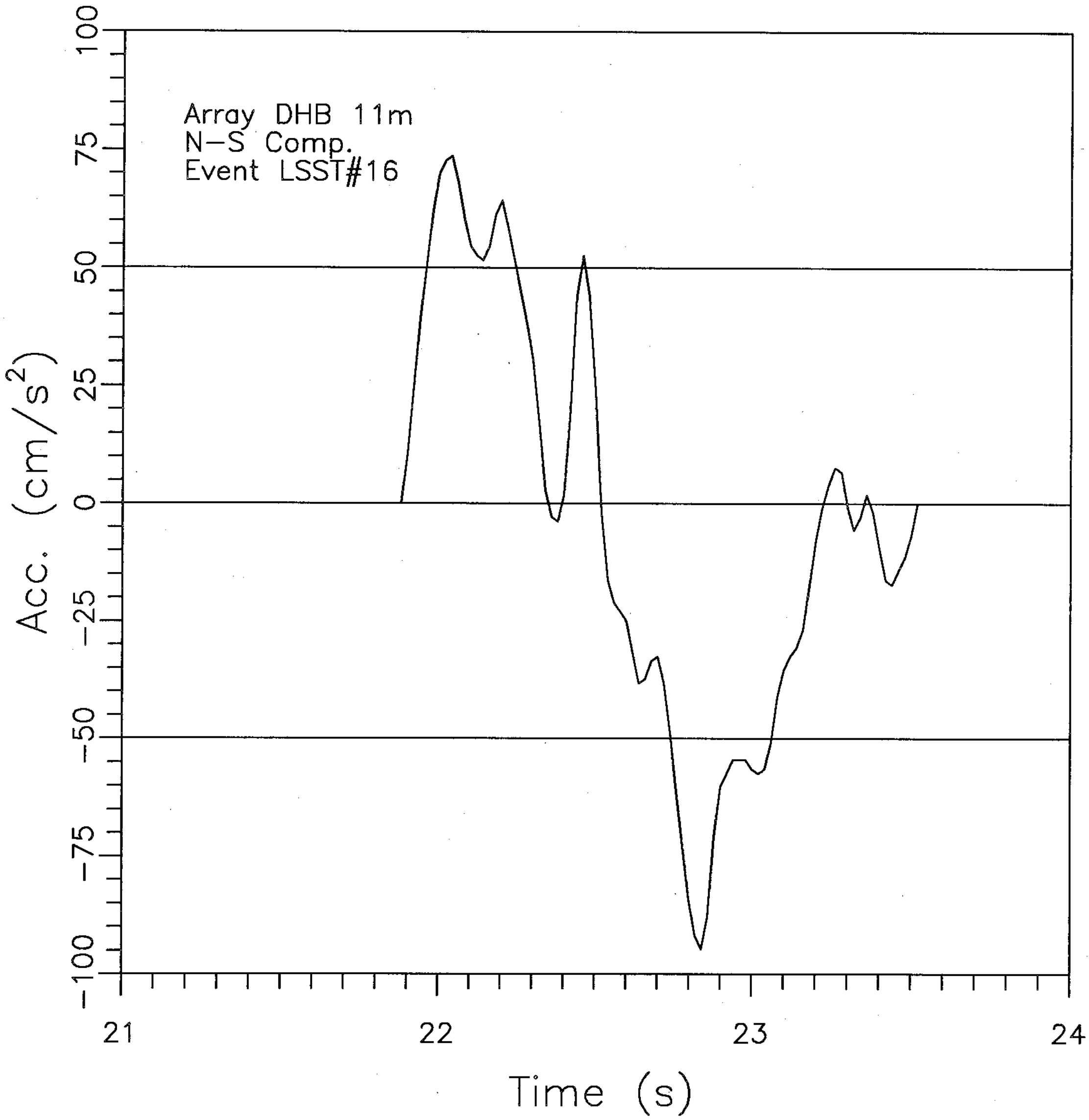


Fig.C.7 Windowed Signal – DHB – 11m – NS comp. – Event #16

Using the windowed signals, velocities were calculated using the cross-correlation and phase methods, with the results shown on Fig.C.4. The results were similar and (again except for the first layer) were about 80% of the values from the resonant frequency method. Presumably this effect can be explained as the strain in the peak wave was likely higher than that used in the resonant frequency method.

Following Idriss(1990), the expected value of damping, for the strain value of 0.1% given by Chang et al, would be about 10%. The spectral ratio slope method was applied to the windowed signals, using the 47m records as the reference signals, for both the N-S and E-W components from event #7. The results are presented in Fig.C.8. For the N-S records, the lower three signals poorly define a line which indicates a damping of less than 1%. For the E-W records the upper 3 signals give a line with a very high slope. Following the method outlined above would give a damping value in excess of 100%. However the equation used to calculate damping, $D_s=kV/(2\pi)$, is only applicable to low damping (say <10%) materials. For higher values of damping, the equation given by Johnston and Toksoz (1981) can be modified as:

$$[B.2] \quad D_s = \frac{kV}{2\left|\pi - \dfrac{k^2V^2}{4\pi}\right|}$$

Applying this equation to the slope given by the E-W records gives a negative value of damping. For the N-S records the slope from 6m to the surface only is similar to that for the E-W records, and it can be seen

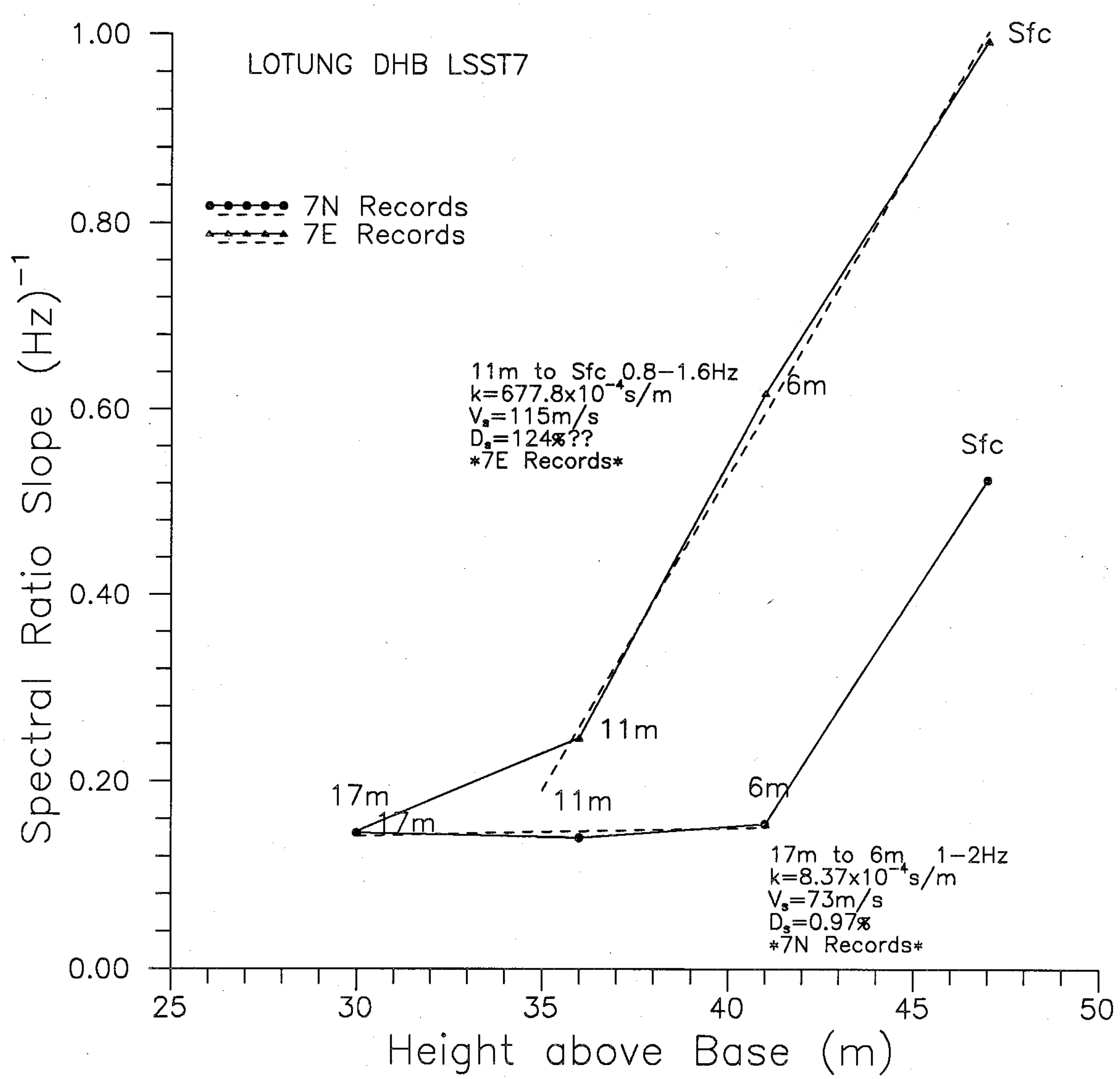


Fig.C.8 Damping from SRS Profiles – NS & EW comp. – Event #7 in Fig.C.5 that the amplification is much greater between these signals than it is for the lower three signals.

It is concluded that amplification, likely due to resonance effects, is occurring in the earthquake events, so that the method of damping calculation developed for SCPT results cannot be applied to earthquake records from an array. It is likely that the amplification is frequency-dependent, so that the spectral ratio slope method cannot remove the amplification effects. Application of more complex methods such as SHAKE or DESRA would require more complete information on the soil stratigraphy and properties.

## APPENDIX D

## PENDER ISLAND EARTHQUAKE

### D.1 Introduction

The best means of confirmation of damping measurements would be a well-instrumented earthquake case history inducing strains near the level of the measurements. Such an ideal case history does not exist in this area , but records are available for the 1976 Pender Island quake. The Pender Island earthquake occurred on May 16,1976 and had a Richter magnitude of between 5.0 and 5.5. The epicentre was under Pender Island at longitude 123.34W and latitude 48.80N. The earthquake was recorded at several sites in the southwest corner of British Columbia. Two sites are of particular interest; Lake Cowichan where the site was underlain by rock, and Annacis Island where the site was underlain by a deep soil deposit where some detailed soil investigations have been carried out. Wallis (1979) analyzed these records as well as those from two other Lower Mainland sites. However, site specific dynamic test results were not available at that time.

### D.2 Record Details

Most of the information on the available records given below was provided in conversations with members of the Geological Survey of Canada (Horner,1990; Baldwin,1990). The Lake Cowichan Telecommunication

Station site is about 56km west of the epicentre. The Annacis Island Industrial Estates site is about 50km north-east of the epicentre.

At both sites the recording instruments are located on the concrete floor slab of a one-storey structure. At the Lake Cowichan site, the recorder was a SMA1 seismograph with a natural frequency of about 26Hz and damping of 60%. At the Annacis Island site, the recorder was an RFT-250 accelerometer with a natural frequency of 20.6-20.9Hz and also damping of 60%. These characteristics should provide a reasonably flat response over the frequency range expected to be of interest (less than 15Hz).

The available records, in the horizontal plane, from the Lake Cowichan site are given in Fig.D.1. To increase the clarity, only the first ten seconds of the 23-second records are shown. It can be seen that the transverse record has some type of offset. In an attempt to correct the offset, the best-fit line through the entire record was subtracted. The corrected transverse record is similar to the longitudinal record, but about 10% greater in the maximum and minimum values.

The longitudinal and transverse records at the Annacis Island site are shown in Fig.D.2. The transverse record is again similar but about 10-20% higher. Only the longitudinal records were used for most of the analyses, except as noted otherwise.

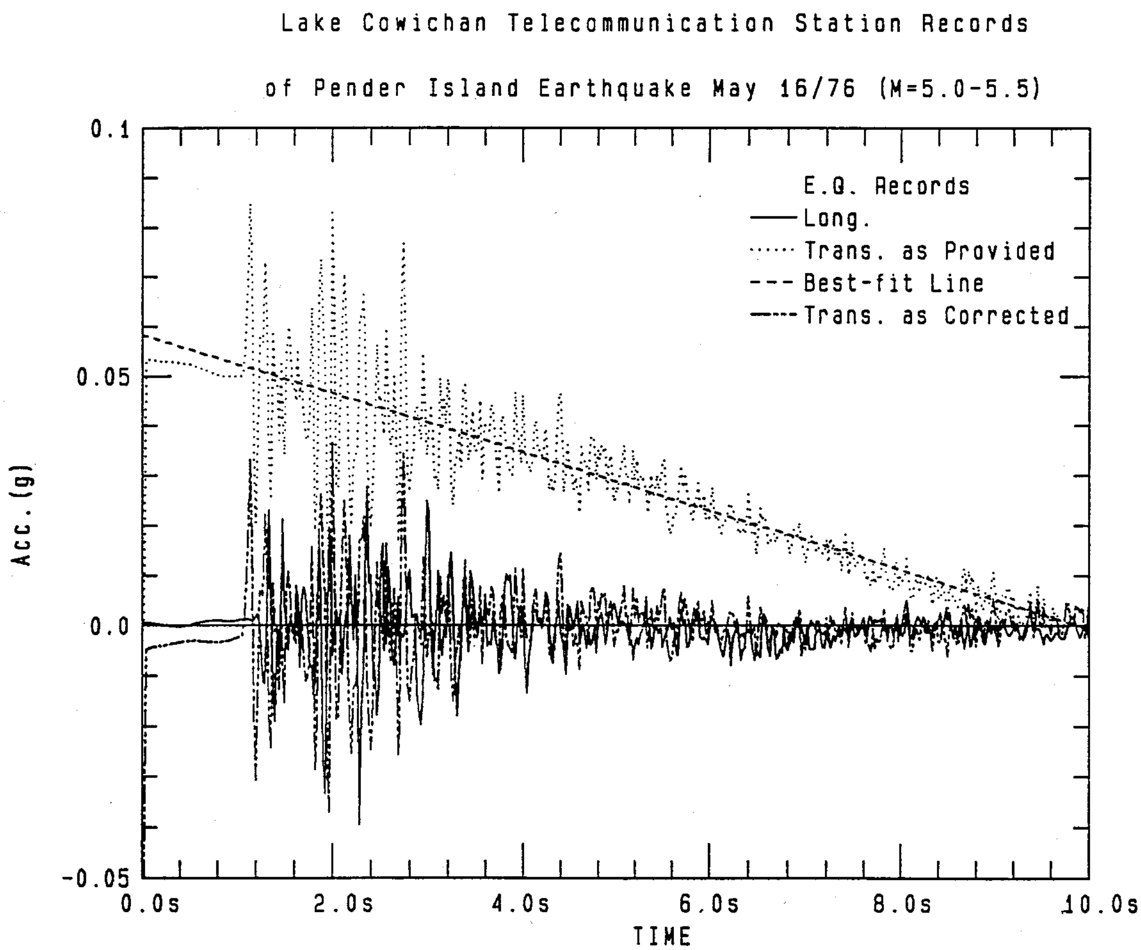


Fig.D.1 Lake Cowichan Records — Pender Island Earthquake

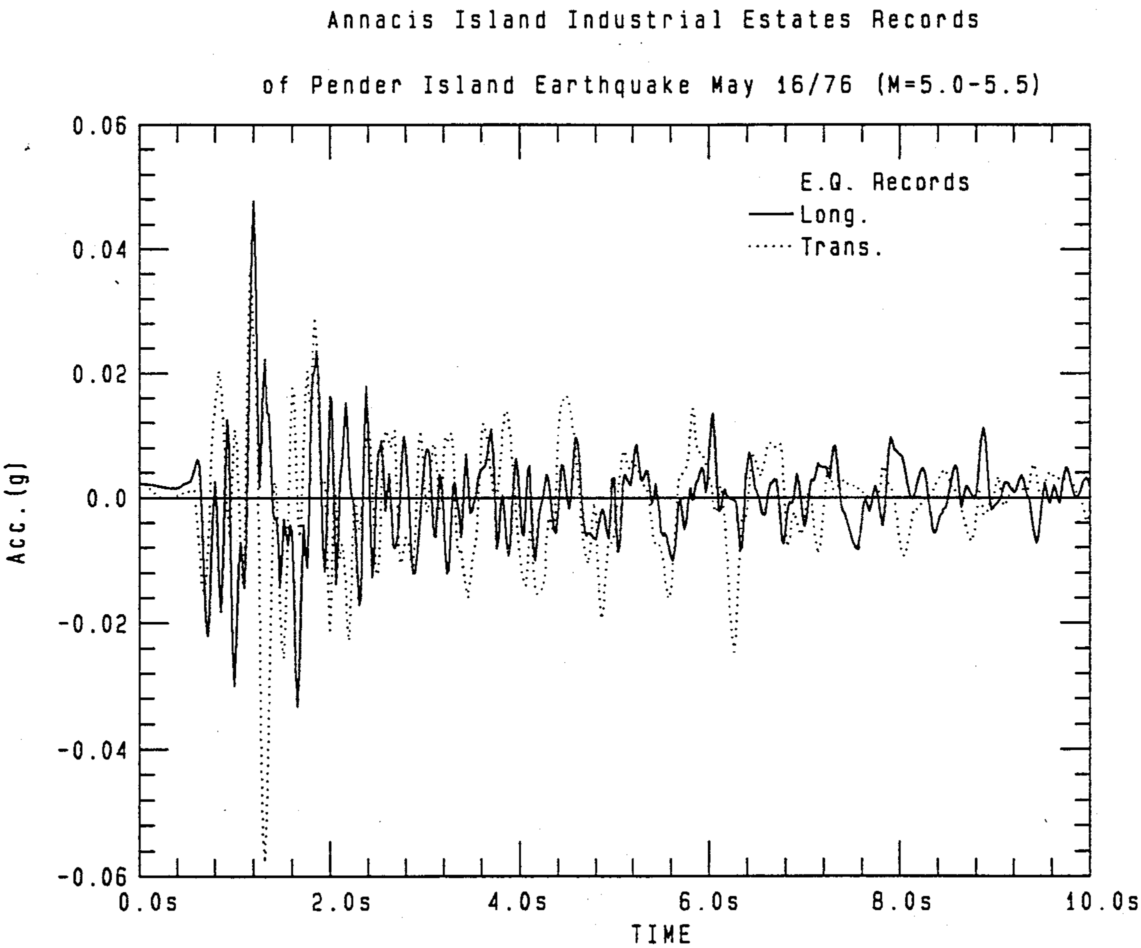


Fig.D.2 Annacis Island Records – Pender Island Earthquake

**D.3 Rock and Soil Conditions**

The reconnaissance geological mapping of the southeast portion of Vancouver Island was given by Mueller(1975). His map shows two reverse faults crossing Pender Island. The bedrock on Pender Island and up the Cowichan Valley is shown as Nanaimo sediments, consisting of conglomerate, sandstone, siltstone and coal. The rock under Annacis Island is at considerable depth (about 220m, Wallis,1979) so that the details of rock type are not known. However it seems likely the rock is similar to the Tertiary bedrock exposed in Vancouver and along the Brunette River, which is also sedimentary - sandstone, siltstone, shale and conglomerate (GSC, 1980).

The south-east corner of Annacis Island has been the subject of detailed geotechnical investigations for the foundations of the Alex Fraser bridge (Bazett and McCammon, 1986). In the fall of 1990, a series of insitu tests were carried out near the north pier of the Alex Fraser bridge by the UBC Insitu Testing Group, including piezo-cone, seismic cone, dilatometer, and SPT soundings. Based on these investigations, surficial geology maps (GSC,1980), and information from other consultants (Morrison,1991), the profile in table D.1 was selected.

For the analysis a static groundwater at a depth of 3m was assumed. The shear wave velocities used are similar to those compiled by Byrne et al (1991).

Table D.1 Soil profile for analysis

| Depth to Base (m) | (ft) | Shear wave vel. (m/s) | (ft/s) | Unit Weight $kN/m^3$ | pcf | General Soil Type |
|---|---|---|---|---|---|---|
| 3 | 10 | 105 | 345 | 19.6 | 125 | Sand |
| 6 | 20 | 120 | 394 | 19.6 | 125 | Sand |
| 9 | 30 | 150 | 492 | 19.6 | 125 | Sand |
| 15 | 49 | 175 | 574 | 19.6 | 125 | Sand |
| 19 | 62 | 200 | 656 | 19.6 | 125 | Sand |
| 26 | 85 | 220 | 722 | 20.4 | 130 | Sand |
| 41 | 135 | 245 | 800 | 20.4 | 130 | Sand |
| 60 | 197 | 283 | 930 | 19.6 | 125 | Clay |
| 80 | 262 | 300 | 985 | 19.6 | 125 | Clay |
| >80 | | 762 | 2500 | | | Dense Till |

Recent resonant column testing was reported by Zavoral (1990). The soil tested was from the Lower 232nd St. site. Based on the GSC mapping the soil here is a part of the Capilano sediments, as is the clay at depth below Annacis Island. Above 2.5m the P.I. was about 40% and below 2.5m the P.I. was about 20%. This latter value is still somewhat higher than that found for the deeper soils at the Annacis Island site, but it was considered that the values for the deeper clays at the 232nd St. site, combined with the shear wave velocities, would give the best available estimates for the dynamic properties of the deeper soils at the Annacis Island site.

For the sands, it can be difficult to obtain undisturbed samples for laboratory testing. Commonly the curves given in Figs.3 (for modulus) and 10(for damping) of Seed and Idriss (1970) have been used. It is possible to adjust the modulus curve to suit the measured shear wave velocities. Fig.D.3 shows a plot of $G_{max}$ versus the square root of mean effective stress for the profile, giving a $K_2$ of 32.6. This

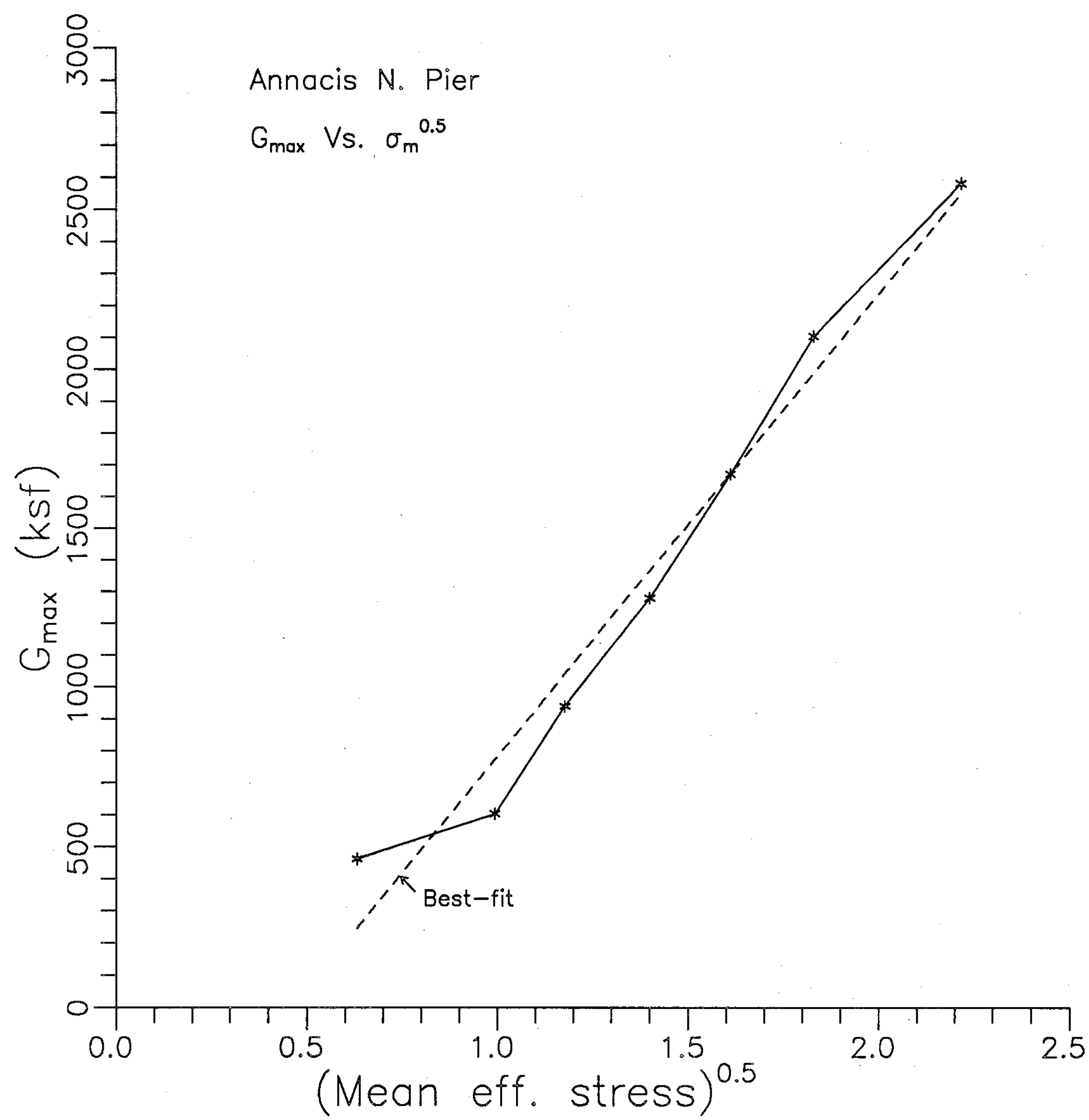


Fig.D.3 $G_{max}$ vs. $\sigma^{0.5}$ for Annacis Island Sand suggests that the sand is quite loose, when compared to the values given by Seed and Idriss.

**D.4 Analysis**

The computer program SHAKE (Schnabel et al, 1972) was used for the analyses. The longitudinal record from the Lake Cowichan site was used as the input motion at the top of the sand/silt till which was considered as an outcropping layer since the record was measured at the surface. The record was not scaled as the distances to the two sites are similar. A maximum error of 5% was allowed in obtaining the strain compatible soil properties.

Several analyses were carried out, using the soil profile given above, a shallower profile, a profile extended down to include the till, and with varying assumptions on the damping in the sand.

**D.5 Evaluation of results**

It is necessary to consider the results in the frequency domain, before considering the results in the time domain. Fig.D.4 shows the ratios of the FFT's of the measured, calculated (standard profile), and shallow model signals to the measured rock signal. The ratios have been smoothed for clarity. Except for the point at 0.95Hz (caused by a severe drop - value of less than 1% of peak - in the rock FFT), both the calculated and shallow ratios show a reasonably smooth variation with frequency, with the peaks corresponding to higher harmonics of the

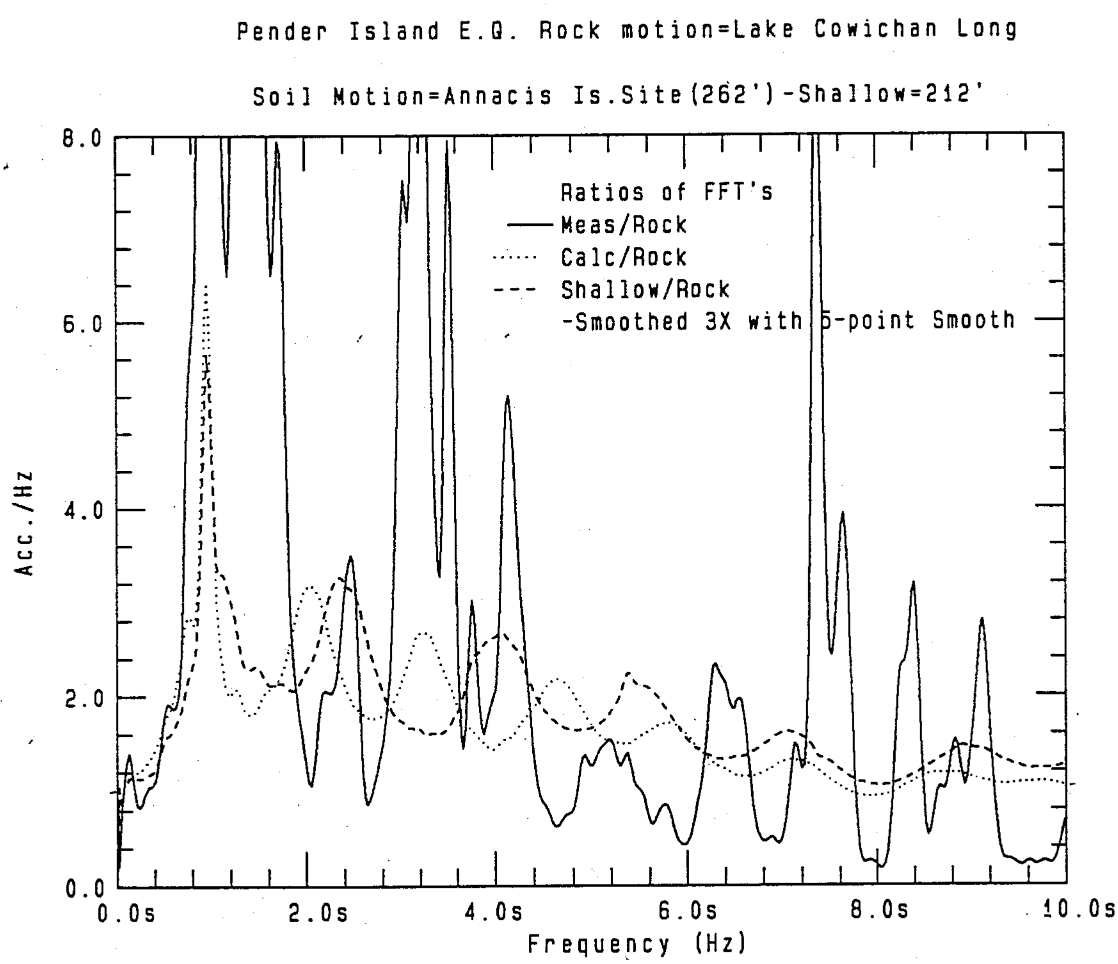


Fig.D.4 Ratios of FFT's to Rock FFT

fundamental frequency. The fundamental frequencies are poorly defined, but the harmonics can be used to estimate the fundamental frequencies as given in Table D.2.

Table D.2. Harmonics and fundamental frequencies

| Model | $3f_n$ | $5f_n$ | $7f_n$ | $f_n$ | $T_n$ |
|---|---|---|---|---|---|
| | | | Hz | | sec |
| Measured | 3.22 | 5.18 | 7.37 | 1.06 | 0.94 |
| Calculated(std.) | 2.05 | 3.25 | 4.64 | 0.67 | 1.50 |
| Shallow | 2.34 | 4.08 | 5.37 | 0.79 | 1.27 |

The magnitudes of the peaks are very similar for the calculated (std.) and shallow curves. The ratio of the measured FFT to the rock FFT is much more erratic, with a peak value (not shown) of 78 at 1.3Hz. The differences can be expressed statistically as given in Table D.3

Table D.3 Comparison of ratios of FFT's to rock FFT

| Model | Mean | Std. Dev. | Coeff. of Variation (%) |
|---|---|---|---|
| Measured | 1.4488 | 4.506 | 311 |
| Calculated(std.) | 0.9629 | 0.916 | 95 |
| Shallow | 1.1101 | 0.857 | 77 |

The erratic nature of the measured/rock ratio suggests that the values may not be related, i.e. the Lake Cowichan record may not be representative of the rock motion under the Annacis Island site.

Another approach to looking at the results is to plot the response spectra of a single-degree-of-freedom structure reacting to the motions. Assuming a damping of 5% for the structure, the resulting spectra are shown in Fig.D.5, along with those given by Wallis (1979). As expected, the spectra agree closely except for the transverse rock motion above 1 sec. This may have been caused in the correction of this signal. Only the longitudinal record is used below.

The measured spectrum is compared with the calculated spectra in Fig.D.6. A number of observations can be made from this figure. First the response with and without the till layer are essentially the same. Secondly the response for the shallow model is also similar, with the small peaks in response at slightly smaller periods. An analysis using the damping curve of Idriss (1990) has almost no effect above 0.7sec, with the increase in response gradually increasing with lower periods below 0.7sec. Fourthly, all of the calculated curves follow the general trend of the rock curve and it would be difficult to pick out the harmonics from these plots. Finally it can be observed that the measured response does not follow the trend of the rock response, and that the fundamental period from the FFT ratios does not clearly compare with the first peak in the response. Again it would appear that the actual rock motion under the site did not have the same frequency

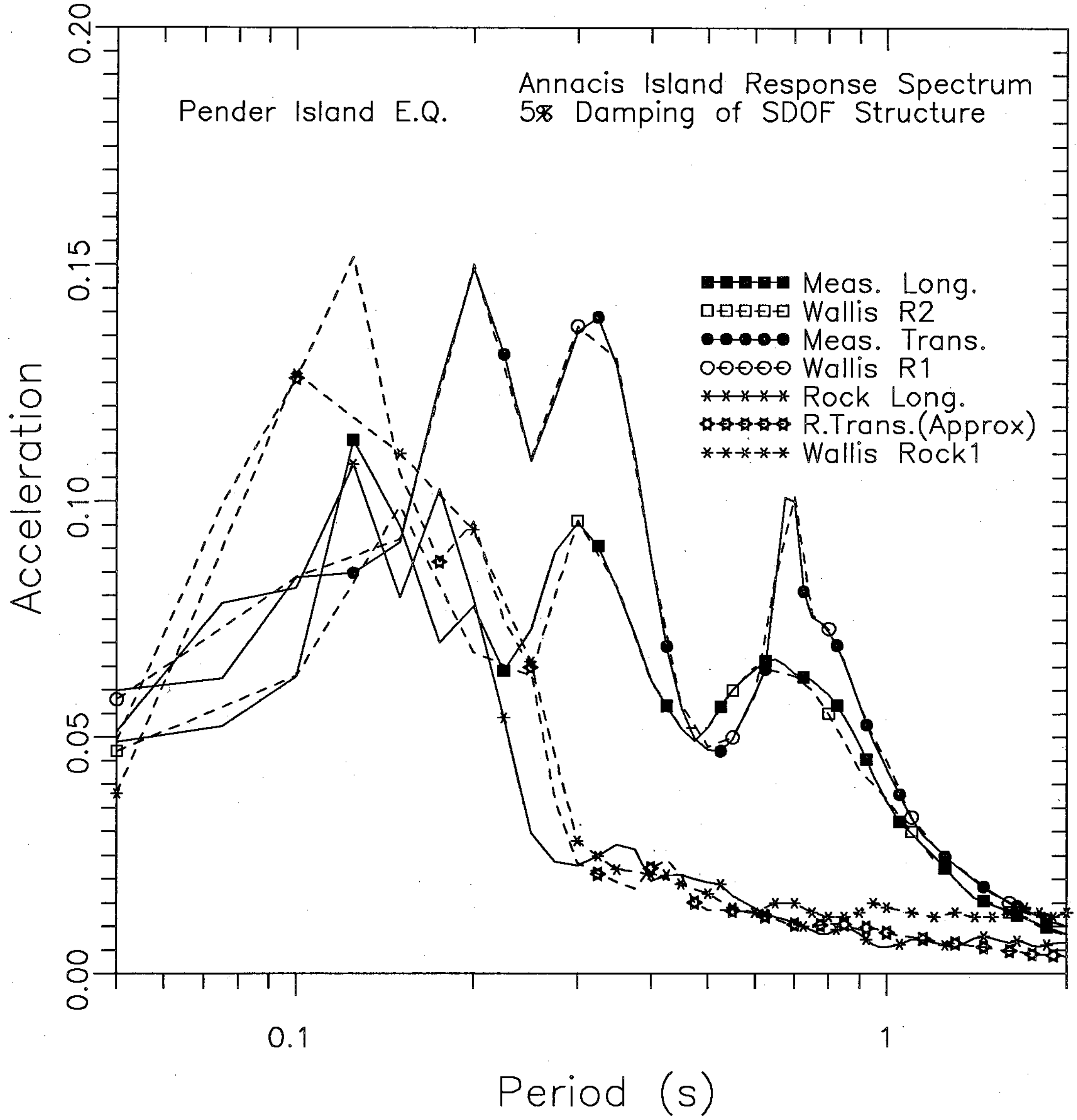


Fig.D.5 Comparison of Computed Response Spectra with Those of Wallis (1979)

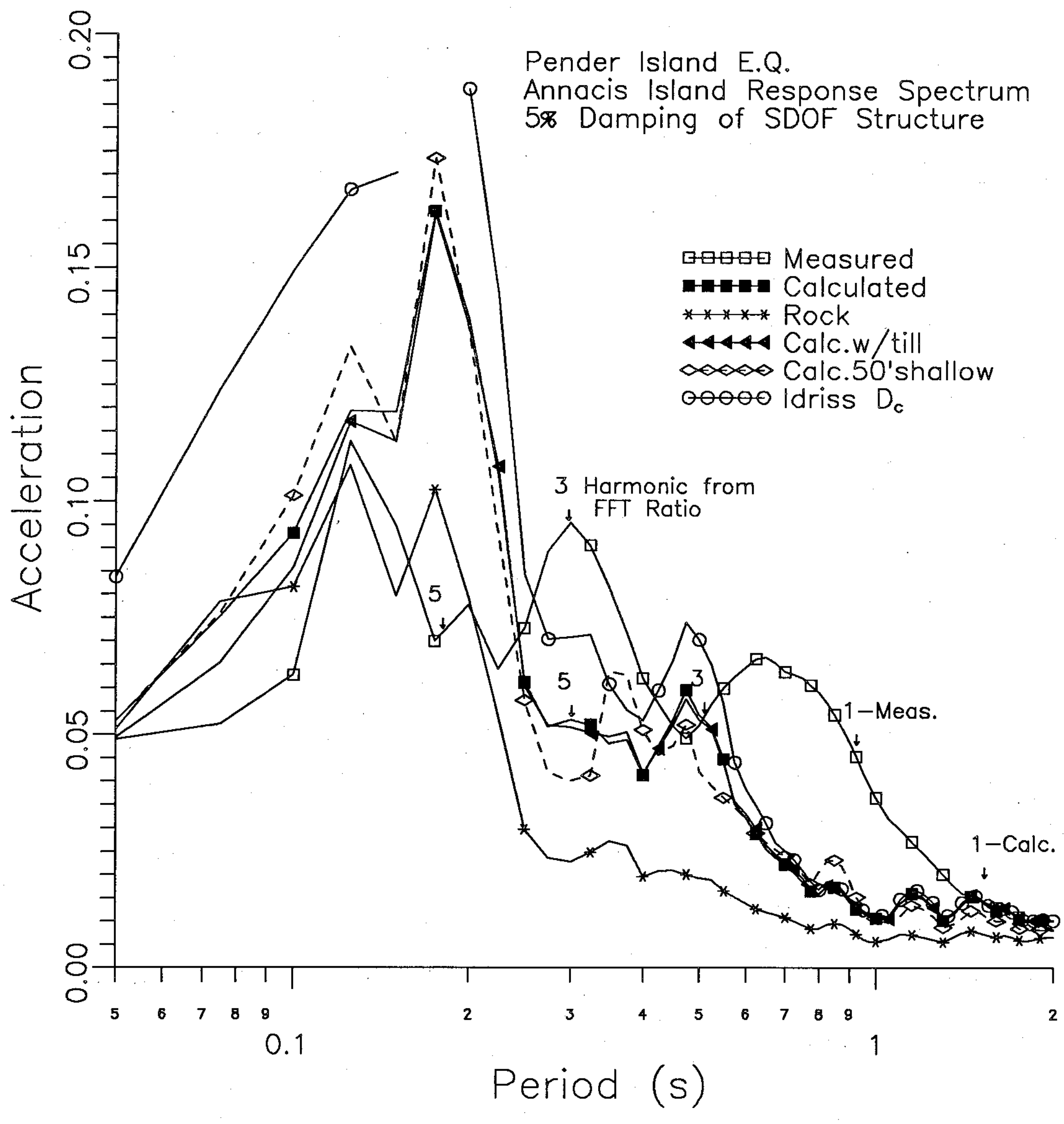


Fig.D.6 Comparison of Measured Response Spectrum with Computed Spectra content as that measured at Lake Cowichan, or the surface motion was not simply the result of vertical propagation of the rock motion.

Very similar results were presented by Taylor et al (1983). They also noted the discrepancy in the measured and calculated results between about 0.5 and 1.1sec.

In Fig.D.7 the ratio of the response spectra are plotted. The ratios of the calculated (std.) and shallow model spectra to the rock spectra are again similar, and show a maximum amplification of about 3. The ratio of the measured spectrum to the rock spectrum is very different and has a maximum amplification of about 7.

The final analysis was carried out to deconvolve the measured soil signal down to the top of the till. Fig.D.8 shows the ratios of the FFT's of the measured rock and the deconvolved signal to the FFT of the measured soil signal. The ratio for the deconvolved signal clearly shows amplification (ratio less than 1) below about 7Hz and deamplification above this frequency. However the ratio for the measured rock signal shows ratios above and below 1 across the full range of frequencies shown, with no apparent pattern.

To confirm the frequencies of the waves causing the anomalous behaviour of the response spectra, a series of filters was applied to the measured signal. A reasonable match (Fig.D.9) was obtained by applying a 0.8-1.8Hz band-reject filter as shown in Fig.D.10.

The evaluation of the results in the frequency domain appears to indicate that the measured soil motion at Annacis Island could not

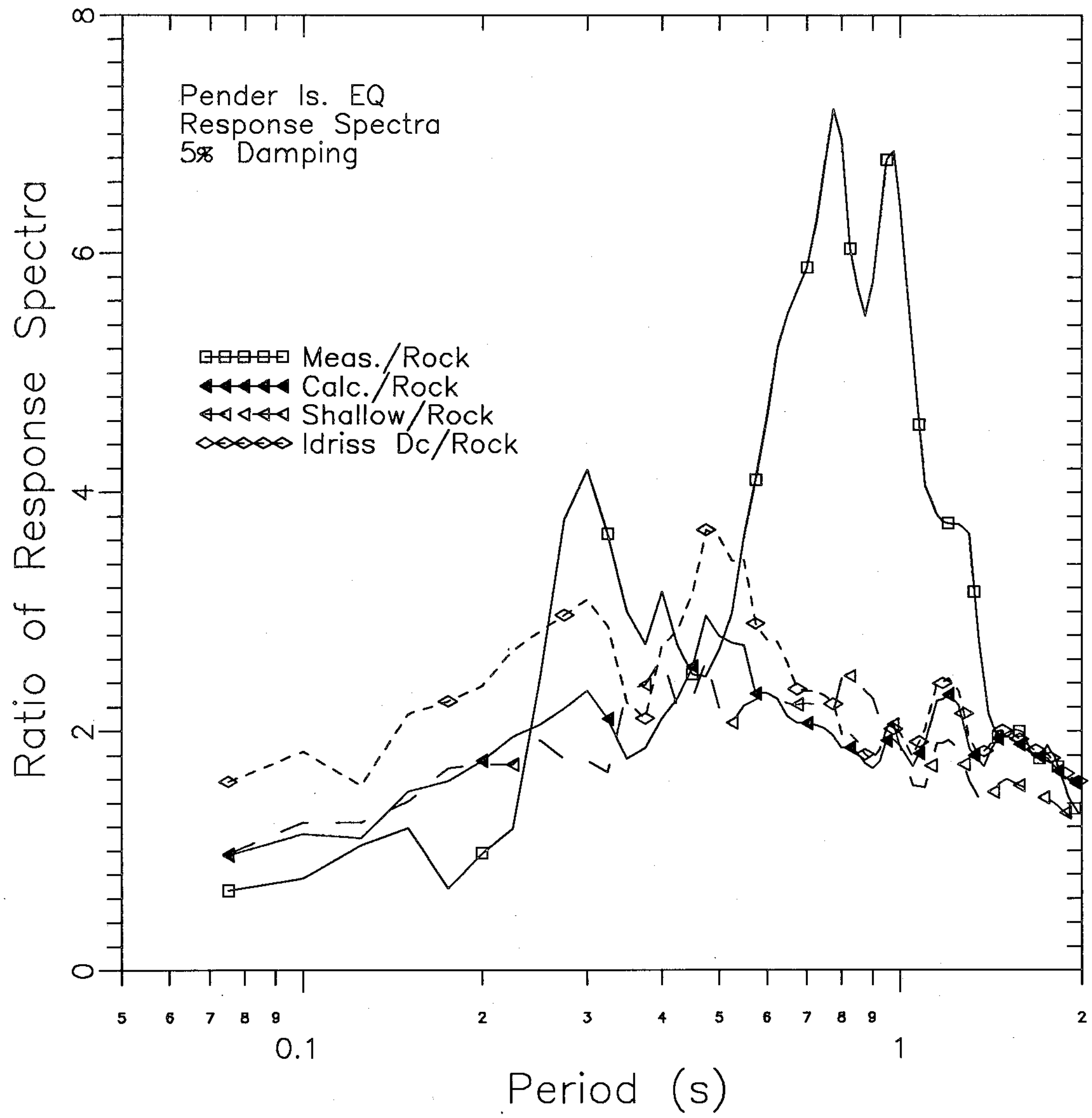


Fig.D.7 Ratios of Response Spectra

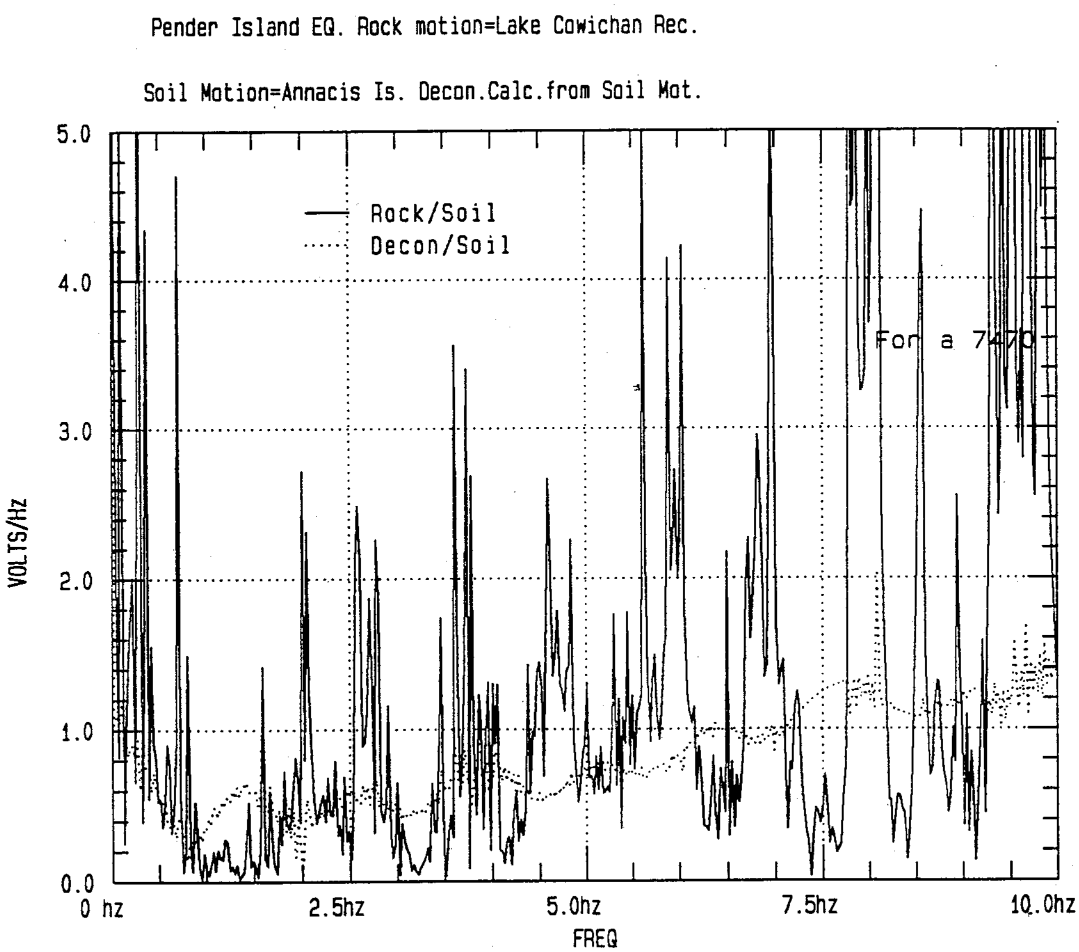


Fig.D.8 Ratios of Rock and Deconvolved Signal FFT's to Measured Soil Signal FFT

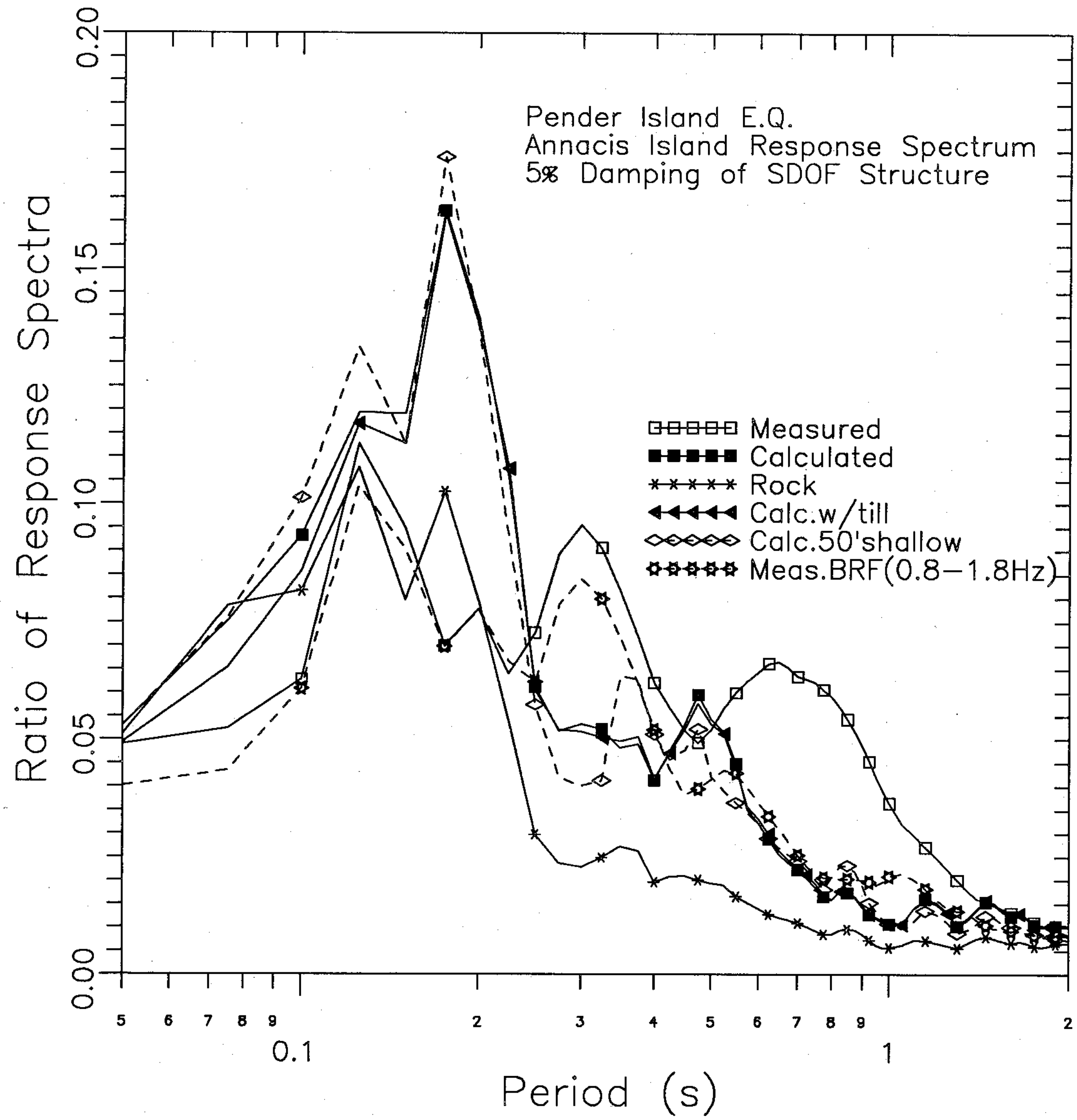


Fig.D.9 Response Spectrum of Filtered Surface Signal

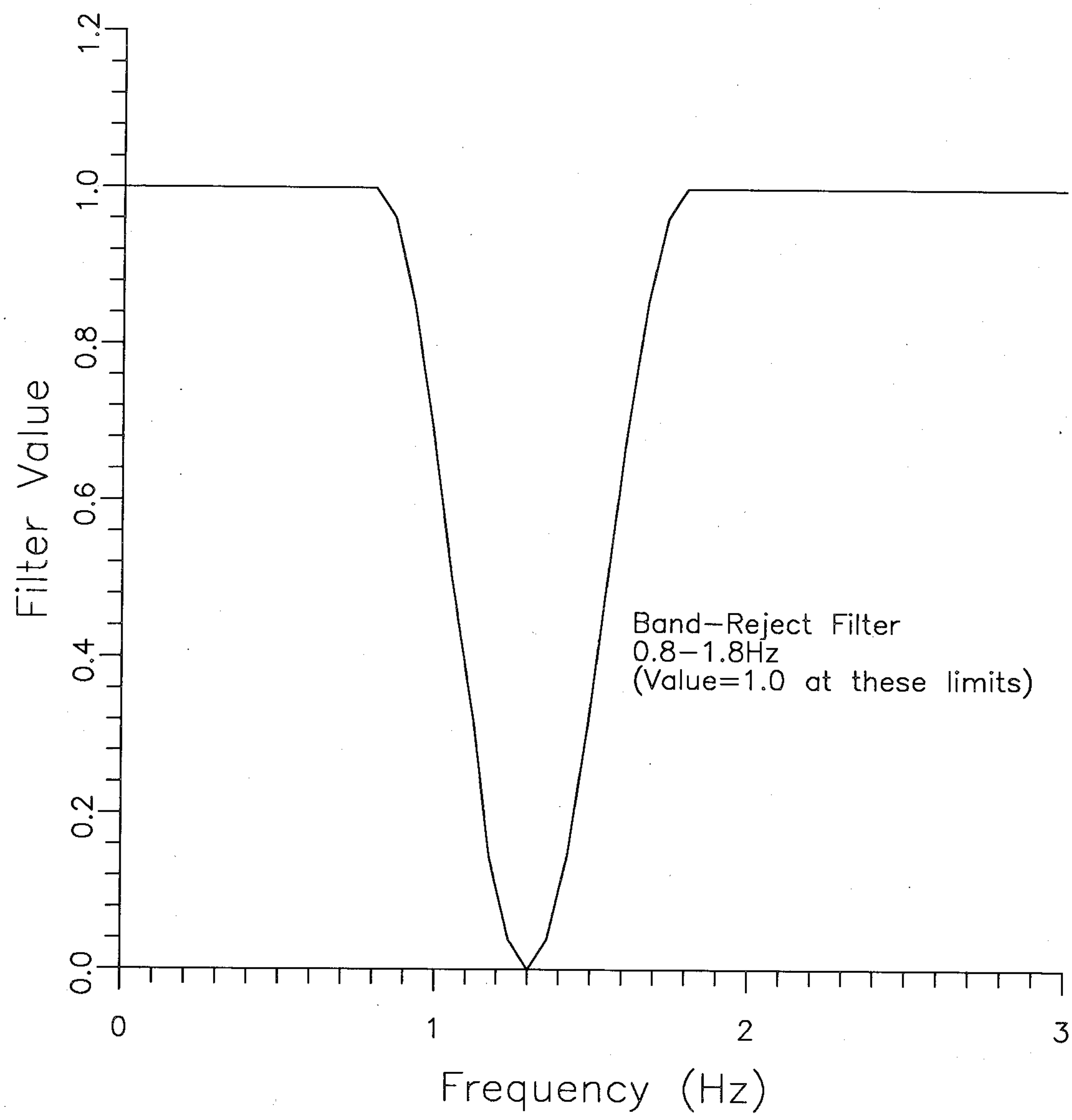


Fig.D.10 Band Reject Filter used to Match Measured and Calculated Record Spectra result from the measured rock motion at Lake Cowichan, at least not with simple vertical propagation through the soil. The measured soil motion appears to have "excess energy" in the 0.8 to 1.8Hz range. Taylor et al (1983) attributed the difference between the measured and calculated response to the presence of surface waves. Although this may be the cause, it is also possible that the rock motion was different at the two locations. It is obvious that care must be exercised if the records are to be scaled to model larger earthquakes and that the records cannot be used to evaluate damping in the soil at Annacis Island.

## APPENDIX E

## SIGNAL PROCESSING MACROS AND PROGRAMS

This appendix presents listings of the final macros and Basic programs used in this research. Some additional details are provided for each macro. If the basic calculations are understood, it is believed that the programs do not require further explanation.

### *E.1 INTRODUCTION TO MACROS*

A macro is a sequence of keystrokes (which control the operations of a menu-driven program) which can be activated by a single keystroke. Both the originally available version (1.21 or VP) and the newer available version (2.03 or VP2) of VU-POINT can be controlled by macros. There were some revisions to the menus and, of course, some additional functions, in VP2 so some adjustments are required in translating the macros between the two versions and some macros written for VP2 cannot be used in VP.

Even within the same version, some adjustments to the macros are necessary. Most commonly the input/output drives will change. The macros have been written with capital letters for the drives e.g iC or owB and must be changed as required. Output filenames will constantly change and a <Pause> function has been used to allow adjustment of the filename. Details of each macro are provided below.

*E.2 AVG4HITS.MAC*

**E.2.1 Macro**

```
<BEGDEF><CtrlF10><TITLE>Avg. 4 Hits<TITLE>
<Esc><Esc><Esc><Esc>
<Text>Input Cone Calib. Factor,l<Text>
<F2>l=0.0979<Enter><Esc><Esc>i4<Pause>ynnnlmmo2o3o4<Pause><Esc><Esc><NoG
uard>
<Esc><Esc>mmj+121(mj+131(mj+141(slo0.25<Enter>oAvgl<Enter>vslol<Enter>
Aog<Enter><Esc>owCm912ca02<Pause>wylmo409.4m<Enter>
<ENDDEF>
```

**E.2.2 Purpose, Requirements and Notes**

-averages 4 records, scales result and saves

- will operate as-is in both VP and VP2

-requires Nicolet 4094 records with 4 files of 4k points in each record, calibration factor for accelerometer (Typically about 0.05-0.1g/v), and endpoint in time for output file.

-will overplot the four files to confirm they are similar - if not, stop and adjust manually (e.g. average of three if one signal does not match)

*E.3 WINDCLIP.MAC*

**E.3.1 Macro**

```
<BEGDEF><CtrlF10><TITLE>windowing by CLIP<TITLE>
<NoGuard><Esc><Esc><Esc><Esc>
<Text>Select original signal to be windowed<Text>
iC<Pause>1n1mm
<Text>Set Horiz.Bounds around Main signal<Text>
uho<Pause>o<Pause><Enter>
<Text>Set Cursor to left bdy.then RTN<Text>
<Pause><AltA>
<Text>Set Cursor to right bdy. then RTN<Text>
<Pause><AltB>mmcmAo0<Enter>o0<Enter>mmcBmo0<Enter>o0<Enter><Esc>owCbg
f3wp15<Pause>yw1mm
<ENDDEF>
```

**E.3.2 Purpose, Requirements and Notes**

-used to isolate main shear wave (start and end selected by user) and place zeros in balance of signal

- will operate as-is in both VP and VP2

-requires Full signal (normally average from above)

*E.4 PHVELFQ2.MAC*

**E.4.1 Macro**

```
<BEGDEF><CtrlF10><TITLE>phvel1<TITLE>
<Esc><Esc><Esc><Esc><NoGuard>
<Text>Select upper data set<Text>
iB<Pause>1<Esc>
<Text>Select lower data set<Text>
<Esc><Esc>iB<Pause>2<Esc>dn1mmo2<Pause><Esc><Esc>mff1mmnnnf*ff2mmnnnf
*ff1cc*mj*123(ff3mcpp*s3o-
1<Enter>pr<Esc><Esc>owcphase.ad<Enter>y3o0<Enter>
o250<Enter>n4<CtrlF9>
<ENDDEF>

<BEGDEF><CtrlF9><TITLE>phvel2<TITLE>
<Esc><Beep>
<Text>Input distance between signals,x<Text>
<CALC>x= <Pause><Esc><CALC>z=x*6.28319<Enter><Esc><Esc>icphase.ad<Enter>
1n1mmmmmmmno1<Enter>po1<Enter>3oFreq.<Enter>mmmmmypi2p<Esc>ms2oz<Enter>
pometres<Enter><Esc><Esc>mmj*234oVelocity<Enter>om/s<Enter>dn4mmmm*o4
0<Enter>o80<Enter><Pause>
<ENDDEF>
```

**E.4.2 Purpose, Requirements and Notes**

-calculates shear wave velocity between two depths as a function of frequency

- will operate as-is in VP2 - cannot use in VP as phase unwrapping not available.

-requires upper & lower data set (normally 1m apart and windowed records from above) and difference in slant distances between depths.

-after end of macro, may manually vary frequency range for average velocity

*E.5 REVNORM2.MAC - CROSS-CORRELATION*

### E.5.1 Macro

```
<BEGDEF><CtrlF10><TITLE>rev.norm1<TITLE>
<Esc><Esc><Esc><Esc><NoGuard>
<REM>ssy2<Text>2 Sets of 8k(!temp2k!)-Preexisting file Conj1.wfm<Text>
<Text>Input End of Beginning Taper,b<Text><REM>
<F2>b=0.0ms<Enter>
<REM><Text>Begin. of End Taper,e<Text><REM>
e=409.4ms<Enter><Esc>
<Text>Select upper data& place in set1<Text>
iC<Pause>1<Esc>mff1mmyyyob<Enter>oe<Enter>f2dn2mo500<Enter><Esc>mfb2c
y<Beep>o60<Pause>o100<Pause>o5<Pause>yob<Esc><Esc>mff2*c1mj*122(ff2ii
o<Esc>owcconj1<Enter>wy1<F2>x=max2<Enter><Esc><CtrlF9>
<ENDDEF>

<BEGDEF><CtrlF9><TITLE>rev.norm2<TITLE>
<NoGuard><Beep>
<Text>Select lower data & place in Set 2<Text>
<Esc><Esc>iC<Pause>2<Esc>mff2mmyyyob<Enter>oe<Enter>f1fb1cypppy2b<Esc>
<Esc>mff2*c1mj*121(ff1iio<F2>y=x*max1<Enter><Esc><Esc><Esc><CtrlF8>
<ENDDEF>

<BEGDEF><CtrlF8><TITLE>rev.norm3<TITLE>
<Esc><Esc><F2>z=1/sqrt(y)<Enter><Esc><Esc>icconj1.wfm<Enter>1<Esc><Esc>
mmj*121(ff1iios1oz<Enter>oCrosscor12<Enter>o
<Enter><F2>t=dt*2048/2<Enter>
<Esc><Esc>mmjslot<Enter>o212<F2>s=-2*t<Enter><Esc>t2os<Enter>mja211oC
orr.CC<Enter><Beep>
<Text>After display use F2, max1 & tmax1 to get cross-cor & time
shift<Text>
dn1mm
<ENDDEF>
```

### E.5.2 Purpose, Requirements and Notes

-calculates shear wave velocity between two depths for a given frequency range

- will operate as-is in VP - minor changes required to run in VP2 (not done as PHVELFQ2 is recommended method)

-set-up for tapers at ends of signals as initially written for full signals (not recommended now), use first and last points in windowed signals

-must preselect frequency range to be used (from observation of FFT's or damping calculations - typically 30-70hz, 40-80Hz, etc.)

-requires upper & lower data set (normally 1m apart and windowed records from above)

- at end the maximum X-corr. coefficient and corresponding time shift are provided

-velocity calculated separately from difference in slant distances between depths and time shift

-Note: if size of sets adjusted in line 2 (ssy?), the corresponding number of points must be adjusted in line 3 of part 3 (dt*?/2)

## *E.6 REDWIND2.MAC*

### E.6.1 Macro

```
<BEGDEF><CtrlF10><TITLE>Redpath method<TITLE>
<Esc><Esc><Esc><Esc><NoGuard>
<Text>Set up for Windowed Cone FFT @ 2.9m<Text>
iCFFT2P029.wfm<Enter>1<Esc>
<Text>Input Lower Waveform<Text>
iC<Pause>2<Esc>mff2mmnnnf*<Esc><Esc>mmj/213(<Esc>owcratio.ad<Enter>y3
mo0<Enter>o500<Enter>ys4icratio.ad<Enter>4<Esc>mmm4mmyn*n<Esc><Esc>ms
4o-1<Enter>nvdn4mo150<Enter><Esc><Esc>mmf4o40<Enter>o80<Enter>co0<Enter>
nncn1c
<ENDDEF>
```

### E.6.2 Purpose, Requirements and Notes

-initial phase of damping calculation using the SRS method

-calculates slope of -ln {ratio[$FFT_{deep}/FFT_{shallow}$]} vs. frequency

- will operate as-is in VP2 - minor modifications for use in VP (available and routinely used)

-requires upper & lower data sets (normally windowed records from above)

-upper data set held constant for sounding and required as FFT

-after end of macro, may manually vary frequency range for slope fitting

-after all depths are calculated, a separate plot is made of the slopes vs. depth

*E.7 BASIC PROGRAM FOR RAYPATH BENDING CORRECTIONS*

### E.7.1 Program Listing

```
DECLARE FUNCTION sum! (nml!, p!, vel(), dz())
OPTION BASE 0
CLS
PRINT ""
PRINT ""
PRINT "RAYBEND-Velocity Calc. w/wo Ray Bending- Telford equations"
PRINT "Written by W.P.Stewart. Latest Revision 09-10-91"
PRINT ""
PRINT ""
CONST ARRAYSZ = 30, OFFSET = 1.1
'
INPUT "Enter Size of Arrays (Lines of data) [30]:  "; iarraysz
IF iarraysz = 0 THEN iarraysz = ARRAYSZ
DIM z(iarraysz), dz(iarraysz), t(iarraysz), dt(iarraysz), vel(iarraysz)
DIM thet(iarraysz), theta2(iarraysz)
INPUT "Print Input Filename"; file1$
OPEN file1$ FOR INPUT AS #1
INPUT "Print Output Filename"; file2$
OPEN file2$ FOR OUTPUT AS #2
INPUT "Enter X-offset [1.1m]"; xoff
IF xoff = 0 THEN xoff = OFFSET
PRINT #2, "Input Data     Calc. Data"
PRINT #2, "Depth    dT     dZ   Time"
INPUT #1, z(0), dt(0)
dz(0) = z(0)
t(0) = dt(0)
PRINT #2, USING "##.#  #.##### #.## #.#####"; z(0), dt(0), dz(0), t(0)
dist = SQR(z(0) ^ 2 + xoff ^ 2)
vel(0) = dist / dt(0)
nd = 1
DO UNTIL EOF(1)
   INPUT #1, z(nd), dt(nd)
   dz(nd) = z(nd) - z(nd - 1)
   t(nd) = t(nd - 1) + dt(nd)
   PRINT #2, USING "##.#  #.##### #.## #.#####"; z(nd), dt(nd), dz(nd),
t(nd)
   nd = nd + 1
LOOP
CLOSE #1
PRINT #2, "Depth   Time   Vray  Vstl    p    Theta"
PRINT #2, USING "##.#  #.##### ###.#"; z(0), t(0), vel(0)
FOR k = 1 TO (nd - 1)
   ic = 1
```

```
   IF z(k) <= 6! THEN
      p = .002
   ELSEIF z(k) <= 9 THEN
      p = .001
   ELSEIF z(k) <= 14 THEN
      p = .0005
   ELSE
      p = .0002
   END IF
100   updif = xoff - sum((k - 1), p, vel(), dz())
   num = (updif / (p * dz(k))) ^ 2
   denom = 1 + (updif / dz(k)) ^ 2
   vel(k) = SQR(num / denom)
   tsum = 0
   FOR j = 0 TO k
      tsum = tsum + dz(j) / (vel(j) * SQR(1 - (p * vel(j)) ^ 2))
   NEXT j
   IF ABS((tsum - t(k)) / t(k)) < .001 THEN GOTO 200
   IF tsum < t(k) THEN
      p = 1.02 * p
   ELSE p = .98 * p
   END IF
   ic = ic + 1
   GOTO 100
200 sint = p * vel(k)
tant = sint / SQR(1 - sint ^ 2)
thet(k) = 57.2958 * ATN(tant)
slvel = (SQR(z(k) ^ 2 + xoff ^ 2) - SQR(z(k - 1) ^ 2 + xoff ^ 2)) /
dt(k)
PRINT #2, USING "##.#  #.##### ###.# ###.# #.##### ##.#"; z(k), t(k),
vel(k), slvel, p, thet(k)
NEXT k
PRINT #2, "Depth dZ  Theta dX SumX"
sumx = 0
FOR i = 0 TO (nd - 1)
   sint = p * vel(i)
   tant = sint / SQR(1 - sint ^ 2)
   theta2(i) = 57.2958 * ATN(tant)
   dx = dz(i) * TAN(theta2(i) / 57.2958)
   sumx = sumx + dx
   PRINT #2, USING "##.# #.### ##.### #.#### #.####"; z(i), dz(i),
theta2(i), dx, sumx
NEXT i
CLOSE #2
END
```

```
FUNCTION sum (nm1, p, v(), dz())
'Computes summation term in Telford Eqn.
sum1 = 0
FOR i = 0 TO nm1
     sum1 = sum1 + p * v(i) * dz(i) / SQR(1 - (p * v(i)) ^ 2)
NEXT i
sum = sum1
END FUNCTION
```

## *E.8 BASIC PROGRAM FOR TRANSMISSIVITY AND DIVERGENCE CORRECTIONS*

### E.8.1 Program Listing

```
PRINT ""
PRINT ""
PRINT "TRANSDIV-Transmissivity & Divergence-From Depths&Velocities"
PRINT "Written by W.P.Stewart. Latest Revision 03-05-90"
PRINT "1st line-title,2nd line-No. of vels.,3rd to N-Depth/vel."
PRINT "Last-final depth"
PRINT ""
'
INPUT "Print Input Filename"; file1$
OPEN file1$ FOR INPUT AS #1
INPUT "Print Output Filename"; file2$
OPEN file2$ FOR OUTPUT AS #2
INPUT "Print Plot Filename"; file3$
OPEN file3$ FOR OUTPUT AS #3
INPUT #1, title$
PRINT #2, title$
PRINT #2, "Depth  Vel   T   ||T SumVZ   Dg     ||T*Dg  R/(||T*Dg) R/||T
R/Dg"
INPUT #1, novel
INPUT #1, d1, v1
INPUT #1, d2, v2
t = 1
pit = 1
PRINT #2, USING "###.#     #.## #.###"; d1, t, pit
PRINT #2, USING "      ####."; v1
   IF v2 = v1 THEN
      t = 1
   ELSE
      r = (v2 - v1) / (v2 + v1)
      t = (1 - ABS(r))
   END IF
pit = pit * t
sumvz = (d2 - d1) * v1
v0 = v1
d0 = d1
dg = 1
PRINT #2, USING "###.#     #.## #.### #### #.###"; d2, t, pit, sumvz, dg
FOR i = 1 TO (novel - 2)
   d1 = d2
   v1 = v2
   PRINT #2, USING "      ####."; v1
   INPUT #1, d2, v2
   sumvz = sumvz + ((d2 - d1) * v1)
   dg = v0 * (d2 - d0) / sumvz
```

```
   td = pit * dg
   corrr = ABS(d2 / td)
   corrt = ABS(d2 / pit)
   corrd = d2 / dg
   IF v2 = v1 THEN
      t = 1
   ELSE
      r = (v2 - v1) / (v2 + v1)
      t = (1 - ABS(r))
   END IF
   pit = pit * t
   PRINT #2, USING "###.#     #.## #.### #### #.###      #.###     ##.#
##.#  ##.#"; d2, t, pit, sumvz, dg, td, corrr, corrt, corrd
   PRINT #3, d2, corrr, corrt, corrd
NEXT i
d1 = d2
v1 = v2
PRINT #2, USING "      ####."; v1
INPUT #1, d2
   sumvz = sumvz + ((d2 - d1) * v1)
   dg = v0 * (d2 - d0) / sumvz
   td = pit * dg
   corrr = ABS(d2 / td)
   corrd = d2 / dg
   PRINT #2, USING "###.#          #.### #### #.###      #.###     ##.#
##.#"; d2, pit, sumvz, dg, td, corrr, corrd
END
```

*E.9 BASIC PROGRAM FOR RANDOM DECREMENT METHOD*

### E.9.1 Program Listing

```
'RANDEC-Random Decrement Analysis-after Yang et al
OPTION BASE 1
CLS
PRINT ""
PRINT ""
PRINT "RANDEC-Random Decrement Analysis-after Yang et al"
PRINT "Written by W.P.Stewart. Latest Revision 09-19-89"
PRINT ""
PRINT ""
CONST ARRAYSZ = 8192
CONST outsize = 1001
'
INPUT "Enter Size of Input Array (Lines of data) [8192]:  "; iarraysz
IF iarraysz = 0 THEN iarraysz = ARRAYSZ
DIM sig(iarraysz)
INPUT "Enter Size of Output Array (Lines of data) [1001]:  "; ioutsize
IF ioutsize = 0 THEN ioutsize = outsize
DIM sigout(ioutsize)
INPUT "Print Input Filename"; file1$
OPEN file1$ FOR INPUT AS #1
INPUT "Enter time step, dt(sec)"; dt
INPUT "Print Output Filename"; file2$
OPEN file2$ FOR OUTPUT AS #2
INPUT "Enter no. of subrecords to be used (even)"; n
INPUT "Enter Amplitude level for Analysis"; ramp
OPEN "CHK.OUT" FOR OUTPUT AS #3
'Delete Header Lines
FOR i = 1 TO 13
   INPUT #1, junk$
NEXT i
nd = 1
DO UNTIL EOF(1)
   INPUT #1, sig(nd)
   nd = nd + 1
LOOP
CLOSE #1
FOR i = 1 TO ioutsize
  sigout(i) = 0
NEXT i
ic = 1
FOR i = 1 TO n
'check for odd
  IF ABS(2 * INT(i / 2) - i) > .01 THEN
   FOR j = ic TO iarraysz
```

```
      IF sig(j) > ramp THEN EXIT FOR
   NEXT j
   ic = j
  ELSE
   FOR j = ic TO iarraysz
     IF sig(j) < ramp THEN EXIT FOR
   NEXT j
   ic = j
  END IF
  PRINT #3, i, ic - 2, sig(ic - 1)
  FOR k = 1 TO ioutsize
     sigout(k) = sigout(k) + sig(ic + k - 2)
  NEXT k
  PRINT i
NEXT i
FOR k = 1 TO ioutsize
   time = (k - 1) * dt
   sigavg = sigout(k) / n
   PRINT #2, USING "##.##### ##.#####"; time, sigavg
NEXT k
CLOSE #2
CLOSE #3
END
```

*E.10 BASIC PROGRAM FOR DAMPING SPIRALS*

### E.10.1 Program Listing

```
PRINT ""
PRINT ""
PRINT "RIMSPIRL-Calculate Real & Imaginary parts of Modal Spiral"
PRINT "Written by W.P.Stewart. Latest Revision 01-03-91"
PRINT ""
PRINT ""
INPUT "Print Plot Filename"; file3$
OPEN file3$ FOR OUTPUT AS #3
INPUT "Damping value as decimal=[0.03]"; damp
IF damp = 0 THEN damp = .03
INPUT "Phase velocity m/s = [167.]"; vel
IF vel = 0 THEN vel = 167!
INPUT "Distance between records m = [5]"; dist
IF dist = 0 THEN dist = 5
INPUT "Ratio of distances upper/lower = [5/10]"; ratio
IF ratio = 0 THEN ratio = .5
INPUT "Trans. & Div. Factor"; td
PRINT #3, CHR$(34) + "damp=", damp, "vel=", vel, "dist=", dist,
"ratio=", ratio, "td=", td
doc = dist / vel
mddoc = -damp * doc
INPUT "Lowest value of w (rad/sec)=[253.11]"; wlow
IF wlow = 0 THEN wlow = 253.11
INPUT "Highest value of w (rad/sec)=[691]"; whigh
IF whigh = 0 THEN whigh = 691
INPUT "Increment of w = [7.66988]"; wstep
IF wstep = 0 THEN wstep = 7.66988
FOR w = wlow TO (whigh + wstep) STEP wstep
   fact = td * ratio * EXP(mddoc * w)
   real = fact * COS(doc * w)
   imag = fact * SIN(doc * w)
   PRINT #3, w, real, imag
NEXT w
CLOSE #3
END
```

## APPENDIX F

## VARIOUS MEASUREMENTS OF DAMPING

The purpose of this appendix is to relate various measurements of damping; wave attenuation ($\alpha$), oscillator (mass, spring, dashpot) models with damping ratio ($\beta$), and cyclic triaxial and pressuremeter tests ($A_{loop}$). The discussion will be limited to shear waves only and will assume a constant hysteresis model (i.e. damping is independent of frequency) as most laboratory testing has indicated this is the behaviour of soil.

### *F.1 VISCOELASTIC MATERIALS IN SHEAR*

For elastic materials in shear, the shear stress $\tau$, is related to the shear strain, $\gamma$, by:

[F.1] $\tau = G\gamma$

For viscoelastic materials, by the correspondence principle (from Bland, 1960):

[F.2] $\tau = G'\gamma$

where: $G'$ = a complex shear modulus.

For constant hysteretic model:

[F.3] $G' = G_1 + i\ G_2$ where $i = \sqrt{-1}$

(no dependence on frequency).

*F.2 WAVE ATTENUATION IN VISCOELASTIC MATERIAL*

This section will present the results for a travelling wave in a viscoelastic material, following O'Connell & Budiansky, 1978. For a sinusoidal shear wave with frequency, $\omega$, in homogeneous viscoelastic material ($\rho$=density), the wave equation can be expressed as:

[F.4] $$\rho(d^2u/dt^2) = G'(d^2u/dx^2)$$

which has the solution:

[F.5] $$u = e^{-\alpha x} * e^{i\omega\{t-x/c\}}$$

where:

[F.5] $$\alpha = \omega V_i/(V_r^2+V_i^2)$$

[F.6] $$c = (V_r^2+V_i^2)/V_r$$

[F.7] $$V_r + iV_i = \sqrt{\{G'/\rho\}}$$

Equating Real and Imaginary parts:

[F.8] $$G_1 = \rho(V_r^2-V_i^2)$$

[F.9] $$G_2 = 2\rho V_r V_i$$

In order to prove that this is the solution we differentiate the equation for u. Let $e^{i\omega t}\ e^{-x(\alpha+i\omega/c)} = Y$ :

Then $$d^2u/dt^2 = Y(-\omega^2)$$

and $$d^2u/dx^2 = Y(\alpha+i\omega/c)^2$$

Therefore we require:

[F.10] $$G'/\rho = -(\omega/\{\alpha+i\omega/c\})^2$$

Inverting this equation gives

[F.11] $$\rho G_1/(G_1^2+G_2^2) = -(\{\alpha/\omega\}^2-\{1/c\}^2) \qquad [A]$$

[F.12] $$-\rho G_2/(G_1^2+G_2^2) = -2\alpha/(c\omega) \qquad [B]$$

Returning to the proposed solution:

[F.13] $G_1 = \rho(V_r^2 - V_i^2)$

[F.14] $G_2 = 2\rho V_r V_i;\ V_r = G_2/(2\rho V_i)$

[F.14] in [F.13] gives:

[F.15] $G1 = \rho[G_2^2/(4\rho^2 V_i^2) - V_i^2]$

Let $V_i^2 = J$

Then $4\rho^2 J + 4G_1\rho J - G_2^2 = 0$

[F.16] $V_i^2 = (1/2\rho)\ (-G_1+\sqrt{\{G_1^2 + G_2^2\}})$

[F.16] in [F.13] gives:

[F.17] $V_r^2 = (1/2\rho)\ (G_1 + \sqrt{\{G_1^2 + G_2^2\}})$

Adding gives:

[F.18] $V_r^2 + V_i^2 = (1/\rho)\ \sqrt{(G_1^2 + G_2^2)}$

Therefore:

[F.19] $(\alpha/\omega)^2 = [(1/\{2\rho\})\ (-G_1+\sqrt{\{G_1^2+G_2^2\}}]\ /\ [(1/\rho^2)\{G_1^2+G_2^2\}]$

[F.20] $(1/c)^2 = [(1/\{2\rho\})\ (G_1+\sqrt{\{G_1^2+G_2^2\}}]\ /\ ((1/\rho^2)\{G_1^2+G_2^2\}]$

[F.21] $-[(\alpha/\omega)^2 - (1/c)^2] = (\rho G_1)/(G_1^2 + G_2^2)$

as required in [A].

And:

[F.22] $-2\alpha/(c\omega) = -2V_i V_r/(V_r^2 + V_i^2)^2$

From previously equating imaginary parts:

[F.23] $V_i V_r = G_2/(2\rho)$

and from squaring eqn.F.18:

[F.24] $(V_r^2 + V_i^2)^2 = (1/\rho^2)(G_1^2 + G_2^2)$

so:

[F.25] $$-2\alpha/(c\omega) = -2[G_2/(2\rho)]/[(1/\rho^2)(G_1^2 + G_2^2)]$$
$$= -\rho G_2/(G_1^2 + G_2^2)$$

as required in [B].

Therefore the proposed solution does satisfy the differential equation, and we have related the attenuation $\alpha$ and the phase velocity c to the viscoelastic constants $G_1$ and $G_2$ as given by equations F.19 and F.20.

## *F.3 COMPLEX OSCILLATOR AND VISCOELASTIC MATERIAL*

This section will develop the concept of the complex oscillator, and compare the resulting modulus to that for a viscoelastic material, following Lysmer (1980). This development will be restricted to harmonic loading ($P = e^{i\omega t}$). A simple one-dimensional model incorporating damping consists of: mass(m), spring(k), and dashpot(c), and has the following equation of motion:

[F.26] $$mu'' + cu' + ku = P\, e^{i\omega t}$$

and the relationship between displacement and loading is given by the transfer function $H(\omega)$:

[F.27] $$P = u\, H(\omega)$$

with:

[F.28] $$H(\omega) = k + i\omega c - \omega^2 m$$

Now, consider a complex oscillator which will be defined by having the following equation of motion:

[F.29] $mu'' + k^*u = P\, e^{i\omega t}$

with:

[F.30] $H^*(\omega) = k^* - \omega^2 m$

Let us now define the fraction of critical damping, $\beta$ (damping ratio, modal damping):

[F.31] $\beta = c/c_c = c/(2\sqrt{\{km\}})$

Now if we let:

[F.32] $k^* = k(1 - 2\beta^2 + i2\beta\sqrt{\{1-\beta^2\}})$

then we can show that the magnitudes of the transfer functions are equal:

[F.33] $\left|H(\omega)\right| = \sqrt{(\{k-\omega^2 m\}^2 + \{\omega c\}^2)}$

[F.34] $\left|H^*(\omega)\right| = \sqrt{(\{k-\omega^2 m\}^2 - 4k\beta^2\{k-\omega^2 m\} + 4k\beta^2 + 4k\beta^2 - 4k^2\beta^4)}$

$$= \sqrt{(\{k-\omega^2 m\}^2 + 4k\beta^2\omega^2 m)}$$

Substitute for $\beta = c/(2\sqrt{\{km\}})$:

$$\left|H^*(\omega)\right| = \sqrt{(\{k-\omega^2 m\} + (\omega c)^2)} = \left|H(\omega)\right|$$

Similarly it can be shown (Lysmer,1980) that the phase difference $\delta\phi$ is given by:

[F.35] $\delta\phi = 2\beta/(1 + \{\omega/\omega_o\})$

But if we assume that $\beta$ is only defined at $\omega=\omega_o$, then

[F.36] $\delta\phi=\beta$

and we will ignore $\delta\phi$ if $\beta$ is small (say <10%).

Comparing the complex spring stiffness, $k^*$, to an equivalent complex modulus for solid materials we can approximate the dashpot models as:

[F.37] $$G^* = G(1-2\beta^2+i2\beta\sqrt{\{1-\beta^2\}}) \simeq G(1+i2\beta)$$

By comparison with the viscoelastic material:

[F.38] $$2\beta \simeq G_2/G_1; \ \beta \simeq G_2/(2G_1)$$

We now wish to relate the damping ratio to wave attenuation. Substituting from eqns. F.13 and F.14:

[F.39] $$\beta \simeq G_2/(2G_1) = 2\rho V_r V_i/(2\rho\{V_r{}^2-V_i{}^2)=V_r V_i/(V_r{}^2-V_i{}^2)$$

and from the definitions of $\alpha$ and c:

[F.40] $$V_i = V_r\ (\alpha c/\omega)$$

and substituting in eqn. F.39 gives:

[F.41] $$\beta = (\alpha c/\omega)/(1 - \{\alpha c/\omega)^2)$$

For commonly measured values we find $\alpha c/\omega \simeq 0.01$, therefore:

[F.42] $$\beta \simeq \alpha c/\omega$$

Now if we consider a complex wavenumber: $\kappa = K + i\alpha'$ and if we let $K = \omega/c$ and $\alpha'=\alpha$, then:

[F.43] $$\alpha'/K = \alpha c/\omega = V_i/V_r \simeq \beta$$

This is likely the justification of Johnston and Toksoz (1981) for using the complex wave number for calculating damping.

## *F.4 OSCILLATOR AND STRESS-STRAIN LOOPS*

This section will use the mass-spring-dashpot oscillator to develop the relationship between the damping ratio and stress-strain loops measured in cyclic triaxial laboratory tests and field pressuremeter tests following the CIVL581 course notes of Byrne (1988). A typical loop is shown in Fig.2.1. This development will be restricted to harmonic loading at the natural frequency, $\omega_o$.

The force in a dashpot is given by $F_d = cu'$ (where $u' = du/dt$). Thus the work done in one cycle of loading is given by the area of the hysteresis loop, $A_{loop}$:

[F.44] $$A_{loop} = \int F_d du = \int cu'u'dt = \int c(u')^2 dt$$

For sinusoidal displacement: $u = U \sin(\omega t)$ and $u' = U\omega \cos(\omega t)$

[F.45] $$(u')^2 = U^2\omega^2 \cos^2(\omega t) = U^2\omega^2(1/2)(1 + \cos\{2\omega t\})$$

Substitute in eqn.F.44 and integrate over 1 period (0-T)

[F.46] $$\int_0^T cU^2\omega^2 \frac{1}{2} (1+\cos\{2\omega t\})dt = \frac{1}{2}cU^2\omega^2 \left| t+ \frac{1}{2\omega} \sin(2\omega t) \right|_0^T$$

Evaluate for $\omega = \omega_o$, and use $T=2\pi/\omega_o$, then

[F.47] $$A_{loop} = cU^2\omega^2 T/2 = cU^2\omega_o\pi = (2\beta\sqrt{\{km\}})\ U^2\ \sqrt{\{km\}}\ \pi$$
$$= 2\pi\beta kU^2$$

[F.48] $$\beta = A_{loop}/(2\pi kU^2)$$

As shown in Fig.2.1, the area of the right triangle below line from origin to tip of the loop is given by:

[F.49] $$A_{tri} = 1/2\ k\ U2$$

[F.50] $$A_{loop}/A_{tri} = 2\pi\beta kU^2/(\{1/2\}kU^2)$$

[F.51] $$\beta = A_{loop}/(4\pi A_{tri})$$

## *F.5 SUMMARY*

Thus we have evaluated the damping coefficient as:

Definition:

$$\beta = c/c_c = c/(2\sqrt{\{km\}})$$

And (for viscoelastic materials at $\omega_o$):

$$\beta \simeq G_2/(2G_1)$$

$$\beta = \alpha c\omega/(\omega^2-\{\alpha c\}^2)/ \simeq \alpha c/\omega$$

$$\beta = A_{loop}/(4\pi A_{tri})$$